2016-07-15

The Drosophila Homolog of the Intellectual Disability Gene ACSL4 Acts in Glia to Regulate Morphology and Neuronal Activity: A Dissertation

Caitlin M. Quigley
University of Massachusetts Medical School

THE *DROSOPHILA* HOMOLOG OF THE INTELLECTUAL DISABILITY GENE *ACSL4* ACTS IN GLIA TO REGULATE MORPHOLOGY AND NEURONAL ACTIVITY

A Dissertation Presented

By

CAITLIN M. QUIGLEY

Submitted to the Faculty of the

University of Massachusetts Graduate School of Biomedical Sciences, Worcester

in partial fulfillment of the requirements for the degree of

DOCTOR OF PHILOSOPHY

JULY 15TH, 2016

MD/PHD PROGRAM

THE *DROSOPHILA* HOMOLOG OF THE INTELLECTUAL DISABILITY GENE *ACSL4* ACTS IN GLIA TO REGULATE MORPHOLOGY AND NEURONAL ACTIVITY

A Dissertation Presented By

CAITLIN M. QUIGLEY

The signatures of the Dissertation Defense Committee signify completion and approval as to style and content of the Dissertation

Hong-Sheng Li, Ph.D., Thesis Advisor

Vivian Budnik, Ph.D., Thesis Advisor

Michael Francis, Ph.D., Member of Committee

David Weaver, Ph.D., Member of Committee

Dorothy Schafer, Ph.D., Member of Committee

Justin Thackeray, Ph.D., Member of Committee

The signature of the Chair of the Committee signifies that the written dissertation meets the requirements of the Dissertation Committee

Patrick Emery, Ph.D., Chair of Committee

The signature of the Dean of the Graduate School of Biomedical Sciences signifies that the student has met all graduation requirements of the school.

Anthony Carruthers, Ph.D.,

Dean of the Graduate School of Biomedical Sciences

MD/PhD Program

July 15th, 2016

DEDICATION

When I began my PhD, I little knew the perseverance, tenacity, and resourcefulness completing it would require. No one person can do this on their own. Accordingly, I dedicate this work to the people in my life who helped me survive it, foremost among them my father, James Quigley, and my friends Tia Brodeur and Michael Gorczyca. I also include my cat, Henry, for giving me a reason to leave the lab occasionally, and always being my failsafe alarm clock.

ACKNOWLEDGEMENTS

I wish to acknowledge the following:

My mentor, Dr. Hong-Sheng Li, for giving me the opportunity to perform this research, and the freedom to investigate the areas of most interest to me.

My co-mentor, Dr. Vivian Budnik, for believing in me and this project from the very beginning, always listening to my ideas and goals with respect, and always pushing me harder to succeed.

Dr. Marc Freeman for lending me his wisdom, guidance, expertise, and extensive stock collection as I forged this project.

The members of my committee for their advice and encouragement over the years.

ABSTRACT

Recent developments in neurobiology make it clear that glia play fundamental and active roles, in the adult and in development. Many hereditary cognitive disorders have been linked to developmental defects, and in at least two cases, Rett Syndrome and Fragile X Mental Retardation, glia are important in pathogenesis. However, most studies of developmental disorders, in particular intellectual disability, focus on neuronal defects. An example is intellectual disability caused by mutations in ACSL4, a metabolic enzyme that conjugates long-chain fatty acids to Coenzyme A (CoA). Depleting *ACSL4* in neurons is associated with defects in dendritic spines, a finding replicated in patient tissue, but the etiology of this disorder remains unclear. In a genetic screen to discover genes necessary for visual function, I identified the *Drosophila* homolog of *ACSL4*, *Acsl*, as a gene important for the magnitude of neuronal transmission, and found that it is required in glia. I determined that *Acsl* is required in a specific subtype of glia in the *Drosophila* optic lobe, and that depletion of *Acsl* from this population causes morphological defects. I demonstrated that *Acsl* is required in development, and that the phenotype can be rescued by human *ACSL4*. Finally, I discovered that ACSL4 is expressed in astrocytes in the mouse hippocampus. This study is highly significant for understanding glial biology and neurodevelopment. It provides information on the role of glia in development, substantiates a novel role for *Acsl* in glia, and advances our understanding of the potential role that glia play in the pathogenesis of intellectual disability.

TABLE OF CONTENTS

LIST OF TABLES

LIST OF FIGURES

PREFACE

All experiments presented herein were designed by myself with input from my mentors and committee, and performed by myself exclusively, including data acquisition and analysis. Dr. Michael Gorczyca and Ms. Melinda Futran generously assisted with blinding data before analysis.

CHAPTER I. INTRODUCTION

1.1. The role of the nervous system

To sustain life, an organism must have the ability to detect information from and interact with its environment. This function is fulfilled by the nervous system in animals, which collects and processes sensory input, and generates behavioral output. Moreover, in complex animals the nervous system institutes high order cognitive operations, allowing us not only to sense and do, but also to think and feel. These functions are mediated by the activity and interaction of only two basic cell types: neurons and glia. Despite their significance, neurons and glia were not described until the late 19th century, and while the importance of neurons was almost immediately recognized, glia were not seriously studied until the mid-1980s, when Albert Einstein's preserved brain was found to have a preponderance of these long-ignored cells (Diamond et al., 1985). In the ensuing decades, research on glia, and the interaction of neurons and glia, has made significant strides, deepening our understanding of how the nervous system accomplishes its astonishing breadth of function.

1.2. Cellular Composition of the Nervous System

1.2.1. Neurons and their functions

Canonically, neurons were believed to be the only cells of the nervous system capable of cell-cell communication. This has since been proven to be incorrect (Hösli et al., 1981; Konnerth et al., 1988); however, neurons are the predominant source of electrical activity within the nervous system, generating both slow gradient potentials that increase in response to stimuli, and fast action potentials that are triggered once stimuli reaches a defined threshold (Stuart et al., 1997). Indeed, the electrical activity of neurons is the primary defining characteristic of this cell population.

Through their electrical properties, neurons are able to communicate the presence of stimuli to other neurons, as well as glia, over long distances. Through the interaction of networks of neurons, information can be processed and interpreted, allowing downstream neurons to generate a response to stimuli. Neurons communicate this information through synapses, a specialized connection between cells. At the synapse, the upstream, or pre-synaptic, neuron releases signaling molecules that traverse the extracellular space to

contact receptors on the downstream, or post-synaptic, neuron (Ackermann et al., 2015). Once the post-synaptic receptors are stimulated, this downstream neuron can propagate the signal onto the next neuron in the synaptic network. In mammals, neurons are polarized, receiving post-synaptic input on specialized processes called dendrites, and generating pre-synaptic output from a separate process called the axon. Mammalian neurons may have multiple dendrites and receive input from many other neurons, but elaborate only one axon. The complexity of this morphology is increased by structures on the dendrites called dendritic spines, at which the post-synaptic machinery is located (Nimchinsky et al., 2002; Govek et al., 2005; Buard et al., 2010). In contrast, many neurons in arthropods such as *Drosophila* are unipolar, and both receive input and generate output from the same structure.

A central organizing principle of complex animal brains is the differentiation between anatomical areas where neuronal processes travel, and areas where they form synaptic connections. Synaptically dense areas are referred to as neuropil, and it is within these structural domains that information is transmitted, processed, and refined.

1.2.2. Glia and their functions

While glia were first identified in the mid-19th century, they were mostly ignored by the field of neuroscience until the last few decades, in large part because it was not clear that glia were capable of participating in the communication and integration of information in the nervous system. Recent research has profoundly expanded our knowledge of glial function, and it is now clear that they play fundamental, active roles in development, function, and maintenance of the nervous system. There are multiple subtypes of glia in the mammalian brain, which serve different functions (Purves et al., 2001). For example, the microglia are the phagocytic cells of the nervous system, and function both to remove debris from surrounding tissue, as well responding to and resolving inflammation and injury. Their sensitivity to changes in the delicate neuronal tissue is paramount, and is believed to be achieved through active physical surveillance of surrounding tissue (Kato et al., 2016; Tay et al., 2016), as well as their expression of ion channels (Madry and Attwell, 2015; Echeverry et al., 2016; Pappalardo et al., 2016). In addition to phagocytosing infectious agents, microglia also engulf and remove the

remains of damaged or apoptotic cells, and extracellular plaques (Gyoneva et al., 2016; Spangenberg and Green, 2016).

In contrast, ensheathing glia, such as oligodendrocytes and Schwann cells, enwrap and support neuronal axons as they travel between neuropil in the brain, and as they travel outside the central nervous system. Ensheathing glia provide myelin sheaths to mammalian axons, which are dense membranous structures encircling neuronal projections. Myelin sheaths are crucial to preventing ion leakage, and increasing the speed of electrical impulses as they travel long distances both within and without the brain (Friess et al., 2016; Mathews and Appel, 2016). Ensheathing glia also provide trophic support to axons, maintaining these structures in a healthy state at long distances from the neuronal cell body (Barateiro et al., 2016).

However, for the purposes of this introduction, I will focus on the function of astrocytes, or neuropil glia, the subtype most heavily involved in neuronal signaling.

i. Astrocyte glia functions in adult physiology

In the adult, astrocytic glia have been demonstrated to function in synaptic communication between neurons. Astrocytic glia are intimately associated with synapses in the neuropil (Allen and Barres, 2005, 2009; Eroglu et al., 2008; Eroglu and Barres, 2010; Halassa and Haydon, 2010; Reichenbach et al., 2010). Their proximity to the synaptic cleft, the extracellular space between synaptic partners, greatly facilitates their role in the clearance of signaling molecules from the synapse. Moreover, glia are the major cell type involved in neurotransmitter recycling, and are capable not only of uptake and metabolism of neurotransmitters, but also return of neurotransmitters to the pre-synaptic neuron (Barres, 2008; Allen and Barres, 2009). These functions have been particularly well established in excitatory glutamate signaling (Marcaggi and Attwell, 2004; Waagepeterson et al., 2005; Bak et al., 2006; Chen et al., 2006; Bringmann et al., 2009; Halassa and Haydon, 2010). These functions are essential for maintaining the ability of neurons to communicate.

Another important function of glia is maintaining extracellular ion homeostasis (Walz, 1989; Silver and Ereciriska, 1992; Simard and Nedergaard, 2004). If the

extracellular concentrations of ions are disturbed, neurons are unable to transfer charged particles across their membranes in sufficient quantities to generate an electrical potential. Glia act to both store ions and maintain regular extracellular concentrations, allowing neurons to continue communicating.

Finally, astrocytic glia function as critical links between the vasculature and neurons. Astrocytes uptake and store glucose, subsequently converting it into lactate, the primary metabolic substrate of neurons (Blanger et al., 2011; Blumrich et al., 2016; Steinman et al., 2016). In this way, astrocytes act as a metabolic sink that can supply energy to neurons in parallel with their levels of activity. Moreover, astrocytes are tightly coupled with the vasculature in the brains, and both regulate the barrier along the vasculature which insulates the brain from toxins or infectious material in the blood stream, and regulate cerebral blood flow, redirecting it to areas of higher neuronal activity (Abbott et al., 2006; Cheslow and Alvarez, 2016; Nuriya and Hirase, 2016).

ii. Astrocyte glia functions in development

Glia serve multiple essential roles in development, some of which are conserved across evolution in diverse species. These conserved functions include axon targeting of developing neurons and synaptic development.

Glia help guide axons during development by providing intermediate targets during axon outgrowth, expressing both attractive and repulsive targeting cues, and often aid in final targeting (Dodd and Jessell, 1988; Araújo and Tear, 2003; Chotard and Salecker, 2008; Pfrieger, 2009). During this process, neurons and glia communicate reciprocally, with neurons providing migration and survival cues to glia (Tsai and Miller, 2002; Pfrieger, 2009).

Glia support synaptic development through both contact-independent and contact-dependent mechanisms, and are essential for all phases of synaptic development, from formation, to maturation, to pruning. In synapse formation, glia facilitate synaptic partnering through their targeting functions, and moreover support dendritic outgrowth and the development of dendritic spines (Murai et al., 2003; Carmona et al., 2009; Buard

et al., 2010). Glia promote synaptic maturation by releasing secreted signals that, for example, enhance the efficacy of transmitter release at the pre-synapse or the expression and stabilization of receptors at the post-synapse (Nägler et al., 2001; Steinmetz et al., 2006; Perez-Gonzalez et al., 2008). A handful of these secreted factors have been identified, including thrombospondin and cholesterol (Mauch, 2001; Christopherson et al., 2005), both of which facilitate maturation of the pre-synapse. Finally, microglia in mammals and neuropil glia in *Drosophila* have been demonstrated to engulf and remove pre-synaptic and axonal debris during development, allowing the nervous system to fine tune its synaptic networks (Eroglu et al., 2008; Schafer and Stevens, 2010, 2014; Schafer et al., 2012).

iii. Roles for glia in developmental disorders and intellectual disability

Given the fundamental roles glia play in development, it is not surprising that they are involved in the pathogenesis of developmental disorders. Glia are strongly implicated in the development of schizophrenia, and potentially bipolar disorder and depression (Dong and Zhen, 2015; Wang et al., 2015). However, the best evidence to date comes from glial malfunction in models of intellectual disability. Rett Syndrome, caused by

mutations in the gene MeCP2, is a severe neurodevelopmental disorder characterized by intellectual disability. MeCP2 was shown to act in astrocytes to non-autonomously influence neuronal dendritic morphology, and glutamate levels (Ballas et al., 2009; Lioy et al., 2011; Makinodan, 2015). Fragile X Syndrome is characterized by learning difficulties, reduced cognitive capacity, and even mood instability and autism. Depletion of the Fragile X Syndrome protein FMRP from astrocytes reduced dendritic arborization and synaptic protein aggregates in co-culture with wild type neurons (Tessier and Broadie, 2008; Cheng et al., 2012). Finally, Alexander Disease, a disorder involving nervous system dysfunction such as seizures and psychomotor retardation, is associated with mutations in the astrocytic gene Glial Fibrillary Acidic Protein (GFAP) (Brenner et al., 2001). Astrocytes bearing this mutation were found to express reduced levels of glutamate transporter, and were unable to regulate glutamate levels in co-culture with neurons (Tian et al., 2010). Together, this body of evidence clearly demonstrates a role for glia in the pathogenesis of intellectual disability.

1.3. Genetic Underpinnings of Intellectual Disability

1.3.1. Prominent genes identified in intellectual disability and their functional groupings

While intellectual disability is a heterogenous disease, and can be linked to mutations in many different genes on many different chromosomes, common phenotypes are observed across populations. As discussed above, defects in dendrites are frequently found in models of intellectual disability (Purpura, 1974; Kaufmann and Moser, 2000), as are defects in excitatory neurotransmitter recycling and neurotransmitter release (Renieri et al., 2005). This clustering of phenotypic effects suggests that the genes underlying intellectual disability can be grouped together by common functions or pathways. Indeed, on the X-chromosome alone, mutations associated with intellectual disability can be grouped into those affecting Rho GTPases and dendritic outgrowth (FMR1, OPHN1, and PAK3), those involved in regulating Rab GTPases and synaptic vesicle transport (GDI1 and IL1RAPL1), and those involved in regulation of gene expression (MeCP2, FMR2, and ARX). In addition, there are genes whose functional effect is more difficult to

classify, termed ‘orphan mechanism’ genes. Among this group, many genes have plausible functions in the nervous system, being associated with neurotransmitter receptors (Discs Large Homolog 3 (DLG3)), or transport of crucial metabolites like creatine (Solute Carrier Family 6 Member 8 (SLC6A8)). The function of the remaining genes is more difficult to interpret. One such gene, Acyl-CoA Synthetase Long-chain 4 (*ACSL4*), encodes a long-chain fatty acid-CoA synthetase, whose function in the nervous system is still being elucidated.

1.3.2. *ACSL4* an X-linked intellectual disability gene

i. Discovery and clinical presentation

ACSL4 was discovered as a gene involved in intellectual disability after mutations in its coding sequence were identified in two unrelated families with non-specific X-linked intellectual disability (Piccini et al., 1998; Meloni et al., 2002). Individuals with either point mutations or deletions were identified, and affected individuals demonstrated non-progressive cognitive deficiency ranging from moderate to severe. It was estimated

that mutations in *ACSL4* are responsible for approximately 1% of all X-linked intellectual disability (Meloni et al., 2002).

ii. What is *ACSL4* and what does it do?

ACSL4 is one of five human ACSL genes. The protein product of *ACSL4*, ACSL4, is a metabolic enzyme that conjugates long-chain fatty acids to Coenzyme A, producing acyl-CoA substrates for lipid catabolism and metabolism (Cao et al., 1998). ACSL4 demonstrates a preference for arachidonic acid (Digel et al., 2009), the most abundant lipid in the mammalian brain. Upon conjugation to CoA, arachidonic acid becomes arachidonoyl-CoA. The predominant splice isoform of ACSL4 in the brain, isoform 2, includes an additional N terminal moiety that changes the putative localization of ACSL4 from the cytoplasm to the endoplasm reticulum (Meloni et al., 2002). Thus, while metabolic functions for *ACSL4* have been documented in other tissues (Mashek et al., 2006; Golej et al., 2011; Küch et al., 2014), such as fatty acid uptake and prostaglandin release, it seems likely that in the brain it is more heavily involved in the production of acyl-CoAs for protein modification.

iii. Why is *ACSL4* a good candidate for study?

Three pieces of evidence indicate that *ACSL4* may be a good candidate for study. First, the burden of disease in families carrying *ACSL4* mutations is severe, and a more in depth understanding of the pathogenesis involved may lead to better treatment options. Indeed, X-linked intellectual disability is predicted to be responsible for 20-25% of all cases of intellectual disability in males, so any insight gained from studying *ACSL4* may have broad applications to other patient populations. Second, *ACSL4* comes from a family of conserved Acyl-CoA synthetases, each containing multiple conserved domains, that have homologs in multiple vertebrate and invertebrate models. The evolutionary conservation points to an essential function, and the presence of homologs in multiple model organisms facilitates the study of endogenous function. Third, what the essential, endogenous function may be is still unknown. Given its role in fatty acid metabolism, *ACSL4* is likely to influence multiple pathways, possibly in a cell- or tissue-specific manner. Thus, the potential for novel discoveries in research devoted to *ACSL4* is high.

1.4. *ACSL4* Regulates Multiple Cellular Processes Through Fatty Acid Channeling

1.4.1. What is fatty acid channeling?

After uptake at the plasma membranes, the intracellular pool of unesterified fatty acids may be metabolized via two pathways. The first pathway is the production of eicosanoids. The eicosanoid pathway oxidizes 20-carbon chain fatty acids into prostaglandins and related metabolites, including thromboxanes and leukotrienes. Together, these molecules are known as 'locally acting hormones', and have well documented activities in blood clotting, inflammation, vasodilation, and apoptosis (Sumida et al., 1993; Cao et al., 2000). Prostaglandins are produced from arachidonic acid, and the first step in this pathway is performed by the cyclooxygenase, or COX, family of enzymes. The second pathway is the production of Acyl-CoA conjugates by the ACSL family of enzymes. Conjugation to CoA is necessary before fatty acids can be used in either lipid catabolism (e.g. production of triglycerides and protein modification), or metabolism (e.g. oxidation to form ATP) (Washizaki et al., 1994; Brash, 2001; Digel

et al., 2009; Grevengoed et al., 2014). Given the strong preference of ACSL4 protein for arachidonic acid, it seems likely that the phenotype of *ACSL4* loss arises from an increase in the intracellular pool of free arachidonic acid, and/or the loss of arachidonoyl-CoA.

1.4.2. Potential processes that can be regulated by free arachidonic acid

Free arachidonic acid can regulate cellular processes directly, or through its metabolism into prostaglandins. While the potential mechanisms through which free arachidonic acid may act in the nervous system are numerous, and include the production of reactive oxygen species (Cocco et al., 1999), activation of the inflammatory response (Kuehl and Egan, 1980), stimulation of blood clotting (Rao and White, 1985), and regulation of arterial smooth muscle cells (Neeli et al., 2003), the two most likely mechanisms involved in this project are discussed below.

i. Gene transcription

In order to regulate fatty acid metabolism, cells rely on multiple sensing and effector systems. One such system involves the regulation of gene transcription (Sumida et al., 1993; Georgiadi and Kersten, 2012). Peroxisome proliferator-activated receptors

(PPARs) are members of the hormone sensing superfamily of transcription factors. PPARs are ligand-activated transcription factors, with a general preference for binding long chain polyunsaturated fatty acids, such as arachidonic acid (Coleman et al., 2002; Hunt and Alexson, 2002). Upon binding their ligand, PPARs bind to PPAR response elements in DNA, and subsequently either repress or activate transcription. Proven targets of PPAR-regulated transcription include genes involved in fatty acid metabolism, such as genes involved in lipid uptake, lipogenesis, peroxisomal β-oxidation, and cholesterol metabolism (Rakhshandehroo et al., 2010; McMullen et al., 2014). However, given the range of pathways affected by fatty acids and their metabolites, it is plausible that PPARs regulate a substantially wider array of genes. Some evidence for this hypothesis is already available, as PPAR-regulated gene transcription is necessary for adipocyte differentiation (Rosen et al., 1999), and PPARs can target genes involved in inflammation (Rakhshandehroo et al., 2010; McMullen et al., 2014). It is thus possible that free arachidonic acid can regulate the transcription of genes involved in neuronal, glial, or general brain development.

ii. Actin dynamics

Arachidonic acid can regulate actin dynamics through its metabolism into prostaglandins (Glenn and Jacobson, 2002). Prostaglandin regulation of the actin cytoskeleton is highly context dependent, with a single prostaglandin, such as PGE_2, capable of both increasing and decreasing actin fiber assembly and myosin contractility in different tissue and cell populations, and even at different developmental time points (Spracklen et al., 2014). Given this complexity, it is difficult to propose an exact pathway through which prostaglandins may influence actin dynamics. Indeed, a context dependent role for prostaglandin-mediated actin regulation in the nervous system seems likely, as it has been demonstrated that application of exogenous arachidonic acid to neuron cell culture increased the outgrowth of neuronal processes at low doses, and inhibited them at high doses (Smalheiser et al., 1996; Meloni et al., 2009). This significant result demonstrates that arachidonic acid and its products can alternately enhance and inhibit actin dynamics and myosin contractility in the nervous system. In the case of enhancement of actin dynamics, cell culture analysis demonstrated that prostaglandins increase actin fiber assembly and cell motility through activation of either protein kinase

A (PKA) or protein kinase C (PKC) (Spracklen et al., 2014). In the case of inhibition of actin dynamics, prostaglandins act through the G-protein coupled prostaglandin receptors EP2 and EP4 to destabilize actin fibers and reduce cell motility (Holla et al., 2005). In support of a potential role for *ACSL4* in actin dynamics, ACSL4 protein puncta were observed to be co-localized with actin puncta in the dendrites of cultured mammalian neurons (Meloni et al., 2009).

1.4.3. Potential functions of arachidonoyl-CoA

Information about the functions of arachidonoyl-CoA is less detailed than that available for arachidonic acid and its eicosanoid metabolites. However, arachidonoyl-CoA is known to be a major component of cell membranes through its incorporation into triglycerides, and is essential for maintaining membrane fluidity (Brash, 2001). Additionally, radiolabeled arachidonic acid was found to be incorporated into proteins, indicating that arachidonoyl-CoA can be used for protein modification (Yamashita et al., 1995). Lipid modification of proteins allows them to embed at the plasma membrane, or be sorted into secretory vesicles (Mann and Beachy, 2004). Thus, lipid modification largely affects proteins at the cell periphery, and in the extracellular environment. Given

the putative localization of ACSL4 protein to the endoplasmic reticulum (Meloni et al., 2009; Zhang et al., 2009), it is reasonable to hypothesize that it is involved in the sorting of membrane and secretory proteins.

1.5. *ACSL4* Functions in Both Neurons and Glia

While the biochemical mechanisms through which *ACSL4* functions in the nervous system are unclear, it has documented roles in both vertebrate and invertebrate neurons. This has led to the conclusion that *ACSL4* and its homologs function exclusively in neurons; however, the design of these studies leaves open the possibility that these genes may also have a function in glia.

1.5.1. Neuronal findings in *ACSL4*-linked intellectual disability

Removal of *ACSL4* via transfection of an RNAi vector in rat hippocampal neurons in cell culture resulted in defects in the growth of dendritic spines (Meloni et al., 2009). In this study, neurons were co-cultured with non-transfected astrocytes, suggesting that this is a cell-autonomous phenotype specific to neurons. In addition, multiple studies

have documented staining of ACSL4 in hippocampal neurons in both human and mouse brains (Cao et al., 2000a; Meloni et al., 2009).

1.5.2. *Drosophila* studies defining a role for the *ACSL4* homolog in neurons

While mammalian studies established a role for *ACSL4* in neurons, extensive characterization of its potential function has been performed in *Drosophila*. In these studies, the morphology and function of neurons were examined in animals with ubiquitous loss of the *ACSL4* homolog *Acsl* in all tissue, including glia. Homozygous null animals did not survive to the third larval instar, so analysis was performed on heterozygous animals containing a null allele over a p-element insertion mutant ($Acsl^{KO}/Acsl^{05847}$). In this context, third larval instar neurons were observed to have a number of phenotypes. First, photoreceptor targeting was observed to be abnormal in the larval brain (Zhang et al., 2009); however, no cell-specific RNAi or rescue was performed to identify the cell types involved in this phenotype. Second, motor neurons in the posterior abdominal segments of the larva were observed to have a defect in synaptic vesicle transport, with a specific reduction in retrograde movement (Liu et al., 2011).

This study further demonstrated reduced growth and stability of synapses in these posterior neurons, and reduced spontaneous and evoked glutamate release.

Third, analysis of anterior motor neurons revealed synaptic overgrowth, which was associated with mislocalization of Rab11, a small GTPase involved in endosome recycling (Liu et al., 2014). Importantly, the levels of activated Bone Morphogenic Protein (BMP) signaling molecules was increased at both posterior and anterior motor neuron synapses. The authors of these studies hypothesized that *Acsl* plays a role in endocytic recycling of BMP receptors; in the absence of *Acsl*, endocytic trafficking of these receptors is impaired, and BMP signaling is increased. In anterior neurons, this results in synaptic overgrowth. Posterior neurons are additionally burdened by defects in transport across the greater distance between their synapses and cell bodies, resulting in malnourishment of posterior neuro-muscular junctions, and a decrease in synaptic growth. Ultimately, a conserved function in endocytic recycling of receptors is proposed for *Acsl* in all neurons, as similar endocytic defects were observed in the photoreceptors of these animals. In photoreceptors, endocytic recycling effects were more severe in animals with RNAi knock-down (KD) of *Acsl* in all photoreceptors, than in mutant clones

of the *Acsl*^{KO} allele. This may be due to partial compensation by wild type tissue surrounding the *Acsl*^{KO} clones. The synaptic overgrowth and undergrowth phenotypes of anterior and posterior larval motor neurons, respectively, was rescued by expression of human *ACSL4* specifically in neurons, and not in the post-synaptic muscle cells or in glia. This result demonstrates functional homology between human *ACSL4* and *Drosophila Acsl* in neurons (Liu et al., 2011, 2014).

1.5.3. Caveats of previous studies, and potential activity of *ACSL4* in glia

While these studies offer compelling evidence that *ACSL4*, and the *Drosophila* homolog *Acsl*, function in neurons, they do not demonstrate conclusively that these genes have no function in glia. While expression of ACSL4 protein was demonstrated in hippocampal neurons of mammalian tissue (Meloni et al., 2009), this analysis was done without the aid of cell-type markers to confirm that expression is restricted to neurons. Furthermore, while removal of *ACSL4* from cultured neurons resulted in a reduction in dendritic spines, no analysis of synapses was performed (Meloni et al., 2009). Thus, while depletion of *ACSL4* causes a morphological defect in mammalian neurons, this may or may not result in a functional defect.

Analysis of *Drosophila* neurons was done in larvae in a mutant background in which *Acsl* was depleted from all tissues (Zhang et al., 2009; Liu et al., 2011, 2014). Expression of *ACSL4* in glia in this background did not rescue the overgrowth phenotype of anterior neurons, while expression of either *Acsl* or *ACSL4* in neurons did. This analysis may seem to indicate that *Acsl* and *ACSL4* function exclusively in neurons, but it cannot rule out that *Acsl* has a separate function in glia unrelated to this phenotype, or that glial *Acsl* may have an effect that relies on the presence of functional *Acsl* in neurons. Furthermore, when the electrophysiological function of posterior motor neurons was assessed in the prior study (Liu et al., 2011), glial expression of either *Acsl* or *ACSL4* was not included in the analysis. Therefore, the possibility remains that *ACSL4* and its homologs function in glia.

1.6. *Drosophila* Optic Lobe as a Model to Study Glial *ACSL4*/*Acsl* Function

In this study, I continue investigating the function of *ACSL4* and its homologs, focusing on their role in glia and in development. These studies were performed in the *Drosophila* optic lobe. The advantages of this model organism and system are discussed below.

1.6.1. Strengths of *Drosophila* for this project

i. Homology of *Drosophila Acsl* with *ACSL4* and *ACSL3*

Drosophila Acsl has ten documented splice variants, labeled A through J (Attrill et al., 2016). While the protein products of these variants have different N-termini, all 10 include conserved, putative ATP and CoA binding domains in the C-terminal regions. Acsl protein isoforms have 51% and 48% identity with ACSL4 protein isoforms 1 and 2, respectively, covering over 98% of the sequence in each case (Table 1.1). Of these 10 Acsl proteins, 6 are predicted to localize to the ER and 4 to the cytosol (Table 1.1). The considerable identity between the protein products of human *ACSL4* and *Drosophila Acsl*

indicates a conservation of function between the two organisms, making *Drosophila* an excellent model system for investigation of the role of *ACSL4* and its homologs in glia.

ACSL3 is the human ACSL protein with closest homology to ACSL4 (66% identities, 80% positives, covering 98% of the query sequence). *Drosophila* Acsl protein also shares homology with ACSL3 at the protein level (isoforms A-I have 49% identity and isoform J has 48% identity, covering 95% of the ACSL3 sequence) (Table 1.1). Indeed, expression of *ACSL3* in mammalian glia has been previously demonstrated, and overexpression of *ACSL3* in glia has been associated with the development of glial cancers, such as glioma (Pei et al., 2009). It is tempting to conclude that the two homologs operate in different cell types in the nervous system: *ACSL4* in neurons, and *ACSL3* in glia. However, expression of *ACSL4* has been recently demonstrated in astrocytes (Zhang et al., 2014; Seeger et al., 2016), making it likely that both *ACSL3* and *ACSL4* function in glia.

ii. Spatial and temporal depletion of *Acsl*

In addition to the homology of Acsl protein with ACSL4 protein, the genetic tools available in *Drosophila* allow spatial and temporal control of RNAi KD, allowing *Acsl* to be specifically depleted from glia or subtypes of glia at specific times. This is achieved through the Gal4/UAS system (Brand and Perrimon, 1993). Gal4 is a transcription factor isolated from yeast that binds and recruits transcription machinery to specific DNA sequences termed Upstream Activating Sequences (UAS). Gal4, and thus UAS-directed, expression can be targeted to distinct cell types by placing tissue specific promoters upstream of the Gal4 encoding element. Moreover, Gal4 expression can be controlled temporally by utilizing the temperature sensitive variant of the Gal4 suppressor Gal80 ($Gal80^{ts}$) (McGuire et al., 2003; Fujimoto et al., 2011). At lower temperatures, $Gal80^{ts}$ retains its function, and acts to suppress Gal4 expression. At higher temperatures, $Gal80^{ts}$ becomes non-functional, and Gal4 expression is released. By transferring flies containing all three elements between low and high temperatures, Gal4 expression can be limited to specific cell populations, and timed to specific developmental stages.

iii. Strengths of the *Drosophila* optic lobe as a model system

The central nervous system of *Drosophila* has been well characterized, and provides multiple systems in which to study the role of *Acsl* in glia. Of these systems, the optic lobe is particularly appealing. First, the electrophysiological activity of the optic lobe can be easily assessed with the electroretinogram (ERG, see more below). Second, the adult morphology of the optic lobe has been well characterized, with extensive documentation of the location and characteristics of multiple subtypes of both neurons and glia. Furthermore, specific Gal4 drivers are available for most of these subtypes, making it possible to identify specific populations and functions regulated by *Acsl*. Finally, the development of the optic lobe has been studied in depth. There is a large body of literature on the generation, differentiation, and migration of neurons and glia, as well as the specification of the post-synaptic compartments, and the development of synapses, and neuropil (reviewed in Section 1.7). Together, the profound body of knowledge of the *Drosophila* optic lobe, combined with the ease of electrophysiological assessment, make it an ideal system to study the role of *Acsl* in glia.

1.6.2. An overview of the adult *Drosophila* optic lobe

i. Adult morphology

The visual system of adult flies can be divided into the retina, in which the light sensing photoreceptors reside, and the optic lobe, which consists of a series of four neuropils: the lamina, medulla, lobula, and lobula plate (Fig 1.1.) (Fischbach and Dittrich, 1989; Rein et al., 1999). Once visual information is collected in the retina, it is transmitted to and processed by the intrinsic neurons of each subsequent neuropil, until ultimately reaching the central brain. Each synaptically dense neuropil is surrounded and supported by glia, which have been particularly well-characterized in the lamina (Tix et al., 1997; Edwards and Meinertzhagen, 2010; Edwards et al., 2012). Glia associated with structures proximal to the lamina have been less studied; however, it is known that glia ensheath the processes of neurons as they traverse the distal optic chiasm, the span between the lamina and medulla, and the proximal optic chiasm, the span between the medulla and lobula, and that glia are adjacent to the other neuropils of the optic lobe.

There are eight distinct subtypes of photoreceptors, labeled R1-R8, which express different combinations of light sensing molecules, or rhodopsins, labeled Rh1-Rh6 (Ranganathan et al., 1995). Photoreceptors R1-R6 express rhodopsin Rh1, and function to sense motion and contrast. Photoreceptors R7 and R8 express combinations of Rh3-Rh6, and function to sense color.

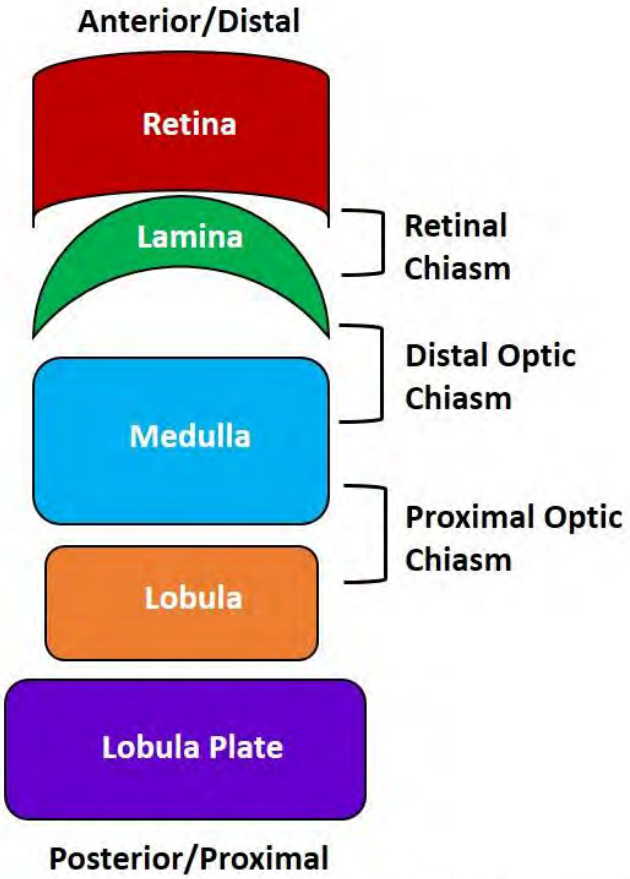

Figure 1.1. Organization of neuropils in the *Drosophila* optic lobe.

Each class of rhodopsin responds to different wavelengths of light. Thus, each subtype of photoreceptors collects information from a subset of the UV-visual light

spectrum. Within the retina, photoreceptors are organized into a repetitive lattice of columnar elements, or ommatidia. While the cell bodies of photoreceptors are located in the ommatidia, they extend axons across the retinal chiasm into either the lamina (R1-R6), or the medulla (R7 and R8) (Fischbach and Dittrich, 1989).

In the lamina, R1-R6 associate with secondary order lamina neurons to form a repetitive lattice of columnar elements termed cartridges. Within the cartridge, photoreceptors release the neurotransmitter histamine, which initiates hyper-polarization of the lamina monopolar cells L1 and L2. These cartridges are supported by three layers of glia: surface and cortex glia, which enwrap the processes of photoreceptors and cell bodies of lamina neurons in the cell body layer of the lamina, and two types of neuropil glia – epithelial and marginal glia (Fig 1.2) (Edwards and Meinertzhagen, 2010; Edwards et al., 2012). Cell bodies of the epithelial glia reside at the distal edge of the lamina neuropil, and cell bodies of the marginal glia reside at the proximal edge. Together, epithelial and marginal glia extend processes into the lamina neuropil. Supportive functions in neuronal signaling such as neurotransmitter recycling have been documented for epithelial glia (Richardt et al., 2002; Edwards and Meinertzhagen, 2010). Epithelial

glia are known to express the enzyme *ebony*, which catabolizes histamine into carcinine, and to return carcinine to the photoreceptor where it is metabolized back into histamine by the enzyme *tan* (Borycz et al., 2002; Richardt et al., 2002; Pantazis et al., 2008).

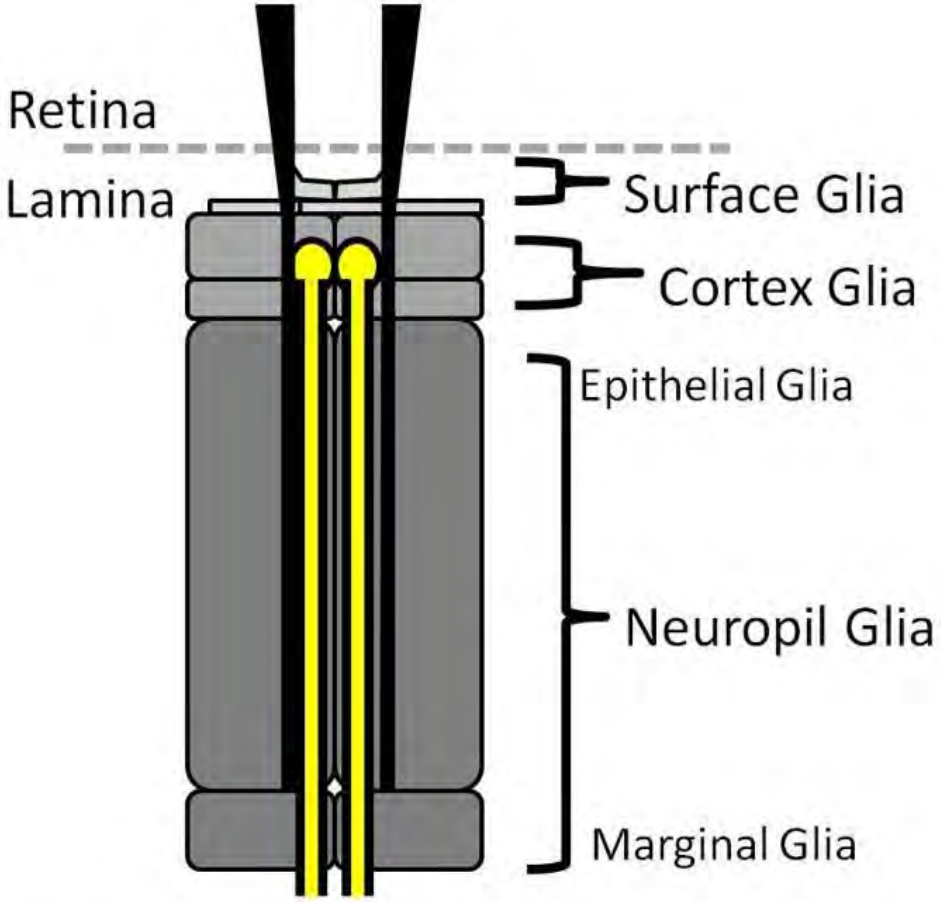

Figure 1.2. Schematic of the adult lamina. Photoreceptors (black) extend terminals from the retina and associate with lamina neurons (yellow) to form a cartridge. The neurons of the lamina are supported by three layers of glia: Surface/cortex glia, epithelial glia, and marginal glia.

Epithelial glia seem to perform this function through a specialized appendage, called a capitate projection, which invaginates into the photoreceptor axon (Fabian-Fine

et al., 2003; Rahman et al., 2012). In contrast, the exact role of marginal glia in the adult lamina is less clear.

The second neuropil of the optic lobe, the medulla, is much larger than the lamina. In cross section, the medulla, like the lamina and retina, is organized into a repetitive lattice of columnar elements, which in this neuropil are simply referred to as columns (Fischbach and Dittrich, 1989; Takemura et al., 2008a). In longitudinal sections, the medulla is organized into ten synaptic layers, M1-M10, with M1 being the most distal and M10 the most proximal layers. Layers M1-M5 are generally grouped together and referred to as the "outer medulla", and layers M6-M10 are referred to as the 'inner medulla'.

While the axons of photoreceptors R1-R6 terminate in the lamina, R7 and R8 extend into the medulla, terminating in layers M6 and M3, respectively (Takemura et al., 2008a). Lamina neurons also extend processes into the medulla, which then associate with, and synapse upon, tertiary order neurons of the medulla. Tertiary order neurons of the medulla then extend into and synapse upon neurons of the lobula, which in turn extend into and synapse upon neurons of the lobula plate. In this fashion, visual

information collected in the retina is passed from neuropil to neuropil, until ultimately reaching the central brain.

ii. Adult electrophysiology

As described above, electrophysiological activity in the optic lobe can be assessed through the ERG. The ERG is a wide field recording of the sum of electrical currents in the retina and neuropils across the optic lobe (see Chapter II. Methods for details on acquisition), and measures the movement of ions in the extra-cellular space. The ERG consists of four parts, each of which represents activity in a different structure (Fig 1.3.). First, at the onset of light stimulation, there is an 'on transient', which is typically 1-4 mV in magnitude. The 'on transient' is believed to be generated by hyper-polarization of lamina neurons in response to photoreceptor depolarization and release of histamine (Heisenberg, 1971; Coombe, 1986; Pantazis et al., 2008). Second, immediately after the 'on transient' there is a 'sustained depolarization', which represents the graded potential of the photoreceptors in the retina. This sustained depolarization is typically 8-12 mV in magnitude. Third, at the offset of light stimulation, there is an 'off transient', which incorporates both the repolarization of the lamina neurons once photoreceptors cease

histamine release, as well as a mix of other signals from across the eye (Heisenberg, 1971; Coombe, 1986; Stuart et al., 2007; Pantazis et al., 2008). The 'off transient' is typically between 2-5 mV in magnitude. Fourth, the trace returns to baseline, which represents the repolarization of the photoreceptors.

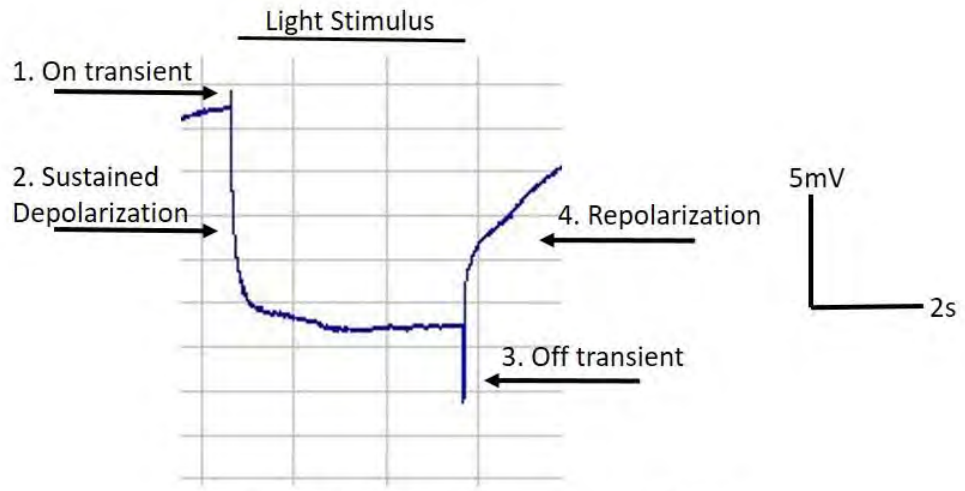

Figure 1.3. The electroretinogram (ERG)

The ERG is recorded from the surface of the eye, and it is best used to measure activity in the closest structures of the visual system, the retina and lamina. Additionally, because it is a wide-field recording, the ERG represents the sum of activity in multiple neuronal subtypes in multiple neuropils, so the activity of a specific group of cells cannot be examined. However, the ease of acquisition and the relative depth of information available in an ERG trace make it a useful tool for examining neuronal signaling in the optic lobe.

Given the ease with which the ERG can be recorded, it has been extensively used to characterize defects in *Drosophila* vision. In particular, loss of the 'on transient' and 'off transient' have been well studied. As expected, genes that mediate histamine signaling or recycling cause a loss of both transients when mutated. These include *hisClA*/*ort*, the histamine receptor on post-synaptic lamina neurons (Gengs et al., 2002; Pantazis et al., 2008), and genes involved in histamine metabolism and recycling in the eye, such as *ebony* and *tan* (discussed above), *ine*, a putative carcinine transporter in photoreceptors, and *hdc*, an enzyme that synthesizes histamine in photoreceptors (Gavin et al., 2007; Romero-Calderón et al., 2007). In addition, *NinaE*/*Rh1*, the light sensing molecule expressed in photoreceptors R1-R6, and *nonA*, an mRNA binding protein that is ubiquitously expressed, cause loss of both the 'on' and 'off' transients (Jones and Rubin, 1990; Rendahl et al., 1992; Campesan et al., 2001).

1.7. Development of the *Drosophila* Optic Lobe

As discussed above, there is a large body of literature on the development of the optic lobe. A general summary of important concepts and discoveries is provided below, as context for my study of the role of glial *Acsl* in development. The development and function of neurons in the nascent optic lobe has been extensively characterized. Briefly, lamina neurons arise in the anterior of the optic lobe, and migrate a short distance to the nascent lamina. Their terminal division is initiated by the entrance of photoreceptor projections into the optic lobe from the developing retina (Huang and Kunes, 1996; Huang et al., 1998a). As they enter the lamina, five lamina neurons associate with photoreceptor terminals to form a cartridge. This process is mediated by signals from photoreceptor terminals, which induce the expression of appropriate ligands on lamina neurons (Huang et al., 1998b; Clandinin and Zipursky, 2000; Umetsu et al., 2006). The specification of cartridges in the lamina has been extensively studied, and several recent reviews have been published that summarize the field (see Melnattur and Lee, 2011). Neurons of the proximal neuropils arise in the posterior of the optic lobe, in the same proliferation center as lamina glia, and migrate short distances to their respective

neuropils. Less is known about the organization of these neurons into their adult columnar elements, although some evidence exists for the expression of specific cues in target layers in the medulla that projecting neurons respond to (Takemura et al., 2008b, reviewed in Melnattur and Lee, 2011). Since the goal of this work is to further elucidate the role of glia, and glial *Acsl*, in development, I will focus the rest of this section on the development and function of glia.

1.7.1. Larval development

i. Timeline

A general theme in larval development of the optic lobe is reliance on innervation from the developing retina. In the developing retina, or eye disc, photoreceptors undergo terminal differentiation in a posterior to anterior wave (Cagan and Ready, 1989; Thomas and Zipursky, 1994). After differentiation, photoreceptors extend their processes through the optic stalk, which connects the eye disc to the optic lobe. Upon entry to the optic lobe, photoreceptor terminals initiate the final stages of development of both their post-synaptic neuronal partners in the lamina (Huang and Kunes, 1996; Huang et al., 1998a),

as well as lamina glia (Perez and Steller, 1996; Suh et al., 2002). The dependence on photoreceptor innervation means that the lamina too develops in a posterior to anterior wave. Photoreceptor differentiation begins in the second larval instar, and innervation of the optic lobe begins by the end of this period.

The concurrent innervation of photoreceptors, differentiation and migration of post-synaptic neurons and glia, targeting of photoreceptors R1-R6 to the lamina and R7 and R8 to the medulla (see below), as well as organization of the post-synaptic compartment (Huang et al., 1998b) , begin during the end of the second larval instar, and continue into pupal development.

ii. Generation and migration of glia

Glia arise in the posterior of the optic lobe in the posterior proliferation center (Winberg et al., 1992; Perez and Steller, 1996). Their specification into glia relies on the expression of the transcription factors Glial Cells Missing (*Gcm*), and Reversed Polarity (*repo*) (Chotard et al., 2005), as well as the signaling molecule Decapentaplegic (DPP) (Yoshida et al., 2005). Glial cell development, as well as migration, is induced by the

presence of photoreceptors in the optic lobe, and relies on expression of the JAB9/CSN5 subunit of the COP9 signalosome in R1-R6 (Suh et al., 2002), as well as Dpp expression (Rangarajan et al., 2001; Yoshida et al., 2005; Yuva-Aydemir et al., 2011). Glia that migrate to the lamina then act as intermediate targets of photoreceptors R1-R6 (see below). Migration of glia out of the posterior proliferation center occurs along the axons of neurons expressing the signaling molecule Wingless (Dearborn and Kunes, 2004). Interestingly, the outgrowth of these axons is also dependent on photoreceptor innervation.

iii. Photoreceptor targeting

At the third larval instar stage, the terminals of photoreceptors R1-R6 are located between the layers of epithelial and marginal glia, while the terminals of photoreceptors R7 and R8 extend into the medulla. A large body of evidence indicates that marginal glia act as temporary targets of R1-R6. The stop signal provided by marginal glia, and the receptors on R1-R6 that interpret this signal, are not known; however, this targeting process appears to involve nitric oxide locally in the lamina (Gibbs and Truman, 1998), as well as expression in the photoreceptors of Brakeless, a nuclear protein expressed by

R1-R6 (Senti et al., 2000), Pak/Dock, a kinase and actin adaptor protein, respectively (Hing et al., 1999), and Jeb, an Alk kinase ligand protein (Bazigou et al., 2007). Expression of nonstop, a ubiquitin-specific protease, is required in marginal glia (Poeck et al., 2001).

1.7.2. Pupal development

i. Timeline

Processes begun in larval development reach their conclusion in pupal development. Photoreceptor ingrowth into the optic lobe is complete by the end of the first 24 hours of pupariation, and R7 and R8 complete their targeting in the appropriate synaptic layers of the medulla before the last 24 hours. Of particular interest to this project are the processes that occur in the latter half of pupal development, during which time lamina neurons extend neurites that interact with the terminals of photoreceptors R1-R6, and synaptogenesis occurs. Given the well documented roles glia play in synaptogenesis, this process is a particularly exciting potential target of glial *Acsl* function.

ii. Synaptic development

In the adult fly, photoreceptor pre-synapses are organized into T-bars, which can be visualized through electron microscopy. The T-bar is formed by a pre-synaptic platform supporting a ribbon, or bar, which together form the shape of a 'T'. The large platform protein bruchpilot (BRP) is an essential component of the pre-synaptic T-bar (Wagh et al., 2006), and immunostaining of BRP is commonly used as a marker for the pre-synapse in the *Drosophila* optic lobe. The post-synapse of the adult fly can be identified by its proximity to the pre-synapse, and by the presence of post-synaptic densities, which are electron dense areas close to the membrane, and/or post-synaptic cisterns, which are membranous structures located beneath the post-synapse and connected to the post-synaptic membrane (Nicol and Meinertzhagen, 1982a; Meinertzhagen and O'Neil, 1991).

Synaptogenesis begins approximately 60 hours after pupal formation (Frohlich and Meinertzhagen, 1982; Meinertzhagen, 1993). During synaptogenesis, the pre-synaptic T-bar develops in concert with post-synaptic densities. In the adult, one pre-synaptic T-bar in the photoreceptor is associated with four post-synaptic densities, which

derive from multiple lamina neuron subtypes, to form a ‘tetrad synapse’ (Meinertzhagen and O’Neil, 1991). Recently, the cell-cell contact proteins Dscam 1 and 2 were found to regulate synaptic specificity at these multi-contact synapses, acting to prevent elements of the same cell from associating with the same synapse (Millard et al., 2010; Schwabe et al., 2013; Bosch et al., 2015). In pupal development, only 24% of T-bars form a tetrad synapse at 87 hours after pupal formation. As synaptogenesis continues, this number increases, reaching 100% by 12 hours before eclosion (Frohlich and Meinertzhagen, 1982; Meinertzhagen, 1993). Early in synaptogenesis, morphology of the pre-synapse is immature, featuring smaller pre-synaptic ribbons and the absence of post-synaptic cisterns, and does not attain its adult form until approximately 12 hours before eclosion (Frohlich and Meinertzhagen, 1982; Meinertzhagen, 1993).

Although electrical activity can be measured in the developing eye of closely related arthropods, and is assumed to also occur in *Drosophila*, synaptogenesis in the optic lobe is activity-independent (Hiesinger et al., 2006). Instead, synapses develop in proportion to the size of the cell surface of pre-synaptic neurons, which indicates that the pre-synaptic photoreceptor terminals are more influential in determining total synapse

number than post-synaptic lamina neurons (Nicol and Meinertzhagen, 1982b; Fröhlich and Meinertzhagen, 1983, 1987; Meinertzhagen and Fröhlich, 1983; Meinertzhagen, 1989, 1993).

Roughly 1.6% of the plasma membrane of photoreceptor terminals is devoted to synaptic active sites (Nicol and Meinertzhagen, 1982a, 1982b; Meinertzhagen, 1993). This percentage is maintained throughout the growth of the terminals during neuropil expansion, suggesting that the number of synapses is actively regulated during development. Given the well-documented roles of glia in engulfment and removal of synapses during development (Eroglu et al., 2008; Schafer and Stevens, 2010, 2014; Schafer et al., 2012), it is possible that the regulation of synapse number is a glia-dependent process. The gross number of synapses peaks at approximately 90 hours after pupal formation, and declines with age (Frohlich and Meinertzhagen, 1982). This decline in the number of synapses is accompanied by an increase in size of the remaining synapses, leaving the percentage of photoreceptor membrane occupied by synapses unchanged (Meinertzhagen, 1989, 1993).

iii. Synaptic plasticity in the adult

Synapses in the optic lobe are not static after eclosion. While there is a small increase of approximately 10% in the number of synapses over the first day of development, after 24 hours of adulthood synaptic number decreases dramatically (Meinertzhagen, 1993; Barth et al., 1997). Synaptic density at 10 days of adulthood is only approximately 25% that of newly eclosed flies (Meinertzhagen, 1989, 1993). In addition, there is evidence of diurnal rhythmicity in the optic lobes, in which the number of synapses change over the course of a day, with peak synaptic density occurring at dawn and dusk (Pyza, 2002; Görlich and Sigrist, 2015).

1.8. Scientific Questions Addressed by this Body of Work

In synthesizing the above information, I developed three lines of inquiry I wished to address with this study. First I wished to address whether *ACSL4* and its homologs have a function in glia. In the following section, I present evidence that *Drosophila Acsl* does in fact have a function in glia, and that expression of human *ACSL4* in glia can

restore this function. Second, I wished to address whether glial *Acsl* functions in development. I present evidence below that conclusively demonstrates glial *Acsl* is required in development. Finally, I wished to address what the potential mechanisms of *ACSL4* are in the nervous system. Based on the phenotype I characterize in the following section I propose that glial *Acsl* functions in synaptogenesis, and possibly gene transcription and actin dynamics in the *Drosophila* optic lobe.

CHAPTER II. METHODS

2.1. Fly Culturing

Flies were cultured on low-yeast medium prepared on site. They were maintained in a 12hr/12hr light/dark cycle at 25^{o}C and 60% humidity, except for heat shift experiments.

2.2. Fly Stocks and Genetics

The following driver lines used in this study were obtained from the Bloomington *Drosophila* Stock Center (BDSC): *repo*-Gal4, *elav*-Gal4, C.S. (Canton-S used as WT), *tubulin*-Gal4, *alrm*-Gal4, *nrv2*-Gal4, Mz97-Gal4, *NorpA*^{7}(referred to as *NorpA*) and *mmd*-Gal4. The following driver lines were a generous gift from Dr. Marc Freeman (University of Massachusetts Medical School): *Gcm*-Gal4, *moody*-Gal4, Mz0709-Gal4, as well as UAS-tdTomato (a fluorescent membrane marker); TIFR-Gal4 and Gal80^{ts}; *repo*-Gal4 flies. Other drivers were obtained from the following sources: *loco*-Gal4 (Dr. Iris Salecker,

Francis Crick Institute), *hisCl1*-Gal4 (Dr. Roger Hardie, University of Cambridge). The following RNAis against *Acsl* were used: JF02811 (BDSC), HMS02307 (BDSC), and GD1638 (Vienna *Drosophila* Resource Center). Additionally, RNAi against *Luciferase* (*Luc* RNAi) for use as a control was obtained from the BDSC (JF03155). Finally, flies overexpressing human *ACSL4* (isoform 2) under UAS control were obtained from the BDSC (stock # 32328). For rescue experiments, a stable line of UAS-*ACSL4* and UAS-JF02811 was created and crossed to TIFR-Gal4> UAS-tdTomato.

2.3. ERG Recording and Quantification

ERG recordings were performed as previously described (Chaturvedi et al., 2014), and standard ERG protocols were followed. Briefly, 1-3 day old adult flies were immobilized on a plastic box with a thin strip of tape. To record voltage change across the eye, a recording glass microelectrode filled with Ringer's solution was placed on the eye surface, and the eye surface was gently scratched. A reference glass electrode filled with the same solution was placed on the thorax away from the wing. Two different protocols

were used to acquire the ERG. In the first, flies were stimulated with 3 5-second pulses of light separated by 7 seconds of darkness. In this protocol, the digital ERG signal was sampled at a rate of 505.5 Hz (sampling every 1.98 ms). In the second protocol, flies were stimulated by 4 5-second pulses of light separated by 15 seconds of darkness. In this protocol, the digital ERG signal was sampled at a rate of 250 Hz (sampling every 4 ms). While these two protocols differ, they both provide adequate recovery time between light pulses and adequately sample the 'on' and 'off' transients, each of which last approximately 100 ms, and thus were used interchangeably. In both protocols, flies were stimulated by light pulses at 4000 lux, and the analog signal was recorded and further amplified using a Warner IE210 Intracellular Electrometer, which filtered the signal at 200 Hz. Before recording from experimental genotypes, the ERG set up was calibrated with C.S. controls.

Before quantifying the ERG phenotype, traces were blinded by a third party so I was unaware of the genotype. Quantification of the 'on transient' and 'off transient' was performed by measuring the amplitude of each transient in each pulse in a trace, after which the values were averaged. In some genotypes, a percentage of traces lacked either the 'on

transient', or both the 'on' and 'off' transients. To represent the penetrance of these phenotypes, traces were binned into either "loss of on transient" or "loss of both transients" categories. Any trace with transients ≥0.1 mV was counted as having transients. Transients <0.1 mV were regarded as potential noise and the trace was counted as "loss of transient/s". Importantly, traces lacking an 'off transient' always additionally lacked an 'on transient', although the reverse was not true.

In some traces, the 'off transient' was cut off or obscured by noise. These traces were excluded from quantification of 'off transient' amplitude, and binning of 'loss of both transients'. Otherwise, all traces were included in quantification. Thus, traces categorized as having a loss of one or both transients were not excluded from quantification of transient magnitude. This was done to ensure that quantification reflected the whole population tested.

'On transients' were classified independently of the magnitude of photoreceptor depolarization for two reasons. First, in observing the controls in each experiment, I frequently observed traces with photoreceptor depolarizations less than 5mV with normal 'on transients'. Second, the post-synaptic receptors on lamina cells are "high gain",

meaning that histamine within the synapse operates cooperatively to increase the open probability of the post-synaptic histamine channel, and that the post-synaptic channel can become saturated early in the light response (Stuart et al., 2007). Indeed, over a prolonged light response the post-synaptic lamina cell will reach peak hyper-polarization, then plateau, multiple times (Stuart et al., 2007). Thus, there is a level of independence between the photoreceptor depolarization and the lamina neuron hyperpolarization that produces the 'on transient'.

2.4. Behavioral Moving Bar Assay

Behavior was tested using the moving bar assay. When presented with a visual stimulus moving in one direction, arthropods, including *Drosophila*, will move in the opposite direction. Thus, when flies are exposed to a visual stimulus of bars moving from left-to-right on a screen, the flies will move from right-to-left. For this assay, my lab developed 8 videos of visual stimuli. Each video featured black or gray bars moving from left-to-right across a white background, then from right-to-left. In the first video, the

contrast between the black bars and white background was 99.00%. In each subsequent video, the contrast between the bars and background was reduced so that any subtle differences in contrast sensitivity could be assessed between genotypes. For this assay, I prepared 50+ adult flies, either less than 3 days old or greater than 1 week old, of TIFR-Gal4> *Luc* RNAi, TIFR-Gal4> *Acsl* RNAi, and *NorpA* genotypes. These flies were anesthetized with CO_2 and transferred to a video screen where they were secured with a clear plastic cover, then the video screen was placed in darkness. The flies were given 30 minutes to recover from anesthetization, then exposed to all 8 videos. Their response was captured on video for later analysis. In total, the assay was performed 3 or 4 times per genotype. To analyze these assays, I calculated the ratio of responding flies (those that moved to the expected edge of the screen) at the end of each video.

2.5. Histology and Imaging

For immunolabeling with antibodies, the brains of 3 day old adults, third instar larvae, or mid-pupal animals were dissected in 1X phosphate-buffered saline (PBS), and fixed in PLB fixation solution (4% paraformaldehyde (PFA), 75 mM lysine, 37 mM sodium phosphate buffer, pH 7.4) for 20 min at room temperature. After 1 hour of blocking at room temperature with 5% fetal bovine serum in 0.3% Triton X-100 in 1X PBS, brains were incubated in primary antibody for 2 days at 4ºC. After three 5-10min washes in 1X PBS containing 0.3% Triton X-100, brains were incubated in FITC/Cy5 secondary antibodies (1:200 (Sigma (F0257), Abcam (ab102732)), with or without phalloidin-rhodamine (1:100) (ThermoFisher R415), for 2 hours at room temperature or overnight at 4ºC. The brains were then washed as previously stated and mounted in Vectashield medium (Vector Laboratories (H-1000)). Upon mounting, the brains were oriented so that the lamina faced up to assist with capturing parallel sections during imaging.

The following primary antibodies were used: mouse anti-BRP 1:10 (Developmental Hybridoma Studies Bank (DHSB) (nc82), guinea pig anti-repo 1:100-

1:500 (a kind gift from Dr. Manzoor Bhat, University of Texas Health Center at San Antonio), and mouse anti-chaoptin 1:10 (DSHB, 24B10).

Mouse tissue fixed in 4% PFA was obtained from Dr. Carlos Lois (California Institute of Technology). After blocking in 10% FBS in 1X PBS for 1 hour at room temperature, samples were transferred to primary antibody solution (goat anti-ACSL4 1:2, Santa Cruz Laboratories (sc-47997) and rabbit anti-GFAP 1:500, Abcam (ab7260)), and incubated at 4^{o}C overnight. As a control, the anti-ACSL4 antibody was pre-absorbed using a commercially available ACSL4 peptide (Santa Cruz Laboratories (sc-47997 P)) at a concentration of 50mM. After washing 3 times for 5-10 min in 1X PBS, the samples were sequentially incubated with secondary antibody to eliminate cross reactivity: first with anti-goat FITC conjugated secondary antibody (Sigma (F2016)) at 1:500 for 1 hour at room temperature, followed by 3 washes for 5-10min each, then with anti-rabbit Cy5 conjugated secondary antibody (Abcam (ab6564)) at 1:100 for 1 hour at room temperature. Samples were then washed for the final time as before, and mounted in Vectashield medium (Vector Laboratories (H-1000)). Coverslips were fixed to the slide with clear nail polish. Slides were stored in darkness at 4^{o}C before and after imaging.

All images were captured using a Zeiss LSM5 PASCAL laser scanning confocal microscope equipped with a Zeiss 63x Plan-Apochromat oil-immersion objective. In all samples, pixel time was 3.20µs, line average was 8, optic slice size was 1µm in every channel, and z-step was .7µm. Larval z-stacks were between 30 and 40 slices, and mid-pupal and adult z-stacks were between 50 and 60 slices. Further settings such as gain, offset, and laser strength were chosen based on control samples, and were used consistently within an experiment allowing for comparison of signal densities in control and *Acsl* RNAi samples. Z coordinates at the beginning and end of each stack were set manually, and were chosen to encompass as much of the lamina and medulla in parallel as possible, depending on the orientation of the sample. Each sample represents 1 optic lobe from 1 animal, so that 1 z-stack was taken per animal. The optic lobe imaged was chosen based on orientation, such that the lamina and medulla could be captured in parallel. By eye, I saw no substantial difference in morphology between optic lobes within a single animal.

I identified the lamina and medulla in mid-pupal and adult samples based primarily on their positions - the lamina is located directly beneath the retina, whereas the medulla is beneath the lamina and separated by the distal optic chiasm. The lamina also has a

notable crescent shape and the medulla is larger. Because the size and shape, although not the relative position, of these neuropils varied in *Acsl* KD animals, I also identified the two neuropils based on staining patterns. For example, BRP signal in the parallel lamina is organized into linear, vertical cartridges, whereas BRP signal in the parallel medulla is organized into horizontal synaptic layers. I also used perspectives from the entire z-stack to assist in identification. I identified the lamina in larval samples through the conspicuous 3 layers of glial nuclei and band of chaoptin signal. I identified the marginal glia layer in larval samples by its distance from the optic stalk and eye disc (the marginal glia layer is furthest from these structures).

2.6. Analysis of Developmental Stages

i. Preparation of third instar larvae

Third instar larvae were prepared by allowing fertilized females to lay eggs for a period of 2 hours to generate a population of staged embryos. After 110 hours, wandering third instar larvae were collected from these vials. Staging was verified by size.

ii. Preparation of pupae

To prepare pupal time points, embryos were staged as before. At the end of larval development, white pupae were identified and allowed to continue development for either 24-26, 48-50, 72-74, or 100-102 hours. Each subsequent time point was verified by the color of pupae and the appearance of morphological structures such as the Malpighian tubules (mid pupal development (50% pupae or P50).

2.7. Temporal Restriction of RNAi Expression

i. Experimental design

Gal80 is a suppressor of Gal4 expression. The temperature sensitive variant of Gal80, $Gal80^{ts}$, will function normally to suppress Gal4 expression at lower temperatures. However, at higher temperatures, $Gal80^{ts}$ is inactivated, and Gal4 expression is released from suppression. By shifting flies between 25ºC and 29ºC, I was able to temporally specify RNAi expression under *repo*-Gal4, which expresses in all glia (Fig 2.1.). For these experiments, I used the RNAi JF02811. Transferring embryos directly after egg laying to

29ºC, thereby initiating *repo*-Gal4 driven RNAi expression at the beginning of development, proved to be fatal, a result consistent with the early lethality of homozygous *Acsl* null animals and our observation that expression of *Acsl* RNAi with tubulin-Gal4 is larval lethal. To compensate for this, I shifted larvae staged to the onset of second larval instar from 25ºC to 29ºC to initiate RNAi expression, where I maintained them until eclosion. To suppress RNAi expression in the adult phases of these animals, I shifted eclosed flies from 29 degrees to 25 degrees, where I maintained them for 10 days. This experimental procedure is referred to as 'developmental expression'. In a complementary experiment, I raised flies at 25ºC until eclosion, effectively suppressing RNAi expression in development. I then shifted these flies to 29ºC for 10 days, allowing RNAi expression exclusively in the adult. This experimental procedure is referred to as 'adult expression'. In each procedure, I analyzed flies driving expression of *Acsl* RNAi with *repo*-Gal4. I included flies driving *Luc* RNAi with *repo*-Gal4 as a control in both procedures. The control animals were subjected to the same temperature shifts at the same time as the *Acsl* RNAi animals.

Controls to address whether these temperature shifts had the desired effect on Gal4 expression were not done in this study, as Gal80^{ts} control of *repo*-Gal4 had been well-established in my lab before these experiments were performed. Additional controls of maintaining flies at 29°C and 25°C throughout development and adulthood were not performed as raising flies at 29°C from egg laying is lethal (see above), and raising flies at 25°C was deemed unnecessary after the 'adult expression' experiments were performed.

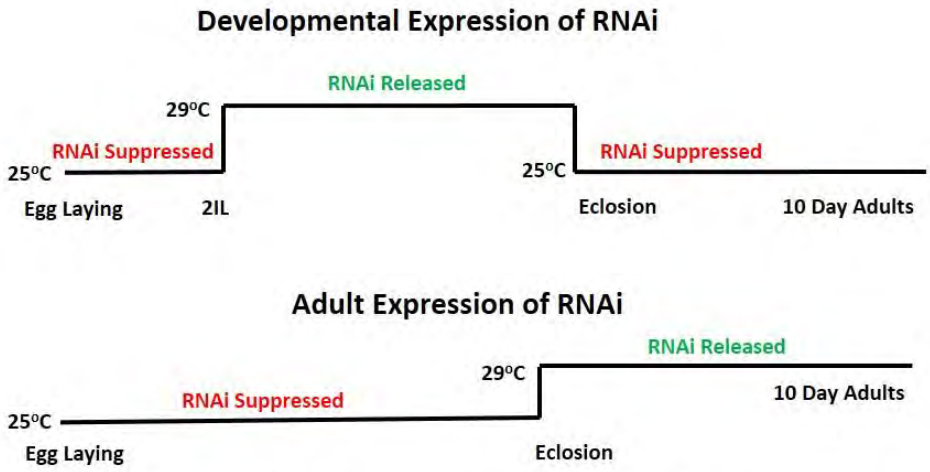

Figure 2.1. Schematic of RNAi temporal restriction. This schematic visualizes the methods for developmental expression of RNAi and adult expression of RNAi. Developmental expression of RNAi animals were heat shifted from second larval instar (2IL) to eclosion. Adult expression of RNAi animals were heat shifted from eclosion to 10 days of adulthood.

ii. Collection for eclosion and 10-day analysis

Because raising flies at higher temperatures increases their rate of development, 'developmental expression' flies were heat-shocked for only 7 days until eclosion. I

collected recently eclosed flies, sorted them by genotype by removing flies with evidence of the *tubby* gene used to mark the balancer chromosome, and performed the ERG and dissection for morphological analysis within 8 hours. I also set aside a subset of these flies for analysis at the 10-day time point.

2.8. Image Analysis

i. Quantification of signal density

To quantify the intensity of signal/area, I utilized the quantification interface of the volumetric analysis software Volocity (Perkin Elmer). Before quantification, each image was assigned a random number by a third party so I was not aware of the genotype. Because the signal intensity is dependent on the depth of the Z-slice within the tissue, I corrected each image stack by removing slices from the beginning or end that had either a mean pixel value above 230 or below 25 (pixel values ranged from 0-255). I identified the lamina and medulla as described above based on location, size, shape, and structural differences. Because both the lamina and medulla are curved structures, and change position in the XY

plane of a Z-stack, I defined each structure with multiple Regions Of Interest (ROIs) in the XY plane, each of which was limited to a subsection of the Z slices. I then identified and combined objects within those ROIs to generate a single 3D object containing either the lamina or the medulla. I verified that this object was limited to either the lamina or the medulla by eye. The mean pixel value, adjusted for volume (μm^3), for either BRP or tdTomato signal was then calculated.

ii. Quantification of nuclei density

To quantify the number of marginal glia, I again used the quantification interface of Volocity. As before, each image was assigned a random number by a third party so I was not aware of the genotype during quantification. Because the entire optic lobe could not be captured in a single image at 63X, I adjusted all nuclei quantification for volume to be representative of the image captured instead of the entire optic lobe. I began by defining multiple Z-limited ROIs in the XY plane of the BRP or chaoptin channel as before, that encompassed either the proximal edge of the lamina, the distal optic chiasm, or the inner medullary neuropil (for pupal analysis I included the entire medullary neuropil as cell bodies were not restricted to just the inner medulla, and for larval analysis I included only

the proximal edge of the lamina). Having defined these ROIs, I then instructed Volocity to find objects in the repo channel within these ROIs using the same threshold and size parameters for each developmental stage. I verified by eye that the objects defined were individual repo nuclei, and that all repo nuclei were accounted for in the ROIs. I then calculated the number of repo objects, and adjusted this number for volume to arrive at a nuclei density in each ROI. For total marginal glia nuclei density in TIFR KD adults and mid-pupal animals, I calculated the average for all ROIs in each sample.

iii. Analysis of morphology

For morphological analysis where quantification was hindered by technical difficulties (e.g. analysis of glial processes), the images were again blinded by a third party. I then sorted and described the morphology of the images before revealing the genotype. In every case, the phenotype of *Acsl* knock-down (KD) was identifiably different from that of controls.

iv. Volume viewer and z-projections

In order to view the morphology of the optic lobe in 3D, I utilized the Volume Viewer plugin and the z-project function in FIJI (National Institutes of Health). I used this method to identify and quantify the number of *Acsl* KD samples with ectopic neuropil, and to verify that the cell bodies of giant optic chiasm glia do not penetrate the medulla at mid-pupal development or in adulthood.

v. Penetrance analysis of morphology

To calculate the penetrance of the mislocalized glia phenotype, I binned blinded images into either those having glial cell bodies in the medulla neuropil, or those having normal morphology of no glial cell bodies in the medulla neuropil. In my observation, control animals had 0 glia in the medulla neuropil, and *Acsl* KD animals had at least 4 mislocalized glial cell bodies per animal. To calculate the penetrance of the ectopic neuropil phenotype, I binned blinded samples into either those having large structures dense in BRP signal in the distal and proximal optic chiasms, or those having normal morphology of no BRP dense structures in the chiasms.

2.9. Statistical Analysis

All experiments where the phenotype was binned and results are expressed as % penetrance were analyzed using the chi-square test (see Appendix A. Table of Experiments). All values for quantification of signal density are expressed as mean ± SEM. The statistical significance for these analyses was assessed using an unpaired, 2-tailed t-test (see Appendix A. Table of Experiments). All values for quantification of repo-positive nuclei are presented as mean ± SEM. Statistical significance for this analysis was assessed using multiple t-tests, one per category of marginal layer, distal optic chiasm, and medullary neuropil, which assumed the same scatter in each population and were adjusted for false discovery rate, or with an unpaired, 2-tailed t-test (see Appendix A. Table of Experiments). The statistical significance of behavior was assessed using 2-factor ANOVA analysis without repeated measures. The factors tested were genotype and contrast difference in the visual stimuli videos. Post-hoc analysis of behavior was performed using Tukey's multiple comparisons test. All experiments were repeated in duplicate from at least 2 independent crosses, with 2 exceptions. The glial subtype specific Gal4 driver screen experiments were collected from 1 to 2 independent crosses, and the NorpA blind

control flies for the behavior assays were collected from a single vial of stock. All statistical analysis and result graphs were generated in GraphPad PRISM.

CHAPTER III. RESULTS

3.1. Glial *Acsl* is Required for Neuronal Signaling

3.1.1. *Acsl* is required in glia for the magnitude of neuronal signaling in the lamina.

Acsl was initially uncovered as a gene regulating visual signaling in a RNAi screen of over 1,000 genes performed by my lab (unpublished data). To determine whether *Acsl* functions in glia as well as in neurons to regulate visual signaling, I specifically depleted *Acsl* from either glia or neurons, and recorded the electrophysiological function of the visual system. I focused my analysis on the 'on' and 'off' transients of the ERG, as these represent activity in post-synaptic neurons and are necessary for visual transmission into the central brain. I was able to target *Acsl* RNAi to different tissues by driving expression with drivers specific to either neurons (*elav*-Gal4), or glia (*repo*-Gal4). Both *elav*-Gal4 and *repo*-Gal4 are generally considered to be specific post-mitotic drivers for neuronal and glial populations. While *repo*-Gal4 appears to be specific to glia, *elav*-Gal4 has been demonstrated to be transiently expressed in embryonic glia (Berger et al., 2007). However, at later stages of development, *elav*-Gal4

and *repo*-Gal4 can be used to drive expression specifically in neurons and glia, respectively.

When *Acsl* RNAi was expressed in neurons, I observed no defects in the 'on transient' of the ERG trace compared to wild type Canton S (C.S.) controls. I observed no absence of the 'on transient' (C.S. n=23 penetrance = 0%, elav-Gal4> *Acsl* RNAi n = 15 penetrance = 0%, p value = >.9999 (Chi-square)) (Fig 3.1. A and D), nor did I observe a decrease in the magnitude of the 'on transient' (C.S. n = 23 mean = 1.452±.1332, *elav*-Gal4> *Acsl* RNAi n = 15 mean = 1.573±.1375, p value = >.5465 (2-tailed t-test)) (Fig 3.1. A and B). However, when *Acsl* RNAi was expressed in glia I observed a loss of the 'on transient', defined as an 'on transient' of <0.1mV (see Chapter II. Methods), in a majority of flies (C.S. n = 23 penetrance = 0%, *repo*-Gal4> *Acsl* RNAi n = 22 penetrance = 82%, p value = <.0001 (Chi-square)) (Fig. 3.1. A and D). I also observed a decrease in the magnitude of the 'on transient' (C.S. n = 23 mean = 1.452±.1332, *repo*-Gal4> *Acsl* RNAi n = 22 mean = .05909±.02917, p value = <.0001 (2-tailed t-test)) (Fig. 3.1. A and B). As discussed above, the 'on transient' is a measurement of the hyperpolarization of lamina neurons in response to photoreceptor release of histamine (Heisenberg, 1971; Coombe,

1986; Pantazis et al., 2008). Thus, I propose that the loss of the 'on transient' when *Acsl* levels are decreased by RNA interference indicates electrophysiological function in the lamina is compromised.

To further characterize electrophysiological function in the lamina, I quantified the 'off transient', which represents the repolarization of lamina neurons after photoreceptors cease releasing histamine, as well as other signals in the optic lobe downstream of the lamina (Stuart et al., 2007; Pantazis et al., 2008). In neuronal knock-down (KD) animals, I found a non-significant decrease in the magnitude of the 'off transient' (C.S. n = 23 mean = 5.483±.4595, elav-Gal4> *Acsl* RNAi n = 14, mean = 3.957±.6114, p value = .0518 (2-tailed t-test)) (Fig 3.1. A and C). Despite this finding, I found no examples of an absent 'off transient' in any traces examined (Fig 3.1. A and D. Appendix A. Table of Experiments). In contrast, when *Acsl* RNAi was expressed in glia, I found a significant reduction in the magnitude of the 'off transient' (C.S. n = 23 mean = 5.483±.4595, repo-Gal4> *Acsl* RNAi n = 22 mean = 2.045±.3857, p value = <.0001 (2-tailed t-test)) (Fig 3.1. A and C). Moreover, I found that 4

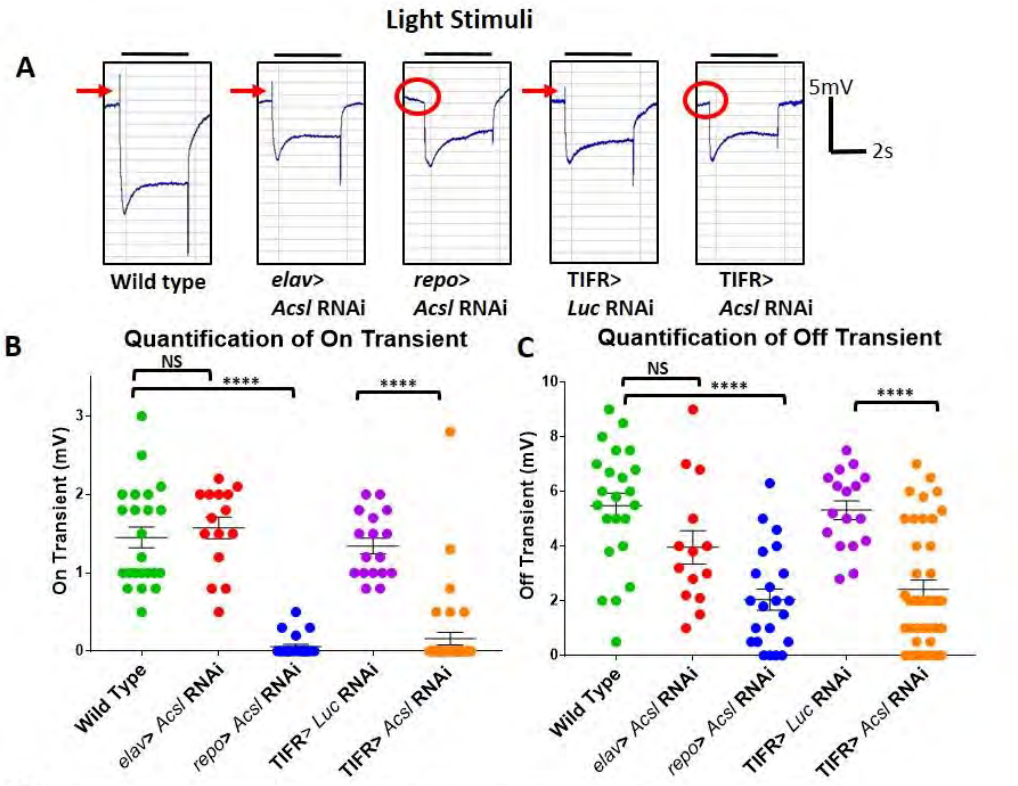

D

Genotype	N number	Loss of On Transient		Loss of On and Off Transients	
Wild Type	23	0%	NS	0%	NS
elav> Acsl RNAi	15	0%	****	0% (n=14)	*
repo> Acsl RNAi	22	82% (18 of 22)		18% (4 of 22)	*
TIFR> *Luc* RNAi	17	0%	****	0%	NS
TIFR> *Acsl* RNAi	40	85% (34 of 40)		20% (8 of 40)	

Figure 3.1. ERG Recordings of laminar signaling in *Acsl* KD. A. ERG traces from wild type, the cell specific screen, and the glial subtype specific screen. The 'on transient' is present in wild type, neuronal *Acsl* KD (*elav> Acsl* RNAi), and control RNAi expression in marginal glia (TIFR> *Luc* RNAi) (see red arrows). Note the absence of the 'on transient' when *Acsl* is depleted in all glia (*repo> Acsl* RNAi) and marginal glia (TIFR> *Acsl* RNAi) (see red circles). **B**. Quantification of the 'on transient' reveals a reduction when *Acsl* is depleted in all glia (*repo> Acsl* RNAi, p value vs. wild type = <.0001), and marginal glia (TIFR> *Acsl* RNAi, p value vs. TIFR> *Luc* RNAi = <.0001). **C**. Quantification of the 'off transient' reveals significant reductions when *Acsl* is depleted from all glia (*repo> Acsl* RNAi, p value vs. wild type = <.0001), and marginal glia (TIFR> *Acsl* RNAi, p value vs. TIFR> *Luc* RNAi = <.0001). *Acsl* KD in neurons exhibits a non-significant reduction (*elav> Acsl* RNAi, p value vs. wild type = .0518). **D**. Table summarizing the penetrance of loss of transients in each genotype. 1 trace was excluded from 'off transient' analysis from the *elav> Acsl* RNAi data set due to noise obscuring the 'off transient'. Loss of the 'on transient' is present with high penetrance when *Acsl* is depleted from all glia (*repo> Acsl* RNAi, p value vs. wild type <.0001), or from marginal glia (TIFR> *Acsl* RNAi, p value vs. TIFR> *Luc* RNAi = <.0001). Loss of both the 'on' and 'off' transients was found in *repo> Acsl* RNAi (p value vs. wild type = .0491) and TIFR> *Acsl* RNAi flies (p value vs. TIFR> *Luc* RNAi = .0899, p value vs. wild type = .0225).

of the 22 glial KD traces examined lacked both the 'on transient' and the 'off transient' (C.S. n = 23 penetrance = 0%, repo-Gal4> *Acsl* RNAi n = 22 penetrance = 18%, p value = .0491 (Chi-square)) (Fig. 3.1. A and D).

A

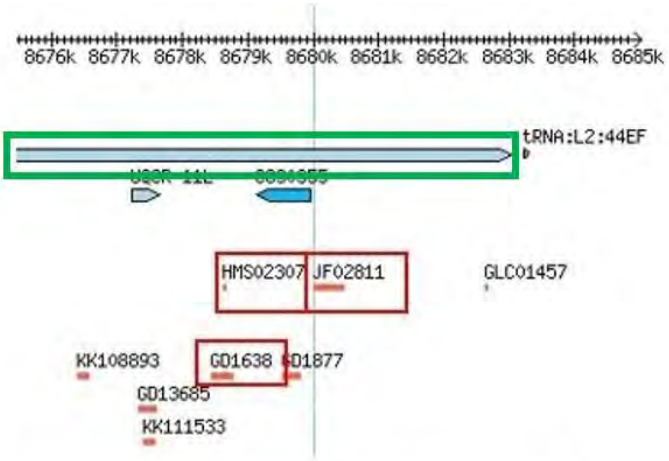

B

Genotype	Loss of On Transient	Loss of On and Off Transient
repo> JF02811	79% (15 of 19)	16% (3 of 19)
repo> HMS02307	80% (8 of 10)	20% (2 of 10)
repo> GD1638	80% (8 of 10)	0% (0 of 10)

Figure 3.2. RNAi's used in this study. A. Visualization of the position of targeted sequences of RNAis on the *Acsl* coding region. RNAis utilized are highlighted in red, and the *Acsl* gene is highlighted in green. All RNAis used target the conserved c-terminus of the protein. Image courtesy of FlyBase (see bibliography). **B**. Summary of the efficacy of RNAis used when driven with *repo*-Gal4. The penetrance of loss of the 'on transient' and loss of both the 'on' and 'off' transients are presented (*repo*> HMS02307 loss of 'on transient' p value = <.0001, loss of both transients p value = .0968; *repo*> GD1638 loss of 'on transient' p value = <.0001, loss of both transients p value = >.9999, all vs. wild type).

These findings in glial *Acsl* KD were confirmed with two additional *Acsl* RNAi lines: HMS02307 (n = 10 80% loss of 'on transient' 20% loss of both transients, p value vs. wild type = <.0001 and .0852, respectively (Chi-square)), and GD1638 (n = 10 80% loss of 'on transient' 0% loss of both transients, p values vs. wild type = <.0001 and .3235, respectively (Chi-square)) (Fig 3.2).

3.1.2. *Acsl* is required in marginal glia.

To determine the specific glial lineage in which *Acsl* is required, I performed a targeted screen driving *Acsl* RNAi in different glial subtypes. I focused on glial subtypes present in, or close to, the lamina, as lamina function appears to be the most severely affected (Table 3.1). Of the multiple additional Gal4 drivers tested, only knock-down (KD) of *Acsl* with TIFR-Gal4 reproduced the ERG phenotype.

TIFR-Gal4 was developed to drive expression in glia in the transient interhemispheric fibrous ring (TIFR) of the mushroom bodies during development (Hitier et al., 2000), and has since been used to drive expression in ensheathing neuropil glia in the central brain (Ziegenfuss et al., 2012). The exact time point at which TIFR-Gal4

becomes active in the optic lobe is not known; however, based on my observations of the developmental phenotype, and of larval brains in which TIFR-Gal4 drove expression of tdTomato prepared in the early third and second larval instar, it is active by the beginning of second larval instar.

In the optic lobe, TIFR-Gal4 drives expression in the marginal glia layer of the lamina, strongly highlighting both cell bodies and processes within the distal optic chiasm and lamina, and the giant optic chiasm (GOC) glia of the proximal optic chiasm (Fig 3.4). This pattern of expression was consistent in all developmental phases I observed. Given that the ERG of *Acsl* RNAi animals has defects in the 'on' and 'off' transients, which are largely generated in the lamina, and the distance of the giant optic chiasm glia from the lamina, I propose that *Acsl* is required in marginal glia for lamina visual function.

In TIFR-Gal4> *Acsl* RNAi animals, I found a significant reduction in the magnitude of the 'on transient' (TIFR-Gal4> *Luc* RNAi n = 17 mean = 1.341±.09965, TIFR-Gal4> *Acsl* RNAi n = 40 mean = .1600±.07965, p value = <.0001 (2-tailed t-test)) (Fig 3.1. A and B), as well as a significant reduction in the magnitude of the 'off

transient' (TIFR-Gal4> *Luc* RNAi n = 17 mean = 5.318±.3426, TIFR-Gal4> *Acsl* RNAi n = 40 mean = 2.420±.3444, p value = <.0001 (2-tailed t-test)) (Fig 3.1. A and C). Furthermore, I found a significant percentage of TIFR-Gal4> *Acsl* RNAi flies lacked the 'on transient' (TIFR-Gal4> *Luc* RNAi n = 17 penetrance = 0%, TIFR-Gal4> *Acsl* RNAi n = 40 penetrance = 85%, p value = <.0001 (Chi-square)) (Table 3.1, Fig 3.1. A and D). I also found that 8 of 40 *Acsl* KD flies were missing both the 'on' and 'off' transients (TIFR-Gal4> *Luc* RNAi n = 17 penetrance = 0%, TIFR-Gal4> *Acsl* RNAi n = 40 penetrance = 20%, p value = .0899 (Chi-square)) (Table 3.1, Fig 3.1. A and D).

The 'off transient' represents secondary signaling both within and downstream of the lamina. While the magnitude of the 'off transient' is significantly reduced in both *repo*-Gal4 and TIFR-Gal4 *Acsl* KD flies, it is still present in the majority of both these populations. Thus, it is likely that the lamina retains some function in most *Acsl* KD flies. Furthermore, I was unable to uncover a defect in visual behavior using the moving bar assay with variable contrast (see Chapter II. Methods). The moving bar assay tests the ability of flies to detect bars moving across a background, and convert that information into behavioral output in which they move in the opposite direction of the bars. The bars

may have variable levels of contrast with the background, allowing one to test the flies' ability to detect both contrast and motion. After exposing the flies to the different visual stimuli, the mean ratio of responding flies was calculated and the results were subjected to a two-factor analysis of variance (2-way ANOVA) (Fig 3.3).

The assay was first performed on aged flies (1 week +) (Fig 3.3. A). Analysis of control RNAi, *Acsl* RNAi, and blind *NorpA* flies that lack all visual signal transmission of this age together demonstrated a significant difference in the factor of genotype ($F(2, 48) = 9.717$, p value = .0003), indicating that the assay was able to differentiate between blind and non-blind flies.

However, analysis of control RNAi and *Acsl* RNAi alone found no difference in the factor of contrast difference ($F(7, 32) = 1.477$, p value = .2107), indicating that the assay was unable to uncover any contrast sensitivity in either control or *Acsl* RNAi flies. Furthermore, post-hoc analysis using Tukey's multiple comparisons test revealed no significant difference in any comparison. Visual transmission can degrade with age in control flies, with a natural degeneration of synapses and ERG transients over time,

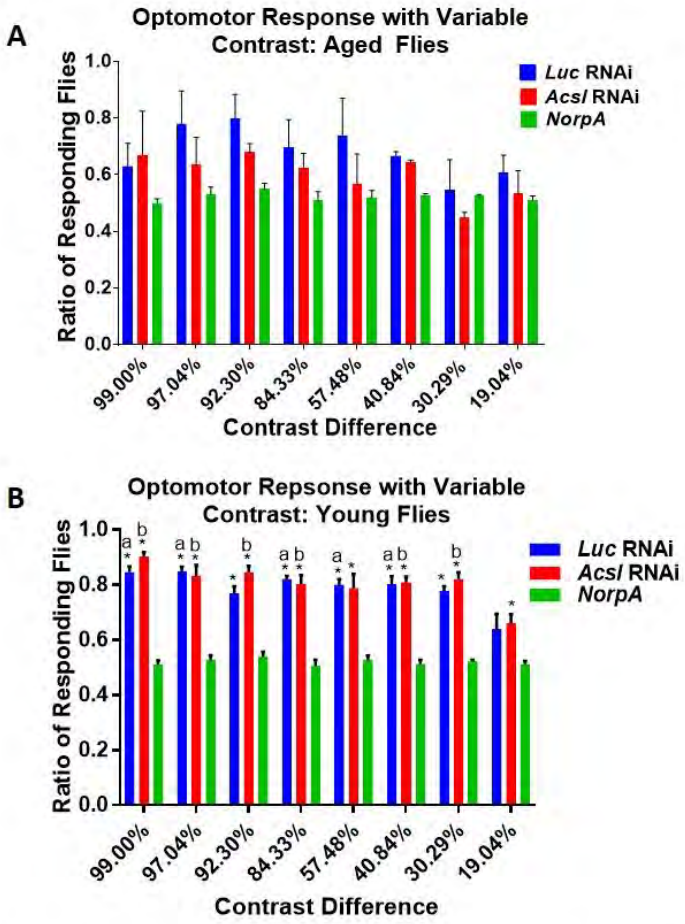

Figure 3.3. *Acsl* KD flies have normal visual behavior. A. Mean ratios of responding aged flies at each contrast difference are plotted. Results were subjected to a two factor ANOVA analysis. The factor of genotype was significant between TIFR-Gal4> *Luc* RNAi and *NorpA* (n=3, p value = <.0001). However, no significant difference was found in the factor of contrast difference, indicating that the assay could not pick up contrast sensitivity in aged flies. **B**. Mean ratios of responding young flies at each contrast difference are plotted. Results were subjected to a two factor ANOVA analysis. The factor of contrast difference was significant between the control (TIFR> *Luc* RNAi) and both TIFR> *Acsl* RNAi flies (n=4, p value = <.0001) and *NorpA* flies (n=4, p value = .0008). The factor of genotype was only significant in comparing the control to *NorpA* (n=4, p value = <.0001). The factor of genotype was not significant in comparing the control to TIFR> *Acsl* RNAi flies (n=4, p value = .2083). The asterisk symbol represents a significant difference in responding flies relative to blind *NorpA* control at each contrast point. The letter 'a' represents a significant difference in responding TIFR> *Luc* RNAi flies relative to the response at the lowest contrast point (19.04%). The letter 'b' represents a significant difference in responding TIFR> *Acsl* RNAi flies relative to the response at the lowest contrast point. All other comparisons, including all *NorpA* responses to all contrast differences, were non-significant (see text).

leading aged flies to respond poorly to visual behavior assays. To address this, the assay was repeated on young flies no older than 3 days post-eclosion.

In young flies, analysis of control RNAi, *Acsl* RNAi, and *NorpA* flies together demonstrated significant differences in the factors of both genotype ($F(2, 72) = 294.4$, p value = <.0001) and contrast difference ($F(7, 72) = 8.283$, p value = <.0001), indicating that the assay was able to pick up contrast sensitivity, and that the response differed between genotypes (Fig 3.3. B). In order to ensure that the blind *NorpA* flies were not solely responsible for the genotype effect, analysis was repeated on control RNAi and *Acsl* RNAi alone. In this analysis, there was a significant main effect of contrast ($F(7, 48) = 9.288$, p value = <.0001), indicating that the assay was able to detect contrast sensitivity in these genotypes. However, the factor of genotype was not significant in comparing control RNAi to *Acsl* RNAi ($F(1, 48) = 1.627$, p value = .2083). These results indicate that the mean ratio of responding flies for each contrast value was not significantly different between TIFR-Gal4> *Luc* RNAi flies and TIFR-Gal4> *Acsl* RNAi flies across this range of contrast values (Fig 3.3. A).

Post-hoc analysis revealed significant differences when comparing both TIFR-Gal4> *Luc* RNAi and TIFR-Gal4> *Acsl* RNAi flies to *NorpA* flies at every contrast level except the lowest, 19.04% contrast (p values all other contrast levels = <.0001, p values at 19.04% contrast = .1614, and .0326, respectively). When comparing response to contrast levels within a genotype, post-hoc analysis revealed that all TIFR-Gal4> *Luc* RNAi and TIFR-Gal4> *Acsl* RNAi responses to higher contrasts differed significantly from their response at the lowest contrast level, 19.04%, with three exceptions noted in Fig 3.3. B (p values ranging from .0481 to <.0001). All other comparisons within genotypes were non-significant, including all comparisons of *NorpA* responses at every contrast level. Finally, assessment of differences in response between TIFR-Gal4> *Luc* RNAi and TIFR-Gal4> *Acsl* RNAi at every contrast level revealed no difference.

Since the screen of glial subtype specific Gal4 drivers was designed to identify a useful driver for further analysis, and not to systematically rule out a potential function for *Acsl* in other glial subtypes, I can only draw tentative conclusions about why no phenotype was observed with the other drivers. Given the low number of samples tested (Table 3.1), it is possible that the other drivers produce a weak phenotype, or a phenotype with low penetrance. Also, it is notable that TIFR-Gal4 shares expression in marginal glia with other Gal4 drivers tested, namely *alrm*-Gal4 and *loco*-Gal4. It is possible that these other drivers do not express as strongly in marginal glia as TIFR-Gal4, or do not turn on

Driver	ERG: loss of 'on transient'	Morphology: mislocalized glia	Expressed in the *Drosophila* optic lobe
repo-Gal4	18 of 22	10 of 10	All Glia, late development
TIFR-Gal4	34 of 40	11 of 11	Marginal and Chiasm Glia
alrm-Gal4	0 of 5	0 of 4	Marginal and Chiasm Glia
Mz0709-Gal4	0 of 4	0 of 4	Surface and Cortex Glia
Gcm-Gal4	0 of 4	0 of 3	Glia and Neurons, early development
hisCl1-Gal4	0 of 4	0 of 3	Epithelial Glia
mmd-Gal4	0 of 4	0 of 3	Epithelial Glia, Medullary Neurons
loco-Gal4	0 of 4	0 of 5	Epithelial and Marginal Glia
moody-Gal4	0 of 4	0 of 3	Surface Glia
Mz97-Gal4	0 of 5	0 of 3	Surface, Cortex, Medullary, and Chiasm Glia
nrv2-Gal4	0 of 4	0 of 3	Cortex Glia

Table 3.1. Glial cell-specific drivers screened. This table presents a summary of selected Gal4 drivers tested to determine the subtype of glia responsible for loss of the 'on transient'.

at the same time in development. Moreover, in the central brain, *alrm*-Gal4 drives expression in 'astrocyte-like' neuropil glia, while TIFR-Gal4 drives expression in 'ensheathing' neuropil glia. Interestingly, the pattern of glial processes I observed when tdTomato, a fluorescent cell-membrane marker, was driven by TIFR-Gal4 indicates that marginal glia extend processes both into the lamina neuropil, as would astrocyte-like glia, and across the distal optic chiasm, as would ensheathing glia (Fig 3.4).

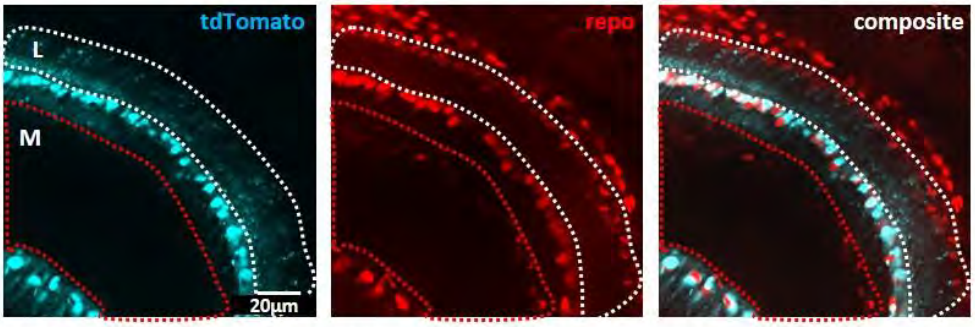

Figure 3.4. TIFR-Gal4 is expressed in Marginal glia and Giant Optic Chiasm glia. Single slice confocal images of UAS-tdTomato driven by TIFR-Gal4 co-stained with repo antibody clearly demonstrates co-localization in marginal glia and giant optic chiasm glia (n = 5). The lamina (L) is outlined in white, with the marginal glial layer directly below. The medulla (M) is outlined in red, with the proximal optic chiasm directly below.

Whether this means that marginal glia are a single population of cells demonstrating both astrocyte-like and ensheathing morphologies, or a mix of two populations that each demonstrate a single morphology, is further explored in the discussion. If the latter case is true, it might help further explain why a phenotype was only seen with TIFR-Gal4.

3.1.3. Conclusions

I have uncovered a requirement for *Acsl* in glia for visual neuron signaling. *Acsl* is specifically required in the marginal glia of the lamina.

3.2. Loss of Glial *Acsl* Causes Morphological Defects

3.2.1. Loss of glial *Acsl* causes mislocalization of marginal glia

To determine a potential cause of the loss of the 'on transient', I examined the morphology of the optic lobe in adult TIFR-Gal4 KD flies. I prepared fly brains in which TIFR-Gal4 drove the expression of either *Acsl* RNAi or *Luc* RNAi, along with tdTomato to highlight TIFR expressing glia cell bodies and processes. I co-stained these brains with antibodies to the glial nuclear protein repo and the pre-synaptic protein bruchpilot (BRP). In the *Drosophila* optic lobe, BRP is used to define synaptically-dense neuropil structures. In these flies, I observed a number of morphological defects (Fig. 3.5). I found that TIFR-expressing glial cell bodies were abnormally localized in the second optic neuropil, the medulla in *Acsl* KD flies (Fig 3.5, Fig 3.6. B). These abnormally localized

glia had complex processes, and repo-positive nuclei. All of the *Acsl* RNAi samples analyzed displayed these mislocalized glia, and none of the control RNAi samples did (*Luc* RNAi n = 8 penetrance = 0%, *Acsl* RNAi n = 11 penetrance = 100%, p value = <.0001) (Fig 3.6. D).

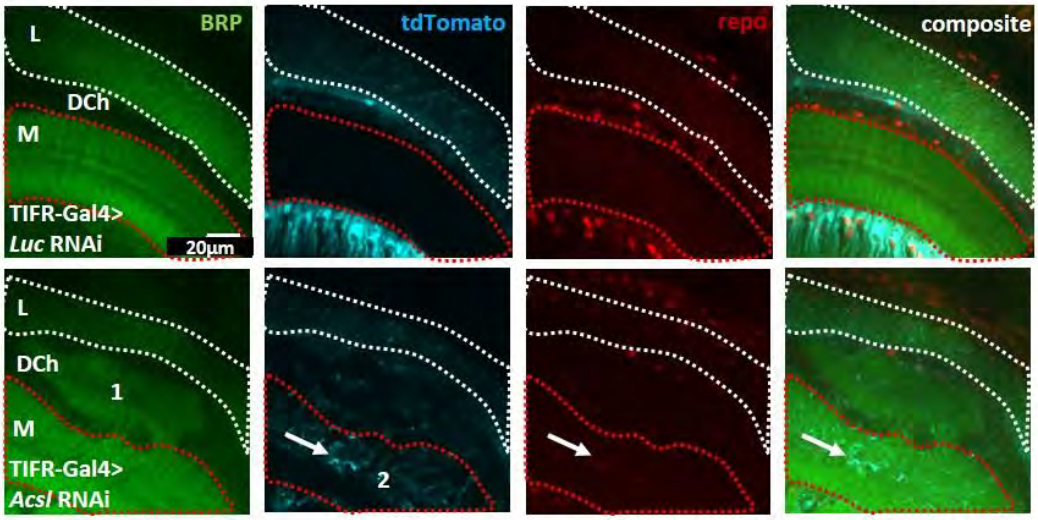

Figure 3.5. *Acsl* KD in Marginal glia causes multiple morphological defects. Single slice images of BRP, tdTomato, and repo. BRP highlights areas of neuropil. tdTomato marks cells expressing TIFR-Gal4. Repo records the location of glial nuclei. The lamina (L) is outlined in white and the medulla (M) in red with the distal chiasm between them (DCh) (neuropils are defined by BRP staining). Numbers indicate the phenotypes addressed in the following figures: 1.) ectopic neuropil (see BRP channel), 2.) mislocalized glia (see tdTomato channel, arrow points to a glial cell mislocalized in the medulla neuropil in *Acsl* KD flies).

To quantify the number of abnormally localized glia, I calculated the density of repo-positive nuclei at the proximal edge of the lamina, in the distal optic chiasm, and the medullary neuropil. Quantification of nuclei number per μm^3 revealed a significant increase in glia mislocalized to the medullary neuropil in *Acsl* RNAi flies vs. *Luc* RNAi

flies (*Luc* RNAi n = 8 mean = 0 ± 0, *Acsl* RNAi n = 10 mean = $1.371x10^{-2}$±.7326, p value = <.0001 (2-tailed t-test)) (Fig 3.6. B).

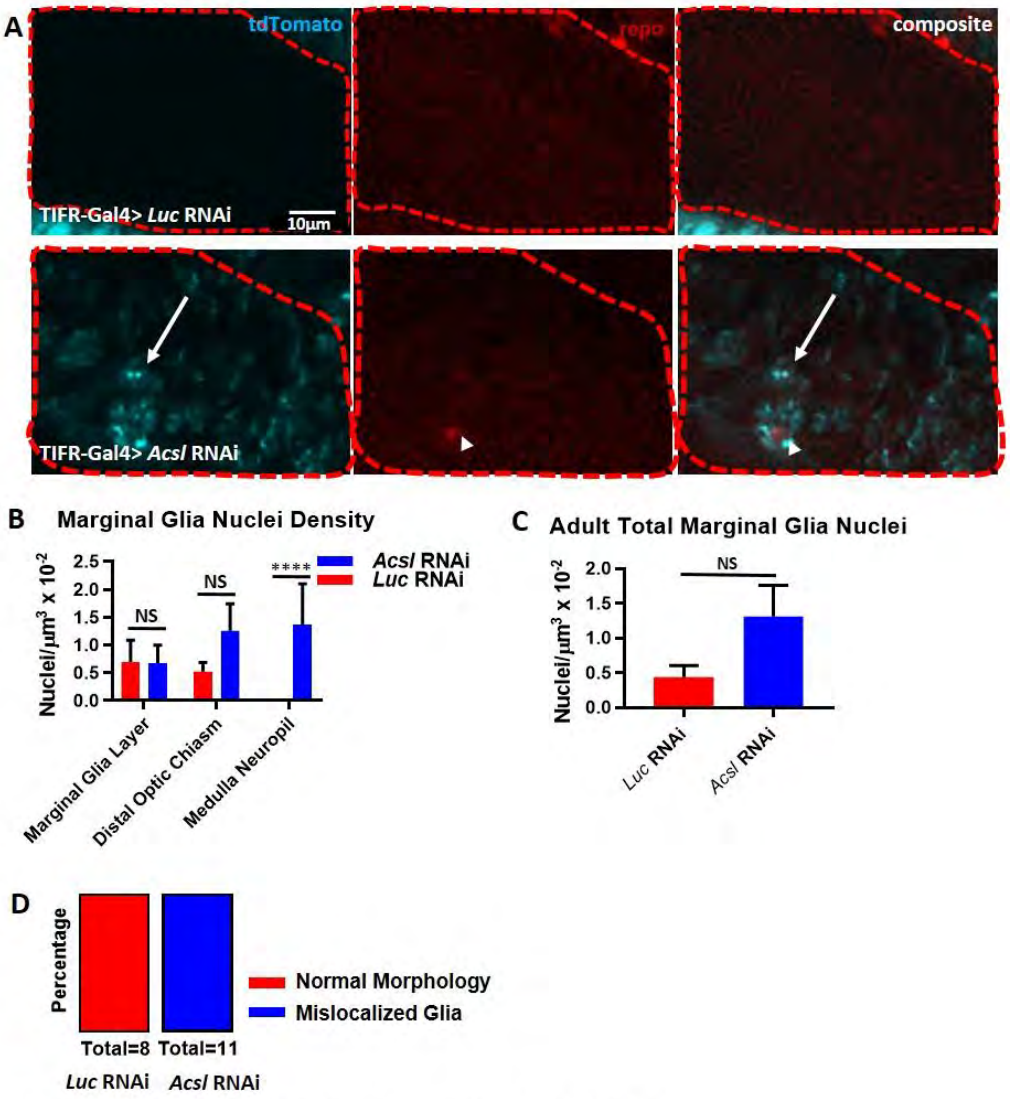

Figure 3.6. *Acsl* KD in Marginal glia causes mislocalized glia.
A. Single slice images of tdTomato and repo. tdTomato marks cells expressing TIFR-Gal4. Repo records the location of glial nuclei. The medulla is outlined in red. Arrowhead points to a glial cell body mislocalized in the medulla neuropil in *Acsl* KD flies. Arrow points to abnormal glial processes. **B**. Quantification of repo+ nuclei at the proximal edge of the lamina, in the distal chiasm, and in the medullary neuropil (*Luc* RNAi n=8, *Acsl* RNAi n=10, p values = .8982, .3917, .0001, respectively). **C**. Quantification of the total number of repo+ nuclei in all three areas demonstrates a non-significant increase (NS) between *Acsl* RNAi and control animals (*Luc* RNAi n=8, *Acsl* RNAi n=10, p value = .1148). D. Penetrance of the mislocalized glia phenotype (*Luc* RNAi n=8, *Acsl* RNAi n=10, p value = <.0001).

However, quantification of glial nuclei in the distal optic chiasm revealed a non-significant increase in *Acsl* RNAi vs. *Luc* RNAi animals (*Luc* RNAi n = 8 mean = $.5268x10^{-2} \pm .1626$, *Acsl* RNAi n = 10 mean = $1.259x10^{-2} \pm .4838$, p value = .3917 (2-tailed t-test)) (Fig 3.6. B). Finally, quantification of nuclei in the marginal glia layer revealed no difference (*Luc* RNAi n = 8 mean = $.6981x10^{-2} \pm .3906$, *Acsl* RNAi n = 10 mean = $.6817x10^{-2} \pm .3211$, p value = .8982 (2-tailed t-test)) (Fig 3.6. B). Quantification of the total number of repo-positive glia in all three areas revealed a non-significant increase in *Acsl* vs. *Luc* RNAi animals (*Luc* RNAi n = 8 mean = $.4356x10^{-2} \pm .1668$, *Acsl* RNAi n = 10 mean = $1.309x10^{-2} \pm .4467$, p value = .1148 (2-tailed t-test)) (Fig 3.6. C).

To determine whether other TIFR-positive cell populations were affected by *Acsl* RNAi expression, I examined the morphology of the giant optic chiasm glia in the proximal optic chiasm. I found their morphology to be abnormal, their processes lacking the regular organization and homogenous distribution within the proximal chiasm seen in controls (Fig 3.7. A). To determine whether the giant optic chiasm glia contribute to the population of mislocalized glia in the adjacent medulla, I quantified the density of repo-positive cell bodies within the proximal optic chiasm. I found no significant difference

between *Acsl* and *Luc* KD animals (*Luc* RNAi n = 7 mean = .4754x10^{-2} ±.2308, *Acsl* RNAi n = 7 mean = .7683x10^{-2}±.1019, p value = .2681 (2-tailed t-test)) (Fig 3.7. B).

The cell bodies of the giant optic chiasm glia may not penetrate the medulla, however I observed that in *Acsl* KD animals the giant optic chiasm glia extend faint processes into the medulla neuropil, whereas in *Luc* KD animals their processes remain

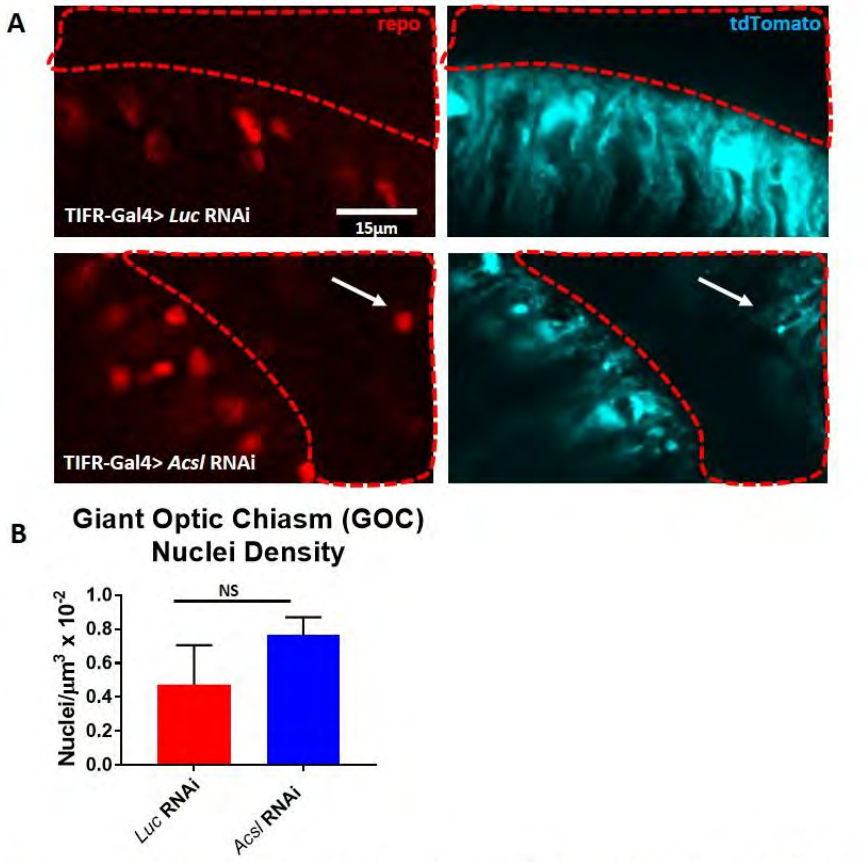

Figure 3.7. Morphological analysis and quantification of Giant Optic Chiasm glia. A. Single slice images of repo antibody staining and tdTomato expressed by TIFR+ giant optic chiasm glia. tdTomato demonstrates disorganized processes in giant optic chiasm glia in *Acsl* KD animals. The medulla is encircled by a red dashed line. Mislocalized glia in the medulla of *Acsl* KD flies are indicated by arrows. **B**. Quantification of the density of repo nuclei in the proximal chiasm reveals a non-significant increase (NS) in *Acsl* vs. *Luc* RNAi animals (*Luc* RNAi n=7, *Acsl* RNAi n=7, p value=.2681).

strictly segregated to the proximal chiasm (Fig 3.7. A). It is possible that *Acsl* KD giant optic chiasm glia communicate with the mislocalized marginal glia via their processes.

There are no significant reductions in the number of nuclei in the marginal glia layer or in the giant optic chiasm glia layer, making the original location of the mislocalized glia in the medullary neuropil difficult to determine. One clue is that the mislocalized glia in the medulla neuropil are clearly connected to the glia occupying the distal chiasm and marginal glial layer through their processes (Fig 3.5, Fig 3.9. A). In contrast, the connection between the GOC glia and mislocalized glia is much weaker. In light of this, I propose that the mislocalized glia in the medulla are marginal glia, but I cannot rule out that giant optic chiasm glia also contribute to this population.

Using signal from tdTomato driven by TIFR-Gal4, I was able to assess the distribution of marginal glia cell bodies and processes in the lamina, distal chiasm, and medullary neuropil. The cell bodies of glia in *Acsl* KD flies were randomly distributed in the distal chiasm. In contrast, in the medulla neuropil the cell bodies of glia were exclusively found in the inner medulla (Fig 3.9. A). BRP staining in the medulla of *Acsl* KD flies is disorganized, and precise identification of the synaptic layers these glial cell

bodies inhabit is not possible (Fig. 3.9. B). However, based on their location I believe them to be located in layers M6 through M8, close to the terminals of R7 and R8.

3.2.2. Glia in the distal chiasm and medulla have abnormal processes

Many glial functions are mediated through their elaboration of processes, including contact-dependent regulation of synaptic development (Garrett and Weiner, 2009; Pfrieger, 2009), recycling of neurotransmitters (Marcaggi and Attwell, 2004; Barres, 2008; Allen and Barres, 2009), and buffering of extracellular ion concentrations (Walz, 1989; Silver and Ereciriska, 1992; Simard and Nedergaard, 2004).

In an effort to indirectly address whether function may be compromised in *Acsl* KD glia, I analyzed the organization and density of their processes. The processes of normally localized marginal glia in control animals permeate the lamina neuropil, and extend from the proximal edge of the lamina to the cell body layer of the medulla. No TIFR-positive processes were observed in the medulla of adult control animals. In both

the lamina and the chiasm, the processes of normally localized marginal glia in control animals are well organized, and exhibit a regular pattern (Fig 3.8, Fig 3.10. A).

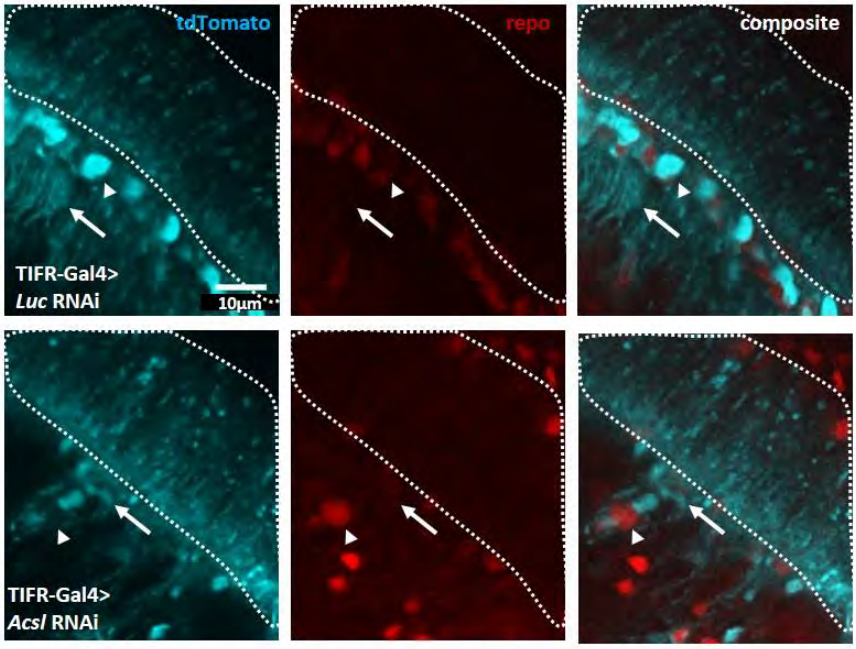

Figure 3.8. TIFR-positive glia in the distal chiasm have abnormal processes in *Acsl* KD. A. Single slice cropped images of BRP and tdTomato demonstrate that glia residing in the chiasm also have abnormal processes (arrows point to processes, arrowheads to cell bodies). Lamina outlined in white, with the distal chiasm directly below. Note the disorganized processes in *Acsl* KD animals.

In the lamina, this pattern is of lines of punctate elements, most likely representing association with lamina cartridges. These lines of puncta were homogenously distributed in the neuropil with a slight increase in density at the proximal edge. In the distal chiasm, this pattern is of regularly spaced smooth columns, most likely representing ensheathing of the processes of R7 and R8. In the distal chiasm of control

animals, the processes of glia extend from the proximal edge of the lamina to the distal edge of the medulla.

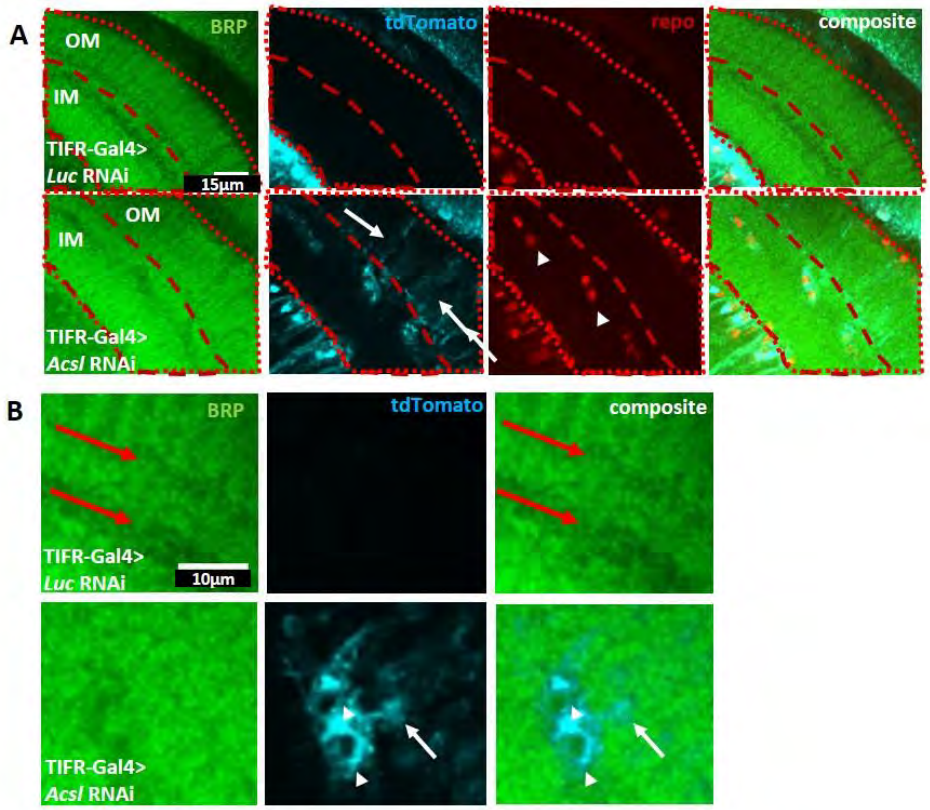

Figure 3.9. TIFR-positive glia in the medulla have abnormal processes in *Acsl* KD. **A**. Single slice images of BRP, tdTomato, and repo demonstrate that glia mislocalized to the medulla have elaborate, abnormal processes (arrows in the tdTomato channel), and cell bodies located to the inner medulla (arrowheads in the repo channel). The whole medulla is outlined in a dotted red line, and the inner medulla in a dashed red line. **B**. Cropped images of BRP and tdTomato signal in the medulla (white arrows point to processes, white arrowheads to cell bodies). Note the complex branching patterns of processes in mislocalized glia in *Acsl* KD animals. Synaptic layers are indicated by red arrows in the *Luc* RNAi animal (see BRP and composite channels). Synaptic layers are absent in *Acsl* KD animals.

In *Acsl* KD animals, these processes continue on to penetrate the outer medulla neuropil (Fig 3.8, Fig 3.10. A). Moreover, in *Acsl* KD animals, these chiasm processes are not organized into smooth columns, nor are they as homogenously distributed

throughout the chiasm as those in controls, instead having large gaps in tdTomato signal. In the medulla, the processes of mislocalized glia are diffuse in the outer medulla, elaborating in complex, branching patterns, but generally do not extend below the cell body into the inner medulla (Fig 3.9. A and B).

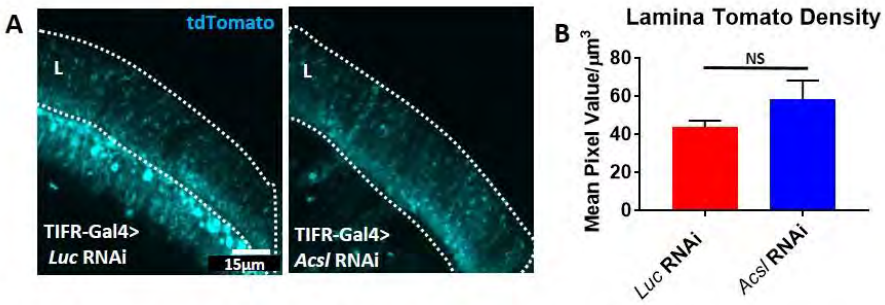

Figure 3.10. Morphological analysis and quantification of Marginal glia processes in the lamina. A. Single slice images of tdTomato expressed by marginal glia demonstrate normally organized processes in the lamina, which is outlined in white. **B**. Quantification of the density of tdTomato signal in the lamina reveals a non-significant increase (NS) in *Acsl* RNAi vs. *Luc* RNAi animals (*Luc* RNAi n = 8, *Acsl* RNAi n = 11, p value = .2477).

Within the lamina neuropil, processes in control animals are well organized and exhibit a regular pattern of linear punctate elements. In *Acsl* KD animals, this basic organization is retained (Fig 3.10. A). Analysis of the total density of tdTomato signal, which labels glial membranes, in the lamina neuropil showed no significant difference between *Acsl* and *Luc* KD animals (*Luc* RNAi n = 8 mean = 43.83 ±3.459, *Acsl* RNAi n = 11 mean = 58.39 ±9.991, p value = .2477 (2-tailed t-test)) (Fig 3.10. B), indicating that glia elaborate sufficient processes in *Acsl* KD flies.

In light of the specific effect of *Acsl* RNAi KD on lamina neuronal signaling, the observation that organization and density of marginal glia processes in the lamina is grossly unchanged is significant. Based on this result, I propose that a physiological or biochemical function of glia, rather than a structural one, is responsible for the loss of the 'on transient'.

3.2.3. The lamina and medulla are anatomically connected by 'ectopic neuropil' when *Acsl* levels are reduced in glia

In control animals, the lamina and medulla neuropil are always clearly separated in space by the distal optic chiasm, which forms two discrete BRP-positive structures. However, in *Acsl* KD animals the chiasm is punctuated by scattered BRP signal. In 55% of *Acsl* KD flies, this BRP signal forms one or more discrete, tuberous structures which occupy the chiasm and physically joins with both the lamina and the medulla (*Luc* RNAi n = 8, *Acsl* RNAi n = 11, p value = .0181 (Chi-square)) (Fig 3.11. A and B). I also observed similar BRP rich structures in the proximal optic chiasm (Fig 3.11. C), which joined with both the medulla and lobula. These structures were large, and generally located towards the periphery of the optic lobe. One of the primary characteristics that

separates neuropils from surrounding areas are their synaptic density. Thus, I have termed these BRP-rich structures ‘ectopic neuropil’.

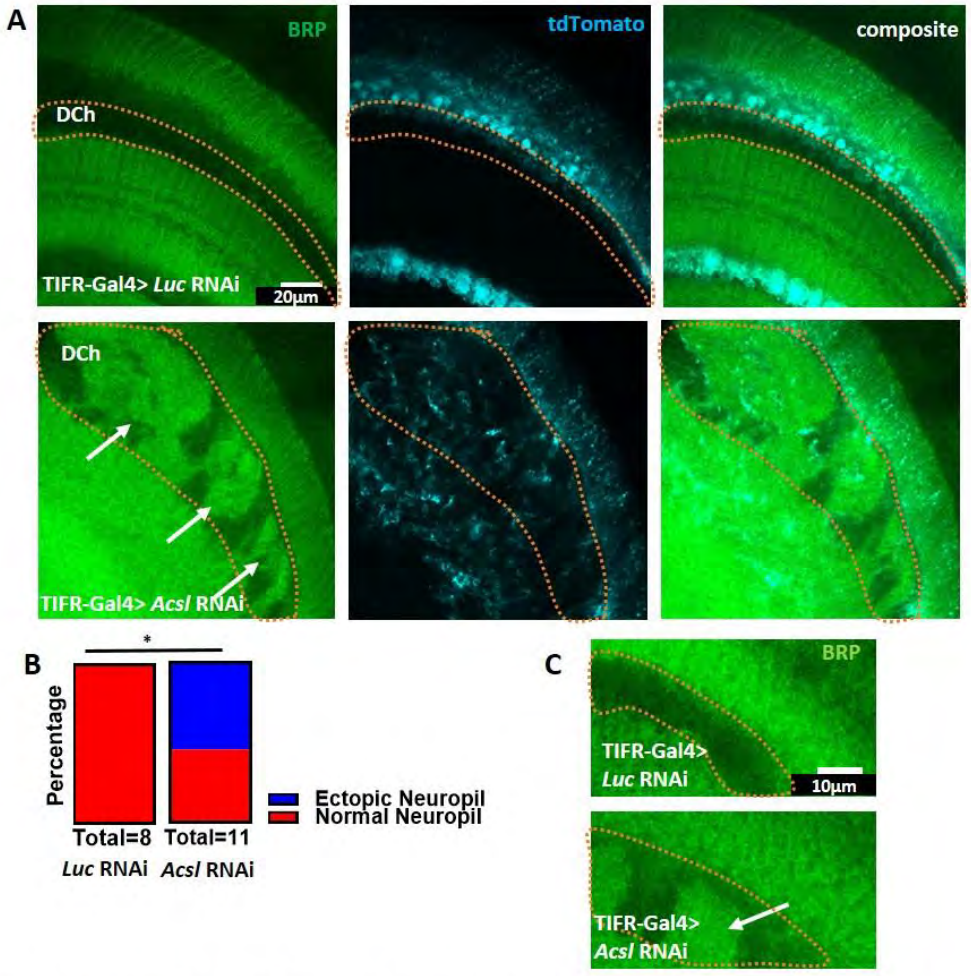

Figure 3.11. Characterization of ‘ectopic’ neuropil in the chiasms of *Acsl* KD flies. **A**. Single slice images of BRP demonstrate the presence of synaptically dense areas in the chiasms which connect to the adjacent neuropil (arrows in the BRP channel). Composite images with tdTomato demonstrate that these ectopic neuropil are rich in TIFR+ processes. The distal optic chiasm is outlined in orange. **B**. Representation of the % penetrance of ectopic neuropils in KD flies (*Luc* RNAi n = 8, *Acsl* RNAi n = 11, p value = .0181). **C**. Ectopic neuropils are also present in the proximal optic chiasm. The distal optic chiasm is outlined by an orange dashed line.

The ectopic neuropils I observed share many features with the medulla, being rich in TIFR-positive glial cell bodies and processes, and lacking the columnar organization of BRP and tdTomato typical of the lamina (Fig 3.11. A). Additionally, the medulla is the common neuropil involved in these ectopic structures, which occupy the chiasms on either side of the medulla as described above. I therefore propose that the ectopic neuropils represent outgrowth of the medulla, perhaps facilitated by mislocalized glia, that then connect with the adjacent neuropil on either side. However, I cannot rule out that ectopic neuropils arise independently of the endogenous neuropils with which they join. Likewise, I cannot conclude that these ectopic neuropils have any electrophysiological activity of their own, or that they allow neuronal signals to pass from the lamina to the medulla.

It is worth noting that the penetrance of ectopic neuropil is different from the penetrance of either the loss of the 'on transient' or the misplacement of glia, both of which are present in over 80% of TIFR *Acsl* KD animals. This may represent variable levels of RNAi expression within the KD population, with the more severely affected individuals exhibiting ectopic neuropils. Therefore, the ectopic neuropils described here

may not be causally related to the ERG phenotype. This result is somewhat surprising, as it could be expected that the ectopic neuropils disrupt electrophysiological barriers around the neuropil, or that they inappropriately propagate signal from one neuropil to another, and thus would directly affect the transients of the ERG. It may instead be the case that these ectopic neuropil are not electrophysiologically active, and thus represent a purely morphological defect with no impact on the ERG or neuronal function.

3.2.4. BRP signal is not significantly reduced in the lamina of *Acsl* KD flies

As discussed above, BRP is a marker for the pre-synapse. Ample evidence demonstrates that the number of synapses developed in the lamina is largely determined by the pre-synapse and pre-synaptic cell (Frohlich and Meinertzhagen, 1982; Fröhlich and Meinertzhagen, 1983, 1987; Meinertzhagen and Fröhlich, 1983; Meinertzhagen, 1993). In many cases, pre-synaptic markers, such as BRP, are used as a measurement of the density of synapses in neuropil of the optic lobe, although effects on the post-synapse cannot be conclusively determined with this method. In order to further explain the loss of the 'on transient' in *Acsl* KD flies, I quantified the density of BRP signal in the lamina using the volumetric analysis (see Chapter II. Methods). To remove the confounding

effects of age-dependent reduction in synaptic density and diurnal synaptic rhythmicity, brains were prepared 3 days after eclosion with age-matched internal controls for comparison. All brains were prepared with ± 2 hours of mid-day to control for diurnal variation in synapse density.

In TIFR-Gal4 *Acsl* KD flies, the density of BRP signal in the lamina neuropil was non-significantly reduced compared to controls (*Luc* RNAi n = 8 mean = 116 ±10.74, *Acsl* RNAi n = 11 mean = 100.2 ±5.281, p value = .1707 (2-tailed t-test)) (Fig 3.12. A and B).

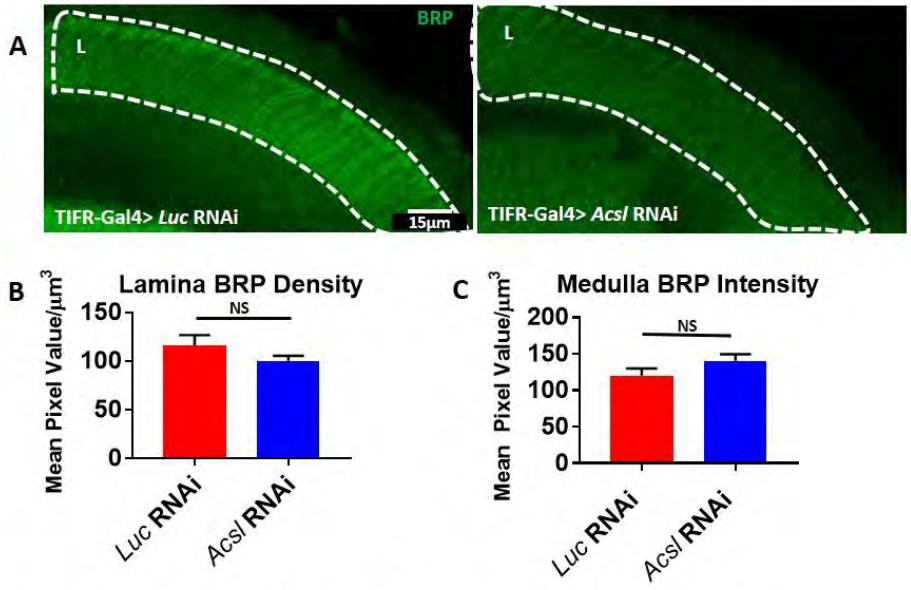

Figure 3.12. BRP density is not significantly changed in *Acsl* KD adults.
A. Single slice images of BRP staining of the lamina demonstrate that BRP density is not significantly reduced, and lamina cartridges are organized normally. The lamina is outlined in white. **B**. Quantification of BRP signal density in the lamina (*Luc* RNAi n = 8, *Acsl* RNAi n = 11, p value = .1707). **C**. Quantification of BRP density in the medulla revealed a non-significant increase (NS) between populations (*Luc* RNAi n = 7, *Acsl* RNAi n = 7, p value = .1577).

It was clear that within the lamina, BRP remained normally organized, arranging into discernible linear cartridges in parallel sections, and homogenously distributed throughout the neuropil (Fig 3.12. A). This result suggests that the association of photoreceptors with lamina neurons and the subsequent development of the lamina cartridges proceeds normally despite glial KD of *Acsl*.

While the electrophysiological phenotype appears to mainly affect the transients of the ERG, which reflect function of the lamina, the medulla was found to contain mislocalized TIFR+ glia in my initial morphological analysis. To determine whether synaptic number was affected in this neuropil, I quantified synaptic density as described previously. This quantification revealed a non-significant increase in *Acsl* vs. *Luc* RNAi populations (*Luc* RNAi n = 7 mean = 120.2±9.79, *Acsl* RNAi n = 7 mean = 140.4±9.132, p value = .1577 (2-tailed t-test)) (Fig 3.12. C). In addition, BRP signal in the medulla of *Acsl* KD flies appears disorganized, without the characteristic horizontal synaptic layers found in controls (Fig 3.9. B, red arrows). The impact of this disorganization is difficult to determine, as the medulla neuropil is too far from the surface of the eye for its activity to be reliably measured in the ERG, and the optomotor assay with contrast difference

(Fig 3.3) is designed to test motion and contrast vision processed by lamina neurons (Melnattur and Lee, 2011; Melnattur et al., 2014).

3.2.5. *ACSL4* rescues the morphology of *Acsl* KD flies

To assess whether there is functional homology of human *ACSL4* and *Drosophila Acsl* in glia, I prepared brains from flies co-expressing human *ACSL4*, *Drosophila Acsl* RNAi or *Luc* RNAi, and tdTomato under TIFR-Gal4, and co-stained these samples with repo and BRP antibodies. I found that while all of the *Acsl* KD fly brains examined had mislocalized glia, only 43% of *ACSL4* rescue flies did, and 0% of control flies did (*Luc* RNAi n = 6, *Acsl* RNAi + *ACSL4* n = 14, *Acsl* RNAi alone n = 11) (Fig 3.13. A and B). The p value between control and *Acsl* RNAi + *ACSL4* flies was .1149 (Chi-square), and the p value between *Acsl* RNAi + *ACSL4* and *Acsl* RNAi alone flies was .0029 (Chi-square), indicating significant rescue of the morphological phenotype by the human homolog (Fig 3.13. B). Moreover, I found evidence of ectopic neuropil in only 1 of the 14 rescue fly brains examined, indicating a reduction in the severity of the phenotype (*Luc* RNAi n = 6 penetrance = 0%, *Acsl* RNAi + *ACSL4* n = 14 penetrance = 7%, *Acsl* RNAi alone n = 11 penetrance = 55%) (Fig 3.13. C). The p value between control and

Acsl RNAi + *ACSL4* flies was >.9999 (Chi-square), and the p value between *Acsl* RNAi + *ACSL4* and *Acsl* RNAi alone flies was .0213 (Chi-square), again indicating a significant rescue of the morphological phenotype (Fig 3.13. C).

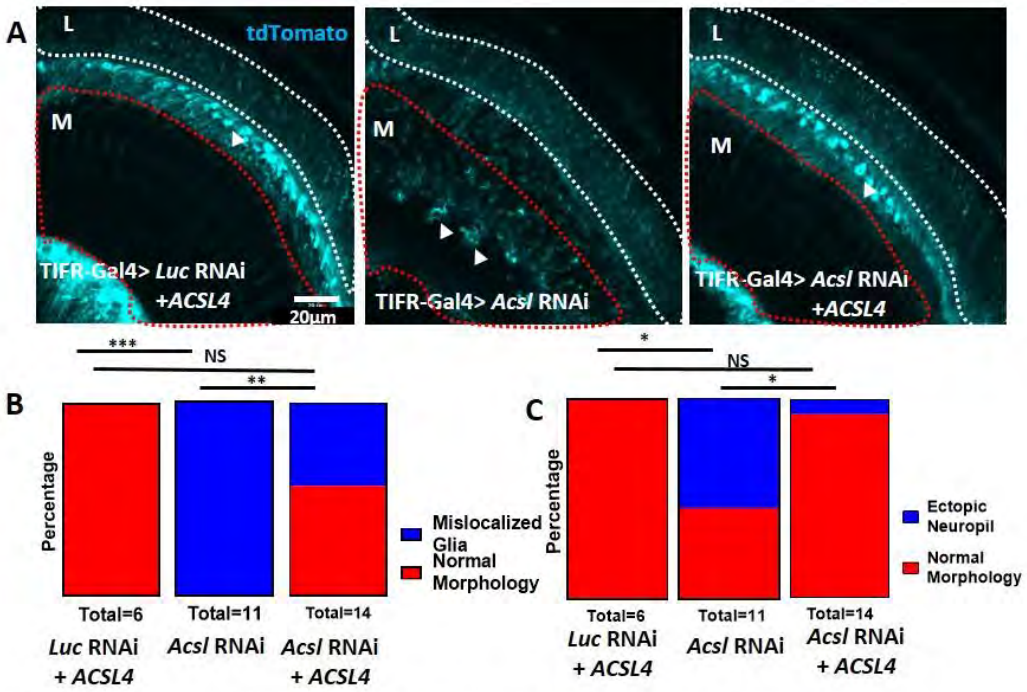

Figure 3.13. Expression of *ACSL4* rescues the morphological phenotype.
A. Single slice images of tdTomato highlight the distribution of TIFR+ cells. Arrowheads point to cell bodies. *ACSL4* expression restores the localization of glia to the proximal edge of the lamina. The lamina is outlined in white, and the medulla in red. **B** Representation of the % penetrance of rescue of the mislocalized glia phenotype (*Luc* RNAi + *ACSL4* n = 6, *Acsl* RNAi + *ACSL4* n = 14, *Acsl* RNAi alone n = 11. P value of *Luc* vs. *Acsl* RNAi rescue = .1149, p value of *Acsl* RNAi + *ACSL4* vs. *Acsl* RNAi alone = .0029, p value of *Luc* RNAi + *ACSL4* vs. *Acsl* RNAi alone = <.0001). **C.** Representation of the % penetrance of rescue of the ectopic neuropil phenotype (*Luc* RNAi + *ACSL4* n = 6, *Acsl* RNAi + *ACSL4* n = 14, *Acsl* RNAi alone n = 11. P value of *Luc* vs. *Acsl* RNAi rescue = >.9999, p value of *Acsl* RNAi + *ACSL4* vs. *Acsl* RNAi alone = .0213, p value of *Luc* RNAi + *ACSL4* vs. *Acsl* RNAi alone = .0427).

3.2.6. Conclusions

Acsl KD in marginal glia causes two major morphological defects: mislocalization of marginal glia in the medullary neuropil, and the development of ectopic neuropil. Of these defects, only the mislocalization of glia is present in a similar penetrance to the ERG phenotype, indicating that ectopic neuropil likely does not underlie this particular physiologic defect. Importantly, all the morphological defects observed in *Acsl* KD flies were rescuable by *ACSL4* expression, demonstrating the functional homology of human *ACSL4* and *Drosophila Acsl* in glia.

3.3. Glial *Acsl* is Required in Development

3.3.1. Marginal glia migrate to the lamina

In *Acsl* KD adults, marginal glia are mislocalized in the medullary neuropil. To determine whether their mislocalization was due to defects in migration, I examined wandering third instar larvae. At this point in time, lamina glia have largely migrated to the nascent lamina, and are arranged in three layers: cortex, epithelial, and marginal. To

determine whether marginal glia successfully migrate to their appropriate layer in the lamina, I prepared larvae expressing either *Acsl* RNAi or *Luc* RNAi, along with tdTomato, using TIFR-Gal4. I co-stained the larval brains with repo and chaoptin, a photoreceptor marker labeling R1-R8 (Van Vactor et al., 1988).

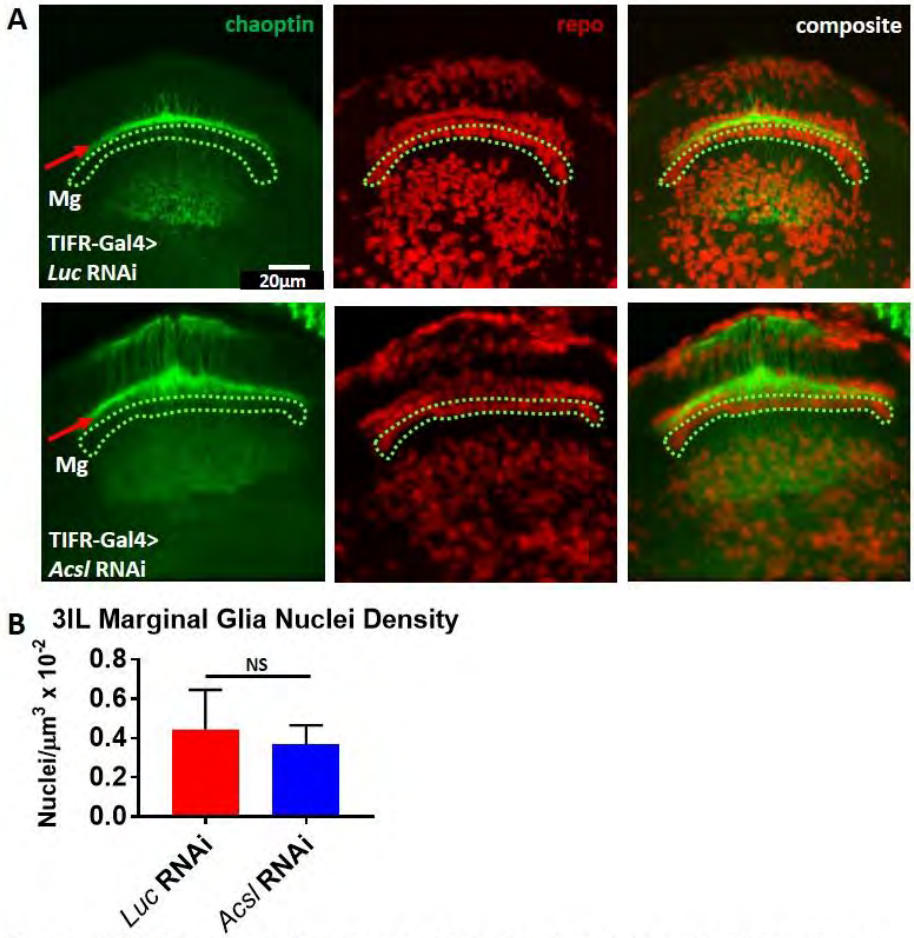

Figure 3.14. Marginal glia migrate to the lamina. A. Z projections of repo and chaoptin in third instar larvae demonstrate that marginal glia migrate to the lamina and act as intermediate targets for photoreceptors in *Acsl* KD flies. The marginal glial layer (Mg) is outlined in green. Terminals of R1-R6 in the lamina are indicated by the red arrow in the chaoptin channel. **B**. Quantification of the density of nuclei in the marginal glia layer reveals a statistically insignificant (NS) decrease in *Acsl* KD flies (*Luc* RNAi n = 8, *Acsl* RNAi n = 13, p value=.7102). Error bars are SEM.

In the wandering third instar larvae, I observed three layers of glia in the developing lamina in control and *Acsl* KD animals (Fig 3.14. A). Quantification of the number of glial nuclei in the marginal glia layer revealed no significant difference

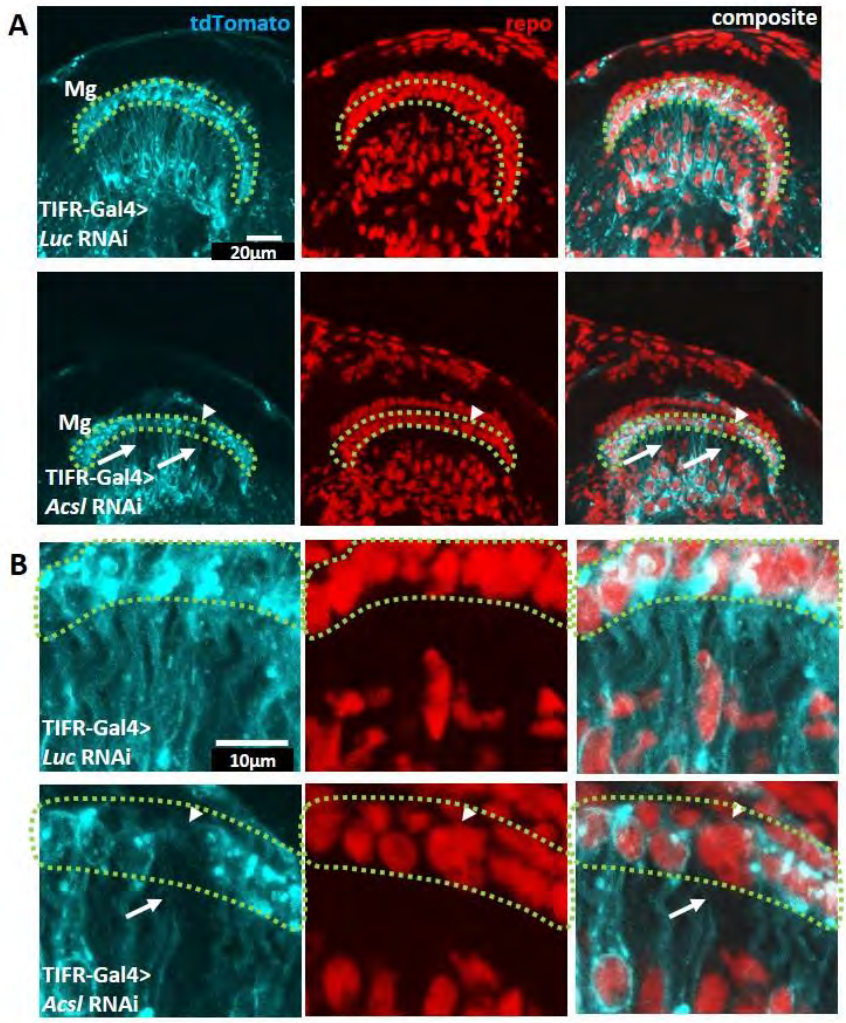

Figure 3.15. Marginal glia processes are abnormal during larval development. A. Z-projections of tdTomato and repo signal highlight the processes and nuclei of TIFR+ marginal glia at the third larval instar. The marginal glia layer (Mg) is outlined in green. The processes of *Acsl* KD animals have abnormal gaps in the marginal glia layer (arrowhead), and in their processes extending below this layer (arrows). **B.** Enlarged images of repo antibody and tdTomato signal in the marginal glia layer (green outline). Arrowheads point to gaps in processes in the marginal glia layer, and arrows to gaps in processes below the marginal glia layer. These gaps are not produced by an absence of cell bodies (see repo channel).

between *Acsl* RNAi vs. *Luc* RNAi populations (*Luc* RNAi n = 8 mean = .4441 ±.2007, *Acsl* RNAi n = 13 mean = $.3692x10^{-2}$ ±.09645, p value = .7102 (2-tailed t-test)) (Fig 3.14. B).

Although marginal glia were present at the lamina in normal numbers, I did observe abnormalities in the organization of their processes (Fig 3.15. A and B). First, in the marginal glia layer of *Acsl* KD larvae I observed gaps in the tdTomato signal. There was no corresponding absence of nuclei in these gaps, indicating that the glial cells were present but were not elaborating processes at the same density as their neighbors (Fig 3.15. A and B, arrowheads). Second, I observed gaps in the tdTomato signal extending below the marginal glia layer, that in some cases were associated with groups of repo+ TIFR- nuclei (Fig 3.15. A and B, arrows). These results suggest that in *Acsl* KD, glial processes are abnormal in the third larval instar.

Marginal glia have a documented function in the third larval instar, acting as temporary targets for photoreceptors R1-R6, which terminate in the lamina until lamina neurons can migrate into the nascent neuropil (Poeck et al., 2001; Rangarajan et al., 2001). In both *Acsl* KD and control animals, chaoptin staining reveals a strong band of

photoreceptor termini between the epithelial and marginal glia layers of the lamina, and normal extension of R7 and R8 into the developing medulla (Fig 3.14. A). Together, these results provide evidence that marginal glia correctly migrate to the lamina, and function to provide a 'stop' signal to photoreceptors R1-R6, in both *Acsl* and *Luc* KD populations.

3.3.2. Marginal glia are mislocalized in mid-pupal development

Having established that marginal glia migrate to their positions at the proximal edge of the lamina in the larvae, I sought to determine whether these glia move from their positions later in development. For this analysis, I prepared brains from multiple stages of pupal development. These brains expressed either *Acsl* RNAi or *Luc* RNAi, as well as tdTomato, under TIFR-Gal4 as before. In addition, I co-stained with repo and chaoptin, as BRP is not expressed until the later stages of pupal development. I focused my analysis on pupae prepared between 48 and 50 hours after pupariation. This time point represents mid-pupal development, or 50% pupae (P50). P50 occurs after the neuropils of the optic lobe rotate from their larval to their adult orientations (Meinertzhagen, 1993). Identifying mislocalization of marginal glia depends upon their relationship to the

lamina; thus, identifying mislocalization while the lamina is in flux is difficult. However, by P50, the pupal brain is morphologically comparable to the adult brain. In P50 brains of

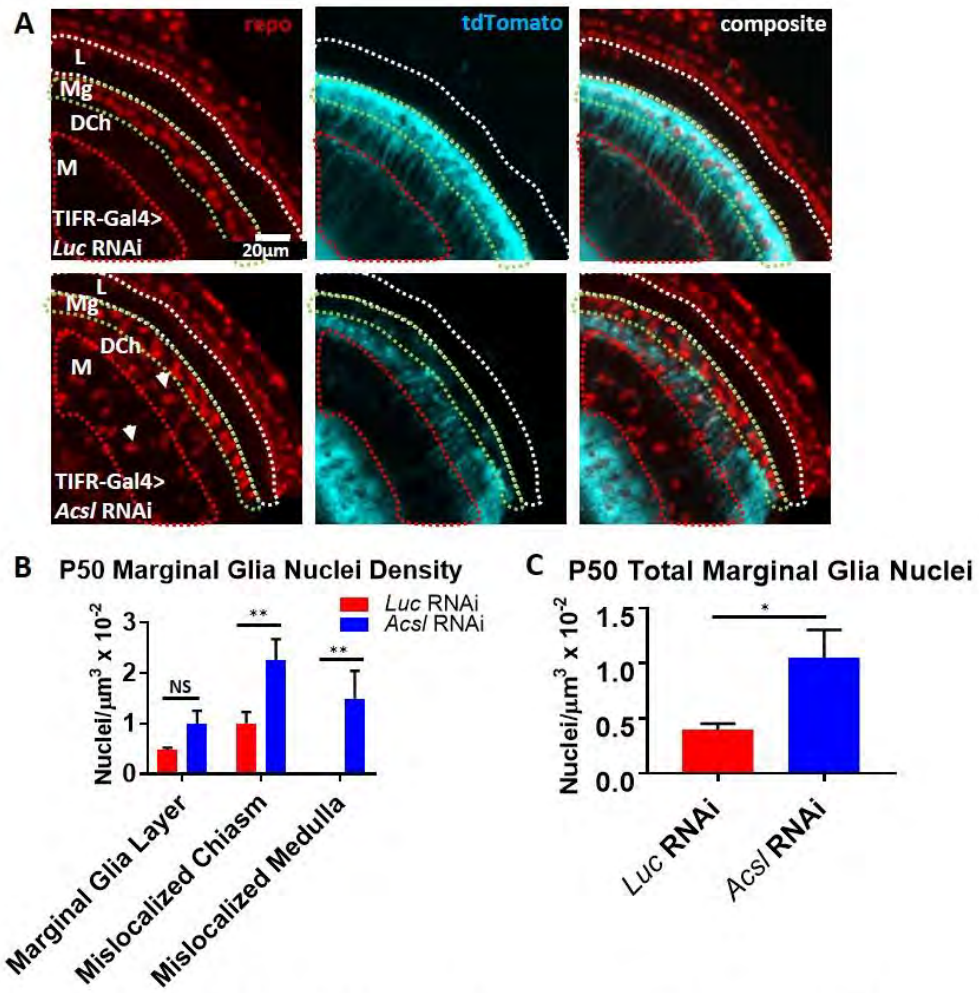

Figure 3.16. Marginal glia have exited the proximal edge of the lamina by P50. **A**. Z-projection images of repo and tdTomato signal at P50 demonstrate that glia have moved into the distal chiasm and medulla in *Acsl* KD animals. The lamina is outlined in white (L), the marginal glia layer in green (Mg), and the medulla in red (M). The distal chiasm is the space between the green and red layers (DCh). Mislocalized cells are indicated by arrowheads in the repo channel. **B**. Quantification of nuclei density demonstrates significant increases in mislocalized glia at this stage (*Luc* RNAi n = 8, *Acsl* RNAi n = 9, p value = .2483, .006850, and .002061, for marginal glial layer, distal chiasm, and medulla neuropil, respectively). **C**. Quantification of the nuclei density in all three areas revealed a significant increase in glia in *Acsl* vs. *Luc* RNAi animals (*Luc* RNAi n = 8, *Acsl* RNAi n = 9, p value = .0302).

Acsl KD flies, marginal glia have exited their normal positions, and occupy the distal optic chiasm and medulla neuropil. Quantification of the density of glial nuclei in the marginal glia layer demonstrated a slight, although not statistically significant, increase relative to control (*Luc* RNAi n = 8 mean = .4839 ±.04411, *Acsl* RNAi n = 9 mean = $.7864x10^{-2}$ ±.1587, p value = .2483 (2-tailed t-test)) (Fig 3.16. B).

Interestingly, expression of tdTomato in this layer is significantly reduced in *Acsl* KD animals (Fig 3.16. A), suggesting either that a non-TIFR expressing population of cells also resides at the proximal edge of the lamina during pupal development, or, more likely, that while the majority of marginal glia cell bodies remain in their appropriate layer at this time, their processes are not as numerous or as developed as glia in control animals. This result may reflect the preparation of glia to exit the proximal edge of the lamina.

In contrast, there were significant increases in mislocalized glia in the chiasm (*Luc* RNAi n = 8 mean = 1.008 ±.2272, *Acsl* RNAi n = 9 mean = $1.93x10^{-2}$ ±.4395, p value = .006850 (2-tailed t-test)) and medulla (*Luc* RNAi n = 8 mean = 0 ± 0, *Acsl* RNAi n = 9 mean = $1.494x10^{-2}$ ±.5513, p value = .002601 (2-tailed t-test)) (Fig 3.16. B).

Quantification of the total number of glial nuclei in all three areas revealed that *Acsl* KD animals have a statistically significant increase (*Luc* RNAi n = 8 mean = 1.492 ±.1933, *Acsl* RNAi n = 9 mean = $4.6x10^{-2}$ ± 1.073, p value = .0129 (2-tailed t-test)) (Fig 3.16. C). In the medulla, the glial cell bodies are largely located in the inner medulla, below synaptic layer M6 where R7 photoreceptors terminate (Fig 3.17) (Fischbach and Dittrich, 1989). In a subset of samples, however, I observed glial cell bodies within layer M6, between R7 termini, or within the outer medulla. This distribution throughout the medulla

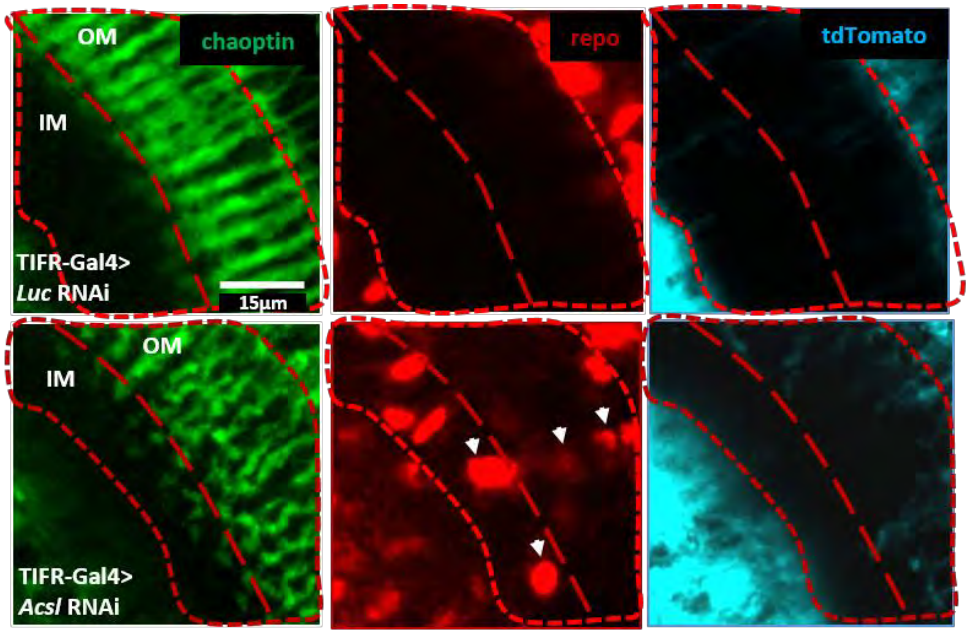

Figure 3.17. Mislocalized glia are located throughout the medulla at P50. Higher magnification z projection images of the medulla of P50 flies. Chaoptin staining labels the termini of R7 and R8 in the medulla, which is outlined in red. Chaoptin staining indicates disrupted photoreceptor termini organization. Mislocalized glia are located both proximal and distal to these termini in the medulla neuropil (arrowheads in the repo channel). Inner and outer medulla are separated by a red dashed line. tdTomato signal in the processes of these glia is weaker than in later stages of development.

at P50 is in sharp contrast to the adult, in which glial cell bodies are exclusively located in the inner medulla (Fig 3.9).

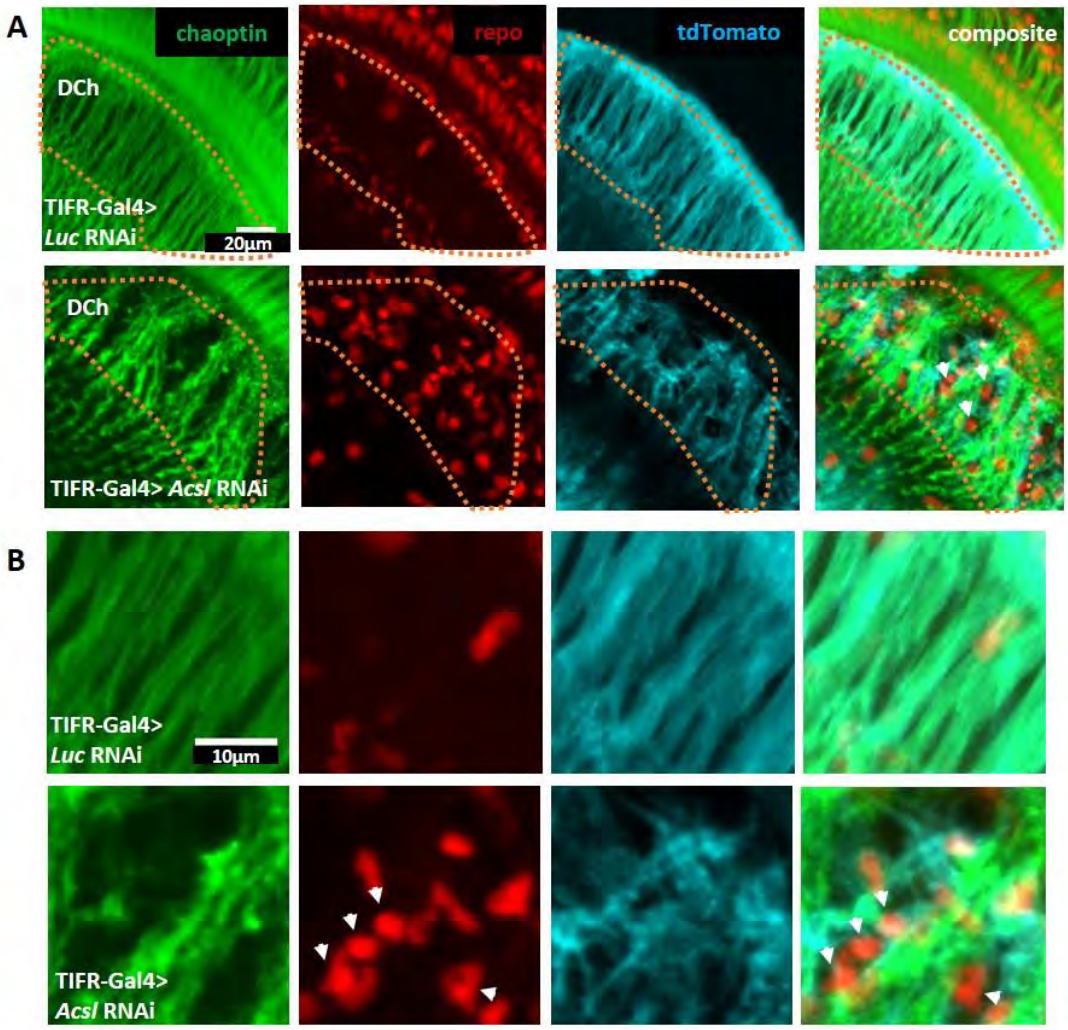

Figure 3.18. TIFR-positive glia are closely associated with R7/R8 projections in the distal optic chiasm. A. Z-projections of the distal chiasm of P50 flies. The distal chiasm is outlined in orange. Chaoptin staining labels the axons of R7 and R8. Axons are disorganized in the chiasm compared to controls, as are the processes of marginal glia. In *Acsl* RNAi animals, the cell bodies of TIFR+ glia are closely associated with R7/R8 projections in the distal chiasm (arrowheads in the composite channel), and their processes are abnormal (see text). **B**. Enlarged images of the distal chiasm in P50 flies. Note the close association of repo+ glial nuclei (white arrowheads) with the processes of R7/R8.

Unlike the adult, the processes of the mislocalized medullary glia in P50 animals are neither complex nor distinct, and do not become so until the last 24 hours of pupal development (Fig 3.17, data not shown). Consistent with the above results, it is possible that the mislocalized glia have recently arrived in the medulla at P50, and are only beginning to incorporate themselves into the surrounding neuropil through the elaboration of processes.

In *Luc* KD control animals, normally localized marginal glia processes traverse the chiasm in an organized fashion at P50, forming smooth columns that are most likely ensheathing the processes of R7/R8, and accompany the terminals of R7 and R8 into the medullary neuropil. In *Acsl* KD animals, the processes of the mislocalized chiasm glia are disorganized at this developmental stage, both within the chiasm itself, and in the medulla (Fig 3.18. A and B). Processes do not organize into regularly spaced, smooth columns in parallel with the lamina cartridges, as in the control animals, but rather appear random, branching perpendicularly to the lamina cartridges, and occasionally accumulating into dense clusters.

As in the third larval instar, photoreceptor targeting at P50 is grossly normal, with clear termination of photoreceptors in the lamina and medulla (Fig 3.17, Fig 3.18. A). However, the organization of R7 and R8 processes as they traverse the distal chiasm in *Acsl* KD animals is disordered, most likely due to physical disruption by mislocalized chiasm glial cell bodies (Fig 3.18. A and B). Indeed, glial cell bodies within the chiasm appear in clusters, and are closely associated with the processes of R7/R8. In spite of this disruption in the chiasm, R7 and R8 terminals still appear to target to the correct medullary synaptic layers, although the terminals are disorganized within the medullary neuropil (Fig. 3.17). In control animals, R7 and R8 termini are regularly spaced, linear, and easily distinguishable from their neighbors. In *Acsl* KD animals, R7 and R8 termini are serpentine, rendering it difficult to distinguish individual termini.

3.3.3. Temporal restriction of *Acsl* RNAi expression to development or adulthood

i. Experimental design

The phenotype of mislocalized glia seen in adult *Acsl* KD animals is present as early as the P50 stage, suggesting that *Acsl* functions in development. To determine this

genetically, I temporally restricted the expression of *Acsl* RNAi or *Luc* RNAi to either development or adult phases, using the Gal80^{ts} system (see Chapter II. Methods, Fig 2.1). In these experiments, the RNAi JF02811 was driven by *repo*-Gal4. ERG and morphology were examined at eclosion and after 10 days of adulthood. For morphological analysis, I co-stained prepared brains with repo and BRP antibodies, to stain glial nuclei and pre-synapses, respectively, and phalloidin-rhodamine to visualize F-actin.

ii. Developmental expression of RNAi

After expressing dsRNA from the onset of second larval instar to eclosion, I analyzed the ERG and morphology of the optic lobe, both at eclosion and after 10 days of adulthood without dsRNA expression. In newly eclosed flies, I observed a significant reduction in the magnitude of the 'on transient' in *Acsl* KD flies (repo-Gal4> *Luc* RNAi n = 15 mean =1.133±.1563, repo-Gal4> *Acsl* RNAi n = 21 mean = .381±.1073, p value = .0002 (2-tailed t-test)) (Fig 3.19. A and B). Additionally, I observed a significant percentage of *Acsl* KD animals with a loss of the 'on transient' (repo-Gal4> *Luc* RNAi n = 15 penetrance = 0%, repo-Gal4> *Acsl* RNAi n = 21 penetrance = 52%, p value = .0008 (Chi-square)) (Fig 3.19. A and D). In contrast, I observed no significant difference in the

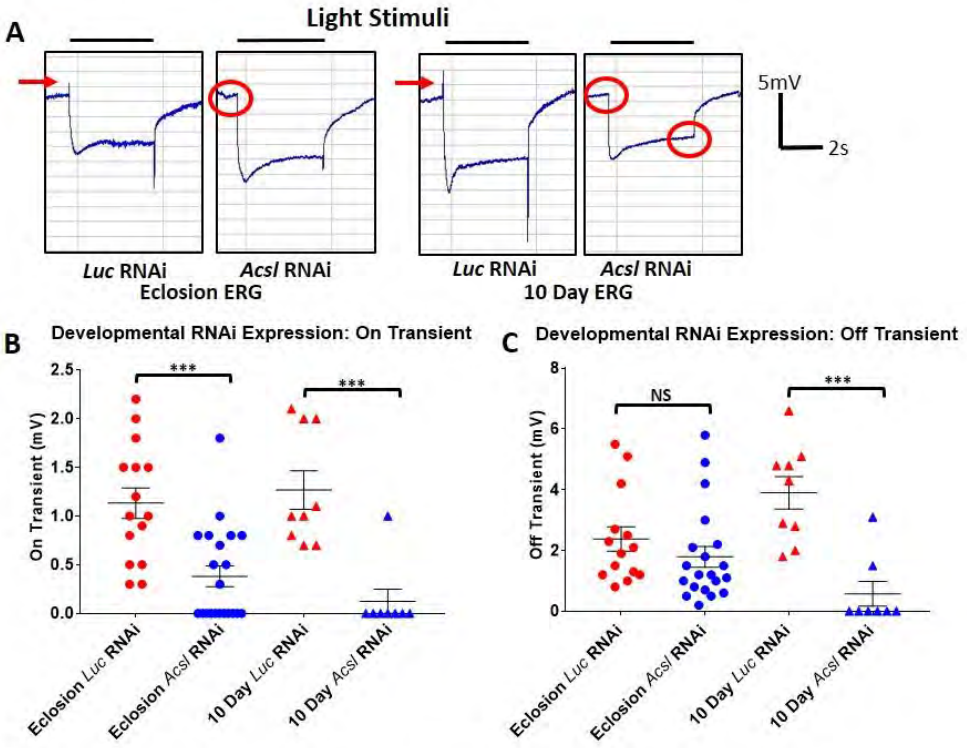

D

Genotype (with *tub*> Gal80^{ts})	N number	Loss of On Transient	Loss of On and Off Transient
repo> *Luc* RNAi Eclosion	15	0%	0% (n=14)
repo> *Acsl* RNAi Eclosion	21	52% (11 of 21) ***	0% (n=20) NS
repo> *Luc* RNAi 10 Day	9	0%	0%
repo> *Acsl* RNAi 10 Day	8	88% (7 of 8) ***	75% (6 of 8) **

Figure 3.19. ERG phenotypes in developmental expression of RNAi. A. In this figure, *Acsl* RNAi was allowed to express only in development, and blocked after eclosion in adults. ERG traces from animals at eclosion and after 10 days of adulthood without RNAi expression. Note the absence of the 'on transient' in *Acsl* RNAi animals at both eclosion and after 10 days of adulthood, and the absence of both transients in 10 day old animals (see red circles). **B**. Quantification of the 'on transient' reveals a significant reduction in *Acsl* RNAi animals at both eclosion and after 10 days of adulthood (p values vs. age matched *Luc* RNAi animals = .0002, and .0003, respectively). **C**. Quantification of the 'off transient' reveals a significant reduction in *Acsl* RNAi animals after 10 days of adulthood (p value vs. age matched *Luc* RNAi animals = .0002), but not at eclosion (p value vs. age matched *Luc* RNAi animals = .2791). **D**. Table summarizing the penetrance of loss of transients in these experiments. At eclosion, 1 trace was excluded from 'off transient' analysis in both *Acsl* and *Luc* RNAi data sets due to noise obscuring the 'off transient'. Loss of the 'on transient' occurs in *Acsl* RNAi animals at both eclosion and 10 days of adulthood (p values vs age matched *Luc* RNAi animals = .0008, and .0003, respectively). After 10 days of adulthood without RNAi expression, both 'on' and 'off' transients are absent in a high percentage of *Acsl* RNAi animals (p value vs. age matched *Luc* RNAi animals = .0023).

magnitude of the ‘off transient’ (repo-Gal4> *Luc* RNAi n = 15 mean = 2.379±.406, repo-Gal4> *Acsl* RNAi n = 21 mean = 1.79±.3453, p value = .2791 (2-tailed t-test)) (Fig 3.19. A and C). Nor did I observe any traces with a loss of both ‘on’ and ‘off’ transients in either the *Luc* RNAi or *Acsl* RNAi populations (Fig 3.19. A and D, Appendix A. Table of Experiments).

After 10 days of adulthood without RNAi expression, I still observed a significant reduction in the magnitude of the ‘on transient’ (repo-Gal4> *Luc* RNAi n = 9 mean = 1.267±.1972, repo-Gal4> *Acsl* RNAi n = 8 mean = .125±.125, p value = .0003 (2-tailed t-test)) (Fig 3.19. A and B), as well as a significant percentage of *Acsl* KD flies with a loss of the ‘on transient’ (repo-Gal4> *Luc* RNAi n = 9 penetrance = 0%, repo-Gal4> *Acsl* RNAi n = 8 penetrance = 88%, p value = .0003 (Chi-square)) (Fig 3.19. A and D).

At this time point, the magnitude of the ‘off transient’ is significantly reduced (repo-Gal4> *Luc* RNAi n = 9 mean = 3.9±.5367, repo-Gal4> *Acsl* RNAi n = 8 mean = .575±.4057, p value = .0002 (2-tailed t-test)) (Fig 3.19. A and C). Moreover, I observed a significant percentage of *Acsl* KD traces with a loss of both the ‘on’ and ‘off’ transients (repo-Gal4> *Luc* RNAi n = 9 penetrance = 0%, repo-Gal4> *Acsl* RNAi n = 8 penetrance

= 75%, p value = .0023 (Chi-square)) (Fig. 3.19. A and D). These results indicate a progression of the phenotype over time, in which visual neuron signaling is more severely affected after 10 days of adulthood, despite the presumed restoration of Acsl protein production after eclosion.

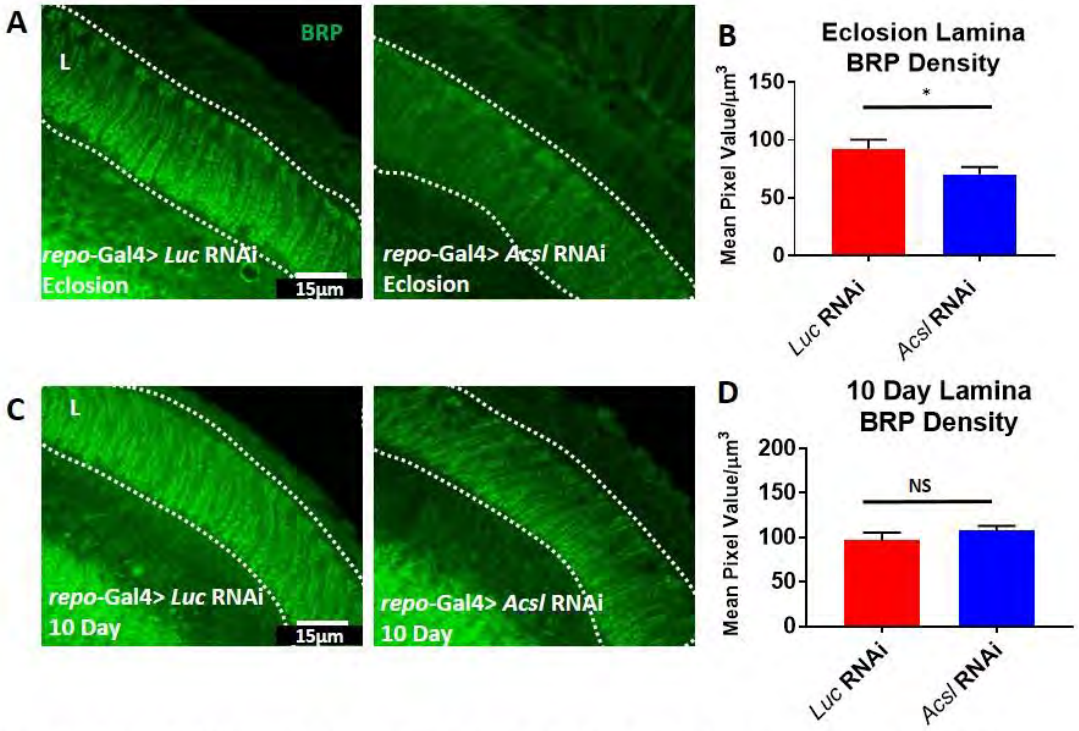

Figure 3.20. BRP Density is reduced after developmental expression of RNAi. A. In this figure, *Acsl* RNAi was allowed to express only in development, and blocked after eclosion in adults. Shown are single slice images of BRP staining in the lamina of newly eclosed flies that experienced RNAi expression in development. **B.** Quantification of BRP density in the lamina at eclosion reveals a significant reduction in *Acsl* RNAi flies (*Luc* RNAi n = 8, *Acsl* RNAi n = 9, p value = .0390). **C.** Shown are single slice images of BRP staining in the lamina after 10 days of adulthood with RNAi suppression. These flies experienced RNAi expression in development, and RNAi suppression in adulthood. **D.** Quantification of BRP density in the lamina after 10 days of suppression reveals no significant decrease (*Luc* RNAi n = 6, *Acsl* RNAi n = 7, p value = .2995).

At eclosion, neither the *Acsl* RNAi nor the *Luc* RNAi populations had mislocalized glia in the chiasm or medulla, nor did I observe ectopic neuropil in any flies (*Luc* RNAi n = 8, *Acsl* RNAi n = 9, p value = >.9999 (Chi-square)) (Fig 3.21. A). However, using volumetric analysis as before, I did find a significant reduction in the density of BRP signal in the lamina at eclosion (*Luc* RNAi n = 8 mean = 92.62±7.682, *csl* RNAi n = 9 mean = 70.2±6.392, p value = .0390 (2-tailed t-test)) (Fig 3.20. A and B). This reduction in BRP density is consistent with the non-significant reduction observed in TIFR-Gal4 adult KD flies; however, the reduction may be more prominent in this experiment because *Acsl* RNAi is driven by the pan-glial driver *repo*-Gal4. It is possible that in the TIFR-Gal4 KD experiments, other glial subtypes compensate for the reduction of *Acsl* function in marginal glia.

Moreover, the separation of the electrophysiological and mislocalized glia phenotypes suggests that *Acsl* regulates physiology and morphology through at least two different mechanisms. This result also indicates that the underlying mechanisms producing the physiological phenotype can be attributed to pupal development, because

in this experiment *Acsl* RNAi expression does not begin until the second larval instar and reduction of Acsl protein would not have been maximal immediately.

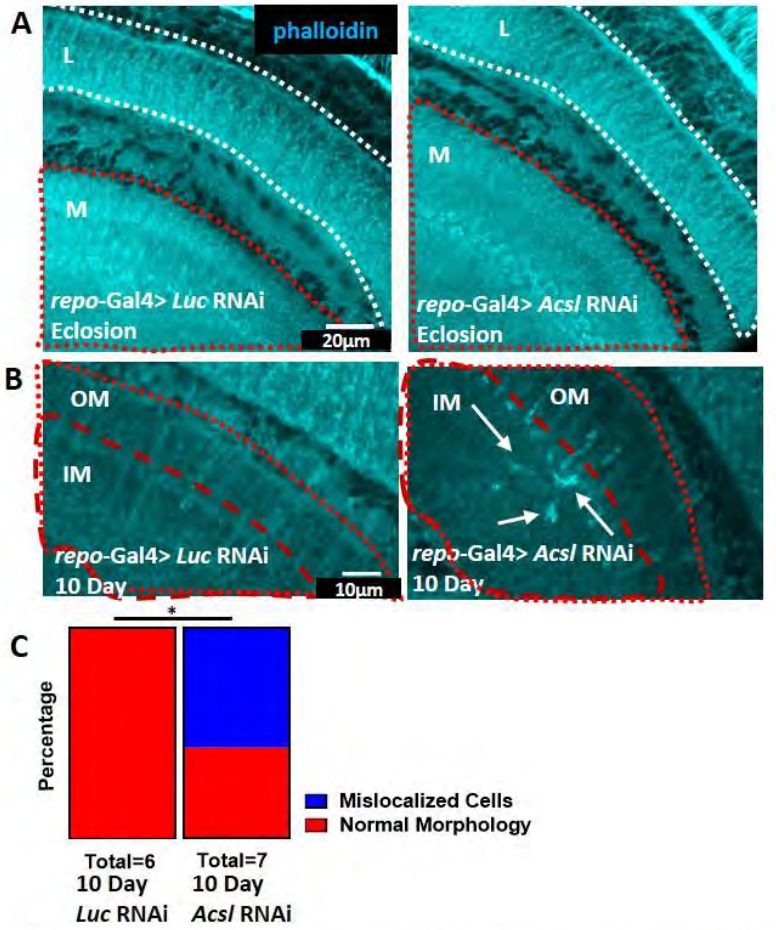

Figure 3.21. Morphological phenotypes in developmental expression of RNAi. A. In this figure, *Acsl* RNAi was allowed to express only in development, and blocked after eclosion in adults. Shown are single slice images of phalloidin staining of newly eclosed flies that experienced RNAi expression in development. Images demonstrate that morphology is normal at this time point (*Luc* RNAi n = 8, *Acsl* RNAi n = 9, p value = >.9999). The lamina is outlined in white and the medulla in red. **B.** High magnification single slice images of phalloidin staining in the medulla of flies after 10 days of adulthood. These flies experienced RNAi expression in development, and suppression of *Acsl* RNAi expression in adulthood. Actin rich cell bodies are present in the inner medulla of flies in which *Acsl* was KD in development (white arrows) (*Luc* RNAi n = 6, *Acsl* RNAi n = 7, p value = .0261). The medulla is circled in a dotted red line, and the inner medulla is circled in a dashed red line. **C.** Representation of the % penetrance of mislocalized cells in 10 day old adult flies that expressed RNAi in development.

After 10 days of adulthood without dsRNA expression, BRP density in control animals was not significantly higher than that in *Acsl* KD animals (*Luc* RNAi n = 6 mean = 96.59±9.13, *Acsl* RNAi n = 7 mean = 107.7±5.373, p value = .2995 (2-tailed t-test)). (Fig 3.20. C and D). Given the progression in the ERG phenotype described above, this result was unexpected, and indicates that reductions in BRP/synapse density are unlikely to be solely responsible for the observed defects in electrophysiology. Further morphological analysis revealed that 57% of 10 day adult *Acsl* KD animals had a population of mislocalized glia in the medulla (*Luc* RNAi n = 6, *Acsl* RNAi n = 7, p value = .0261 (Chi-square)) (Fig 3.21. B and C). This result is significant for three reasons. First, it demonstrates that *Acsl* KD in development has long term effects on morphology in the adult, regardless of resumption of Acsl protein expression. Second, it demonstrates that glia lacking *Acsl* expression in development are capable of motility in the adult, even if *Acsl* expression is restored. Third, the long temporal separation between *Acsl* RNAi expression and the appearance of mislocalized glia suggests that *Acsl* regulates at least this aspect of morphology through a long-term mechanism.

iii. Adult expression of RNAi

After suppressing RNAi throughout development, and releasing *Acsl*-targeting dsRNA expression in adulthood, I analyzed the ERG and optic lobe morphology, both at eclosion and after 10 days of adult RNAi expression. As expected, at eclosion I observed no significant difference in the magnitude of the 'on transient' (repo-Gal4> *Luc* RNAi n = 10 mean = 1.24±.1887, repo-Gal4> *Acsl* RNAi n = 16 mean = 1.25±.1571, p value = .9682 (2-tailed t-test)) (Fig 3.22. A and B), or in the magnitude of the 'off transient' (repo-Gal4> *Luc* RNAi n = 10 mean = 3.10±.6939, repo-Gal4> *Acsl* RNAi n = 15 mean = 3.693±.4682, p value = .4684 (2-tailed t-test)) (Fig 3.22. A and C).

Nor did I observe any traces with either a loss of the 'on transient' or a loss of the 'on' and 'off' transients in any trace examined (Fig 3.22. A and D, Appendix A. Table of Experiments). After 10 days of RNAi expression in the adult, I did not observe a reduction in the magnitude of the 'on transient' (repo-Gal4> *Luc* RNAi n = 11 mean = 1.391±.2078, repo-Gal4> *Acsl* RNAi n = 18 mean = 1.30±.1901, p value = .7586 (2-tailed t-test)) (Fig 3.22. A and B), or in the magnitude of the 'off transient' (repo-Gal4> *Luc* RNAi n = 11 mean = 3.218±.4319, repo-Gal4> *Acsl* RNAi n = 18 mean = 2.60±.3711,

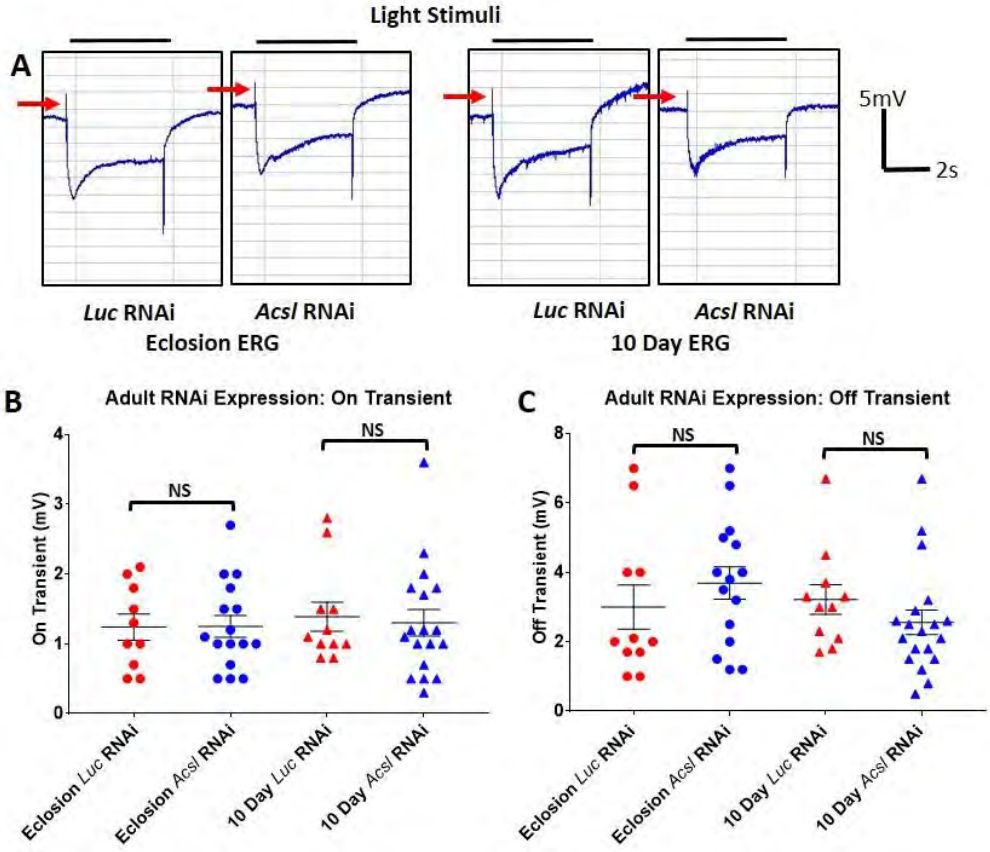

D

Genotype (with *tub*> Gal80^{ts})	N number	Loss of On Transient	Loss of On and Off Transient
repo> *Luc* RNAi Eclosion	10	0% NS	0% NS
repo> *Acsl* RNAi Eclosion	16	0%	0% (n=15)
repo> *Luc* RNAi 10 Day	11	0% NS	0% NS
repo> *Acsl* RNAi 10 Day	18	0%	0%

Figure 3.22. The ERG is normal in adult expression of RNAi. A. In this figure, *Acsl* RNAi was allowed to express only in adulthood, and began at eclosion. ERG traces from animals at eclosion and after 10 days of adulthood with RNAi expression. Note the presence of the 'on transient' in *Acsl* RNAi animals at both eclosion and after 10 days of adulthood (see red arrows). **B**. Quantification of the 'on transient' reveals no difference in *Acsl* RNAi animals at both eclosion and after 10 days of adulthood (p values vs. age matched *Luc* RNAi animals = .9682, and .7586, respectively). **C**. Quantification of the 'off transient' reveals no reduction in *Acsl* RNAi animals at eclosion or after 10 days of adulthood (p value vs. age matched *Luc* RNAi animals = .3773, and .2561, respectively). **D**. Table summarizing the penetrance of loss of transients in these experiments. 1 trace was excluded from 'off transient' analysis from the *Acsl* RNAi eclosion data set due to noise obscuring the 'off transient'. No loss of transients was recorded in *Acsl* RNAi animals at either eclosion or after 10 days of adulthood with RNAi expression.

p value = .2984 (2-tailed t-test)) (Fig 3.22. A and C). I also did not observe any traces with a loss of the 'on transient' or both transients (Fig 3.22. A and D, Appendix A. Table of Experiments). Analysis of morphology revealed no defect in *Acsl* RNAi flies at either eclosion or in 10 day old flies, whether in BRP density in the lamina, or in the proportion of animals with mislocalized glia (Fig 3.23. A and B) (see Appendix A. Table of Experiments for more information). These results suggest that *Acsl* is not required in the adult, either for the presence of the 'on transient', the normal localization of glia, or normal synaptic density.

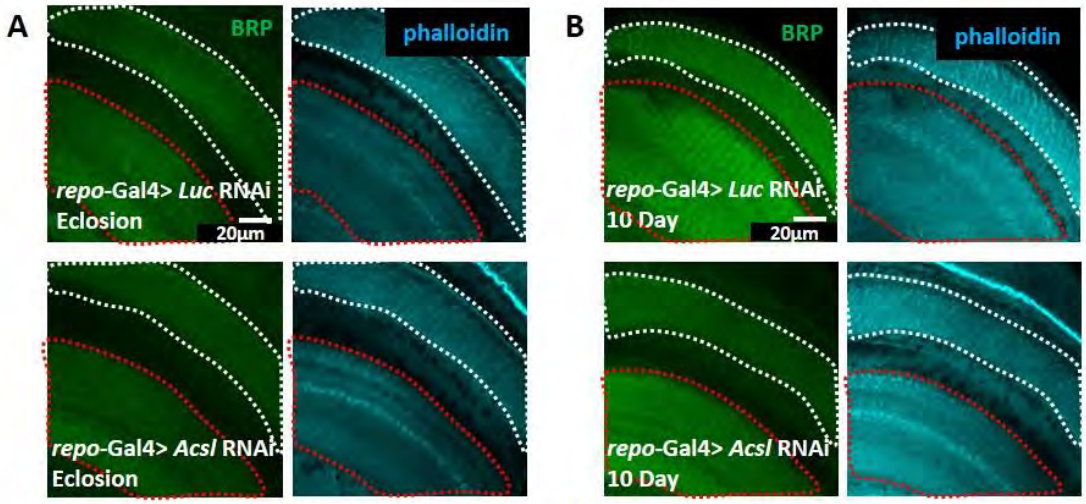

Figure 3.23. Morphology is normal in adult expression of RNAi. A. In this figure, *Acsl* RNAi expression was blocked in development and began in adulthood, after eclosion. Shown are single slice images of BRP and phalloidin at eclosion which reveal no apparent difference in BRP density, or any evidence of cells occupying the medulla neuropil (*Luc* RNAi n = 8, *Acsl* RNAi n = 12, p value BRP density = .6556, p value mislocalized glia = >.9999). **B.** Shown are single slice images after 10 days of adult expression of RNAi which similarly show no morphological phenotype (*Luc* RNAi n = 7, *Acsl* RNAi n = 6, p value BRP density = .2680, p value mislocalized glia = >.9999).

3.3.4. Conclusions

Consistent with the finding that *Acsl* KD does not affect glial migration, I found no evidence of a defect in photoreceptor targeting, and could observe the wild type two layers of chaoptin staining in both larvae and pupae. While *Acsl* does not appear to have a significant effect on glial migration, I have substantial evidence that it does mediate the stability of glial localization. Glia are mislocalized by P50 when *Acsl* RNAi is expressed throughout development, and are mislocalized by 10 days of adulthood, but not at eclosion, when *Acsl* RNAi is expressed between second larval instar and eclosion.

The delay between *Acsl* RNAi expression and glial mislocalization in the latter experiment suggests that *Acsl* regulates glial stability through a long-term mechanism, such as gene expression or modification of extra-cellular proteins with low turnover.

While it is clear that *Acsl* is required during development, this gene appears to function through at least two separate pathways to mediate its electrophysiologic effects, loss of the ‘on transient’, and morphologic effect, misplacement of glia. Furthermore, the electrophysiologic and morphologic effects can be tentatively divided in the early and

late developmental mechanisms. First, loss of the ‘on transient’ and the reduction in BRP signal both appear to arise in late development, based on the results of late-developmental expression of *Acsl*-dsRNA reported here, and the observation that BRP is not expressed in the optic lobe until late pupal development (Meinertzhagen, 1993). Second, while marginal glia are present at the lamina in normal number by the wandering third instar stage, their processes are abnormal, perhaps indicating alterations in actin dynamics. The fact that morphological defects in marginal glia are present at this stage is consistent with an early developmental mechanism for the glial mislocalization seen in the adult. Finally, loss of *Acsl* in glia at the P50 stage seems to confer some survival benefit, as the total density of marginal glia are increased. This benefit must be temporary, however, since in the adult stage, there is no significant difference in the total density of marginal glia.

3.4. ACSL4 is Expressed in Mammalian Glia

3.4.1. ACSL4 staining co-localizes with mammalian glial markers

While I have demonstrated functional homology between human *ACSL4* and *Drosophila Acsl*, expression of ACSL4 protein in human glia had not been confirmed previously through immunohistochemistry. To determine whether ACSL4 protein is expressed in human glia, I co-stained wild type mouse brain sections with GFAP, an astrocyte glial marker, and ACSL4 antibodies (n = 4). As a control, I pre-absorbed the ACSL4 antibody with a commercially available peptide used to raise the ACSL4 antisera, to demonstrate specificity of the antibody (n = 2). I examined hippocampal sections, which are rich in GFAP-positive astrocytes, and were previously shown to contain ACSL4-expressing cells (Cao et al., 2000a; Meloni et al., 2009).

I found extensive co-localization of ACSL4 with GFAP-positive astrocyte processes and cell bodies, as well as ACSL4 staining of neuronal cell bodies (Fig.3.24. A and B). When pre-absorbed, ACSL4 staining of GFAP-positive astrocytes was largely eliminated (Fig 3.24. C). These results are consistent with the high-throughput mRNA

expression data recently published (Zhang et al., 2014; Seeger et al., 2016), which confirms that ACSL4 is indeed expressed in astrocytes, although not as strongly as in neurons.

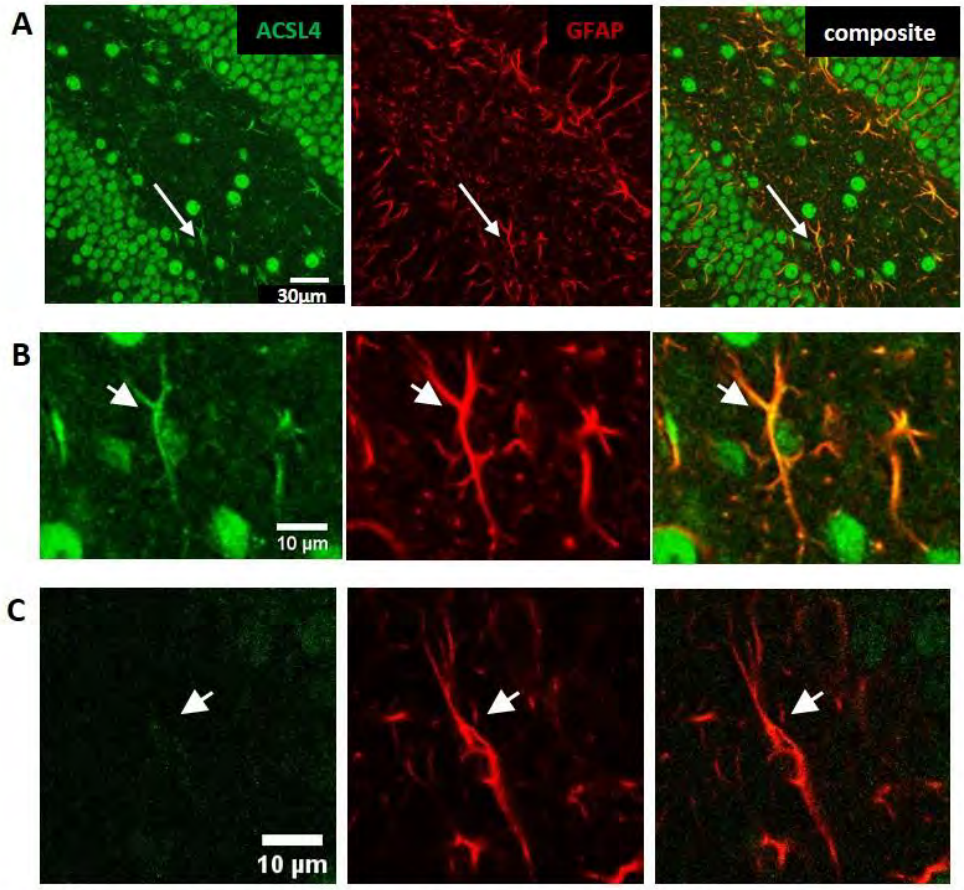

Figure 3.24. ACSL4 colocalizes with mammalian glial markers. A. Shown are single slice images of ACSL4 and GFAP staining of the mouse hippocampus demonstrate which clear localization of ACSL4 with GFAP+ cell bodies and processes. White arrow points to an astrocyte expressing ACSL4 (wild type mouse brain tissue n = 4). **B**. Higher magnification single slice images of a GFAP+ astrocyte with co-localization of ACSL4 (short arrow). **C**. Shown are single slice image of preabsorbed ACSL4 antibody with GFAP. Staining from the astrocyte is eliminated (short arrow, wild type mouse brain tissue n = 2).

3.4.2. Conclusions

The results of co-staining analysis suggest that mammalian ACSL4 is expressed in GFAP+ astrocytes in the mouse hippocampus, indicating that ACSL4 may also play a currently unknown role in mammalian nervous system development and function. Based on the work presented in this thesis, it is plausible that ACSL4 regulates the development or pruning of synapses, stabilization of glia through cell-cell contacts, or the regulation of neuropil boundaries.

CHAPTER IV. DISCUSSION

4.1. Context for this Study

Of the many genes implicated in intellectual disability, there remain a subset for whom the function is unknown. One such gene is *ACSL4*, a long-chain fatty acid CoA synthetase with a preference for arachidonic acid (Cao et al., 1998; Piccini et al., 1998; Meloni et al., 2002; Golej et al., 2011). While the biochemical mechanisms regulated by *ACSL4* and its homologs are unknown, there is substantial evidence that it functions in neuronal development to regulate the production of dendritic spines in mammals (Meloni et al., 2009), and the endocytic recycling of BMP receptors in *Drosophila* (Liu et al., 2011, 2014). These studies concluded that *ACSL4* and its homologs function exclusively in neurons based on the following results: immunohistochemical analysis of the distribution of ACSL4 protein exhibited a pattern consistent with neuronal expression, although not exclusive of glial expression, and expression of either *ACSL4* or *Acsl* in *Drosophila* glia did not rescue the neuronal phenotype. However, the design of these studies leaves open the possibility that *ACSL4* and its homologs function in glia.

4.2. Questions Addressed by this Study

This study originated in an RNAi screen to identify genes that when depleted affected visual neuronal signaling. This study was designed to address the following questions. First, does *ACSL4* and its homolog *Acsl* have a function in glia? While *Acsl* has well-documented roles to play in neurons (see above), prior to this study there was no evidence in either vertebrate or invertebrate systems that *Acsl* or its homologs function in glia.

Second, this study was designed to determine whether glial *Acsl* plays a role in development. While this seemed likely given the current body of literature (see above), it was unproven speculation. Through morphological analysis and temporal restriction of RNAi expression, I was able to demonstrate that glial *Acsl* does have essential functions in glia in development that ultimately affect adult structure and function.

Third, this study was designed to identify potential mechanisms of *Acsl* function in the nervous system. Through careful analysis of the morphological phenotype and

BRP staining, I was able to postulate a role for glial *Acsl* in regulation of synaptic development and localization of glia.

4.3. Major Results and Conclusions of this Study

4.3.1. *Acsl* is required in glia for visual signaling

By restricting *Acsl* RNAi expression to either neurons or glia, I was able to demonstrate that *Acsl* is required in glia for the normal magnitude of visual signaling in the lamina. When *Acsl* is globally depleted from glia by driving RNAi with *repo*-Gal4, the amplitude of the 'on transient' of the ERG, a wide-field electrical signal generated in the lamina, was significantly reduced, and absent in 79% of flies (Fig. 3.1). In contrast, I observed no defects in the 'on transient' when *Acsl* was depleted from neurons using the pan-neuronal driver *elav*-Gal4 (Fig. 3.1). Similarly, I observed a significant reduction in the magnitude of the 'off transient' in glial *Acsl* KD flies, and the absence of both transients in 16% of these flies. Using cell-subtype specific drivers, I was able to isolate

the ERG phenotype to the marginal glia of the lamina using the driver TIFR-Gal4 (Fig 3.1, Table 3.1.).

Loss of the 'on transient' is a phenotype with much history, and many other genes have been analyzed which, when mutated or depleted by RNAi, cause a loss of the 'on transient'. These include *hisClA*/*ort*, the histamine receptor on post-synaptic lamina neurons (Gengs et al., 2002; Pantazis et al., 2008), *NinaE*/*Rh1*, the light sensing molecule expressed in photoreceptors R1-R6, and *nonA*, an mRNA binding protein that is ubiquitously expressed (Rendahl et al., 1992; Campesan et al., 2001; Mazzoni et al., 2008), and genes involved in histamine metabolism and recycling in the eye, such as *ebony*, *tan*, *ine*, and *hdc* (Borycz et al., 2002, 2012; Richardt et al., 2002; Chaturvedi et al., 2014). All of the above mutations lead to a reliable loss of both the 'on transient' and 'off transient', indicating that all transmission of visual information downstream of the retina is abolished. In contrast, in glial *Acsl* KD, only the 'on transient' is lost with high penetrance, indicating that visual transmission may still be occurring in most flies, but at an unrecordable level (Fig 3.1). This is consistent with my finding that visual behavior is normal (Fig 3.3).

Functional homology between *ACSL4* and *Acsl* has been well-documented in neurons (Liu et al., 2011, 2014). In contrast, whether *ACSL4* can substitute for *Acsl* in glia was unknown. Over-expression of RNAi resistant human *ACSL4* along with *Acsl* RNAi in marginal glia using TIFR-Gal4 resulted in partial rescue of the morphological phenotype. I observed misplaced glia in only 43% of *ACSL4* rescue flies (Fig 3.13.) versus 100% in non-rescued *Acsl* KD flies. Similarly, I observed ectopic neuropil in only 7% of *ACSL4* rescue flies, versus 55% in *Acsl* KD flies.

4.3.2. Loss of *Acsl* causes morphological defects

During normal development, marginal glia migrate to the proximal edge of the nascent lamina in larval stages and remain there throughout pupal development and adulthood (Winberg et al., 1992; Perez and Steller, 1996). When *Acsl* is depleted from marginal glia, their cell bodies exit the proximal edge of the lamina by mid-pupal development, moving into the adjacent distal optic chiasm and medullary neuropil (Fig. 3.16). Within the adult medulla, their cell bodies reside proximal to the terminals of photoreceptors R7 and R8, in the inner medulla (Fig. 3.9. A). The processes of these mislocalized glia are complex and abundant, permeating both the distal chiasm and the

outer medullary neuropil, and do not exhibit the regular organization observed in marginal glia in the control animals, or in the normally localized glia in *Acsl* KD adult animals (Fig. 3.9. B).

In a subset of *Acsl* KD animals, there are discrete structures of BRP signal located in the distal and proximal chiasm that connect with the lamina and the medulla, and the medulla and lobula (Fig. 3.11.). Given that these structures are rich in BRP expression, and BRP expression is characteristic of neuropil, it is likely that these structures represent ectopic neuropil. These ectopic neuropils share more characteristics with the medulla than they do with the other neuropils, making it possible that they originated from the second optic neuropil, although I cannot rule out the possibility that these structures originate independently of either the lamina, medulla, or lobula.

4.3.3. *Acsl* is required in development

To determine whether the mislocalization of marginal glia is due to a failure to migrate to their proper positions, I examined third instar larvae and found no reduction in the number of nuclei in the marginal glia layer of the developing lamina (Fig. 3.14).

Furthermore, I observed no defect in photoreceptor targeting, observing two bands of termination in the lamina and the medulla.

By mid-pupal development, marginal glia become mislocalized, occupying the distal chiasm and medulla (Fig. 3.16. A and B). At this time point, glial nuclei are largely located in the inner medulla, but there are nuclei present in the outer medulla as well (Fig. 3.17). The processes of the mislocalized medullary glia are faint at this time, and do not become prominent until the last 24 hours of pupal development (Fig. 3.17, data not shown).

Restricting *Acsl* RNAi expression to either development or adulthood confirms the requirement for *Acsl* in development. When *Acsl* RNAi is active from the onset of second larval instar until eclosion (but not in adulthood), 52% of flies exhibit a loss of the 'on transient' at eclosion (Fig. 3.19. A and D). Morphological analysis revealed a significant reduction in the density of BRP signal in lamina in this population, but no evidence that glial cells were misplaced (Fig 3.20. A and B., Fig 3.21. A). After suppressing *Acsl* RNAi expression for 10 days after eclosion, I found that 88% of flies

exhibited a loss of the 'on transient' (Fig. 3.19. A and D), and that 75% lacked both the 'on' and 'off' transients.

Moreover, I found that 57% of 10 day old adult flies that expressed RNAi in development had evidence for misplacement of glial cell bodies in the medulla, in spite of the fact that *Acsl* RNAi expression had been suppressed after eclosion (Fig 3.21. B and C). The mislocalization of glia after 10 days of adulthood in flies expressing *Acsl* RNAi only in development is intriguing, and it would be interesting to expand this analysis to flies continuously expressing *Acsl* RNAi, to determine whether there is further motility of marginal glia in adulthood.

4.3.4. ACSL4 co-localizes with mammalian glial markers

Finally, I analyzed the co-localization of signal from ACSL4 and GFAP antibodies in the mouse hippocampus. I found significant co-localization of ACSL4 with GFAP-positive astrocyte cell bodies and processes (Fig. 3.24. A and B). Pre-absorption of the ACSL4 antibody eliminated staining in the glia, suggesting that staining was specific (Fig 3.24. C).

4.4. Novel Contributions and Implications of this Study for the Field of Neurobiology

4.4.1. Novel contributions of this study

i. *Acsl* functions in glia

This study is the first to demonstrate a role for *Acsl* in glia. The function of *Acsl*/*ACSL4* in neurons has been explored in both mammals and *Drosophila* (Meloni et al., 2009; Liu et al., 2011, 2014). *ACSL4* has been found to regulate dendritic spines in mammalian neurons, and *Acsl* was observed to mediate synaptic vesicle transport and synaptic development in *Drosophila* neurons. In these prior studies *Acsl* was either depleted from cultured mammalian neurons using RNAi transfection, or from all *Drosophila* tissues using mutants. This is the first study to specifically remove *Acsl* from glia, and document a phenotypic effect.

ii. Glial *Acsl* modulates neuronal signaling

In this study, I demonstrate that depleting *Acsl* from glia produces a measurable effect on neuronal function. Glia have been shown to exhibit small depolarizations in other systems (Hösli et al., 1981; Konnerth et al., 1988; Silies and Klämbt, 2011). I cannot rule out that in the *Drosophila* eye glia also have small depolarizations which may be recorded in the ERG, as the ERG is a wide-field recording of the sum of signals from across the eye. However, while there is evidence that glia can modulate the ERG (Pantazis et al., 2008), there is no evidence that the ERG trace is exclusively generated by glia, and eliminating a small amount of glial electrical activity from a limited number of glial subtypes is unlikely to account for the magnitude of the reduction in the 'on' and 'off' transients I observed. Therefore, in this study I provide the first documentation of glial *Acsl* mediating neuronal signaling.

How glial *Acsl* mediates neuronal signaling remains unclear. I observed no differences in the structure or density of glial processes in the lamina, and a non-significant reduction in BRP density in the same neuropil. Moreover, when *Acsl* RNAi expression was limited to development, I observed separation of the ERG and

morphological defects. Indeed, none of the morphological defects described here (mislocalization of glia, ectopic neuropil, or reduction in BRP density) exactly correlates with the ERG defect, and it is thus not possible to conclude that the morphological phenotype causes the electrophysiological phenotype. However, it is possible that a physiologic function of glia, rather than a structural one, is affected. Potentially, glial regulation of extracellular ions such as chloride and calcium is affected, or clearance of extracellular histamine or other neurotransmitters.

iii. *Acsl* has specific roles in glial subtypes

I began this study by depleting *Acsl* RNAi from all glial cells using the pan-glial driver *repo*-Gal4. I was able to reproduce the phenotype observed in these flies by driving *Acsl* RNAi in marginal glia with TIFR-Gal4. This suggests that the physiologic and morphologic phenotypes I describe here are not due to global and non-specific glial defects and decompensation, but rather to the loss of one or more specific functions in a glial subtype.

iv. *ACSL4* has functional homology with *Acsl* in glia, and can rescue loss of *Acsl* function in multiple pathways

As stated above, *ACSL4* was previously demonstrated to have functional homology with *Drosophila Acsl* in neurons. Interestingly, human ACSL3, with which *Drosophila* Acsl protein shares 49% identity at the protein level, was not functionally homologous in *Drosophila* motor neurons, and over-expression of this gene in neurons did not rescue the phenotype (Liu et al., 2011). This result is consistent with studies demonstrating a function for *ACSL3* in mammalian glia (Pei et al., 2009), and it is tempting to conclude that the two mammalian genes operate exclusively in either neurons or glia. Attempts to study human *ACSL3* in this project were unsuccessful. However, in this study I demonstrate that *ACSL4* can replace *Acsl* function in glia, and can rescue morphological phenotypes that are potentially downstream of separate mechanisms.

v. Marginal glia are important regulators of optic lobe neuropil physiology and morphology

The optic lobe of *Drosophila* is a widely used and well-studied system. The lamina in particular has been used to dissect mechanisms of migration (Perez and Steller, 1996; Huang et al., 1998a; Tayler, 2004), axon targeting (Hing et al., 1999; Senti et al., 2000; Poeck et al., 2001; Tayler and Garrity, 2003; Yoshida et al., 2005), synapse development (Frohlich and Meinertzhagen, 1982; Meinertzhagen, 1989, 1993; Hiesinger et al., 2006), and neuron-glia interactions (Huang et al., 1998a; Suh et al., 2002; Borycz et al., 2012; Chaturvedi et al., 2014; Dutta et al., 2015). The glia of the lamina have also been extensively studied, the body of literature mostly focusing on the role of epithelial glia (Stuart et al., 2007; Pantazis et al., 2008; Edwards and Meinertzhagen, 2010; Borycz et al., 2012). In this study, I substantiate novel roles for marginal glia in regulation of lamina neuron physiology and the bounding of neuropils, as well as a potential role in synaptogenesis or synapse maintenance in the lamina. Furthermore, I provide evidence that the organization of synaptic layers is disrupted when *Acsl* is depleted from marginal glia, and that the processes of R7 and R8 are disorganized both in the distal optic chiasm

and within the medullar neuropil. Whether these defects are a primary function of marginal glia or secondary to their mislocalization remains to be determined.

vi. Glial *Acsl* is necessary for the stability of glia in their specified positions

Depletion of *Acsl* from marginal glia results in their mislocalization from the proximal edge of the lamina into the distal optic chiasm and medullary neuropil. This result demonstrates that expression of *Acsl* is necessary for the retention of marginal glia in their normal positions. Given the close proximity of mislocalized marginal glia with the axons of photoreceptors R7 and R8 both in the distal chiasm and the medulla, it is likely that these glia move along the terminals of these neurons as they travel outside of their normal positions. In the *Drosophila* optic lobe, glial movement along neuronal axons has been demonstrated previously (Dearborn and Kunes, 2004). It is notable that marginal glia move toward the central brain into the distal chiasm and medulla, rather than away from the central brain into the lamina. This may be due to a preference for R7 and R8 termini as substrates for movement, response to a chemoreceptor gradient, or simply physical exclusion from the tightly packed lamina. Further study is needed to

conclusively demonstrate that mislocalized glia maintain contact with the processes of R7/R8 throughout development.

vii. Glial *Acsl* regulates the organization of glial processes

By using the density of tdTomato signal to measure the density of marginal glia processes, I was able to determine that there is no significant difference in the elaboration of glial processes in the lamina neuropil, nor was there significant disorganization, in *Acsl* KD flies. However, glia that mislocalized away from the marginal glia layer elaborated complex processes, and comparing the organization of processes between normally localized and mislocalized populations of marginal glia revealed distinctive disorganization in the mislocalized population. Together these results indicate that *Acsl* is in some way involved in the regulation of glial processes, either through their elaboration, their retraction, or in the determination of the direction they elaborate in. Potentially, *Acsl* mediates this effect by increasing the pool of free intracellular arachidonic acid, which then regulates actin dynamics through its metabolism into prostaglandins (Glenn and Jacobson, 2002).

viii. Glial *Acsl* is important for the separation of neuropils, acting to either establish or maintain neuropil boundaries

In 55% of *Acsl* KD animals, BRP dense structures physically connect the lamina and medulla, and medulla and lobula. These BRP dense structures most likely represent ectopic neuropil. Given that the medulla is the common neuropil involved in these growths, I propose that the ectopic neuropil are outgrowths of the medulla. However, whether these ectopic neuropils represent an outgrowth of endogenous neuropils (the lamina, medulla, and lobula), or an independent growth cannot be determined conclusively by the present set of data. In order to determine this, time lapse microscopy would need to be performed during late pupal development as BRP begins to be expressed. By tracking the growth of neuropils, it would be possible to determine whether the medulla produces outgrowths that then join with the adjacent neuropils (lamina distally, and lobula proximally), or whether independent BRP structures arise in the distal and proximal optic chiasms.

I did not observe ectopic neuropil in control populations, indicating that glial *Acsl* has a role in establishing the boundaries or neuropil, and/or the inhibition of their

development. In the absence of *Acsl*, this inhibition is released, allowing ectopic neuropil to arise.

ix. Glial *Acsl* has morphological effects on neurons

While KD of *Acsl* with TIFR-Gal4 did not produce a significant reduction in BRP density in the adult, depletion of *Acsl* with *repo*-Gal4 during development results in a reduction in the density of BRP signal in the lamina. This disparity in RNAi effect between the two experiments may indicate that only a subset of synapses are reduced in the TIFR-Gal4 KD adults, and this effect is masked by no reduction in other synaptic populations. Indeed, the 'on transient' has been demonstrated to be the result of photoreceptors synapsing upon the lamina neurons L1 and L2; however, there are many other neurons in the lamina that synapse upon each other and provide feedback to photoreceptors. At the level of light microscopy, these synaptic populations cannot be distinguished with BRP staining. Moreover, TIFR-Gal4 KD is specific to marginal glia, and the presence of *Acsl* in other glial subtypes may have compensated for depletion in marginal glia.

The reduction in BRP signal seen with *repo*-Gal4 KD during development is possibly due to regulation of BRP protein, but given the essential role that glia play in the development, maturation, and removal of synapses, it is also plausible that the observed reduction in signal is due to regulation of the pre-synapse in synaptogenesis or synaptic pruning.

Additionally, the processes of R7 and R8 are disorganized in the distal optic chiasm and within the medullary neuropil. This may be a result of improper glial ensheathment of R7 and R8 termini, or simply a result of the mislocalization of glia causing physical disruption of the termini in the distal chiasm and medulla.

x. Glial *Acsl* is required in development

I demonstrate here that glial *Acsl* is required in development of the optic lobe of *Drosophila* for the 'on transient' of the ERG, the normal localization of glia, normal neuropil boundaries, and normal synaptic density. Glial *Acsl* does not appear to be required in the adult for these functions, although confounding factors in the adult, such as a difference in either Acsl protein turn over or *repo*-Gal4 driver strength, cannot be

ruled out. Based on the current set of data, however, it is likely that glial *Acsl* is involved almost exclusively in development. I have presented evidence that *Acsl* is not only important for morphological development of neurons, glia, and neuropil, but also for visual neuron signaling. I have also presented evidence that these functions arise through different mechanisms, as I was able to demonstrate separation of morphological and electrophysiological defects when *Acsl* RNAi expression is restricted to development. Whether these phenotypes are mediated by separate pathways (e.g. actin regulation vs. protein modification), or the same pathway with different targets (i.e. protein modification of separate membrane or extracellular proteins) remains to be proven. What is clear is that glial *Acsl* has a central role in development, and causes obvious defects in adulthood.

xi. ACSL4 expression in GFAP-positive astrocytes can be demonstrated through immunohistochemistry

Previous studies have demonstrated expression of ACSL4 in astrocytes via high-throughput screen of the transcriptome (Zhang et al., 2014), although at a lower level than in neurons. Prior to this study, no one had yet performed co-localization analysis of

mammalian glial markers and ACSL4 antibodies. In my analysis, I demonstrate that ACSL4 is clearly co-localized with GFAP signal, further solidifying the body of evidence for expression of ACSL4 in glia.

4.4.2. Potential developmental mechanisms affected

While it is clear that *Acsl* functions in development, direct evidence for which developmental processes it regulates remains to be gathered. I have presented evidence that BRP signal density in the adult lamina is significantly reduced in developmental *Acsl* KD with the pan-glial driver *repo*-Gal4. I propose that this phenotype is caused by defects in the regulation of one of the following developmental processes.

i. Synaptic development

In motor neurons of third instar larvae, *Acsl* was shown to increase synaptic growth in anterior neurons, and decrease it in posterior neurons (Liu et al., 2011, 2014). This difference was postulated to be due to an exaggeration of defects in retrograde transport in posterior neurons, as their axons are substantially longer. In glial *Acsl* KD,

synaptic density was only observed to decrease, making the potential functions of glial *Acsl* on synaptogenesis easier to interpret.

Glia play well documented roles in synapse development, both through contact-independent and -dependent mechanisms (Christopherson et al., 2005; Eroglu et al., 2008; Garrett and Weiner, 2009). The potential biochemical pathways that *Acsl* could regulate that would result in this phenotype are discussed below, and largely involve protein modification through the production of arachidonoyl-CoA. It is possible that *Acsl* provides necessary acyl modifications to proteins secreted by glia that enhance synaptic development, such as the thrombospondin family of proteins (Christopherson et al., 2005), which in *Drosophila* has homology with Cysteine knot C-terminal (*Ccn)*. Interestingly, glial KD of *Ccn* also produces a loss of the 'on transient' (unpublished data), although any potential interactions between *Acsl* and *Ccn* remain to be proven.

Another potential pathway that would result in a decrease in synaptic development is the production of acyl modifications for plasma membrane proteins, allowing them to be targeted and inserted into the periphery of the cell. Integral glial membrane proteins, such as γ-protocadherins, have already been demonstrated to

promote synaptic development in mammals (Garrett and Weiner, 2009), and may additionally provide an anchoring mechanism for glia that, when disrupted, promotes mislocalization. Moreover, there is evidence that expression of the cell-cell interaction proteins Dscam 1 and 2 in post-synaptic neurons have a role in specification of synaptic partners in the lamina (Millard et al., 2010). While a similar role for cell-cell contact proteins in glia has not been established in the lamina, the precedent set by the above study indicates that this hypothesis is plausible.

ii. Synaptic pruning

Conversely, *Acsl* could inhibit engulfment and removal of the pre-synapse. In *Drosophila*, there is an extensive body of literature on the role of glia in phagocytosing axonal debris during axon pruning in development in the central brain (Edenfeld et al., 2005; Freeman, 2006). Additionally, glia were found to engulf and remove the pre-synapse during development of the larval neuro-muscular junction (Fuentes-Medel et al., 2009). Finally, *Acsl* already has a demonstrated role in endocytic recycling of BMP receptors in neurons during synaptic maturation (Liu et al., 2014), making a similar function in phagocytosing the pre-synapse in glia plausible.

4.4.3. Potential biochemical mechanisms affected

Depletion of *Acsl* may affect the levels of two different important intracellular molecules, causing either an increase in the intracellular pool of free arachidonic acid, or a decrease in the level of arachidonoyl-CoA (Fig 4.1). On a subcellular level, arachidonic acid is an essential component of cell membranes, and contributes greatly to their fluidity through its four flexible cis double bonds (Brash, 2001). On a tissue level, arachidonic acid is involved in the inflammatory response though its metabolism into prostaglandins by the COX family of enzymes, and has established roles in regulating multiple cellular processes, such as apoptosis and actin remodeling (Cao et al., 2000b; Glenn and Jacobson, 2002). Finally, like other fatty acids, arachidonic acid will activate nuclear PPAR receptors (Georgiadi and Kersten, 2012).

Acsl conjugates arachidonic acid to CoA to form arachidonoyl-CoA, which can then be used in a variety of biological processes, such as the formation of triglycerides, β-oxidation in the mitochondrion for generation of ATP, and protein modification. *Acsl* has been demonstrated to localize to the ER (Meloni et al., 2009), which suggests that its molecular products may be more heavily involved in protein modification than in the

production of triglycerides or lipid metabolism. Together, the potential biochemical mechanisms regulated by *Acsl* through either free arachidonic acid or arachidonoyl-CoA are numerous. For this discussion, I will focus on three potential mechanisms: regulation of actin dynamics, modulation of gene transcription, and protein modification (Fig 4.1.)

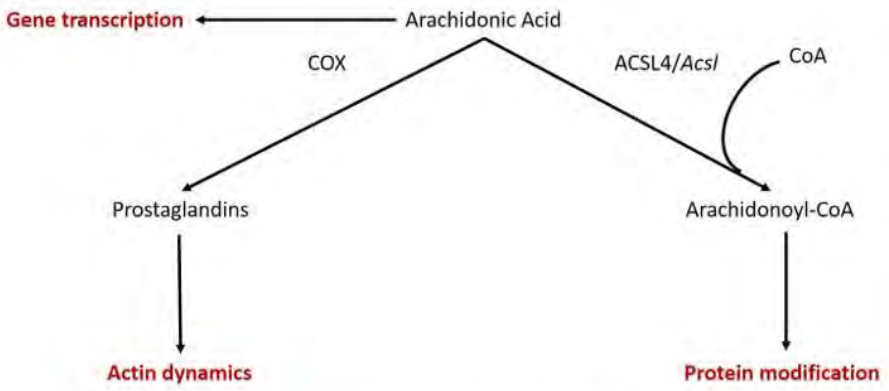

Figure 4.1. *ACSL4/Acsl* and fatty acid channeling.

i. Regulation of actin dynamics

The motility of the marginal glia in *Acsl* KD, as well the disorganization of their processes, suggests that *Acsl* may regulate the cytoskeleton. Arachidonic acid can regulate actin dynamics through its metabolism into prostaglandins (Glenn and Jacobson, 2002). The classes of prostaglandins have been demonstrated to differentially regulate the actin cytoskeleton in a cell type, and prostaglandin type, specific manner. Moreover, in

Drosophila oogenesis, prostaglandins have been demonstrated to have temporal specificity, having different effects at different stages of oocyte development (Spracklen et al., 2014). Despite this complexity, it is clear that prostaglandins can promote the formation of actin stress fibers and myosin contractility through activation of PKA and PKC (Glenn and Jacobson, 2003). It is possible that an increased intracellular pool of free arachidonic acid following *Acsl* KD can be metabolized into prostaglandins, and thus promote motility in *Acsl* KD marginal glia.

ii. Modulation of gene transcription

In addition to being essential for membrane development and energy metabolism, fatty acids are important signaling molecules (Sumida et al., 1993). Through binding and activation of PPAR nuclear receptors, fatty acids are known to regulate gene expression (Georgiadi and Kersten, 2012). The effect of fatty acids on transcription of genes involved in metabolism has been extensively studied, and both upregulation and downregulation of transcription has been documented. Whether fatty acids can regulate the transcription of non-metabolic genes has not yet been determined, although it seems likely given that fatty acid-mediated gene regulation is necessary for adipocyte

differentiation (Rosen et al., 1999). It is possible that an increase in arachidonic acid following *Acsl* depletion either decreases the transcription of genes encoding stabilizing cell-cell contact proteins, such as cadherins and integrins, or increases the expression of genes related to motility.

iii. Protein modification

Both membranous and secreted proteins are typically modified with a lipid moiety, which allows them to embed either in the plasma membrane or in secretory vesicles (Mann and Beachy, 2004). This lipid modification is provided by various fatty acid-CoA conjugates. Evidence that arachidonoyl-CoA participates in protein modification was found in isolated rat liver microsomes (Yamashita et al., 1995), although the range of proteins that can be modified by arachidonoyl-CoA remains unknown. Based on this, I hypothesize that Acsl protein provides essential arachidonoyl-CoA modification to one or more plasma membrane or secreted proteins, which in the absence of *Acsl* are mislocalized and unable to perform their usual functions. This potential mechanism may affect stabilizing cell-cell contact proteins that help maintain

marginal glia in place, glial proteins that mediate contact dependent synaptogenesis or synaptic maturation, or secreted proteins with a variety of functions.

4.4.4. Implications of this study for the field of Neurobiology

The study of glia in neurobiology is a relatively recent phenomenon, and there remains much to be elucidated about their roles in adult physiology, as well as development, and the regulation of these roles. Their importance, however, is made clear by the prominence of glial dysfunction in neurologic disease ranging from neurodegenerative disorders (Miller et al., 2004; Nagai et al., 2007; Sloan and Barres, 2013), to neurodevelopmental disorders such as bipolar disorder (Dong and Zhen, 2015), schizophrenia (Wang et al., 2015), and intellectual disability (Brenner et al., 2001; Bergmann et al., 2003; Govek et al., 2004; Ballas et al., 2009; Tian et al., 2010; Lioy et al., 2011). In this study, I elucidate a role for ACSL4 and its homologs in glia. This novel finding expands our understanding of the pathogenesis of ACSL4-linked intellectual disability to potentially include glia. Moreover, the phenotypes documented here may be observed in other intellectual disability models where glia have not been previously studied, or even other neurodevelopmental disorders without intellectual disability. Thus

this work provides a foundation for further study of the role of glia both specifically in ACSL4-linked intellectual disability, and broadly in neurodevelopmental disorders as a whole.

4.5. Restrictions on Conclusions From This Study

4.5.1. TIFR-Gal4 is not specific to marginal glia

While TIFR-Gal4 strongly expresses in marginal glia, it also expresses in the giant chiasm glia of the proximal optic chiasm. Moreover, the processes of TIFR-positive glia both penetrate the lamina neuropil, consistent with 'astrocyte-like' neuropil glia, as well as condense at the proximal edge of the lamina and traverse the distal optic chiasm, consistent with 'ensheathing' neuropil glia (Edwards and Meinertzhagen, 2010). This pattern may reflect that marginal glia are both 'astrocyte-like' and 'ensheathing', or it may reflect that the marginal glia layer is actually composed of two separate glial subclasses, each of which express TIFR-Gal4 and exhibit either 'astrocyte-like' or

‘ensheathing’ morphologies. In this latter case, it would be difficult to further resolve the glial subtype involved.

If marginal glia can be further subdivided into two classes of glia, it may help to explain why the loss of the ‘on transient’ was not seen in the drivers *alrm*-Gal4 or *loco*-Gal4, both of which share expression in marginal glia with TIFR-Gal4. Based on the patterns of glial processes, it seems that TIFR-Gal4 expresses in both ‘astrocyte-like’ and ‘ensheathing’ glia within the marginal glia layer. In contrast, *alrm*-Gal4 and *loco*-Gal4 have both been used to drive expression in ‘astrocyte-like’ glia, and may be missing expression in the ‘ensheathing’ glia subtype. All three of these drivers are considered to be strong, although subtle differences in their expression within marginal glia was not assessed. While all three drivers are known to express by larval development, when optic lobe glia are differentiating and migrating, their expression in embryonic development was not assessed in this study. Thus, it is possible that these drivers differ in either early expression onset, or subtly in expression strength in marginal glia, or in expression between subsets of marginal glia.

While I have demonstrated that giant optic chiasm glia processes are affected in *Acsl* KD, their distance from the lamina does not suggest a role in regulating neuronal signaling or the density of BRP in this neuropil, and indeed no function for giant optic chiasm glia in neuronal signaling has been elucidated to date. Moreover, I found no significant reduction in the density of repo-positive nuclei in the proximal chiasm, suggesting that giant optic chiasm glia do not contribute to the population of misplaced cells. Together, these data suggest that *Acsl* KD in marginal glia is the source of the ERG phenotype and reduced BRP density, and the primary source of mislocalized glia in the distal optic chiasm and medulla.

4.5.2. Heat shift experiments have limited temporal specificity

I was unable to drive *Acsl* RNAi expression in heat shift experiments from embryonic development without inducing lethality. Therefore, in this project "developmental expression" of *Acsl* RNAi does not include the earliest stages of development. Furthermore, while RNAi expression was initiated at the beginning of second larval instar, I can expect a delay between onset of *Acsl* RNAi expression and depletion of Acsl protein, which would depend in large part on the degradation of Acsl

protein already produced earlier in development. I observed only aspects of the *Acsl* KD phenotype in these flies upon eclosion. While useful in allowing us to divide early (embryonic and larval) from late (pupal) development, and thus propose specific developmental functions affected, this experimental design does not allow for more specificity in determining when in development *Acsl* is necessary.

Similarly, I can expect a delay between Gal80^{ts} suppression of RNAi production and the resumption of *Acsl* function, dependent on the production of new Acsl protein. For this reason, I cannot pinpoint exactly when in adulthood *Acsl* function returns. Moreover, the turnover of Acsl protein in the adult may be different from that in development, leading to longer periods before an effect of RNAi is seen, and the strength of *repo*-Gal4 may differ between development and adulthood.

4.5.3. No effect on behavior was demonstrated

Although the 'on transient' of the ERG was absent with a penetrance over 80%, I was unable to uncover a behavioral defect in either young or aged TIFR-Gal4 KD flies. That aged flies responded poorly to the behavioral assay is unsurprising, given the

degeneration of the ERG and lamina synaptic density over the lifespan of *Drosophila*. However, the data collected from young flies clearly demonstrates no behavioral defect in *Acsl* KD flies.

The behavioral assays I used tested motion and contrast vision, which are generally thought to be mediated by photoreceptors R1-R6, and separate from color vision mediated by R7 and R8. It is worth noting that within the lamina, where R1-R6 terminate, the morphological defects are not as severe as in the medulla, where R7 and R8 terminate, and that the ERG is a poor tool to record electrical activity in neuropils further from the surface of the eye than the lamina, such as the medulla. It would be interesting to test color vision based behavior (see section 4.6.3 in Future Directions for this Body of Work).

It is also worth noting that the behavior assays used tested large populations of flies, and a phenotype with low penetrance could be masked. However, we can conclude with the current body of data that neuronal activity in the lamina is affected in glial *Acsl* KD, and we can postulate that the ‘on transient’ may not be entirely abolished, thus allowing visual information to pass into the central brain.

4.5.4. More than one biochemical and developmental pathway may be involved in producing the phenotypes observed

Lipid metabolism is central to the activity of cells, and affects multiple processes on a tissue, cell, and biochemical level. Indeed, in this document I have explored multiple ways in which *Acsl* KD may affect lipid metabolism, and what the outcome of each may be. While *Acsl* regulating a single pathway is the reductionist answer, it may not be correct. *Acsl* KD may in fact be influencing multiple pathways to produce the phenotypes observed in this body of work. Determining which pathways are affected, and how they may interact, is further explored in section 4.6. Future Directions for this Body of Work.

4.5.5. *Drosophila Acsl* shares homology with *ACSL3* as well as *ACSL4*

As outlined in the introduction, 9 isoforms of *Drosophila* Acsl protein share 48% protein identity with human ACSL4 isoform 2, while 9 isoforms share 49% with human ACSL3 (Table 1.1). Moreover, human ACSL4 and ACSL3 share 66% identity with each other. This opens the possibility that the phenotype observed in this work could be rescued by either ACSL4 or ACSL3. Due to technical difficulties, I was unable to test

rescue of the phenotype with ACSL3, although given the level of protein homology some rescue would have likely been observed. Indeed, in a previous study, overexpression of either human *ACSL4* or *ACSL3* was able to rescue the lethality of homozygous $Acsl^{KO}$ mutants, as well as lipid storage in the larval wing disc (Zhang et al., 2009). However, the goal of this project is not to establish which human ACSL proteins have functional homology with *Drosophila* Acsl in glia, but rather to specifically demonstrate that human ACSL4 has functional homology in glia, in an effort to elucidate the pathogenesis of intellectual disability caused by mutations in *ACSL4*.

A separate question is why mutations in *ACSL4*, but not *ACSL3*, cause intellectual disability. This is not likely to be simply a matter of differences in mutation frequency based on genomic location. While *ACSL4* is encoded on the X chromosome, and *ACSL3* on the 2nd chromosome, mutations in *ACSL3* have been documented as well, although they result in cancer rather than intellectual disability. The answer is more likely to be found in RNA splicing isoforms. All ACSL proteins have multiple isoforms, each with context dependent expression in different tissues (Digel et al., 2009). Moreover, these

isoforms are targeted to different locations in the cell, and most likely fulfill different functions (Digel et al., 2009).

Notably, ACSL4 isoform 2, which is enriched in the brain, is predicted to target to the ER and ACSL3 to the cytoplasm. It is thus possible that the two proteins have both overlapping and separate functions, and can produce different effects on development and glial function. Similarly, the multiple isoforms derived from the *Drosophila Acsl* gene suggest that each has a different function. Indeed, the 10 Acsl protein isoforms are predicted to localize the two main locations: the ER and the cytosol. Moreover, the N termini and 5' untranslated regions of each isoform vary considerably. Of the 10 Acsl protein isoforms, 6 are predicted to localize to the ER and 4 to the cytosol (Table 1.1). In this context, it is notable that the *ACSL4* isoform 2 rescue experiments reported here provided partial rescue. Potentially, *ACSL4* was only able to compensate for the functions of a subset of *Acsl* isoforms.

4.5.6. Modest sample size

Due to technical difficulties, the sample size of some imaging experiments is modest. In some cases, the modest sample sizes were enough to uncover statistically significant differences in signal or nuclei density, while in others it seems likely that the sample size is insufficient and results would benefit from further experimentation.

Protein Isoform	Identity with ACSL4 isoform 1	Identity with ACSL4 isoform 2	% Identity with ACSL3	Predicted localization
Acsl-A	51%	48%	49%	Cytosol
Acsl-B	51%	48%	49%	Cytosol
Acsl-C	51%	48%	49%	ER
Acsl-D	51%	48%	49%	ER
Acsl-E	51%	48%	49%	Cytosol
Acsl-F	51%	48%	49%	ER
Acsl-G	51%	48%	49%	ER
Acsl-H	51%	48%	49%	Cytosol
Acsl-I	51%	48%	49%	ER
Acsl-J	51%	47%	48%	ER
ACSL4-1	100%	100%	67%	Cytosol
ACSL4-2	100%	100%	66%	ER
ACSL3	67%	66%	100%	Cytosol

Table 4.1. % Identity and predicted localization of Acsl protein isoforms. This table presents the % identity of each Drosophila Acsl protein isoform with human ACSL4 protein isoforms 1 and 2, and human ACSL3 protein. Also presented is the predicted localization of each protein isoform.

Despite these difficulties, I was able to demonstrate clear defects in the morphology and electrophysiology of *glial Acsl* KD flies, and link these defects to a developmental mechanism.

4.5.7. Quantification of transient magnitude is subject to many variables

As a wide field recording, the ERG is dependent on many variables, including contact between the recording electrode and the eye, the orientation of the eye to light stimuli, and the orientation of the lamina. While I ensured that there were no defects in the ERG equipment by calibrating every session with wild type flies, that does not rule out that subsequent flies tested were oriented differently. Thus, comparing magnitudes across ERG traces is subject to many caveats. To compensate for this, I supplemented quantification of transient amplitude by binning the traces into either absence or presence of the transients. Despite variability in the magnitude of the transients in control flies, likely due to variables mentioned above, I never observed a complete loss of the transients. In contrast, loss of one or both transients were robust phenotypes with high penetrance in glial *Acsl* KD flies. Based on these results, I am confident that visual neuron signaling is indeed altered in glial *Acsl* KD flies.

4.6. Future Directions

4.6.1. Further investigate the reduction in BRP density

The reduction in BRP signal density in the lamina I observed after restricting *Acsl* RNAi expression to development is a significant aspect of the phenotype, which may explain the loss of the 'on transient', and bears further analysis. First, to verify that the pre-synapse is reduced and not BRP protein itself, volumetric analysis of the expression of other pre-synaptic proteins should be performed. Analysis with commonly available antibodies to proteins such as cysteine string protein (CSP), which associates with synaptic vesicles, and *syntaxin* (DSyd-1), involved in vesicle docking and fusion, are appropriate. It would also be beneficial to measure the distribution and density of the post-synapse in the lamina with an antibody to *hisClA/Ort* (Hong et al., 2006b).

After verifying the phenotype through immunohistochemistry, further verification through electron microscopy could be performed. Observation of synapses through electron microscopy would allow not only quantification, but also finer analysis of their morphology and structure. In addition, at the level of electron microscopy, synapses

between different populations of neurons in the lamina can be quantified, in particular the synapse between photoreceptors R1-R6 and lamina monopolar cells L1 and L2.

Whether the reduction in BRP signal in *Acsl* KD flies arises from defects in synaptic development or in synaptic pruning is unknown. This question could be addressed by staining synaptic proteins during pupal development as synapses are being produced (Frohlich and Meinertzhagen, 1982; Meinertzhagen, 1993), and performing quantitative analysis. If there is a significant decrease in synaptic protein signals throughout development, it would indicate that there are defects in the development of synapses. In contrast, if synaptic proteins are initially present at normal levels, but decrease abnormally over time, it would indicate excessive pruning of synapses by glia. Whether glia are indeed engulfing synapses or axons would need to be proven by demonstrating the presence of either pre- or post-synaptic material within glial cell bodies or processes. Given the close association of cells in the developing and adult lamina, this would most likely need to be done by utilizing clonal analysis, in which a single glial cell or small number of glial cells could be highlighted and analyzed. Notably, TIFR-Gal4 expresses in ensheathing glia in the central brain, and ensheathing glia were demonstrated

to express *Draper*, *Shark*, and *dCed-6*, all of which are involved in the engulfment of axonal debris (Doherty et al., 2009).

4.6.2. Investigate the mislocalization of glia

While the mislocalization of glia does not appear to be responsible for the loss of the 'on transient', it is still an important aspect of the phenotype and warrants further analysis. It is possible that *Acsl* provides important lipid modifications for stabilizing cell-cell contact proteins, and that depletion of *Acsl* results in an inability of these proteins to reach or imbed into the cell membrane. In addition, glia are believed to facilitate synaptic development through contact-dependent mechanisms, which rely on the expression of cell-cell contact proteins such as γ-protocadherins in mammals (Garrett and Weiner, 2009). Thus, analysis of the expression of cell-cell contact proteins in *Acsl* KD glia could shed light on multiple aspects of the observed phenotype.

Since free arachidonic acid has documented functions in regulating actin dynamics (Glenn and Jacobson, 2002), and depletion of *Acsl* conceivably increases the intra-cellular pool of free arachidonic acid, analyzing actin dynamics in *Acsl* KD glia,

particularly in the observed mislocalized glia, could be a fruitful avenue of analysis. Staining with phalloidin would allow for analysis of increased F-actin density in mislocalized glia and their processes. This approach will label all actin in the entire optic lobe; a more specific approach would be to express moesin-GFP in marginal glia, along with either *Acsl* or *Luc* RNAi, using TIFR-Gal4. Moesin connects the actin cytoskeleton to the plasma membrane (Amieva et al., 1999). By expressing moesin-GFP and measuring the density of GFP signal at the cell periphery, it is possible to analyze the extent of actin interaction with the plasma membrane, a necessary antecedent for cell motility (Zhao et al., 2011).

4.6.3. Test vision mediated by R7 and R8

The 'on transient' of the ERG largely measures the hyperpolarization of lamina neurons in response to photoreceptors R1-R6, and the 'off transient' measures their repolarization as well as other signals from across the eye. However, in *Acsl* KD flies the processes of R7 and R8, which mediate color vision, appear to be ensheathed by abnormal glial processes as they project across the distal optic chiasm, and the terminals of R7 and R8 in the medulla are closely associated with mislocalized glia. Moreover,

BRP signal in the medulla is disorganized to the extent that synaptic layers can no longer by determined, and R7 and R8 termini in the medulla neuropil are disorganized. Thus, it is possible that visual information mediated by R7 and R8 is disrupted, and it would be fruitful to assay the extent of the disruption. Color vision, mediated by R7 and R8, is generally considered to be independent of motion vision, mediated by R1-R6 (Rister et al., 2007; Berger et al., 2008; Kelber and Henze, 2013; Melnattur et al., 2014), and most visual behavioral assays are geared to test motion vision. However, behavioral assays to measure color vision exist by testing phototaxis toward different wavelengths of light.

4.6.4. Investigate the effect of *Acsl* KD on fatty acid channeling

Through its role in fatty acid channeling, *Acsl* has two major biochemical functions. The first is to regulate the pool of free fatty acids in the cell. The second is to produce fatty acid-CoA conjugates, for use in both energy metabolism and protein modifications (Coleman et al., 2002; Grevengoed et al., 2014). Since *Acsl* has an established affinity for arachidonic acid, its biochemical functions most likely involve either intracellular free arachidonic acid, or arachidonoyl-CoA. Free arachidonic acid and arachidonoyl-CoA are involved in different processes, which are described above.

Identifying whether the populations of one of these molecules is differentially affected in *Acsl* KD would greatly assist in determining a specific pathway responsible for the observed phenotype.

It is possible to measure global levels of free arachidonic acid and arachidonoyl-CoA in the brain through lipid extraction and mass spectrometry. In the *Drosophila* brain, glia represent only 10% of the total cell population (Edwards and Meinertzhagen, 2010), which makes it likely that any difference in the levels of these molecules in this cell population would be difficult to uncover from whole brain lipid extract. An alternate method is to isolate glial cells through fluorescence activated cell sorting (FACS) before lipid extraction. This approach may also present difficulties, as separating glia from neurons requires long incubations with proteinases, and causes cells to undergo a stress response. Another approach is to stain the brain with a fat soluble dye such as Oil Red O. This would allow visualization of all neutral fatty acids, including arachidonic acid. If there is a large enough increase in the pool of free arachidonic acid following *Acsl* KD, it may produce a visible increase in Oil Red O staining, which could be specifically localized to glia by co-staining with glial markers.

Another approach would be to analyze genetic interactions between pathways of arachidonic acid metabolism. *Pxt*, a *Drosophila* COX-like enzyme, was recently described in ovarian tissue (Tootle and Spradling, 2008). It is possible that *Pxt* also functions in the *Drosophila* optic lobe. By combining KD of both *Pxt* and *Acsl*, the level of free arachidonic acid in the cell could be substantially increased over KD of either *Pxt* or *Acsl* alone. If an increase in free arachidonic acid is responsible for the phenotype, then combined KD of *Pxt* and *Acsl* should exacerbate the phenotype. If the metabolism of free arachidonic acid into prostaglandins is responsible for the phenotype, then combined KD of *Pxt* and *Acsl* should provide rescue of the phenotype.

If candidate cell-cell contact or synaptogenic proteins are identified in section 4.6.2, a reporter system could be used to assay whether PPARs regulate the expression of the associated genes. By cloning the promoter areas of candidate genes upstream of a *Luciferase* or GFP reporter, expression of the reporter could be assayed in the presence or absence of different PPAR transcription factors, allowing *in vitro* demonstration of PPAR regulation of the genes. In a similar vein, the incorporation of radiolabeled arachidonoyl-

CoA into the candidate proteins could be assessed via western blot to determine if loss of protein modification has a role in producing the observed phenotype.

Finally, one could test whether the enzymatic activity of *Acsl* is necessary by overexpressing a mutant *Acsl* with either a point mutation in or deletion of its important catalytic domains in an *Acsl* KD background. If *Acsl* enzymatic activity is required to rescue the phenotype, then no rescue should be observed with the enzymatically inactive *Acsl*.

4.6.5. Measure function in mammals

Ultimately, to demonstrate that *ACSL4* is required in mammalian glia, it would be necessary to develop a glial specific knock-down or knock-out genetic model. If *ACSL4* were specifically removed either from all glia, or specifically from astrocytes, it would be possible to analyze these animals for similar defects in glial placement, neuronal signaling, density of pre-synapses, and neuropil separation. Although there are no recorded visual effects in *ACSL4*-mediated intellectual disability, the visual system of mammalian models has also been well studied, and could provide a starting place for

detailed analysis of the role of *ACSL4* in mammalian glia. It is possible to record the electrical activity of mammalian eyes; however, morphological analysis would be most appropriate in the neuropil rich areas, perhaps in the lateral geniculate nucleus of the thalamus or the visual cortex of the occipital lobes, as these are most analogous to the neuropil of the *Drosophila* optic lobe. Moreover, in a mammalian system, the effect of glial *ACSL4* on the development of dendritic spines could be assessed, either in the visual cortex or in the hippocampus, as previous studies observed defects in cultured rat hippocampal neurons (Meloni et al., 2009). This would be particularly illuminating, as a reduction in the number of dendritic spines is the primary neuronal phenotype observed in *in vitro ACSL4* neuronal knock-down (Meloni et al., 2009), as well as in patient tissue (Purpura, 1974). It would also be instructive to compare removal of *ACSL4* from glia with removal of *ACSL3* from glia, in order to further elucidate the glial functions of these two enzymes.

4.6.6. Measure cognitive capacity in animal models

Thus far, I have measured visual activity and behavior in flies. However, visual defects are not the defining characteristic of *ACSL4* mediated intellectual disability.

Accordingly, measuring learning and memory in flies, as well as mice, that have either *Acsl* or *ACSL4* specifically removed from glia, would be an interesting area of study. Additional study of social deficits, especially in mammalian models, might provide further insight into the role of glia in intellectual disability caused by mutations in *ACSL4*.

4.6.7. Measure endosomal trafficking in glia

Since a function for *Drosophila Acsl* in endosomal trafficking has been proposed in neurons, it would be interesting to test whether *Acsl* has a similar function in glia. In Liu et al., 2014, they analyzed the distribution of several endosomal markers, including the early endosome marker Rab5, and the late endosome markers Dor, Hook, and Spinster, and found them to be abnormal compared to controls. Of these, analysis of Spinster would be most interesting, as it already has proven expression and function in optic lobe glia during development (Yuva-Aydemir et al., 2011).

4.6.8. Correlate physiological phenotype with morphological phenotype

In many experiments in this body of work, there is evidence of variable penetrance of the phenotype. My efforts to raise an antibody to *Drosophila Acsl* were unsuccessful, so I was unable to verify to what extent protein levels of *Acsl* were reduced in individual flies. It is still possible to correlate the ERG phenotype and morphological phenotype by identifying individual flies, recording the ERG, and immediately dissecting. It would be interesting to compare the severity of the physiological and morphological phenotypes: do flies with ectopic neuropil reliably have a loss of 'on transient'? Are there morphological differences in flies with loss of both the 'on' and 'off' transients? Is BRP density more reduced in flies with a loss of both transients? A similar analysis with *ACSL4* rescue flies, in which rescue of morphology could be correlated with rescue of the ERG, would be interesting.

It would also be interesting to correlate ERG and morphology with behavior. Unfortunately, the behavioral assays used in this project require pooling at least 50 flies and measuring their behavior simultaneously. However, assays that record the behavior of individual flies exist, such as the Visual Alert Response Assay developed in my lab

(see Chaturvedi et al., 2014). Moreover, the phototaxis assay proposed in section 4.6.3 above could be adapted to measure individual flies; thus, both motion and color vision could be tested.

4.6.9. Further investigate the impact on the post-synapse and post-synaptic neurons

In this study, synapses were measured using the pre-synaptic marker BRP. While there is ample evidence that the pre-synapse and pre-synaptic cell are the major determinates of synapse number during development of the lamina (Frohlich and Meinertzhagen, 1982; Fröhlich and Meinertzhagen, 1983, 1987; Meinertzhagen and Fröhlich, 1983; Meinertzhagen, 1993), I cannot conclusively determine whether there are similar defects in the density of the post-synapse without further experimentation. To directly assess the post-synapse, I could either stain with an antibody raised to the post-synaptic histamine receptor on lamina neurons (Hong et al., 2006a), or I could quantify the post-synapse on electron microscopy images. The latter method offers a further benefit in that it would allow me to assess whether there were any structural defects in the post-synapse, as well as a defect in density.

The post-synaptic lamina neurons elaborate processes that invaginates into the photoreceptor terminals, and on which the post-synapse develops. While arthropods do not develop dendrites or dendritic spines, as do mammals, these processes are analogous structures. Since defects in the number and development of dendritic spines are a recurring phenotype in tissue taken from intellectual disability patients, assessing the density and distribution of post-synaptic processes in glial *Acsl* KD flies could be an interesting and fruitful endeavor.

4.6.10. Expand rescue experiments

In this study I present evidence that *ACSL4* can rescue the morphological phenotype. However, further study to determine whether *ACSL4* can also rescue the electrophysiological phenotype would be beneficial. Given the multiple pathways *Acsl* is likely to regulate, it would be enlightening to further rescue with individual *Acsl* isoforms, as well as to confirm their putative subcellular localizations. In this way, it would be possible to directly link an isoform to a particular function of *Acsl*, and to correlate these functions with the potential functions of *ACSL4* isoforms 1 and 2, and *ACSL3*.

4.7. Concluding Remarks

The central purpose of the nervous system is to collect and process data, and generate a response. Through the interpretation of both simple (e.g. sensory stimulus) and complex (e.g. emotional stimulus) data, the nervous system allows us to interact with our environment, as well as providing us with a rich internal experience. When the function of the nervous system is disrupted the effects are profound, both on the affected individual and their community. Better understanding of the pathophysiology of nervous system disorders is thus of critical importance. Previous work has demonstrated that glial defects significantly contribute to the development of nervous system disorders, such as intellectual disability. In this study, I substantiated a novel role for a gene known to cause intellectual disability, *ACSL4*/*Acsl*, in glia, and found that it affected neuronal signaling and both neuronal and glial morphology. These findings have significant implications for understanding the potential role glia play in pathophysiology of *ACSL4*-linked intellectual disability, and developmental disorders of the nervous system in general.

BIBLIOGRAPHY

Abbott NJ, Rönnbäck L, Hansson E (2006) Astrocyte–endothelial interactions at the blood–brain barrier. Nat Rev Neurosci 7:41–53.

Ackermann F, Waites CL, Garner CC (2015) Presynaptic active zones in invertebrates and vertebrates. EMBO Rep 16:1–16 Available at: http://www.ncbi.nlm.nih.gov/pubmed/26160654.

Allen NJ, Barres BA (2005) Signaling between glia and neurons: focus on synaptic plasticity. Curr Opin Neurobiol 15:542–548.

Allen NJ, Barres BA (2009) Neuroscience: glia — more than just brain glue. Nature 457:675–677 Available at: http://www.nature.com/doifinder/10.1038/457675a.

Amieva MR, Litman P, Huang L, Ichimaru E, Furthmayr H (1999) Disruption of dynamic cell surface architecture of NIH3T3 fibroblasts by the N-terminal domains of moesin and ezrin: in vivo imaging with GFP fusion proteins. J Cell Sci 112 (Pt 1:111–125.

Araújo SJ, Tear G (2003) Axon guidance mechanisms and molecules: lessons from invertebrates. Nat Rev Neurosci 4:910–922 Available at: http://www.nature.com/doifinder/10.1038/nrn1243.

Attrill H, Falls K, Goodman JL, Millburn GH, Antonazzo G, Rey AJ, Marygold SJ (2016) FlyBase: establishing a Gene Group resource for *Drosophila melanogaster*. Nucleic Acids Res 44:D786–D792 Available at: http://nar.oxfordjournals.org/lookup/doi/10.1093/nar/gkv1046.

Bak LK, Schousboe A, Waagepetersen HS (2006) The glutamate/GABA-glutamine cycle: aspects of transport, neurotransmitter homeostasis and ammonia transfer. J Neurochem 98:641–653 Available at: http://doi.wiley.com/10.1111/j.1471-4159.2006.03913.x.

Ballas N, Lioy DT, Grunseich C, Mandel G (2009) Non-cell autonomous influence of MeCP2-deficient glia on neuronal dendritic morphology. Nat Neurosci 12:311–317 Available at: http://www.pubmedcentral.nih.gov/articlerender.fcgi?artid=3134296&tool=pmcentrez&rendertype=abstract.

Barateiro A, Brites D, Fernandes A (2016) Oligodendrocyte development and myelination in neurodevelopment: molecular mechanisms in health and disease. Curr Pharm Des 22:656–679 Available at: http://www.ncbi.nlm.nih.gov/pubmed/26635271.

Barres BA (2008) The mystery and magic of glia: a perspective on their roles in health

and disease. Neuron 60:430–440 Available at: http://dx.doi.org/10.1016/j.neuron.2008.10.013.

Barth M, Hirsch H V, Meinertzhagen IA, Heisenberg M (1997) Experience-dependent developmental plasticity in the optic lobe of *Drosophila melanogaster*. J Neurosci 17:1493–1504 Available at: http://www.ncbi.nlm.nih.gov/pubmed/9006990.

Bazigou E, Apitz H, Johansson J, Loren CE, Hirst EMA, Chen PL, Palmer RH, Salecker I (2007) Anterograde Jelly belly and Alk Receptor Tyrosine Kinase signaling mediates retinal axon targeting in *Drosophila*. Cell 128:961–975.

Berger C, Renner S, Lüer K, Technau GM (2007) The commonly used marker ELAV is transiently expressed in neuroblasts and glial cells in the *Drosophila* embryonic CNS. Dev Dyn 236:3562–3568 Available at: http://doi.wiley.com/10.1002/dvdy.21372.

Berger J, Senti KA, Senti G, Newsome TP, Asling B, Dickson BJ, Suzuki T (2008) Systematic identification of genes that regulate neuronal wiring in the *Drosophila* visual system. PLoS Genet 4.

Bergmann C, Zerres K, Senderek J, Rudnik-Schoneborn S, Eggermann T, Häusler M, Mull M, Ramaekers VT (2003) Oligophrenin 1 (OPHN1) gene mutation causes syndromic X-linked mental retardation with epilepsy, rostral ventricular enlargement and cerebellar hypoplasia. Brain 126:1537–1544.

Blanger M, Allaman I, Magistretti PJ (2011) Brain energy metabolism: focus on astrocyte-neuron metabolic cooperation. Cell Metab 14:724–738.

Blumrich E-M, Kadam R, Dringen R (2016) The protein tyrosine kinase inhibitor Tyrphostin 23 strongly accelerates glycolytic lactate production in cultured primary astrocytes. Neurochem Res Available at: http://link.springer.com/10.1007/s11064-016-1972-3.

Borycz J, Borycz JA, Loubani M, Meinertzhagen IA (2002) Tan and Ebony genes regulate a novel pathway for transmitter metabolism at fly photoreceptor terminals. J Neurosci 22:10549–10557.

Borycz J, Borycz JA, Edwards TN, Boulianne GL, Meinertzhagen IA (2012) The metabolism of histamine in the *Drosophila* optic lobe involves an ommatidial pathway: β-alanine recycles through the retina. J Exp Biol 215:1399–1411 Available at: http://www.ncbi.nlm.nih.gov/pubmed/22442379.

Bosch DS, van Swinderen B, Millard SS (2015) Dscam2 affects visual perception in *Drosophila melanogaster*. Front Behav Neurosci 9:149 Available at: http://journal.frontiersin.org/article/10.3389/fnbeh.2015.00149/abstract.

Brand AH, Perrimon N (1993) Targeted gene expression as a means of altering cell fates and generating dominant phenotypes. Development 118:401–415 Available at:

http://www.ncbi.nlm.nih.gov/pubmed/8223268.

Brash AR (2001) Arachidonic acid as a bioactive molecule. J Clin Invest 107:1339–1345.

Brenner M, Johnson AB, Boespflug-Tanguy O, Rodriguez D, Goldman JE, Messing A (2001) Mutations in GFAP, encoding glial fibrillary acidic protein, are associated with Alexander disease. Nat Genet 27:117–120 Available at: http://www.ncbi.nlm.nih.gov/pubmed/11138011.

Bringmann A, Pannicke T, Biedermann B, Francke M, Iandiev I, Grosche J, Wiedemann P, Albrecht J, Reichenbach A (2009) Role of retinal glial cells in neurotransmitter uptake and metabolism. Neurochem Int 54:143–160 Available at: http://linkinghub.elsevier.com/retrieve/pii/S0197018608002027.

Buard I, Steinmetz CC, Claudepierre T, Pfrieger FW (2010) Glial cells promote dendrite formation and the reception of synaptic input in purkinje cells from postnatal mice. Glia 58:538–545.

Cagan RL, Ready DF (1989) The emergence of order in the *Drosophila* pupal retina. Dev Biol 136:346–362.

Campesan S, Dubrova Y, Hall JC, Kyriacou CP (2001) The nonA gene in *Drosophila* conveys species-specific behavioral characteristics. Genetics 158:1535–1543.

Cao Y, Murphy KJ, McIntyre TM, Zimmerman GA, Prescott SM (2000a) Expression of fatty acid-CoA ligase 4 during development and in brain. FEBS Lett 467:263–267.

Cao Y, Pearman a T, Zimmerman G a, McIntyre TM, Prescott SM (2000b) Intracellular unesterified arachidonic acid signals apoptosis. Proc Natl Acad Sci U S A 97:11280–11285.

Cao Y, Traer E, Zimmerman GA, McIntyre TM, Prescott SM (1998) Cloning, expression, and chromosomal localization of human Long-Chain Fatty Acid-CoA Ligase 4 (FACL4). Genomics 49:327–330 Available at: http://linkinghub.elsevier.com/retrieve/pii/S0888754398952685.

Carmona MA, Murai KK, Wang L, Roberts AJ, Pasquale EB (2009) Glial ephrin-A3 regulates hippocampal dendritic spine morphology and glutamate transport. Proc Natl Acad Sci U S A 106:12524–12529 Available at: http://www.pubmedcentral.nih.gov/articlerender.fcgi?artid=2718351&tool=pmcentrez&rendertype=abstract.

Chaturvedi R, Reddig K, Li H-S (2014) Long-distance mechanism of neurotransmitter recycling mediated by glial network facilitates visual function in *Drosophila*. Proc Natl Acad Sci U S A 111:2812–2817 Available at: http://www.pubmedcentral.nih.gov/articlerender.fcgi?artid=3932938&tool=pmcentrez&rendertype=abstract.

Chen CJ, Ou YC, Lin SY, Liao SL, Huang YS, Chiang AN (2006) L-Glutamate activates

RhoA GTPase leading to suppression of astrocyte stellation. Eur J Neurosci 23:1977–1987.

Cheng C, Sourial M, Doering LC (2012) Astrocytes and developmental plasticity in Fragile X. Neural Plast 2012:1–12 Available at: http://www.hindawi.com/journals/np/2012/197491/.

Cheslow L, Alvarez JI (2016) Glial-endothelial crosstalk regulates blood–brain barrier function. Curr Opin Pharmacol 26:39–46 Available at: http://linkinghub.elsevier.com/retrieve/pii/S1471489215001125.

Chotard C, Leung W, Salecker I (2005) glial cells missing and gcm2 cell autonomously regulate both glial and neuronal development in the visual system of *Drosophila*. Neuron 48:237–251.

Chotard C, Salecker I (2008) Glial cell development and function in the *Drosophila* visual system. Neuron Glia Biol 3:17–25 Available at: http://www.pubmedcentral.nih.gov/articlerender.fcgi?artid=2265801&tool=pmcentrez&rendertype=abstract.

Christopherson KS, Ullian EM, Stokes CCA, Mullowney CE, Hell JW, Agah A, Lawler J, Mosher DF, Bornstein P, Barres BA (2005) Thrombospondins are astrocyte-secreted proteins that promote CNS synaptogenesis. Cell 120:421–433.

Clandinin TR, Zipursky SL (2000) Afferent growth cone interactions control synaptic specificity in the *Drosophila* visual system. Neuron 28:427–436 Available at: http://www.ncbi.nlm.nih.gov/pubmed/11144353.

Cocco T, Di M, Papa P, Lorusso M (1999) Arachidonic acid interaction with the mitochondrial electron transport chain promotes reactive oxygen species generation. Free Radic Biol Med 27:51–59 Available at: http://linkinghub.elsevier.com/retrieve/pii/S0891584999000349.

Coleman RA, Lewin TM, Van Horn CG, Gonzalez-Baró MR (2002) Do long-chain acyl-CoA synthetases regulate fatty acid entry into synthetic versus degradative pathways? J Nutr 132:2123–2126.

Coombe PE (1986) The large monopolar cells L1 and L2 are responsible for ERG transients in *Drosophila*. J Comp Physiol A 159:655–665.

Dearborn R, Kunes S (2004) An axon scaffold induced by retinal axons directs glia to destinations in the *Drosophila* optic lobe. Development 131:2291–2303 Available at: http://dev.biologists.org/content/131/10/2291.long.

Diamond M, Schiebel A, Murphy G, Harvey T (1985) On the brain of a scientist: Albert Einstein. Exp Neurol 88:198–204.

Digel M, Ehehalt R, Stremmel W, Füllekrug J (2009) Acyl-CoA synthetases: fatty acid uptake and metabolic channeling. Mol Cell Biochem 326:23–28.

Dodd J, Jessell T (1988) Axon guidance and the patterning of neuronal projections in vertebrates. Science (80-) 242:692–699 Available at: http://www.sciencemag.org/cgi/doi/10.1126/science.3055291.

Doherty J, Logan MA, Taşdemir OE, Freeman MR (2009) Ensheathing glia function as phagocytes in the adult *Drosophila* brain. J Neurosci 29:4768–4781 Available at: http://www.pubmedcentral.nih.gov/articlerender.fcgi?artid=2674269&tool=pmcentrez&rendertype=abstract.

Dong X-H, Zhen X-C (2015) Glial pathology in bipolar disorder: potential therapeutic implications. CNS Neurosci Ther 21:393–397 Available at: http://doi.wiley.com/10.1111/cns.12390.

Dutta S, Rieche F, Eckl N, Duch C, Kretzschmar D (2015) Glial expression of Swiss-cheese (SWS), the *Drosophila* orthologue of Neuropathy Target Esterase, is required for neuronal ensheathment and function. Available at: http://www.ncbi.nlm.nih.gov/pubmed/26634819.

Echeverry S, Rodriguez MJ, Torres YP (2016) Transient Receptor Potential Channels in microglia: roles in physiology and disease. Neurotox Res Available at: http://link.springer.com/10.1007/s12640-016-9632-6.

Edenfeld G, Stork T, Klämbt C (2005) Neuron-glia interaction in the insect nervous system. Curr Opin Neurobiol 15:34–39.

Edwards TN, Meinertzhagen IA (2010) The functional organisation of glia in the adult brain of *Drosophila* and other insects. Prog Neurobiol 90:471–497 Available at: http://dx.doi.org/10.1016/j.pneurobio.2010.01.001.

Edwards TN, Nuschke AC, Nern A, Meinertzhagen IA (2012) Organization and metamorphosis of glia in the *Drosophila* visual system. J Comp Neurol 520:2067–2085.

Ellis JM, Mentock SM, Depetrillo MA, Koves TR, Sen S, Watkins SM, Muoio DM, Cline GW, Taegtmeyer H, Shulman GI, Willis MS, Coleman RA (2011) Mouse cardiac acyl coenzyme a synthetase 1 deficiency impairs fatty acid oxidation and induces cardiac hypertrophy. Mol Cell Biol 31:1252–1262 Available at: http://www.pubmedcentral.nih.gov/articlerender.fcgi?artid=3067914&tool=pmcentrez&rendertype=abstract.

Eroglu C, Barres B a (2010) Regulation of synaptic connectivity by glia. Nature 468:223–231.

Eroglu C, Barres BA, Stevens B (2008) Glia as active participants in the development and function of synapses. In: Structural and functional organization of the synapse, pp 683–714. Boston, MA: Springer US. Available at: http://link.springer.com/10.1007/978-0-387-77232-5_23.

Fabian-Fine R, Verstreken P, Hiesinger PR, Horne JA, Kostyleva R, Zhou Y, Bellen HJ, Meinertzhagen IA (2003) Endophilin promotes a late step in endocytosis at glial invaginations in *Drosophila* photoreceptor terminals. J Neurosci 23:10732–10744.

Fischbach K-F, Dittrich APM (1989) The optic lobe of *Drosophila melanogaster*. I. A Golgi analysis of wild-type structure. Cell Tissue Res 258 Available at: http://link.springer.com/10.1007/BF00218858.

Freeman MR (2006) Sculpting the nervous system: Glial control of neuronal development. Curr Opin Neurobiol 16:119–125.

Friess M, Hammann J, Unichenko P, Luhmann HJ, White R, Kirischuk S (2016) Intracellular ion signaling influences myelin basic protein synthesis in oligodendrocyte precursor cells. Cell Calcium Available at: http://linkinghub.elsevier.com/retrieve/pii/S0143416016301002.

Fröhlich A, Meinertzhagen I (1983) Quantitative features of synapse formation in the fly's visual system. I. The presynaptic photoreceptor terminal. J Neurosci 3:2336–2349.

Frohlich A, Meinertzhagen IA (1982) Synaptogenesis in the first optic neuropile of the fly's visual system. J Neurocytol 11:159–180.

Fröhlich A, Meinertzhagen IA (1987) Regulation of synaptic frequency: Comparison of the effects of hypoinnervation with those of hyperinnervation in the fly's compound eye. J Neurobiol 18:343–357 Available at: http://doi.wiley.com/10.1002/neu.480180403.

Fuentes-Medel Y, Logan MA, Ashley J, Ataman B, Budnik V, Freeman MR (2009) Glia and muscle sculpt neuromuscular arbors by engulfing destabilized synaptic boutons and shed presynaptic debris. PLoS Biol 7:e1000184 Available at: http://dx.plos.org/10.1371/journal.pbio.1000184.

Fujimoto E, Gaynes B, Brimley CJ, Chien C-B, Bonkowsky JL (2011) Gal80 intersectional regulation of cell-type specific expression in vertebrates. Dev Dyn 240:2324–2334 Available at: http://doi.wiley.com/10.1002/dvdy.22734.

Garrett AM, Weiner JA (2009) Control of CNS Synapse Development by γ-protocadherin-mediated astrocyte-neuron contact. J Neurosci 29:11723–11731 Available at: http://www.jneurosci.org/cgi/doi/10.1523/JNEUROSCI.2818-09.2009.

Gavin BA, Arruda SE, Dolph PJ (2007) The role of carcinine in signaling at the *Drosophila* photoreceptor synapse. PLoS Genet 3:e206 Available at: http://dx.plos.org/10.1371/journal.pgen.0030206.

Gengs C, Leung HT, Skingsley DR, Iovchev MI, Yin Z, Semenov EP, Burg MG, Hardie RC, Pak WL (2002) The target of *Drosophila* photoreceptor synaptic transmission is a histamine-gated chloride channel encoded by ort (hclA). J Biol Chem 277:42113–

42120.

Georgiadi A, Kersten S (2012) Mechanisms of gene regulation by fatty acids. Adv Nutr 3:127–134.

Gibbs SM, Truman JW (1998) Nitric Oxide and Cyclic GMP regulate retinal patterning in the optic lobe of *Drosophila*. Neuron 20:83–93.

Glenn HL, Jacobson BS (2002) Arachidonic acid signaling to the cytoskeleton: the role of cyclooxygenase and cyclic AMP-dependent protein kinase in actin bundling. Cell Motil Cytoskeleton 53:239–250.

Glenn HL, Jacobson BS (2003) Cyclooxygenase and cAMP-dependent protein kinase reorganize the actin cytoskeleton for motility in HeLa cells. Cell Motil Cytoskeleton 55:265–277.

Golej DL, Askari B, Kramer F, Barnhart S, Vivekanandan-Giri A, Pennathur S, Bornfeldt KE (2011) Long-chain acyl-CoA synthetase 4 modulates prostaglandin E_2 release from human arterial smooth muscle cells. J Lipid Res 52:782–793.

Görlich A, Sigrist S (2015) BRP-170 and BRP190 isoforms of Bruchpilot protein differentially contribute to the frequency of synapses and synaptic circadian plasticity in the visual system of *Drosophila*. Front Cell Neurosci 9:1–8.

Govek E-E, Newey SE, Akerman CJ, Cross JR, Van der Veken L, Van Aelst L (2004) The X-linked mental retardation protein oligophrenin-1 is required for dendritic spine morphogenesis. Nat Neurosci 7:364–372 Available at: http://www.ncbi.nlm.nih.gov/pubmed/15034583\nhttp://www.nature.com/neuro/journal/v7/n4/extref/nn1210-S1.jpg\nhttp://www.nature.com/neuro/journal/v7/n4/extref/nn1210-S2.pdf\nhttp://www.nature.com/neuro/journal/v7/n4/extref/nn1210-S3.pdf\nhttp://www.nature.

Govek EE, Newey SE, Van Aelst L (2005) The role of the Rho GTPases in neuronal development. Genes Dev 19:1–49.

Grevengoed TJ, Klett EL, Coleman R a (2014) Acyl-CoA metabolism and partitioning. Annu Rev Nutr 34:1–30 Available at: http://www.ncbi.nlm.nih.gov/pubmed/24819326.

Gyoneva S, Swanger SA, Zhang J, Weinshenker D, Traynelis SF (2016) Altered motility of plaque-associated microglia in a model of Alzheimer's disease. Neuroscience 330:410–420 Available at: http://www.sciencedirect.com/science/article/pii/S0306452216302202.

Halassa MM, Haydon PG (2010) Integrated brain circuits: astrocytic networks modulate neuronal activity and behavior. Annu Rev Physiol 72:335–355 Available at: http://www.annualreviews.org/doi/abs/10.1146/annurev-physiol-021909-135843.

Hansson E (2003) Glial neuronal signaling in the central nervous system. FASEB J 17:341–348 Available at: http://www.fasebj.org/cgi/doi/10.1096/fj.02-0429rev.

Heisenberg M (1971) Separation of receptor and lamina potentials in the electroretinogram of normal and mutant *Drosophila*. J Exp Biol 55:85–100 Available at: http://www.ncbi.nlm.nih.gov/pubmed/5001616.

Hiesinger PR, Zhai RG, Zhou Y, Koh TW, Mehta SQ, Schulze KL, Cao Y, Verstreken P, Clandinin TR, Fischbach KF, Meinertzhagen IA, Bellen HJ (2006) Activity-independent prespecification of synaptic partners in the visual map of *Drosophila*. Curr Biol 16:1835–1843.

Hing H, Xiao J, Harden N, Lim L, Lawrence Zipursky S (1999) Pak functions downstream of Dock to regulate photoreceptor axon guidance in *Drosophila*. Cell 97:853–863.

Hitier R, Simon AF, Savarit F, Préat T (2000) no-bridge and linotte act jointly at the interhemispheric junction to build up the adult central brain of *Drosophila melanogaster*. Mech Dev 99:93–100 Available at: http://www.ncbi.nlm.nih.gov/pubmed/11091077.

Holla VR, Wang D, Brown JR, Mann JR, Katkuri S, DuBois RN (2005) Prostaglandin E2 regulates the complement inhibitor CD55/decay-accelerating factor in colorectal cancer. J Biol Chem 280:476–483.

Hong S, Bang S, Paik D, Kang J, Hwang S, Jeon K, Chun B, Hyun S, Lee Y, Kim J (2006a) Histamine and its receptors modulate temperature- preference behaviors in *Drosophila*. Neuroscience 26:7245–7256.

Hösli L, Hösli E, Andrès PF, Landolt H (1981) Evidence that the depolarization of glial cells by inhibitory amino acids is caused by an efflux of K+ from neurones. Exp brain Res 42:43–48 Available at: http://www.ncbi.nlm.nih.gov/pubmed/7215508.

Huang Z et al. (1998a) Signals transmitted along retinal axons in *Drosophila*: hedgehog signal reception and the cell circuitry of lamina cartridge assembly. Development 125:3753–3764 Available at: http://www.ncbi.nlm.nih.gov/pubmed/9729484.

Huang Z, Kunes S (1996) Hedgehog, transmitted along retinal axons, triggers neurogenesis in the developing visual centers of the *Drosophila* brain. Cell 86:411–422.

Huang Z, Shilo BZ, Kunes S (1998b) A retinal axon fascicle uses spitz, an EGF receptor ligand, to construct a synaptic cartridge in the brain of *Drosophila*. Cell 95:693–703.

Hunt MC, Alexson SEH (2002) The role Acyl-CoA thioesterases play in mediating intracellular lipid metabolism. Prog Lipid Res 41:99–130.

Jones KR, Rubin GM (1990) Molecular analysis of no-on-transient A, a gene required for normal vision in *Drosophila*. Neuron 4:711–723 Available at:

http://linkinghub.elsevier.com/retrieve/pii/089662739090197N.

Kato G, Inada H, Wake H, Akiyoshi R, Miyamoto A, Eto K, Ishikawa T, Moorhouse AJ, Strassman AM, Nabekura J (2016) Microglial contact prevents excess depolarization. eNeuro 3:1–9.

Kaufmann WE, Moser HW (2000) Dendritic anomalies in disorders associated with mental retardation. Cereb cortex 10:981–991.

Kelber A, Henze MJ (2013) Colour vision: parallel pathways intersect in *Drosophila*. Curr Biol 23:R1043–R1045 Available at: http://dx.doi.org/10.1016/j.cub.2013.10.025.

Konnerth A, Orkand PM, Orkand RK (1988) Optical recording of electrical activity from axons and glia of frog optic nerve: potentiometric dye responses and morphometrics. Glia 1:225–232 Available at: http://www.ncbi.nlm.nih.gov/pubmed/2852172.

Küch EM, Vellaramkalayil R, Zhang I, Lehnen D, Brügger B, Stremmel W, Ehehalt R, Poppelreuther M, Füllekrug J (2014) Differentially localized acyl-CoA synthetase 4 isoenzymes mediate the metabolic channeling of fatty acids towards phosphatidylinositol. Biochim Biophys Acta - Mol Cell Biol Lipids 1841:227–239 Available at: http://dx.doi.org/10.1016/j.bbalip.2013.10.018.

Kuehl F, Egan R (1980) Prostaglandins, arachidonic acid, and inflammation. Science (80-) 210:978–984 Available at: http://www.sciencemag.org/cgi/doi/10.1126/science.6254151.

Lai S-L, Lee T (2006) Genetic mosaic with dual binary transcriptional systems in *Drosophila*. Nat Neurosci 9:703–709.

Lioy DT, Garg SK, Monaghan CE, Raber J, Foust KD, Kaspar BK, Hirrlinger PG, Kirchhoff F, Bissonnette JM, Ballas N, Mandel G (2011) A role for glia in the progression of Rett's syndrome. Nature 475:497–500 Available at: http://www.pubmedcentral.nih.gov/articlerender.fcgi?artid=3268776&tool=pmcentrez&rendertype=abstract.

Liu Z, Huang Y, Hu W, Huang S, Wang Q, Han J, Zhang YQ (2014) dAcsl, the *Drosophila* ortholog of acyl-CoA synthetase long-chain family member 3 and 4, inhibits synapse growth by attenuating bone morphogenetic protein signaling via endocytic recycling. J Neurosci 34:2785–2796 Available at: http://www.ncbi.nlm.nih.gov/pubmed/24553921.

Liu Z, Huang Y, Zhang Y, Chen D, Zhang YQ (2011) *Drosophila* Acyl-CoA synthetase long-chain family member 4 regulates axonal transport of synaptic vesicles and is required for synaptic development and transmission. J Neurosci 31:2052–2063.

Madry C, Attwell D (2015) Receptors, ion channels, and signaling mechanisms underlying microglial dynamics. J Biol Chem 290:12443–12450.

Makinodan M (2015) Potential primary roles of glial cells in the mechanisms of psychiatric disorders. Front Cell Neurosci 9:1–11.

Mann RK, Beachy PA (2004) Novel lipid modifications of secreted protein signals. Annu Rev Biochem 73:891–923 Available at: http://www.annualreviews.org/doi/10.1146/annurev.biochem.73.011303.073933.

Marcaggi P, Attwell D (2004) Role of glial amino acid transporters in synaptic transmission and brain energetics. Glia 47:217–225 Available at: http://doi.wiley.com/10.1002/glia.20027.

Mashek DG, Li LO, Coleman RA (2006) Rat long-chain acyl-CoA synthetase mRNA, protein, and activity vary in tissue distribution and in response to diet. J Lipid Res 47:2004–2010 Available at: http://www.ncbi.nlm.nih.gov/pubmed/16772660.

Mathews ES, Appel B (2016) Cholesterol biosynthesis supports myelin gene expression and axon ensheathment through modulation of P13K/Akt/mTor signaling. J Neurosci 36:7628–7639 Available at: http://www.jneurosci.org/cgi/doi/10.1523/JNEUROSCI.0726-16.2016.

Mauch DH (2001) CNS synaptogenesis promoted by glia-derived cholesterol. Science (80-) 294:1354–1357 Available at: http://www.sciencemag.org/cgi/doi/10.1126/science.294.5545.1354.

Mazzoni EO, Celik A, Wernet MF, Vasiliauskas D, Johnston RJ, Cook TA, Pichaud F, Desplan C (2008) Iroquois complex genes induce co-expression of rhodopsins in *Drosophila*. PLoS Biol 6:825–835.

McGuire SE, Le PT, Osborn AJ, Matsumoto K, Davis RL (2003) Spatiotemporal rescue of memory dysfunction in *Drosophila*. Science (80-) 302:1765–1768 Available at: http://www.sciencemag.org/cgi/doi/10.1126/science.1089035.

McMullen PD, Bhattacharya S, Woods CG, Sun B, Yarborough K, Ross SM, Miller ME, McBride MT, Lecluyse EL, Clewell RA, Andersen ME (2014) A map of the PPAR transcription regulatory network for primary human hepatocytes. Chem Biol Interact 209:14–24 Available at: http://dx.doi.org/10.1016/j.cbi.2013.11.006.

Meinertzhagen IA (1989) Fly photoreceptor synapses: their development, evolution, and plasticity. J Neurobiol 20:276–294.

Meinertzhagen IA (1993) The development of the optic lobe. In: The development of *Drosophila melanogaster*, Volume 2 (Bate M, Arias AM, eds), pp 1363–1490. Cold Spring Harbor, NY: Cold Spring Laboratory Press.

Meinertzhagen IA, Fröhlich A (1983) The regulation of synapse formation in the fly's visual system. Trends Neurosci 6:223–228 Available at: http://linkinghub.elsevier.com/retrieve/pii/0166223683900991.

Meinertzhagen IA, O'Neil SD (1991) Synaptic organization of columnar elementsin the

lamina of the wild type in *Drosophila melanogaster*. J Comp Neurol 305:232–263.

Melnattur K V., Lee C-H (2011) Visual circuit assembly in *Drosophila*. Dev Neurobiol 71:1286–1296 Available at: http://doi.wiley.com/10.1002/dneu.20894.

Melnattur K V., Pursley R, Lin T-Y, Ting C-Y, Smith PD, Pohida T, Lee C-H (2014) Multiple redundant medulla projection neurons mediate color vision in *Drosophila*. J Neurogenet 28:374–388 Available at: http://www.tandfonline.com/doi/full/10.3109/01677063.2014.891590.

Meloni I, Muscettola M, Raynaud M, Longo I, Bruttini M, Moizard M-P, Gomot M, Chelly J, des Portes V, Fryns J-P, Ropers H-H, Magi B, Bellan C, Volpi N, Yntema HG, Lewis SE, Schaffer JE, Renieri A (2002) FACL4, encoding fatty acid-CoA ligase 4, is mutated in nonspecific X-linked mental retardation. Nat Genet 30:436–440.

Meloni I, Parri V, De Filippis R, Ariani F, Artuso R, Bruttini M, Katzaki E, Longo I, Mari F, Bellan C, Dotti CG, Renieri A (2009) The XLMR gene ACSL4 plays a role in dendritic spine architecture. Neuroscience 159:657–669 Available at: http://dx.doi.org/10.1016/j.neuroscience.2008.11.056.

Millard SS, Lu Z, Zipursky SL, Meinertzhagen IA (2010) *Drosophila* Dscam proteins regulate postsynaptic specificity at multiple-contact synapses. Neuron 67:761–768 Available at: http://dx.doi.org/10.1016/j.neuron.2010.08.030.

Miller DW, Cookson MR, Dickson DW (2004) Glial cell inclusions and the pathogenesis of neurodegenerative diseases. Neuron Glia Biol 1:13–21 Available at: http://www.journals.cambridge.org/abstract_S1740925X04000043.

Murai KK, Nguyen LN, Irie F, Yamaguchi Y, Pasquale EB (2003) Control of hippocampal dendritic spine morphology through ephrin-A3/EphA4 signaling. Nat Neurosci 6:153–160.

Nagai M, Re DB, Nagata T, Chalazonitis A, Jessell TM, Wichterle H, Przedborski S (2007) Astrocytes expressing ALS-linked mutated SOD1 release factors selectively toxic to motor neurons. Nat Neurosci 10:615–622 Available at: http://www.nature.com/doifinder/10.1038/nn1876.

Nägler K, Mauch DH, Pfrieger FW (2001) Glia-derived signals induce synapse formation in neurones of the rat central nervous system. J Physiol 533:665–679 Available at: http://doi.wiley.com/10.1111/j.1469-7793.2001.00665.x.

Neeli I, Yellaturu CR, Rao GN (2003) Arachidonic acid activation of translation initiation signaling in vascular smooth muscle cells. Biochem Biophys Res Commun 309:755–761 Available at: http://www.ncbi.nlm.nih.gov/pubmed/13679036.

Nicol D, Meinertzhagen IA (1982a) An analysis of the number and composition of the synaptic populations formed by photoreceptors of the fly. J Comp Neurol 207:29–44

Available at: http://doi.wiley.com/10.1002/cne.902070104.

Nicol D, Meinertzhagen IA (1982b) Regulation in the number of fly photoreceptor synapses: the effects of alterations in the number of presynaptic cells. J Comp Neurol 207:45–60 Available at: http://doi.wiley.com/10.1002/cne.902070105.

Nimchinsky EA, Sabatini BL, Svoboda K (2002) Structure and function of dendritic spines. Annu Rev Physiol 64:313–353 Available at: http://www.ncbi.nlm.nih.gov/pubmed/11826272.

Nuriya M, Hirase H (2016) Involvement of astrocytes in neurovascular communication. In: Progress in Brain Research, pp 41–62 Available at: http://linkinghub.elsevier.com/retrieve/pii/S0079612316000364.

Pantazis A, Segaran A, Liu C-H, Nikolaev A, Rister J, Thum AS, Roeder T, Semenov E, Juusola M, Hardie RC (2008) Distinct roles for two histamine receptors (hclA and hclB) at the *Drosophila* photoreceptor synapse. J Neurosci 28:7250–7259.

Pappalardo LW, Black JA, Waxman SG (2016) Sodium channels in astroglia and microglia. Glia: Available at: http://doi.wiley.com/10.1002/glia.22967.

Pei Z, Sun P, Huang P, Lal B, Laterra J, Watkins PA (2009) Acyl-CoA synthetase VL3 knockdown inhibits human glioma cell proliferation and tumorigenicity. Cancer Res 69:9175–9182.

Perez SE, Steller H (1996) Migration of glial cells into retinal axon target field in *Drosophila melanogaster*. J Neurobiol 30:359–373.

Perez-Gonzalez AP, Albrecht D, Blasi J, Llobet A (2008) Schwann cells modulate short-term plasticity of cholinergic autaptic synapses. J Physiol 586:4675–4691 Available at: http://doi.wiley.com/10.1113/jphysiol.2008.160044.

Pfrieger FW (2009) Roles of glial cells in synapse development. Cell Mol Life Sci 66:2037–2047.

Piccini M, Vitelli F, Bruttini M, Pober BR, Jonsson JJ, Villanova M, Zollo M, Borsani G, Ballabio A, Renieri A (1998) FACL4, a new gene encoding long-chain acyl-CoA synthetase 4, is in a family with Alport syndrome, elliptocytosis, and mental retardation. Genomics 47:350–358.

Poeck B, Fischer S, Gunning D, Zipursky SL, Salecker I (2001) Glial cells mediate target layer selection of retinal axons in the developing visual system of *Drosophila*. Neuron 29:99–113.

Purpura DP (1974) Dendritic spine “dysgenesis” and mental retardation. Science 186:1126–1128.

Purves D, Augustine G, D F (2001) Neuroglial cells. In: Neuroscience. Sinaur Associates.

Pyza E (2002) Dynamic structural changes of synaptic contacts in the visual system of insects. Microsc Res Tech 58:335–344.

Rahman M, Ham H, Liu X, Sugiura Y, Orth K, Krämer H (2012) Visual neurotransmission in *Drosophila* requires expression of Fic in glial capitate projections. Nat Neurosci 15:871–875 Available at: http://www.pubmedcentral.nih.gov/articlerender.fcgi?artid=3578554&tool=pmcentrez&rendertype=abstract.

Rakhshandehroo M, Knoch B, Müller M, Kersten S (2010) Peroxisome Proliferator-Activated Receptor Alpha target genes. PPAR Res 2010:1–20 Available at: http://www.hindawi.com/journals/ppar/2010/612089/.

Ranganathan R, Malicki DM, Zuker CS (1995) Signal transduction in *Drosophila* photoreceptors. Annu Rev Neurosci 18:283–317 Available at: http://www.annualreviews.org/doi/abs/10.1146/annurev.ne.18.030195.001435.

Rangarajan R, Courvoisier H, Gaul U (2001) Dpp and Hedgehog mediate neuron-glia interactions in *Drosophila* eye development by promoting the proliferation and motility of subretinal glia. Mech Dev 108:93–103.

Rao GH, White JG (1985) Role of arachidonic acid metabolism in human platelet activation and irreversible aggregation. Am J Hematol 19:339–347 Available at: http://www.ncbi.nlm.nih.gov/pubmed/3161324.

Reichenbach A, Derouiche A, Kirchhoff F (2010) Morphology and dynamics of perisynaptic glia. Brain Res Rev 63:11–25 Available at: http://dx.doi.org/10.1016/j.brainresrev.2010.02.003.

Rein K, Zöckler M, Heisenberg M (1999) A quantitative three-dimensional model of the *Drosophila* optic lobes. Curr Biol 9:93-S2 Available at: http://linkinghub.elsevier.com/retrieve/pii/S0960982299800219.

Rendahl KG, Jones KR, Kulkarni SJ, Bagully SH, Hall JC (1992) The dissonance mutation at the no-on-transient-A locus of *D. melanogaster*: genetic control of courtship song and visual behaviors by a protein with putative RNA-binding motifs. J Neurosci 12:390–407.

Renieri A, Pescucci C, Longo I, Ariani F, Mari F, Meloni I (2005) Non-syndromic X-linked mental retardation: from a molecular to a clinical point of view. J Cell Physiol 204:8–20.

Richardt A, Rybak J, Störtkuhl KF, Meinertzhagen IA, Hovemann BT (2002) Ebony protein in the *Drosophila* nervous system: optic neuropile expression in glial cells. J Comp Neurol 452:93–102.

Rister J, Pauls D, Schnell B, Ting CY, Lee CH, Sinakevitch I, Morante J, Strausfeld NJ, Ito K, Heisenberg M (2007) Dissection of the peripheral motion channel in the

visual system of *Drosophila melanogaster*. Neuron 56:155–170.

Romero-Calderón R, Shome RM, Simon AF, Daniels RW, DiAntonio A, Krantz DE (2007) A screen for neurotransmitter transporters expressed in the visual system of *Drosophila melanogaster* identifies three novel genes. Dev Neurobiol 67:550–569 Available at: http://doi.wiley.com/10.1002/dneu.20342.

Rosen ED, Sarraf P, Troy AE, Bradwin G, Moore K, Milstone DS, Spiegelman BM, Mortensen RM (1999) PPARγ is required for the differentiation of adipose tissue in vivo and in vitro. Mol Cell 4:611–617 Available at: http://linkinghub.elsevier.com/retrieve/pii/S1097276500802117.

Schafer DP, Lehrman EK, Kautzman AG, Koyama R, Mardinly AR, Yamasaki R, Ransohoff RM, Greenberg ME, Barres BA, Stevens B (2012) Microglia sculpt postnatal neural circuits in an activity and complement-dependent manner. Neuron 74:691–705 Available at: http://dx.doi.org/10.1016/j.neuron.2012.03.026.

Schafer DP, Stevens B (2010) Synapse elimination during development and disease: immune molecules take centre stage. Biochem Soc Trans 38:476–481 Available at: http://www.ncbi.nlm.nih.gov/pubmed/20298206.

Schafer DP, Stevens B (2014) Phagocytic glial cells: sculpting synaptic circuits in the developing nervous system. Curr Opin Neurobiol 23:1034–1040.

Schwabe T, Neuert H, Clandinin TR (2013) A network of cadherin-mediated interactions polarizes growth cones to determine targeting specificity. Cell 154:351–364 Available at: http://linkinghub.elsevier.com/retrieve/pii/S0092867413007137.

Seeger DR, Murphy CC, Murphy EJ (2016) Astrocyte arachidonate and palmitate uptake and metabolism is differentially modulated by dibutyryl-cAMP treatment. Prostaglandins, Leukot Essent Fat Acids 110:16–26 Available at: http://linkinghub.elsevier.com/retrieve/pii/S0952327816300047.

Senti K, Keleman K, Eisenhaber F, Dickson BJ (2000) brakeless is required for lamina targeting of R1-R6 axons in the *Drosophila* visual system. Development 127:2291–2301 Available at: http://www.ncbi.nlm.nih.gov/pubmed/10804172.

Silies M, Klämbt C (2011) Adhesion and signaling between neurons and glial cells in *Drosophila*. Curr Opin Neurobiol 21:11–16.

Silver IA, Ereciriska M (1992) Ion homeostasis in rat brain in vivo: intra- and extracellular [Ca2+] and [H+] in the hippocampus during recovery from short-term, transient ischemia. J Cereb Blood Flow Metab 12:759–772 Available at: http://jcb.sagepub.com/lookup/doi/10.1038/jcbfm.1992.107.

Simard M, Nedergaard M (2004) The neurobiology of glia in the context of water and ion homeostasis. Neuroscience 129:877–896 Available at: http://linkinghub.elsevier.com/retrieve/pii/S0306452204008462.

Sloan SA, Barres BA (2013) Glia as primary drivers of neuropathology in TDP-43 proteinopathies. Proc Natl Acad Sci 110:4439–4440 Available at: http://www.pnas.org/cgi/doi/10.1073/pnas.1301608110\npapers3://publication/doi/10.1073/pnas.1301608110.

Smalheiser NR, Dissanayake S, Kapil A (1996) Rapid regulation of neurite outgrowth and retraction by phospholipase A2-derived arachidonic acid and its metabolites. Brain Res 721:39–48.

Spangenberg EE, Green KN (2016) Inflammation in Alzheimer's disease: lessons learned from microglia-depletion models. Brain Behav Immun Available at: http://linkinghub.elsevier.com/retrieve/pii/S0889159116301970.

Spracklen AJ, Kelpsch DJ, Chen X, Spracklen CN, Tootle TL (2014) Prostaglandins temporally regulate cytoplasmic actin bundle formation during *Drosophila* oogenesis. Mol Biol Cell 25:397–411 Available at: http://www.pubmedcentral.nih.gov/articlerender.fcgi?artid=3907279&tool=pmcentrez&rendertype=abstract.

Steinman MQ, Gao V, Alberini CM (2016) The role of lactate-mediated metabolic coupling between astrocytes and neurons in long-term memory formation. Front Integr Neurosci 10:10 Available at: http://journal.frontiersin.org/article/10.3389/fnint.2016.00010/abstract.

Steinmetz CC, Buard I, Claudepierre T, Nägler K, Pfrieger FW (2006) Regional variations in the glial influence on synapse development in the mouse CNS. J Physiol 577:249–261 Available at: http://doi.wiley.com/10.1113/jphysiol.2006.117358.

Stuart AE, Borycz J, Meinertzhagen IA (2007) The dynamics of signaling at the histaminergic photoreceptor synapse of arthropods. Prog Neurobiol 82:202–227.

Stuart G, Spruston N, Sakmann B, Häusser M (1997) Action potential initiation and backpropagation in neurons of the mammalian CNS. Trends Neurosci 20:125–131 Available at: http://linkinghub.elsevier.com/retrieve/pii/S0166223696100758.

Suh GSB, Poeck B, Chouard T, Oron E, Segal D, Chamovitz DA, Zipursky SL (2002) *Drosophila* JAB1/CSN5 acts in photoreceptor cells to induce glial cells. Neuron 33:35–46.

Sumida C, Graber R, Nunez E (1993) Role of fatty acids in signal transduction: modulators and messengers. Prostaglandins, Leukot Essent Fat Acids 48:117–122.

Takemura SY, Lu Z, Meinertzhagen IA (2008a) Synaptic circuits of the *Drosophila* optic lobe: the input terminals to the medulla. J Comp Neurol 509:493–513.

Tay TL, Savage J, Hui CW, Bisht K, Tremblay M-È (2016) Microglia across the lifespan: from origin to function in brain development, plasticity and cognition. J Physiol

Available at: http://doi.wiley.com/10.1113/JP272134.

Tayler TD (2004) Compartmentalization of visual centers in the *Drosophila* brain requires Slit and Robo proteins. Development 131:5935–5945 Available at: http://www.ncbi.nlm.nih.gov/pubmed/15525663\nhttp://www.pubmedcentral.nih.gov/articlerender.fcgi?artid=PMC1201521\nhttp://dev.biologists.org/cgi/doi/10.1242/dev.01465.

Tayler TD, Garrity PA (2003) Axon targeting in the *Drosophila* visual system. Curr Opin Neurobiol 13:90–95.

Tessier CR, Broadie K (2008) *Drosophila* fragile X mental retardation protein developmentally regulates activity-dependent axon pruning. Development 135:1547–1557 Available at: http://www.pubmedcentral.nih.gov/articlerender.fcgi?artid=3988902&tool=pmcentrez&rendertype=abstract.

Thomas BJ, Lawrence Zipursky S (1994) Early pattern formation in the developing *Drosophila* eye. Trends Cell Biol 4:389–394.

Tian R, Wu X, Hagemann TL, Sosunov AA, Messing A, McKhann GM, Goldman JE (2010) Alexander disease mutant glial fibrillary acidic protein compromises glutamate transport in astrocytes. J Neuropathol Exp Neurol 69:335–345 Available at: http://www.pubmedcentral.nih.gov/articlerender.fcgi?artid=3342699&tool=pmcentrez&rendertype=abstract.

Tix S, Eule E, Fischbach KF, Benzer S (1997) Glia in the chiasms and medulla of the *Drosophila melanogaster* optic lobes. Cell Tissue Res 289:397–409.

Tootle TL, Spradling AC (2008) *Drosophila* Pxt: a cyclooxygenase-like facilitator of follicle maturation. Development 135:839–847 Available at: http://www.pubmedcentral.nih.gov/articlerender.fcgi?artid=2818214&tool=pmcentrez&rendertype=abstract.

Tsai H-H, Miller RH (2002) Glial cell migration directed by axon guidance cues. Trends Neurosci 25:173–175 Available at: http://linkinghub.elsevier.com/retrieve/pii/S0166223600020968.

Umetsu D, Murakami S, Sato M, Tabata T (2006) The highly ordered assembly of retinal axons and their synaptic partners is regulated by Hedgehog/Single-minded in the *Drosophila* visual system. Development 133:791–800.

Van Vactor D, Krantz DE, Reinke R, Lawrence Zipursky S (1988) Analysis of mutants in chaoptin, a photoreceptor cell-specific glycoprotein in *Drosophila*, reveals its role in cellular morphogenesis. Cell 52:281–290.

Waagepetersen H, Qu H, Sonnewald U, Shimamoto K, Schousboe A (2005) Role of

glutamine and neuronal glutamate uptake in glutamate homeostasis and synthesis during vesicular release in cultured glutamatergic neurons. Neurochem Int 47:92–102 Available at: http://linkinghub.elsevier.com/retrieve/pii/S0197018605000975.

Wagh DA, Rasse TM, Asan E, Hofbauer A, Schwenkert I, D??rrbeck H, Buchner S, Dabauvalle MC, Schmidt M, Qin G, Wichmann C, Kittel R, Sigrist SJ, Buchner E (2006) Bruchpilot, a protein with homology to ELKS/CAST, is required for structural integrity and function of synaptic active zones in *Drosophila*. Neuron 49:833–844.

Walz W (1989) Role of glial cells in the regulation of the brain ion microenvironment. Prog Neurobiol 33:309–333 Available at: http://linkinghub.elsevier.com/retrieve/pii/0301008289900051.

Wang C, Aleksic B, Ozaki N (2015) Glia-related genes and their contribution to schizophrenia. Psychiatry Clin Neurosci:448–461.

Washizaki K, Smith QR, Rapoport SI, Purdon a D (1994) Brain arachidonic acid incorporation and precursor pool specific activity during intravenous infusion of unesterified [3H]arachidonate in the anesthetized rat. J Neurochem 63:727–736 Available at: http://www.ncbi.nlm.nih.gov/pubmed/8035197.

Winberg ML, Perez SE, Steller H (1992) Generation and early differentiation of glial cells in the first optic ganglion of *Drosophila melanogaster*. Development 115:903–911 Available at: http://www.ncbi.nlm.nih.gov/pubmed/1451666.

Yamashita a, Watanabe M, Tonegawa T, Sugiura T, Waku K (1995) Acyl-CoA binding and acylation of UDP-glucuronosyltransferase isoforms of rat liver: their effect on enzyme activity. Biochem J 312 (Pt 1:301–308 Available at: http://www.pubmedcentral.nih.gov/articlerender.fcgi?artid=1136259&tool=pmcentrez&rendertype=abstract.

Yoshida S, Soustelle L, Giangrande A, Umetsu D, Murakami S, Yasugi T, Awasaki T, Ito K, Sato M, Tabata T (2005) DPP signaling controls development of the lamina glia required for retinal axon targeting in the visual system of *Drosophila*. Development 132:4587–4598.

Yuva-Aydemir Y, Bauke A-C, Klämbt C (2011) Spinster controls Dpp signaling during glial migration in the *Drosophila* eye. J Neurosci 31:7005–7015.

Zhang Y, Chen D, Wang Z (2009) Analyses of mental dysfunction-related ACSL4 in *Drosophila* reveal its requirement for Dpp/BMP production and visual wiring in the brain. Hum Mol Genet 18:3894–3905.

Zhang Y, Chen K, Sloan SA, Bennett ML, Scholze AR, O'Keeffe S, Phatnani HP, Guarnieri P, Caneda C, Ruderisch N, Deng S, Liddelow SA, Zhang C, Daneman R, Maniatis T, Barres BA, Wu JQ (2014) An RNA-sequencing transcriptome and splicing database of glia, neurons, and vascular cells of the cerebral cortex. J

Neurosci 34:11929–11947 Available at: http://www.jneurosci.org/cgi/doi/10.1523/JNEUROSCI.1860-14.2014.

Zhao H, Pykäläinen A, Lappalainen P (2011) I-BAR domain proteins: linking actin and plasma membrane dynamics. Curr Opin Cell Biol 23:14–21.

Ziegenfuss JS, Doherty J, Freeman MR (2012) Distinct molecular pathways mediate glial activation and engulfment of axonal debris after axotomy. Nat Neurosci 15:979–987 Available at: http://www.nature.com/doifinder/10.1038/nn.3135.

APPENDIX A. TABLE OF EXPERIMENTS

Experiment/Genotype	N	Penetrance of phenotype	Mean	SEM	P value	Type of Analysis
Cell type screen: C.S. wild type control. 'On transient' mean.	23	N/A	1.452	0.1332	N/A	N/A
Cell type screen: C.S. wild type control. 'Off transient' mean.	23	N/A	5.483	0.4595	N/A	N/A
Cell type screen: C.S. wild type control. Loss of 'on transient'.	23	0% loss of 'on transient'	N/A	N/A	N/A	N/A
Cell type screen: C.S. wild type control. Loss of 'on' and 'off' transients.	23	0% loss of both transients	N/A	N/A	N/A	N/A
Cell type screen: *repo*-Gal4> *Acsl* RNAi. 'On transient' mean.	22	N/A	0.05909	0.02917	<0.0001 vs. wild type	Unpaired, two-tailed, t-test
Cell type screen: *repo*-Gal4> *Acsl* RNAi. 'Off transient' mean.	22	N/A	2.045	0.3857	<0.0001 vs. wild type	Unpaired, two-tailed, t-test
Cell type screen: *repo*-Gal4> *Acsl* RNAi. Loss of 'on transient'.	22	82% loss of 'on transient'	N/A	N/A	<0.0001 vs. wild type	Chi-square (Fischer's exact test)
Cell type screen: *repo*-Gal4> *Acsl* RNAi. Loss of 'on' and 'off' transients.	22	18% loss of both transients	N/A	N/A	0.0491 vs. wild type	Chi-square (Fischer's exact test)
Cell type screen: *elav*-Gal4> *Acsl* RNAi. 'On transient' mean.	15	N/A	1.573	0.1375	0.5465 vs. wild type	Unpaired, two-tailed, t-test
Cell type screen: *elav*-Gal4> *Acsl* RNAi. 'Off transient' mean.	14	N/A	3.957	0.6114	0.0518 vs. wild type	Unpaired, two-tailed, t-test
Cell type screen: *elav*-Gal4> *Acsl* RNAi. Loss of 'on transient'.	15	0% loss of 'on transient'	N/A	N/A	>0.9999 vs. wild type	Chi-square (Fischer's exact test)
Cell type screen: *elav*-Gal4> *Acsl* RNAi. Loss of 'on' and 'off' transients.	14	0% loss of both transients	N/A	N/A	>0.9999 vs. wild type	Chi-square (Fischer's exact test)

Experiment/Genotype	**N**	**Penetrance of phenotype**	**Mean**	**SEM**	**P value**	**Type of Analysis**
Glial subtype screen: TIFR-Gal4> *Acsl* RNAi. 'On transient' mean.	40	N/A	0.1600	0.07965	<0.0001 vs. TIFR> *Luc* RNAi	Unpaired, two-tailed, t-test
Glial subtype screen: TIFR-Gal4> *Acsl* RNAi. 'Off transient' mean.	40	N/A	2.420	0.3444	<0.0001 vs. TIFR> *Luc* RNAi	Unpaired, two-tailed, t-test
Glial subtype screen: TIFR-Gal4> *Acsl* RNAi. Loss of 'on transient'.	40	85% loss of 'on transient'	N/A	N/A	<0.0001 vs. TIFR> *Luc* RNAi	Chi-square (Fischer's exact test)
Glial subtype screen: TIFR-Gal4> *Acsl* RNAi. Loss of 'on' and 'off' transients.	40	20% loss of both transients	N/A	N/A	0.0899 vs. TIFR> *Luc* RNAi 0.0225 vs. wild type	Chi-square (Fischer's exact test)
Glial subtype screen: TIFR-Gal4> *Luc* RNAi. 'On transient' mean.	17	N/A	1.341	0.09965	0.8410 vs. wild type	Unpaired, two-tailed, t-test
Glial subtype screen: TIFR-Gal4> *Luc* RNAi. 'Off transient' mean.	17	N/A	5.318	0.3426	0.8173 vs. wild type	Unpaired, two-tailed, t-test
Glial subtype screen: TIFR-Gal4> *Luc* RNAi. Loss of 'on transient'.	17	0% loss of 'on transient'	N/A	N/A	>0.9999 vs. wild type	Chi-square (Fischer's exact test)
Glial subtype screen: TIFR-Gal4> *Luc* RNAi. Loss of 'on' and 'off' transients.	17	0% loss of both transients	N/A	N/A	>0.9999 vs. wild type	Chi-square (Fischer's exact test)
Glial subtype screen: *Alrm*-Gal4> *Acsl* RNAi. Loss of 'on transient'.	5	0% loss of 'on transient'	N/A	N/A	>0.9999 vs. wild type	Chi-square (Fischer's exact test)
Glial subtype screen: *Gcm*-Gal4> *Acsl* RNAi. Loss of 'on transient'.	4	0% loss of 'on transient'	N/A	N/A	>0.9999 vs. wild type	Chi-square (Fischer's exact test)
Glial subtype screen: *hisCl1*-Gal4> *Acsl* RNAi. Loss of 'on transient'.	4	0% loss of 'on transient'	N/A	N/A	>0.9999 vs. wild type	Chi-square (Fischer's exact test)
Glial subtype screen: *loco*-Gal4> *Acsl* RNAi. Loss of 'on transient'.	4	0% loss of 'on transient'	N/A	N/A	>0.9999 vs. wild type	Chi-square (Fischer's exact test)
Glial subtype screen: *mmd*-Gal4> *Acsl* RNAi. Loss of 'on transient'.	4	0% loss of 'on transient'	N/A	N/A	>0.9999 vs. wild type	Chi-square (Fischer's exact test)

Experiment/Genotype	N	Penetrance of phenotype	Mean	SEM	P value	Type of Analysis
Glial subtype screen: *moody*-Gal4> *Acsl* RNAi. Loss of 'on transient'.	4	0% loss of 'on transient'	N/A	N/A	>0.9999 vs. wild type	Chi-square (Fischer's exact test)
Glial subtype screen: mz97-Gal4> *Acsl* RNAi. Loss of 'on transient'.	5	0% loss of 'on transient'	N/A	N/A	>0.9999 vs. wild type	Chi-square (Fischer's exact test)
Glial subtype screen: mz0709-Gal4> *Acsl* RNAi. Loss of 'on transient'.	4	0% loss of 'on transient'	N/A	N/A	>0.9999 vs. wild type	Chi-square (Fischer's exact test)
Glial subtype screen: *Nrv2*-Gal4> *Acsl* RNAi. Loss of 'on transient'.	4	0% loss of 'on transient'	N/A	N/A	>0.9999 vs. wild type	Chi-square (Fischer's exact test)
Alternate RNAis: *repo*-Gal4> HMS02307 (41885). Loss of 'on transient'.	10	80% loss of 'on transient'	N/A	N/A	<0.0001 vs. wild type	Chi-square (Fischer's exact test)
Alternate RNAis: *repo*-Gal4> HMS02307 (41885). Loss of 'on' and 'off' transients.	10	20% loss of both transients	N/A	N/A	0.0852 vs. wild type	Chi-square (Fischer's exact test)
Alternate RNAis: *repo*-Gal4> GD1638 (3222). Loss of 'on transient'.	10	80% loss of 'on transient'	N/A	N/A	<0.0001 vs. wild type	Chi-square (Fischer's exact test)
Alternate RNAis: *repo*-Gal4> GD1638 (3222). Loss of 'on' and 'off' transients.	10	0% loss of both transients	N/A	N/A	.3235 vs. wild type	Chi-square (Fischer's exact test)
Behavior, Optomotor response, young flies: TIFR-Gal4> *Luc* RNAi		N/A	.848 to .638	.056 to .012	Factor 1 (contrast difference): <.0001 Factor 2 (genotype): <.0001 Interaction: .0064 All vs. TIFR> *Acsl* RNAi and *NorpA*	2-Way ANOVA without repeated measures

Experiment/Genotype	**N**	**Penetrance of phenotype**	**Mean**	**SEM**	**P value**	**Type of Analysis**
Behavior, Optomotor response, young flies: TIFR-Gal4> *Luc* RNAi		N/A	.848 to .638	.056 to .012	Significant differences in response at higher contrast levels to lowest contrast level (p values .0075 to <.0001) Significant differences at each contrast level vs. *NorpA* (p values <.0001, except 19.04% contrast p value = .1614).	Tukey's multiple comparisons test
Behavior, Optomotor response, young flies: TIFR-Gal4> *Acsl* RNAi		N/A	.903 to .660	.052 to .017	Factor 1 (contrast difference): <.0001 Factor 2 (genotype): .2083 Interaction: .6724 All vs. TIFR> *Luc* RNAi	2-Way ANOVA without repeated measures
Behavior, Optomotor response, young flies: TIFR-Gal4> *Acsl* RNAi		N/A	.903 to .660	.052 to .017	Significant differences in response at higher contrast levels to lowest contrast level (p values .0481 to <.0001). Significant differences at each contrast level vs. *NorpA* (p values <.0001, except 19.04% contrast p value = .0326).	Tukey's multiple comparisons test

Experiment/Genotype	**N**	**Penetrance of phenotype**	**Mean**	**SEM**	**P value**	**Type of Analysis**
Behavior, Optomotor response, young flies: *NorpA*		N/A	.538 to .505	.022 to .005	Factor 1 (contrast difference): .0008 Factor 2 (genotype): <.0001 Interaction: .0008 All vs. TIFR> *Luc* RNAi	2-Way ANOVA without repeated measures
Behavior, Optomotor response, young flies: *NorpA*		N/A	.538 to .505	.022 to .005	No significant difference in comparison of any contrast level response with any other within genotype (p values >.9999).	Tukey's multiple comparisons test
Behavior, Optomotor response, aged flies: TIFR-Gal4> *Luc* RNAi		N/A	.547 to .800	.015 to .133	Factor 1 (contrast difference): .1685 Factor 2 (genotype): .0003 Interaction: .9025 All vs. TIFR> *Acsl* RNAi and *NorpA*	2-Way ANOVA without repeated measures
Behavior, Optomotor response, aged flies: TIFR-Gal4> *Luc* RNAi		N/A	.547 to .800	.015 to .133	No significant difference found in any comparison.	Tukey's multiple comparisons test
Behavior, Optomotor response, aged flies: TIFR-Gal4> *Acsl* RNAi		N/A	.450 to .680	.009 to .155	Factor 1 (contrast difference): .2107 Factor 2 (genotype): .0714 Interaction: .9536 All vs. TIFR> *Luc* RNAi	2-Way ANOVA without repeated measures

Experiment/Genotype	**N**	**Penetrance of phenotype**	**Mean**	**SEM**	**P value**	**Type of Analysis**
Behavior, Optomotor response, aged flies: TIFR-Gal4> *Acsl* RNAi		N/A	.450 to .680	.009 to .155	No significant difference found in any comparison.	Tukey's multiple comparisons test
Behavior, Optomotor response, aged flies: *NorpA*		N/A	.500 to .550	.003 to .031	Factor 1 (contrast difference): .4332 Factor 2 (genotype): <.0001 Interaction: .6693 All vs. TIFR> *Luc* RNAi	2-Way ANOVA without repeated measures
Behavior, Optomotor response, aged flies: *NorpA*		N/A	.500 to .550	.003 to .031	No significant difference found in any comparison.	Tukey's multiple comparisons test
TIFR-Gal4 is expressed in marginal and Giant Optic Chiasm Glia: TIFR-Gal4> tdTomato	5	N/A	N/A	N/A	N/A	N/A
Mislocalized glia: TIFR-Gal4> *Luc* RNAi	8	0% mislocalized glia	N/A	N/A	N/A	N/A
Mislocalized glia: TIFR-Gal4> *Acsl* RNAi	11	100% mislocalized glia	N/A	N/A	<.0001 vs. TIFR-Gal4> *Luc* RNAi	Chi-Square (Fischer's exact test)
Quantification of Glial nuclei in the distal optic lobe: TIFR-Gal4> *Luc* RNAi	8	N/A	Marginal Glia Layer: 0.6981 Distal Chiasm: 0.5268 Medulla neuropil: 0	Marginal Glia Layer: 0.3906 Distal Chiasm: 0.1626 Medulla neuropil: 0	N/A	N/A

Experiment/Genotype	**N**	**Penetrance of phenotype**	**Mean**	**SEM**	**P value**	**Type of Analysis**
Quantification of Glial nuclei in the distal optic lobe: TIFR-Gal4> *Acsl* RNAi	10	N/A	Marginal Glia Layer: 0.6817 Distal Chiasm: 1.259 Medulla neuropil: 1.371	Marginal Glia Layer: 0.3211 Distal Chiasm: 0.4838 Medulla neuropil: .7326	Marginal Glia Layer: 0.8982 Distal Chiasm: 0.3917 Medulla neuropil: .0001 All vs. TIFR-Gal4> *Luc* RNAi	Multiple t-tests, adjusted for false discovery rate
Quantification of glial nuclei in all 3 layers: TIFR-Gal4> *Luc* RNAi	8	N/A	.4356	.1668	N/A	N/A
Quantification of glial nuclei in all 3 layers: TIFR-Gal4> *Acsl* RNAi	10	N/A	1.309	.4467	.1148 vs. TIFR-Gal4> *Luc* RNAi	Unpaired, , 2 tailed t-test
Quantification of Giant Optic Chiasm nuclei: TIFR-Gal4> *Luc* RNAi	7	N/A	.4754	.2308	N/A	N/A
Quantification of Giant Optic Chiasm nuclei: TIFR-Gal4> *Acsl* RNAi	7	N/A	.7683	.1019	.2681 vs. TIFR-Gal4> *Luc* RNAi	Unpaired, 2 tailed t-test
TIFR+ glia have disorganized processes: TIFR-Gal4> *Luc* RNAi	8	N/A	N/A	N/A	N/A	N/A
TIFR+ glia have disorganized processes: TIFR-Gal4> *Acsl* RNAi	11	N/A	N/A	N/A	N/A	N/A
TIFR+ glial process in the lamina are unchanged: TIFR-Gal4> *Luc* RNAi	8	N/A	43.83	3.459	N/A	N/A
TIFR+ glial process in the lamina are unchanged: TIFR-Gal4> *Acsl* RNAi	11	N/A	58.39	9.991	.2477 vs. TIFR-Gal4> *Luc* RNAi	Unpaired, 2 tailed t-test
Characterization of ectopic neuropil: TIFR-Gal4> *Luc* RNAi	8	0% ectopic neuropil	N/A	N/A	N/A	N/A

Experiment/Genotype	**N**	**Penetrance of phenotype**	**Mean**	**SEM**	**P value**	**Type of Analysis**
Characterization of ectopic neuropil: TIFR-Gal4> *Acsl* RNAi	11	55% ectopic neuropil	N/A	N/A	.0181 vs. TIFR-Gal4> *Luc* RNAi	Chi-square (Fischer's exact test)
BRP density is not changed in TIFR KD adults Lamina: TIFR-Gal4> *Luc* RNAi	8	N/A	116	10.74	N/A	N/A
BRP density is not changed in TIFR KD adults Lamina: TIFR-Gal4> *Acsl* RNAi	11	N/A	100.2	5.281	.1707 vs. TIFR-Gal4> *Luc* RNAi	Unpaired, 2 tailed t-test
BRP density is not changed in TIFR KD adults Medulla: TIFR-Gal4> *Luc* RNAi	7	N/A	120.2	9.79	N/A	N/A
BRP density is not changed in TIFR KD adults Medulla: TIFR-Gal4> *Acsl* RNAi	7	N/A	140.4	9.132	.1577	Unpaired, 2 tailed t-test
ACSL4 rescues the mislocalized glia phenotype: TIFR-Gal4> *Luc* RNAi, *ACSL4*	6	0% mislocalized glia	N/A	N/A	N/A	N/A
ACSL4 rescues the mislocalized glia phenotype: TIFR-Gal4> *Acsl* RNAi, *ACSL4*	14	43% mislocalized glia	N/A	N/A	.1149 vs. TIFR-Gal4> *Luc* RNAi, *ACSL4*	Chi-square (Fischer's exact test)
ACSL4 rescues the mislocalized glia phenotype: TIFR-Gal4> *Acsl* RNAi alone	11	100% mislocalized glia	N/A	N/A	.0029 vs. TIFR-Gal4> *Acsl* RNAi, *ACSL4*	Chi-square (Fischer's exact test)
ACSL4 rescues the ectopic neuropil phenotype: TIFR-Gal4> *Luc* RNAi, *ACSL4*	6	0% ectopic neuropil	N/A	N/A	N/A	N/A
ACSL4 rescues the ectopic neuropil phenotype: TIFR-Gal4> *Acsl* RNAi, *ACSL4*	14	7% ectopic neuropil	N/A	N/A	>.9999 vs. TIFR-Gal4> *Luc* RNAi, *ACSL4*	Chi-square (Fischer's exact test)

Experiment/Genotype	**N**	**Penetrance of phenotype**	**Mean**	**SEM**	**P value**	**Type of Analysis**
ACSL4 rescues the ectopic neuropil phenotype: TIFR-Gal4> *Acsl* RNAi alone	11	55% ectopic neuropil	N/A	N/A	.0213 vs. TIFR-Gal4> *Acsl* RNAi, *ACSL4*	Chi-square (Fischer's exact test)
Quantification of 3IL marginal glia nuclei: TIFR-Gal4> *Luc* RNAi	8	N/A	.4441	.2007	N/A	N/A
Quantification of 3IL marginal glia nuclei: TIFR-Gal4> *Acsl* RNAi	13	N/A	.3692	.09645	.7102 vs. TIFR> *Luc* RNAi	Unpaired, 2 tailed t-test
Glial processes are abnormal during 3IL: TIFR-Gal4> *Luc* RNAi	8	N/A	N/A	N/A	N/A	N/A
Glial processes are abnormal during 3IL: TIFR-Gal4> *Acsl* RNAi	13	N/A	N/A	N/A	N/A	N/A
P50 quantification of Glial nuclei in the distal optic lobe: TIFR-Gal4> *Luc* RNAi	8	N/A	Marginal Glia Layer: 0.4839 Distal Chiasm: 1.008 Medulla neuropil: 0	Marginal Glia Layer: .04411 Distal Chiasm: 0.2272 Medulla neuropil: 0	N/A	N/A
P50 quantification of Glial nuclei in the distal optic lobe: TIFR-Gal4> *Acsl* RNAi	9	N/A	Marginal Glia Layer: 0.7864 Distal Chiasm: 1.93 Medulla neuropil: 1.494	Marginal Glia Layer: 0.1587 Distal Chiasm: 0.4395 Medulla neuropil: 0.5513	Marginal Glia Layer: 0.2483 Distal Chiasm: 0.006850 Medulla neuropil: 0.002601 All vs. TIFR-Gal4> *Luc* RNAi	Multiple t-tests, adjusted for false discovery rate
P50 quantification of Glial nuclei in all 3 layers: TIFR-Gal4> *Luc* RNAi	8	N/A	0.3989	.0525	N/A	N/A

Experiment/Genotype	**N**	**Penetrance of phenotype**	**Mean**	**SEM**	**P value**	**Type of Analysis**
P50 quantification of Glial nuclei in all 3 layers: TIFR-Gal4> *Acsl* RNAi	9	N/A	1.052	.2522	.0302 vs. TIFR-Gal4> *Luc* RNAi	Unpaired, 2 tailed t-test
P50 mislocalized glia are located throughout the medulla: TIFR-Gal4> *Luc* RNAi	8	N/A	N/A	N/A	N/A	N/A
P50 mislocalized glia are located throughout the medulla: TIFR-Gal4> *Acsl* RNAi	9	N/A	N/A	N/A	N/A	N/A
P50 TIFR+ glia are closely associated with R7/R8 processes: TIFR-Gal4> *Luc* RNAi	8	N/A	N/A	N/A	N/A	N/A
P50 TIFR+ glia are closely associated with R7/R8 processes: TIFR-Gal4> *Acsl* RNAi	9	N/A	N/A	N/A	N/A	N/A
Developmental Expression of RNAi: Eclosion: *repo*> *Luc* RNAi ERG. 'On transient' mean.	15	N/A	1.133	0.1563	N/A	
Developmental Expression of RNAi: Eclosion: *repo*> *Luc* RNAi ERG. 'Off transient' mean.	14	N/A	2.379	0.406	N/A	N/A
Developmental Expression of RNAi: Eclosion: *repo*> *Luc* RNAi ERG. Loss of 'on transient'.	15	0% loss of 'on transient'	N/A	N/A	N/A	N/A
Developmental Expression of RNAi: Eclosion: *repo*> *Luc* RNAi ERG. Loss of 'on' and 'off' transients.	14	0% loss of both transients	N/A	N/A	N/A	N/A

Experiment/Genotype	**N**	**Penetrance of phenotype**	**Mean**	**SEM**	**P value**	**Type of Analysis**
Developmental Expression of RNAi: Eclosion: *repo*> *Acsl* RNAi ERG. 'On transient' mean.	21	N/A	0.381	0.1073	0.0002 vs. *repo*> *Luc* RNAi	Unpaired, 2 tailed t-test
Developmental Expression of RNAi: Eclosion: *repo*> *Acsl* RNAi ERG. 'Off transient' mean.	20	N/A	1.79	0.3453	0.2791 vs. *repo*> *Luc* RNAi	Unpaired, 2 tailed t-test
Developmental Expression of RNAi: Eclosion: *repo*> *Acsl* RNAi ERG. Loss of 'on transient'.	21	52% loss of 'on transient'	N/A	N/A	0.0008 vs. *repo*> *Luc* RNAi	Chi-square (Fischer's exact test)
Developmental Expression of RNAi: Eclosion: *repo*> *Acsl* RNAi ERG. Loss of 'on' and 'off' transients.	20	0% loss of both transients	N/A	N/A	>0.9999 vs. *repo*> *Luc* RNAi	Chi-square (Fischer's exact test)
Developmental Expression of RNAi: 10 Day: *repo*> *Luc* RNAi ERG. 'On transient' mean.	9	N/A	1.267	0.1972	N/A	N/A
Developmental Expression of RNAi: 10 Day: *repo*> *Luc* RNAi ERG. 'Off transient' mean.	9	N/A	3.9	0.5367	N/A	N/A
Developmental Expression of RNAi: 10 Day: *repo*> *Luc* RNAi ERG. Loss of 'on transient'.	9	0% loss of 'on transient'	N/A	N/A	N/A	N/A
Developmental Expression of RNAi: 10 Day: *repo*> *Luc* RNAi ERG. Loss of 'on' and 'off' transients.	9	0% loss of both transients	N/A	N/A	N/A	N/A
Developmental Expression of RNAi: 10 Day: *repo*> *Acsl* RNAi ERG. 'On transient' mean.	8	N/A	0.125	0.125	0.0003 vs. *repo*> *Luc* RNAi	Unpaired, 2 tailed t-test

Experiment/Genotype	**N**	**Penetrance of phenotype**	**Mean**	**SEM**	**P value**	**Type of Analysis**
Developmental Expression of RNAi: 10 Day: *repo*> *Acsl* RNAi ERG. 'Off transient' mean.	8	N/A	0.575	0.4057	0.0002 vs. *repo*> *Luc* RNAi	Unpaired, 2 tailed t-test
Developmental Expression of RNAi: 10 Day: *repo*> *Acsl* RNAi ERG. Loss of 'on transient'.	8	88% loss of 'on transient'	N/A	N/A	0.0003 vs. *repo*> *Luc* RNAi	Chi-square (Fischer's exact test)
Developmental Expression of RNAi: 10 Day: *repo*> *Acsl* RNAi ERG. Loss of 'on' and 'off' transients.	8	75% loss of both transients	N/A	N/A	0.0023 vs. *repo*> *Luc* RNAi	Chi-square (Fischer's exact test)
Developmental Expression of RNAi: Eclosion: *repo*-Gal4> *Luc* RNAi BRP Density	8	N/A	92.62	7.682	N/A	N/A
Developmental Expression of RNAi: Eclosion: *repo*-Gal4> *Acsl* RNAi BRP Density	9	N/A	70.2	6.392	.0390 vs. *repo*-Gal4> *Luc* RNAi	Unpaired, 2 tailed t-test
Developmental Expression of RNAi: 10 day: *repo*-Gal4> *Luc* RNAi BRP Density	6	N/A	96.59	9.13	N/A	N/A
Developmental Expression of RNAi: 10 day: *repo*-Gal4> *Acsl* RNAi BRP Density	7	N/A	107.7	5.373	.2995 vs. *repo*-Gal4> *Luc* RNAi	Unpaired, 2 tailed t-test
Developmental Expression of RNAi: Eclosion: *repo*-Gal4> *Luc* RNAi mislocalized glia	8	0% mislocalized glia	N/A	N/A	N/A	N/A
Developmental Expression of RNAi: Eclosion: *repo*-Gal4> *Acsl* RNAi mislocalized glia	9	0% mislocalized glia	N/A	N/A	>.9999 vs *repo*-Gal4> *Luc* RNAi	Chi-square (Fischer's exact test)

Experiment/Genotype	**N**	**Penetrance of phenotype**	**Mean**	**SEM**	**P value**	**Type of Analysis**
Developmental Expression of RNAi: 10 day: *repo*-Gal4> *Luc* RNAi mislocalized glia	6	0% mislocalized glia	N/A	N/A	N/A	N/A
Developmental Expression of RNAi: 10 day: *repo*-Gal4> *Acsl* RNAi mislocalized glia	7	57% mislocalized glia	N/A	N/A	.0261 vs. *repo*-Gal4> *Luc* RNAi	Chi-square
Adult Expression of RNAi: Eclosion: *repo*-Gal4> *Luc* RNAi ERG. 'On transient' mean.	10	N/A	1.24	0.1887	N/A	N/A
Adult Expression of RNAi: Eclosion: *repo*-Gal4> *Luc* RNAi ERG. 'Off transient' mean.	10	N/A	3.1	0.6939	N/A	N/A
Adult Expression of RNAi: Eclosion: *repo*-Gal4> *Luc* RNAi ERG. Loss of 'on transient'.	10	0% loss of 'on transient'	N/A	N/A	N/A	N/A
Adult Expression of RNAi: Eclosion: *repo*-Gal4> *Luc* RNAi ERG. Loss of 'on' and 'off' transients.	10	0% loss of both transients	N/A	N/A	N/A	N/A
Adult Expression of RNAi: Eclosion: *repo*-Gal4> *Acsl* RNAi ERG. 'On transient' mean.	16	N/A	1.25	0.1571	0.9682 vs. *repo*> *Luc* RNAi	Unpaired, 2 tailed t-test
Adult Expression of RNAi: Eclosion: *repo*-Gal4> *Acsl* RNAi ERG. 'Off transient' mean.	15	N/A	3.693	0.4682	0.4684 vs. *repo*> *Luc* RNAi	Unpaired, 2 tailed t-test
Adult Expression of RNAi: Eclosion: *repo*-Gal4> *Acsl* RNAi ERG. Loss of 'on transient'.	16	0% loss of 'on transient'	N/A	N/A	>0.9999 vs. *repo*> *Luc* RNAi	Chi-square (Fischer's exact test)

Experiment/Genotype	**N**	**Penetrance of phenotype**	**Mean**	**SEM**	**P value**	**Type of Analysis**
Adult Expression of RNAi: Eclosion: *repo*-Gal4> *Acsl* RNAi ERG. Loss of 'on' and 'off' transients.	15	0% loss of both transients	N/A	N/A	>0.9999 vs. *repo*> *Luc* RNAi	Chi-square (Fischer's exact test)
Adult Expression of RNAi: 10 Day: *repo*-Gal4> *Luc* RNAi ERG. 'On transient' mean.	11	N/A	1.391	0.2078	N/A	N/A
Adult Expression of RNAi: 10 Day: *repo*-Gal4> *Luc* RNAi ERG. 'Off transient' mean.	11	N/A	3.218	0.4319	N/A	N/A
Adult Expression of RNAi: 10 Day: *repo*-Gal4> *Luc* RNAi ERG. Loss of 'on transient'.	11	0% loss of 'on transient'	N/A	N/A	N/A	N/A
Adult Expression of RNAi: 10 Day: *repo*-Gal4> *Luc* RNAi ERG. Loss of 'on' and 'off' transients.	11	0% loss of both transients	N/A	N/A	N/A	N/A
Adult Expression of RNAi: 10 Day: *repo*-Gal4> *Acsl* RNAi ERG. 'On transient' mean.	18	N/A	1.3	0.1901	0.7586 vs. *repo*> *Luc* RNAi	Unpaired, 2 tailed t-test
Adult Expression of RNAi: Eclosion: *repo*-Gal4> *Acsl* RNAi ERG. 'Off transient' mean.	18	N/A	2.6	0.3711	0.2561 vs. *repo*> *Luc* RNAi	Unpaired, 2 tailed t-test
Adult Expression of RNAi: 10 Day: *repo*-Gal4> *Acsl* RNAi ERG. Loss of 'on transient'.	18	0% loss of 'on transient'	N/A	N/A	>0.9999 vs. *repo*> *Luc* RNAi	Chi-square (Fischer's exact test)
Adult Expression of RNAi: 10 Day: *repo*-Gal4> *Acsl* RNAi ERG. Loss of 'on' and 'off' transients.	18	0% loss of both transients	N/A	N/A	>0.9999 vs. *repo*> *Luc* RNAi	Chi-square (Fischer's exact test)

Experiment/Genotype	N	Penetrance of phenotype	Mean	SEM	P value	Type of Analysis
Adult Expression of RNAi: Eclosion: *repo*-Gal4> *Luc* RNAi BRP density	8	N/A	87.22	8.968	N/A	N/A
Adult Expression of RNAi: Eclosion: *repo*-Gal4> *Acsl* RNAi BRP density	12	N/A	83.13	4.374	.6556 vs. *repo*-Gal4> *Luc* RNAi	Unpaired, 2 tailed t-test
Adult Expression of RNAi: 10 day: *repo*-Gal4> *Luc* RNAi BRP density	7	N/A	108.1	11.58	N/A	N/A
Adult Expression of RNAi: 10 day: *repo*-Gal4> *Acsl* RNAi BRP density	6	N/A	91.03	8.164	.2680 vs *repo*-Gal4> *Luc* RNAi	Unpaired, 2 tailed t-test
Adult Expression of RNAi: Eclosion: *repo*-Gal4> *Luc* RNAi mislocalized glia	8	0% mislocalized glia	N/A	N/A	N/A	N/A
Adult Expression of RNAi: Eclosion: *repo*-Gal4> *Acsl* RNAi mislocalized glia	12	0% mislocalized glia	N/A	N/A	>.9999 vs *repo*-Gal4> *Luc* RNAi	Chi-square (Fischer's exact test)
Adult Expression of RNAi: 10 day: *repo*-Gal4> *Luc* RNAi mislocalized glia	7	0% mislocalized glia	N/A	N/A	N/A	N/A
Adult Expression of RNAi: 10 day: *repo*-Gal4> *Acsl* RNAi mislocalized glia	6	0% mislocalized glia	N/A	N/A	>.9999 vs *repo*-Gal4> *Luc* RNAi	Chi-square (Fischer's exact test)
ACSL4 colocalizes with mammalian glial markers: Wild type mouse, no pre-absorption	4	N/A	N/A	N/A	N/A	N/A
ACSL4 colocalizes with mammalian glial markers: Wild type mouse, with pre-absorption	2	N/A	N/A	N/A	N/A	N/A

APPENDIX B. ERG TRACES

Genotype: C.S. wild type

Phenotype: with transient

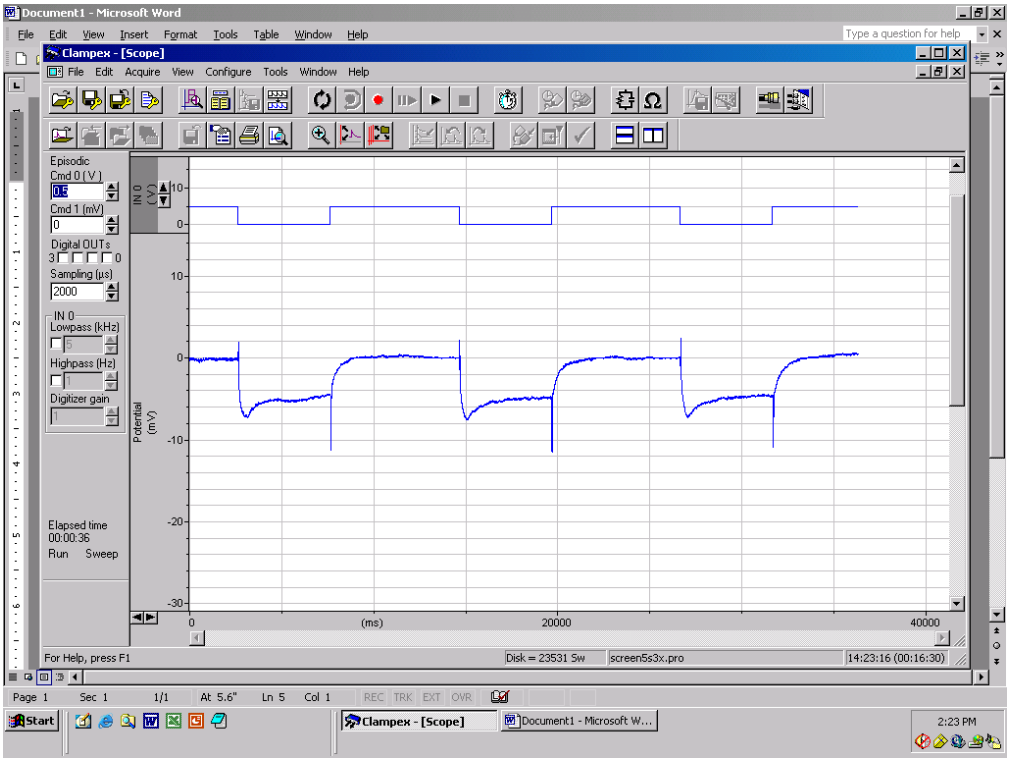

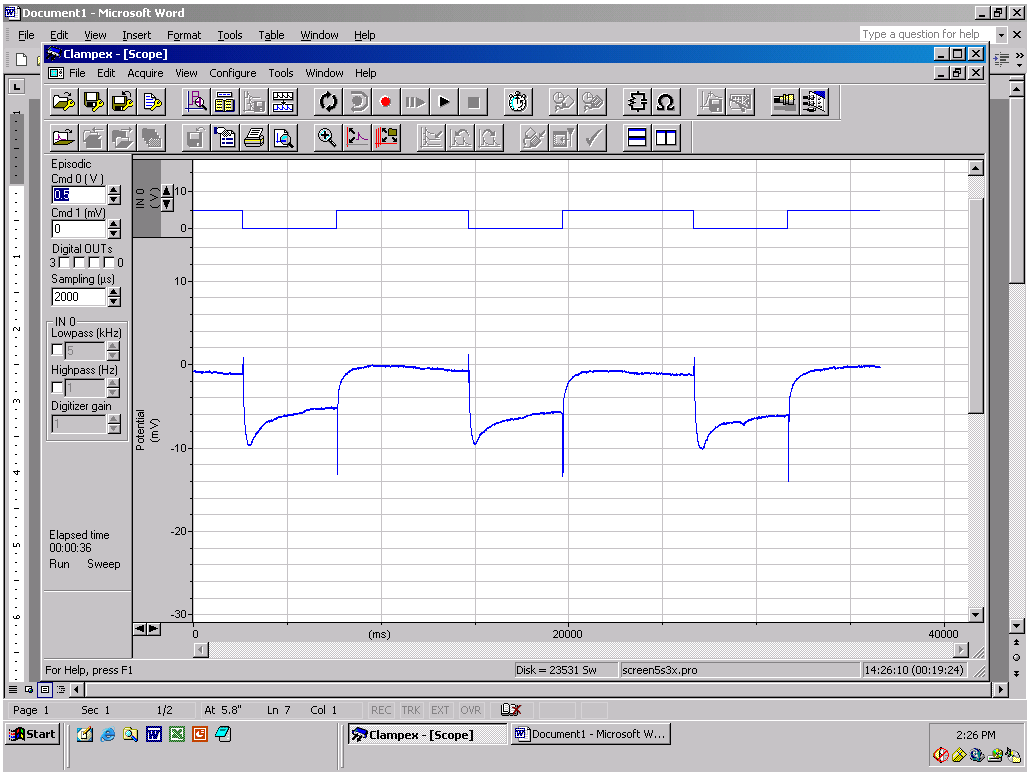
Document1 - Microsoft Word
Clampex - [Scope]
Episodic
Cmd 0 (V)
0.5
Cmd 1 (mV)
0
Digital OUTs
Sampling (µs)
2000
IN 0
Lowpass (kHz)
Highpass (Hz)
Digitizer gain
Elapsed time
00:00:36
Run Sweep
Potential (mV)
(ms)
For Help, press F1
Disk = 23531 Sw
screen5s3x.pro
14:26:10 (00:19:24)
2:26 PM

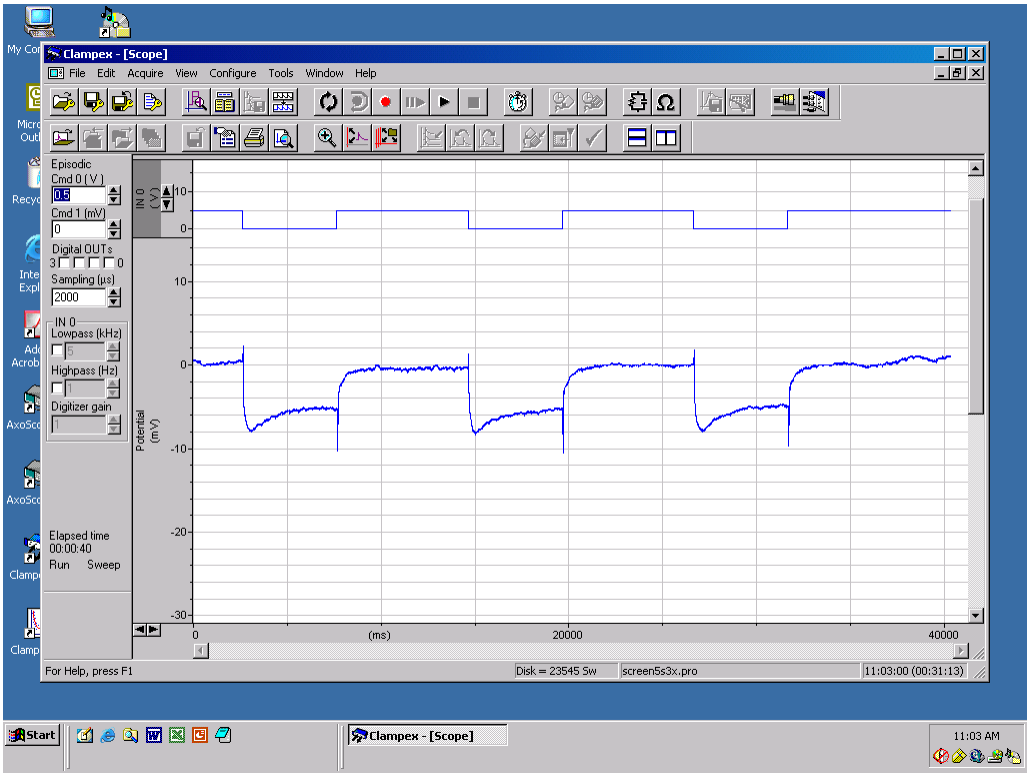
Clampex - [Scope]
Episodic
Cmd 0 (V)
0.5
Cmd 1 (mV)
0
Digital OUTs
Sampling (µs)
2000
IN 0
Lowpass (kHz)
Highpass (Hz)
Digitizer gain
Elapsed time
00:00:40
Run Sweep
Potential (mV)
(ms)
For Help, press F1
Disk = 23545 Sw
screen5s3x.pro
11:03:00 (00:31:13)
11:03 AM

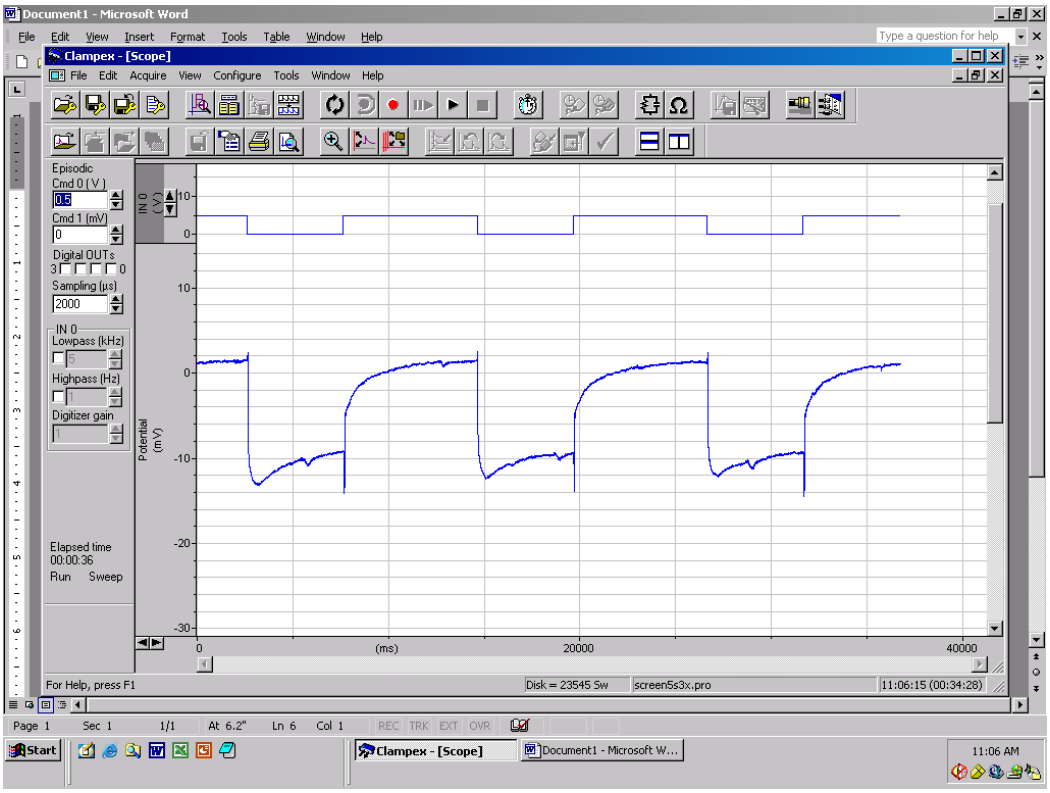
Document1 - Microsoft Word
Clampex - [Scope]
Episodic
Cmd 0 (V)
Cmd 1 (mV)
Digital OUTs
Sampling (µs)
2000
IN 0
Lowpass (kHz)
Highpass (Hz)
Digitizer gain
Elapsed time
00:00:36
Run Sweep
Potential (mV)
(ms)
For Help, press F1
Disk = 23545 Sw
screen5s3x.pro
11:06:15 (00:34:28)
Page 1 Sec 1 1/1 At 6.2" Ln 6 Col 1
Start
11:06 AM

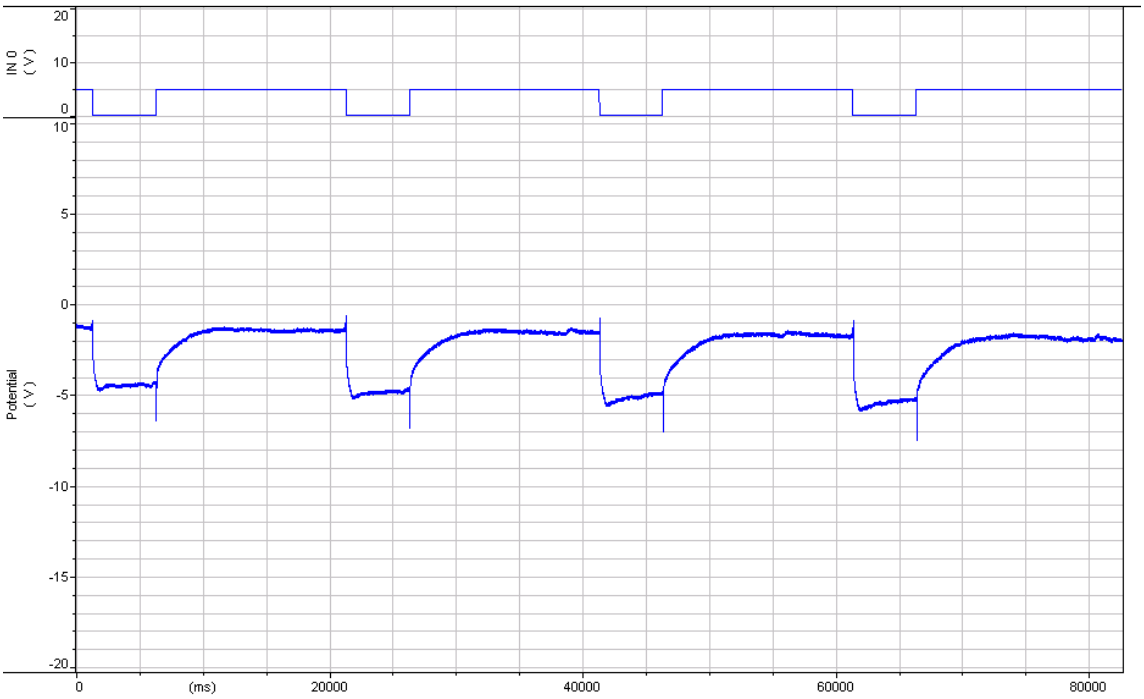
IN 0 (V)
Potential (V)
(ms)
0
20000
40000
60000
80000

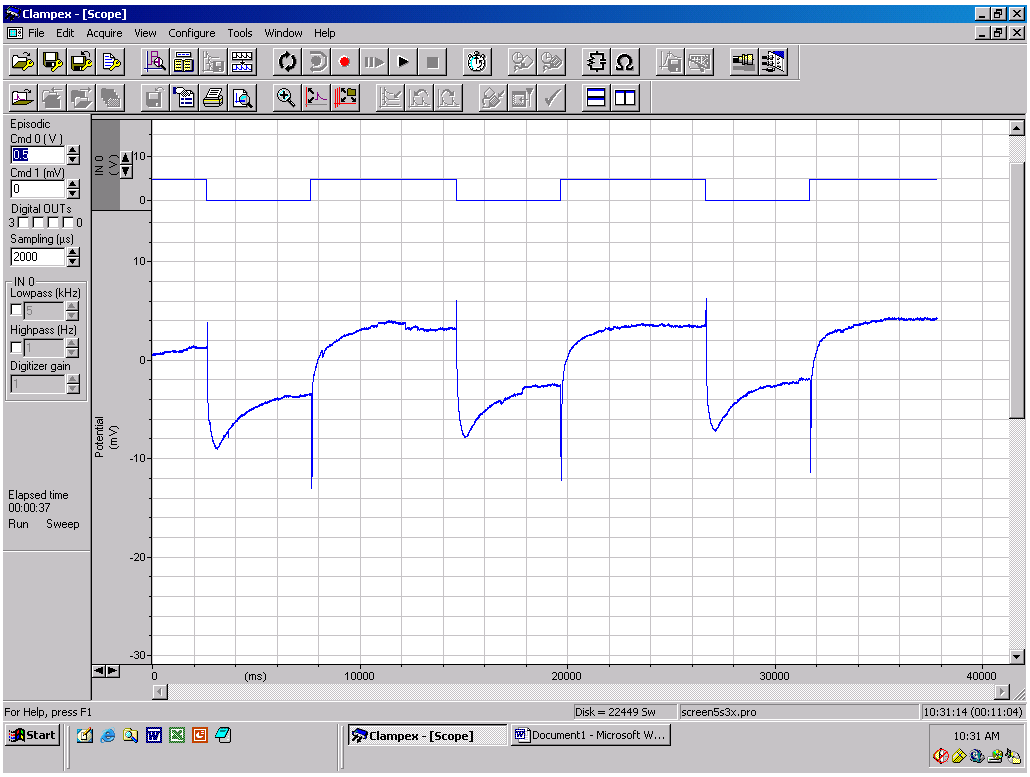
Clampex - [Scope]
File Edit Acquire View Configure Tools Window Help
Episodic
Cmd 0 (V)
Cmd 1 (mV)
Digital OUTs
Sampling (µs)
2000
IN 0
Lowpass (kHz)
Highpass (Hz)
Digitizer gain
Elapsed time
00:00:37
Run Sweep
IN 0 (V)
Potential (mV)
10
0
-10
-20
-30
0
(ms)
10000
20000
30000
40000
For Help, press F1
Disk = 22449 Sw
screen5s3x.pro
10:31:14 (00:11:04)
Start
Clampex - [Scope]
Document1 - Microsoft W...
10:31 AM

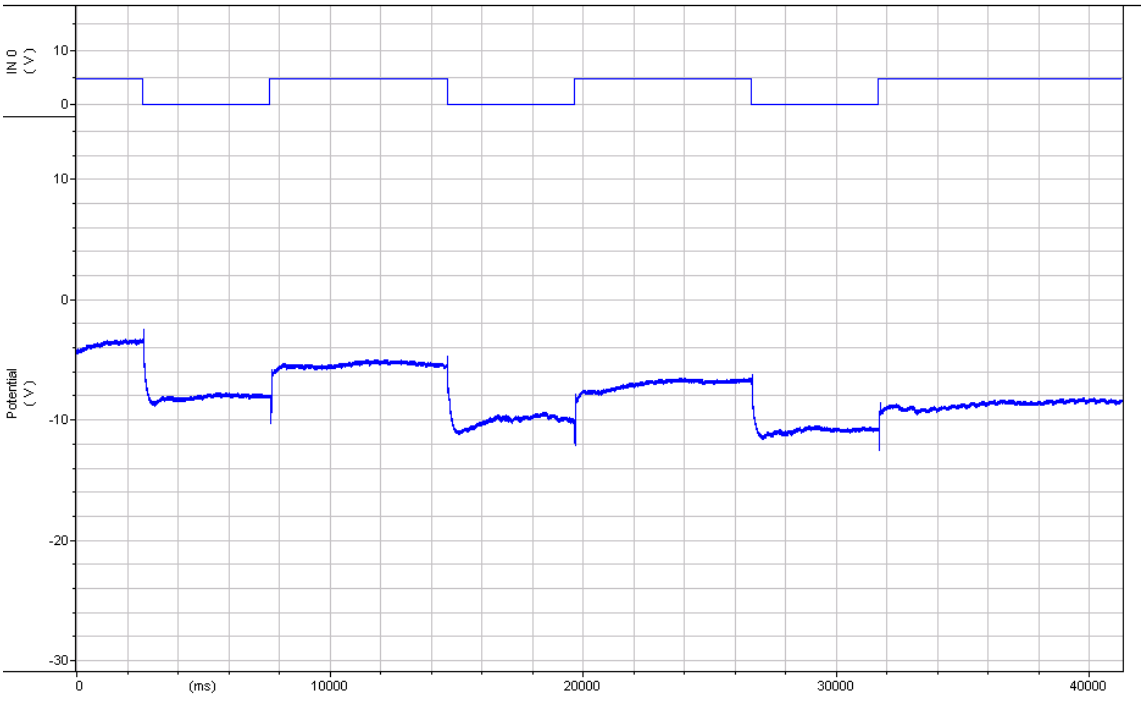
IN 0 (V)
10
0
Potential (V)
10
0
-10
-20
-30
0
(ms)
10000
20000
30000
40000

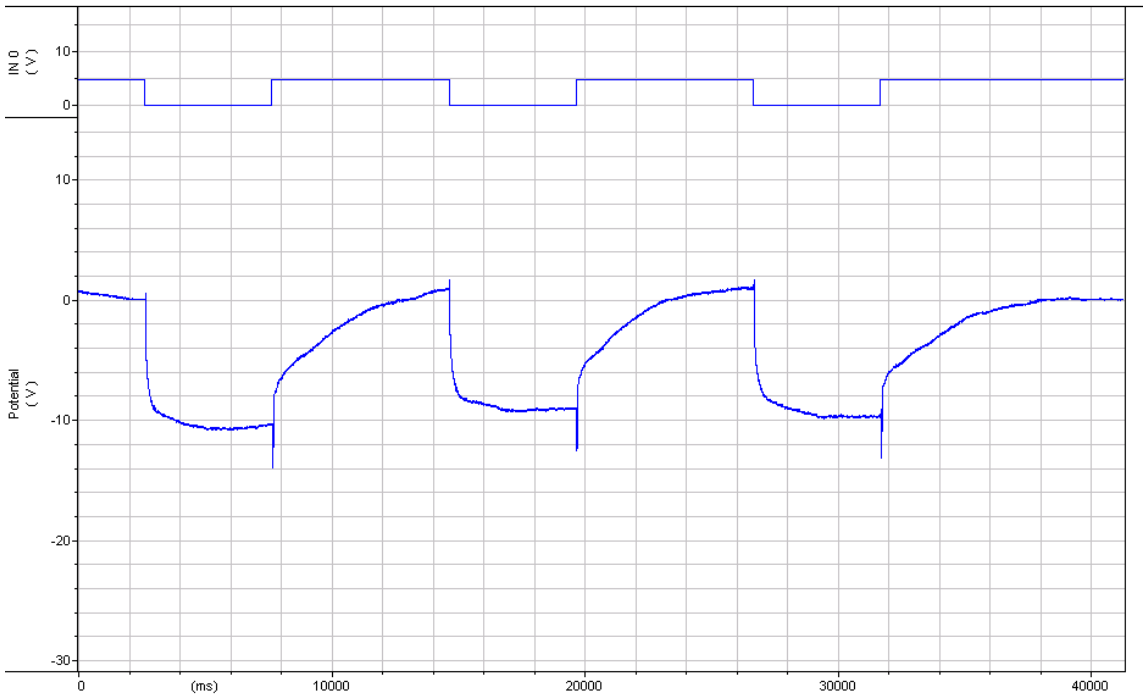
IN 0
(V)
10
0
10
0
-10
-20
-30
Potential
(V)
0
(ms)
10000
20000
30000
40000

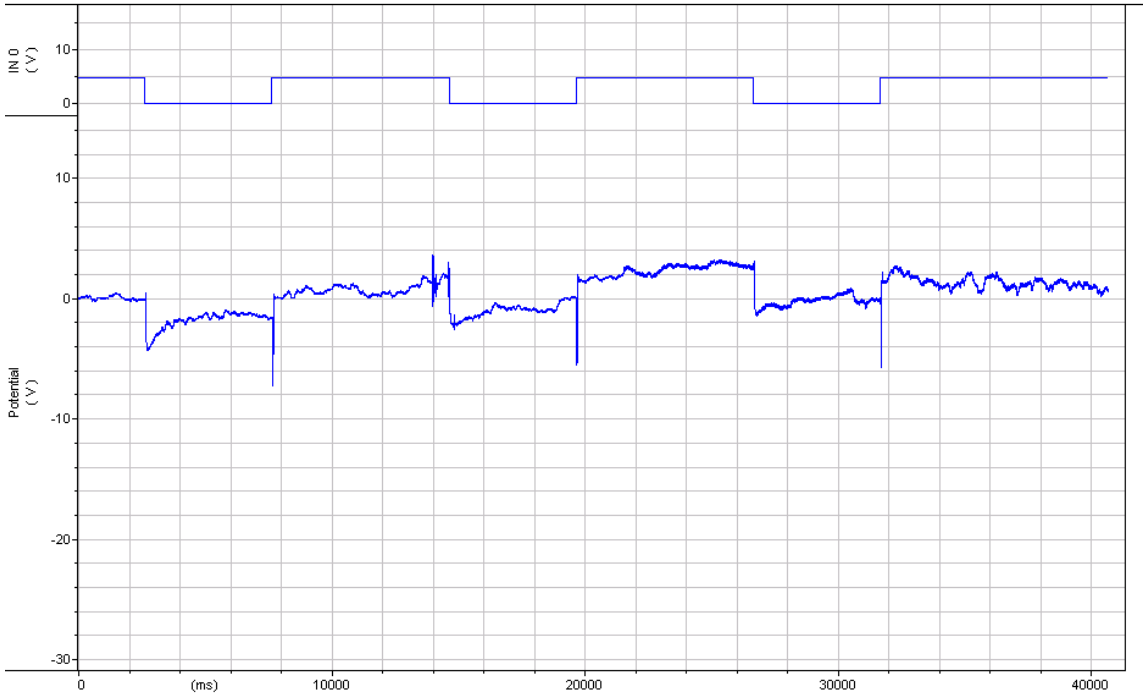
IN 0
(V)
10
0
10
0
-10
-20
-30
Potential
(V)
0
(ms)
10000
20000
30000
40000

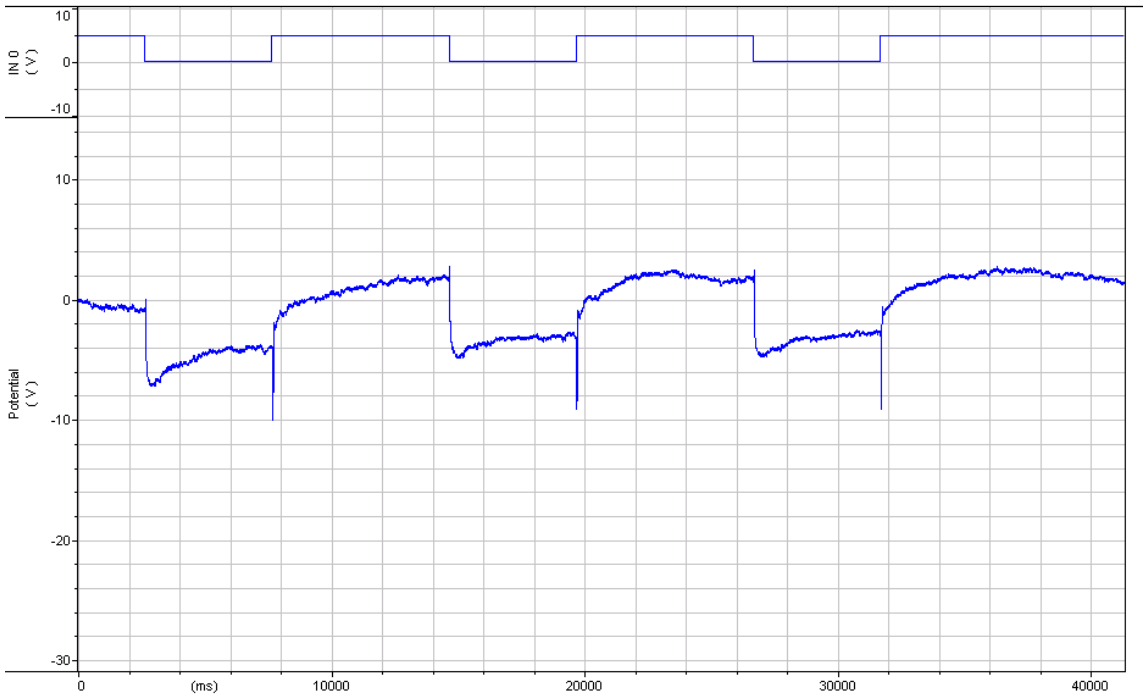
IN 0
(V)
10
0
-10
10
0
-10
-20
-30
Potential
(V)
0
(ms)
10000
20000
30000
40000

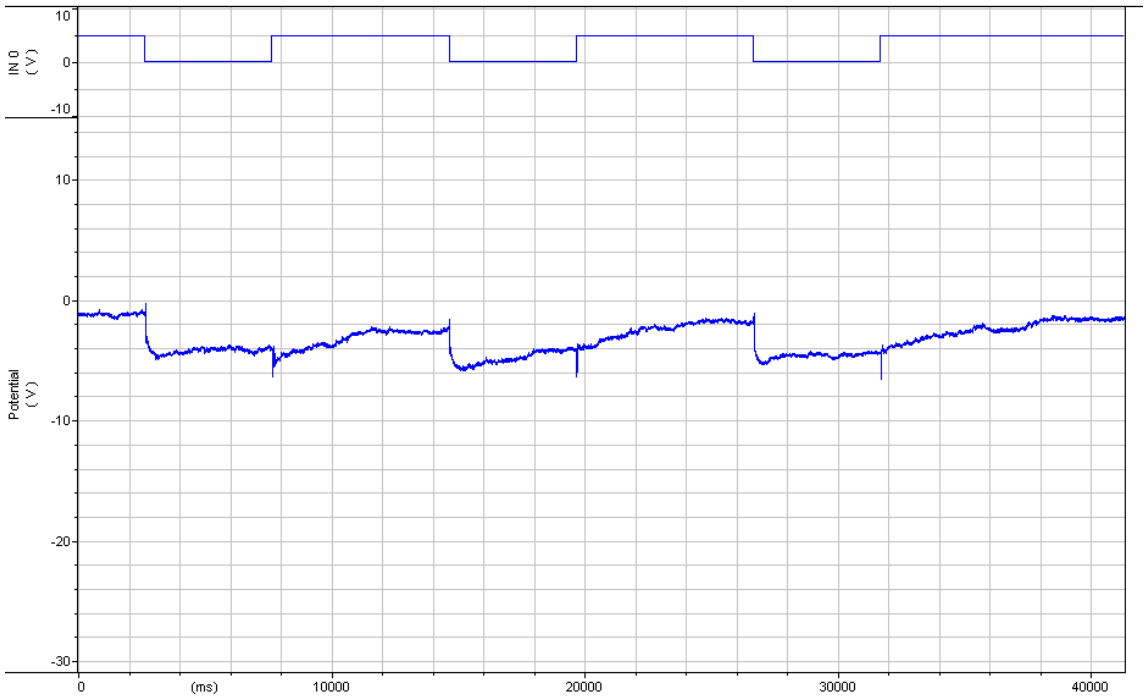
IN 0
(V)
10
0
-10
10
0
-10
-20
-30
Potential
(V)
0
(ms)
10000
20000
30000
40000

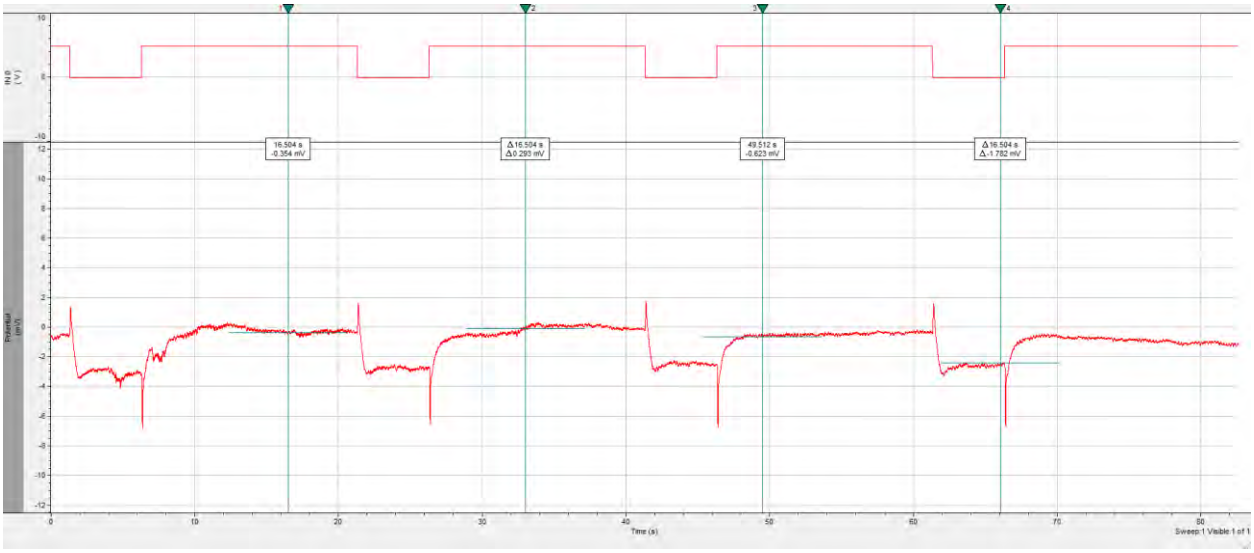

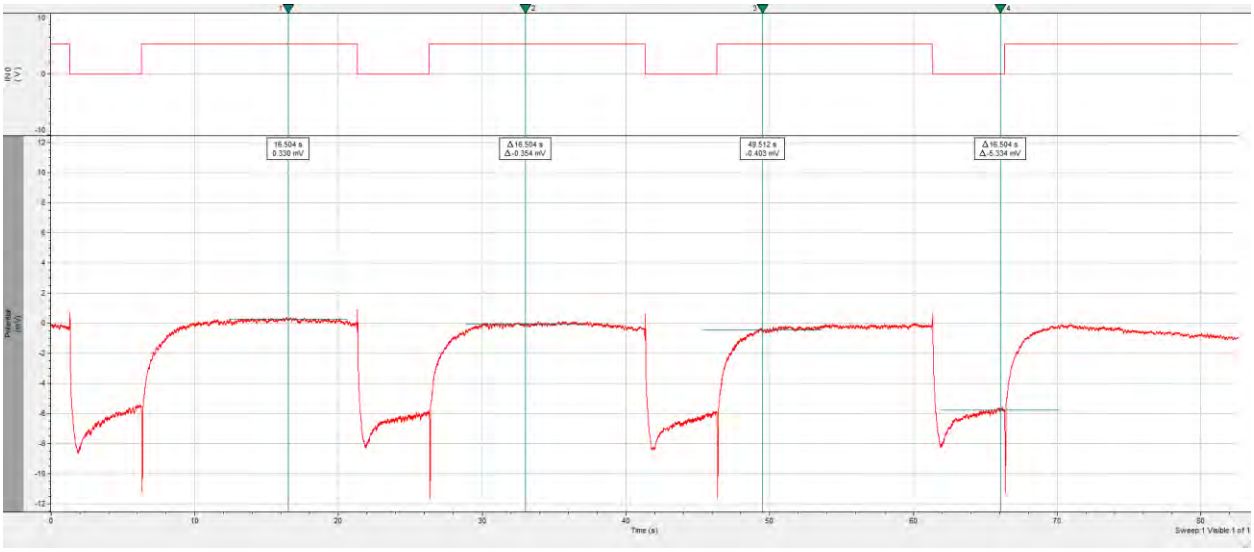

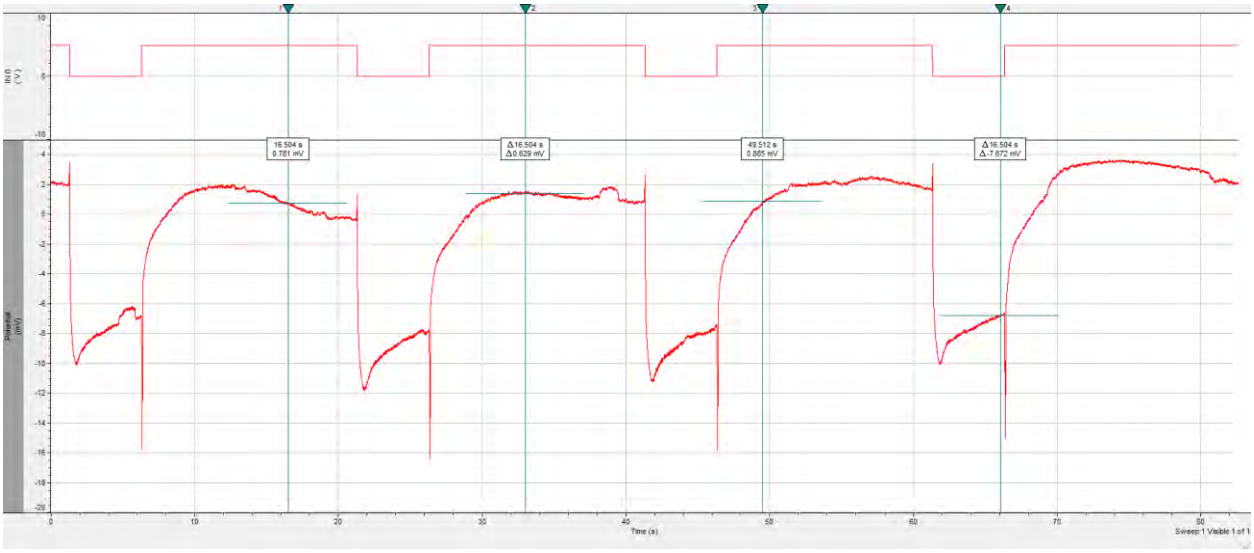
16.504 s
0.781 mV
Δ16.504 s
Δ0.629 mV
49.512 s
0.885 mV
Δ16.504 s
Δ-7.672 mV
Time (s)

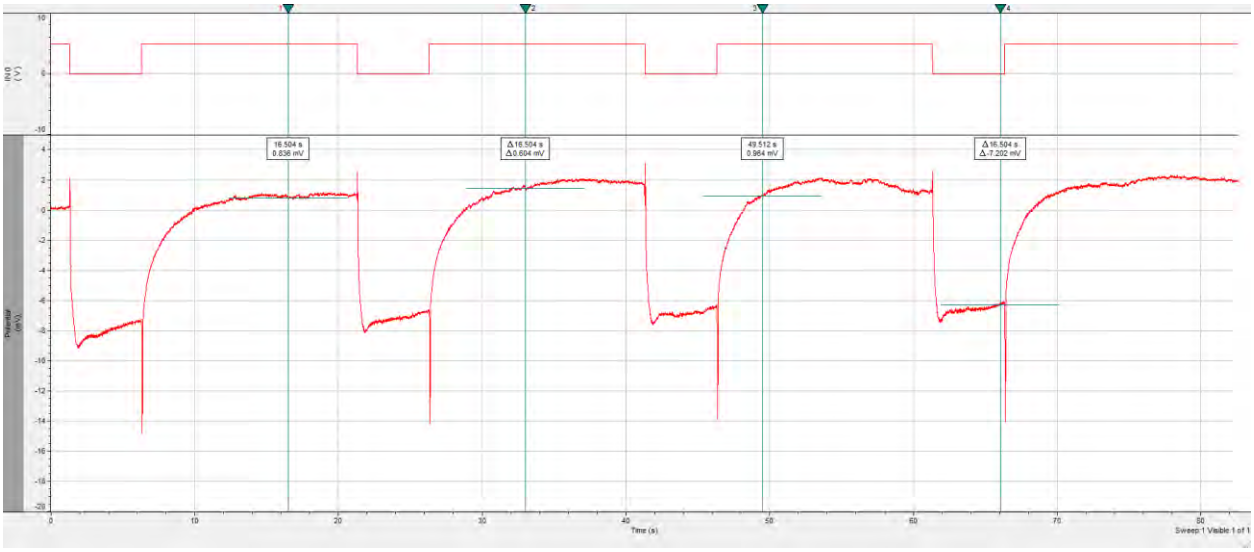
16.504 s
0.836 mV
Δ16.504 s
Δ0.604 mV
49.512 s
0.964 mV
Δ16.504 s
Δ-7.202 mV
Time (s)

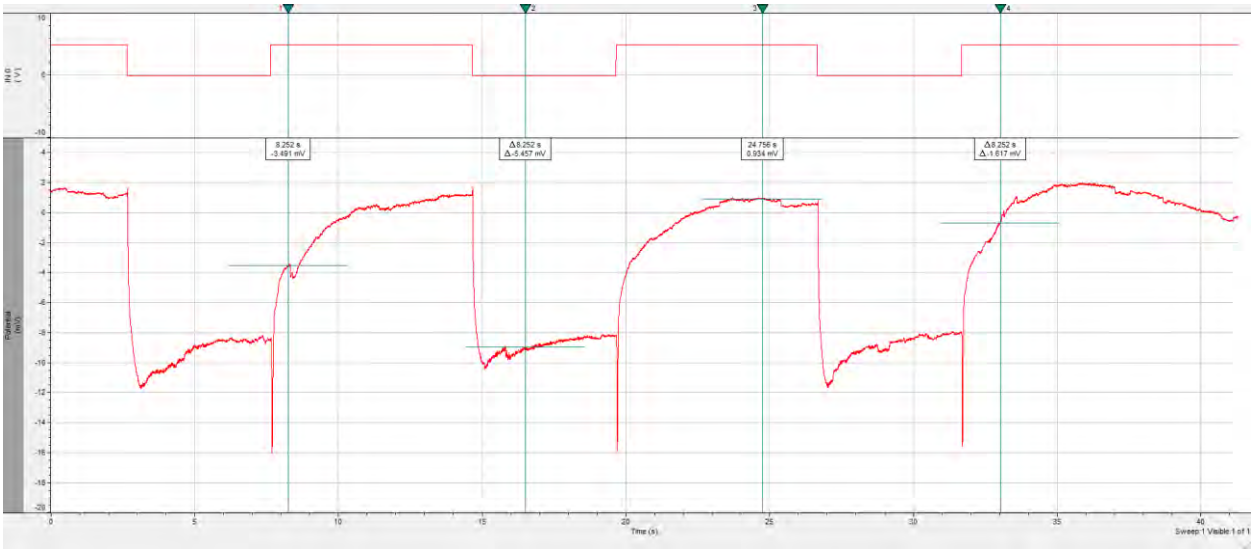
8.252 s
-0.491 mV
Δ8.252 s
Δ-5.457 mV
24.756 s
0.934 mV
Δ8.252 s
Δ-1.617 mV
Time (s)

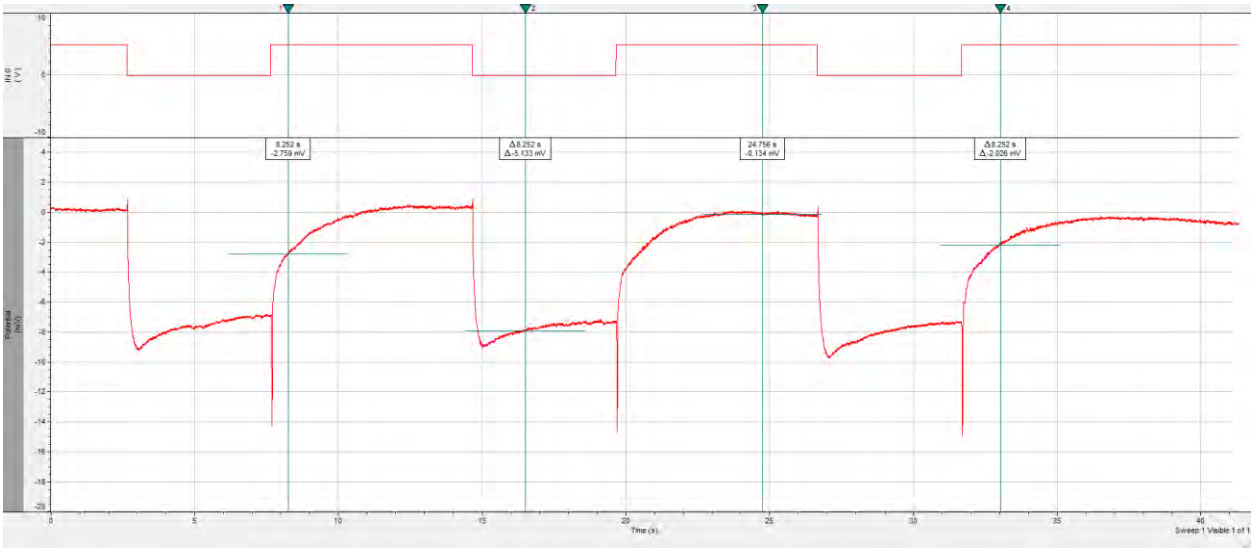
8.252 s
-2.759 mV
Δ8.252 s
Δ-5.133 mV
24.756 s
-0.134 mV
Δ8.252 s
Δ-2.926 mV
Time (s)

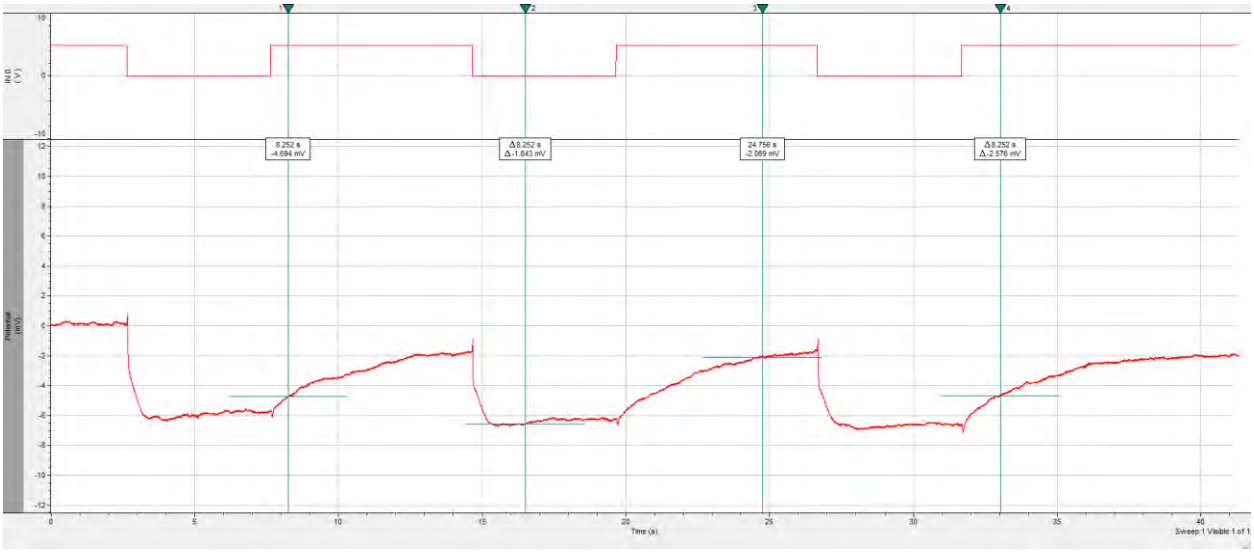
8.252 s
-4.694 mV
Δ8.252 s
Δ-1.843 mV
24.756 s
-2.069 mV
Δ8.252 s
Δ-2.576 mV
Time (s)

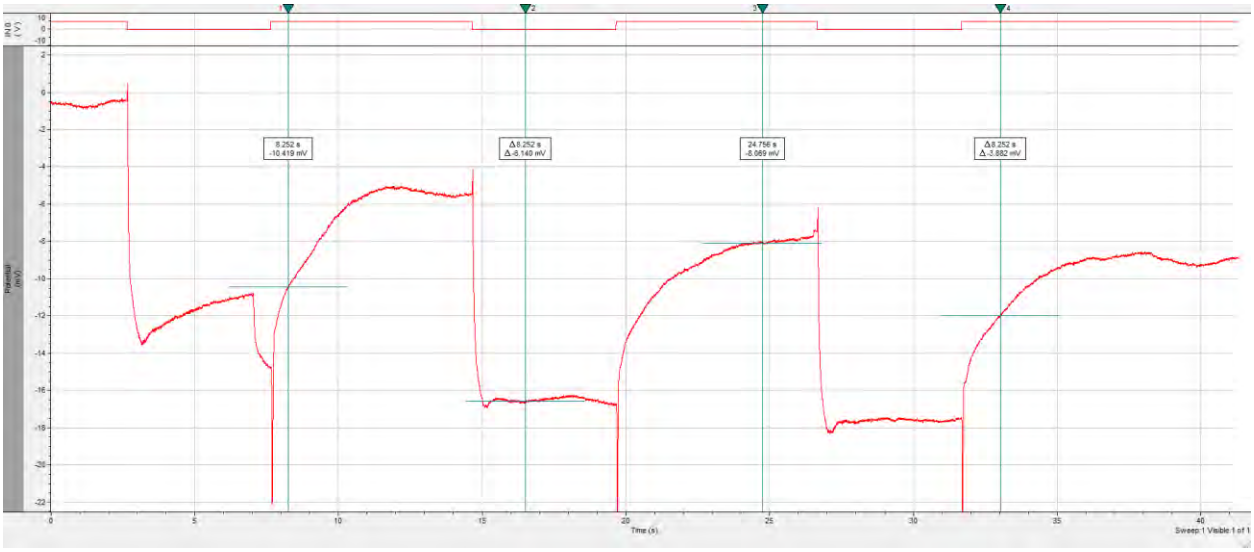
8.252 s
-10.419 mV
Δ8.252 s
Δ-8.140 mV
24.756 s
-8.069 mV
Δ8.252 s
Δ-3.882 mV
Time (s)

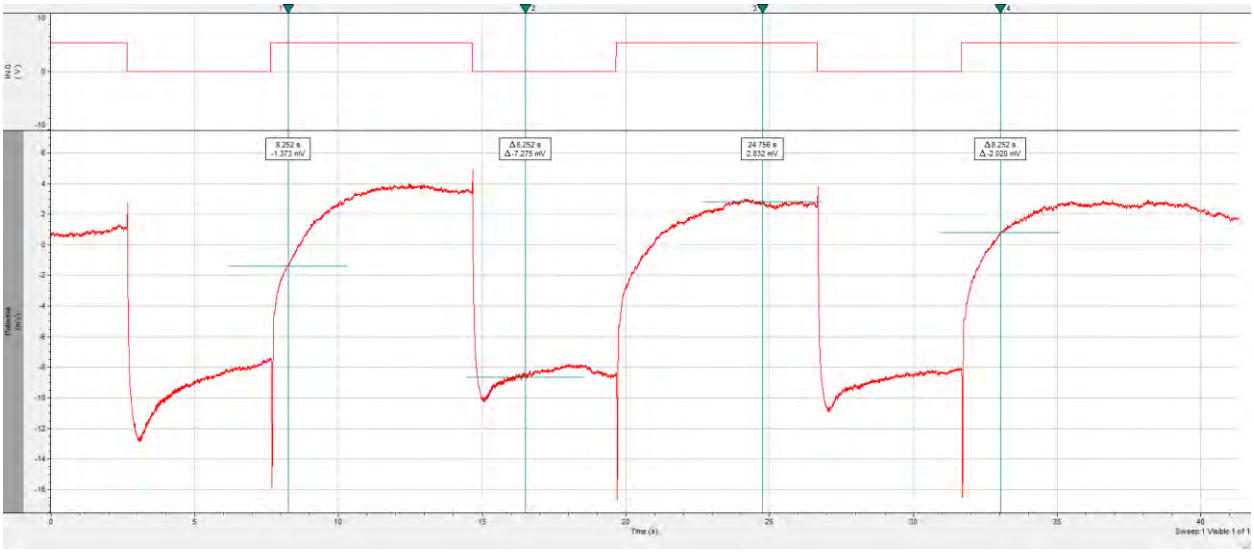
8.252 s
-1.373 mV
Δ8.252 s
Δ-7.275 mV
24.756 s
2.832 mV
Δ8.252 s
Δ-2.020 mV
Time (s)

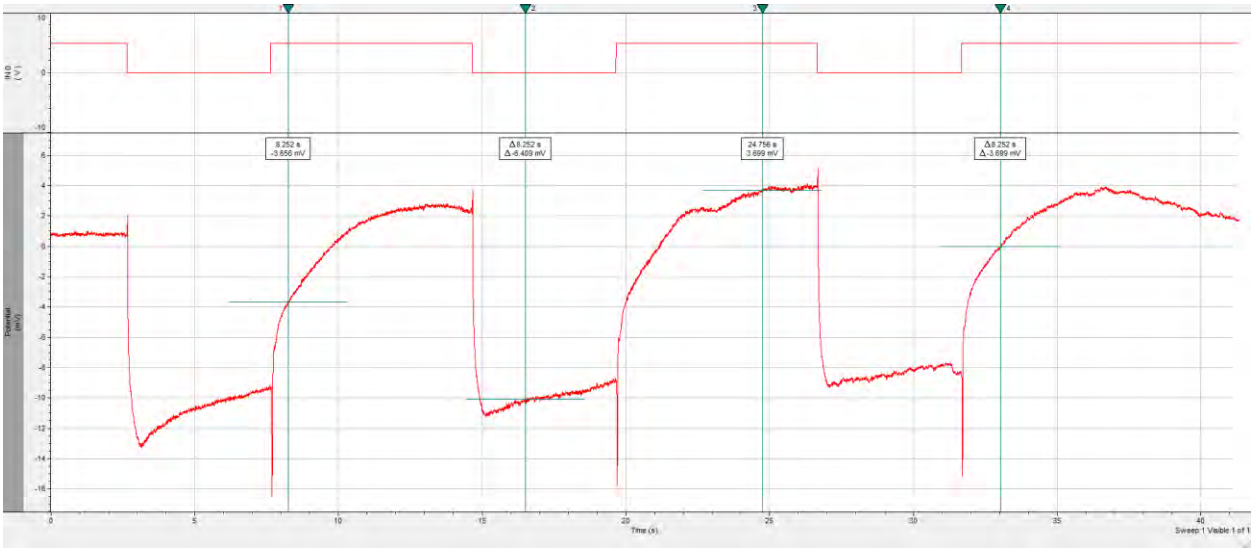
8.252 s
-3.855 mV
Δ8.252 s
Δ-6.409 mV
24.756 s
3.699 mV
Δ8.252 s
Δ-3.699 mV
Time (s)

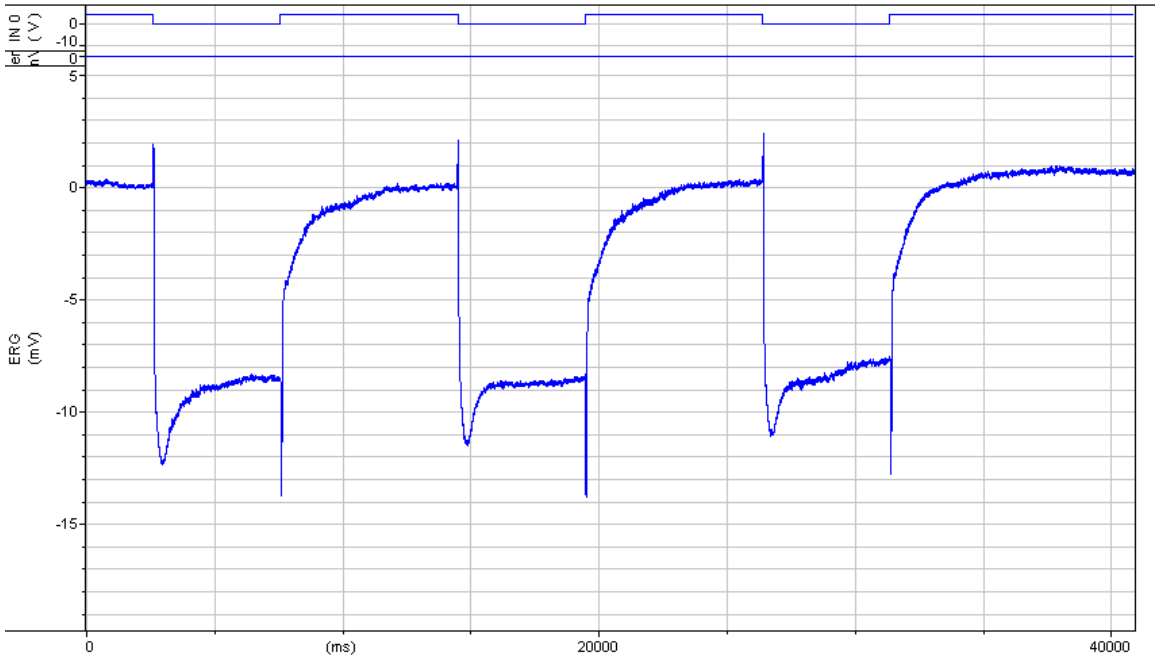
ef IN 0
n\ (V)
0
-10
0
5
0
-5
-10
-15
ERG
(mV)
0
(ms)
20000
40000

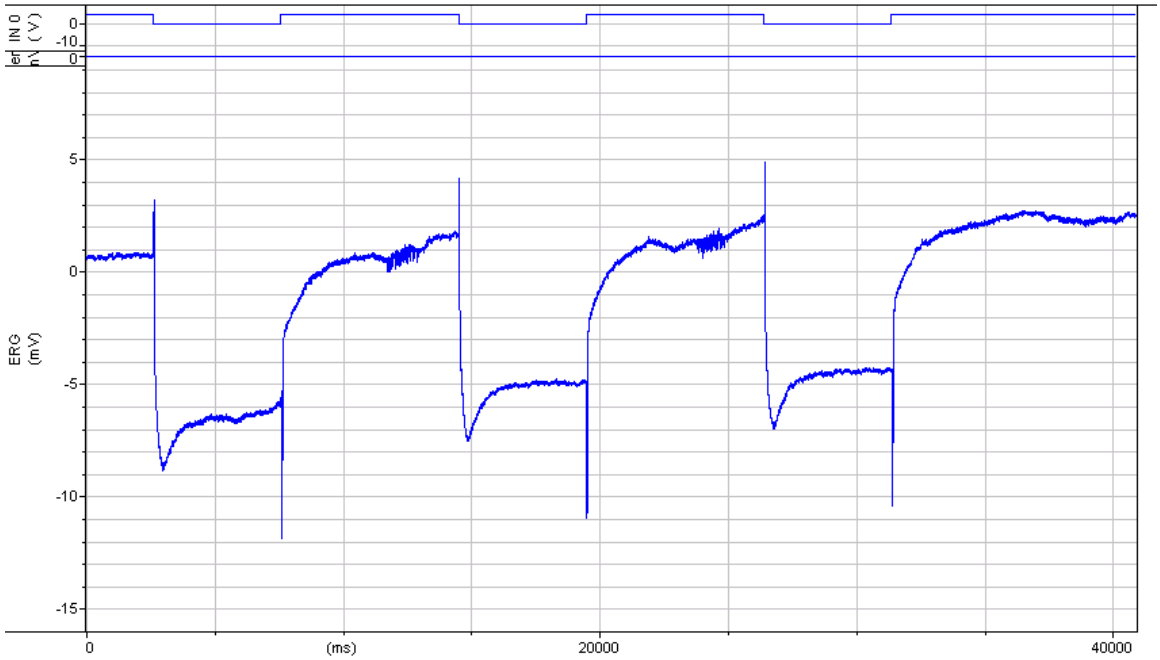
ef IN 0
n\ (V)
0
-10
0
5
0
-5
-10
-15
ERG
(mV)
0
(ms)
20000
40000

Genotype: *elav*-Gal4> *Acsl* RNAi

Phenotype: with transient

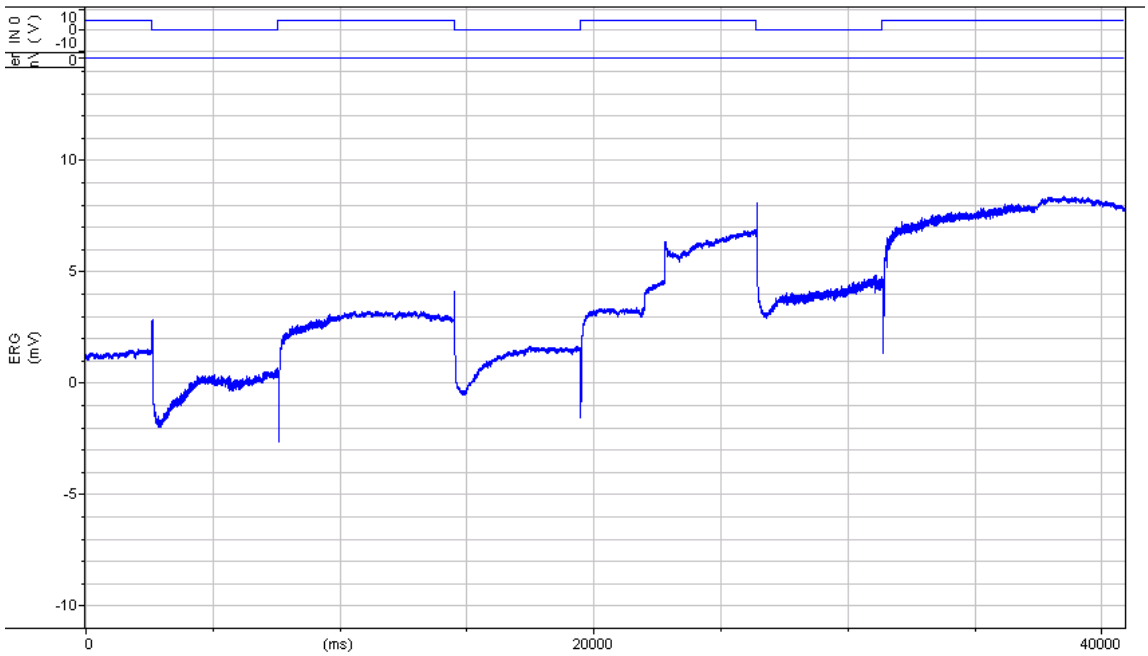

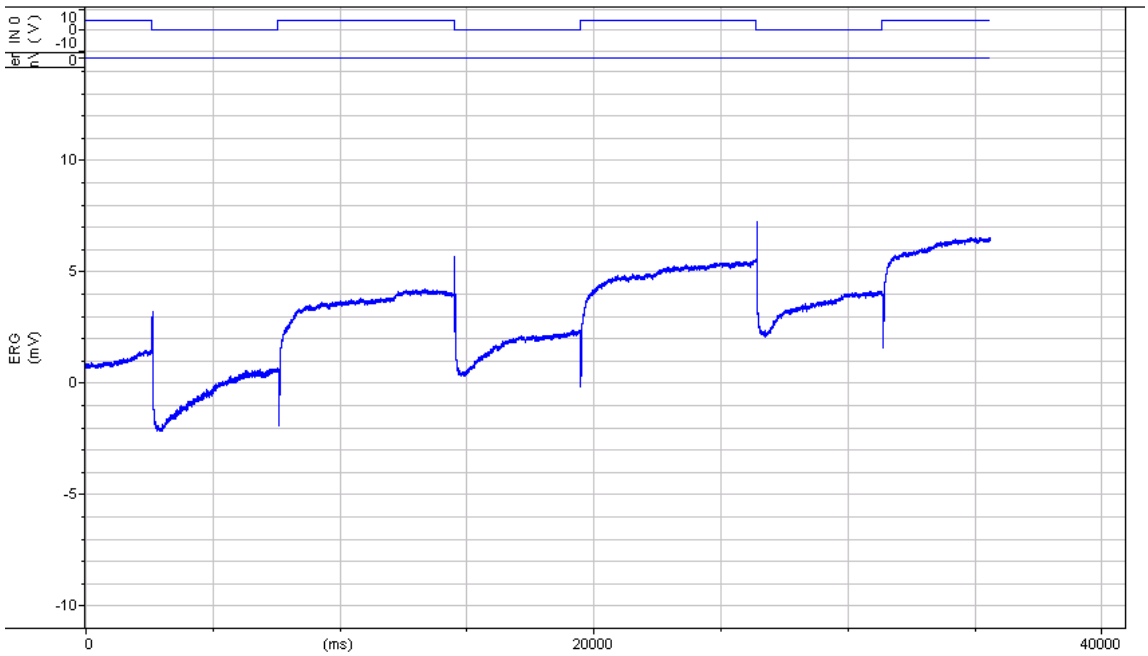

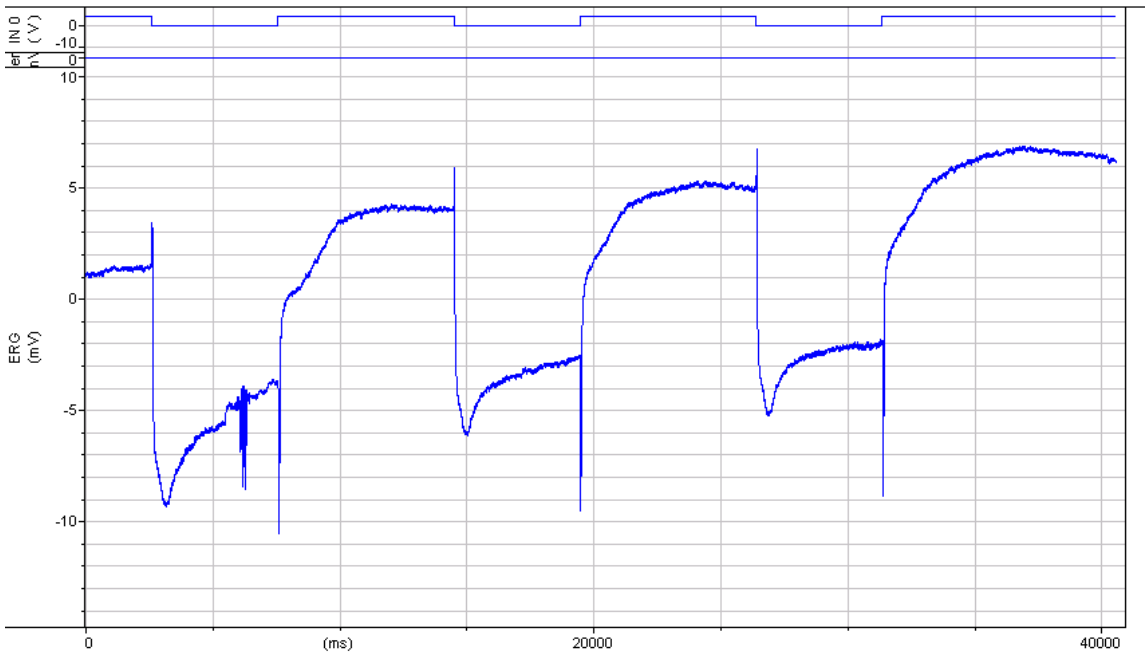
IN 0 (V)
0
-10
0
10
5
0
-5
-10
ERG (mV)
0
(ms)
20000
40000

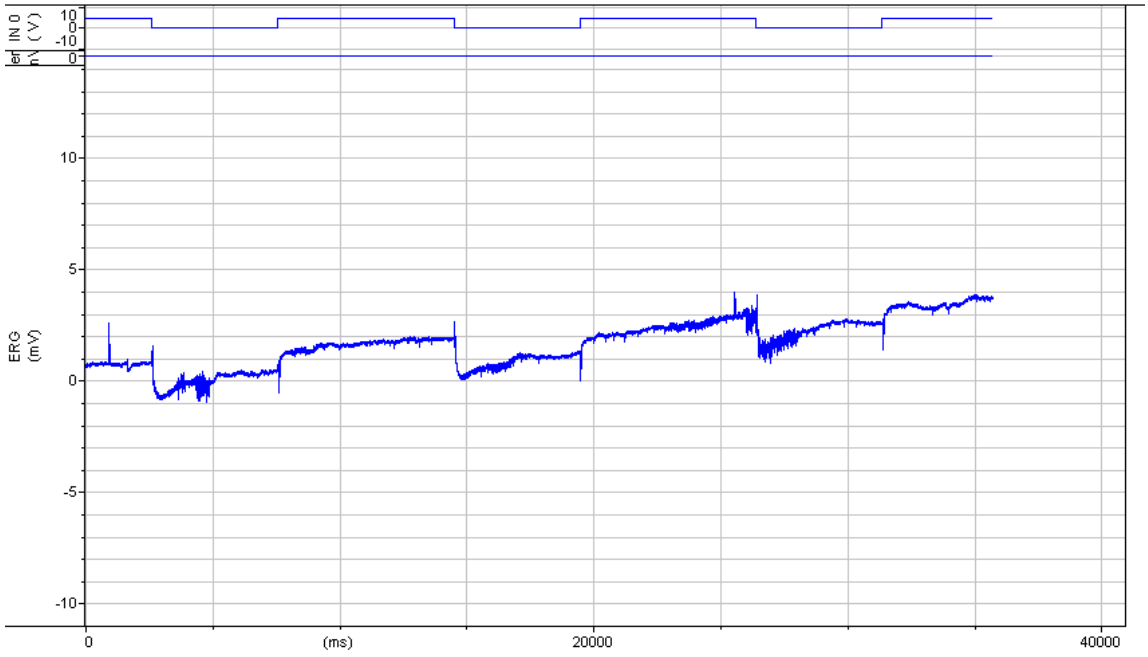
IN 0 (V)
10
0
-10
0
10
5
0
-5
-10
ERG (mV)
0
(ms)
20000
40000

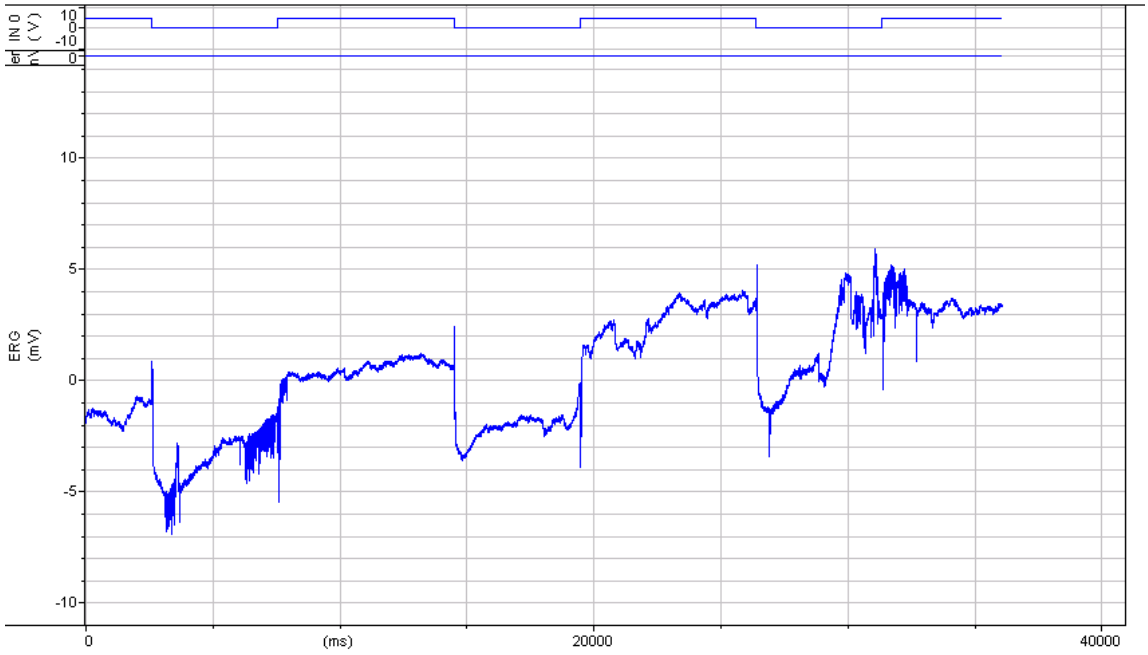
IN 0 (V)
10
0
-10
0
10
5
0
-5
-10
ERG (mV)
0
(ms)
20000
40000

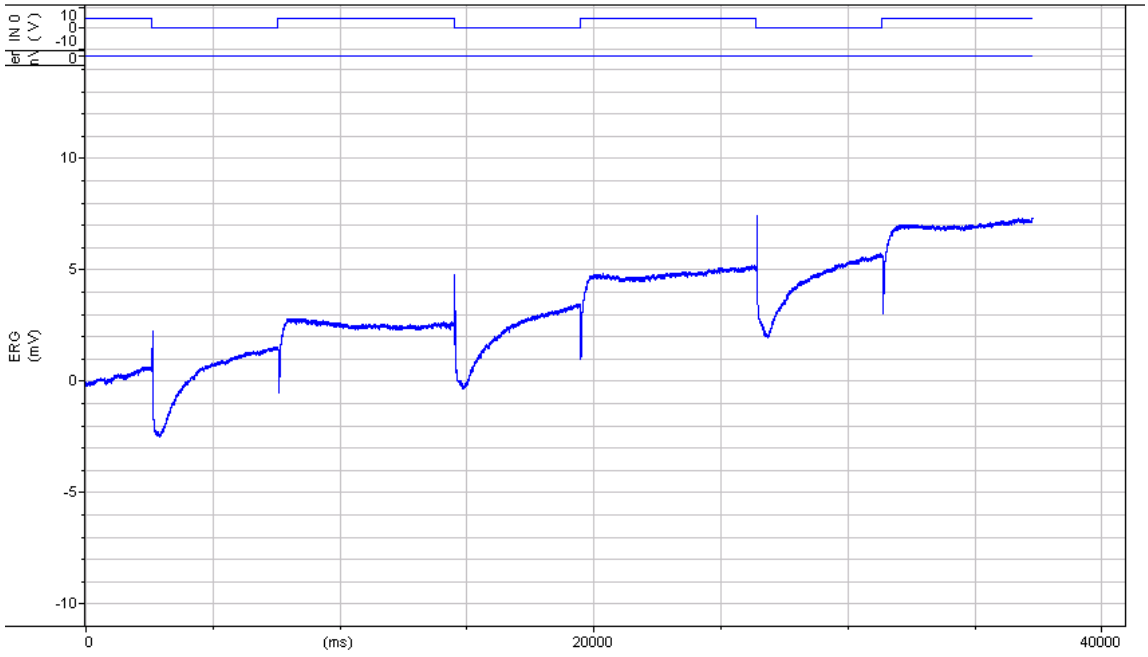
IN 0 (V)
10
0
-10
0
10
5
0
-5
-10
ERG (mV)
0
(ms)
20000
40000

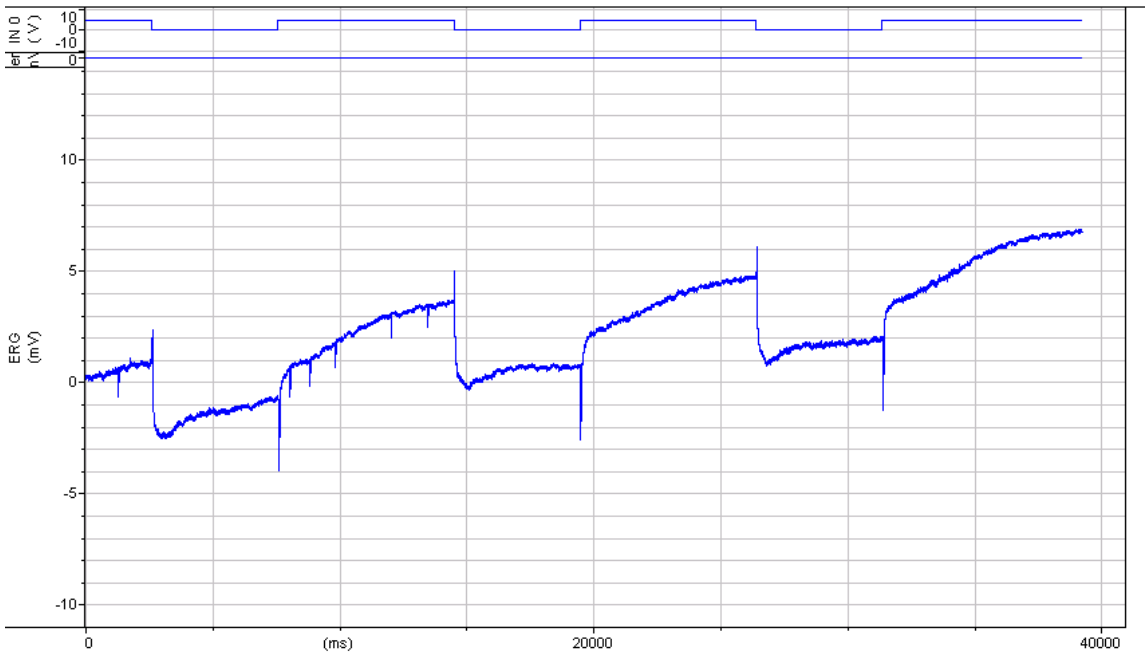
IN 0
(V)
10
0
-10
0
10
5
0
-5
-10
ERG
(mV)
0
(ms)
20000
40000


IN 0
(V)
10
0
10
5
0
-5
-10
-15
Potential
(mV)
0
(ms)
20000
40000
60000
80000

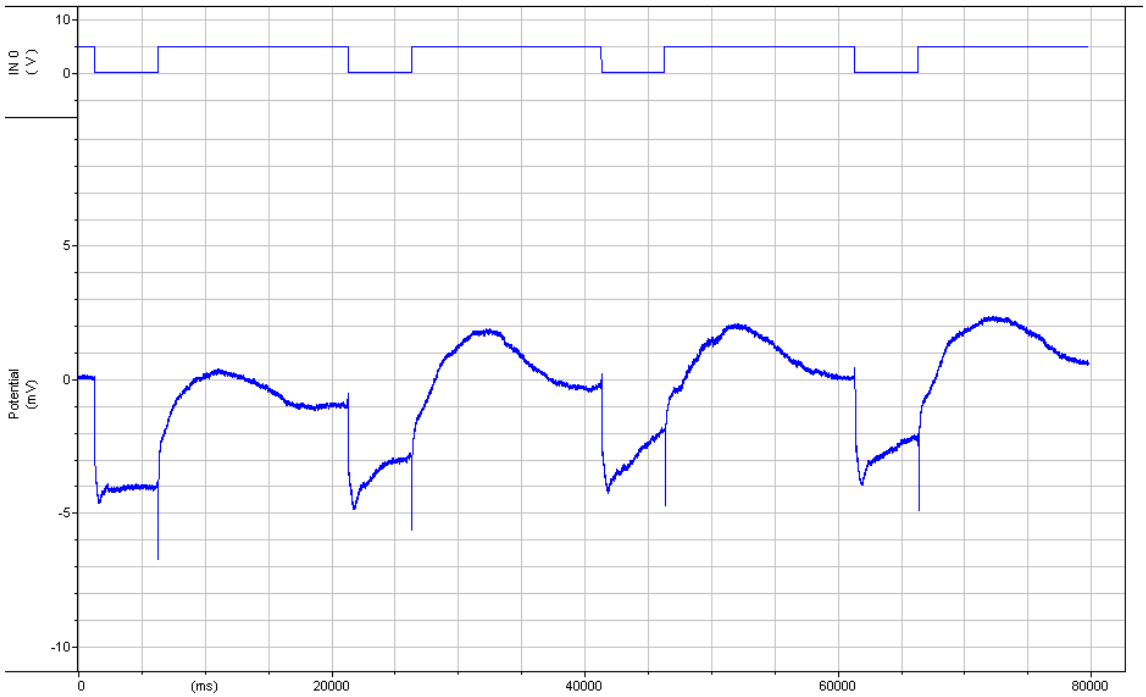
IN 0
(V)
10
0
5
0
-5
-10
Potential
(mV)
0
(ms)
20000
40000
60000
80000

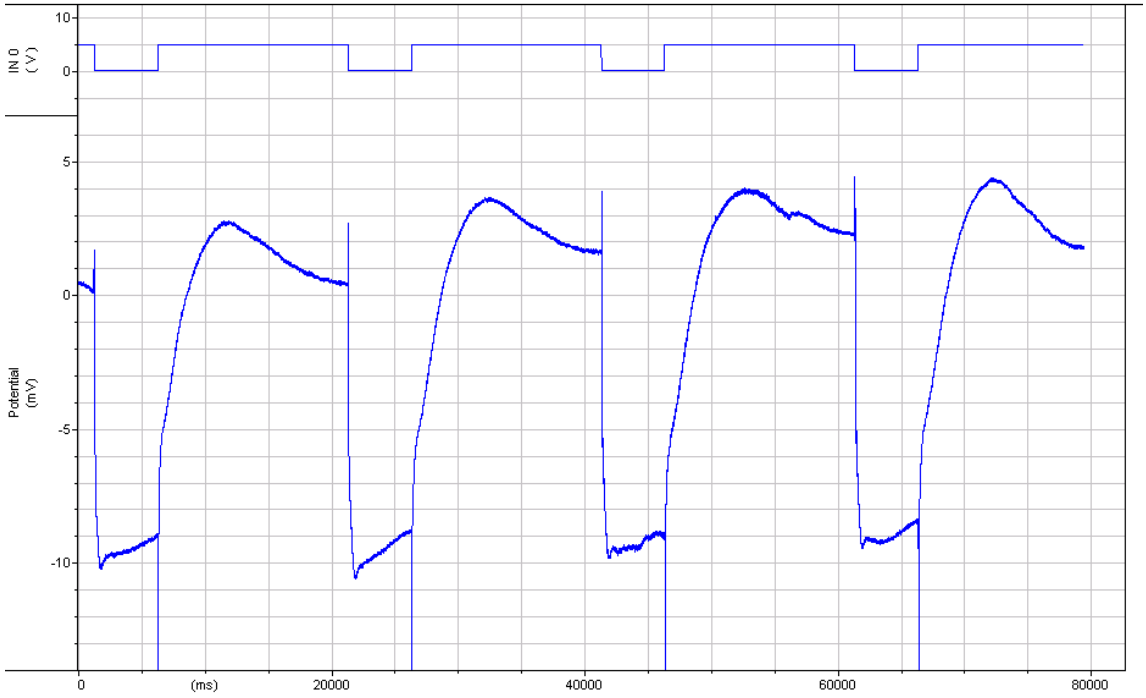
IN 0
(V)
10
0
5
0
-5
-10
Potential
(mV)
0
(ms)
20000
40000
60000
80000

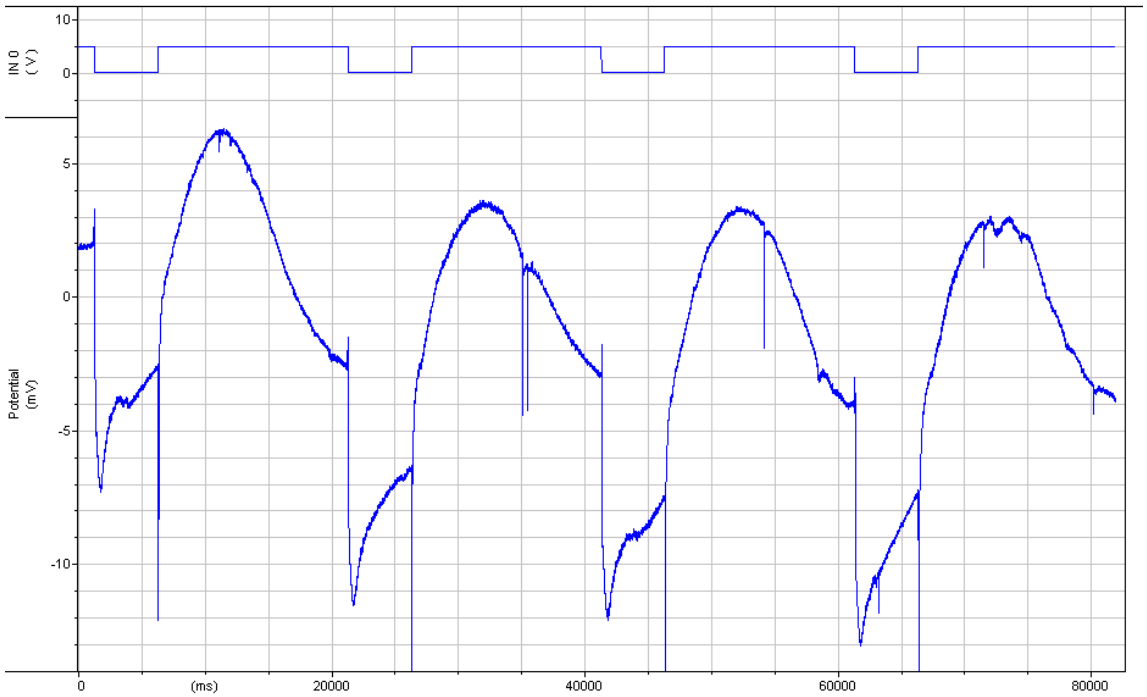
IN 0
(V)
10
0
5
0
-5
-10
Potential
(mV)
0
(ms)
20000
40000
60000
80000

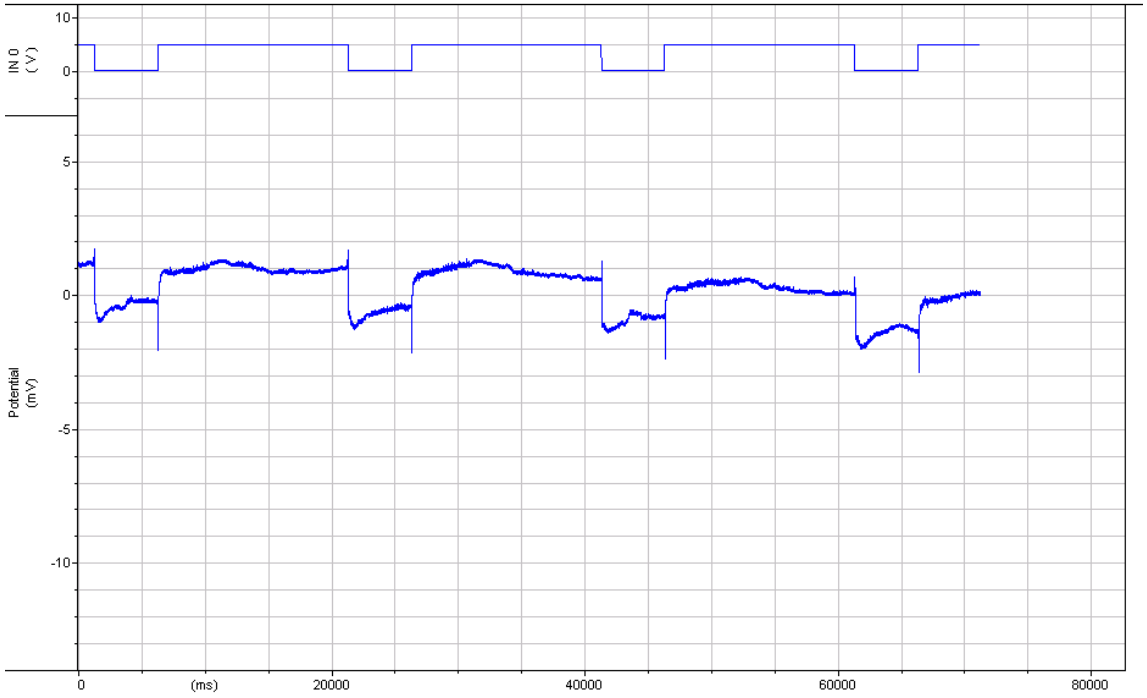
IN 0
(V)
10
0
5
0
-5
-10
Potential
(mV)
0
(ms)
20000
40000
60000
80000

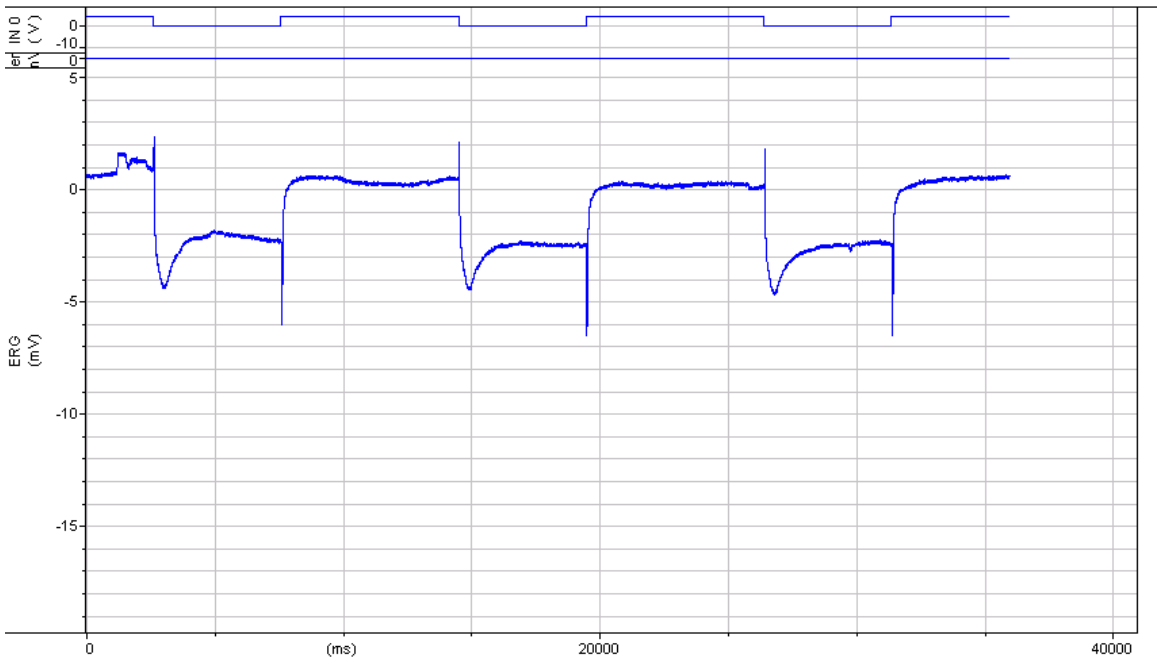
Ref IN 0
(V)
0
-10
0
5
0
-5
-10
-15
ERG
(mV)
0
(ms)
20000
40000

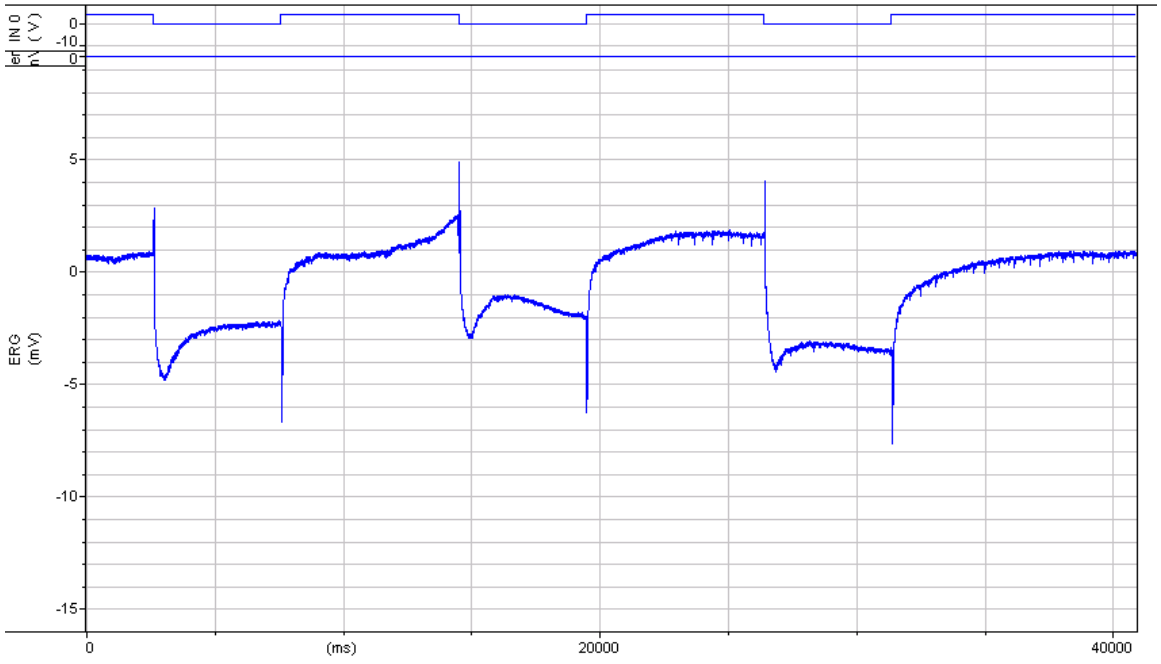
Ref IN 0
(V)
0
-10
0
5
0
-5
-10
-15
ERG
(mV)
0
(ms)
20000
40000

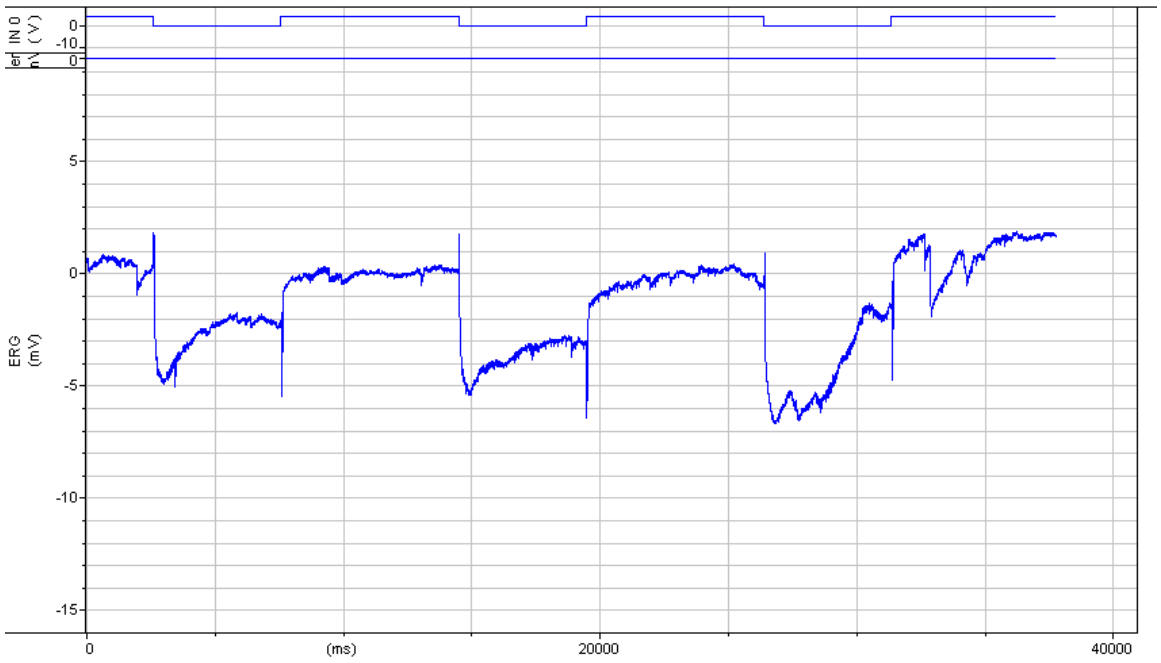
IN 0 (V)
0
-10
Ref
0
5
0
-5
-10
-15
ERG (mV)
0
(ms)
20000
40000

Genotype: *repo*-Gal4> *Acsl* RNAi

Phenotype: with transient

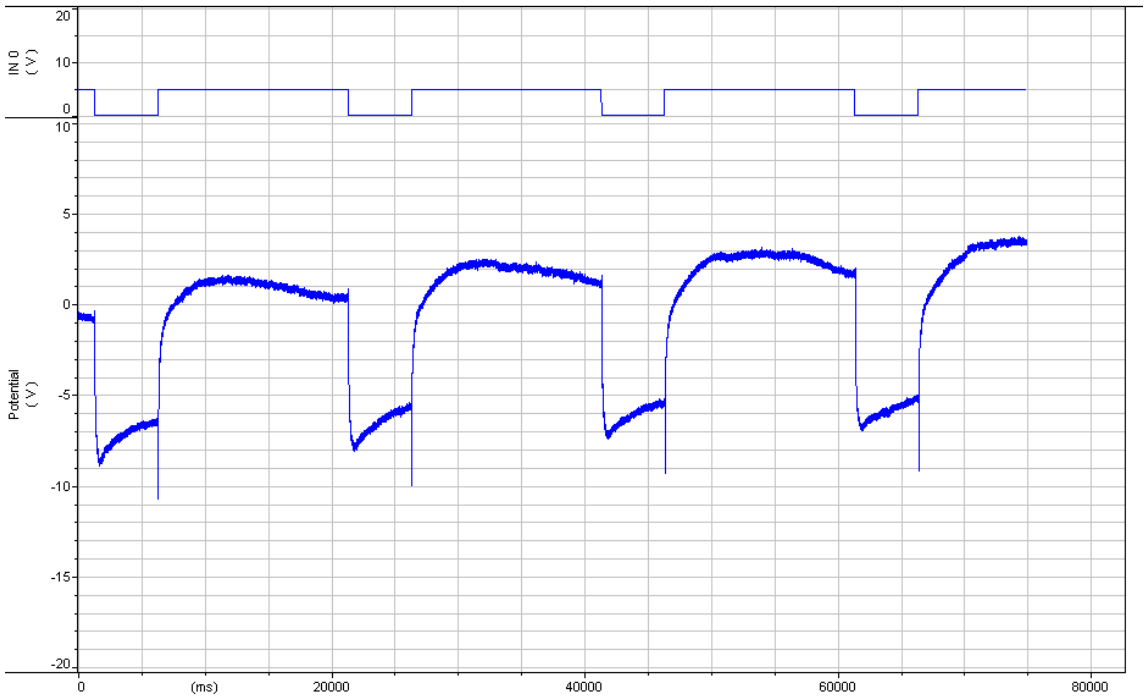

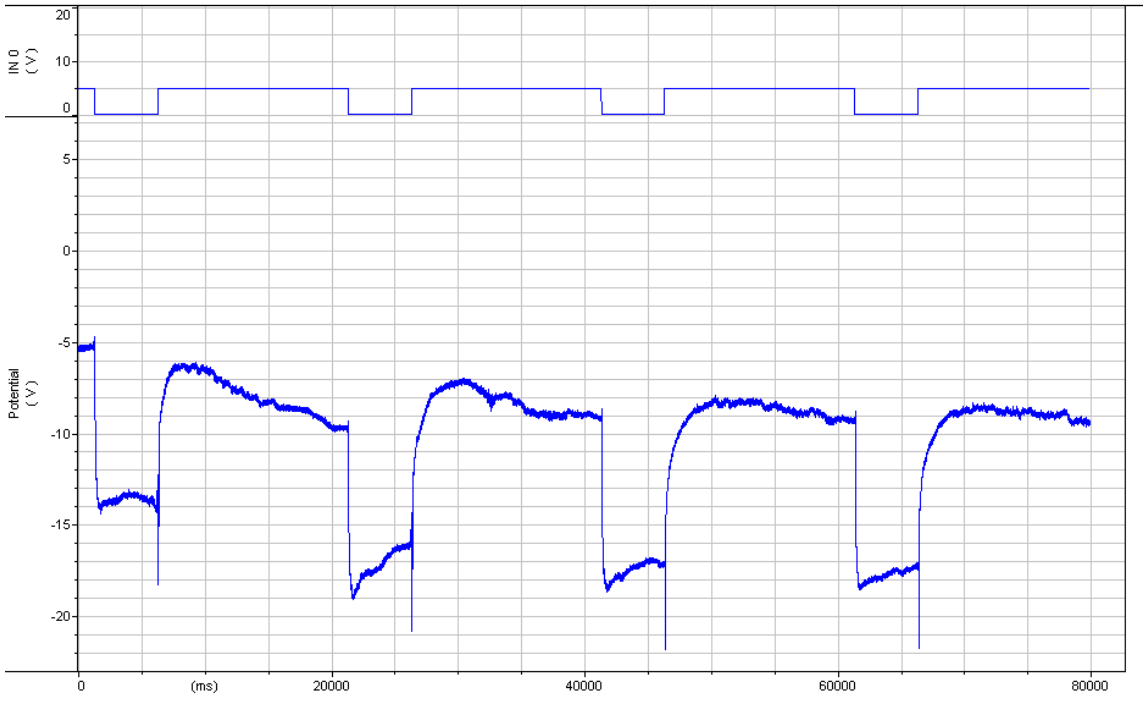

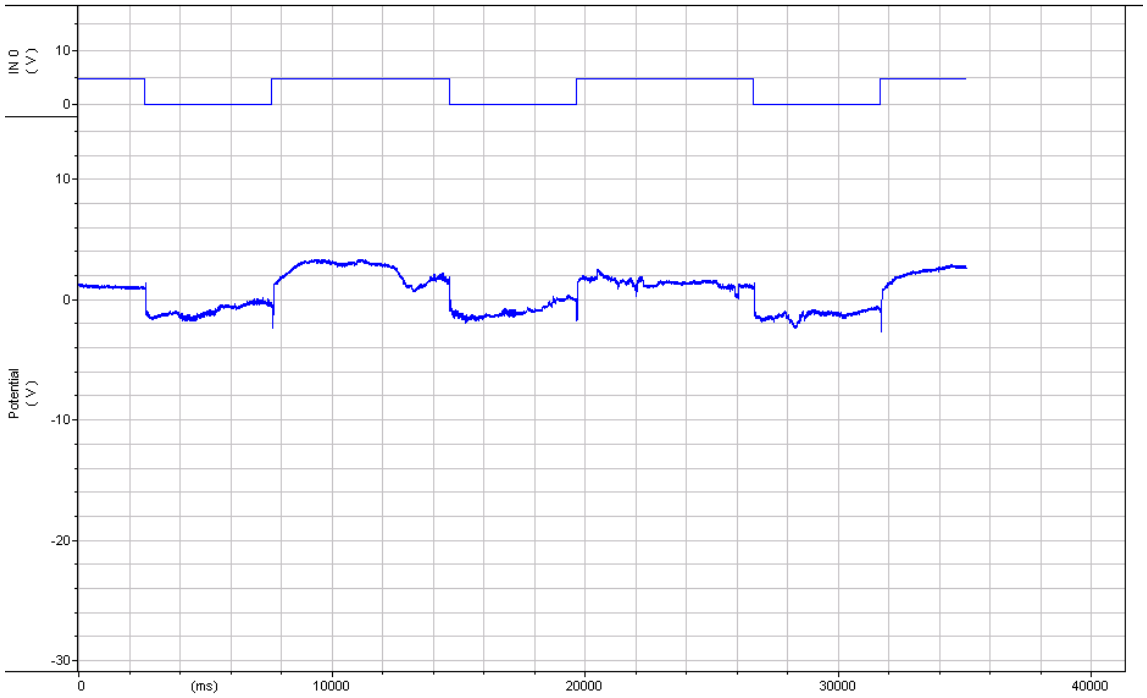
IN 0
(V)
10
0
10
0
Potential
(V)
-10
-20
-30
0
(ms)
10000
20000
30000
40000

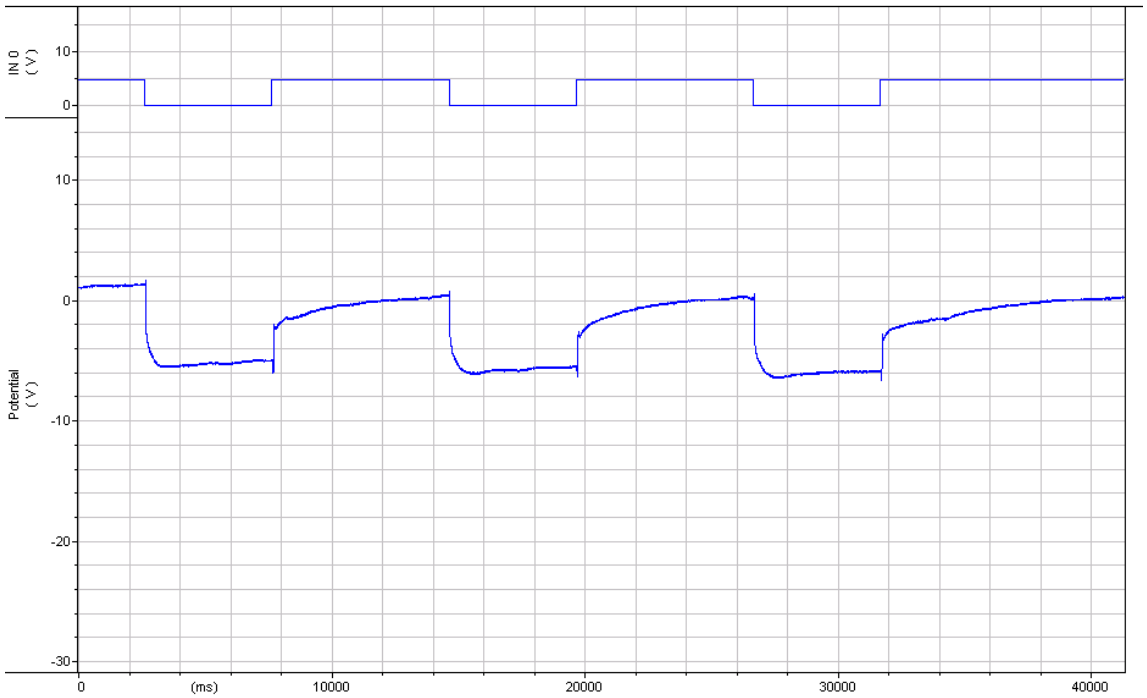
IN 0
(V)
10
0
10
0
Potential
(V)
-10
-20
-30
0
(ms)
10000
20000
30000
40000

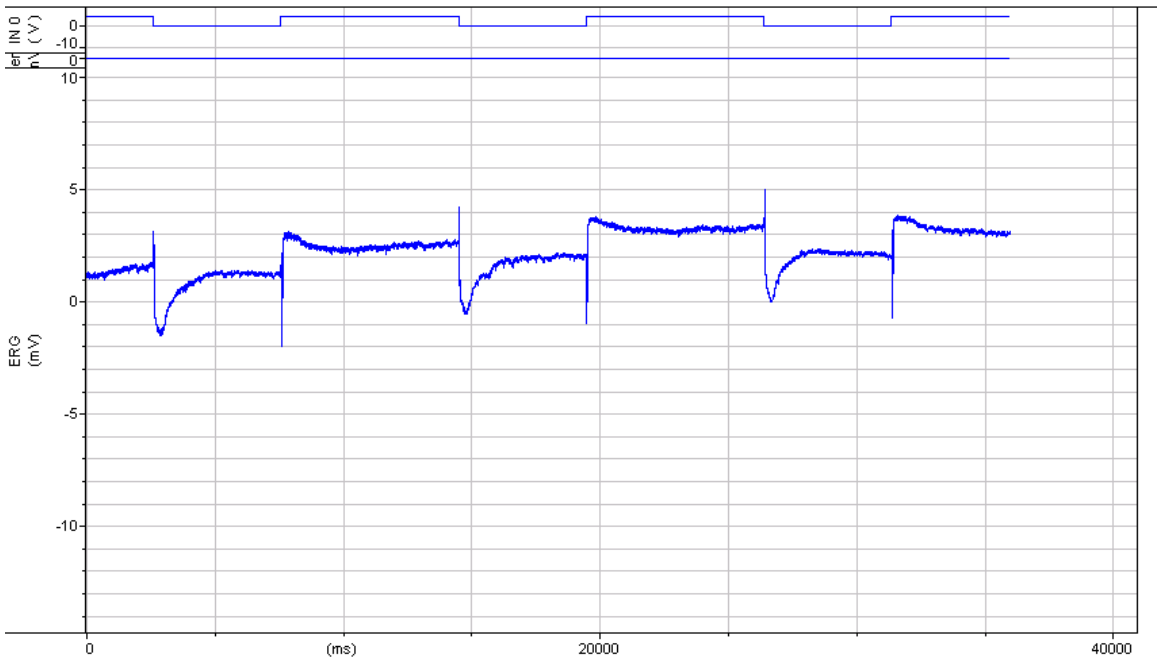
IN 0
(V)
0
-10
0
10
5
0
-5
-10
ERG
(mV)
0
(ms)
20000
40000

Genotype: *repo*-Gal4> *Acsl* RNAi

Phenotype: loss of ‘on transient’

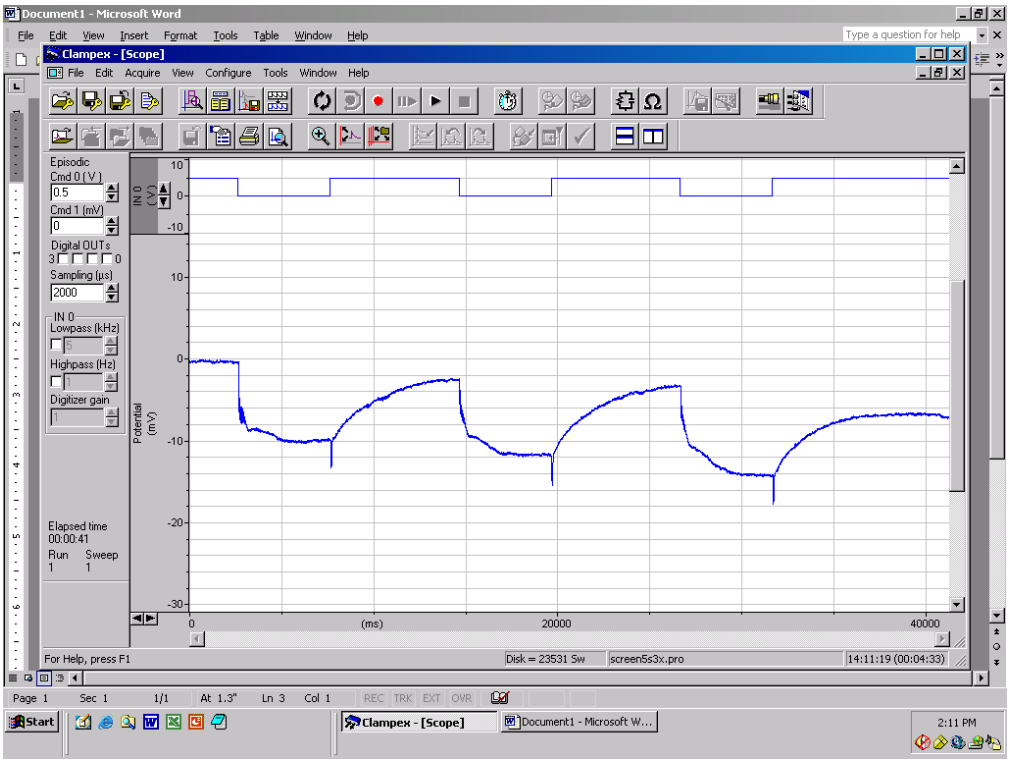

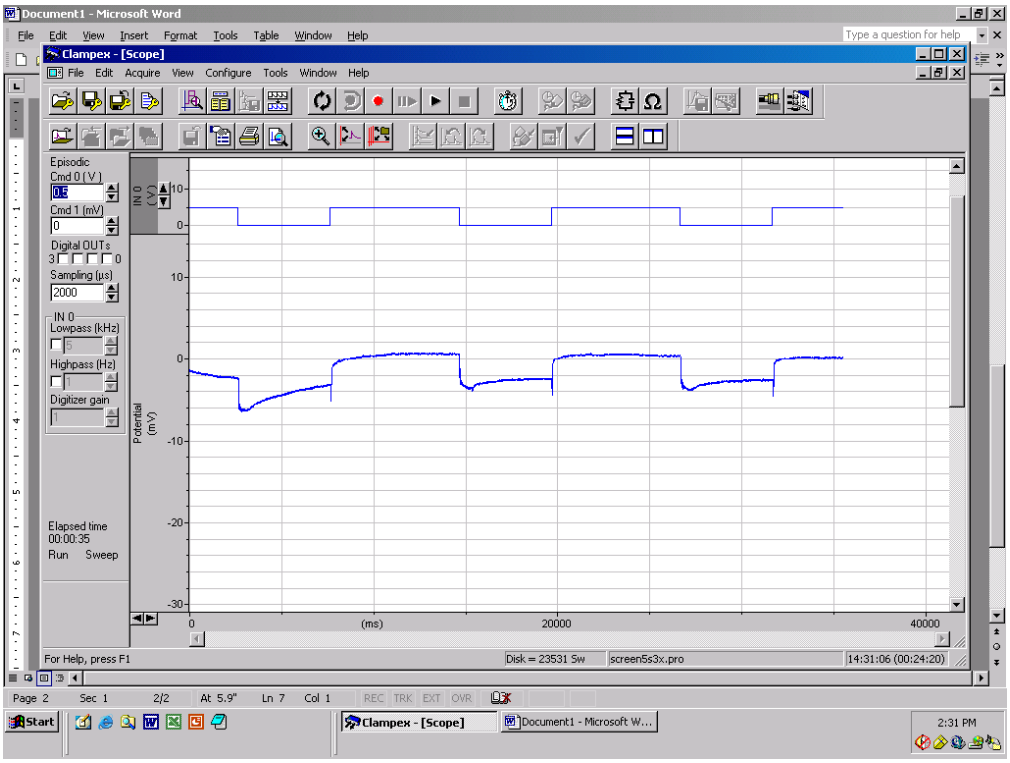
Document1 - Microsoft Word
Clampex - [Scope]
Episodic
Cmd 0 (V)
Cmd 1 (mV)
Digital OUTs
Sampling (µs)
2000
IN 0
Lowpass (kHz)
Highpass (Hz)
Digitizer gain
Elapsed time
00:00:35
Run Sweep
Potential (mV)
(ms)
For Help, press F1
Disk = 23531 Sw
screen5s3x.pro
14:31:06 (00:24:20)
2:31 PM

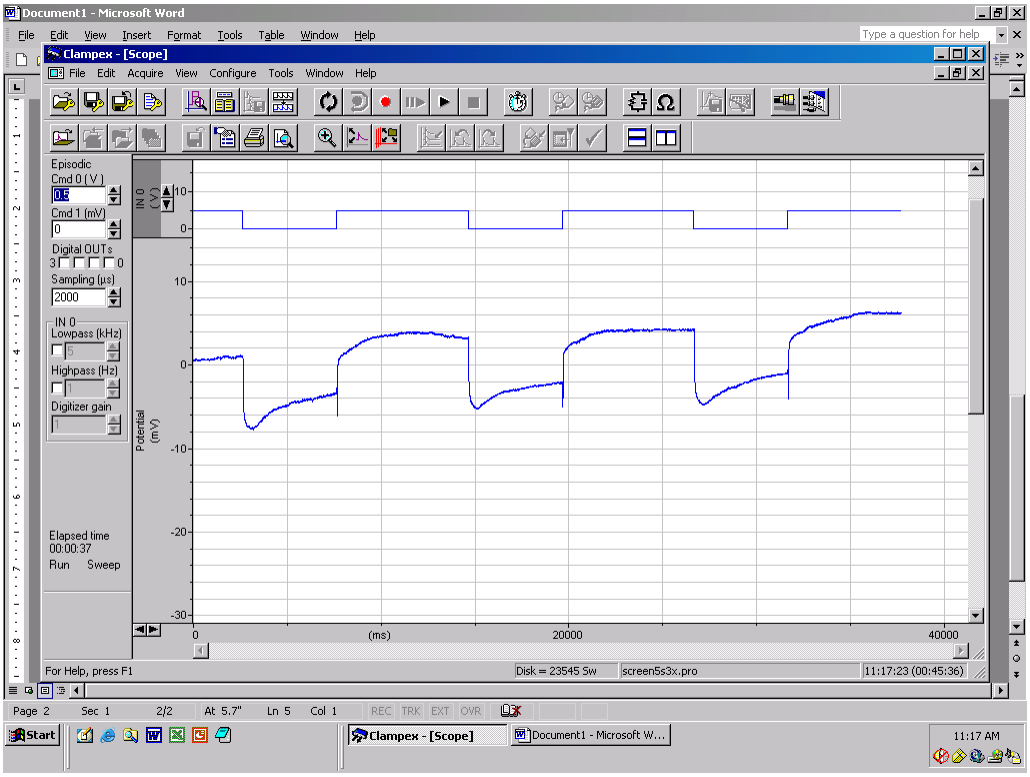
Document1 - Microsoft Word
Clampex - [Scope]
Episodic
Cmd 0 (V)
Cmd 1 (mV)
Digital OUTs
Sampling (µs)
2000
IN 0
Lowpass (kHz)
Highpass (Hz)
Digitizer gain
Elapsed time
00:00:37
Run Sweep
Potential (mV)
(ms)
For Help, press F1
Disk = 23545 Sw
screen5s3x.pro
11:17:23 (00:45:36)
11:17 AM

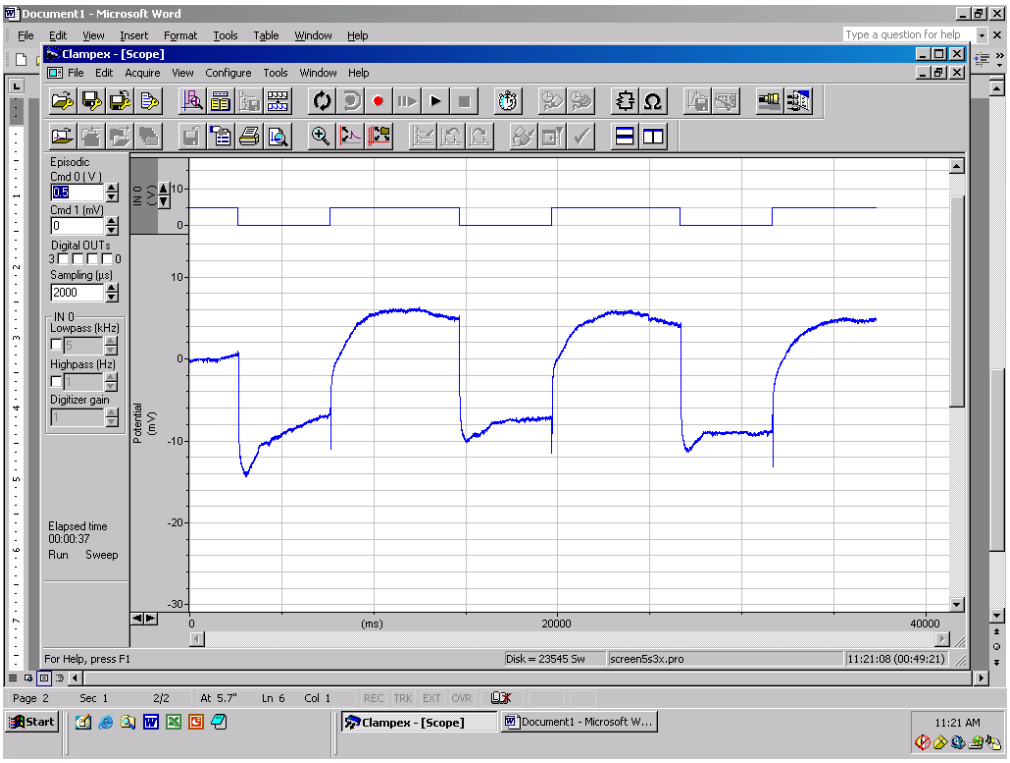
Document1 - Microsoft Word
Clampex - [Scope]
Episodic
Cmd 0 (V)
Cmd 1 (mV)
Digital OUTs
Sampling (µs)
2000
IN 0
Lowpass (kHz)
Highpass (Hz)
Digitizer gain
Elapsed time
00:00:37
Run Sweep
Potential (mV)
(ms)
For Help, press F1
Disk = 23545 Sw
screen5s3x.pro
11:21:08 (00:49:21)
Page 2 Sec 1 2/2 At 5.7" Ln 6 Col 1
11:21 AM

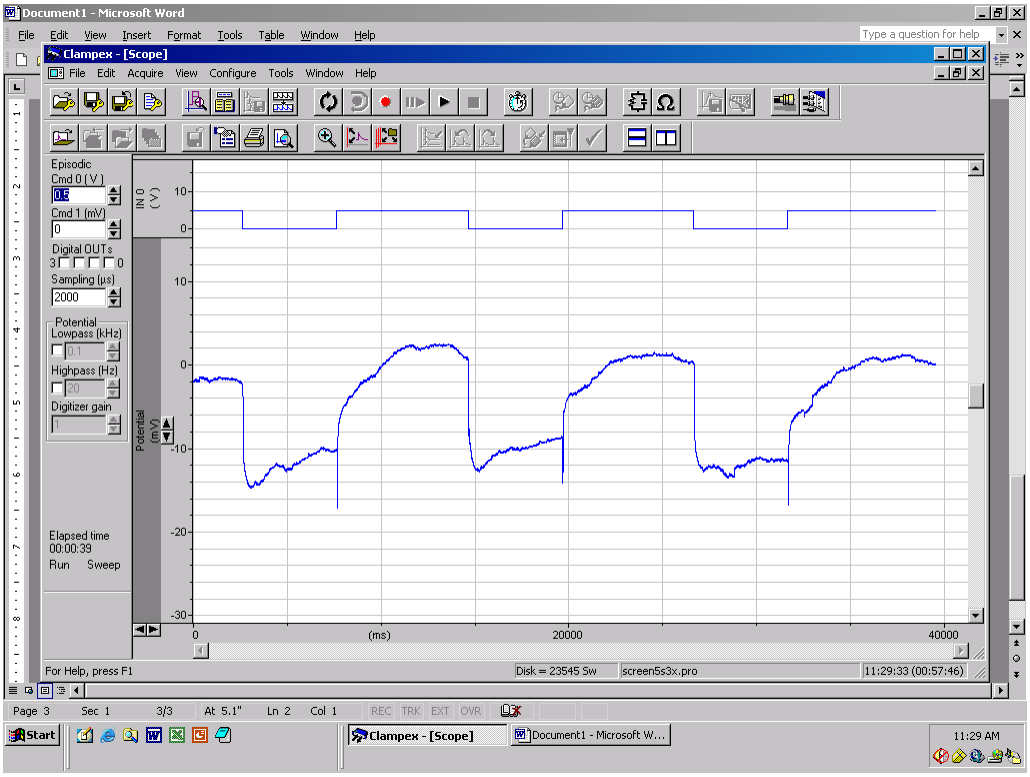
Document1 - Microsoft Word
Clampex - [Scope]
Episodic
Cmd 0 (V)
Cmd 1 (mV)
Digital OUTs
Sampling (µs)
2000
Potential
Lowpass (kHz)
Highpass (Hz)
Digitizer gain
Elapsed time
00:00:39
Run Sweep
Potential (mV)
(ms)
For Help, press F1
Disk = 23545 Sw
screen5s3x.pro
11:29:33 (00:57:46)
Page 3 Sec 1 3/3 At 5.1" Ln 2 Col 1
11:29 AM

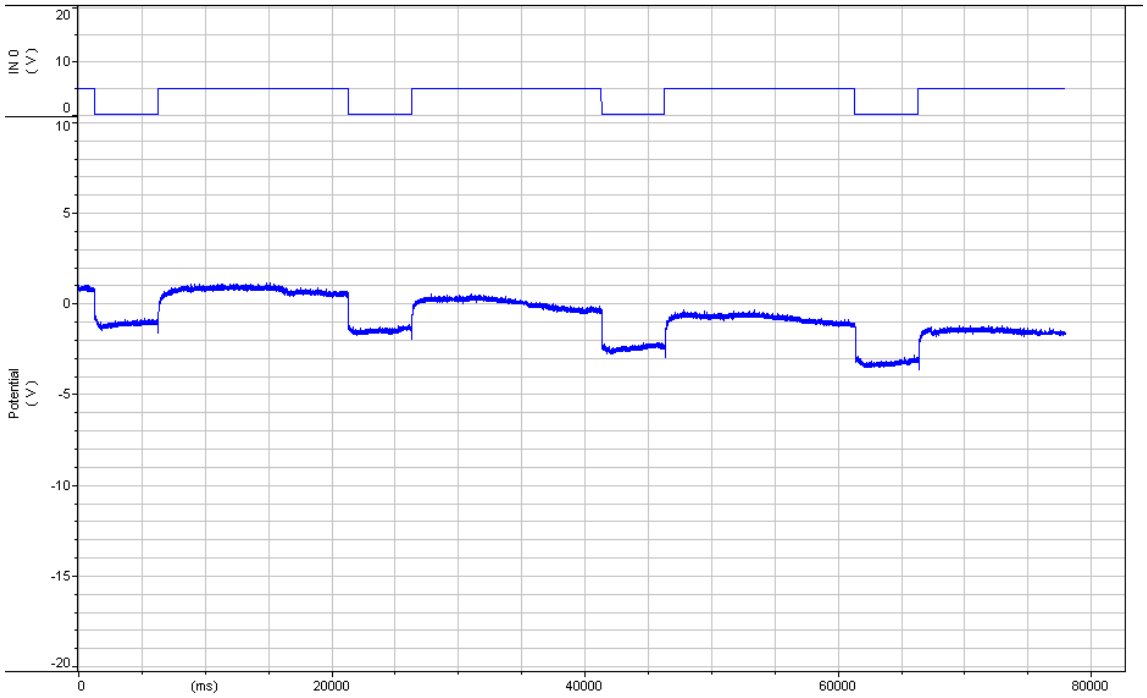
IN 0
(V)
20
10
0
10
5
0
-5
-10
-15
-20
Potential
(V)
0
(ms)
20000
40000
60000
80000

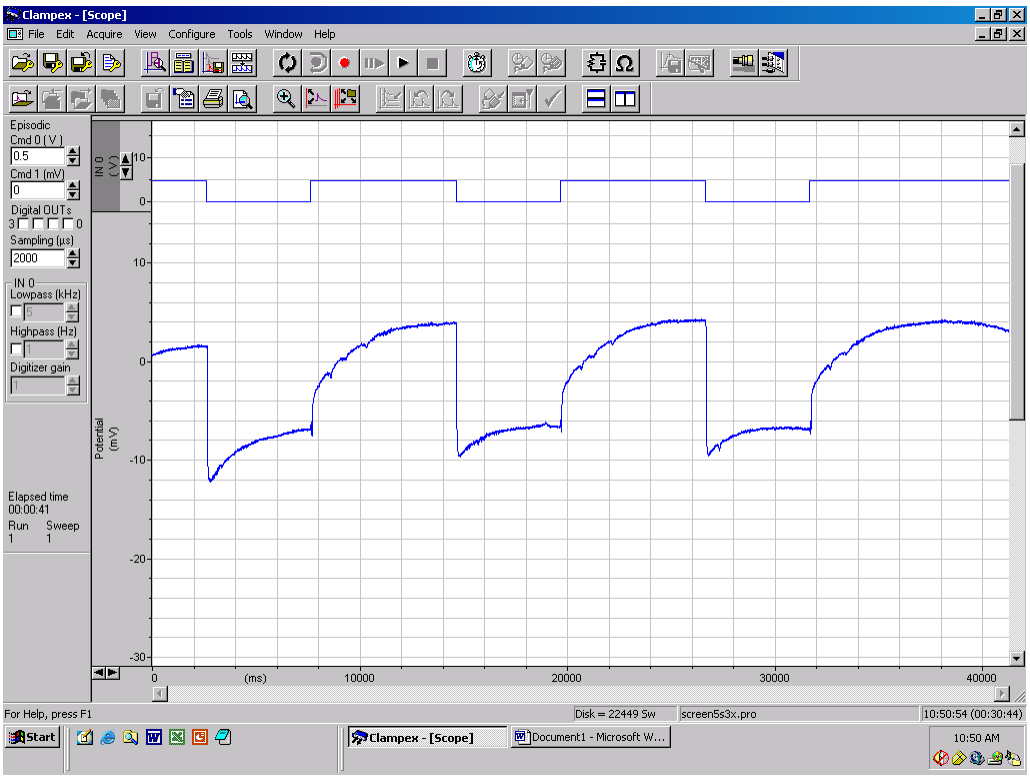
Clampex - [Scope]
File Edit Acquire View Configure Tools Window Help
Episodic
Cmd 0 (V)
0.5
Cmd 1 (mV)
0
Digital OUTs
3 0
Sampling (µs)
2000
IN 0
Lowpass (kHz)
Highpass (Hz)
Digitizer gain
Elapsed time
00:00:41
Run
1
Sweep
1
IN 0
(V)
Potential
(mV)
(ms)
10000
20000
30000
40000
For Help, press F1
Disk = 22449 Sw
screen5s3x.pro
10:50:54 (00:30:44)
Start
Clampex - [Scope]
Document1 - Microsoft W...
10:50 AM

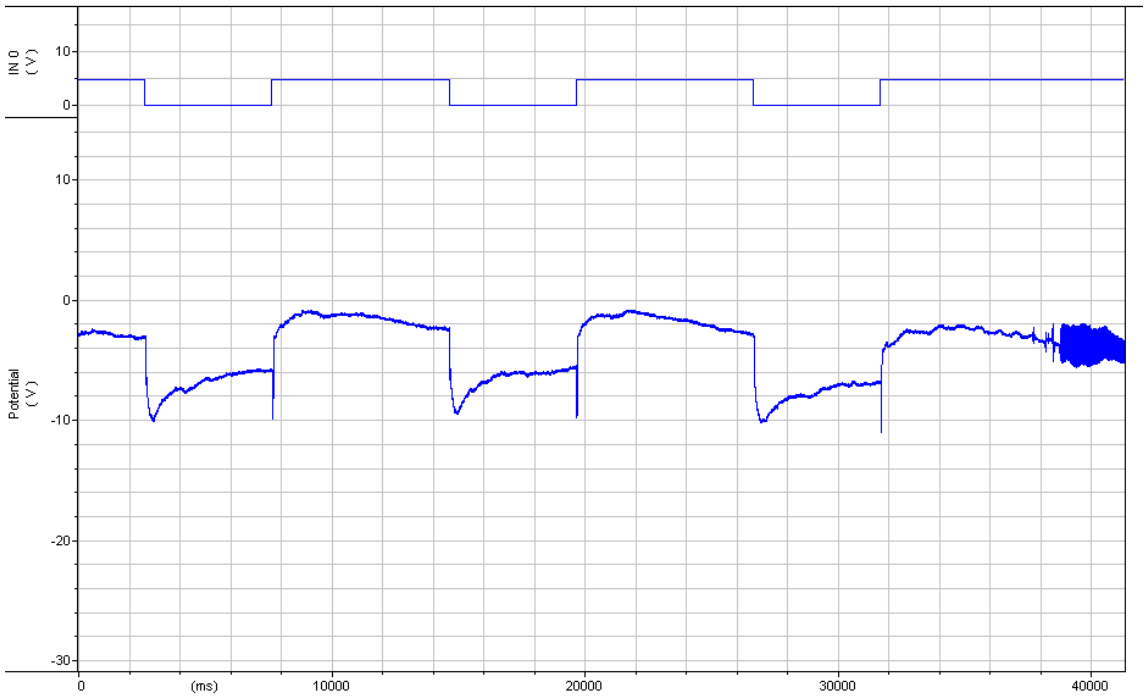
IN 0
(V)
10
0
10
0
-10
-20
-30
Potential
(V)
0
(ms)
10000
20000
30000
40000

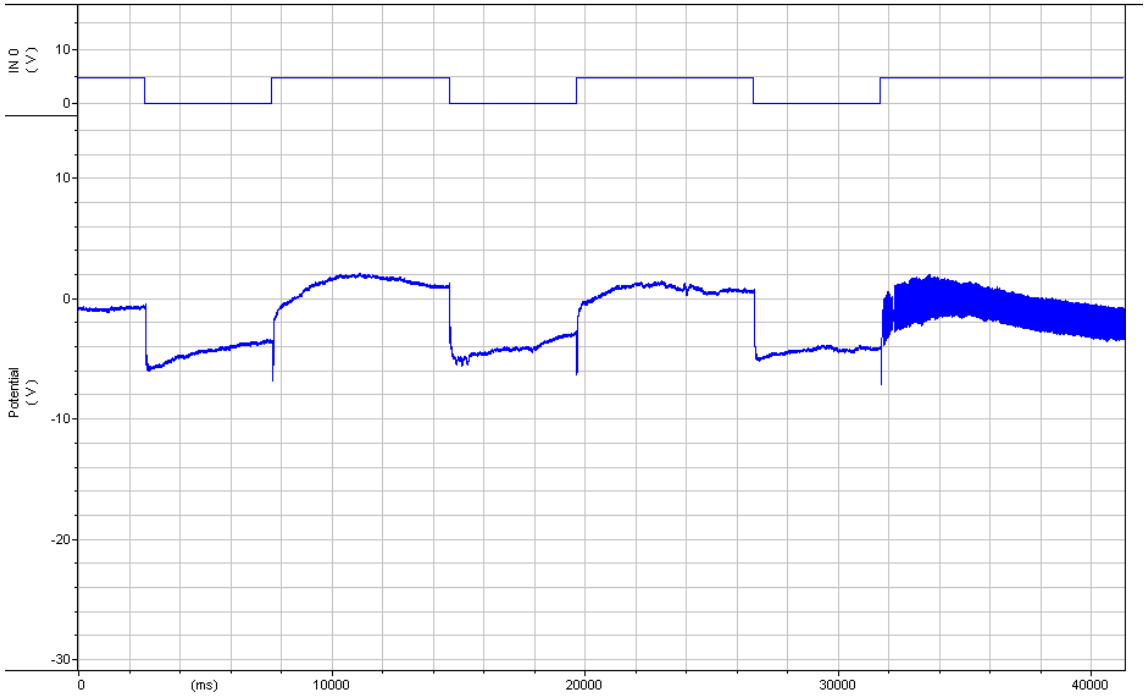
IN 0
(V)
10
0
10
0
-10
-20
-30
Potential
(V)
0
(ms)
10000
20000
30000
40000

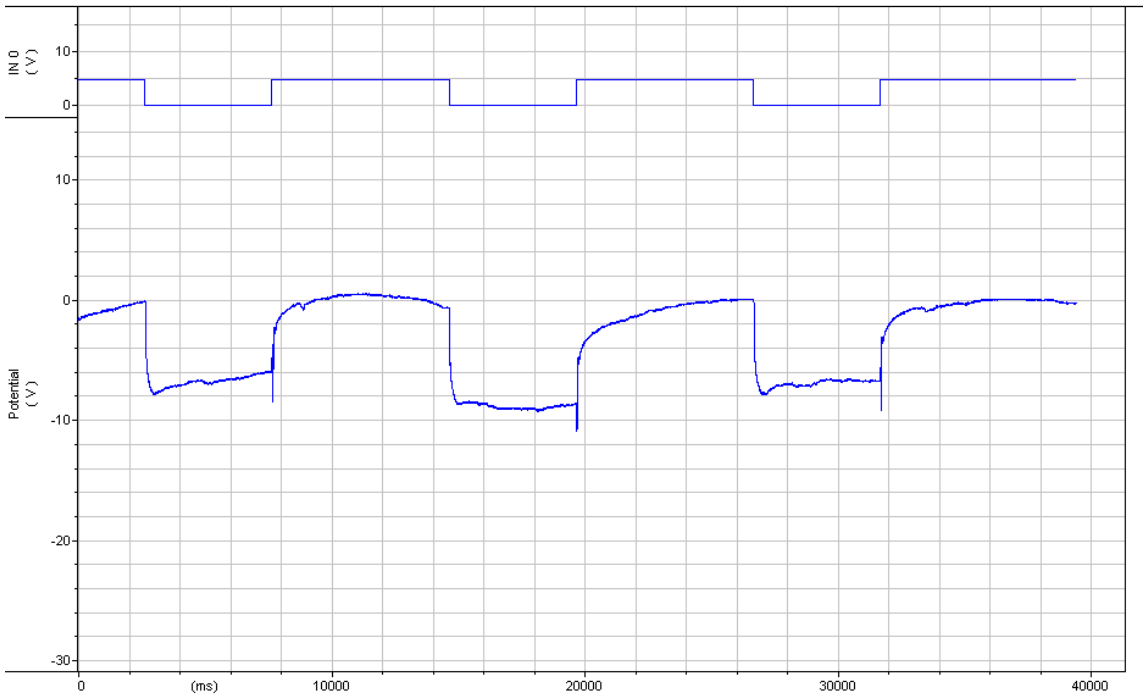
IN 0
(V)
10
0
10
0
Potential
(V)
-10
-20
-30
0
(ms)
10000
20000
30000
40000

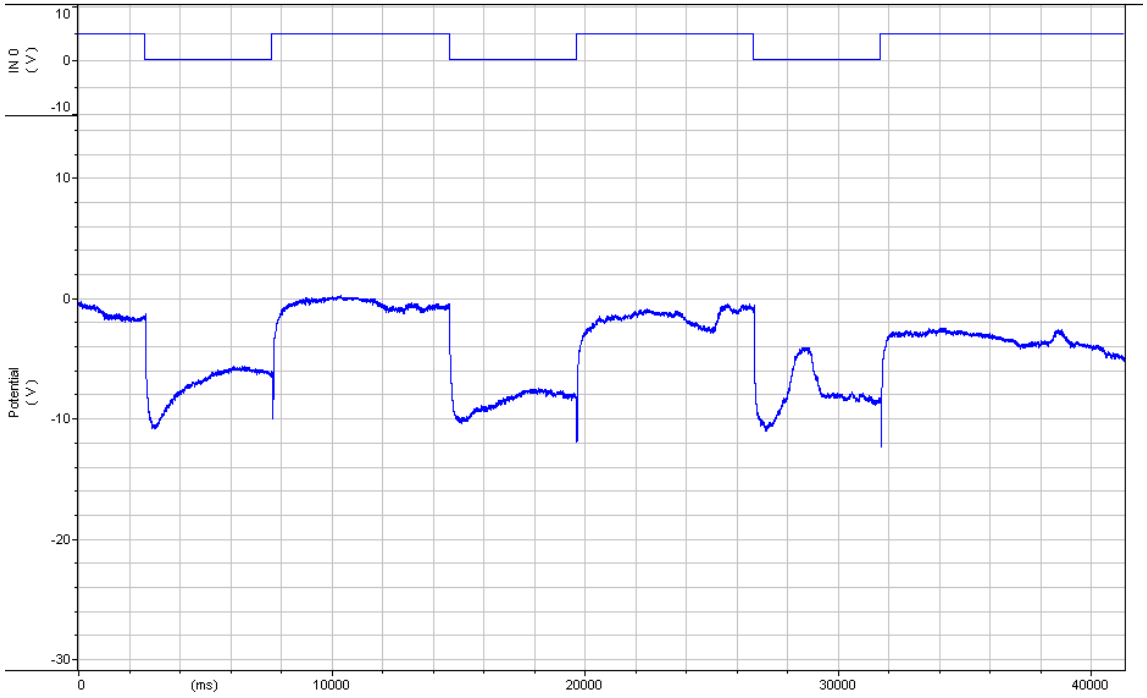
IN 0
(V)
10
0
-10
10
0
Potential
(V)
-10
-20
-30
0
(ms)
10000
20000
30000
40000

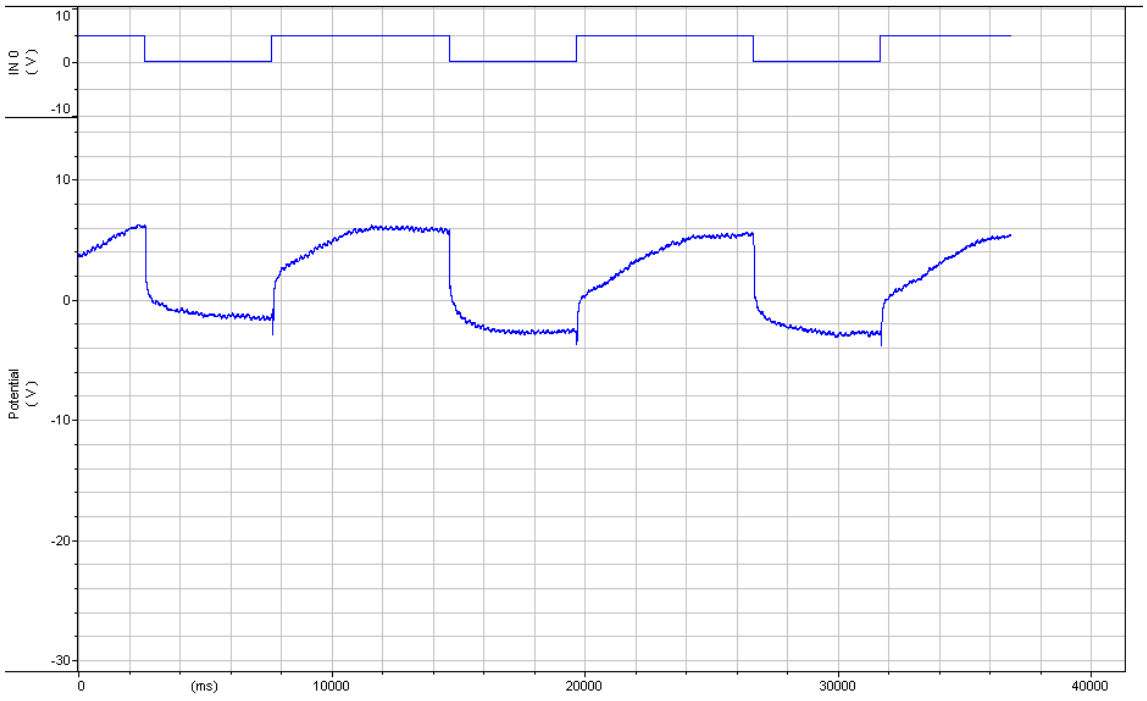
IN 0
(V)
10
0
-10
10
0
-10
-20
-30
Potential
(V)
0
(ms)
10000
20000
30000
40000

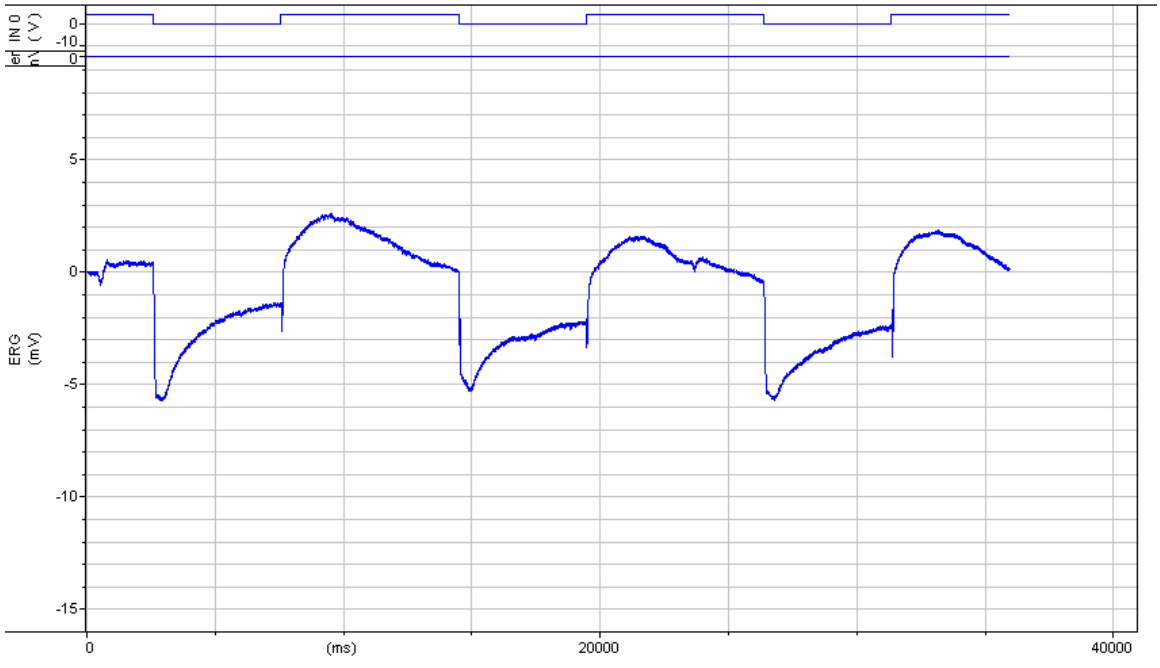
IN 0
(V)
0
-10
0
5
0
-5
-10
-15
ERG
(mV)
0
(ms)
20000
40000

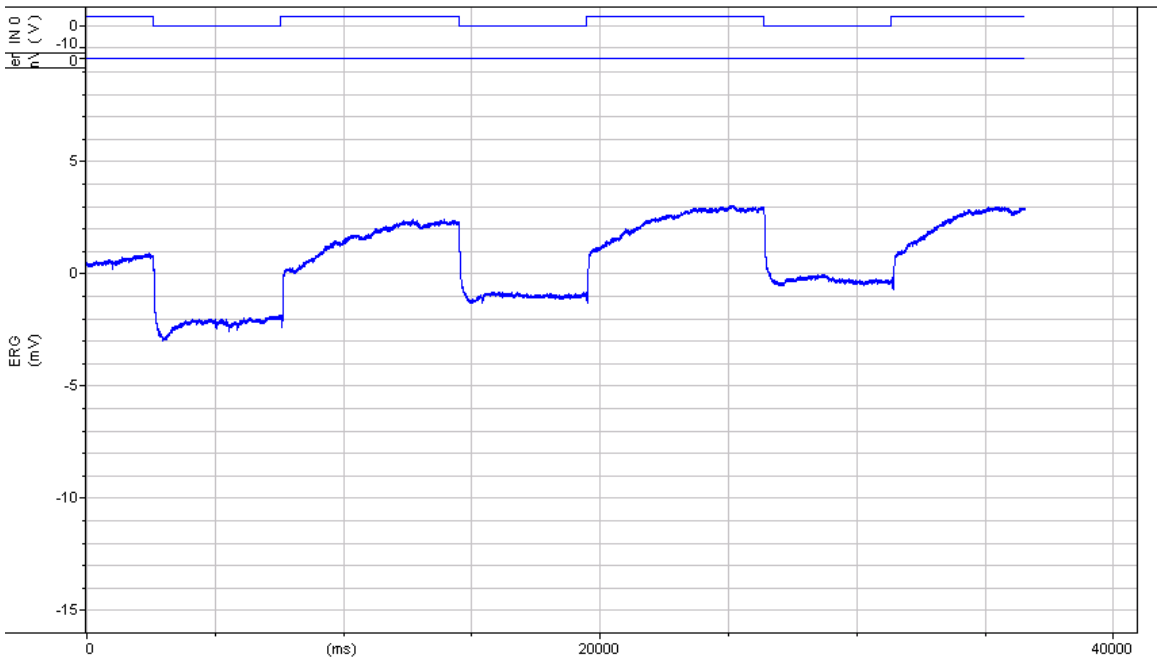
IN 0
(V)
0
-10
0
5
0
-5
-10
-15
ERG
(mV)
0
(ms)
20000
40000

Genotype: *repo*-Gal4> *Acsl* RNAi

Phenotype: loss of ‘on’ and ‘off’ transients

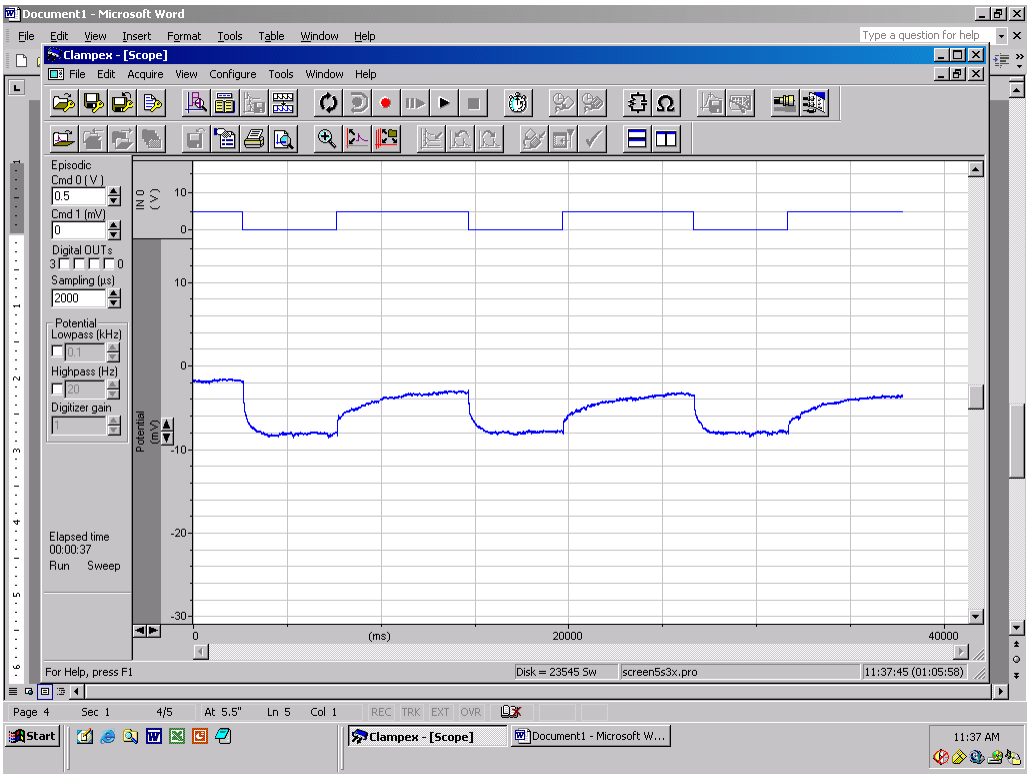

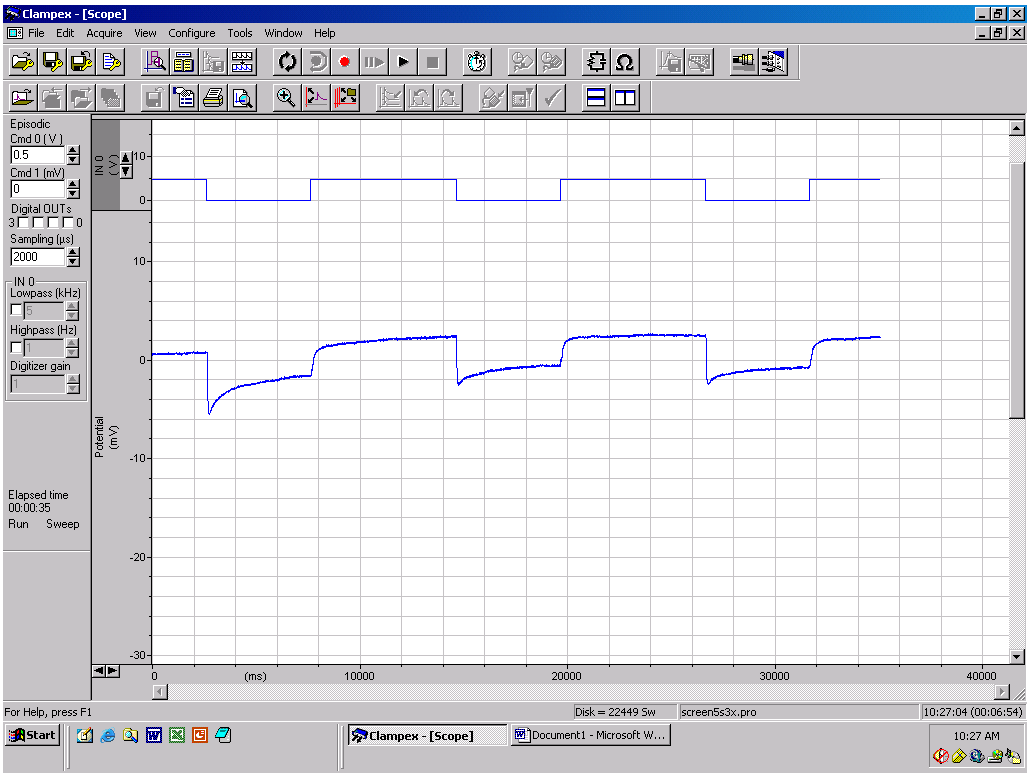
Clampex - [Scope]
File Edit Acquire View Configure Tools Window Help
Episodic
Cmd 0 (V)
0.5
Cmd 1 (mV)
0
Digital OUTs
Sampling (µs)
2000
IN 0
Lowpass (kHz)
Highpass (Hz)
Digitizer gain
Elapsed time
00:00:35
Run Sweep
IN 0 (V)
Potential (mV)
(ms)
For Help, press F1
Disk = 22449 Sw
screen5s3x.pro
10:27:04 (00:06:54)
Start
Clampex - [Scope]
Document1 - Microsoft W...
10:27 AM

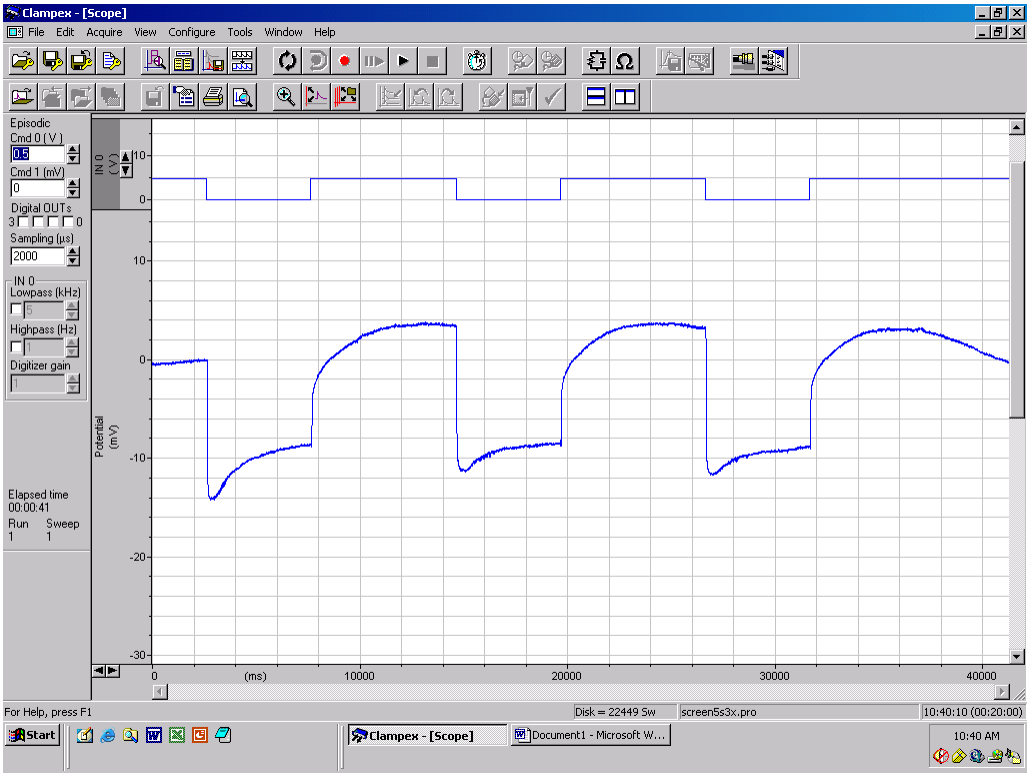
Clampex - [Scope]
File Edit Acquire View Configure Tools Window Help
Episodic
Cmd 0 (V)
0.5
Cmd 1 (mV)
0
Digital OUTs
Sampling (µs)
2000
IN 0
Lowpass (kHz)
Highpass (Hz)
Digitizer gain
Elapsed time
00:00:41
Run Sweep
1 1
IN 0 (V)
Potential (mV)
(ms)
For Help, press F1
Disk = 22449 Sw
screen5s3x.pro
10:40:10 (00:20:00)
Start
Clampex - [Scope]
Document1 - Microsoft W...
10:40 AM

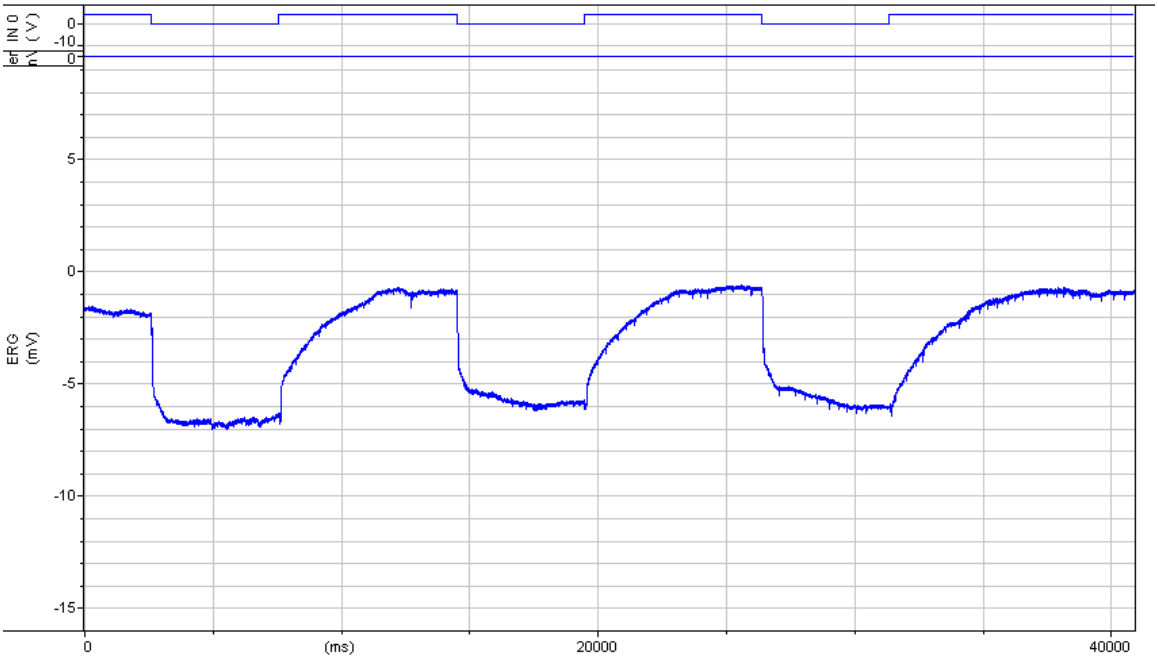
IN 0
(V)
0
-10
0
5
0
-5
-10
-15
ERG
(mV)
0
(ms)
20000
40000

Genotype: TIFR-Gal4> *Luc* RNAi

Phenotype: with transient

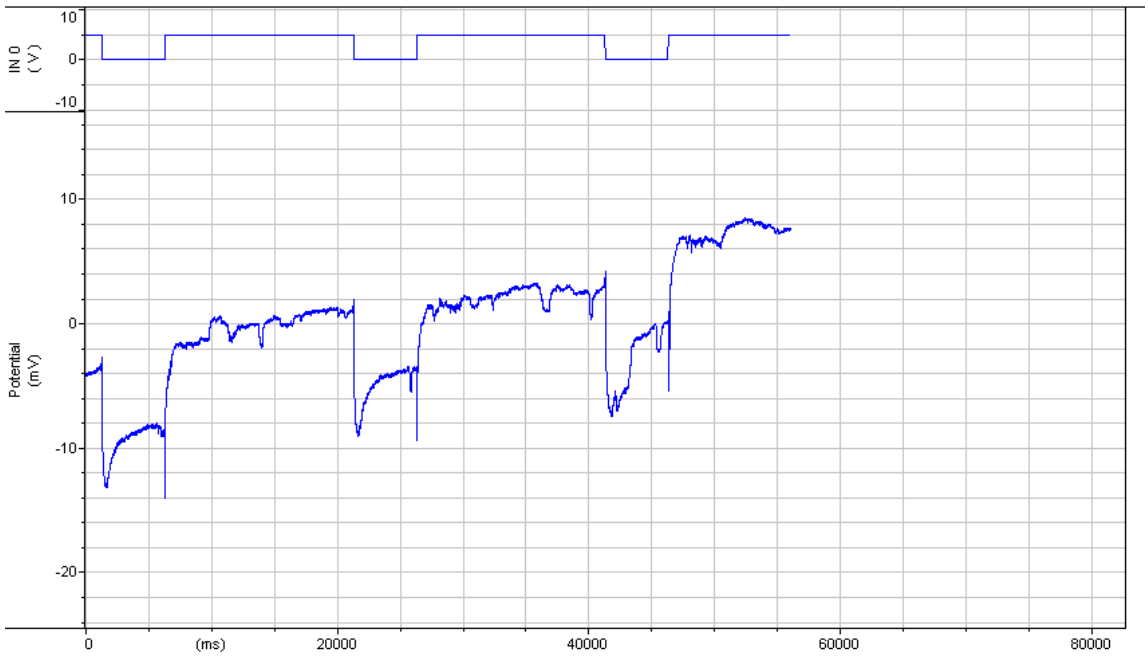

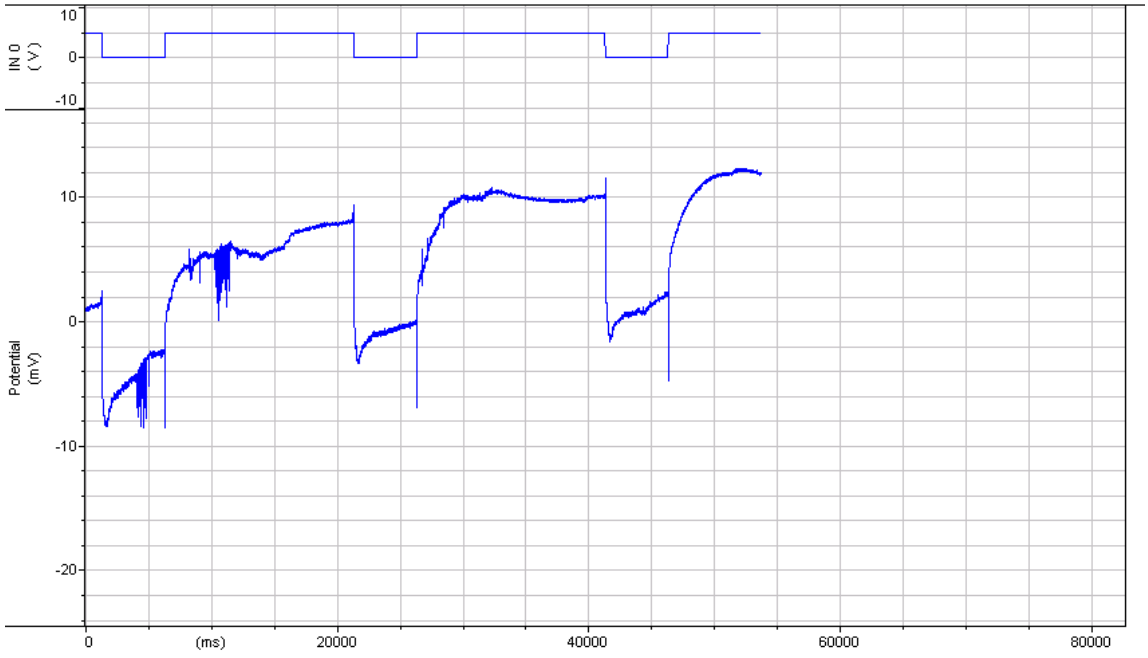

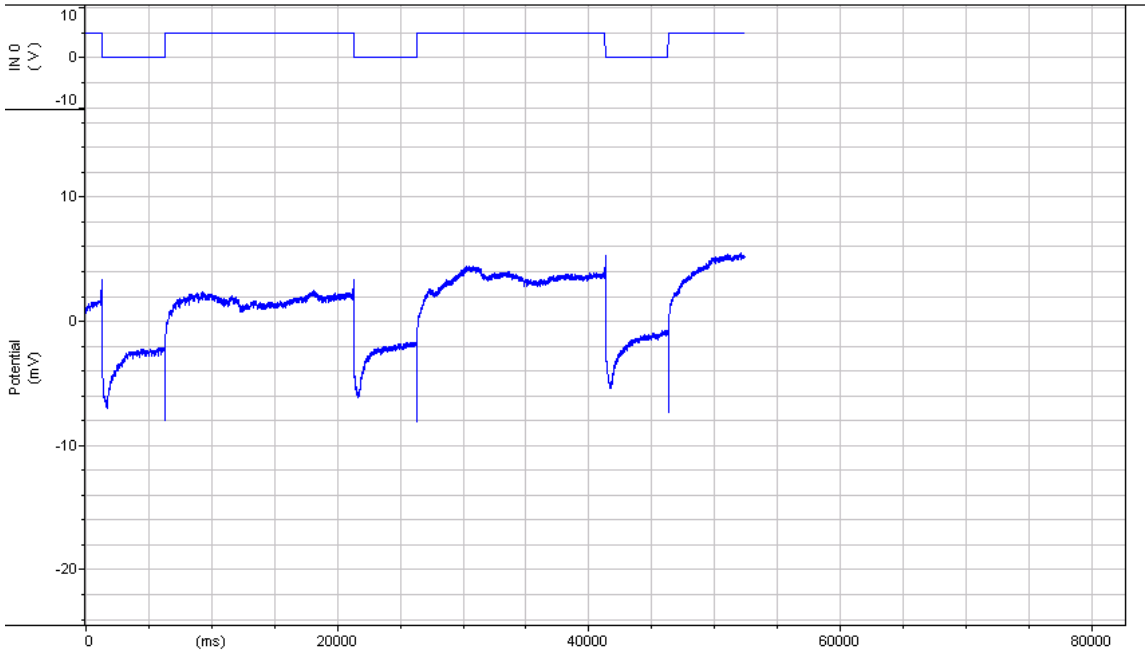
IN 0
(V)
10
0
-10
10
0
-10
-20
Potential
(mV)
0
(ms)
20000
40000
60000
80000

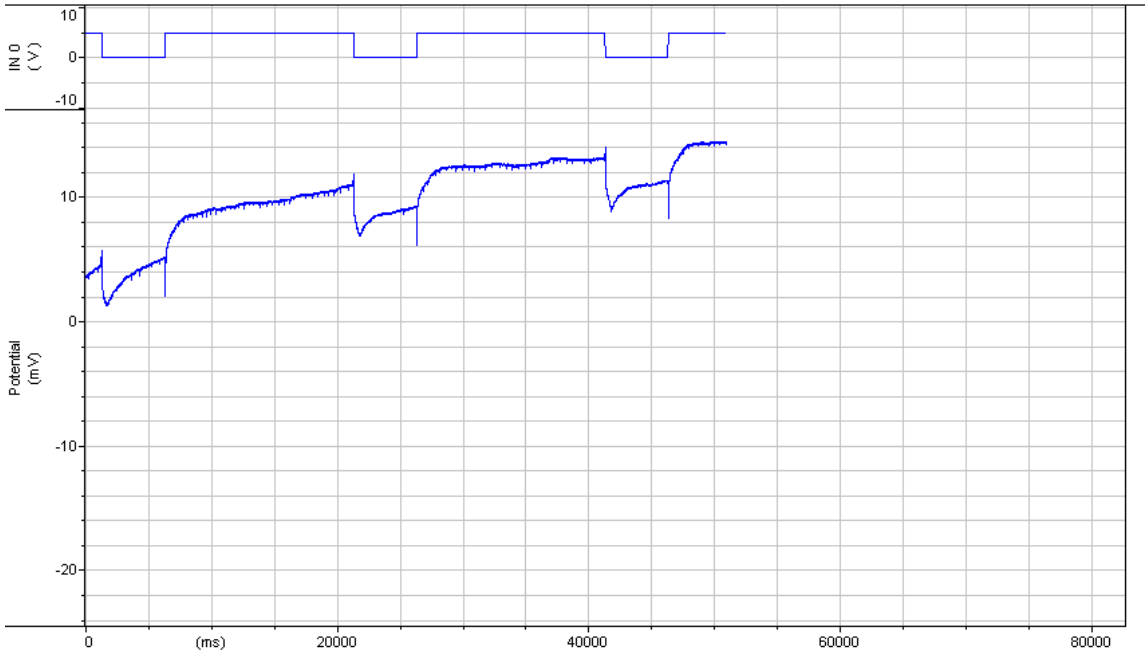
IN 0
(V)
10
0
-10
10
0
-10
-20
Potential
(mV)
0
(ms)
20000
40000
60000
80000

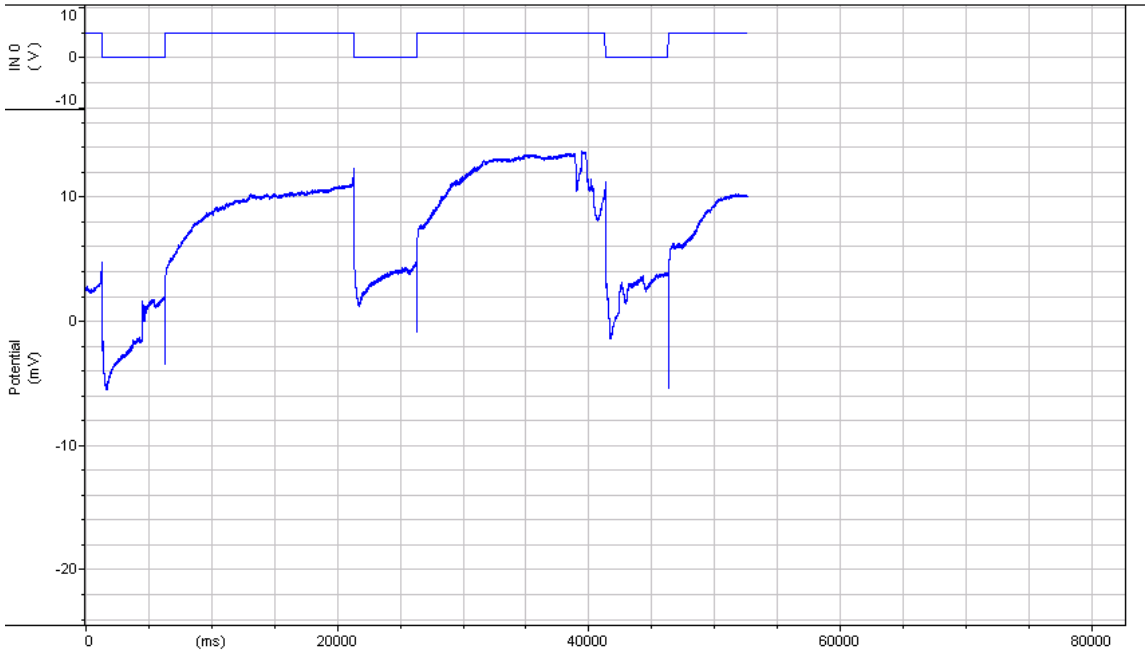
IN 0
(V)
10
0
-10
10
0
-10
-20
Potential
(mV)
0
(ms)
20000
40000
60000
80000

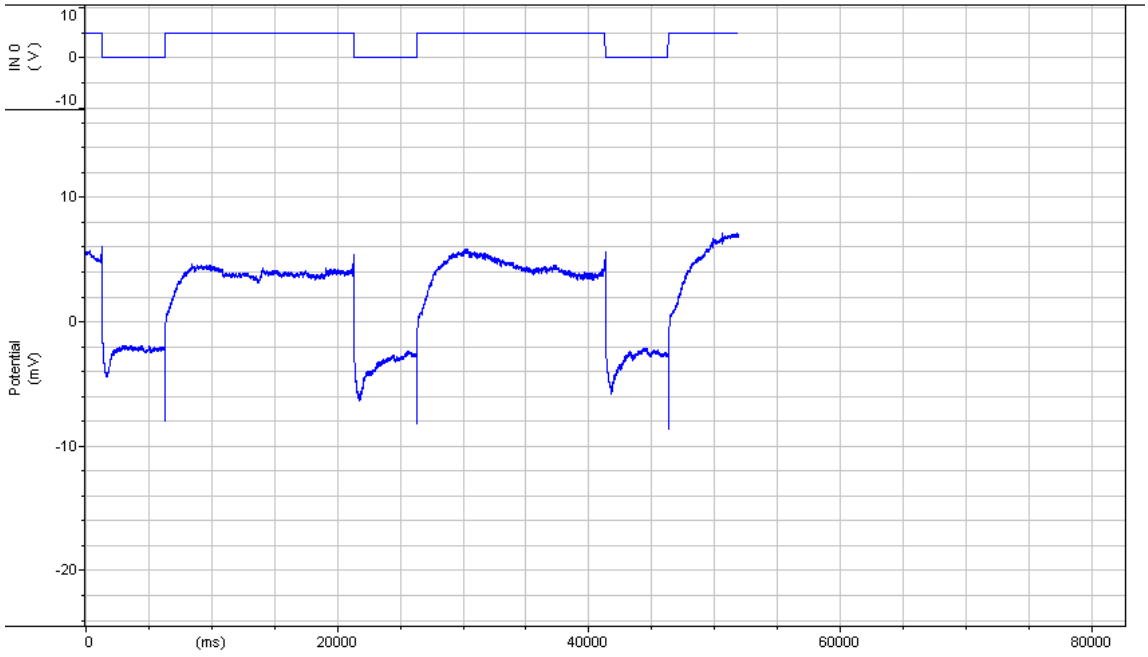
IN 0
(V)
10
0
-10
10
0
-10
-20
Potential
(mV)
0
(ms)
20000
40000
60000
80000

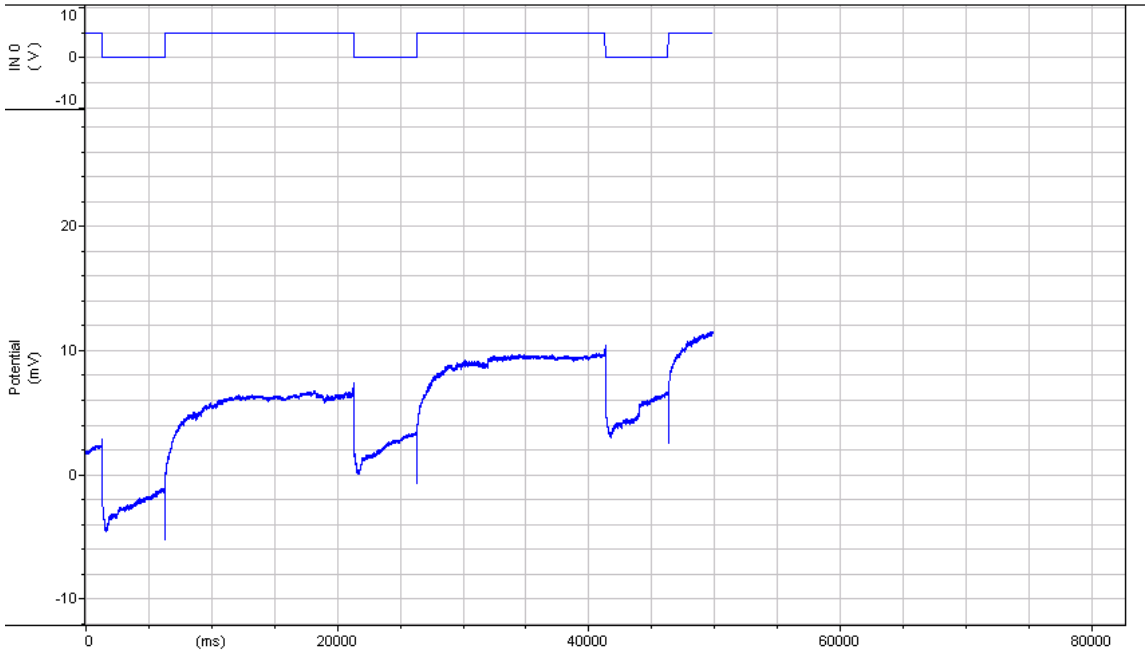
IN 0
(V)
10
0
-10
20
Potential
(mV)
10
0
-10
0
(ms)
20000
40000
60000
80000

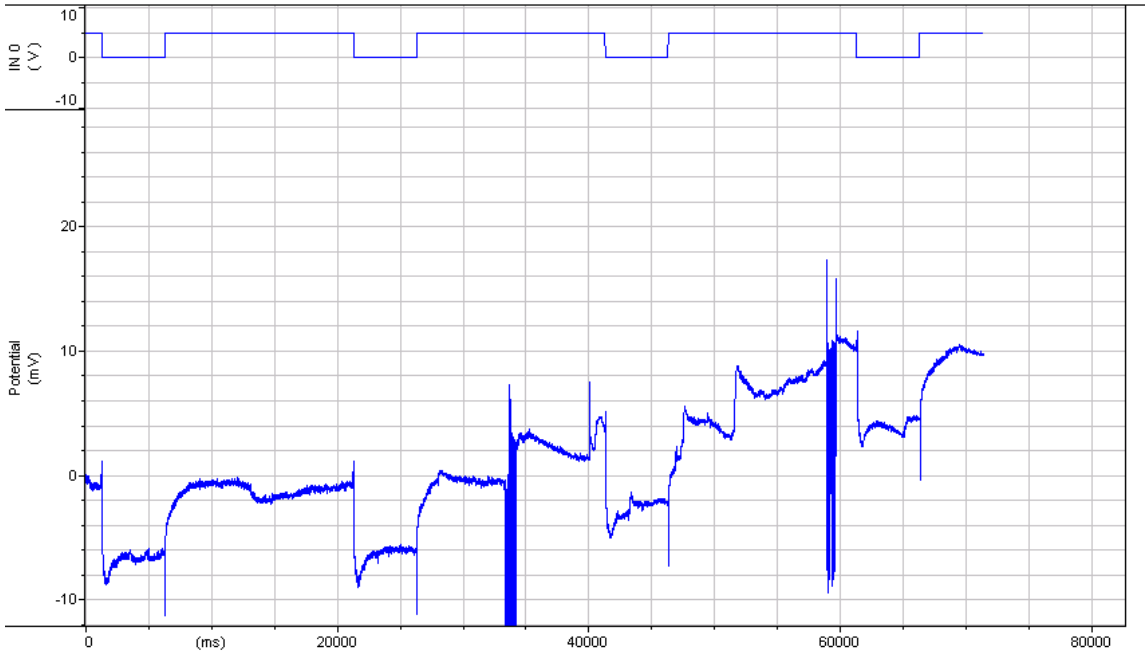
IN 0
(V)
10
0
-10
20
Potential
(mV)
10
0
-10
0
(ms)
20000
40000
60000
80000

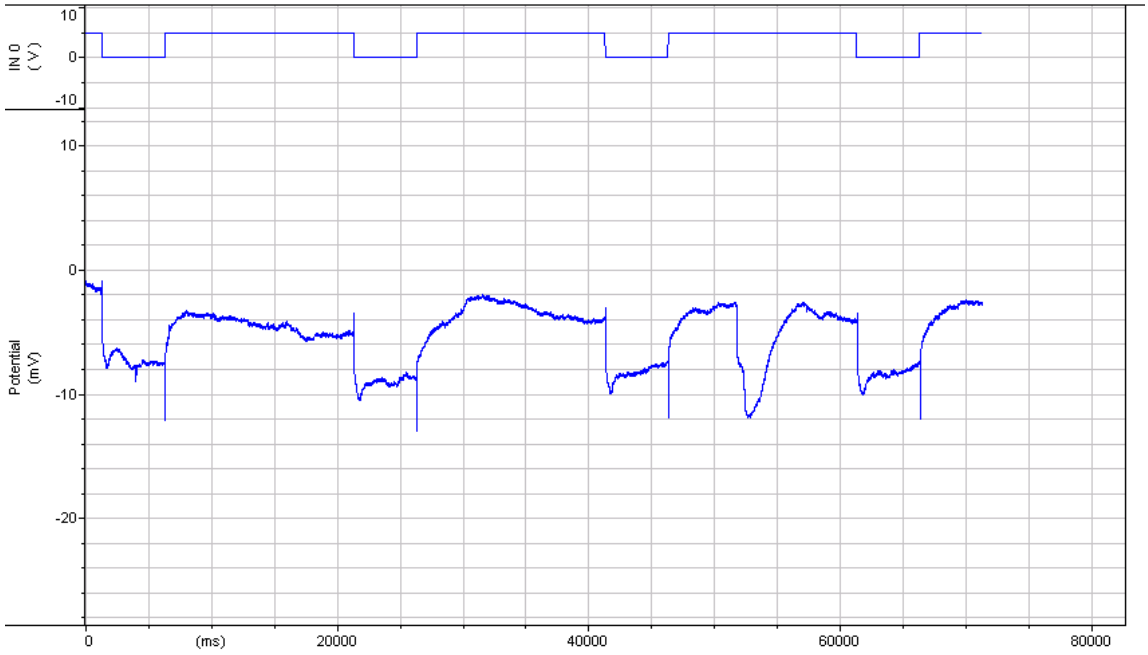
IN 0
(V)
10
0
-10
10
0
-10
-20
Potential
(mV)
0
(ms)
20000
40000
60000
80000

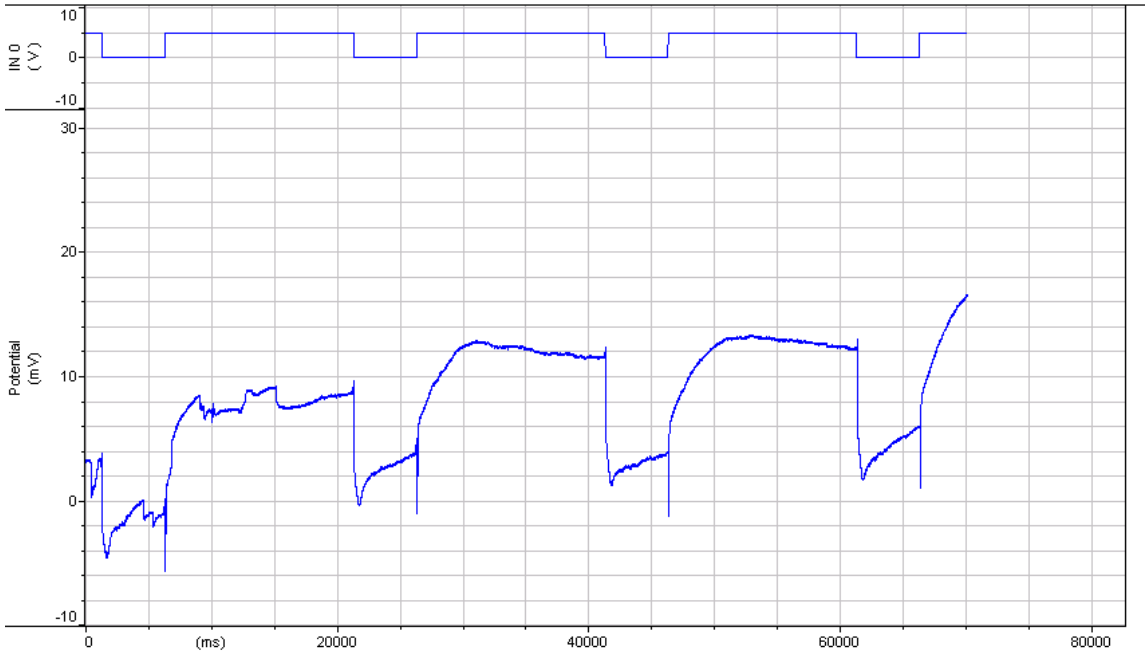
IN 0
(V)
10
0
-10
30
20
10
0
-10
Potential
(mV)
0
(ms)
20000
40000
60000
80000

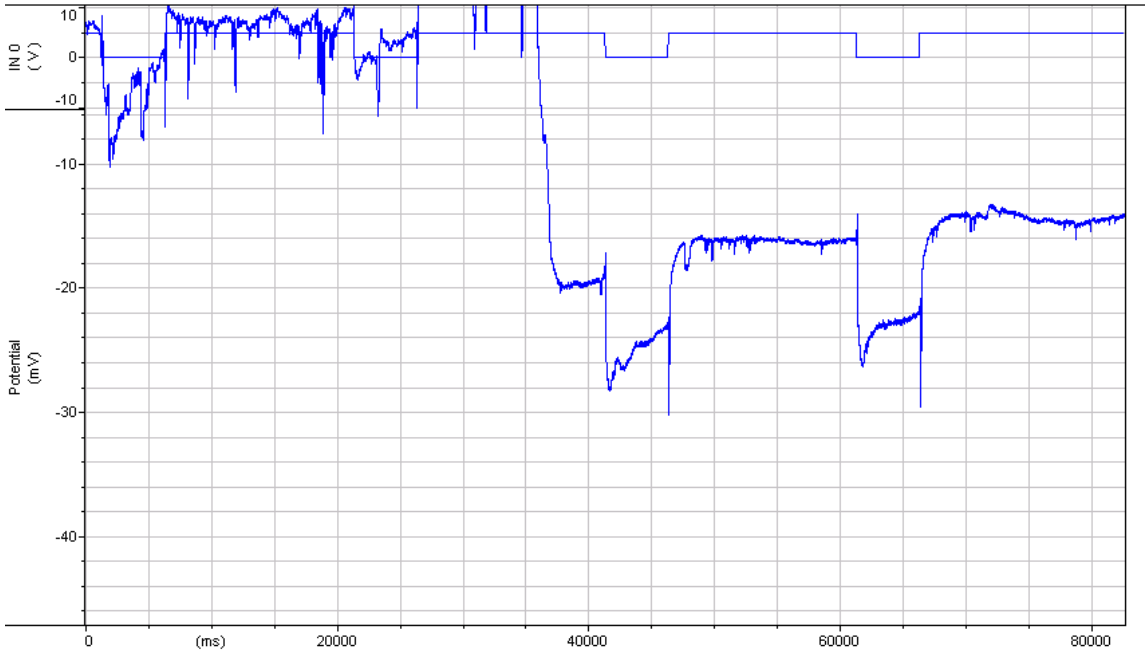
IN 0
(V)
10
0
-10
-10
-20
-30
-40
Potential
(mV)
0
(ms)
20000
40000
60000
80000

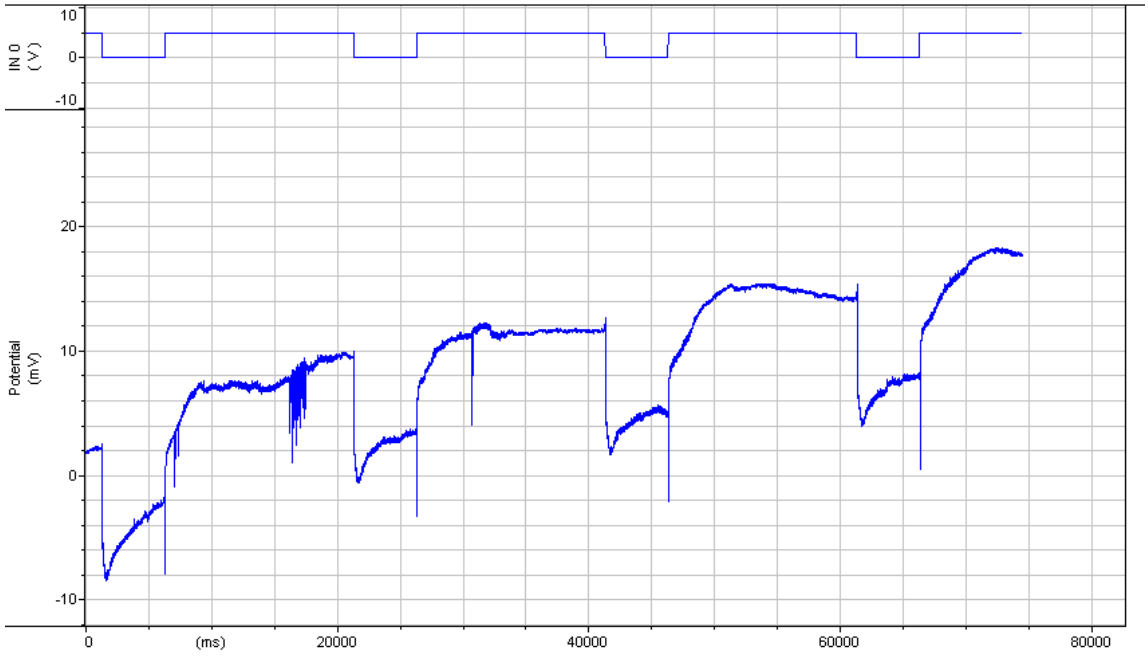
IN 0
(V)
10
0
-10
20
10
0
-10
Potential
(mV)
0
(ms)
20000
40000
60000
80000

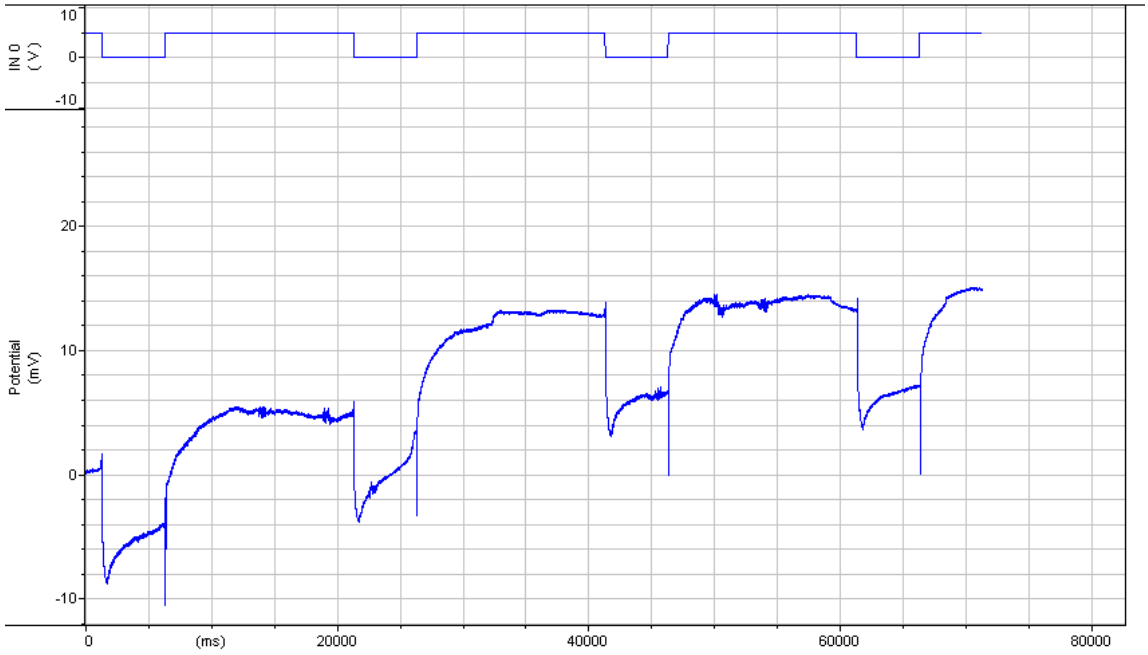
IN 0
(V)
10
0
-10
20
Potential
(mV)
10
0
-10
0
(ms)
20000
40000
60000
80000

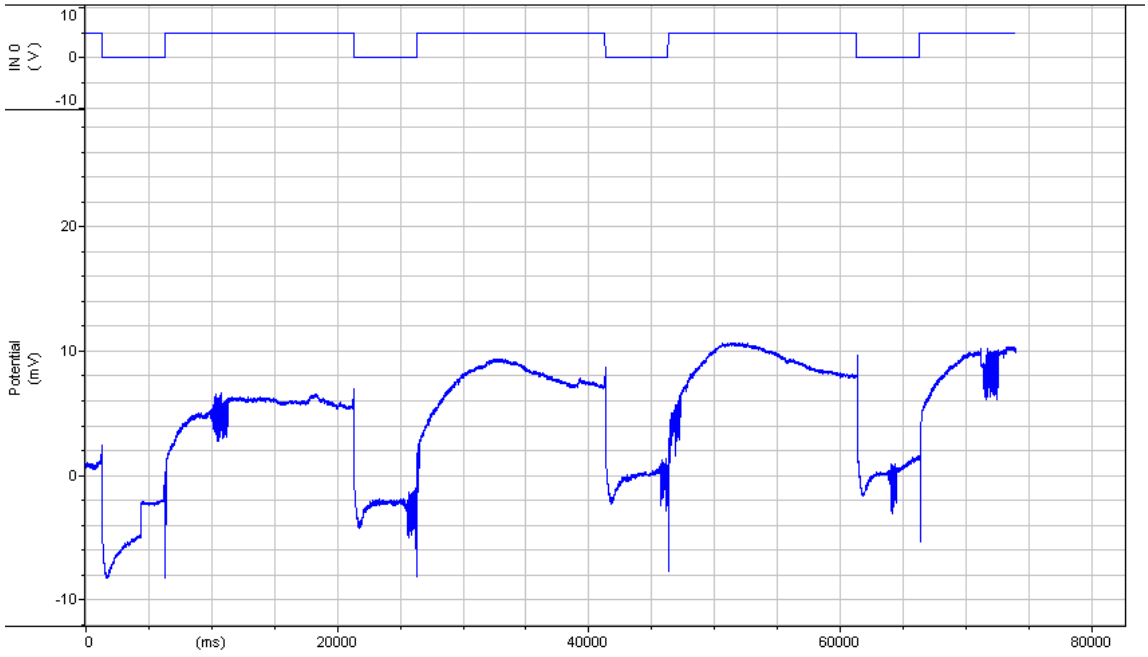
IN 0
(V)
10
0
-10
20
Potential
(mV)
10
0
-10
0
(ms)
20000
40000
60000
80000

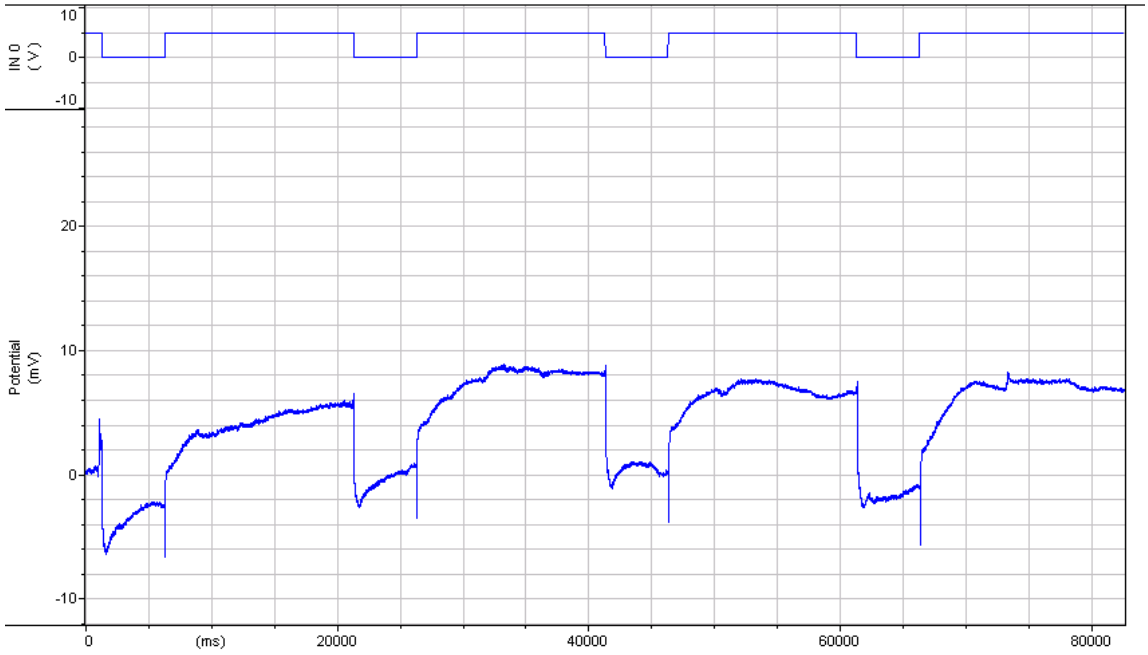
IN 0
(V)
10
0
-10
20
Potential
(mV)
10
0
-10
0
(ms)
20000
40000
60000
80000

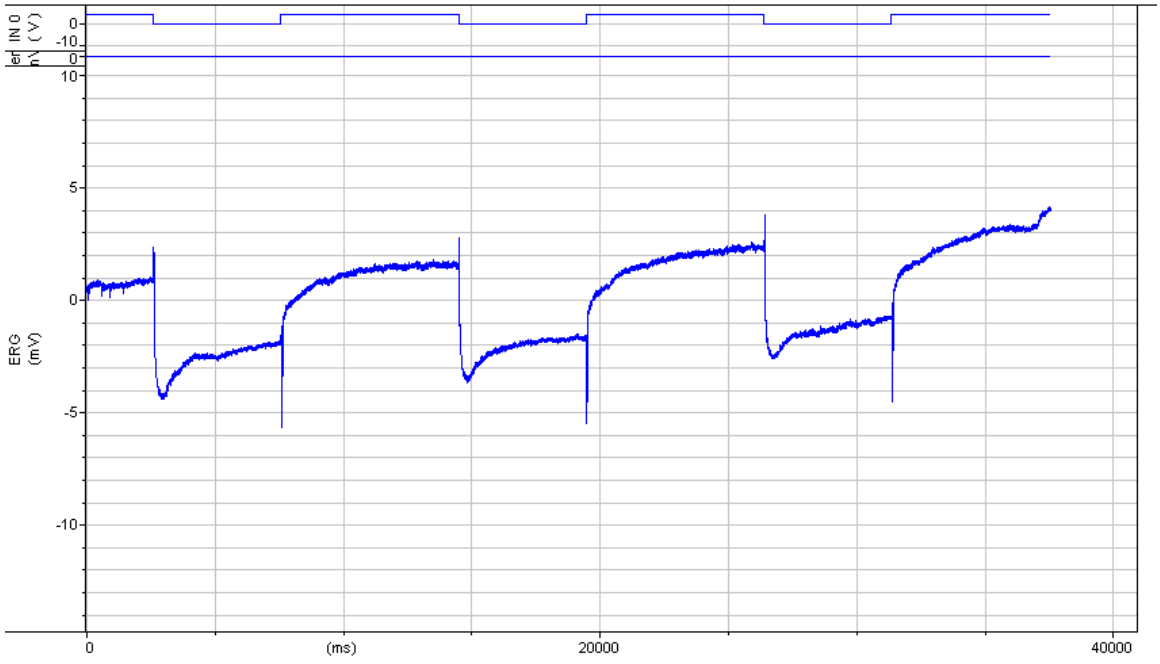
IN 0
(V)
0
-10
0
10
5
ERG
(mV)
0
-5
-10
0
(ms)
20000
40000

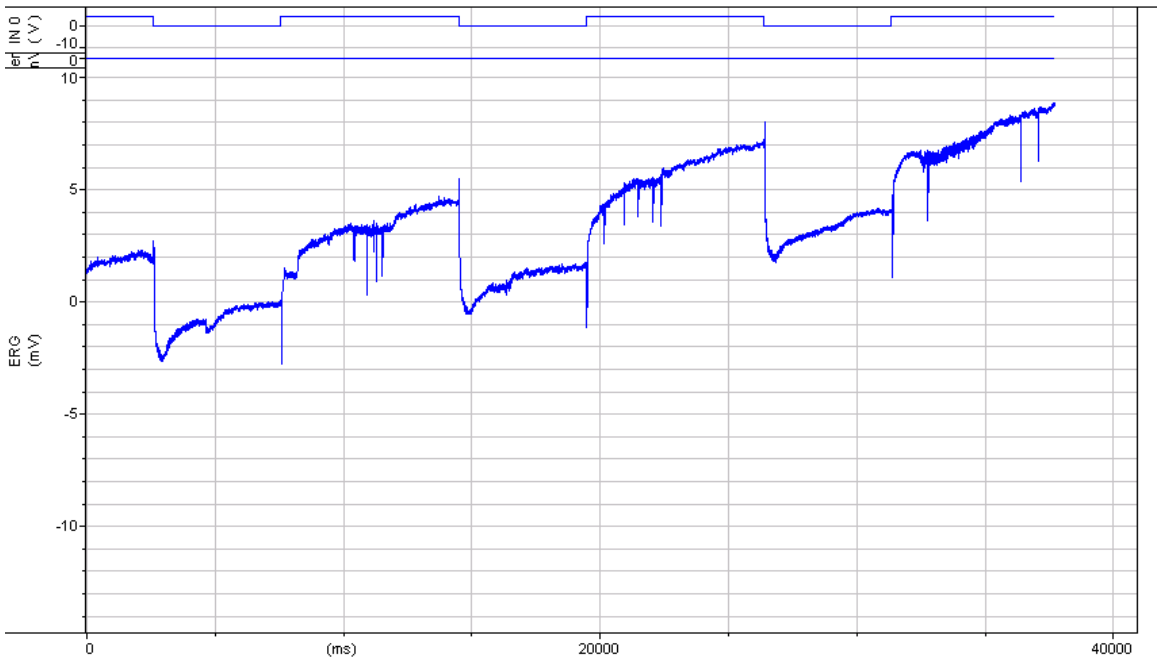
IN 0 (V)
0
-10
ref
0
10
5
0
-5
-10
ERG (mV)
0
(ms)
20000
40000

Genotype: TIFR-Gal4> *Acsl* RNAi

Phenotype: with transient

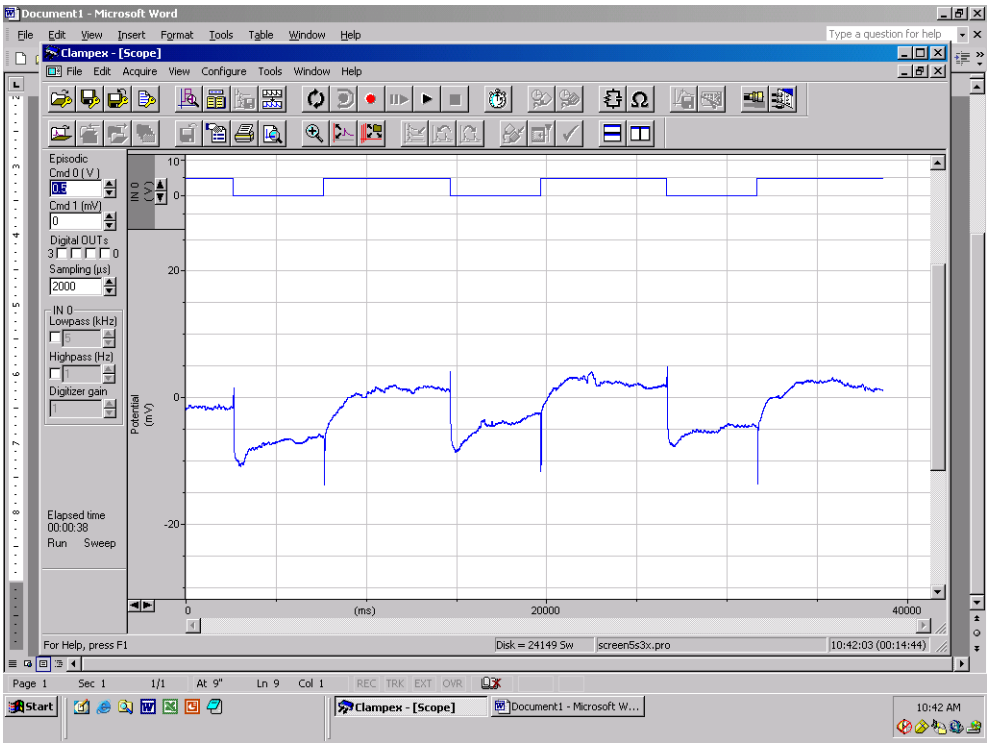

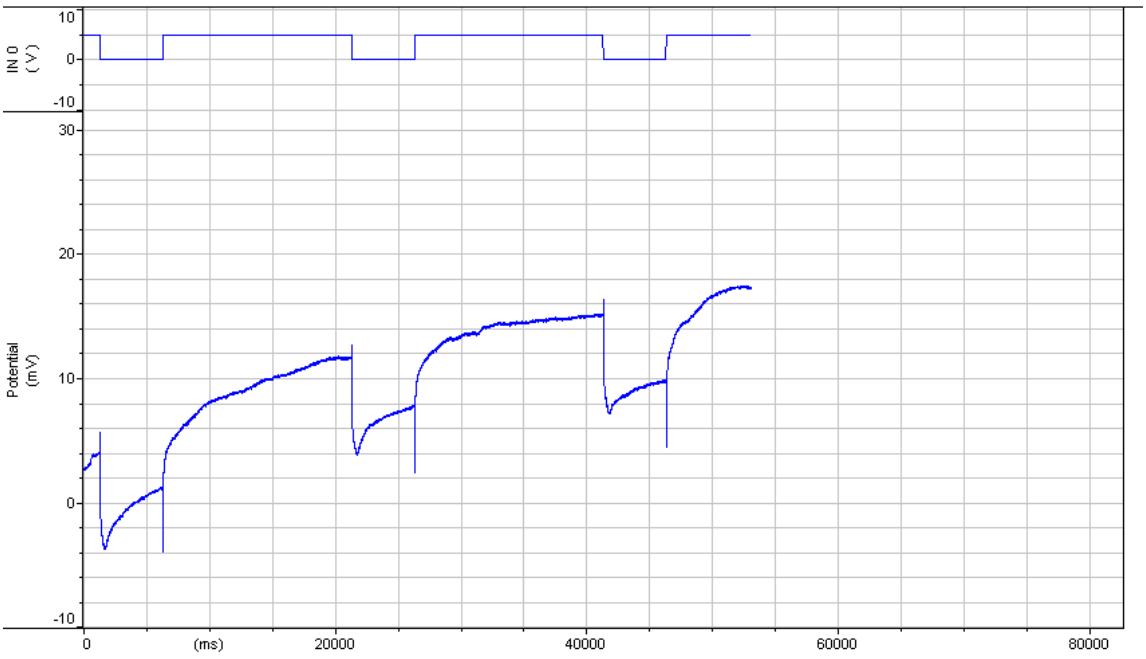

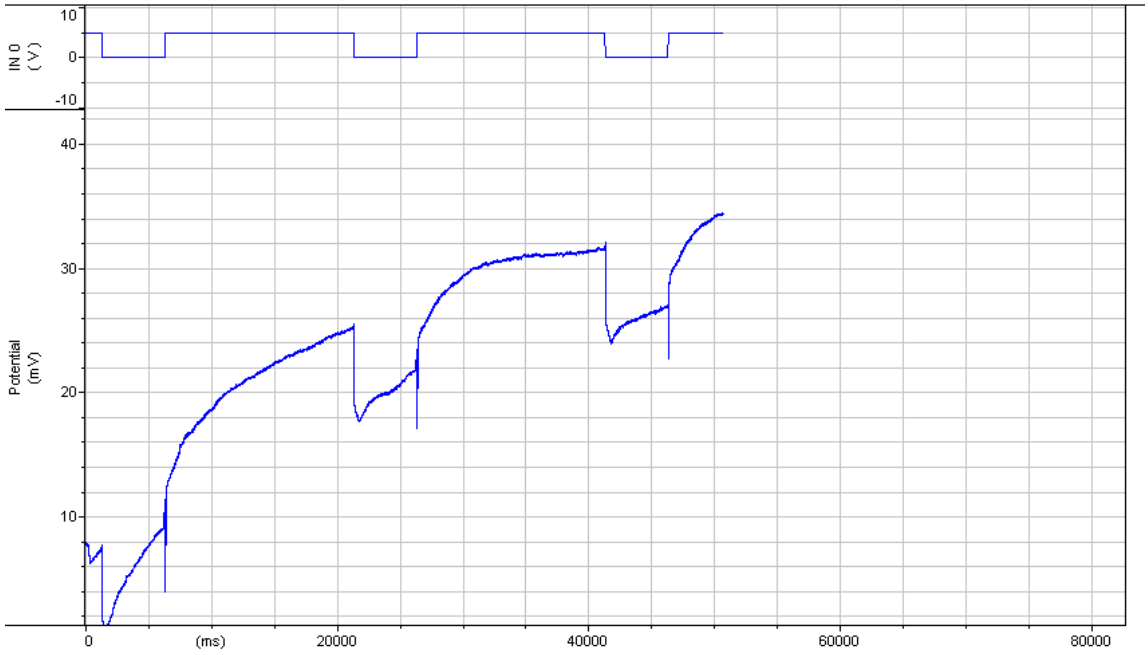
IN 0
(V)
10
0
-10
40
30
20
10
Potential
(mV)
0
(ms)
20000
40000
60000
80000

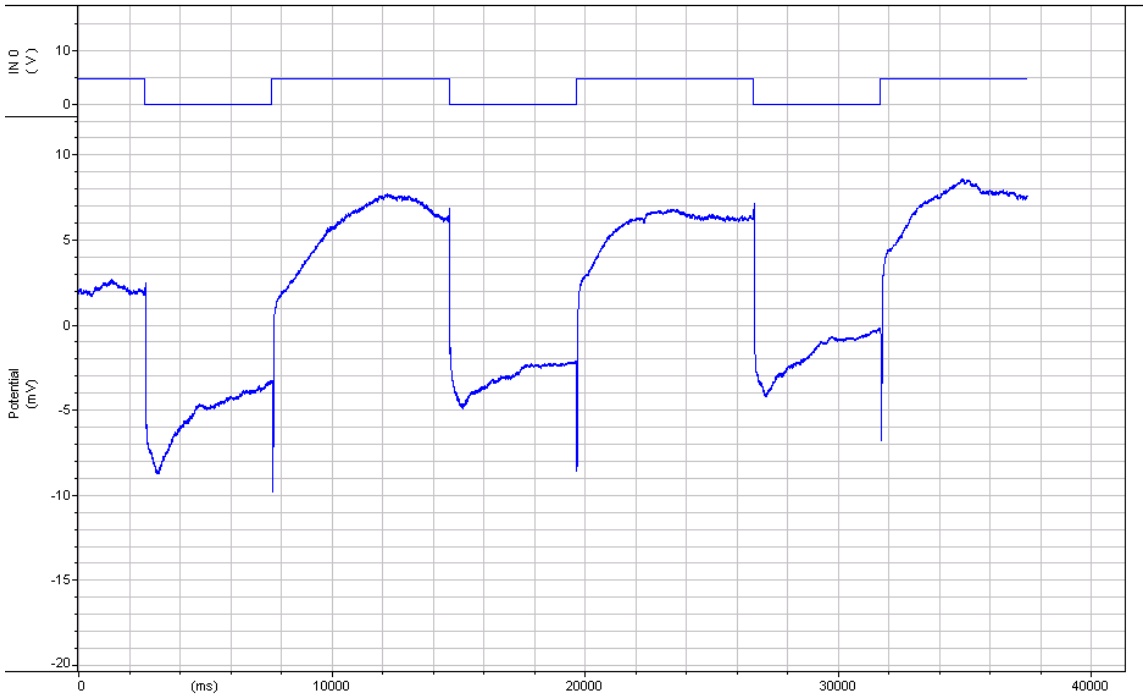
IN 0
(V)
10
0
10
5
0
-5
-10
-15
-20
Potential
(mV)
0
(ms)
10000
20000
30000
40000

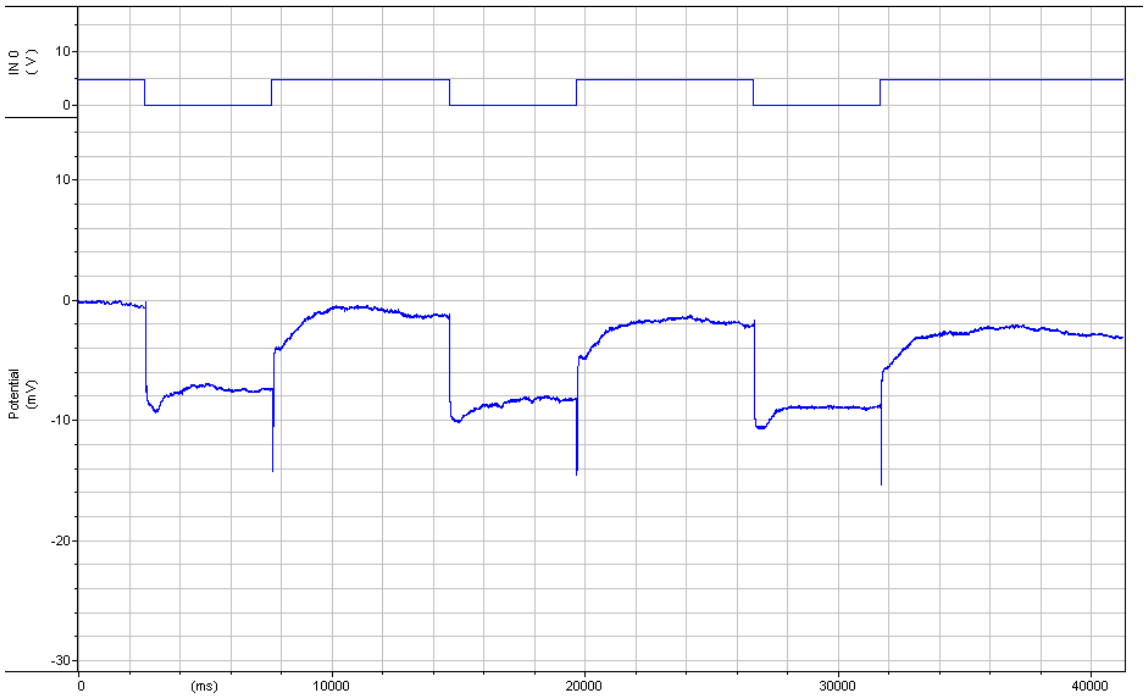
IN 0
(V)
10
0
10
0
Potential
(mV)
-10
-20
-30
0
(ms)
10000
20000
30000
40000

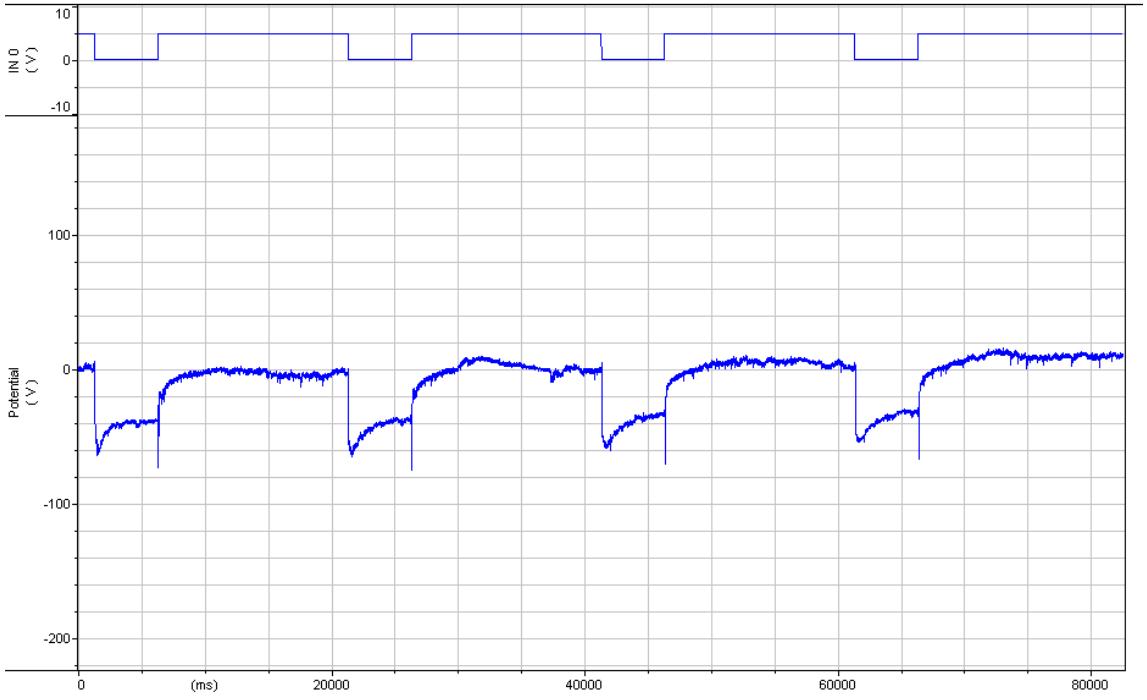
IN 0
(V)
10
0
-10
100
0
Potential
(V)
-100
-200
0
(ms)
20000
40000
60000
80000

Genotype: TIFR-Gal4> *Acsl* RNAi

Phenotype: loss of ‘on transient’

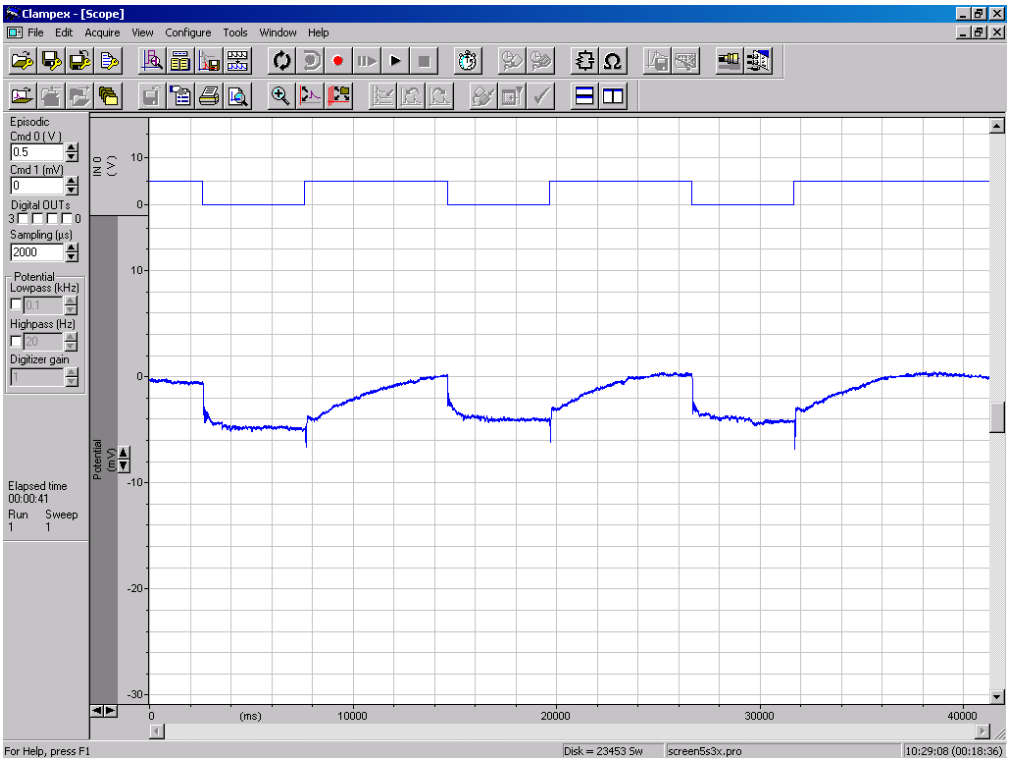

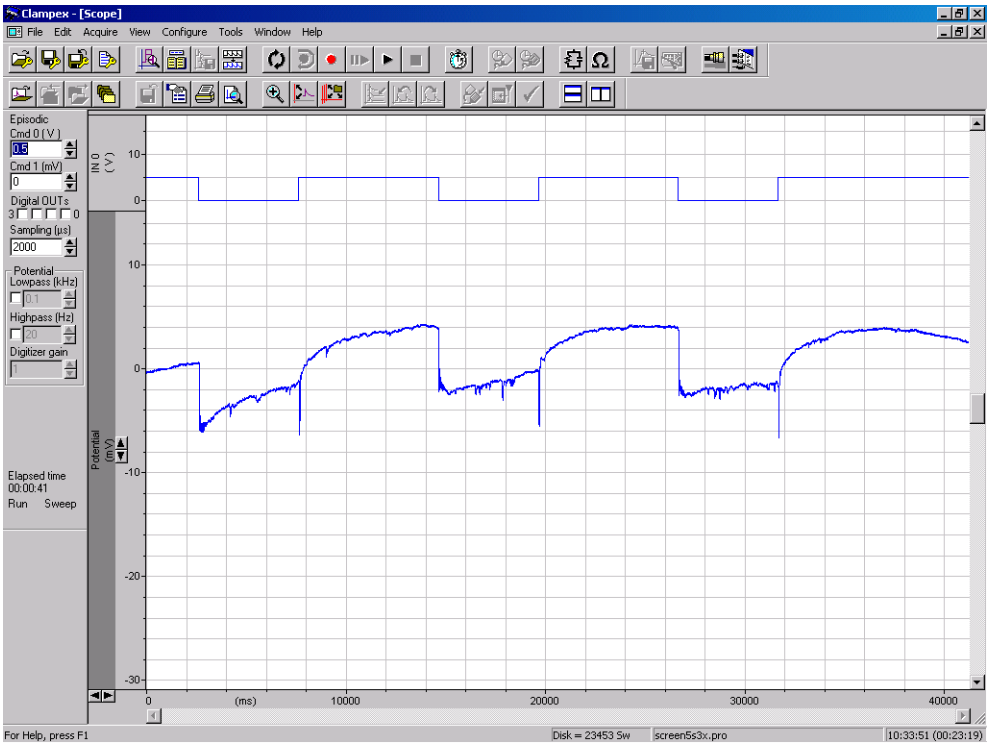
Clampex - [Scope]
File Edit Acquire View Configure Tools Window Help
Episodic
Cmd 0 (V)
0.5
Cmd 1 (mV)
0
Digital OUTs
Sampling (µs)
2000
Potential
Lowpass (kHz)
Highpass (Hz)
Digitizer gain
Elapsed time
00:00:41
Run Sweep
IN 0 (V)
Potential (mV)
(ms)
For Help, press F1
Disk = 23453 Sw
screen5s3x.pro
10:33:51 (00:23:19)

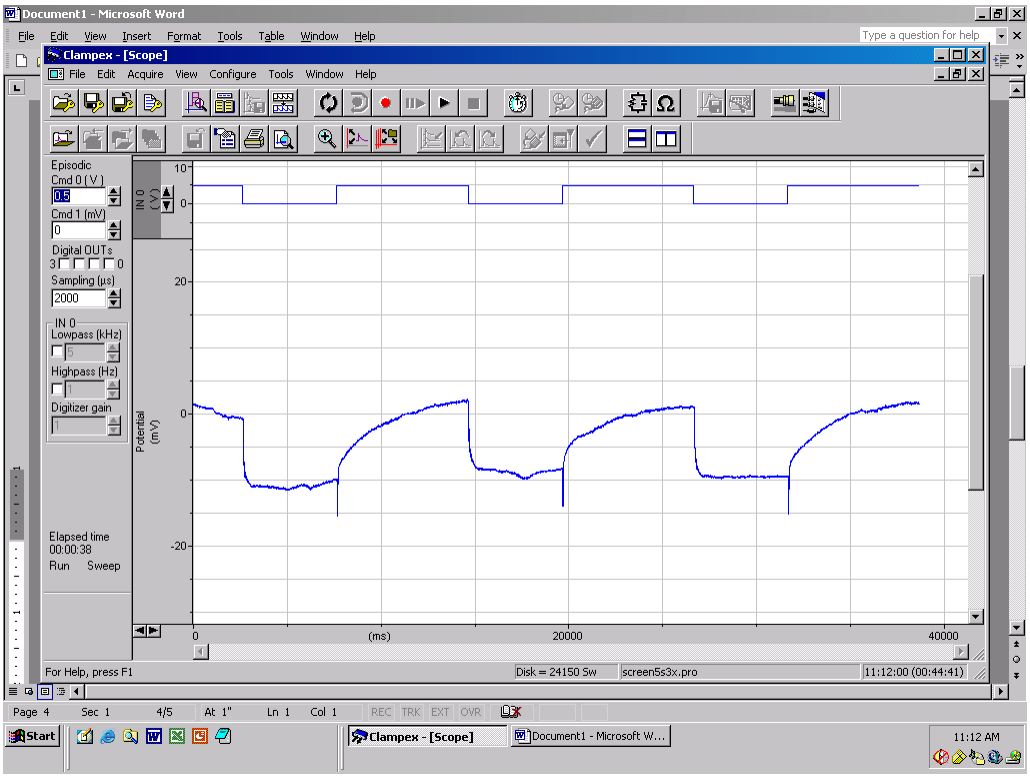
Document1 - Microsoft Word
File Edit View Insert Format Tools Table Window Help
Type a question for help
Clampex - [Scope]
File Edit Acquire View Configure Tools Window Help
Episodic
Cmd 0 (V)
0.5
Cmd 1 (mV)
0
Digital OUTs
Sampling (µs)
2000
IN 0
Lowpass (kHz)
Highpass (Hz)
Digitizer gain
Elapsed time
00:00:38
Run Sweep
IN 0 (V)
Potential (mV)
(ms)
For Help, press F1
Disk = 24150 Sw
screen5s3x.pro
11:12:00 (00:44:41)
Page 4 Sec 1 4/5 At 1" Ln 1 Col 1 REC TRK EXT OVR
Start
Clampex - [Scope]
Document1 - Microsoft W...
11:12 AM

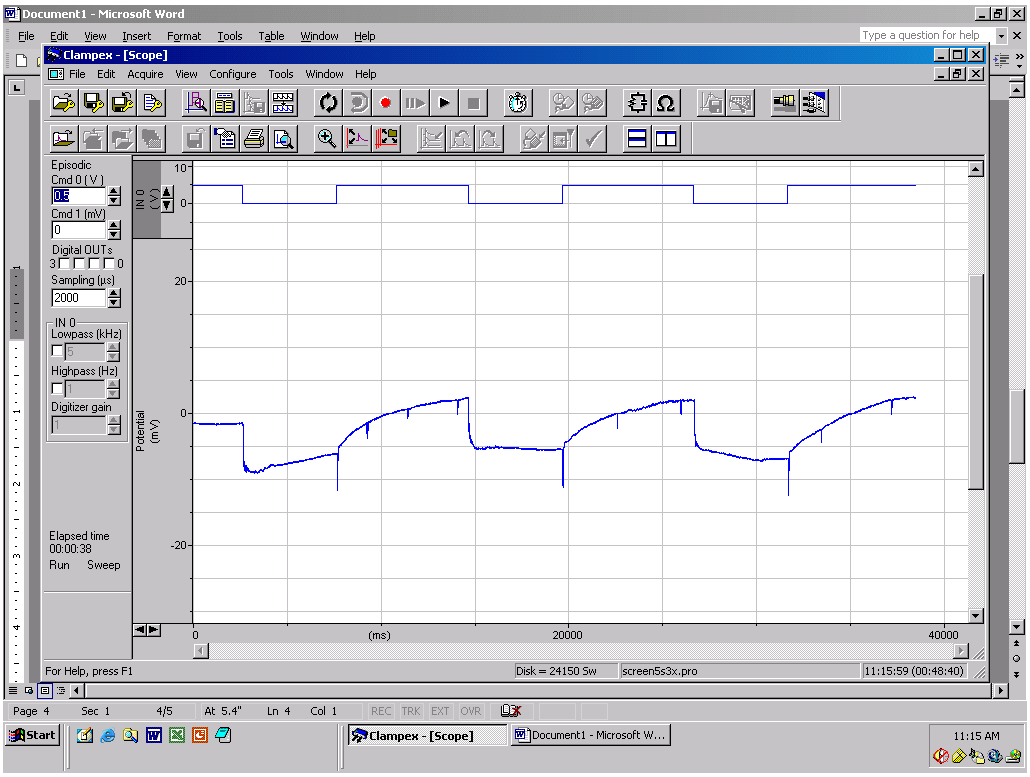
Document1 - Microsoft Word
Clampex - [Scope]
Episodic
Cmd 0 (V)
0.5
Cmd 1 (mV)
0
Digital OUTs
Sampling (µs)
2000
IN 0
Lowpass (kHz)
Highpass (Hz)
Digitizer gain
Elapsed time
00:00:38
Run Sweep
Potential (mV)
(ms)
20000
40000
For Help, press F1
Disk = 24150 Sw
screen5s3x.pro
11:15:59 (00:48:40)
11:15 AM

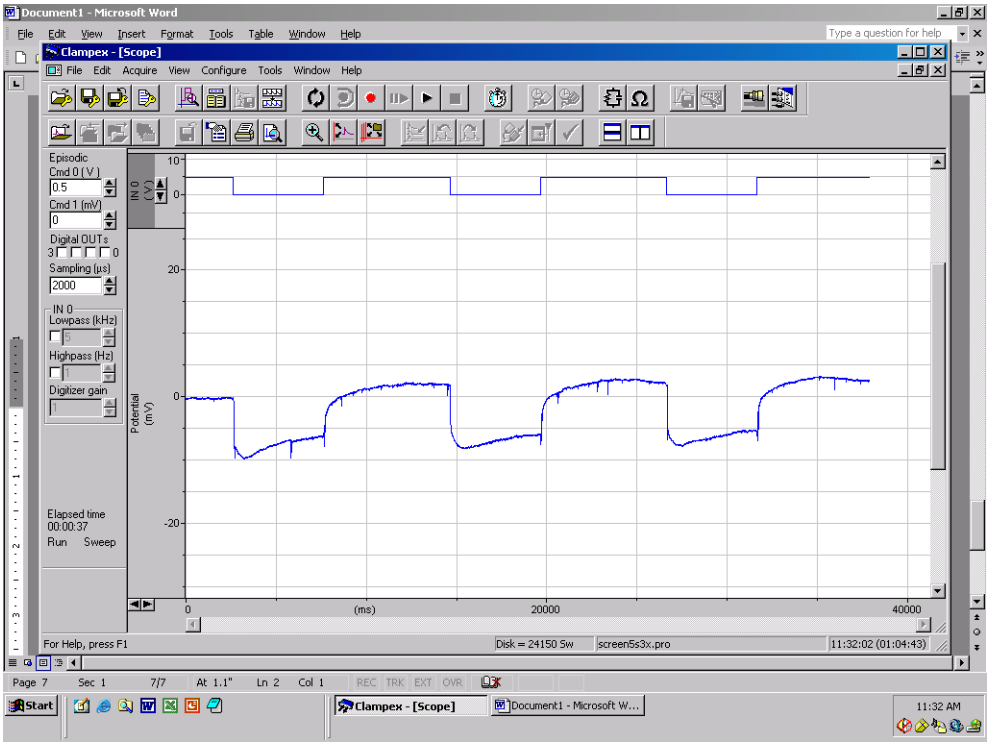
Document1 - Microsoft Word
Clampex - [Scope]
Episodic
Cmd 0 (V)
0.5
Cmd 1 (mV)
0
Digital OUTs
Sampling (µs)
2000
IN 0
Lowpass (kHz)
Highpass (Hz)
Digitizer gain
Elapsed time
00:00:37
Run Sweep
Potential (mV)
(ms)
20000
40000
For Help, press F1
Disk = 24150 Sw
screen5s3x.pro
11:32:02 (01:04:43)
11:32 AM

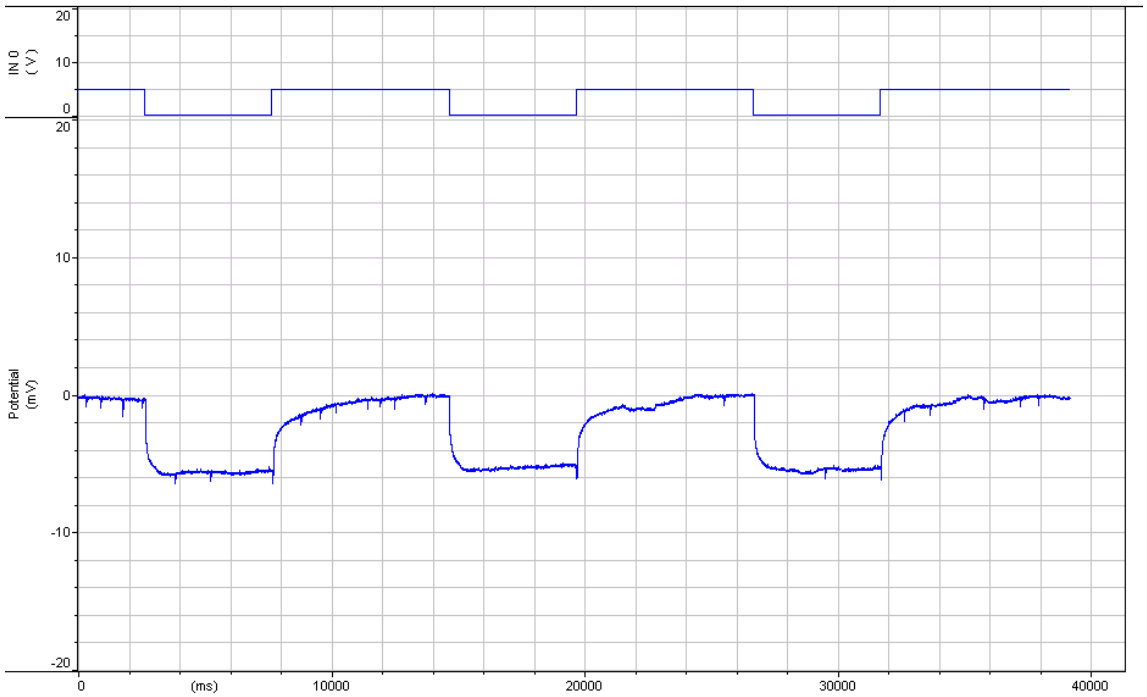
IN 0
(V)
20
10
0
Potential
(mV)
20
10
0
-10
-20
0
(ms)
10000
20000
30000
40000

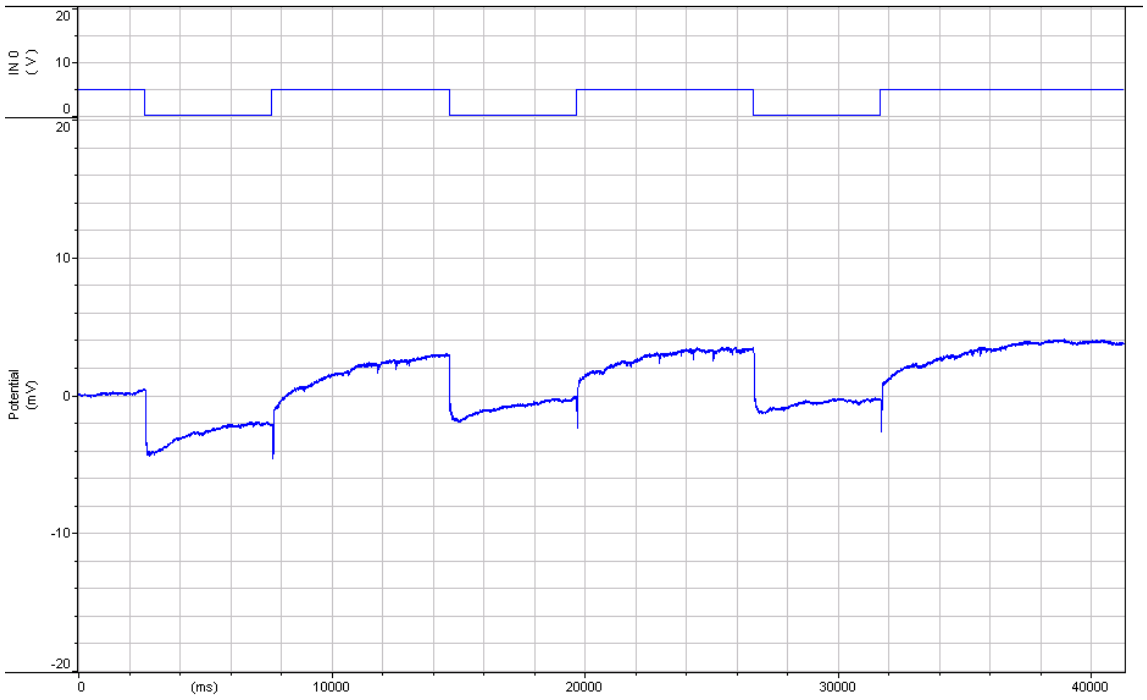
IN 0
(V)
20
10
0
Potential
(mV)
20
10
0
-10
-20
0
(ms)
10000
20000
30000
40000

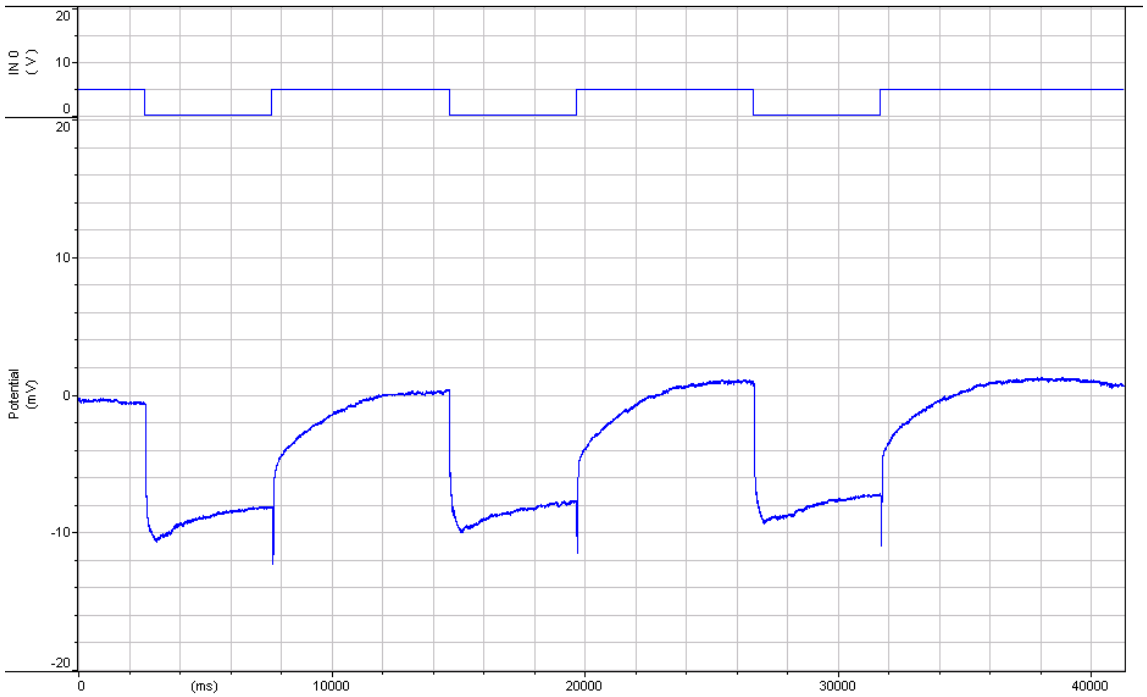
IN 0
(V)
20
10
0
Potential
(mV)
20
10
0
-10
-20
0
(ms)
10000
20000
30000
40000

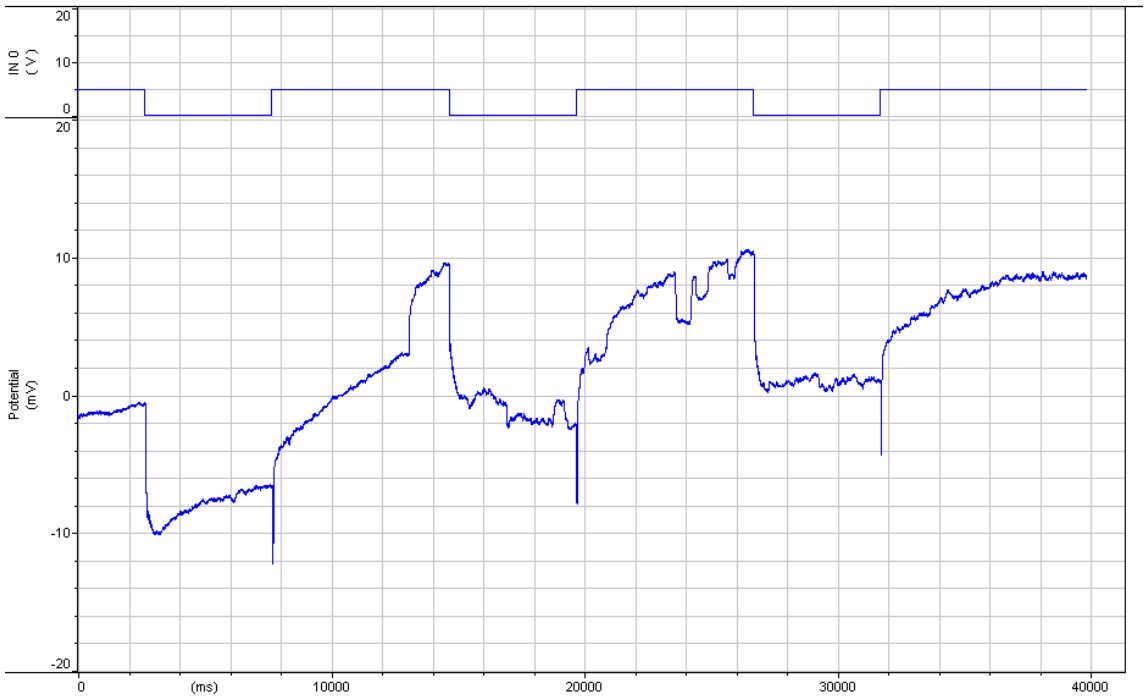
IN 0
(V)
20
10
0
Potential
(mV)
20
10
0
-10
-20
0
(ms)
10000
20000
30000
40000

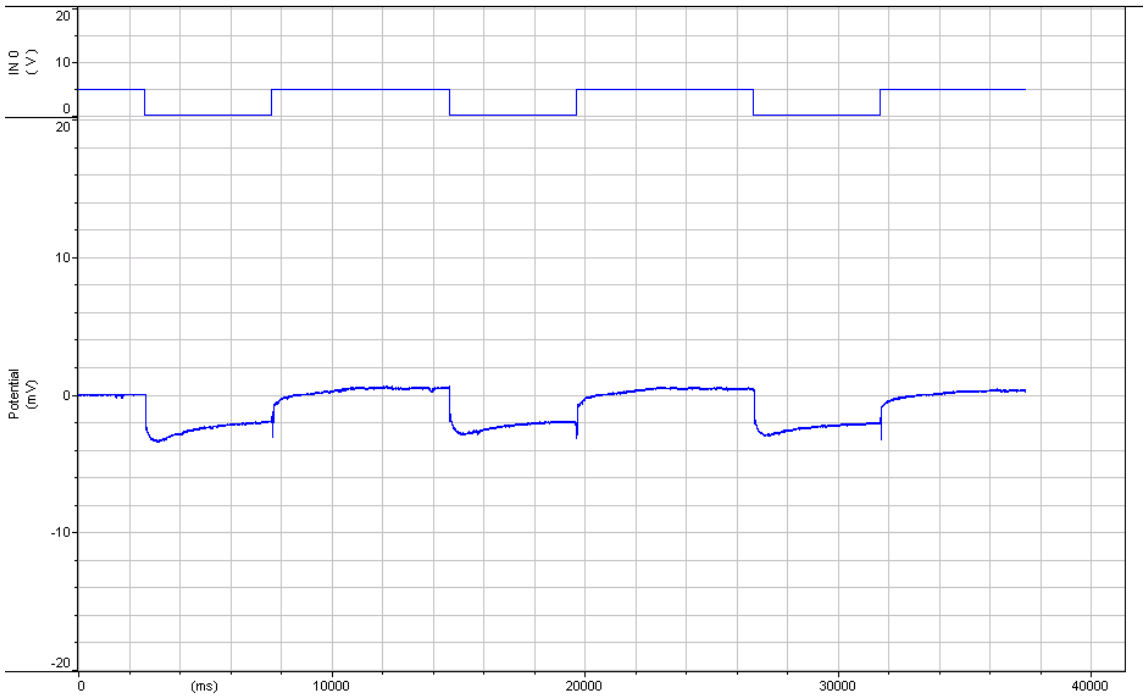
IN 0
(V)
20
10
0
Potential
(mV)
20
10
0
-10
-20
0
(ms)
10000
20000
30000
40000

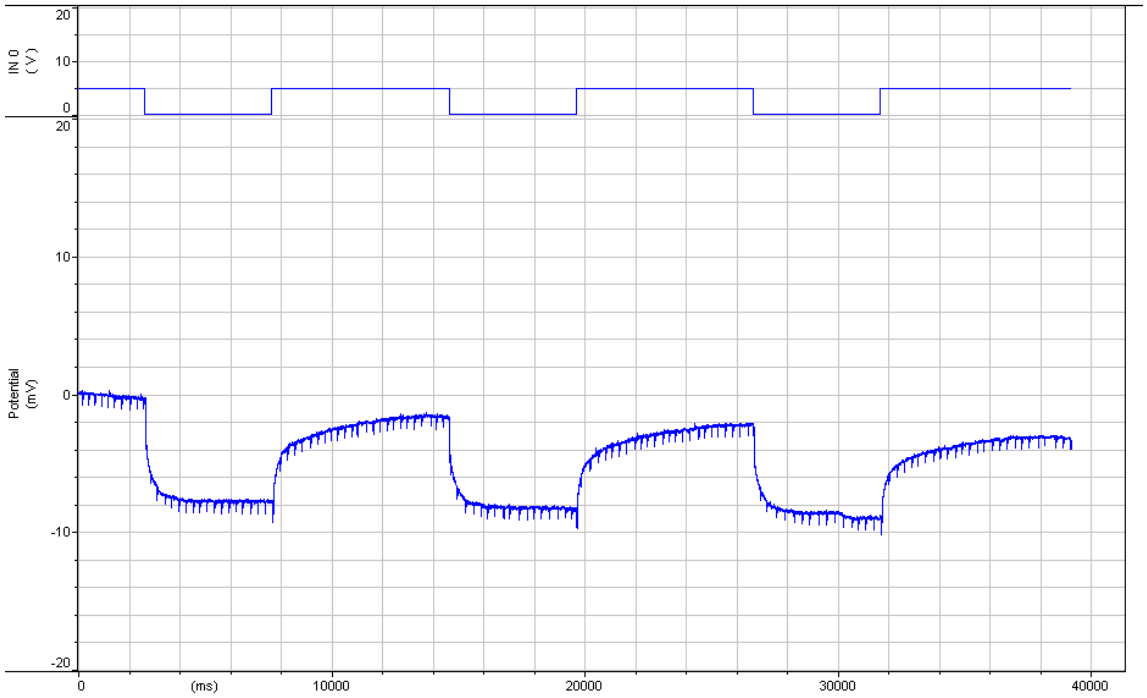
IN 0
(V)
20
10
0
Potential
(mV)
20
10
0
-10
-20
0
(ms)
10000
20000
30000
40000

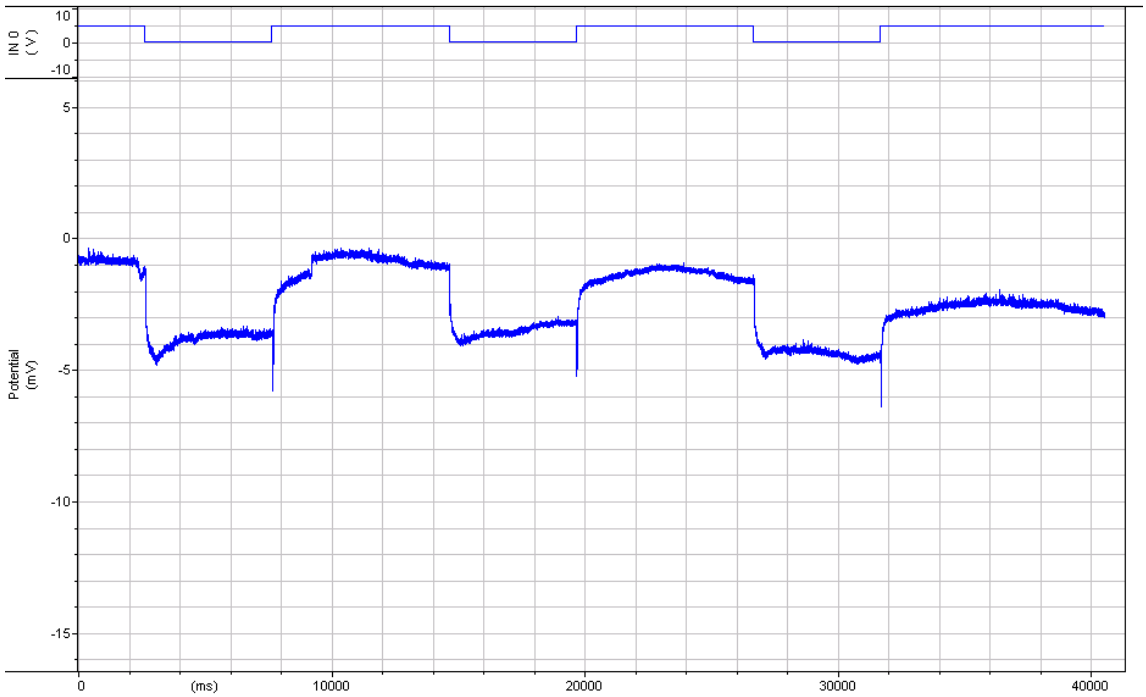
IN 0
(V)
10
0
-10
5
0
-5
-10
-15
Potential
(mV)
0
(ms)
10000
20000
30000
40000

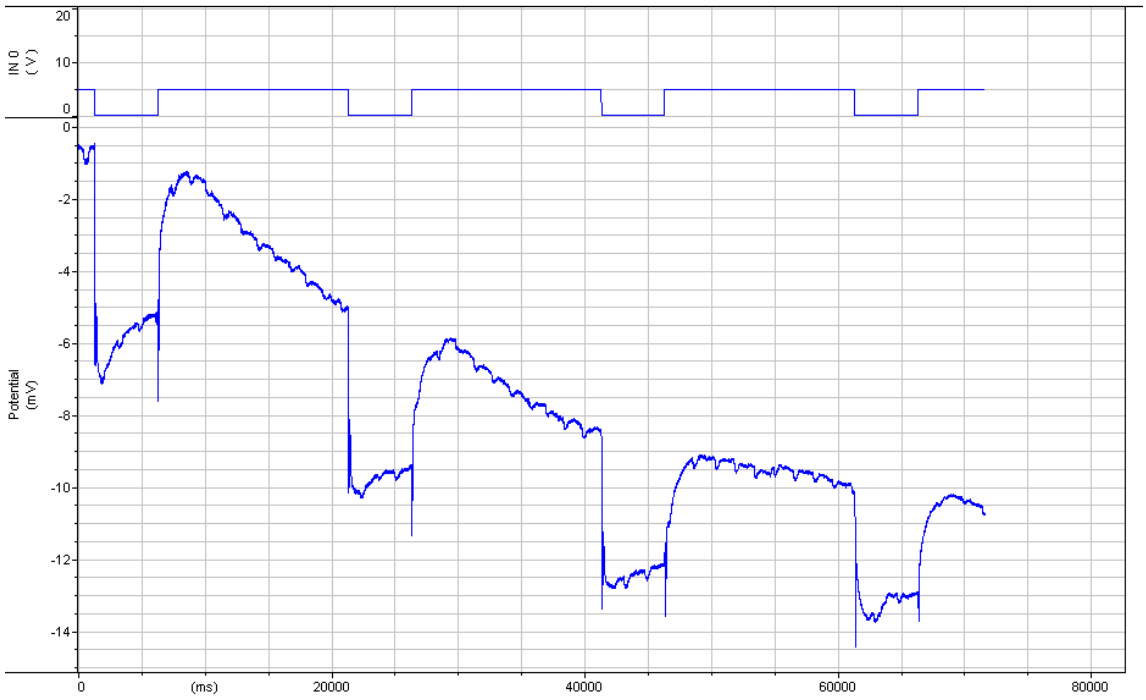
IN 0
(V)
20
10
0
0
-2
-4
-6
-8
-10
-12
-14
Potential
(mV)
0
(ms)
20000
40000
60000
80000

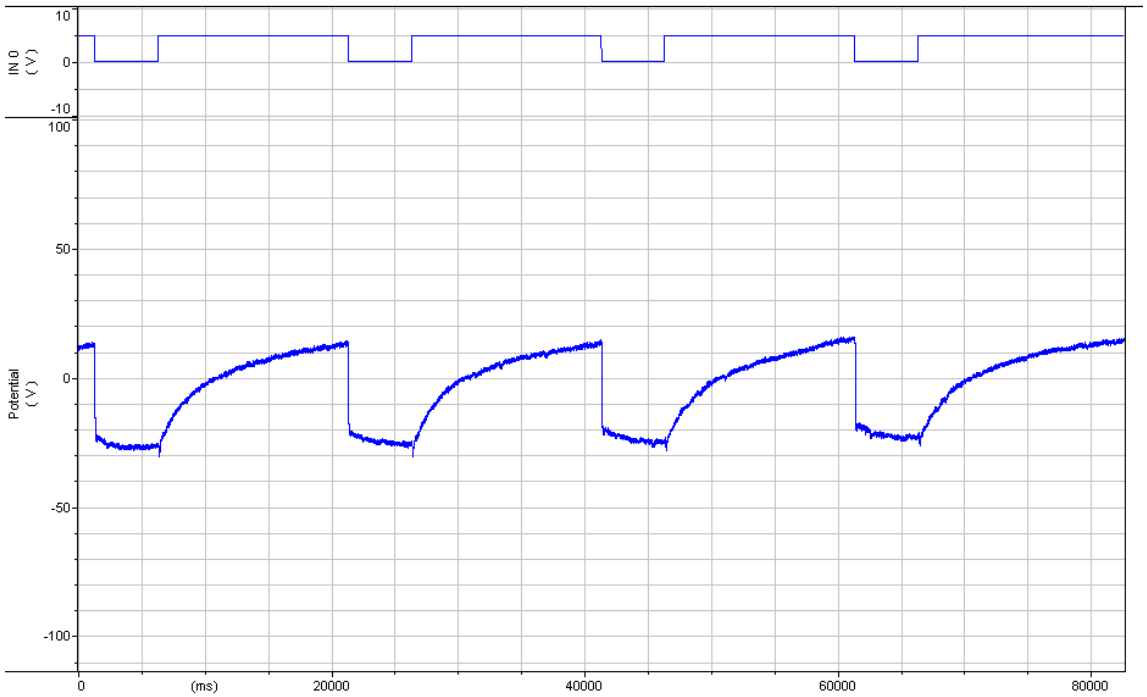
IN 0
(V)
10
0
-10
Potential
(V)
100
50
0
-50
-100
0
(ms)
20000
40000
60000
80000

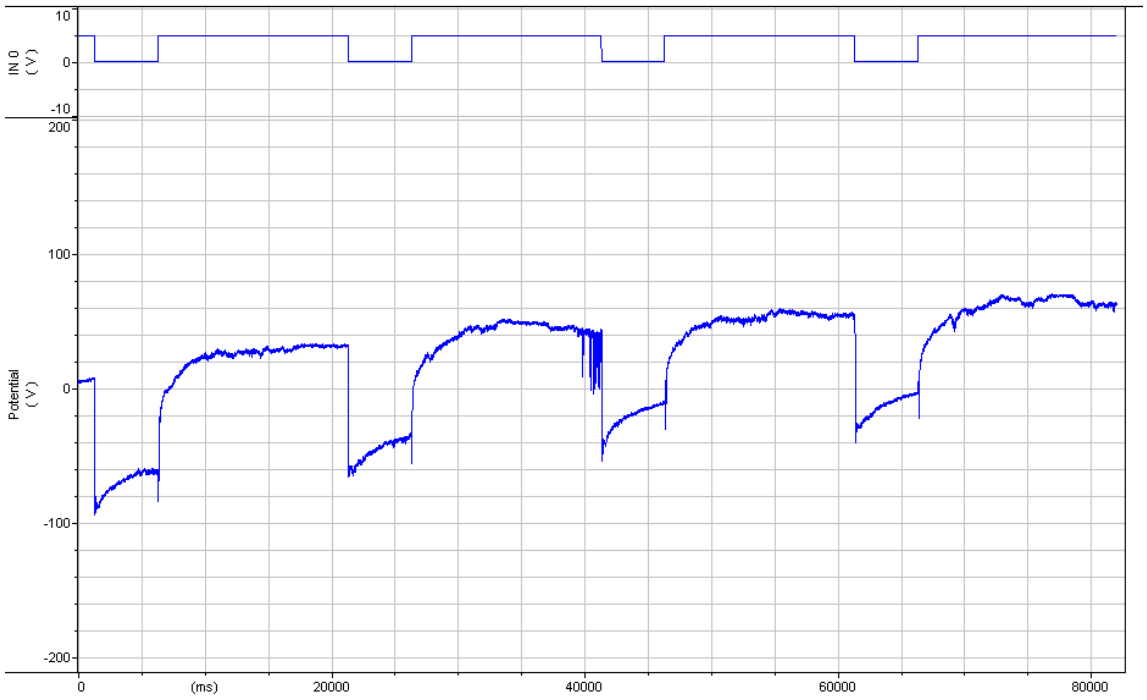
IN 0
(V)
10
0
-10
Potential
(V)
200
100
0
-100
-200
0
(ms)
20000
40000
60000
80000

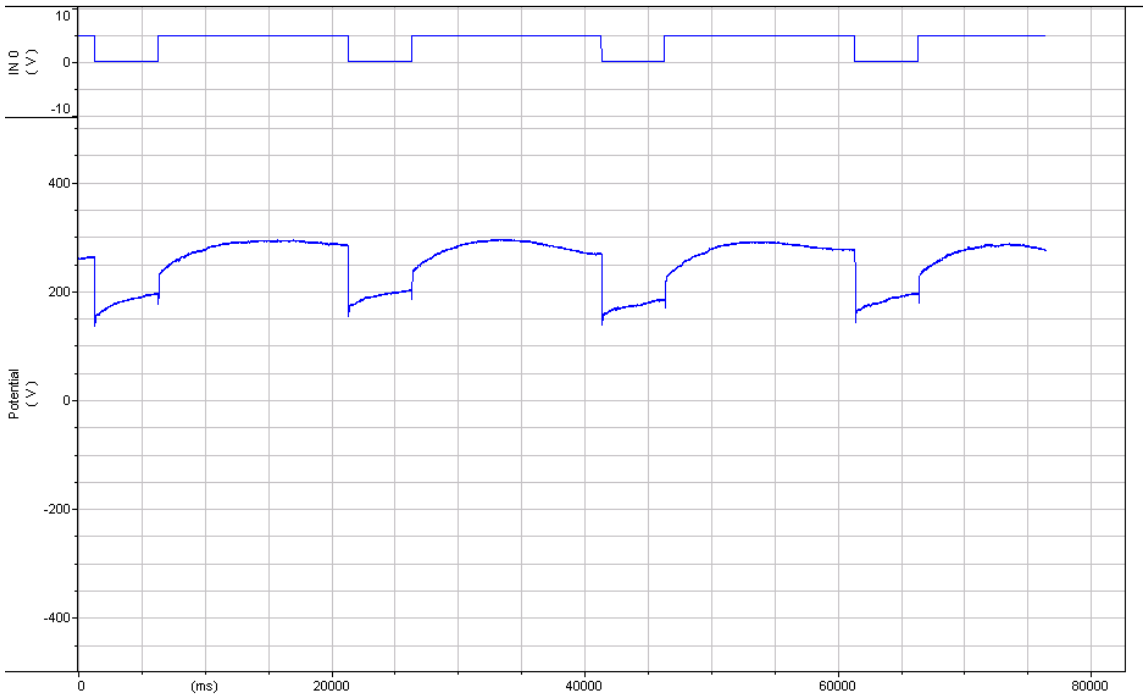
IN 0
(V)
10
0
-10
400
200
0
-200
-400
Potential
(V)
0
(ms)
20000
40000
60000
80000

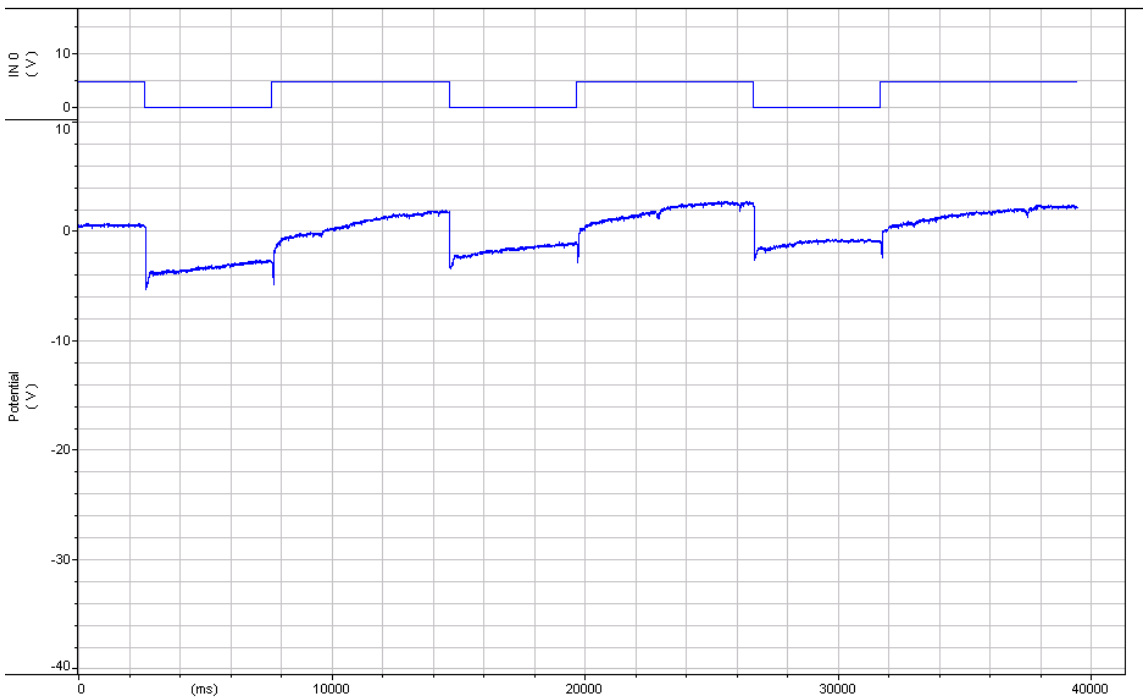
IN 0
(V)
10
0
10
0
-10
-20
-30
-40
Potential
(V)
0
(ms)
10000
20000
30000
40000

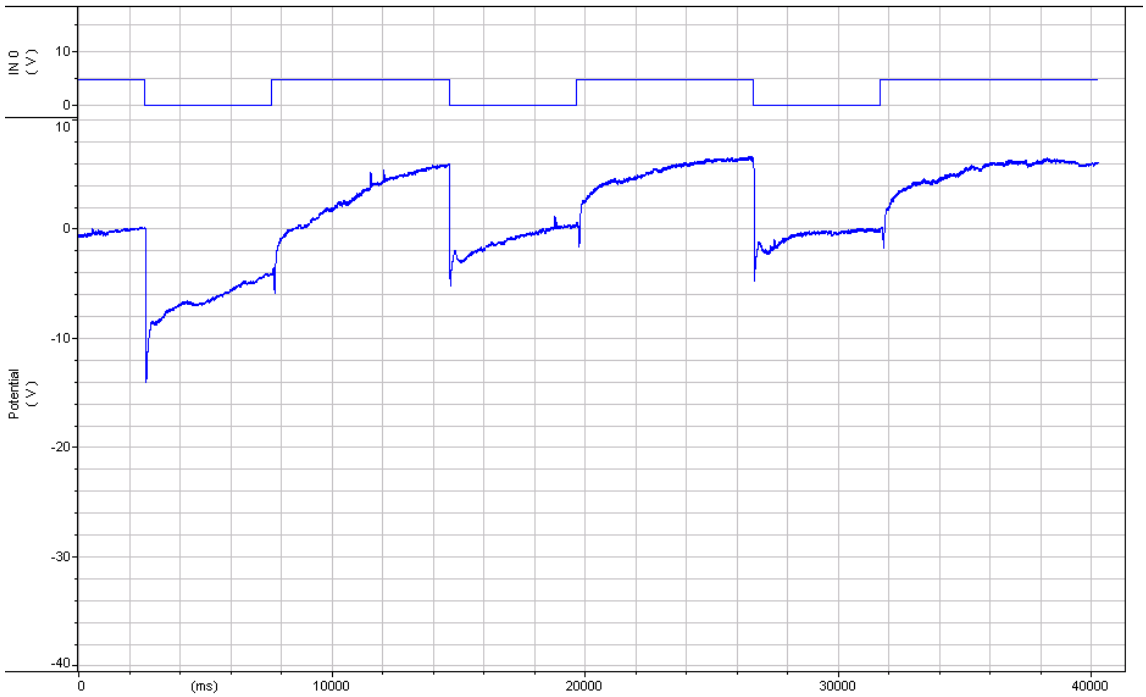
IN 0
(V)
10
0
10
0
-10
-20
-30
-40
Potential
(V)
0
(ms)
10000
20000
30000
40000

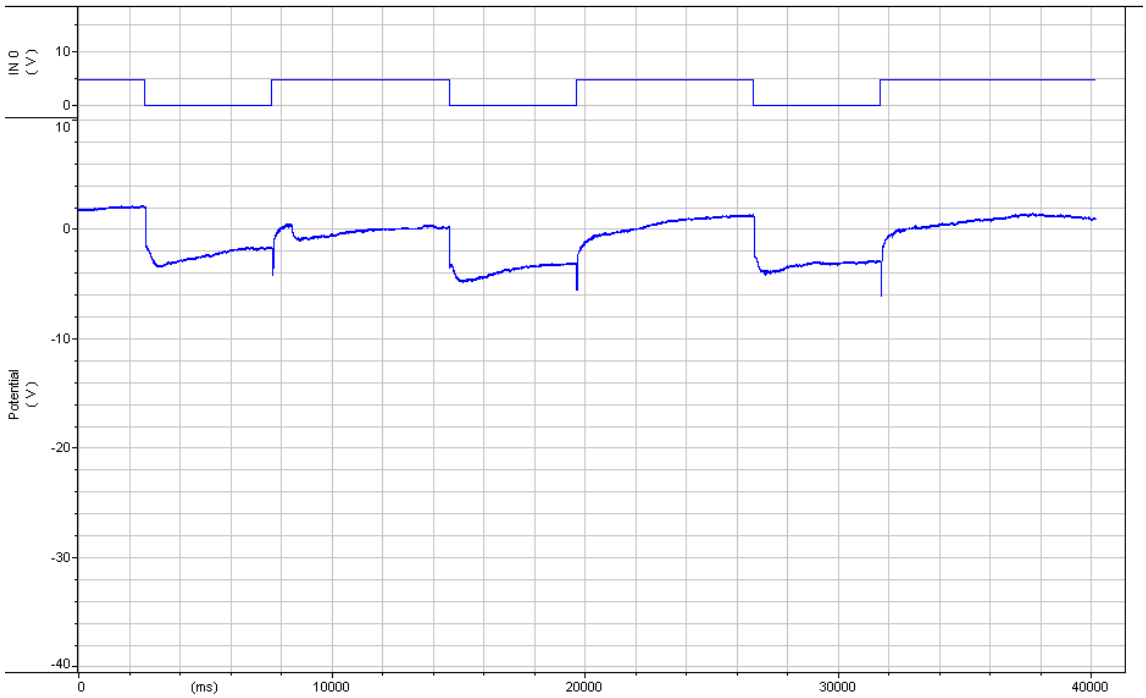
IN 0
(V)
10
0
10
0
-10
-20
-30
-40
Potential
(V)
0
(ms)
10000
20000
30000
40000

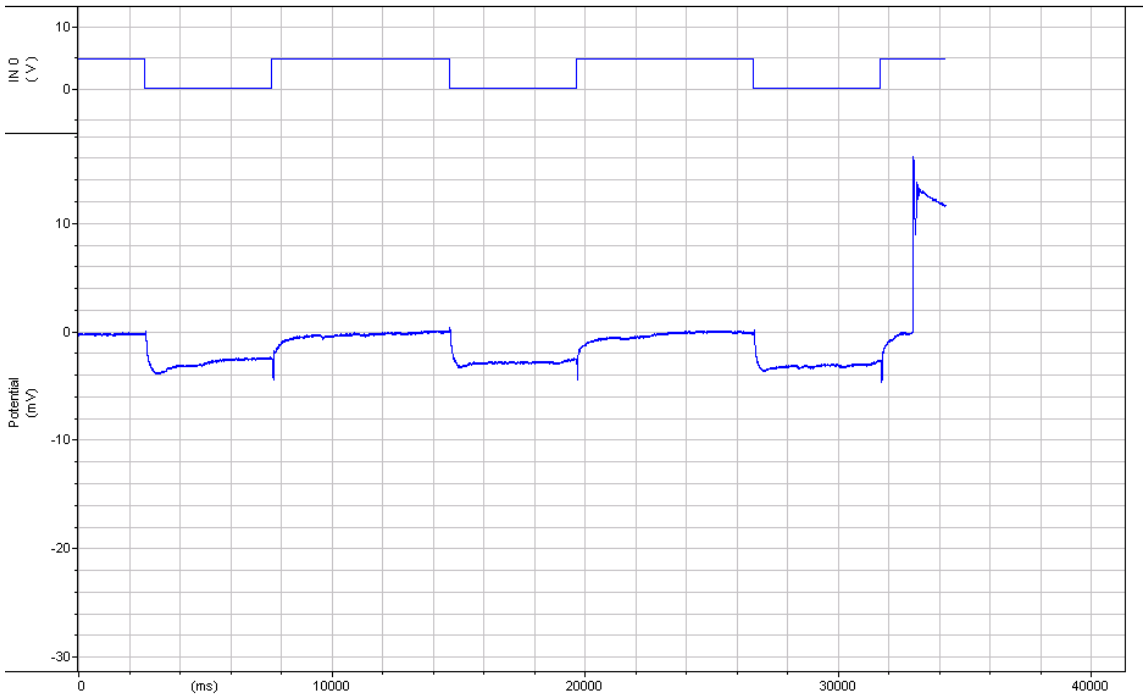
IN 0
(V)
10
0
10
0
-10
-20
-30
Potential
(mV)
0
(ms)
10000
20000
30000
40000

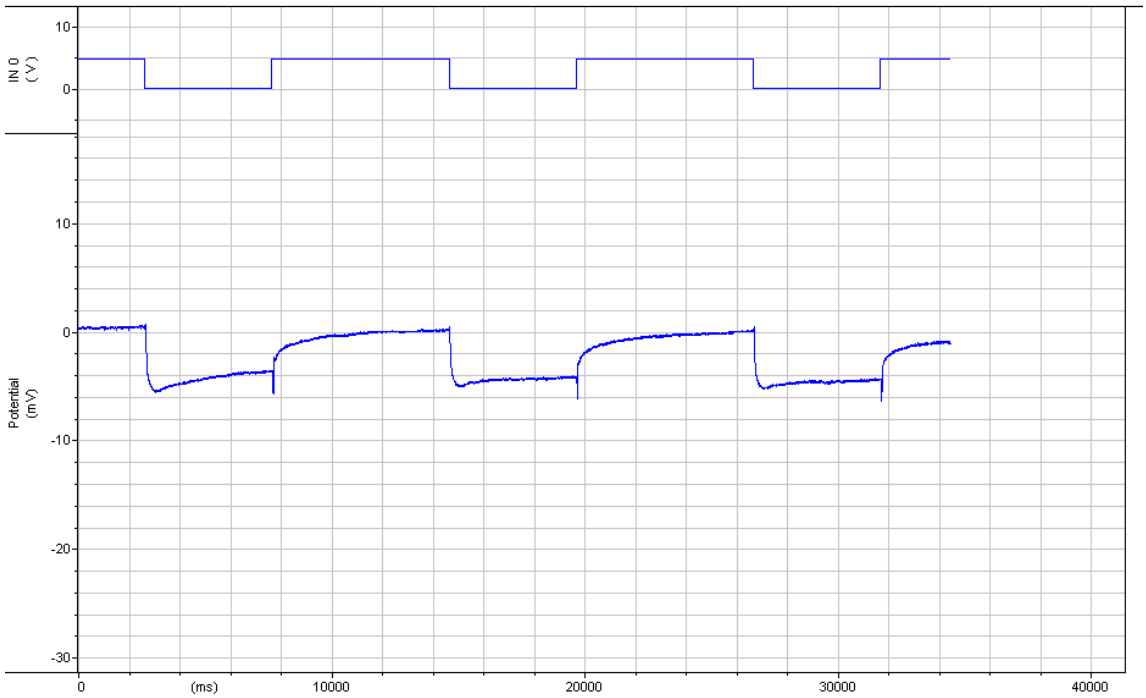
IN 0
(V)
10
0
10
0
-10
-20
-30
Potential
(mV)
0
(ms)
10000
20000
30000
40000

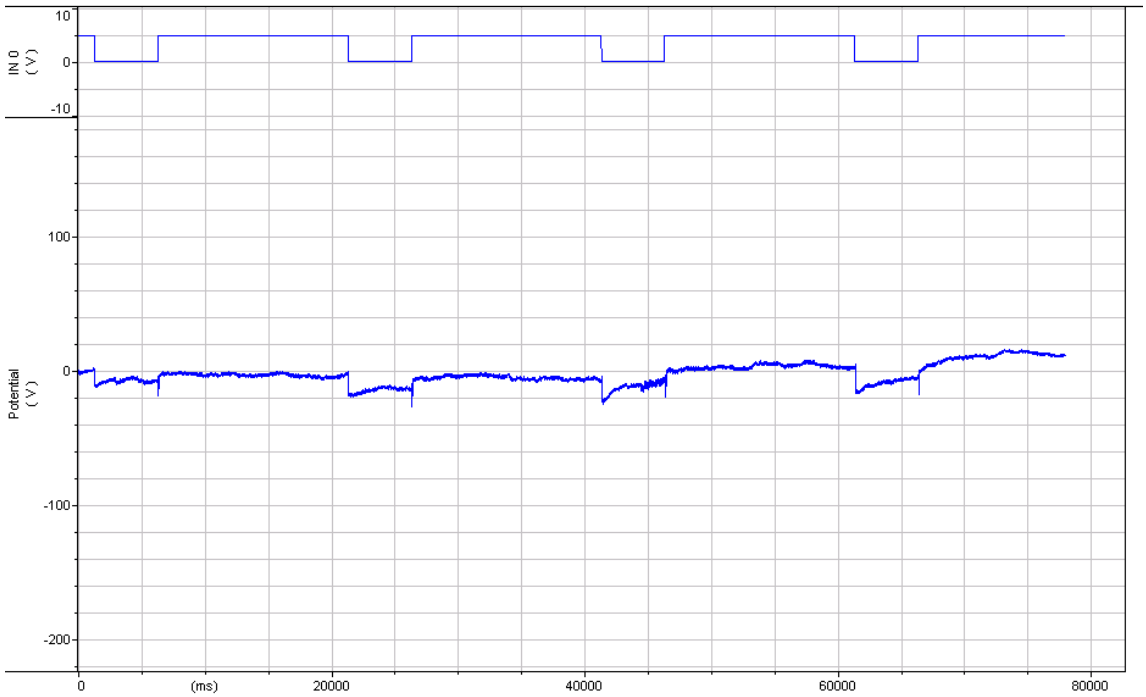
IN 0
(V)
10
0
-10
100
0
-100
-200
Potential
(V)
0
(ms)
20000
40000
60000
80000

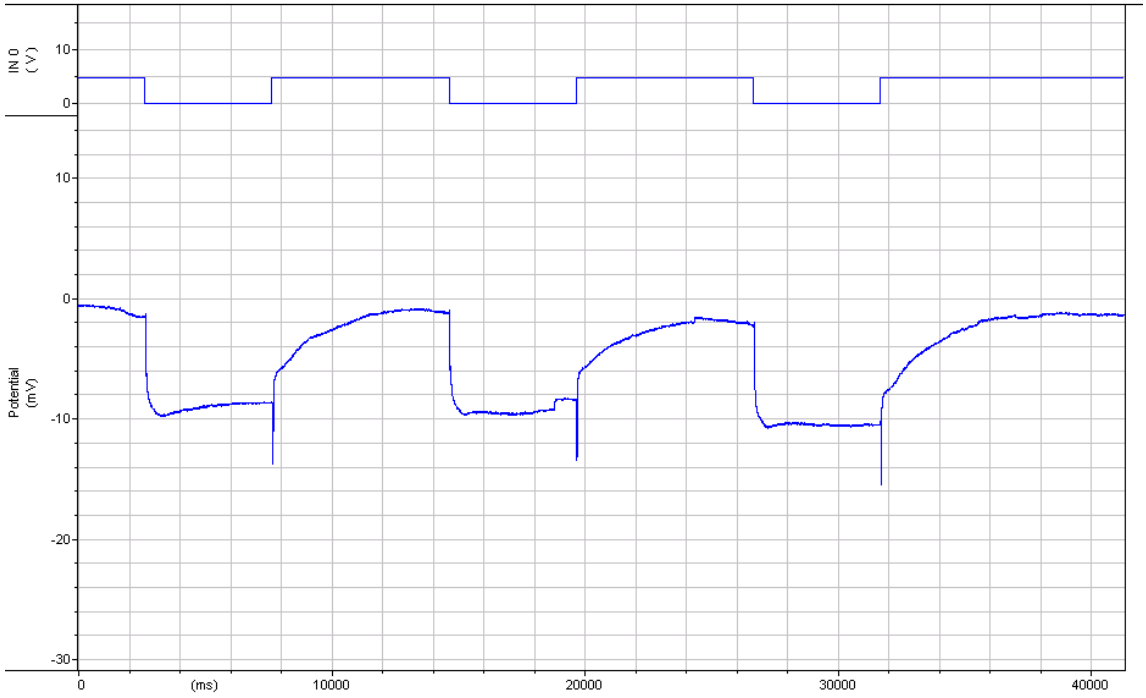
IN 0
(V)
10
0
10
0
-10
-20
-30
Potential
(mV)
0
(ms)
10000
20000
30000
40000

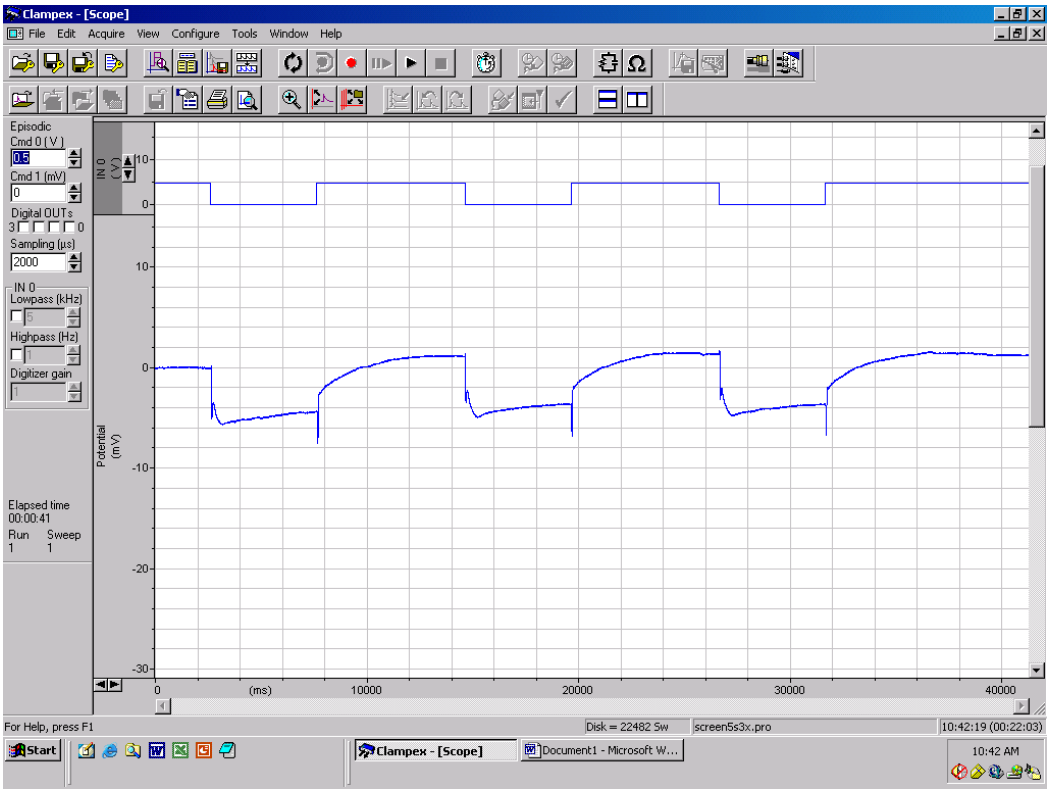
Clampex - [Scope]
File Edit Acquire View Configure Tools Window Help
Episodic
Cmd 0 (V)
0.5
Cmd 1 (mV)
0
Digital OUTs
3 0
Sampling (µs)
2000
IN 0
Lowpass (kHz)
Highpass (Hz)
Digitizer gain
Elapsed time
00:00:41
Run Sweep
1 1
IN 0 (V)
Potential (mV)
10
0
10
0
-10
-20
-30
0
(ms)
10000
20000
30000
40000
For Help, press F1
Disk = 22482 Sw
screen5s3x.pro
10:42:19 (00:22:03)
Start
Clampex - [Scope]
Document1 - Microsoft W...
10:42 AM

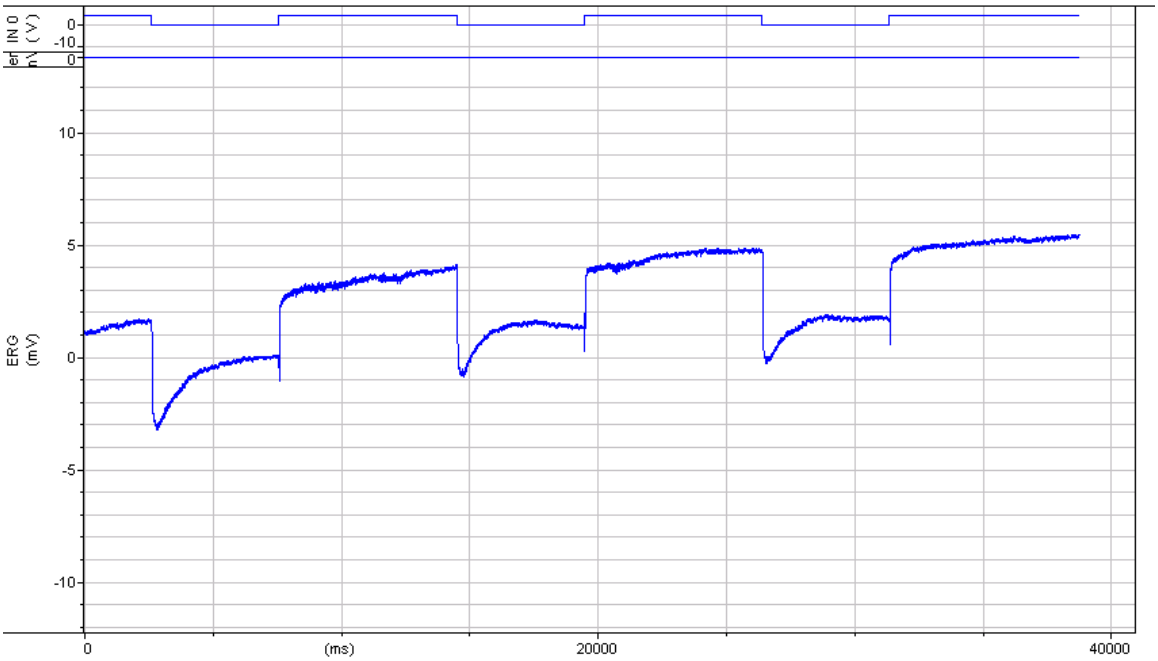
IN 0 (V)
0
-10
0
10
5
0
-5
-10
ERG (mV)
0
(ms)
20000
40000

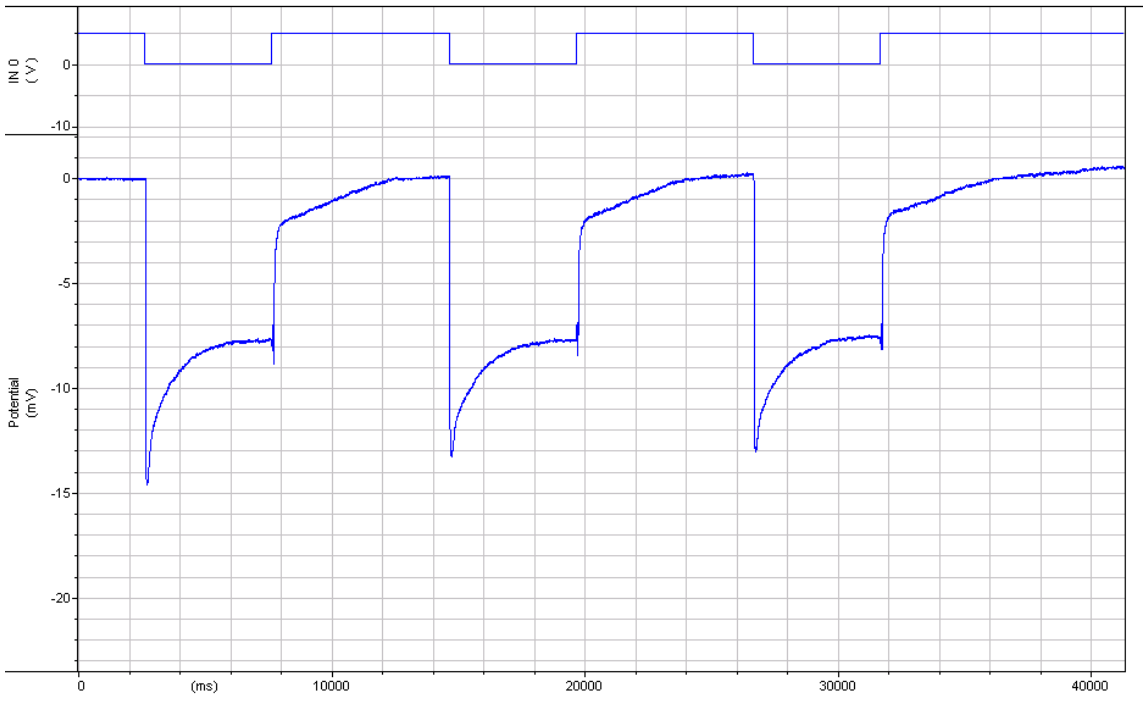
IN 0
(V)
0
-10
0
-5
-10
-15
-20
Potential
(mV)
0
(ms)
10000
20000
30000
40000

Genotype: TIFR-Gal4> *Acsl* RNAi

Phenotype: loss of ‘on’ and ‘off’ transients

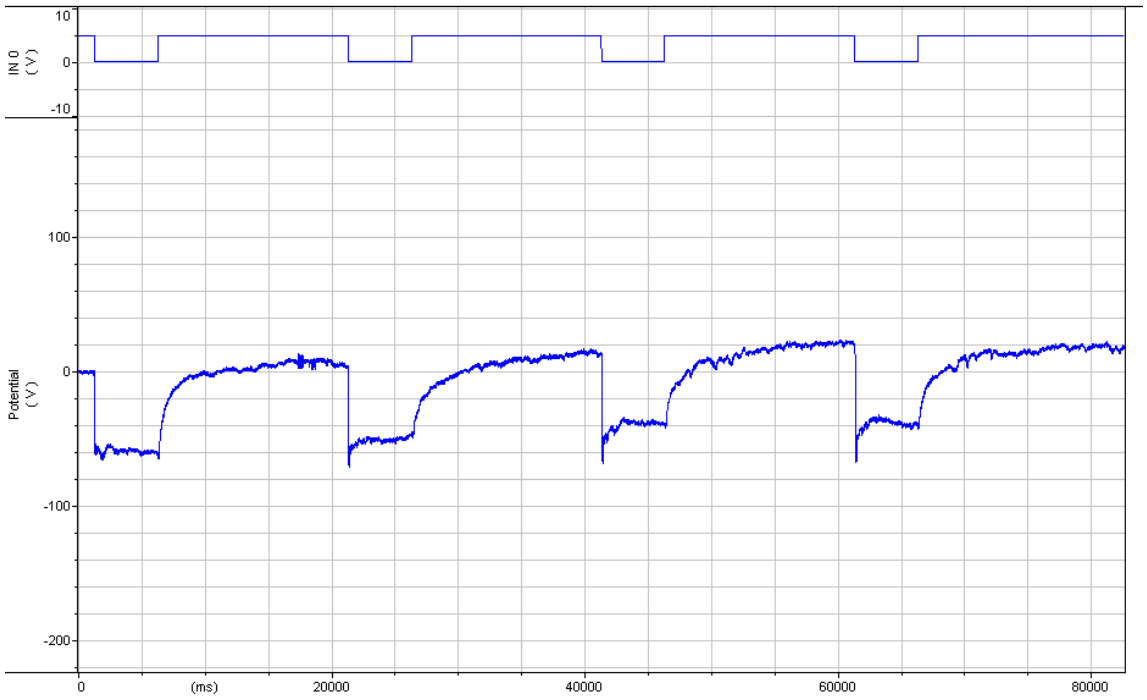

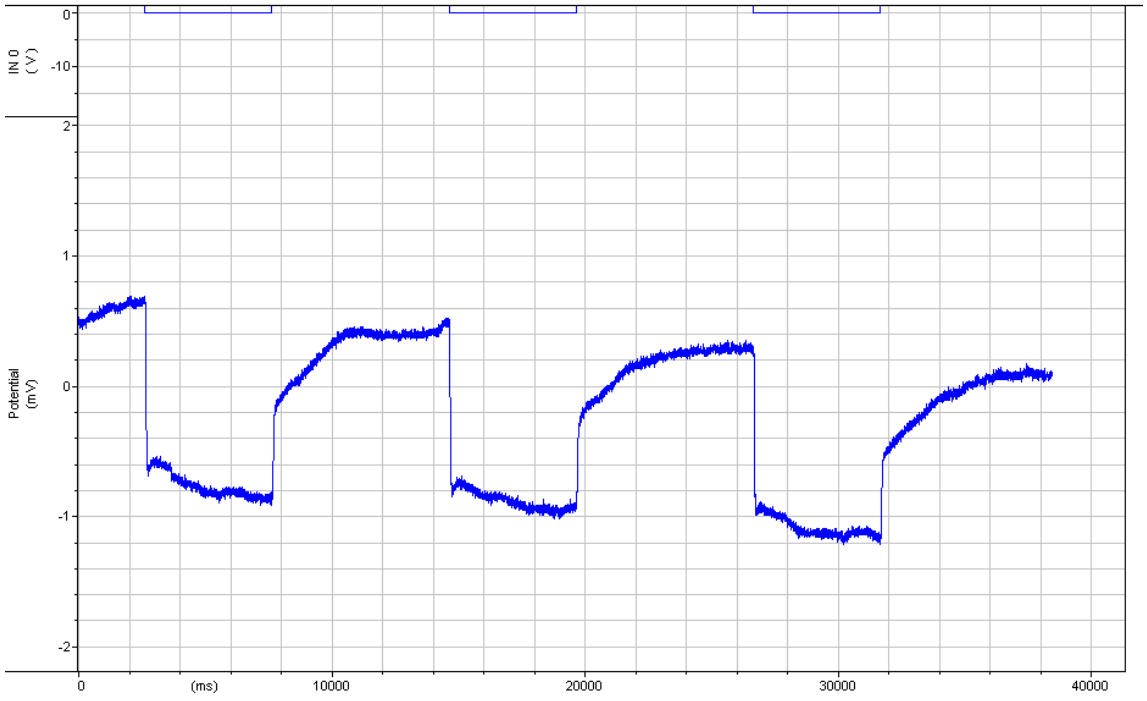

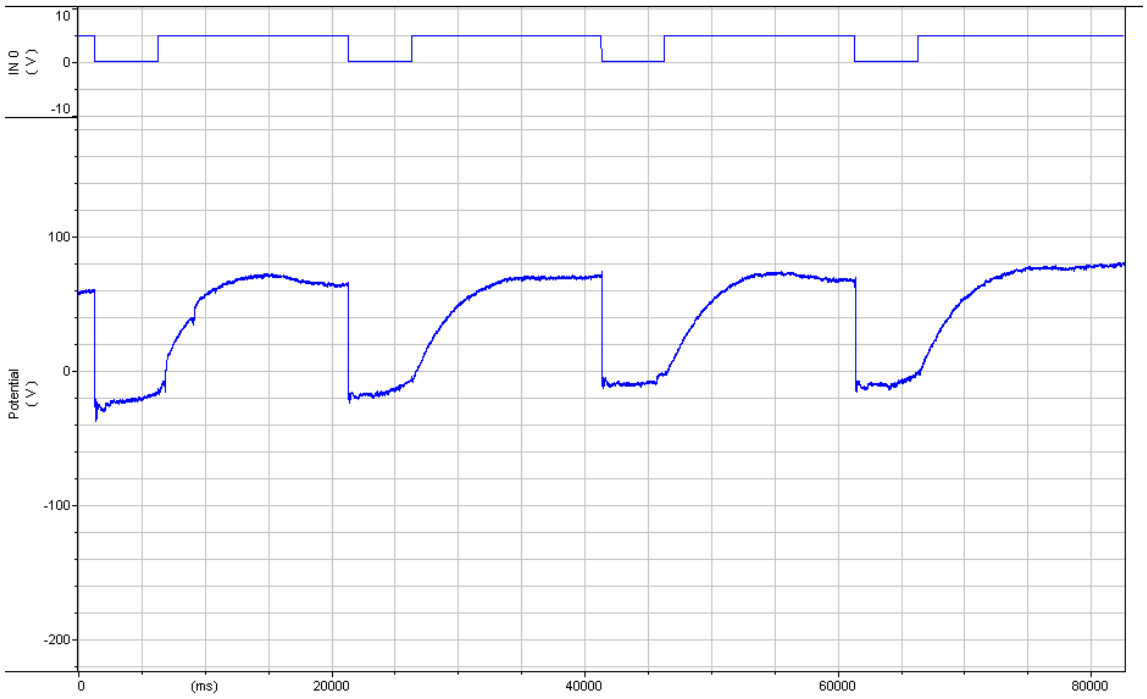
IN 0
(V)
10
0
-10
100
0
-100
-200
Potential
(V)
0
(ms)
20000
40000
60000
80000

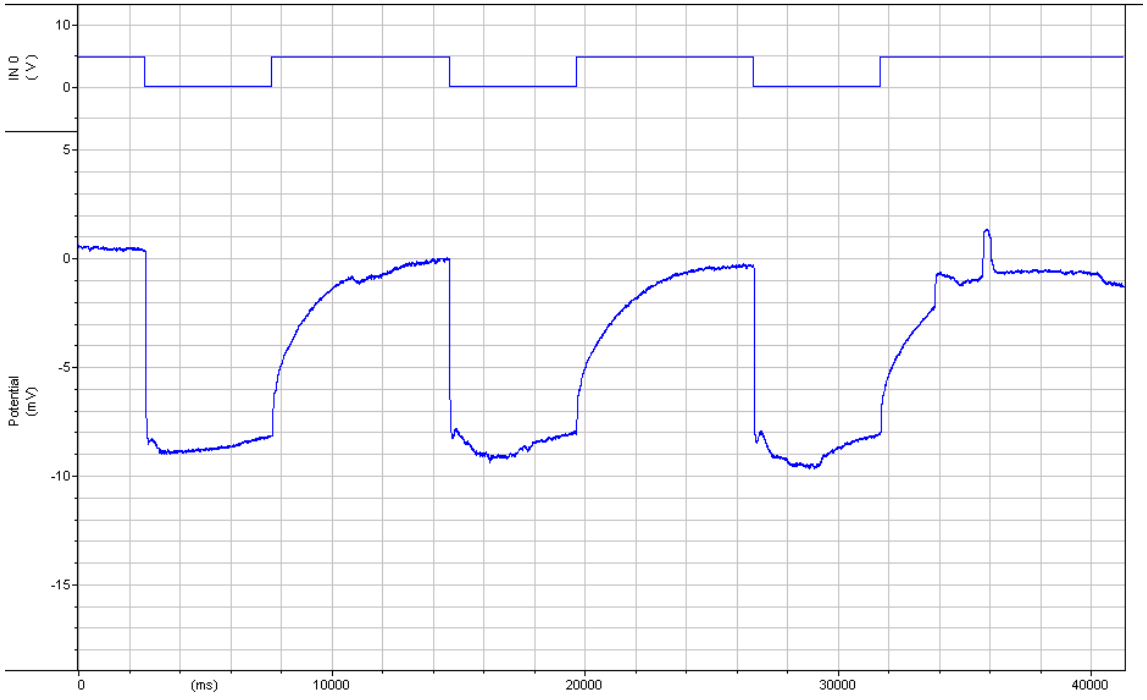
IN 0
(V)
10
0
5
0
-5
-10
-15
Potential
(mV)
0
(ms)
10000
20000
30000
40000

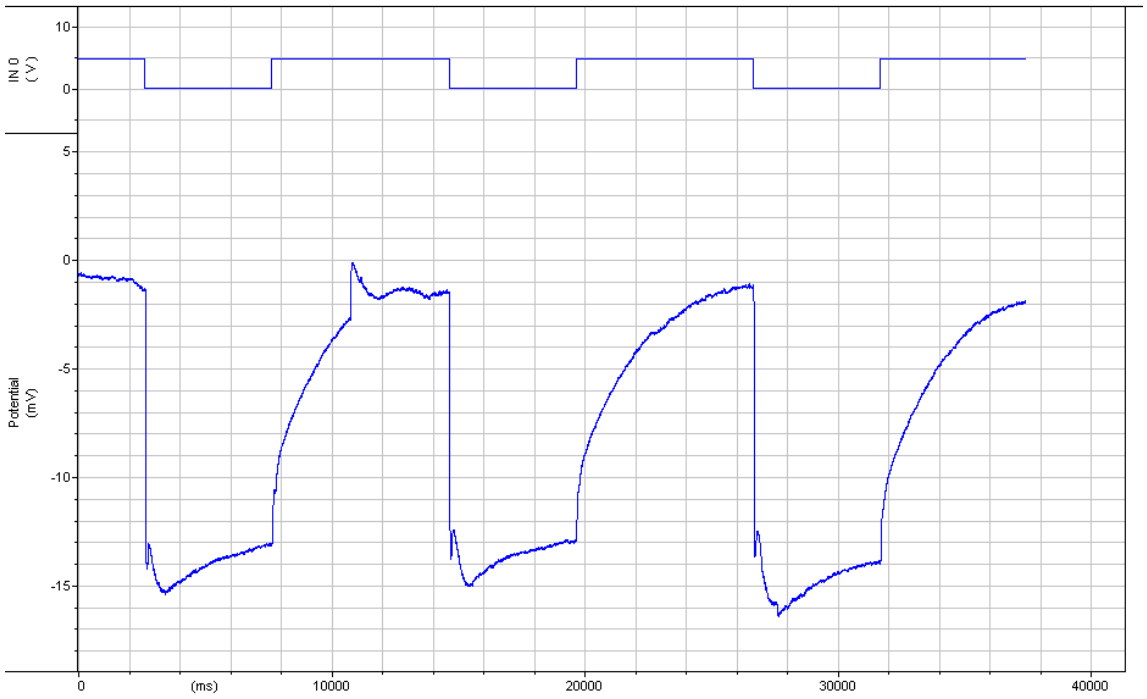
IN 0
(V)
10
0
5
0
-5
-10
-15
Potential
(mV)
0
(ms)
10000
20000
30000
40000

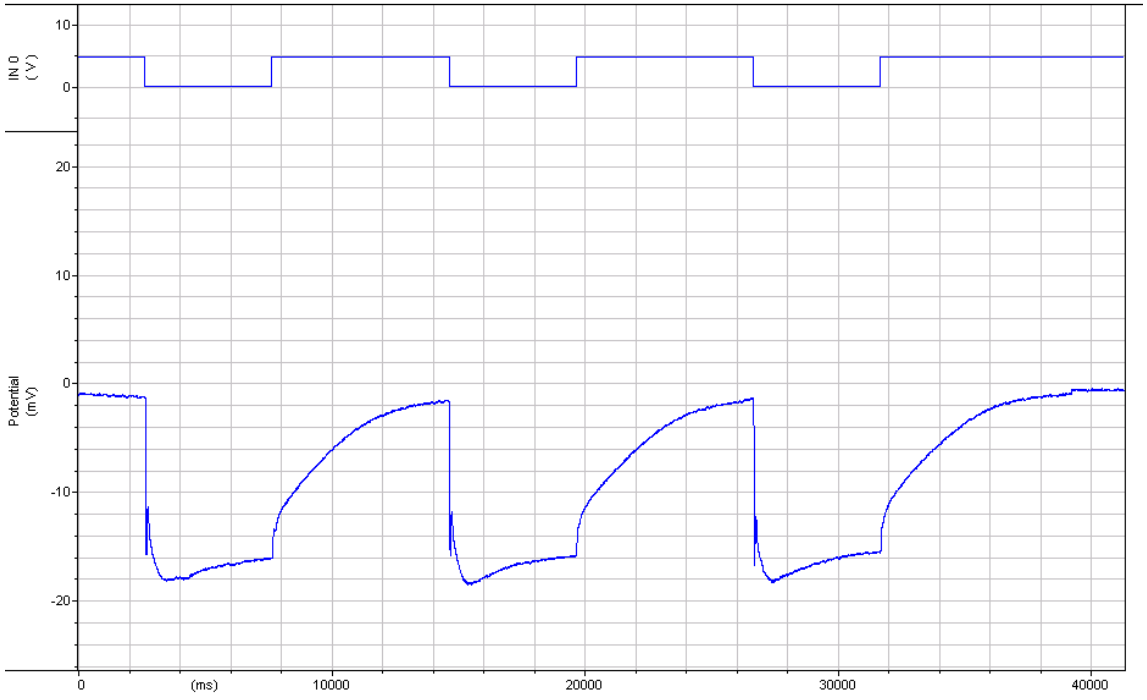
IN 0
(V)
10
0
20
10
0
-10
-20
Potential
(mV)
0
(ms)
10000
20000
30000
40000

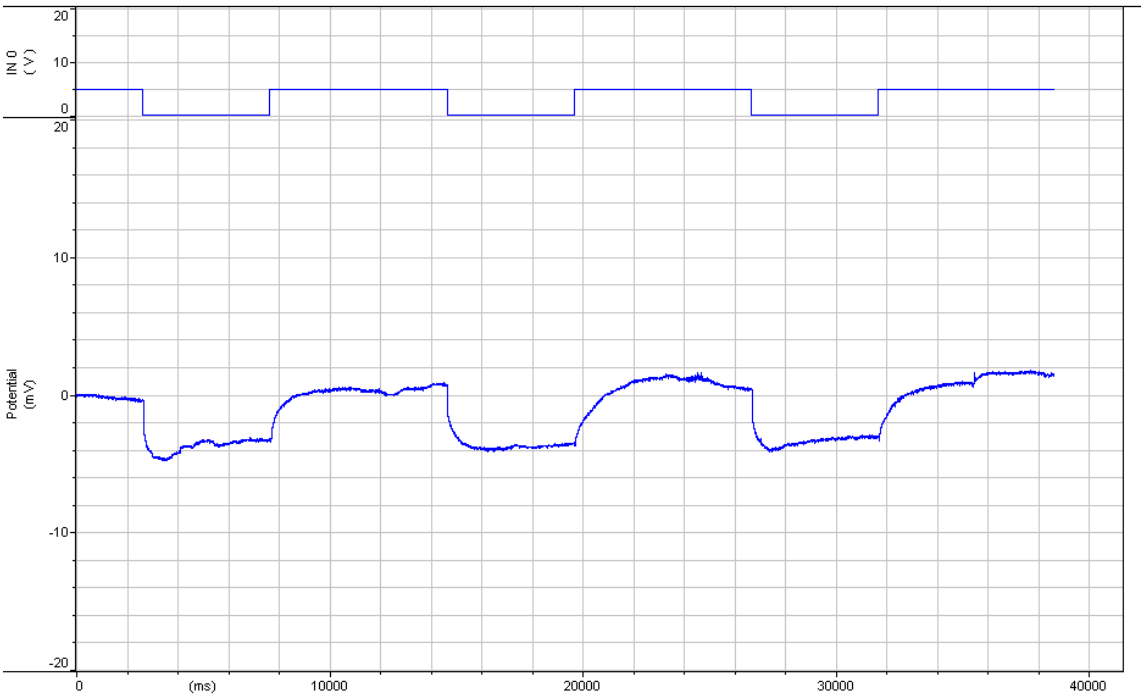
IN 0
(V)
20
10
0
20
10
0
-10
-20
Potential
(mV)
0
(ms)
10000
20000
30000
40000

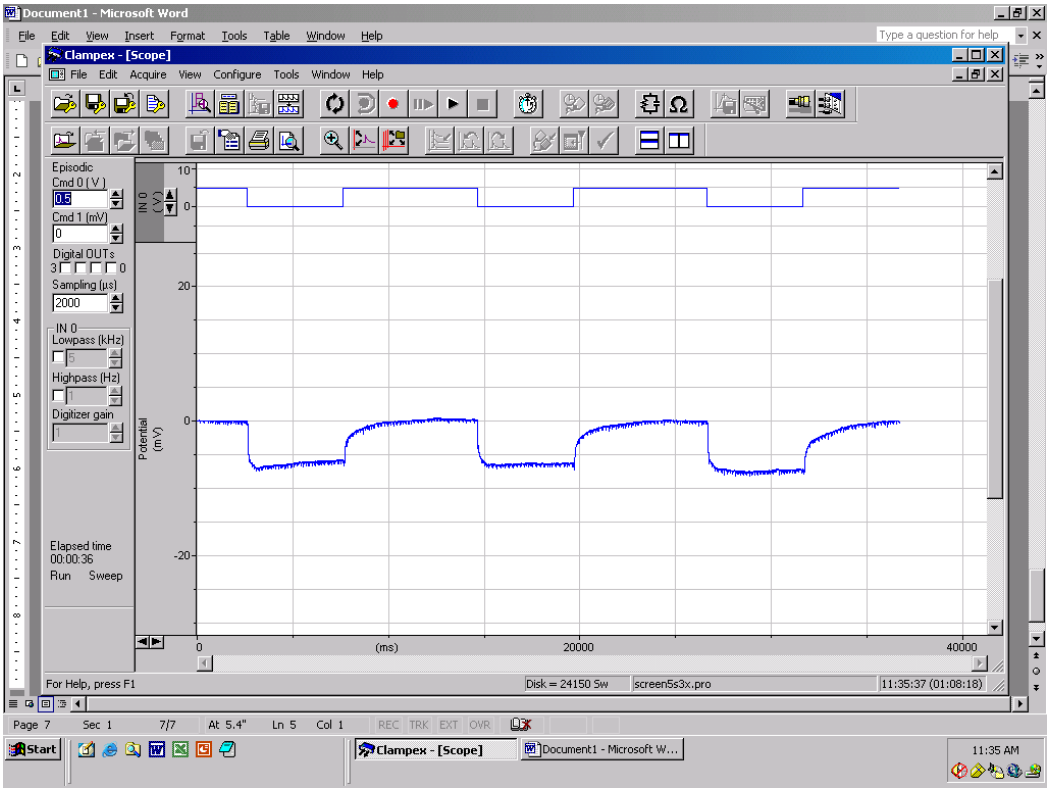
Document1 - Microsoft Word
File Edit View Insert Format Tools Table Window Help
Clampex - [Scope]
File Edit Acquire View Configure Tools Window Help
Episodic
Cmd 0 (V)
0.5
Cmd 1 (mV)
0
Digital OUTs
Sampling (µs)
2000
IN 0
Lowpass (kHz)
Highpass (Hz)
Digitizer gain
Elapsed time
00:00:36
Run Sweep
IN 0
(V)
Potential
(mV)
10
0
20
0
-20
(ms)
20000
40000
For Help, press F1
Disk = 24150 Sw
screen5s3x.pro
11:35:37 (01:08:18)
Page 7 Sec 1 7/7 At 5.4" Ln 5 Col 1
REC TRK EXT OVR
Start
Clampex - [Scope]
Document1 - Microsoft W...
11:35 AM

Genotype: *repo*-Gal4> 41885 (HMS02307)

Phenotype: with transient

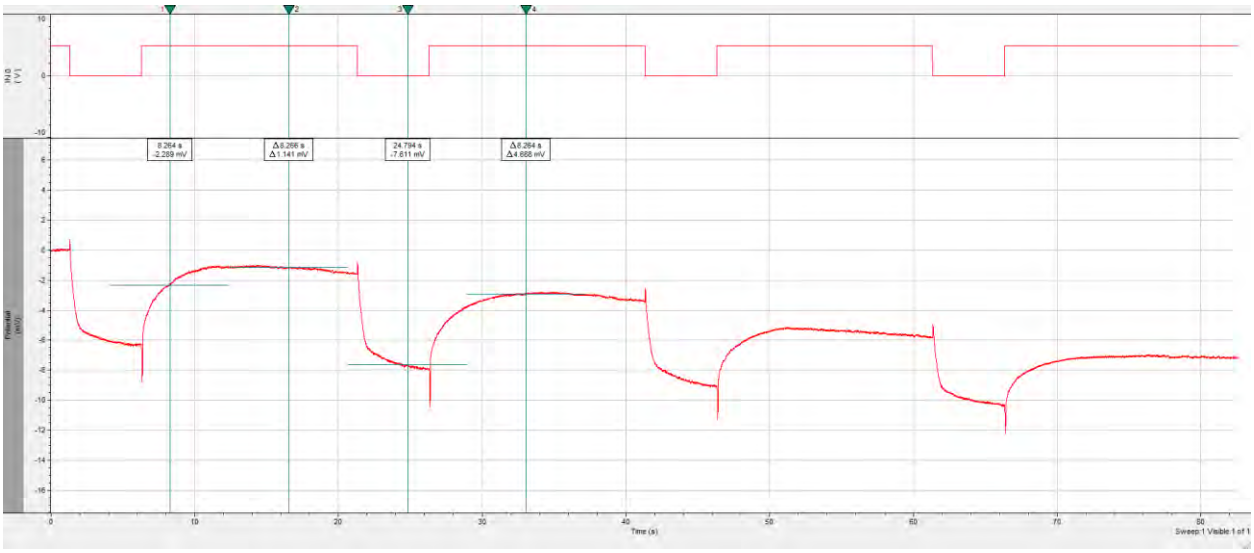

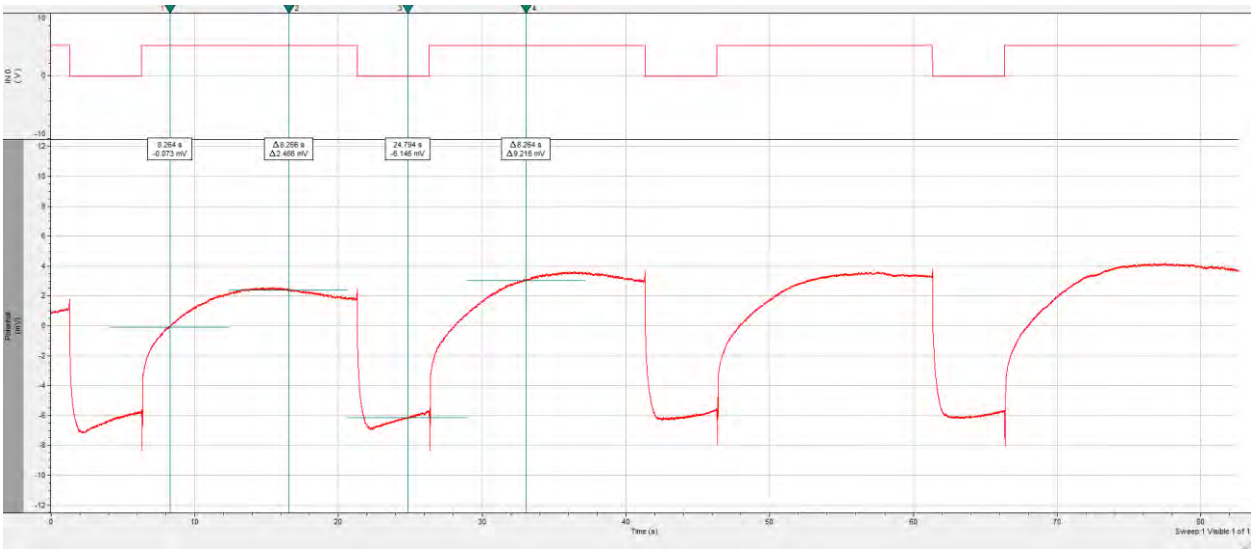

Genotype: *repo*-Gal4> 41885 (HMS02307)

Phenotype: loss of ‘on transient’

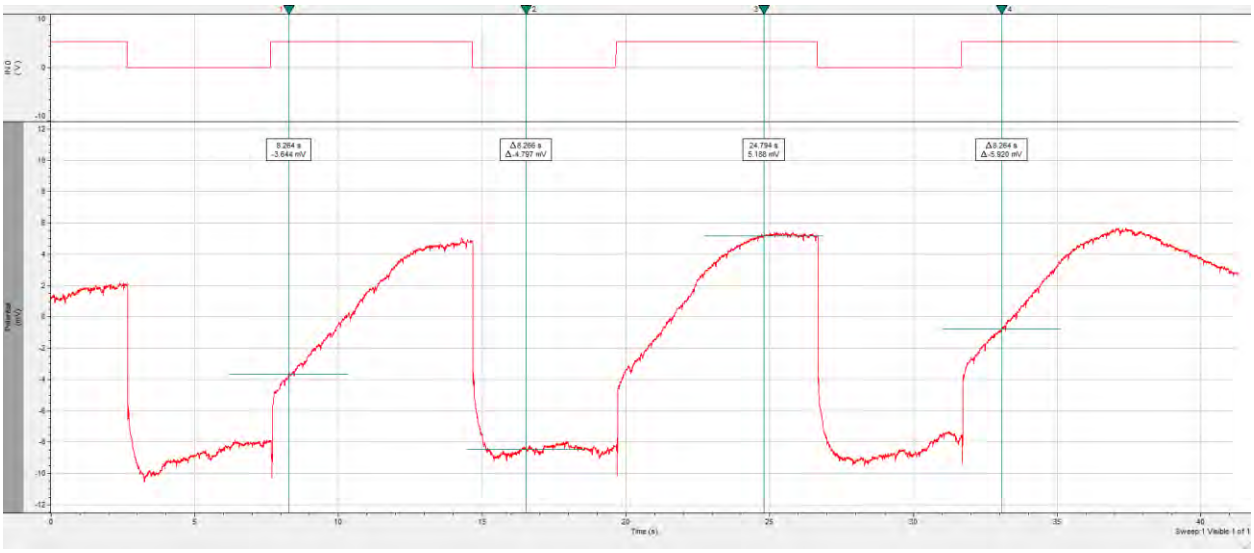

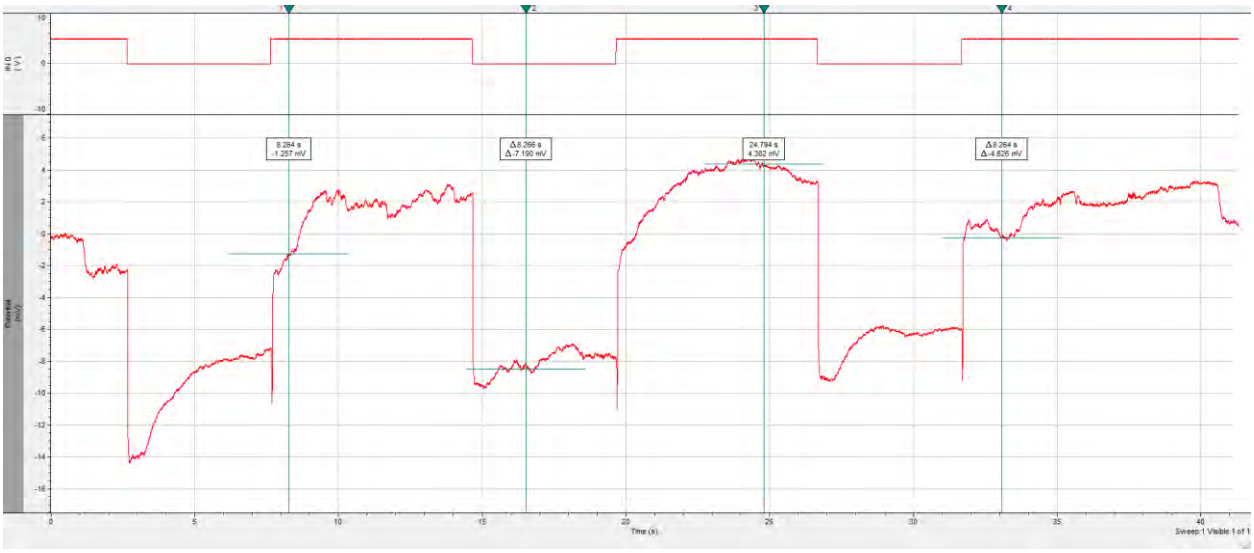

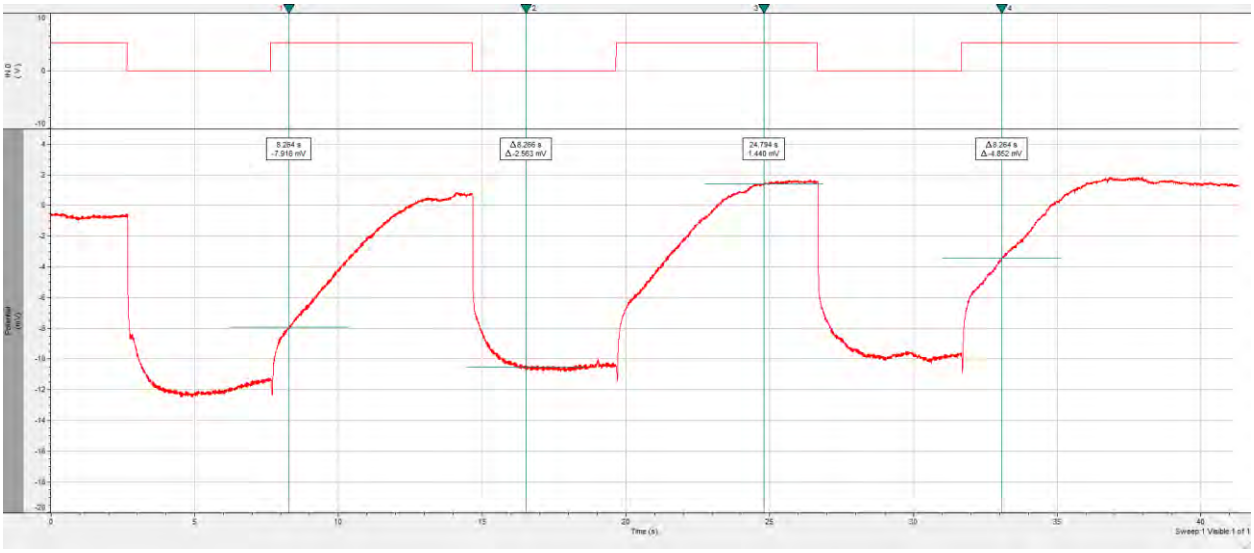
8.284 s
-7.916 mV
Δ8.266 s
Δ-2.563 mV
24.794 s
1.440 mV
Δ8.264 s
Δ-4.852 mV
Time (s)

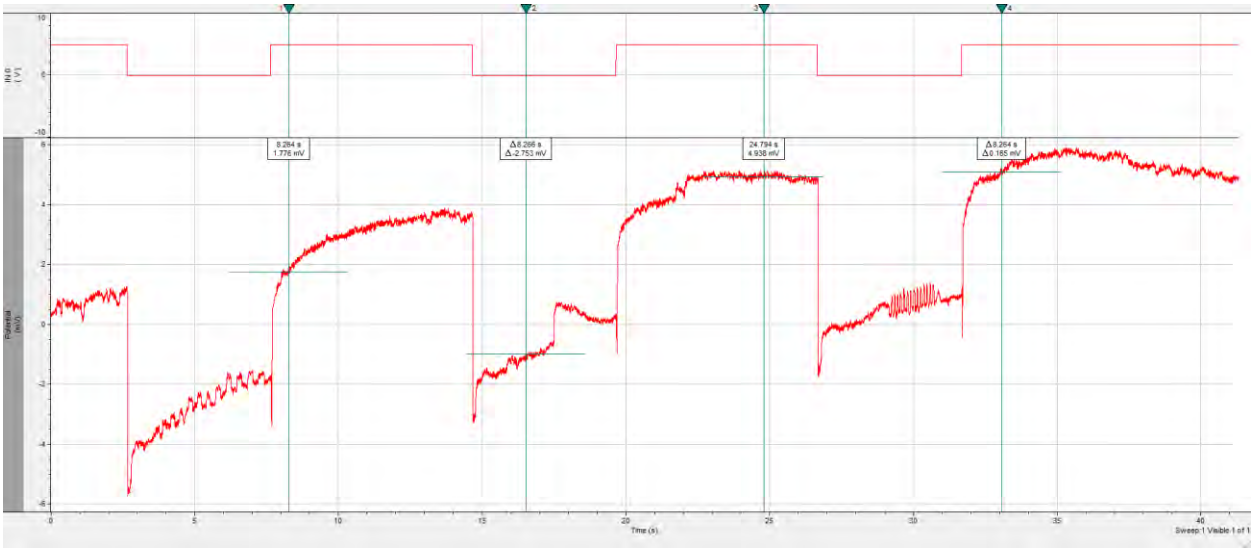
8.284 s
1.776 mV
Δ8.266 s
Δ-2.753 mV
24.794 s
4.938 mV
Δ8.264 s
Δ0.185 mV
Time (s)

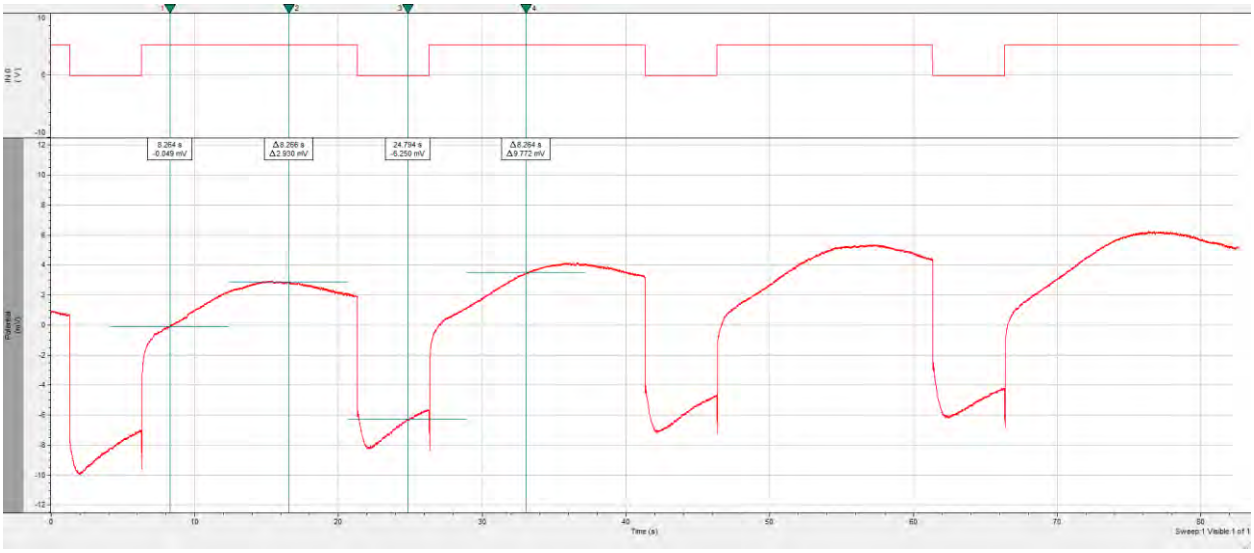

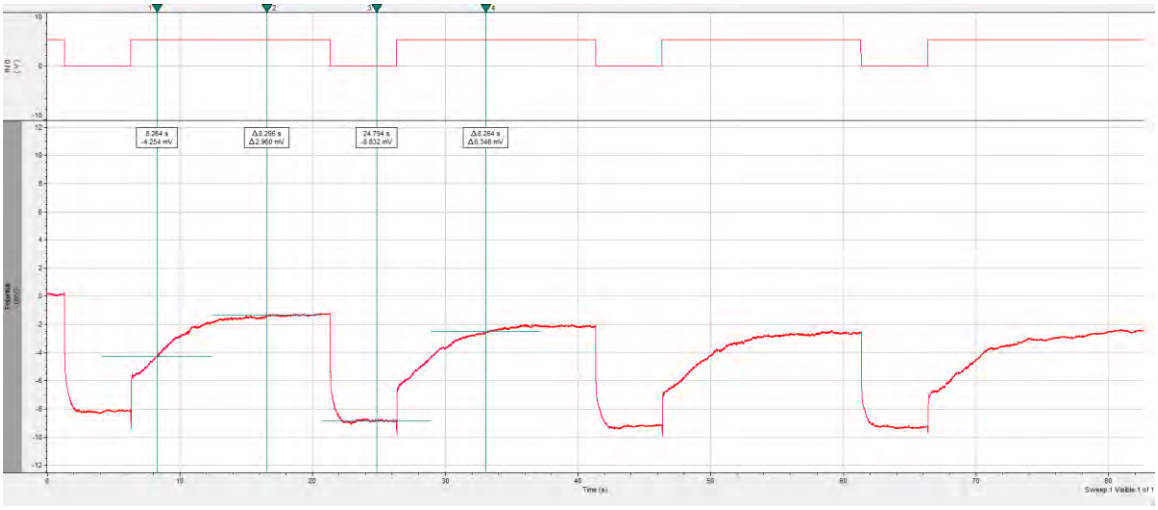

Genotype: *repo*-Gal4> 41885 (HMS02307)

Phenotype: loss of ‘on’ and ‘off’ transients

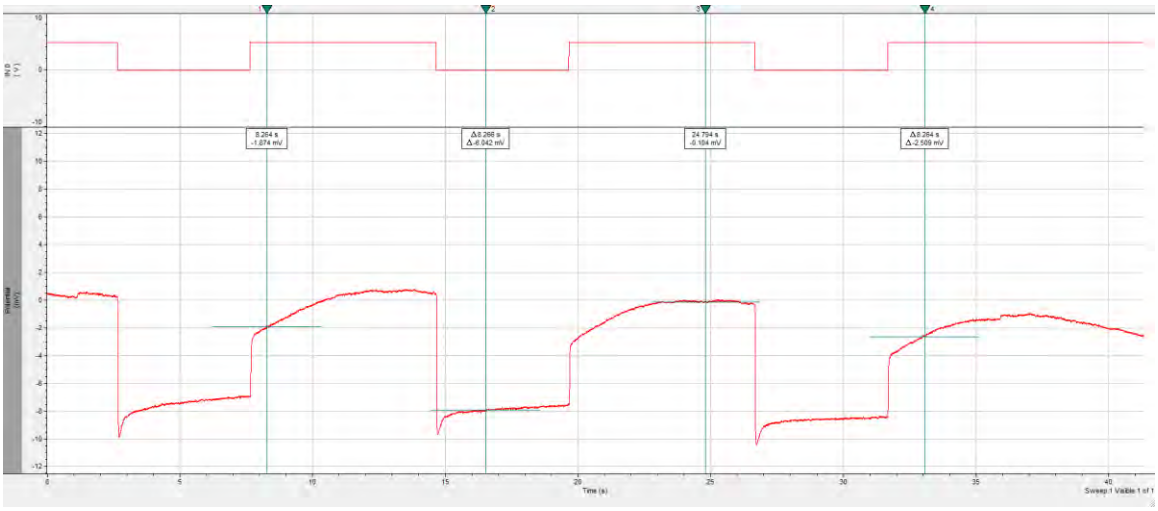

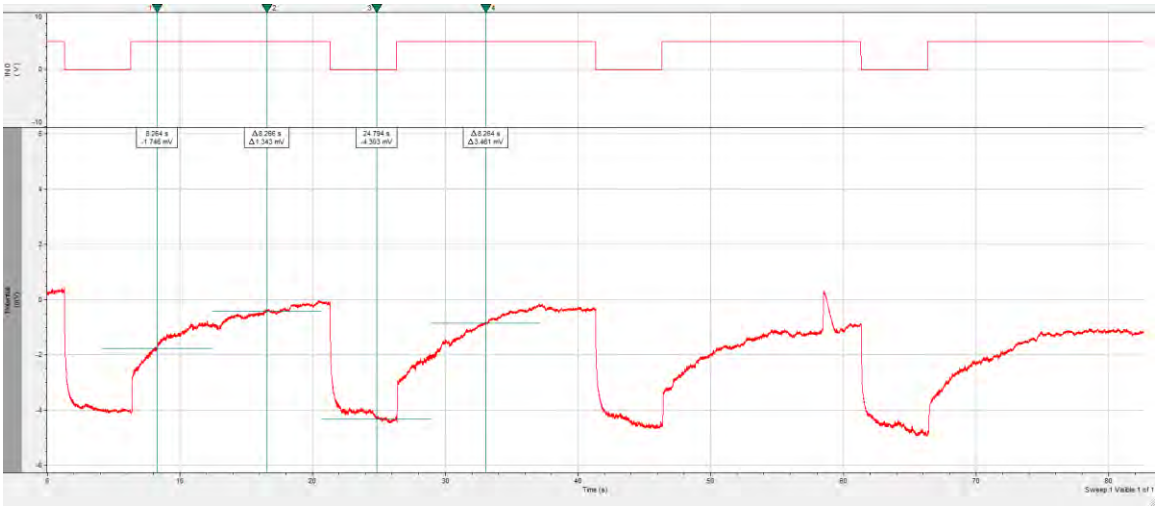

repo-Gal4> 3222 (GD1638)

Phenotype: with transient

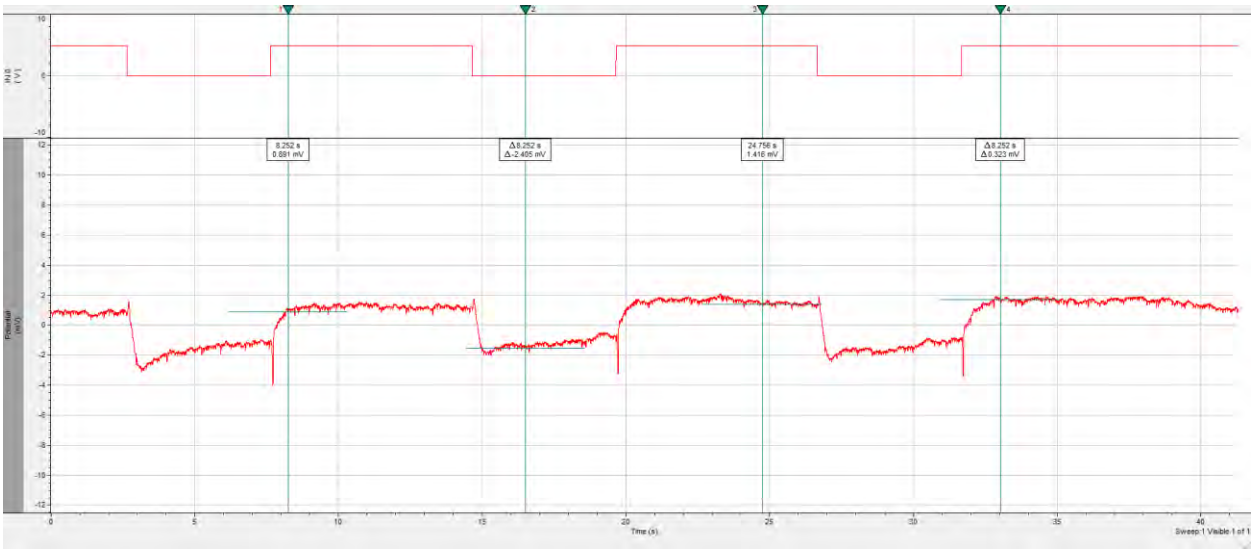

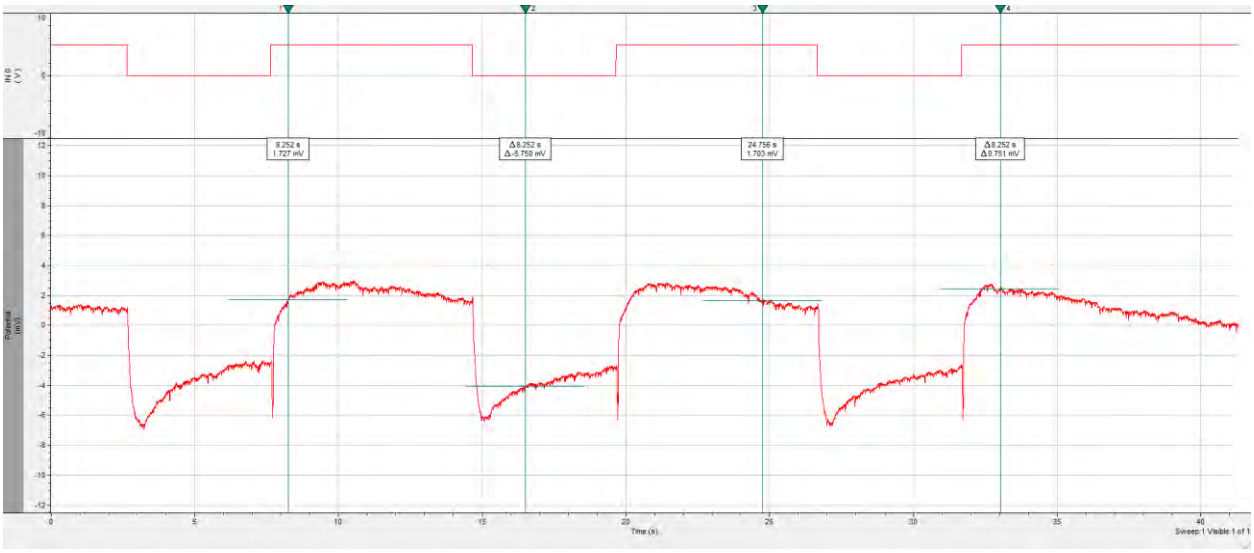

repo-Gal4> 3222 (GD1638)

Phenotype: loss of ‘on transient’

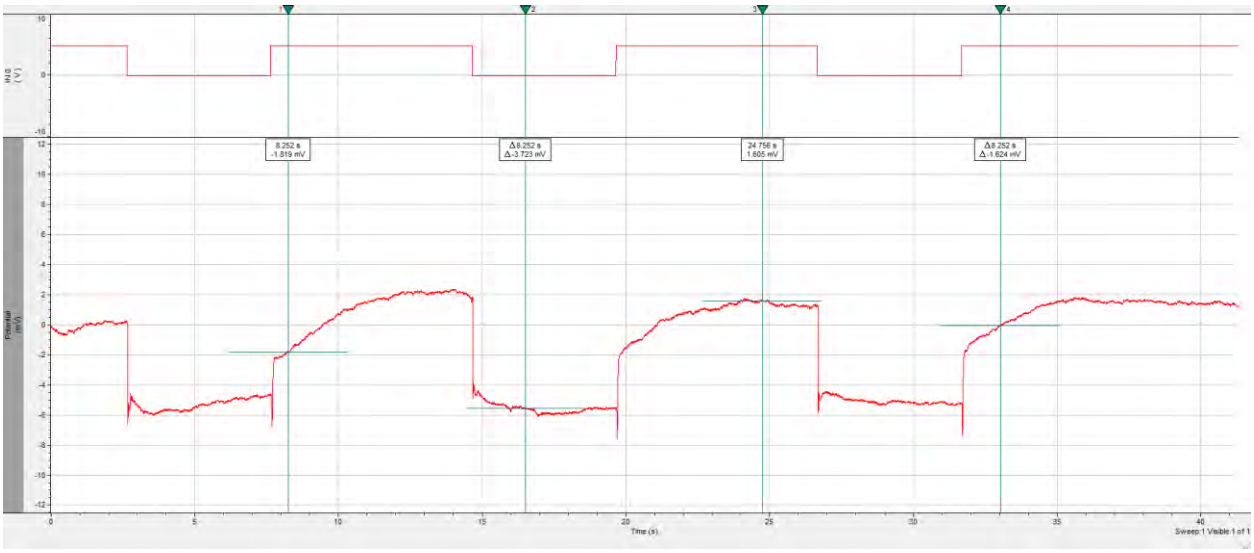

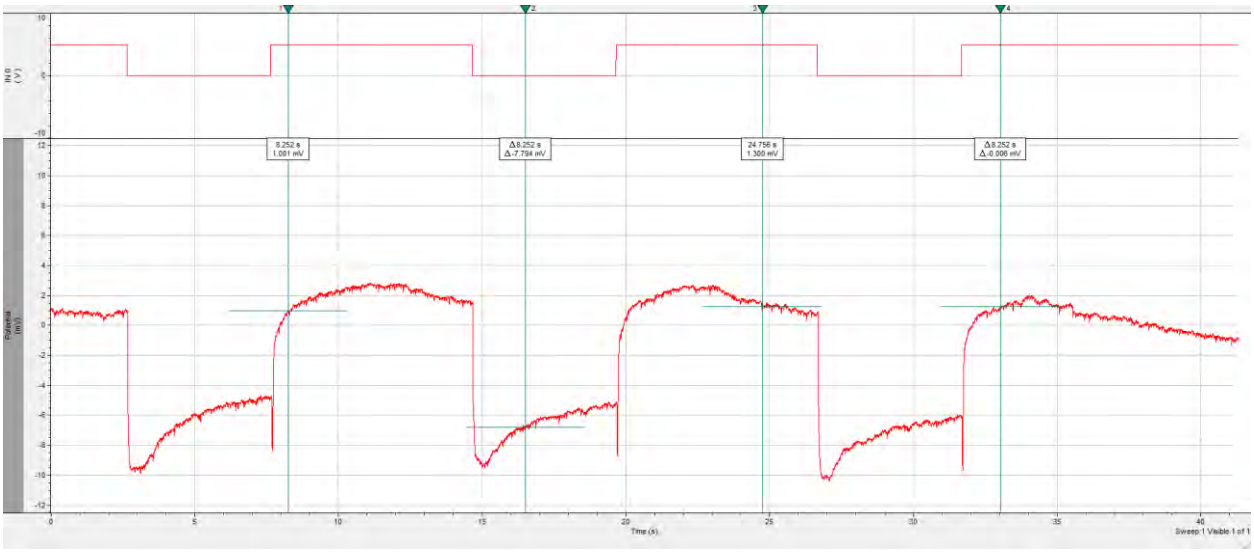

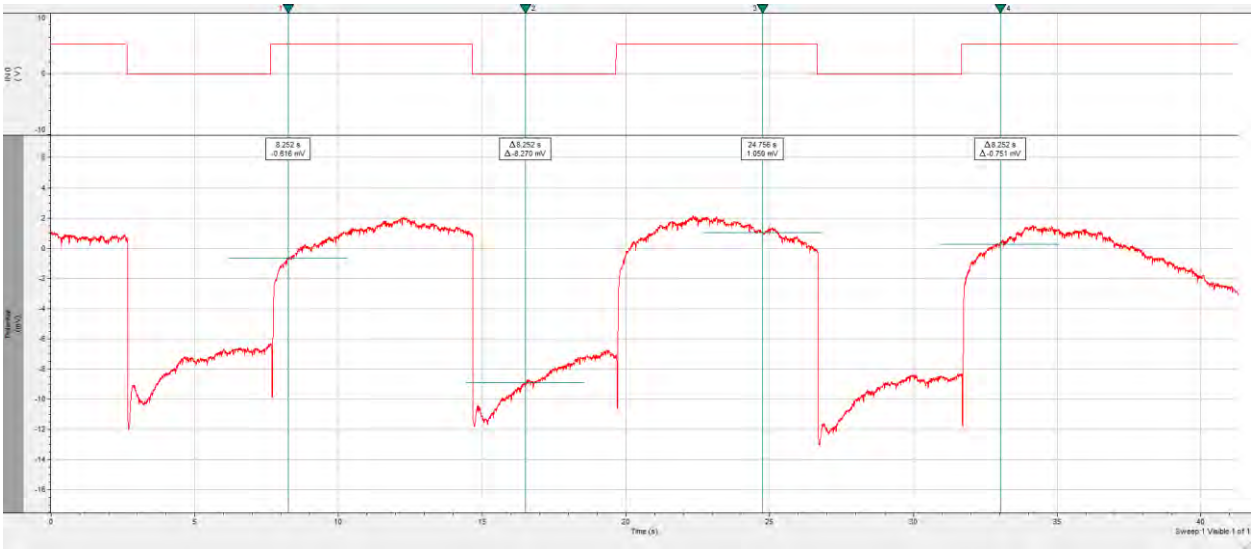
8.252 s
-0.616 mV
Δ8.252 s
Δ-8.270 mV
24.756 s
1.059 mV
Δ8.252 s
Δ-0.751 mV
Time (s)

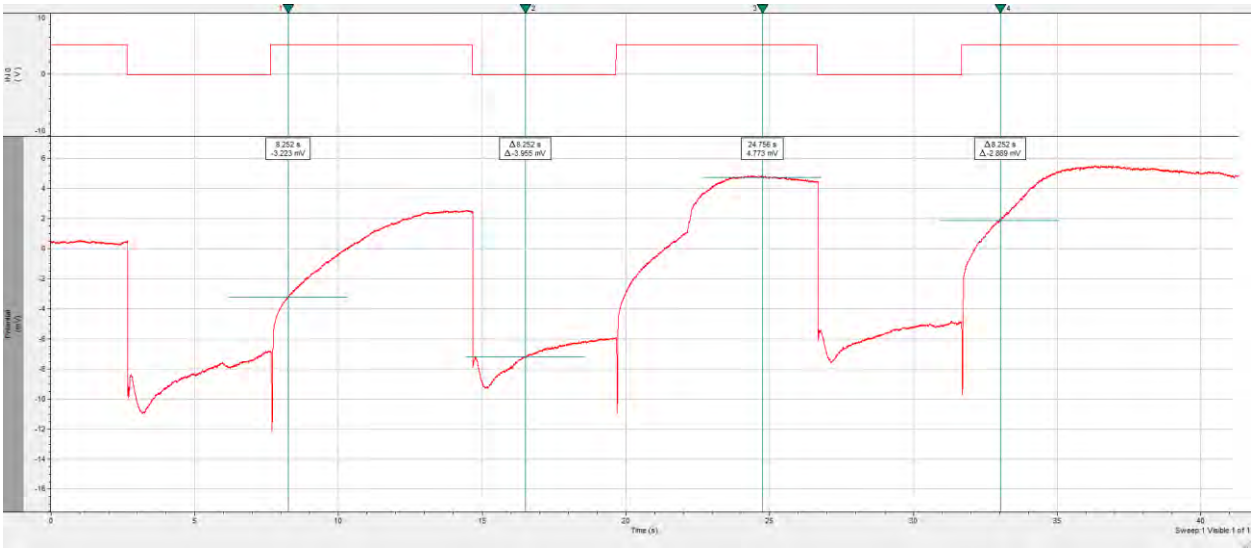
8.252 s
-3.223 mV
Δ8.252 s
Δ-3.955 mV
24.756 s
4.773 mV
Δ8.252 s
Δ-2.889 mV
Time (s)

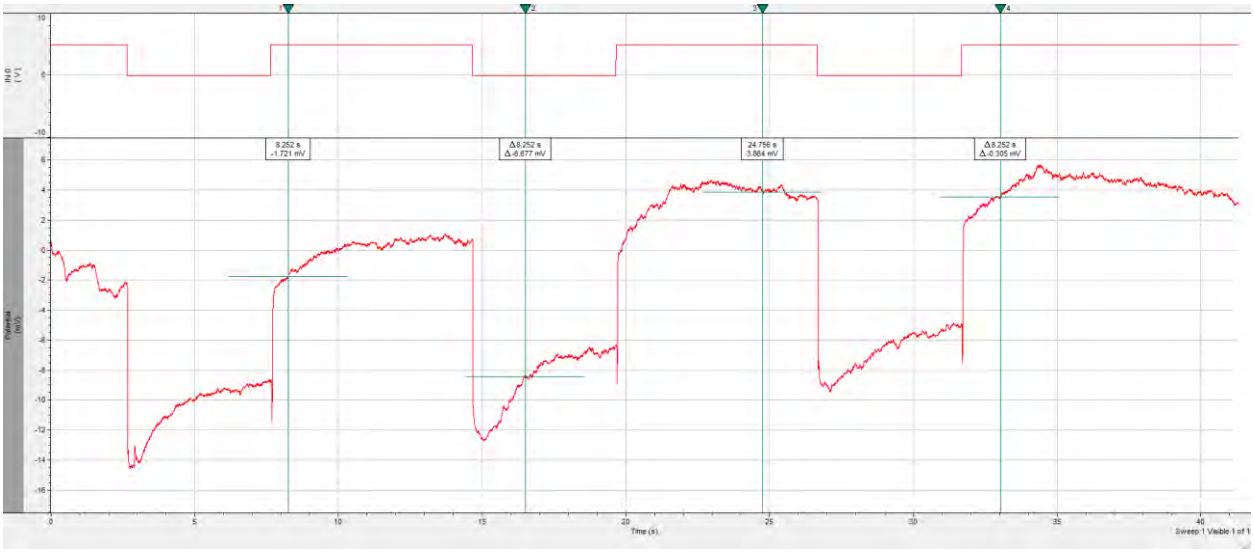

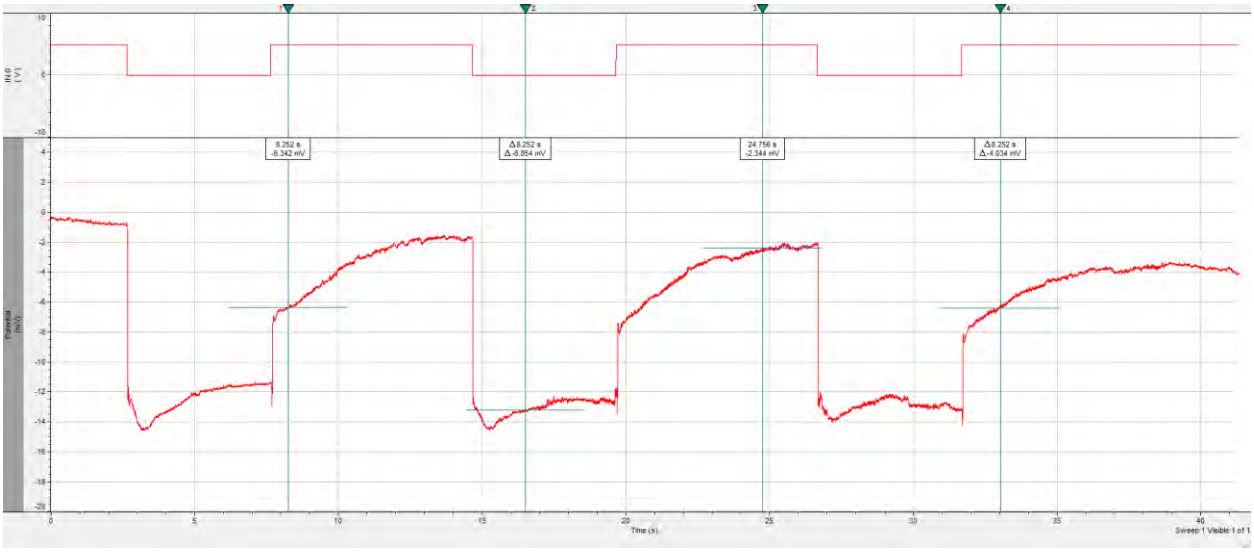

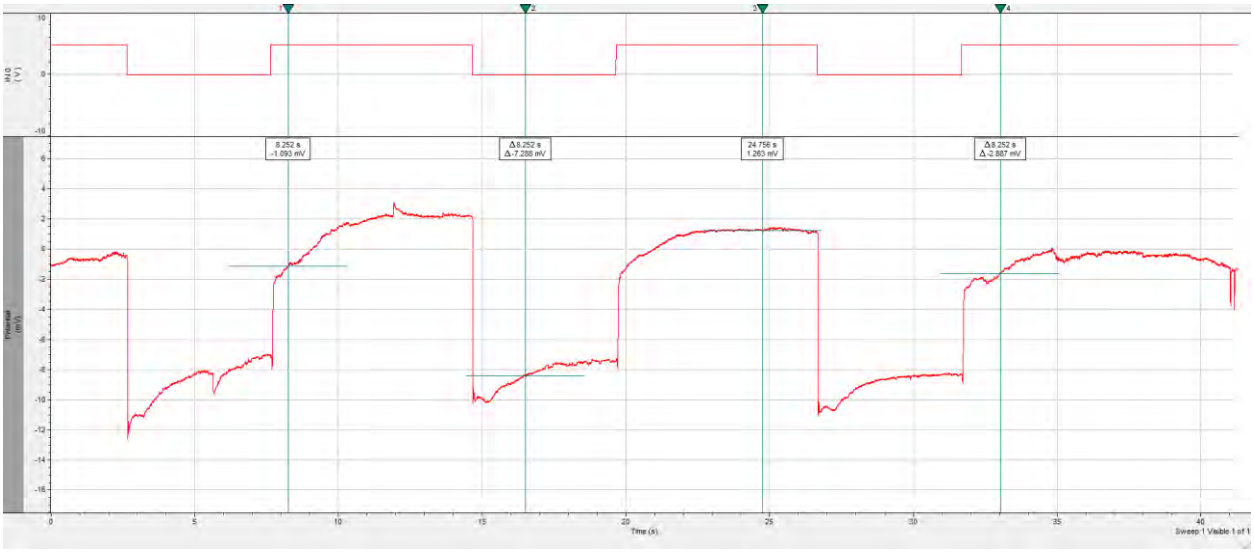
8.252 s
-1.093 mV
Δ8.252 s
Δ-7.288 mV
24.756 s
1.263 mV
Δ8.252 s
Δ-2.887 mV
Time (s)

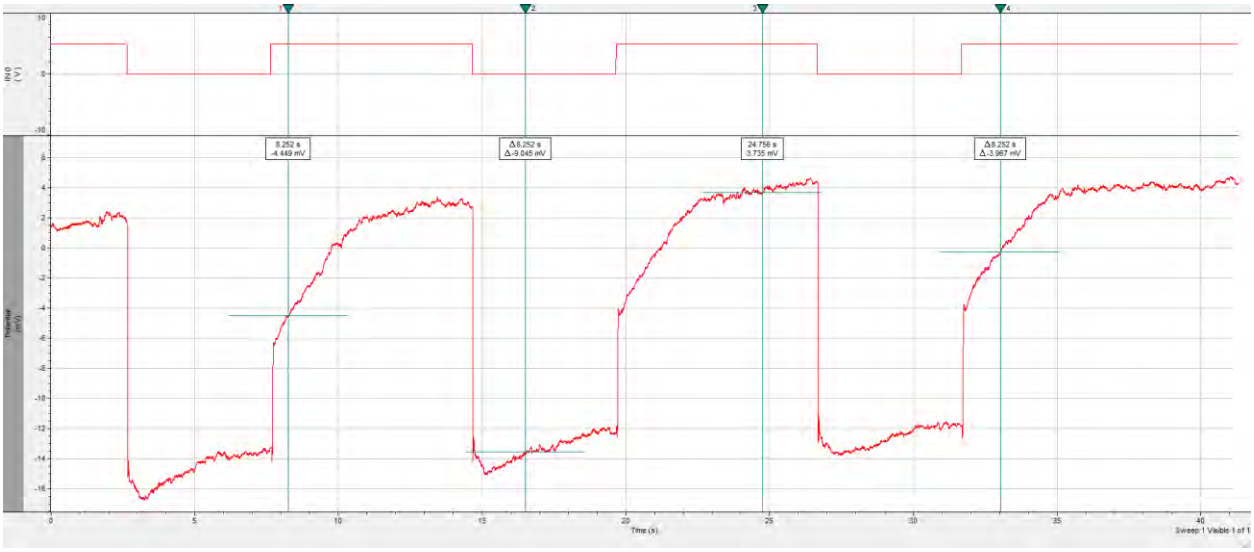
8.252 s
-4.449 mV
Δ8.252 s
Δ-9.045 mV
24.756 s
3.735 mV
Δ8.252 s
Δ-3.967 mV
Time (s)

Genotype: *alrm*-Gal4> *Acsl* RNAi

Phenotype: with transient

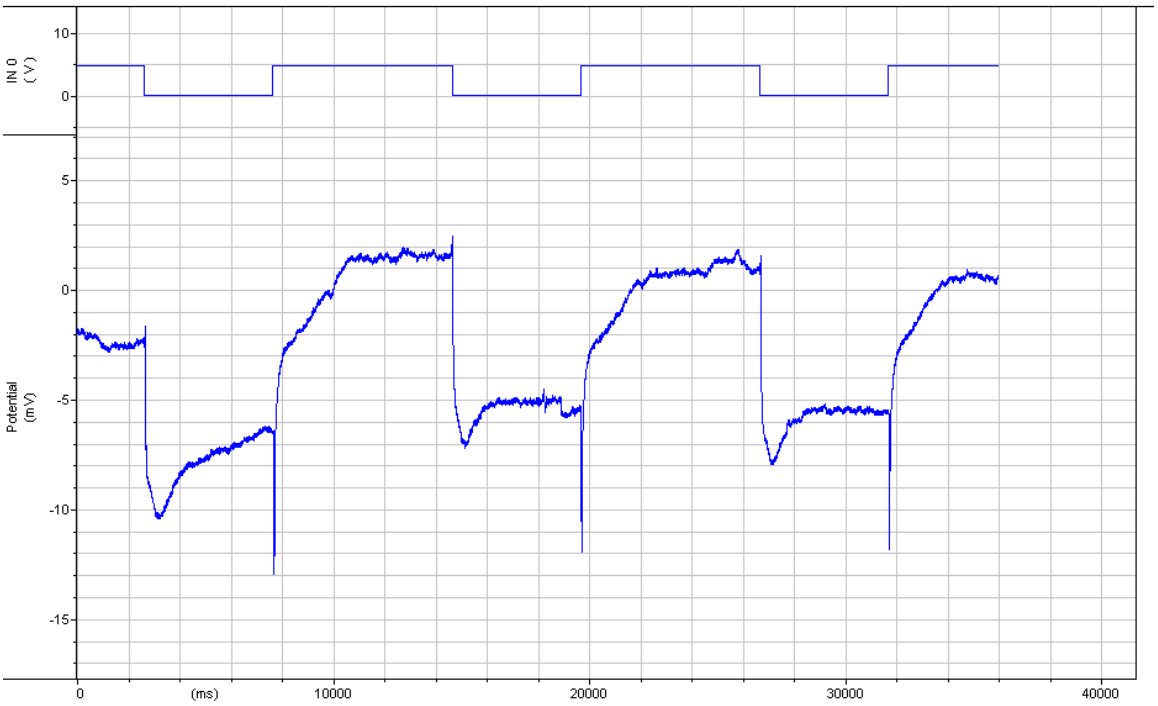

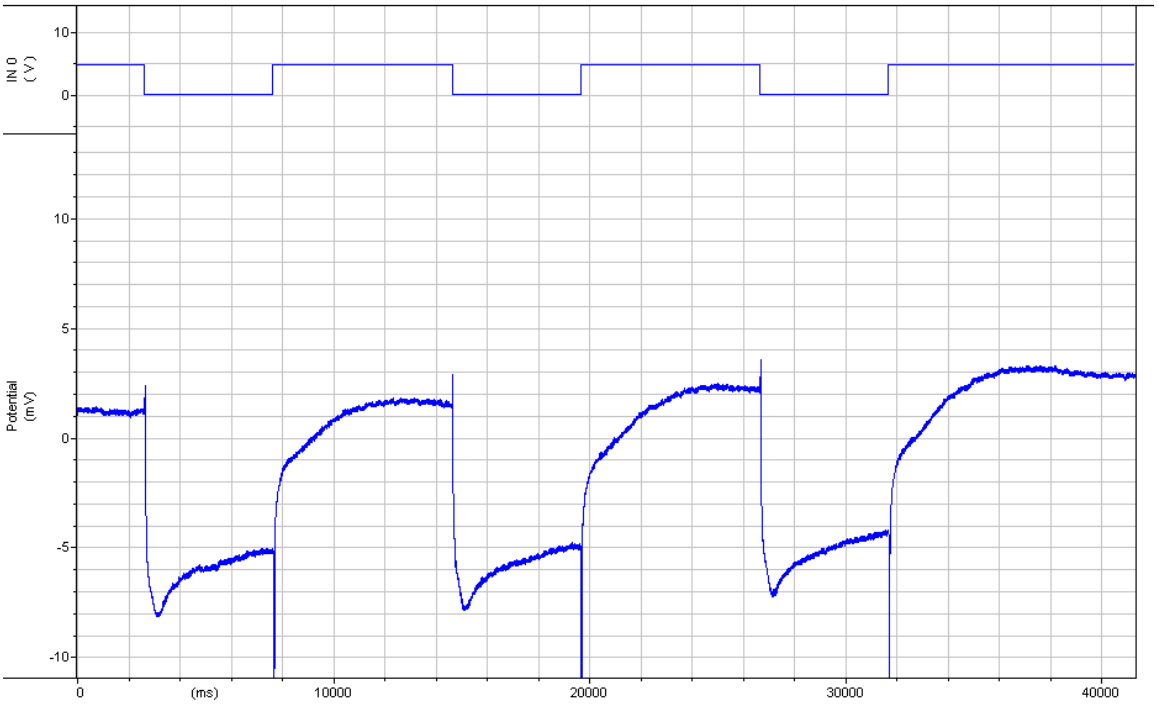

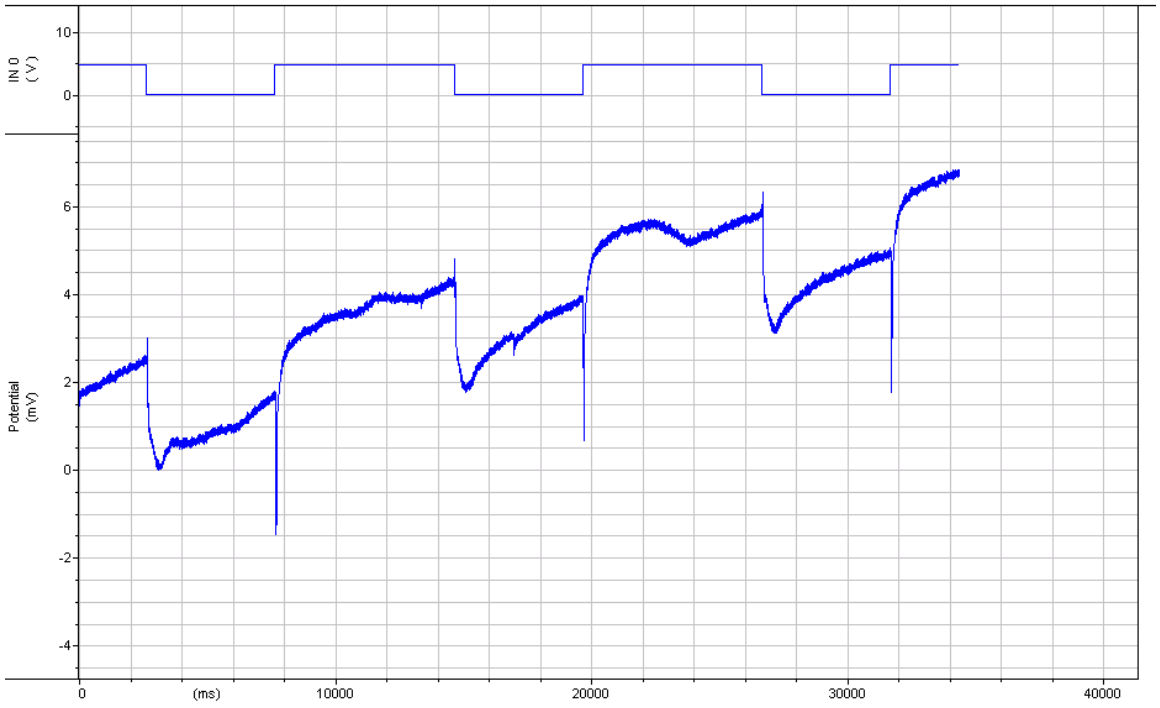
IN 0
(V)
10
0
6
4
2
0
-2
-4
Potential
(mV)
0
(ms)
10000
20000
30000
40000

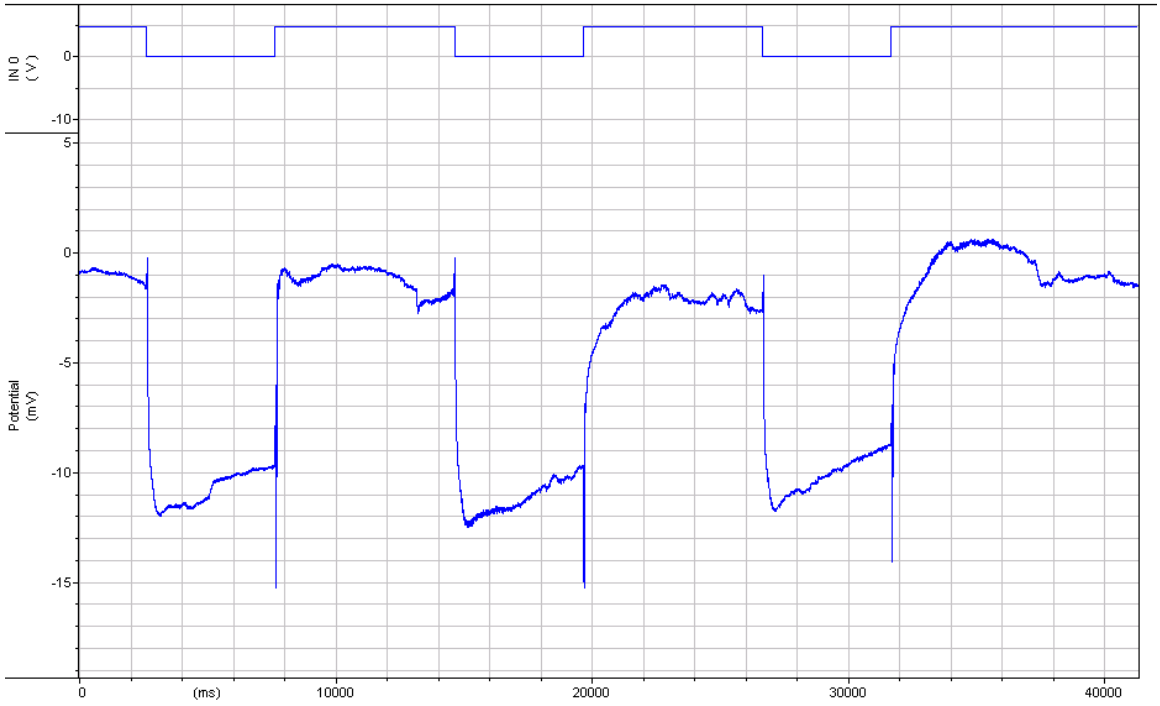
IN 0
(V)
0
-10
5
0
-5
-10
-15
Potential
(mV)
0
(ms)
10000
20000
30000
40000

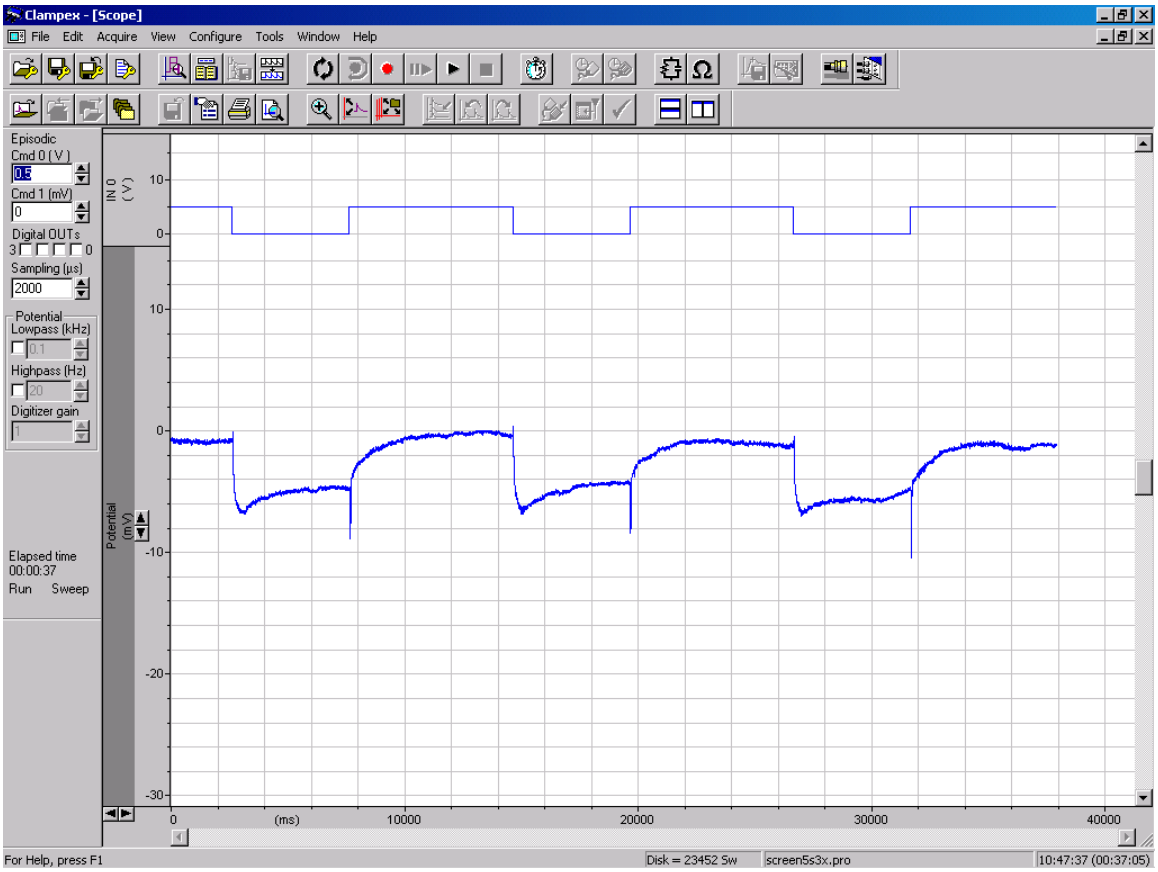
Clampex - [Scope]
File Edit Acquire View Configure Tools Window Help
Episodic
Cmd 0 [V]
0.5
Cmd 1 (mV)
0
Digital OUTs
3 0
Sampling (µs)
2000
Potential
Lowpass (kHz)
0.1
Highpass (Hz)
20
Digitizer gain
1
Elapsed time
00:00:37
Run Sweep
IN 0 (V)
Potential (mV)
10
0
10
0
-10
-20
-30
0
(ms)
10000
20000
30000
40000
For Help, press F1
Disk = 23452 Sw
screen5s3x.pro
10:47:37 (00:37:05)

Genotype: *Gcm*-Gal4> *Acsl* RNAi

Phenotype: with transient

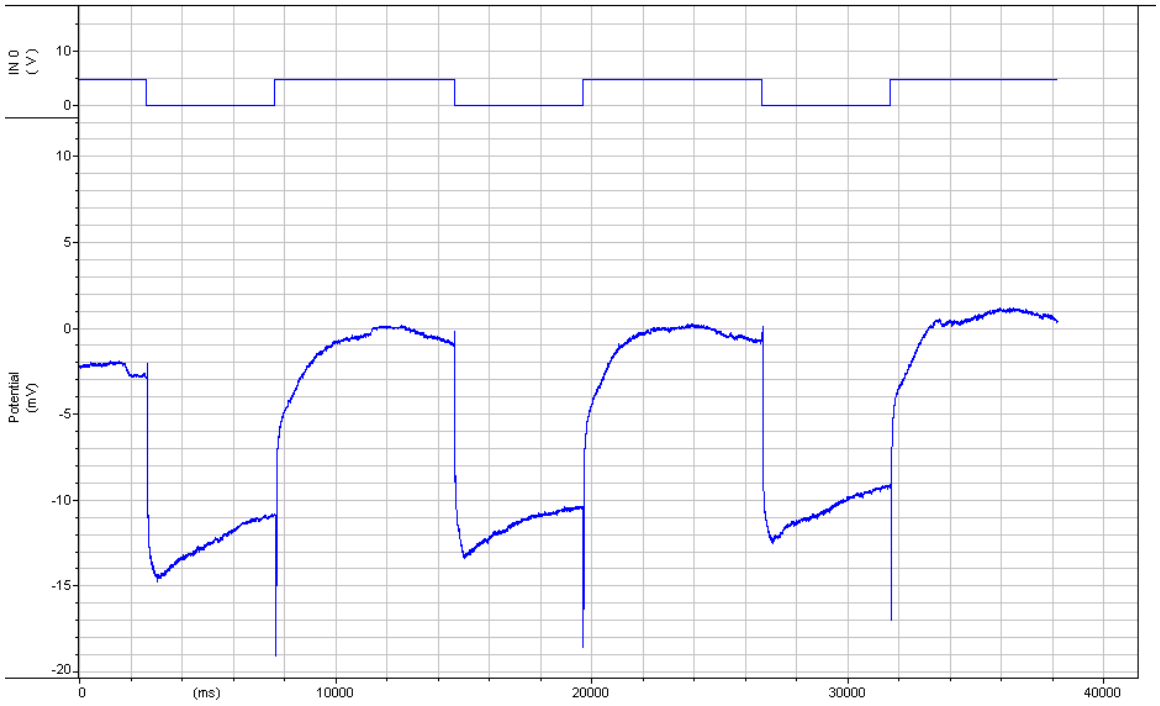

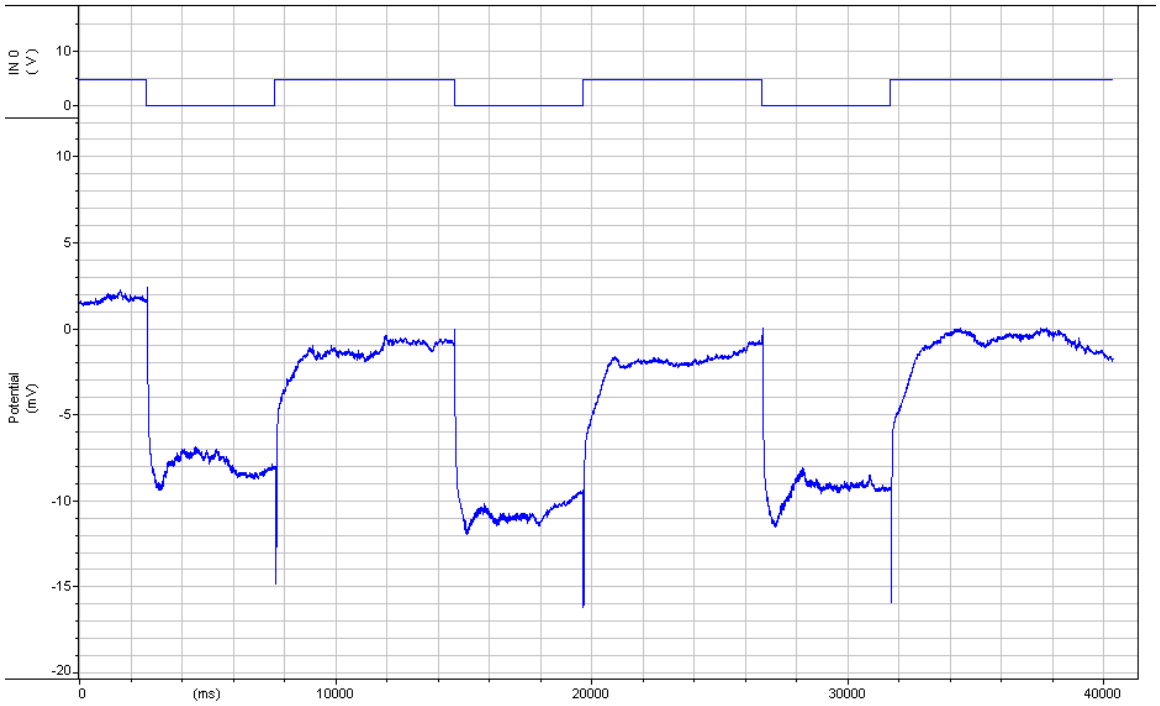


IN 0
(V)
10
0
10
5
0
-5
-10
-15
-20
Potential
(mV)
0
(ms)
10000
20000
30000
40000

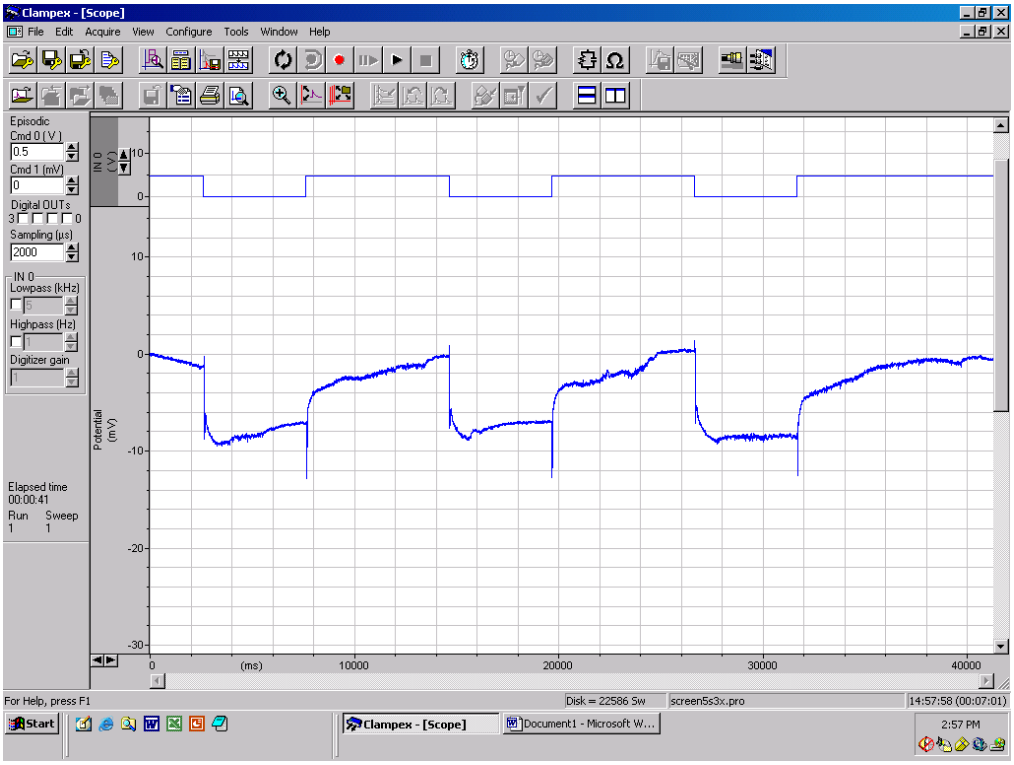
Clampex - [Scope]
File Edit Acquire View Configure Tools Window Help
Episodic
Cmd 0 (V)
0.5
Cmd 1 (mV)
0
Digital OUTs
3 0
Sampling (µs)
2000
IN 0
Lowpass (kHz)
Highpass (Hz)
Digitizer gain
Elapsed time
00:00:41
Run Sweep
1 1
IN 0
(V)
10
0
10
0
-10
-20
-30
Potential
(mV)
0
(ms)
10000
20000
30000
40000
For Help, press F1
Disk = 22586 Sw
screen5s3x.pro
14:57:58 (00:07:01)
Start
Clampex - [Scope]
Document1 - Microsoft W...
2:57 PM

Genotype: *hisCl1*-Gal4> *Acsl* RNAi

Phenotype: with transient

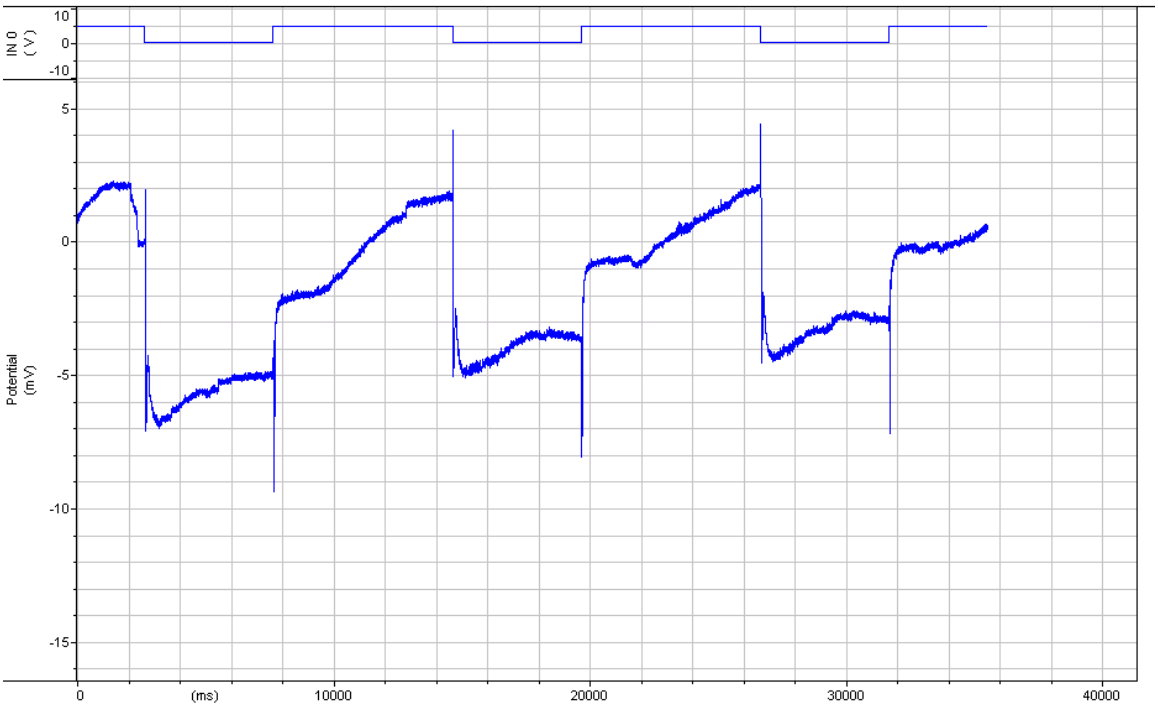

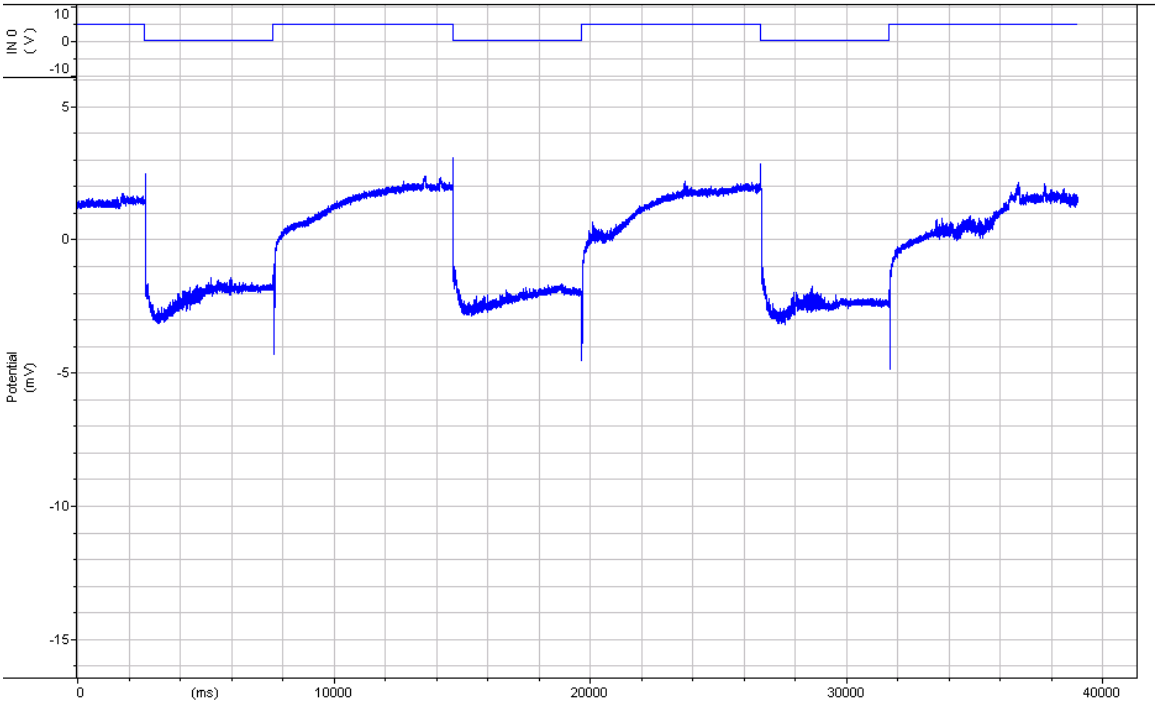

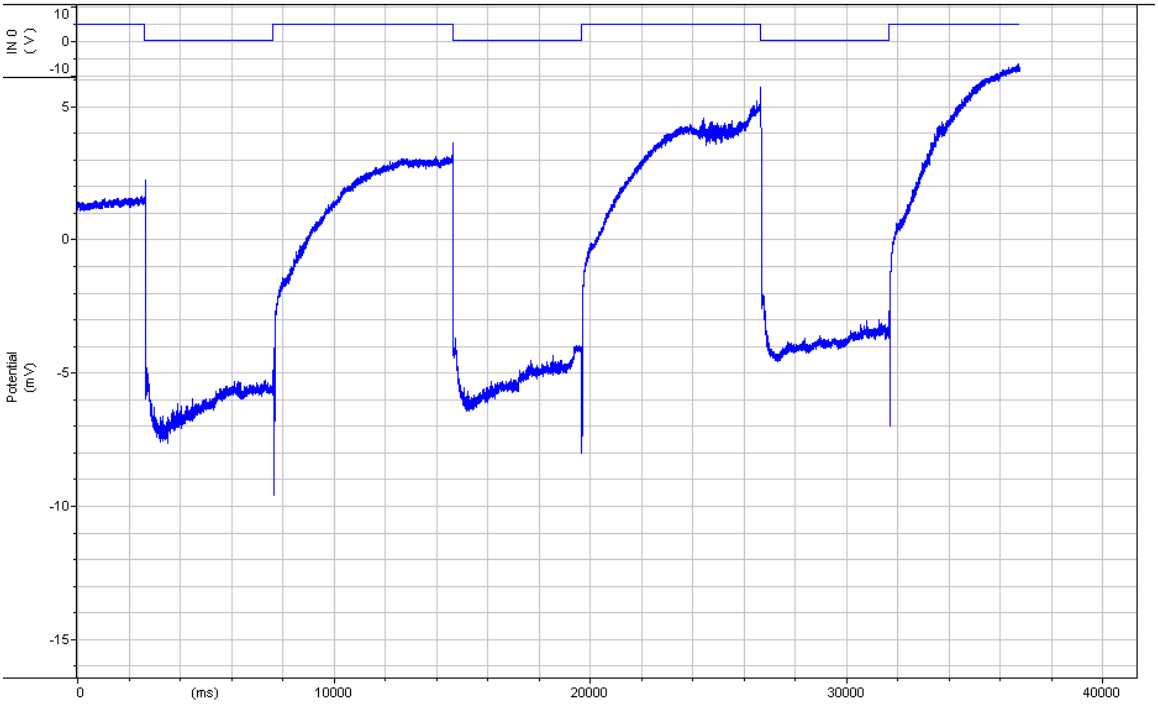
IN 0
(V)
10
0
-10
5
0
-5
-10
-15
Potential
(mV)
0
(ms)
10000
20000
30000
40000

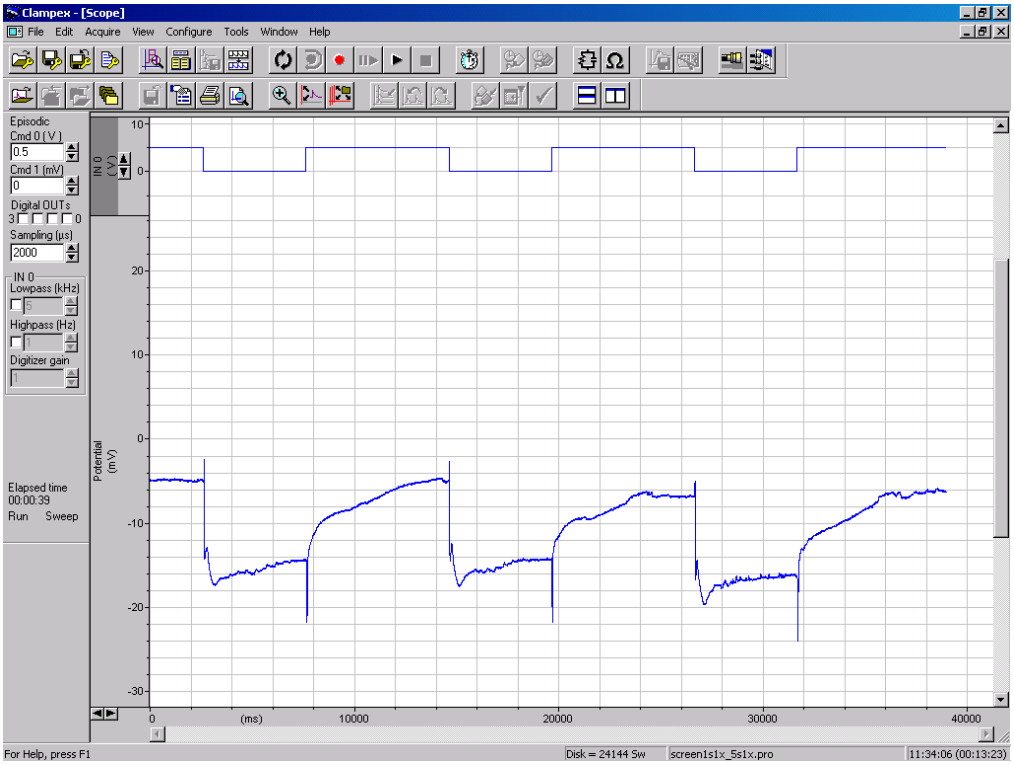
Clampex - [Scope]
File Edit Acquire View Configure Tools Window Help
Episodic
Cmd 0 (V)
0.5
Cmd 1 (mV)
0
Digital OUTs
Sampling (µs)
2000
IN 0
Lowpass (kHz)
Highpass (Hz)
Digitizer gain
Elapsed time
00:00:39
Run Sweep
IN 0
(V)
Potential
(mV)
(ms)
For Help, press F1
Disk = 24144 Sw
screen1s1x_5s1x.pro
11:34:06 (00:13:23)

Genotype: *loco*-Gal4> *Acsl* RNAi

Phenotype: with transient

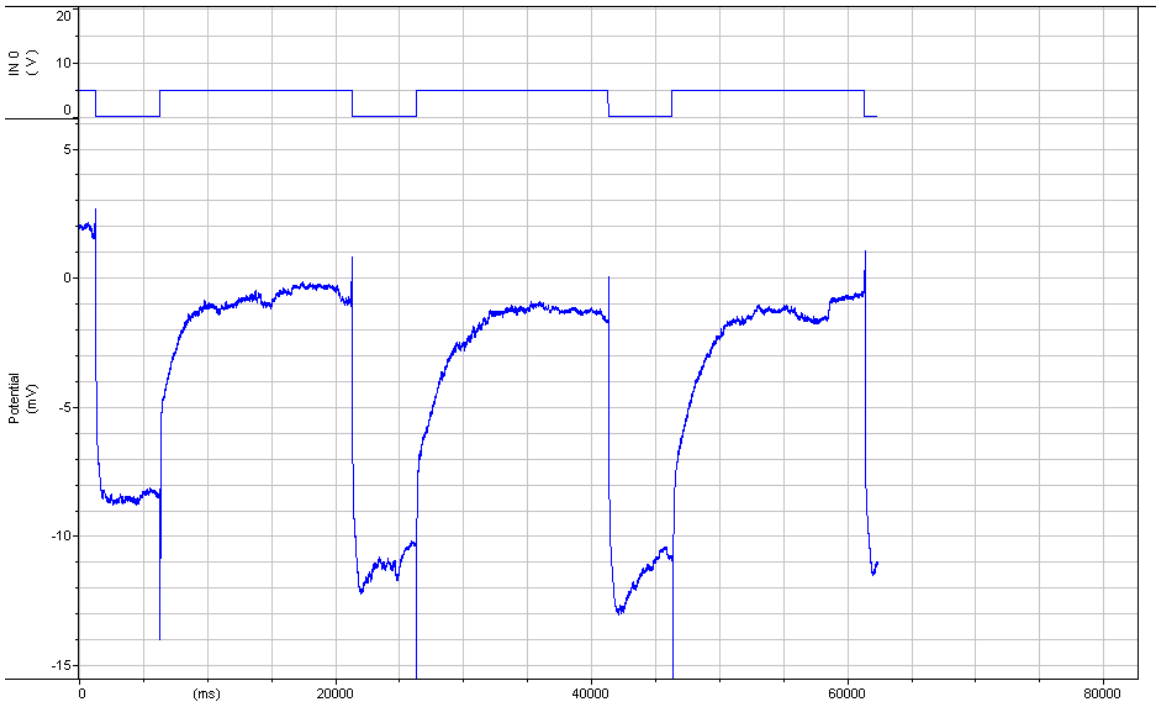

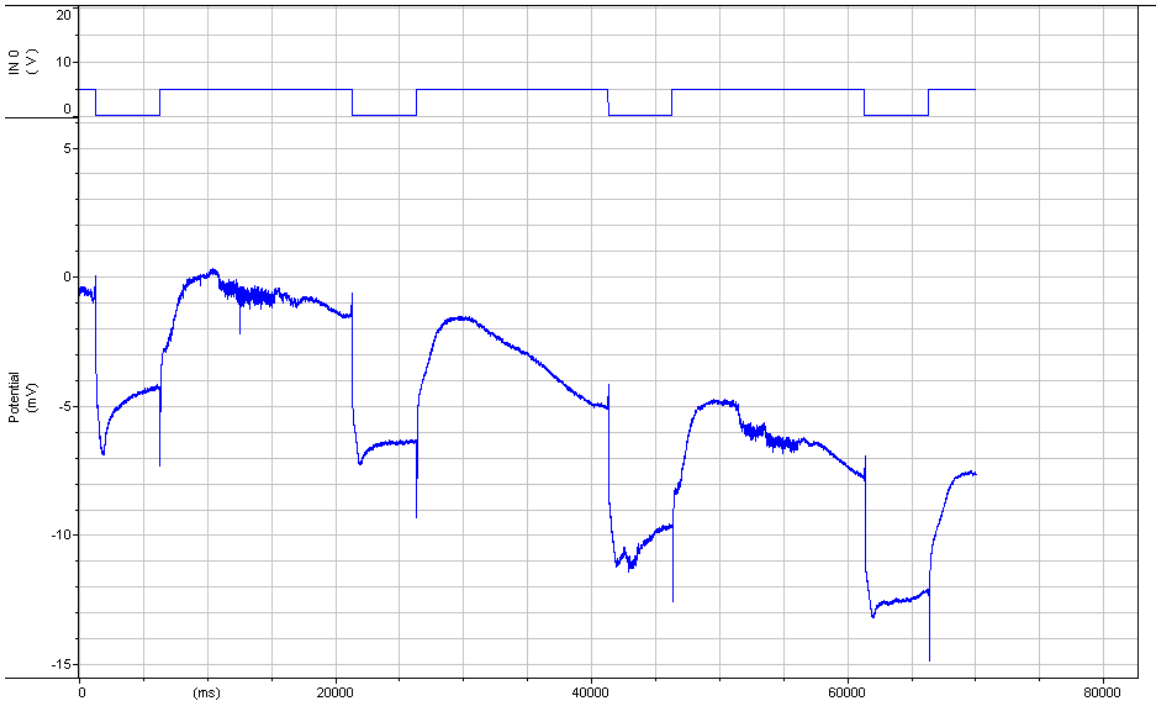

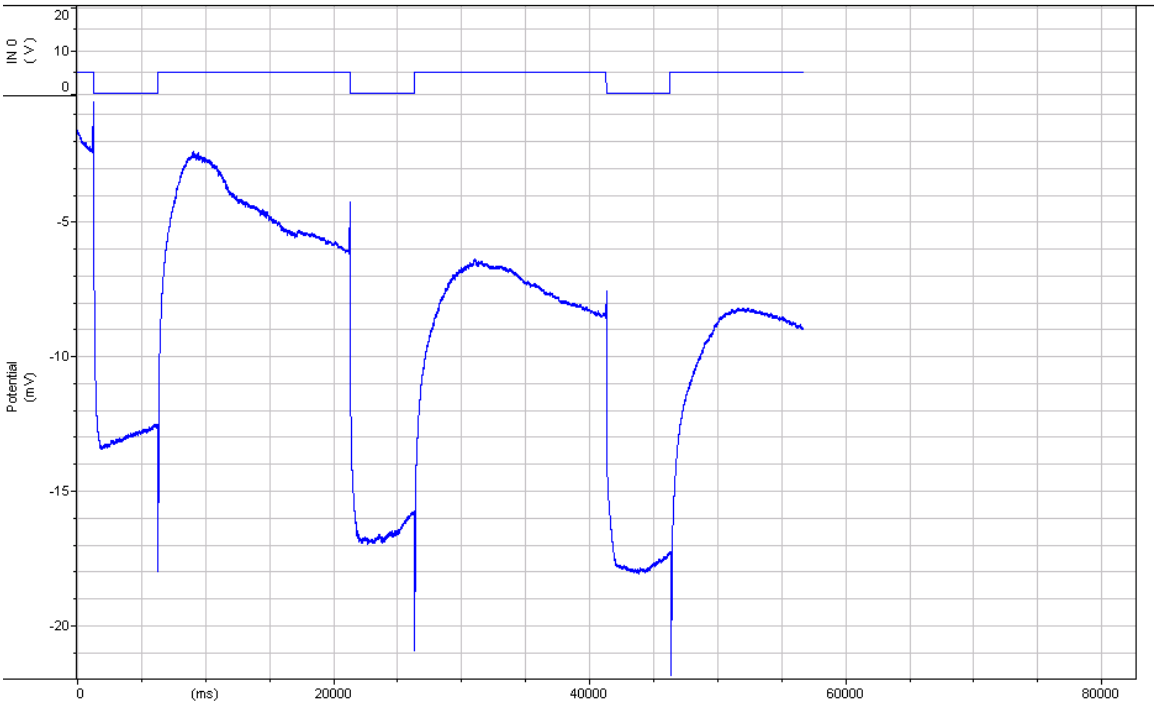
IN 0
(V)
20
10
0
-5
-10
-15
-20
Potential
(mV)
0
(ms)
20000
40000
60000
80000

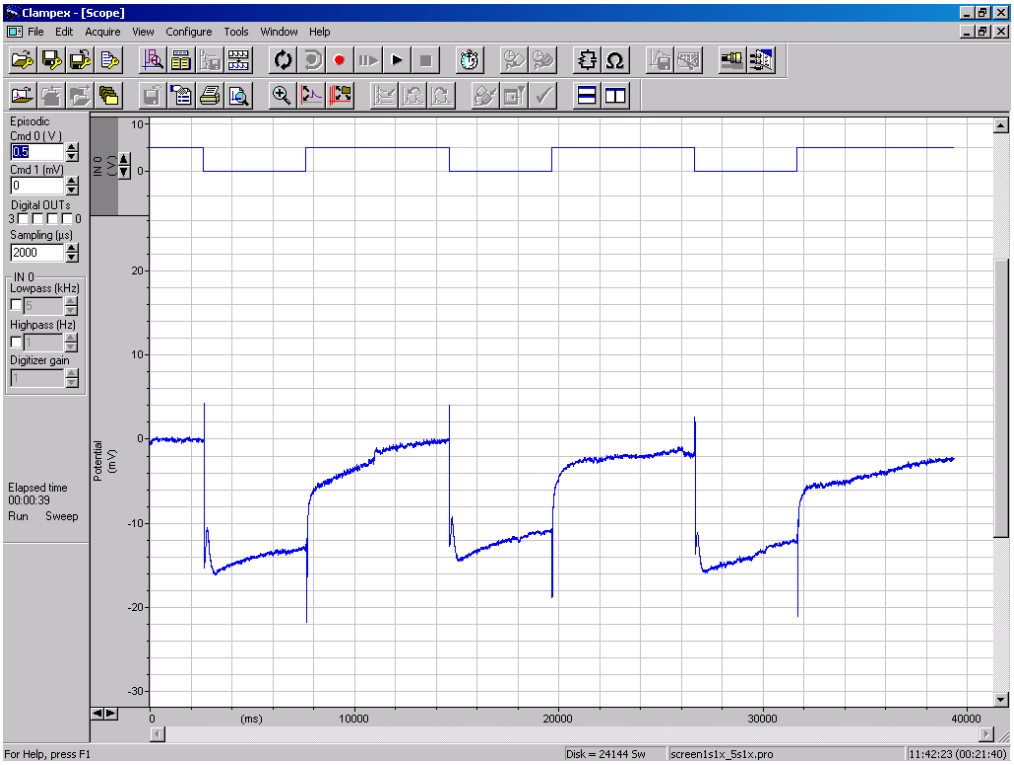
Clampex - [Scope]
File Edit Acquire View Configure Tools Window Help
Episodic
Cmd 0 (V)
0.5
Cmd 1 (mV)
0
Digital OUTs
3 0
Sampling (µs)
2000
IN 0
Lowpass (kHz)
Highpass (Hz)
Digitizer gain
Elapsed time
00:00:39
Run Sweep
IN 0
(V)
Potential
(mV)
10
0
20
10
0
-10
-20
-30
0
(ms)
10000
20000
30000
40000
For Help, press F1
Disk = 24144 Sw
screen1s1x_5s1x.pro
11:42:23 (00:21:40)

Genotype: *mmd*-Gal4> *Acsl* RNAi

Phenotype: with transient

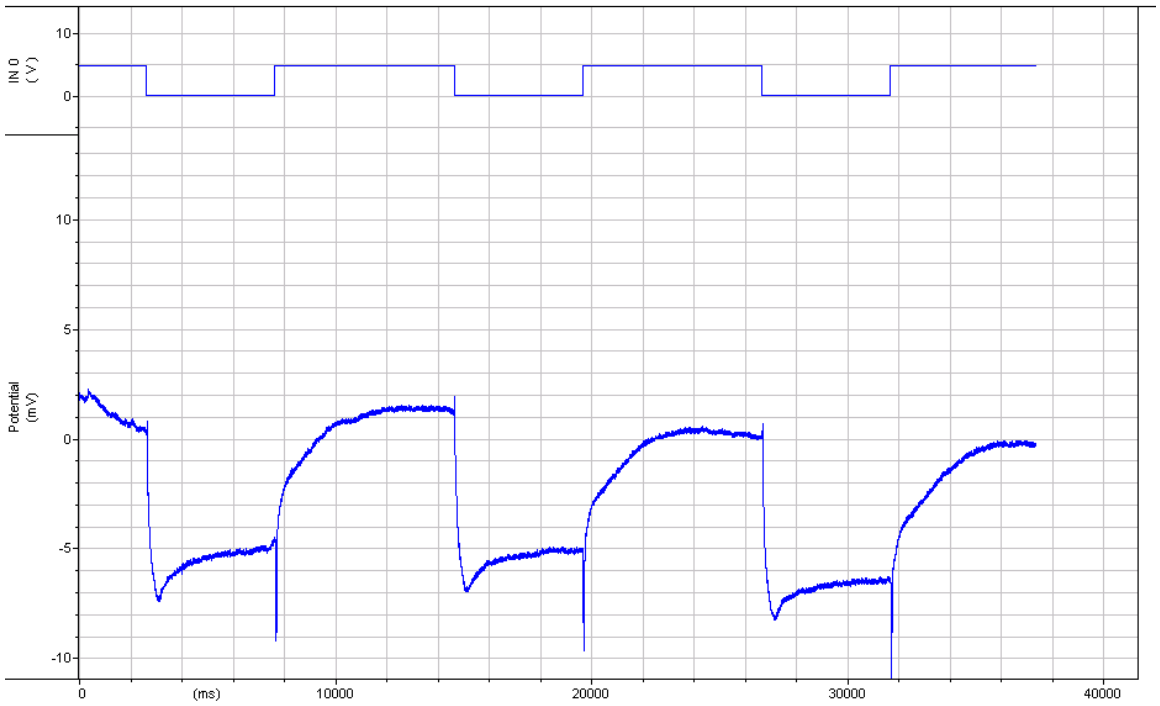

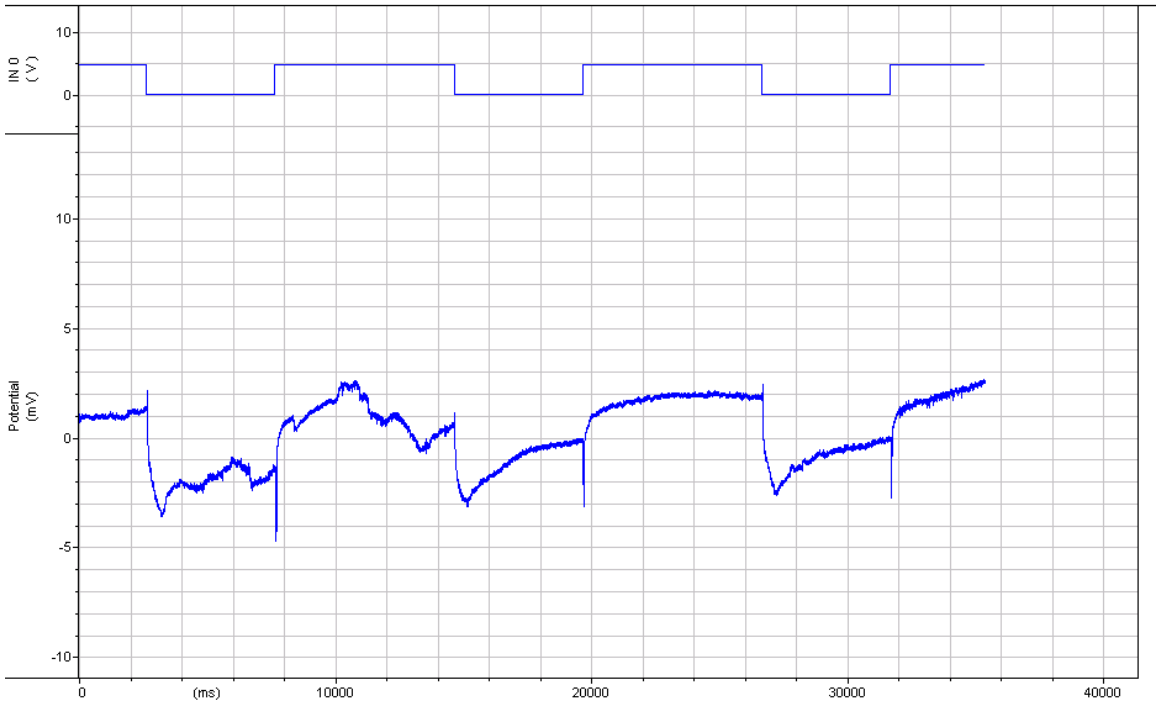

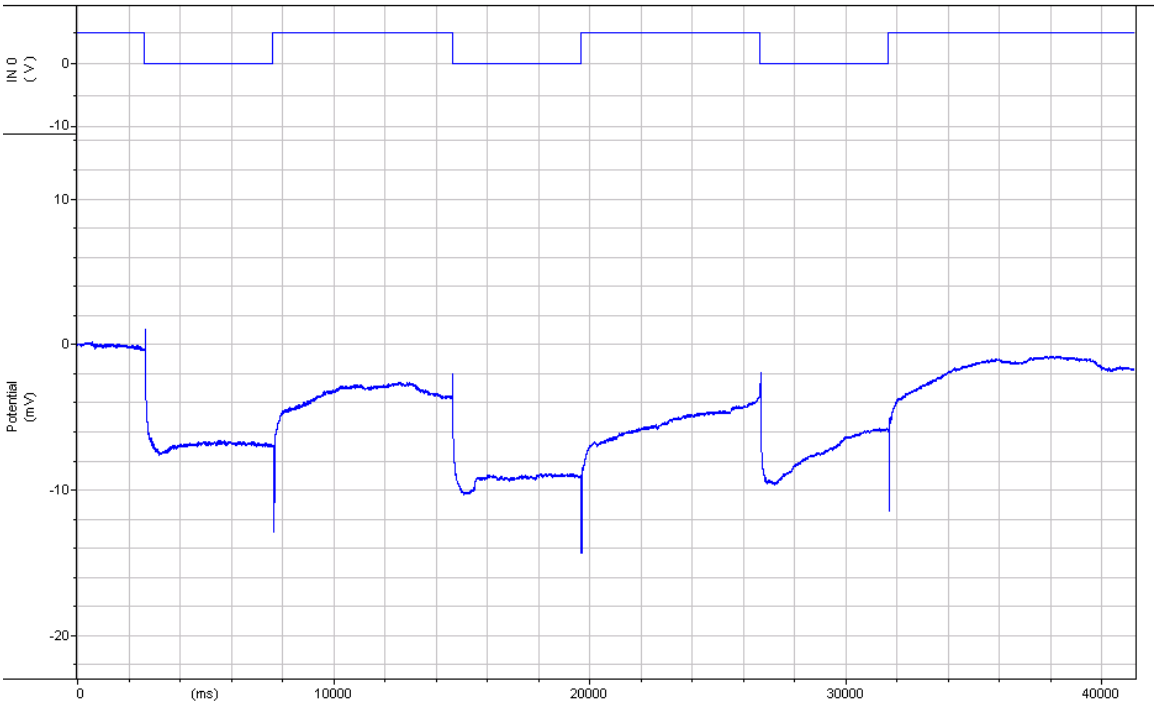
IN 0
(V)
0
-10
10
0
Potential
(mV)
-10
-20
0
(ms)
10000
20000
30000
40000

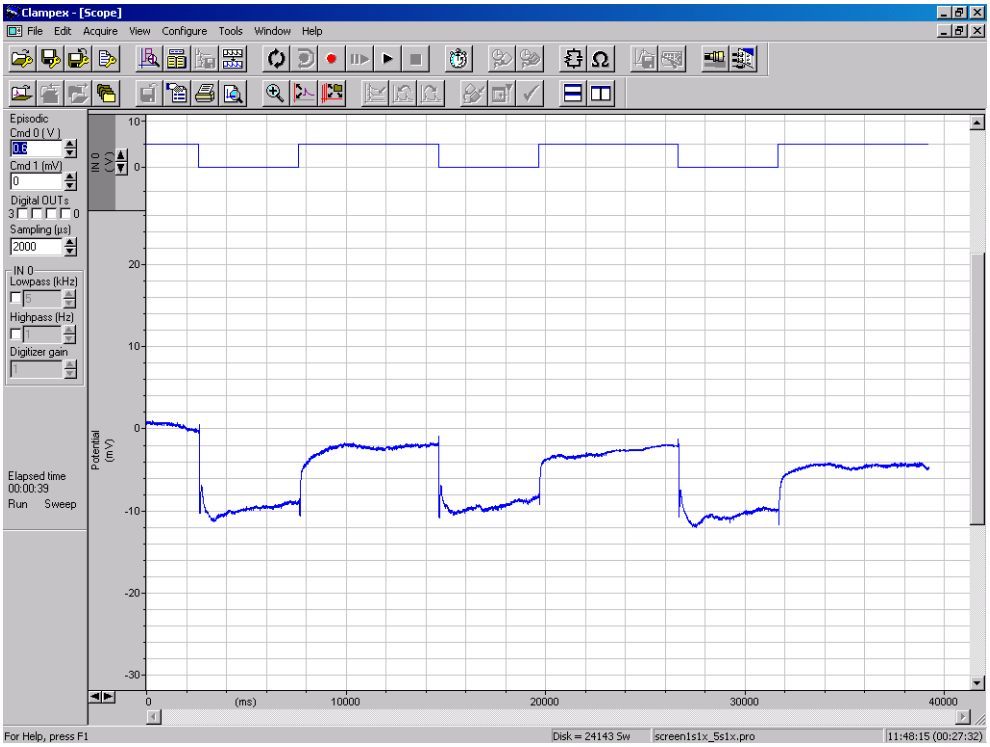
Clampex - [Scope]
File Edit Acquire View Configure Tools Window Help
Episodic
Cmd 0 (V)
0.0
Cmd 1 (mV)
0
Digital OUTs
3 0
Sampling (µs)
2000
IN 0
Lowpass (kHz)
Highpass (Hz)
Digitizer gain
Elapsed time
00:00:39
Run Sweep
IN 0
(V)
Potential
(mV)
10
0
20
10
0
-10
-20
-30
0
(ms)
10000
20000
30000
40000
For Help, press F1
Disk = 24143 Sw
screen1s1x_5s1x.pro
11:48:15 (00:27:32)

Genotype: *moody*-Gal4> *Acsl* RNAi

Phenotype: with transient

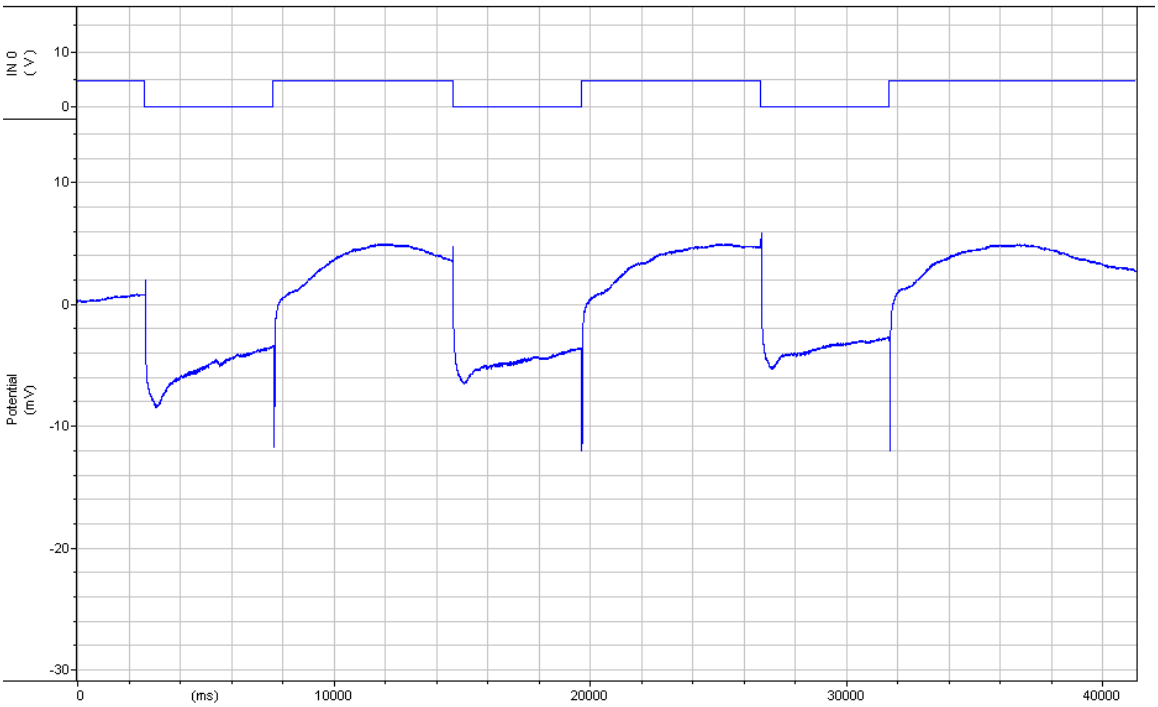

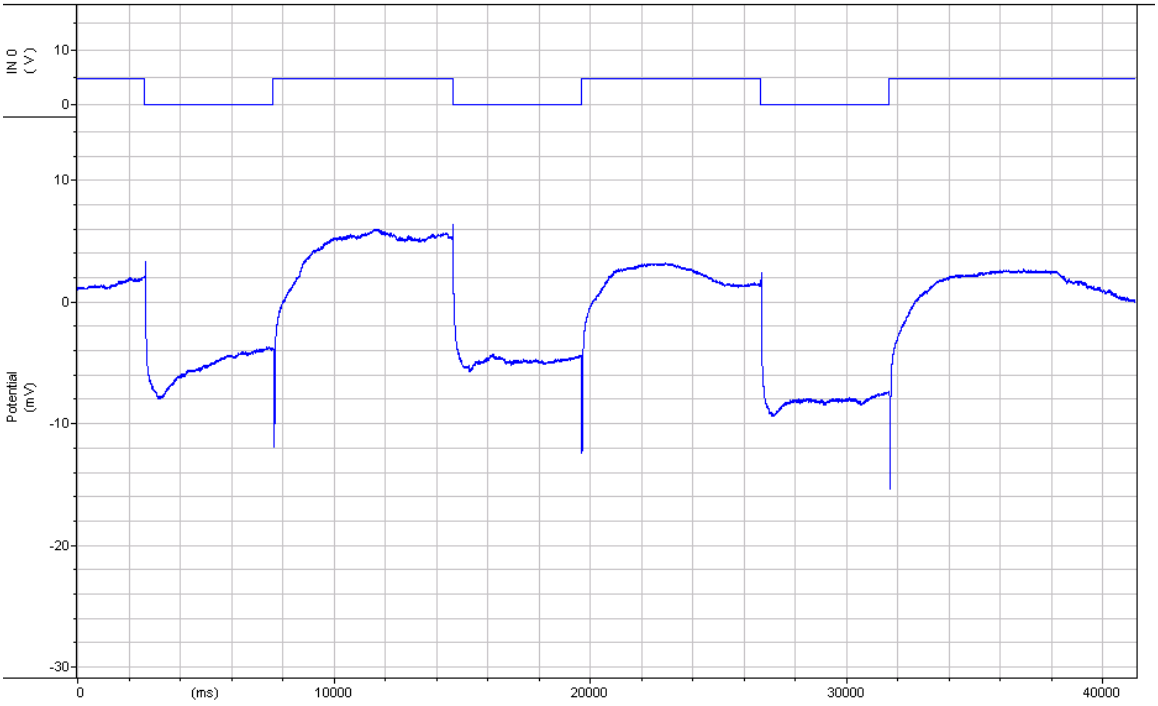

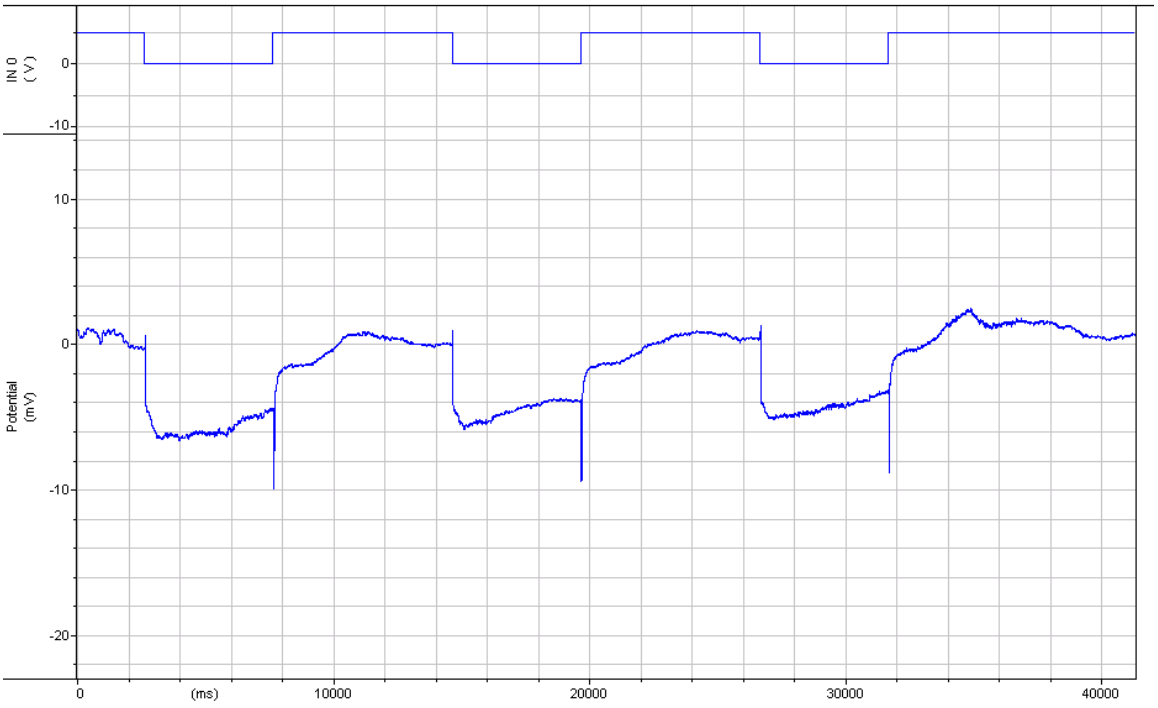
IN 0
(V)
0
-10
10
0
Potential
(mV)
-10
-20
0
(ms)
10000
20000
30000
40000

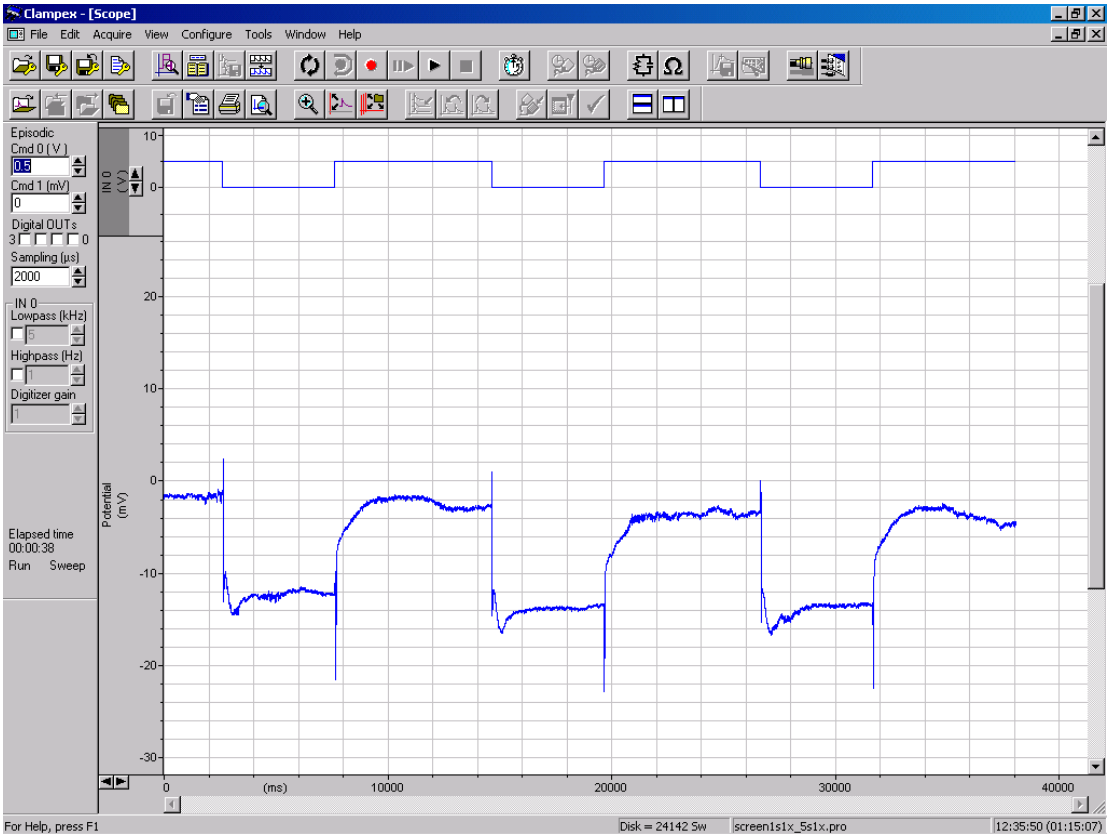
Clampex - [Scope]
File Edit Acquire View Configure Tools Window Help
Episodic
Cmd 0 (V)
0.5
Cmd 1 (mV)
0
Digital OUTs
3 0
Sampling (µs)
2000
IN 0
Lowpass (kHz)
5
Highpass (Hz)
1
Digitizer gain
1
Elapsed time
00:00:38
Run Sweep
IN 0
(V)
Potential
(mV)
10
0
20
10
0
-10
-20
-30
0
(ms)
10000
20000
30000
40000
For Help, press F1
Disk = 24142 Sw
screen1s1x_5s1x.pro
12:35:50 (01:15:07)

Genotype: Mz97-Gal4> *Acsl* RNAi

Phenotype: with transient

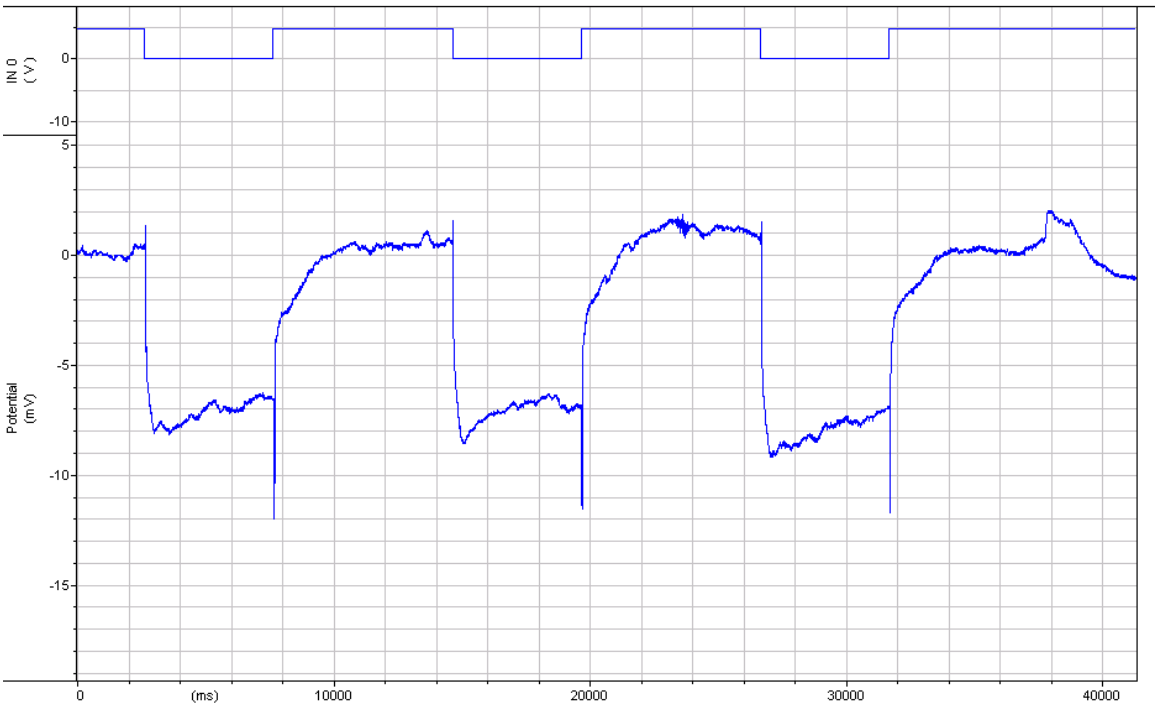

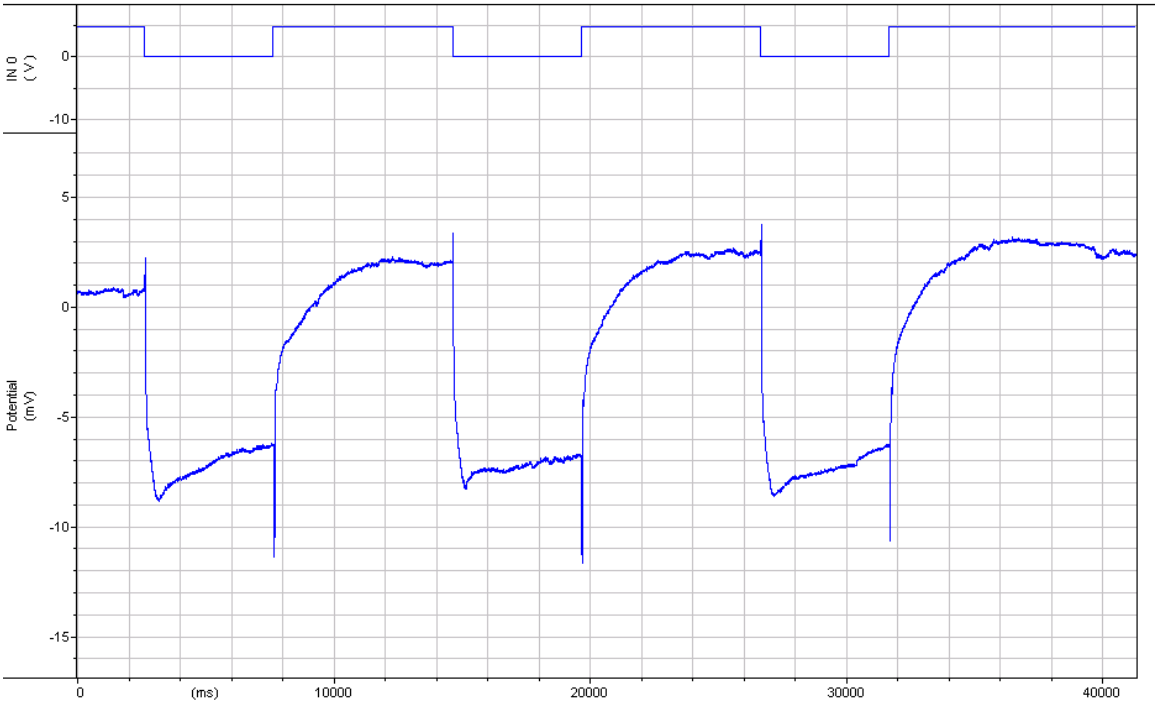

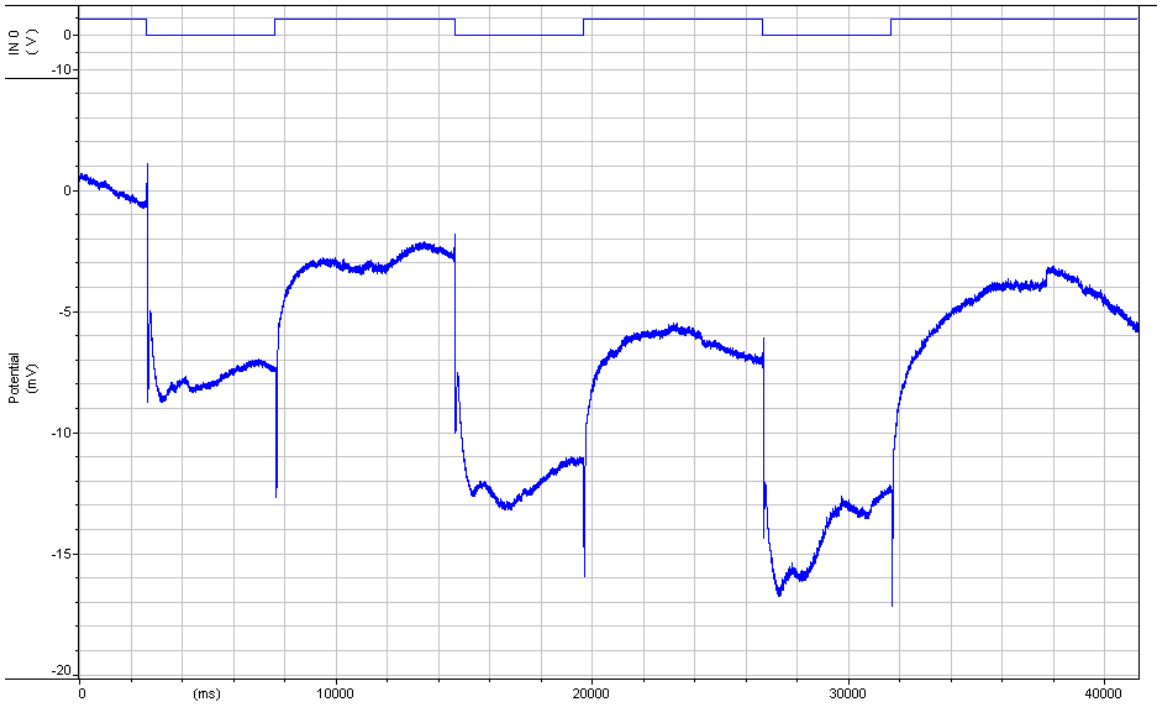
IN 0
(V)
0
-10
0
-5
-10
-15
-20
Potential
(mV)
0
(ms)
10000
20000
30000
40000


IN 0
(V)
0
-10
0
-5
-10
-15
-20
Potential
(mV)
0
(ms)
10000
20000
30000
40000

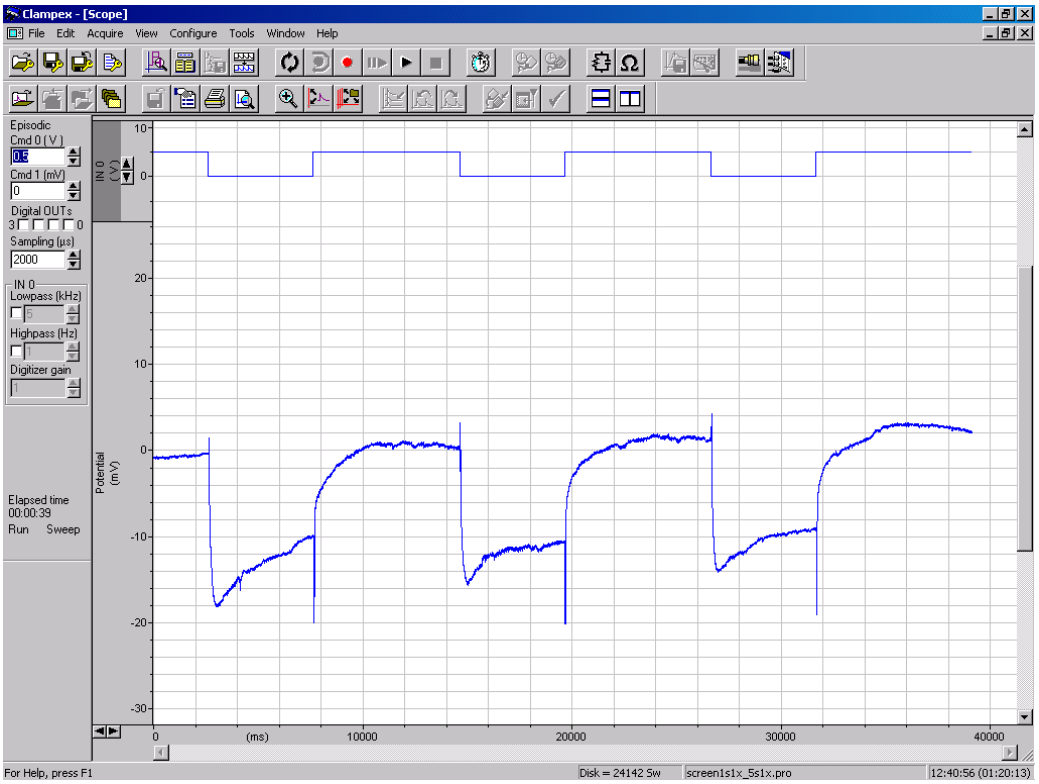
Clampex - [Scope]
File Edit Acquire View Configure Tools Window Help
Episodic
Cmd 0 (V)
0.5
Cmd 1 (mV)
0
Digital OUTs
3 0
Sampling (µs)
2000
IN 0
Lowpass (kHz)
5
Highpass (Hz)
1
Digitizer gain
1
Elapsed time
00:00:39
Run Sweep
IN 0 (V)
Potential (mV)
10
0
20
10
0
-10
-20
-30
0
(ms)
10000
20000
30000
40000
For Help, press F1
Disk = 24142 Sw
screen1s1x_5s1x.pro
12:40:56 (01:20:13)

Genotype: Mz0709-Gal4> *Acsl* RNAi

Phenotype: with transient

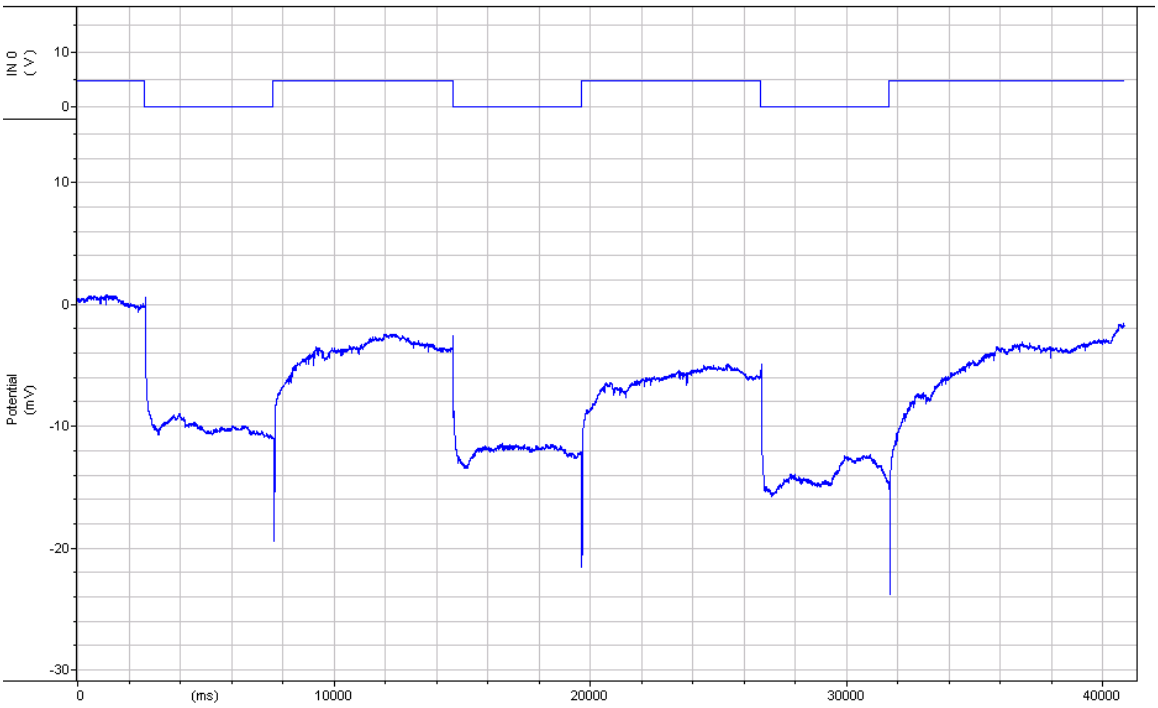

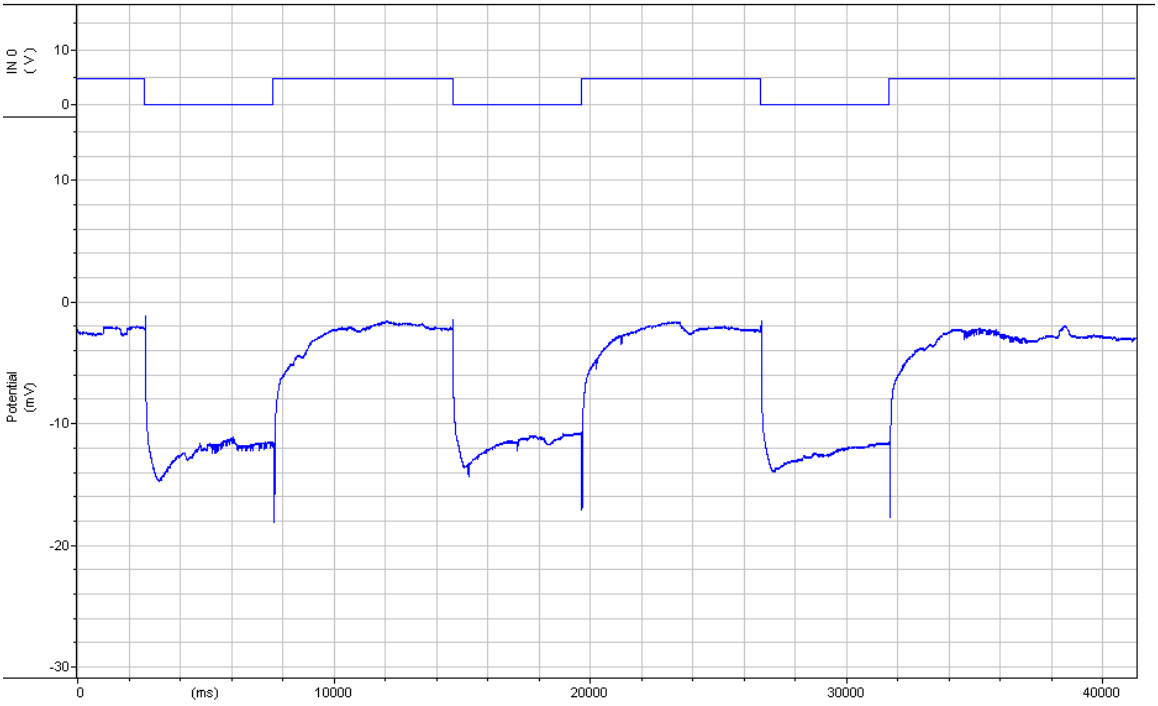

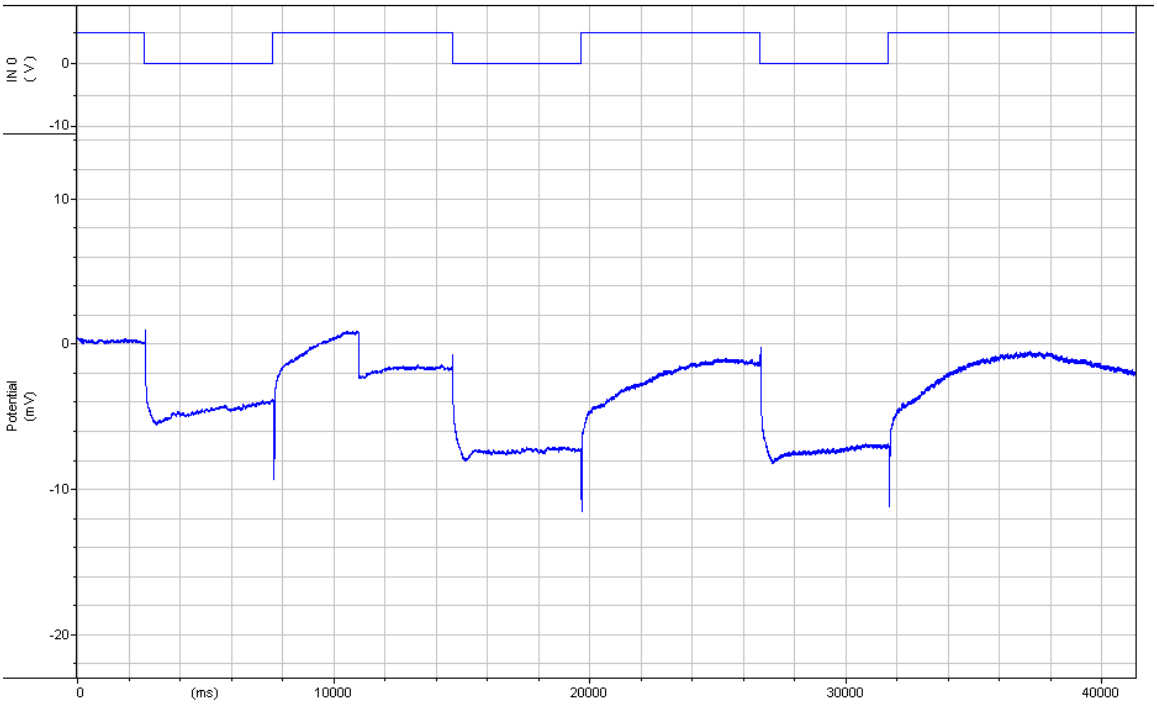
IN 0
(V)
0
-10
10
0
-10
-20
Potential
(mV)
0
(ms)
10000
20000
30000
40000

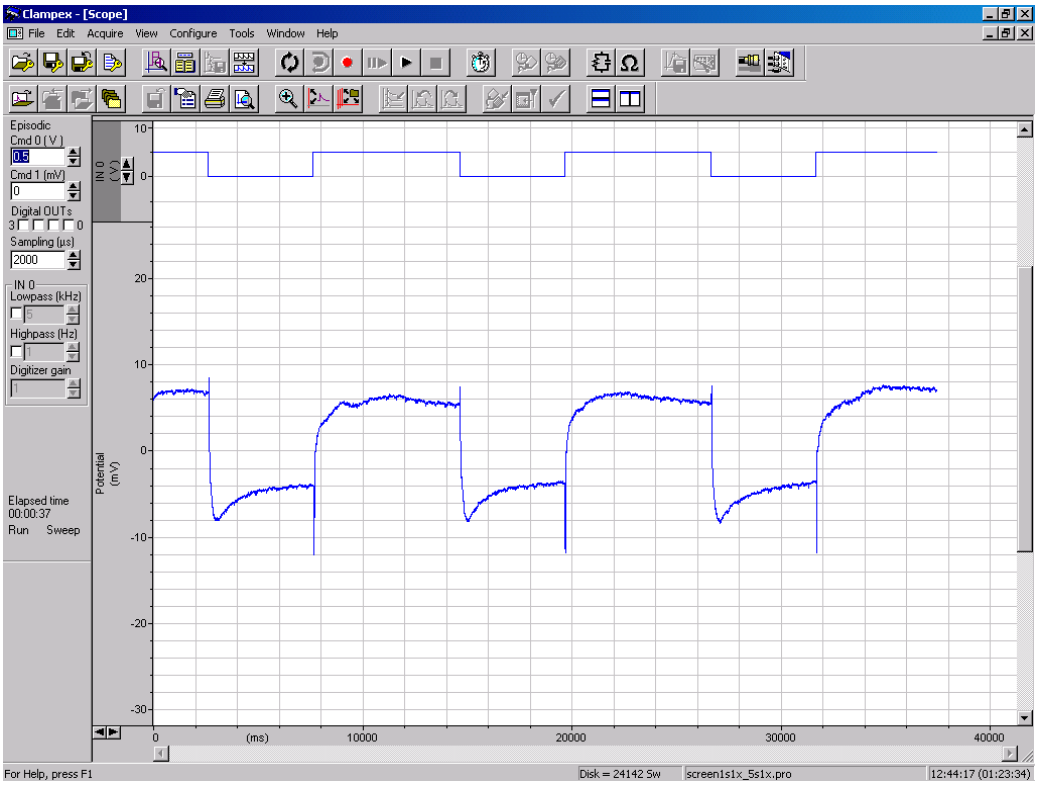
Clampex - [Scope]
File Edit Acquire View Configure Tools Window Help
Episodic
Cmd 0 (V)
0.5
Cmd 1 (mV)
0
Digital OUTs
3 0
Sampling (µs)
2000
IN 0
Lowpass (kHz)
Highpass (Hz)
Digitizer gain
Elapsed time
00:00:37
Run Sweep
IN 0
(V)
Potential
(mV)
10
0
20
10
0
-10
-20
-30
0
(ms)
10000
20000
30000
40000
For Help, press F1
Disk = 24142 Sw
screen1s1x_5s1x.pro
12:44:17 (01:23:34)

Genotype: *nrv2*-Gal4> *Acsl* RNAi

Phenotype: with transient

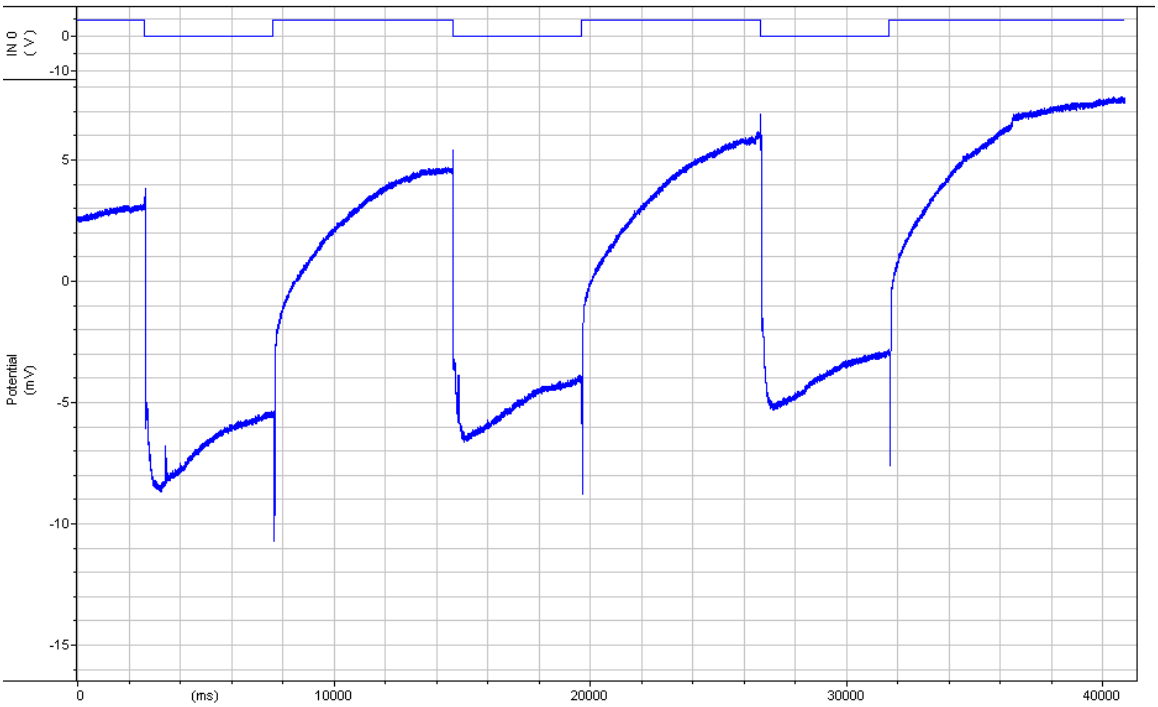

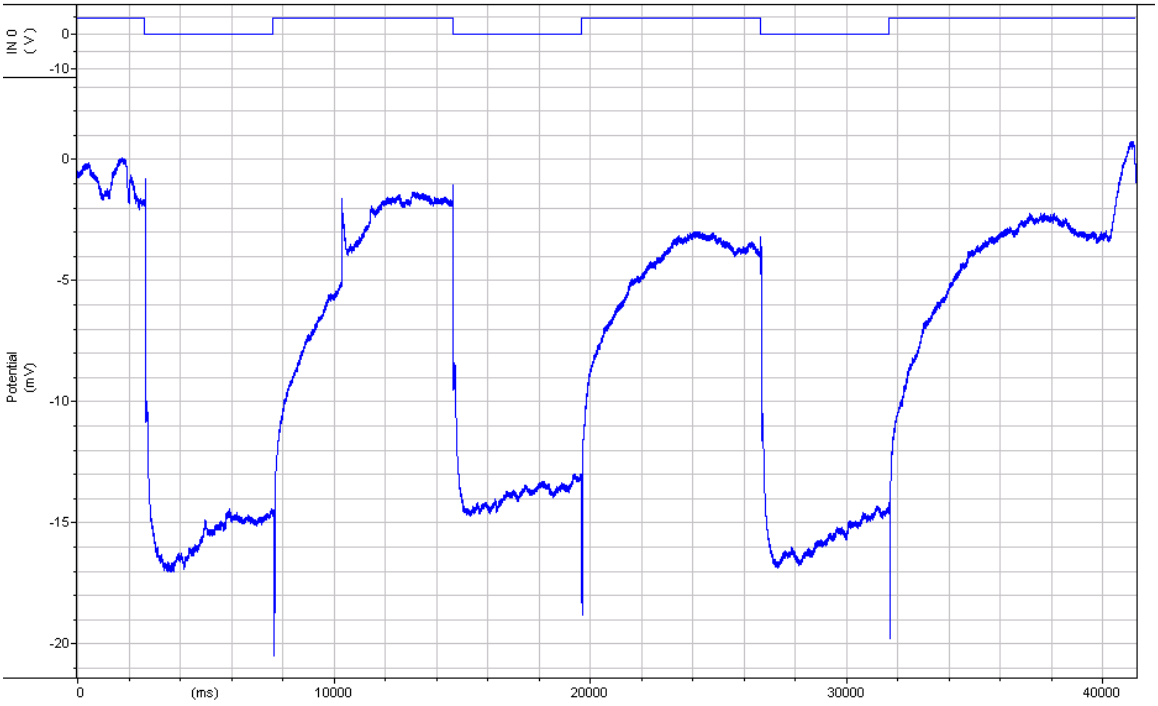


IN 0
(V)
10
0
-10
0
-5
-10
-15
Potential
(mV)
0
(ms)
10000
20000
30000
40000

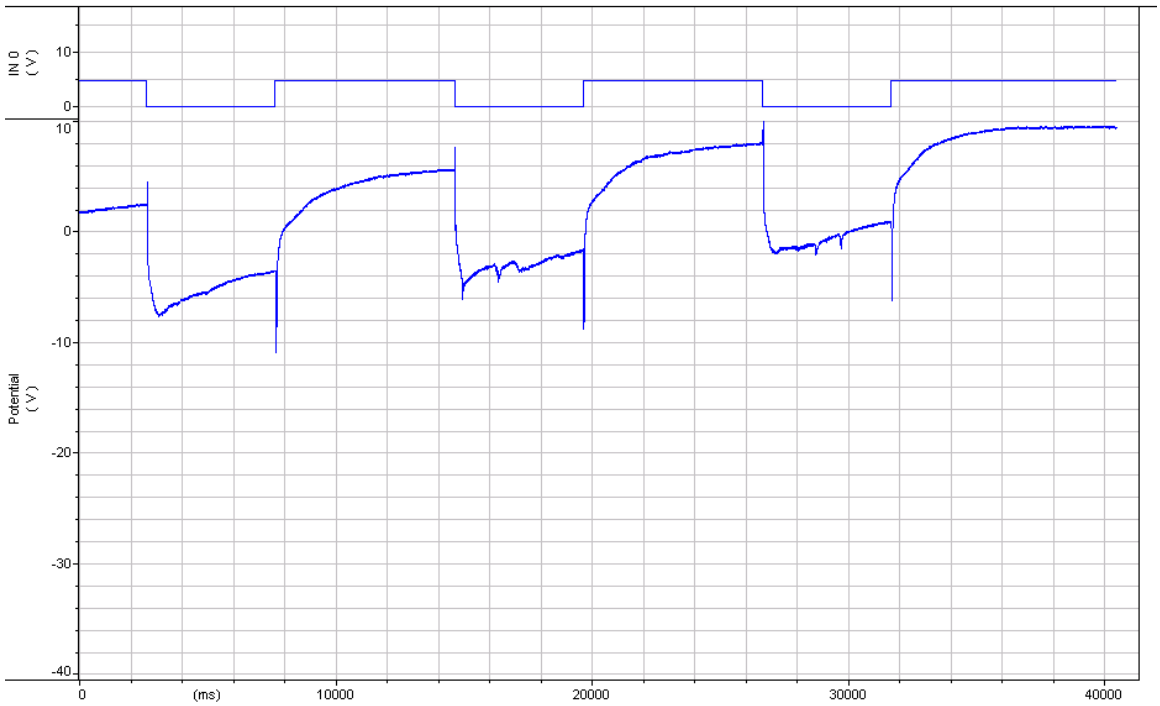
IN 0
(V)
10
0
10
0
-10
-20
-30
-40
Potential
(V)
0
(ms)
10000
20000
30000
40000

Genotype: tubGal80ts; *repo*-Gal4> *Luc* RNAi

Experiment: developmental heat shift, eclosion

Phenotype: with transient

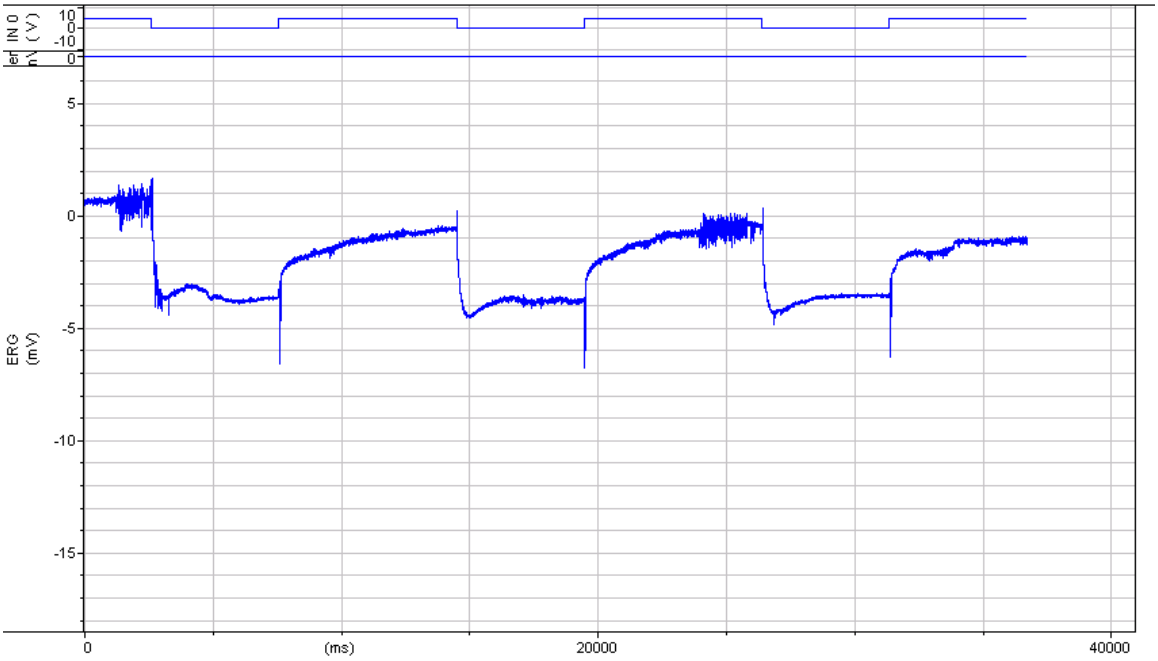

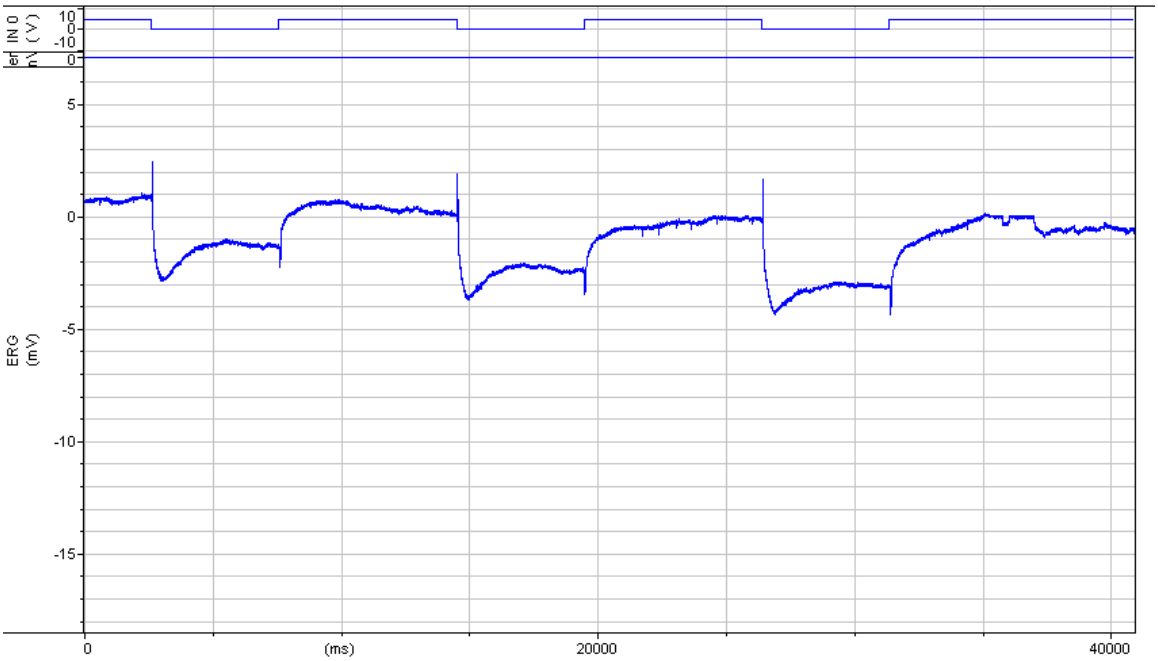

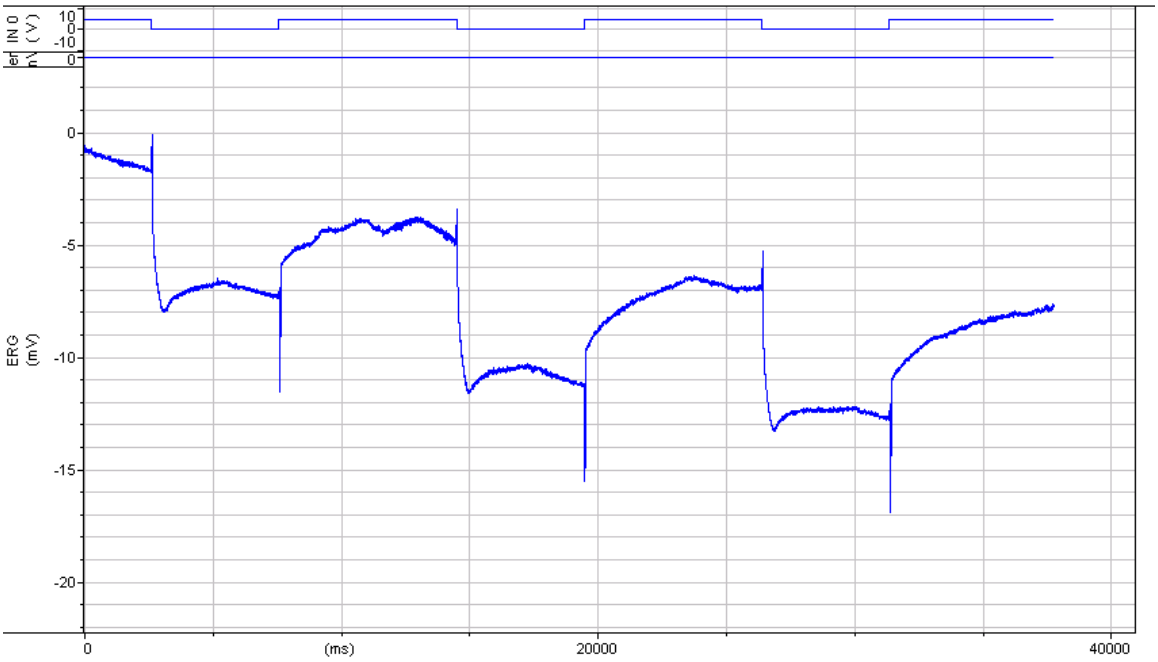
IN 0
(V)
10
0
-10
0
0
-5
-10
-15
-20
ERG
(mV)
0
(ms)
20000
40000

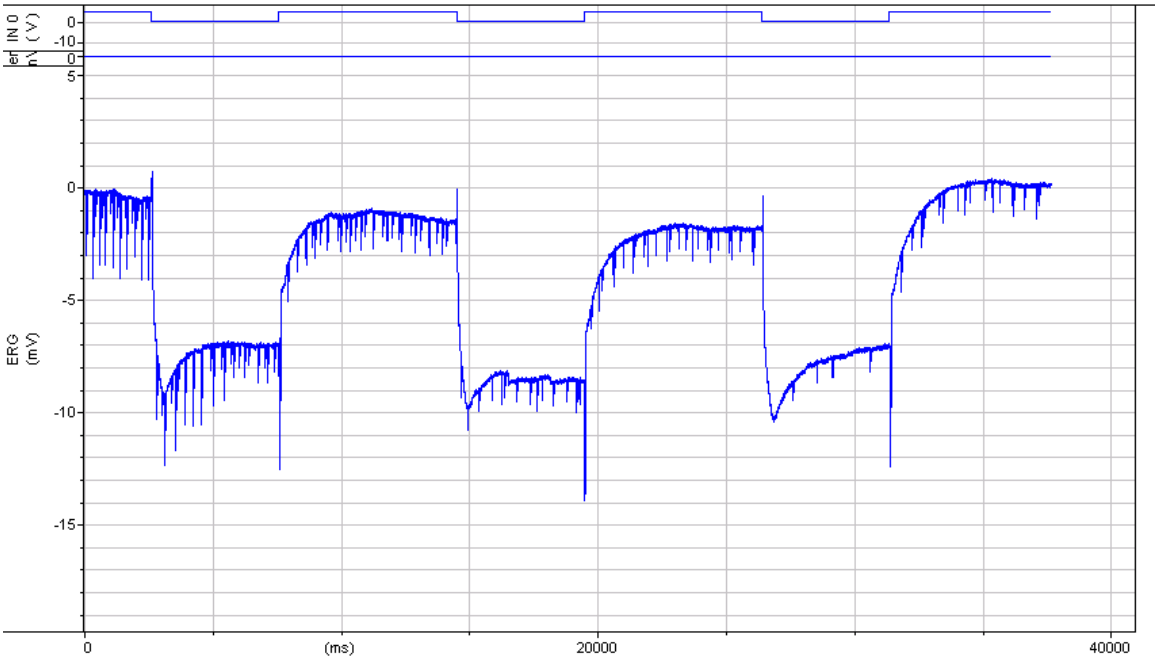
IN 0
(V)
0
-10
0
5
0
-5
-10
-15
ERG
(mV)
0
(ms)
20000
40000

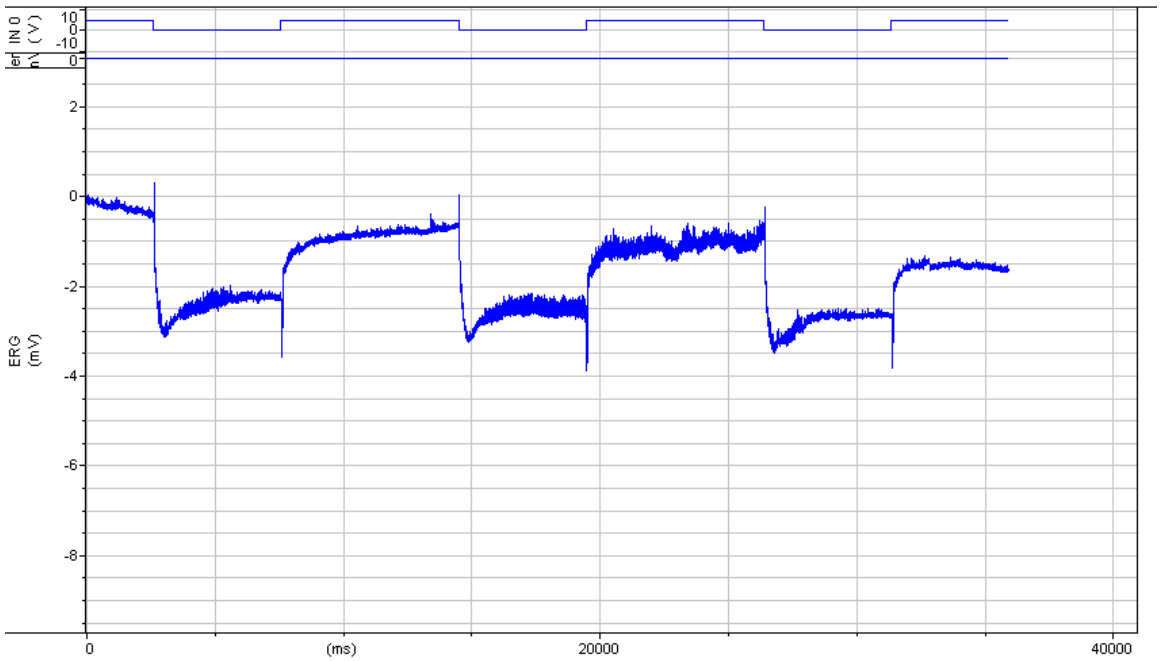
IN 0 (V)
10
0
-10
0
2
0
-2
-4
-6
-8
ERG (mV)
0
(ms)
20000
40000

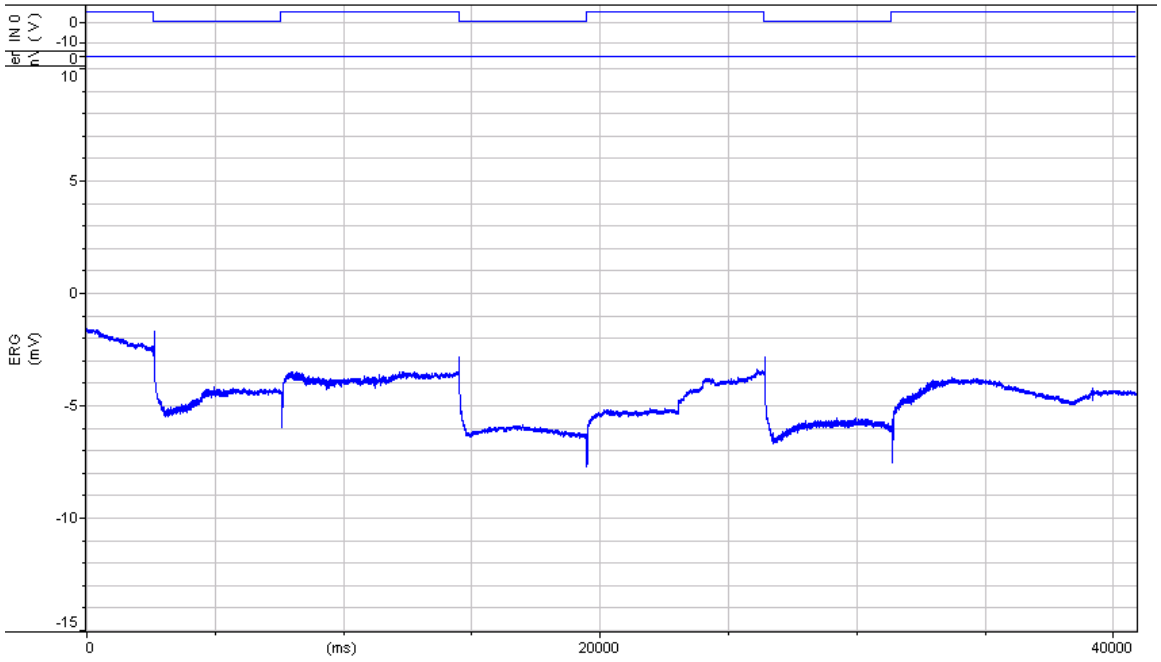
IN 0 (V)
0
-10
0
10
5
0
-5
-10
-15
ERG (mV)
0
(ms)
20000
40000

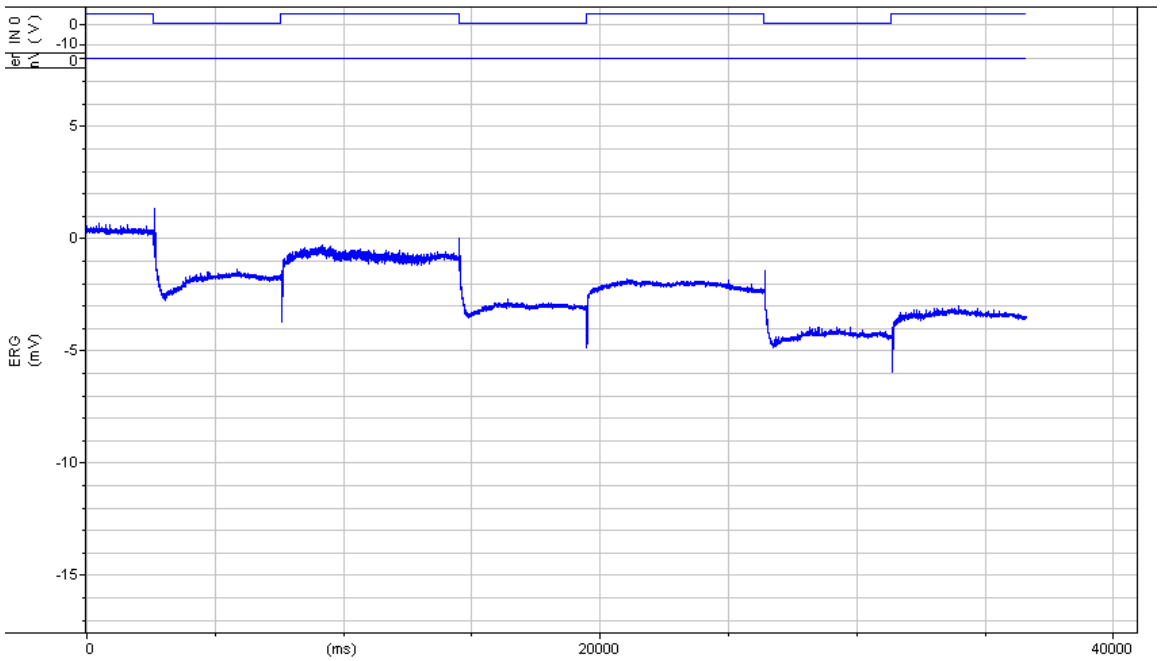
ref IN 0
(V)
0
-10
0
5
0
-5
-10
-15
ERG
(mV)
0
(ms)
20000
40000

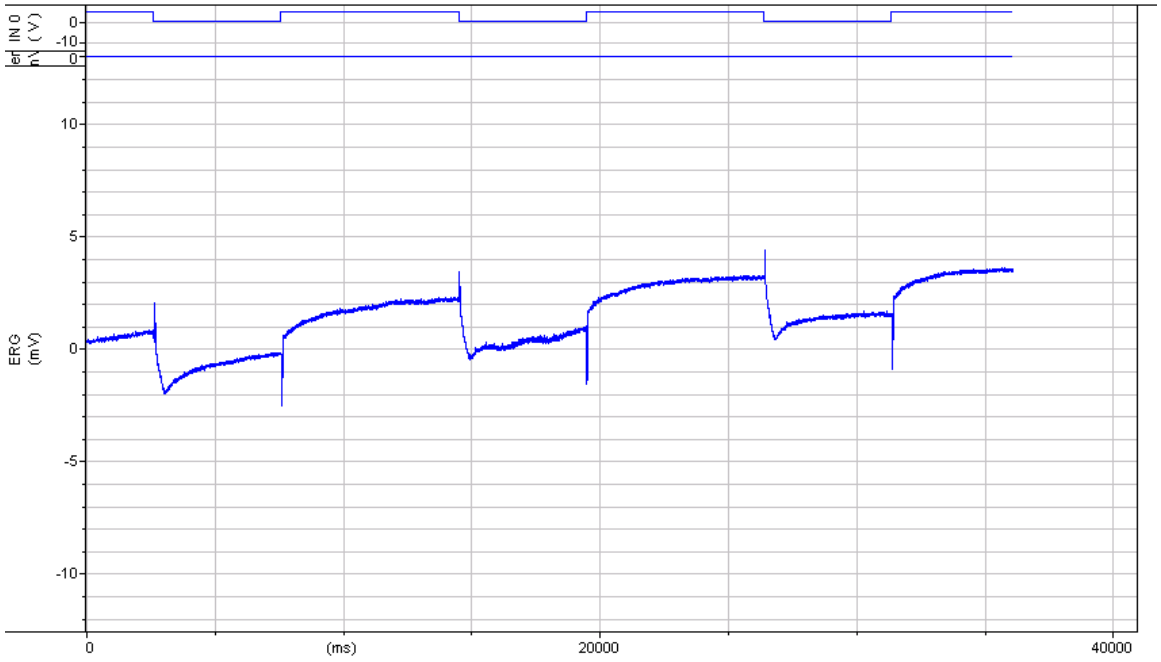
ref IN 0
(V)
0
-10
0
10
5
0
-5
-10
ERG
(mV)
0
(ms)
20000
40000

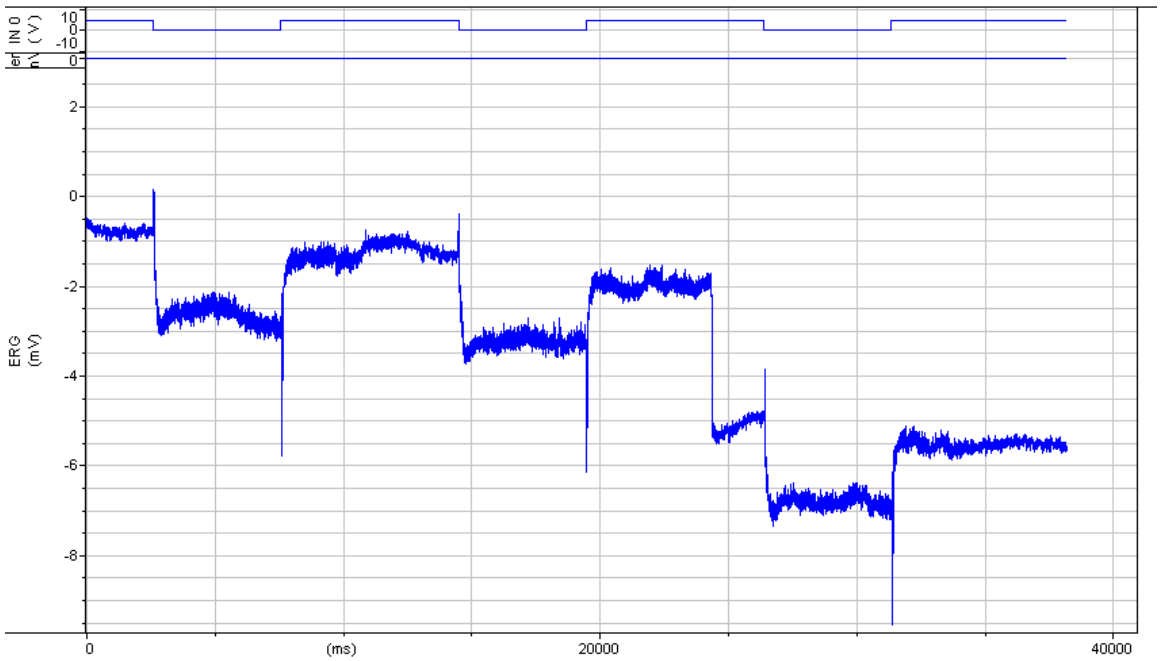
IN 0
(V)
10
0
-10
0
2
0
-2
-4
-6
-8
ERG
(mV)
0
(ms)
20000
40000

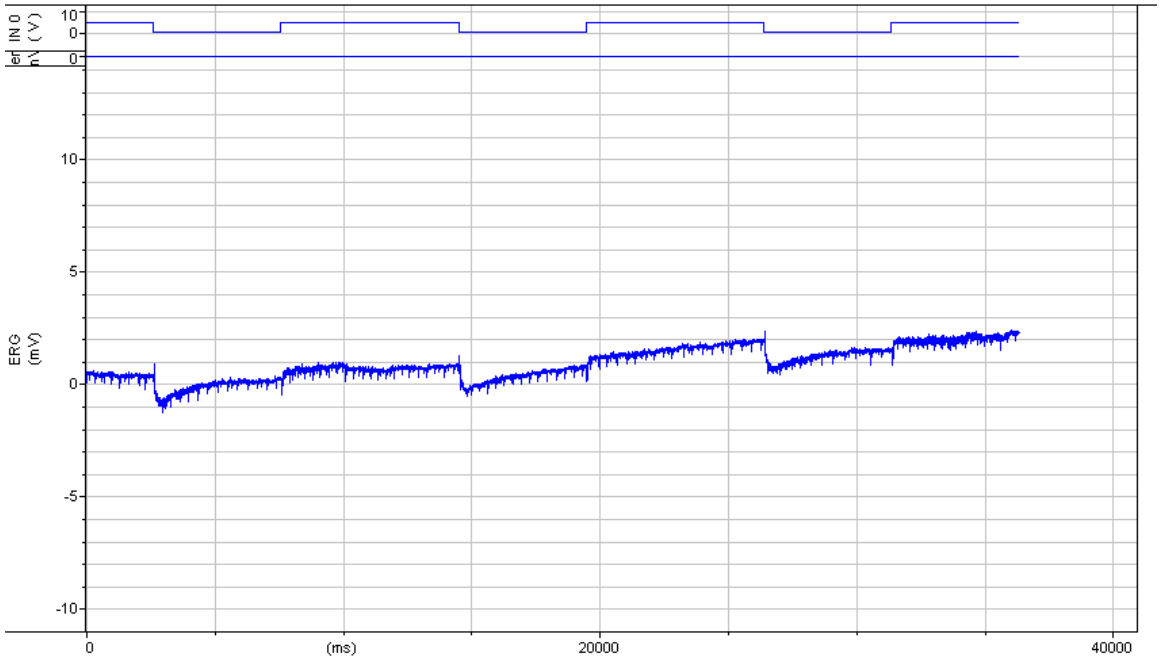
IN 0
(V)
10
0
0
10
5
0
-5
-10
ERG
(mV)
0
(ms)
20000
40000

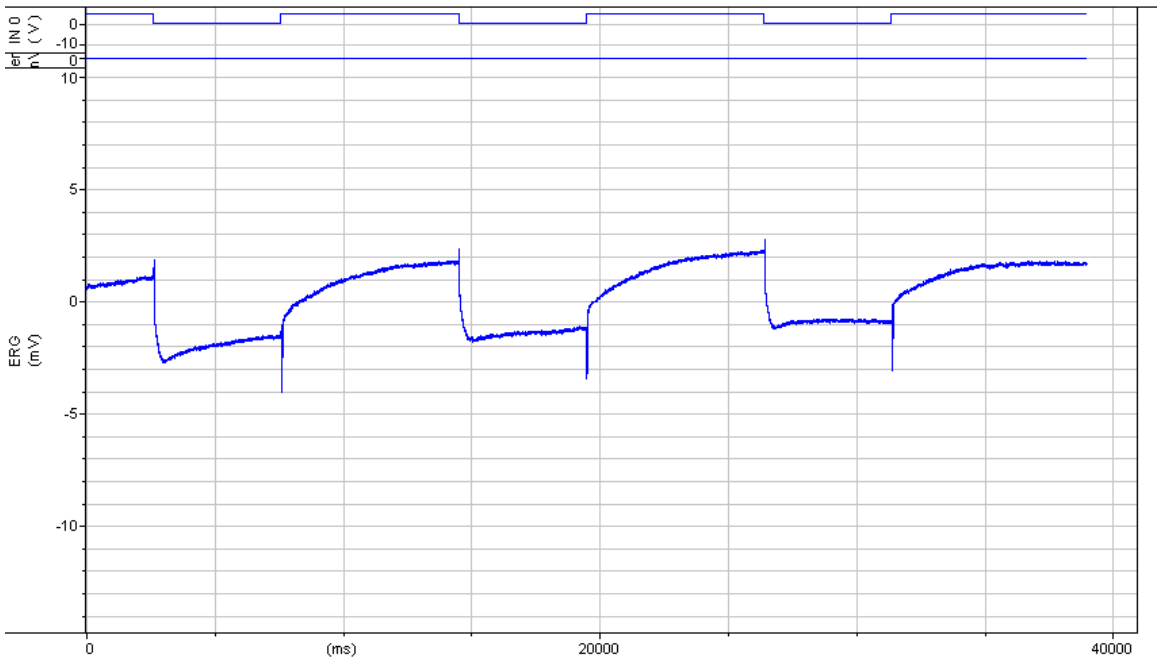
IN 0 (V)
ERG (mV)
(ms)
0
20000
40000

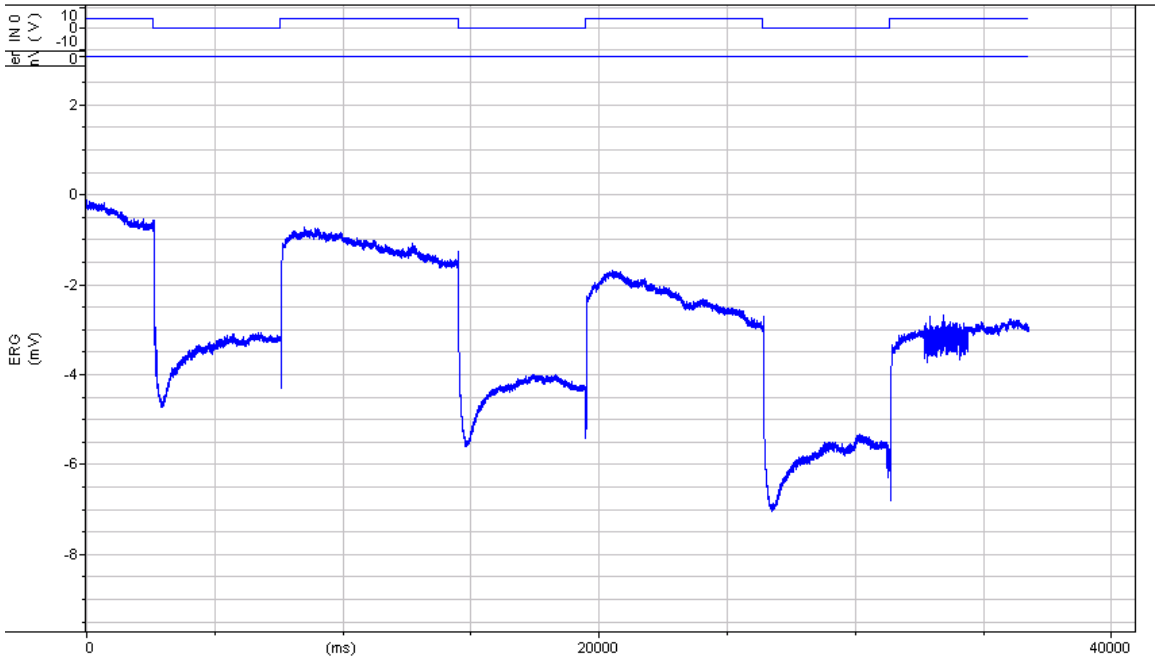
IN 0 (V)
ERG (mV)
(ms)
0
20000
40000

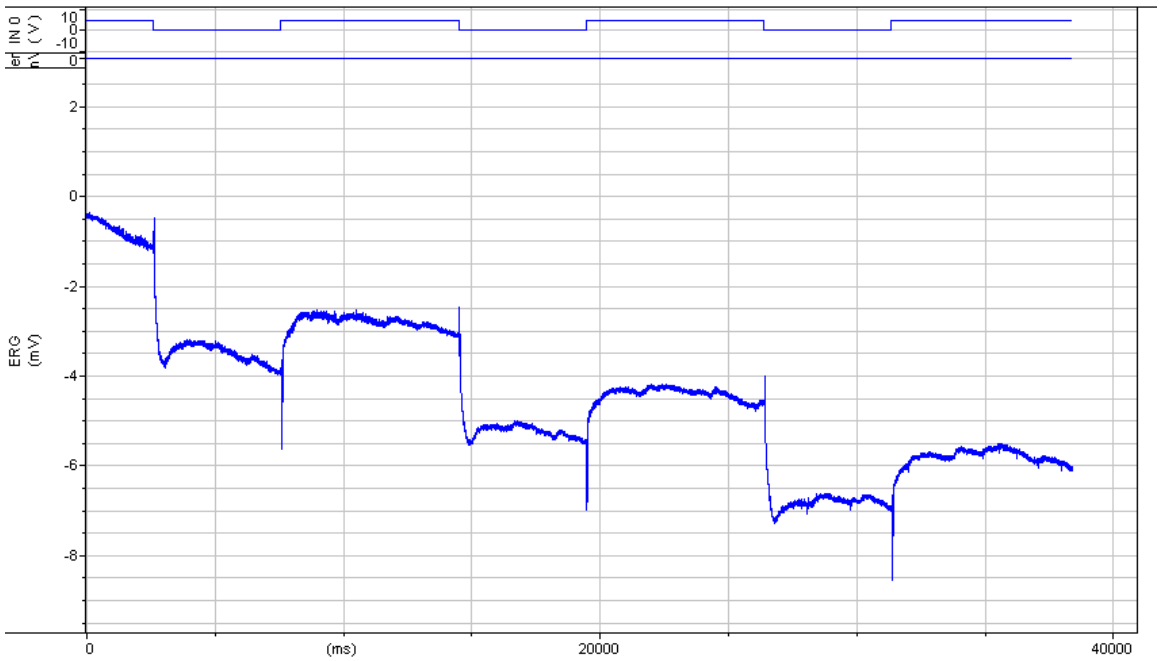
Ref IN 0
mV (V)
10
0
-10
0
2
0
-2
-4
-6
-8
ERG
(mV)
0
(ms)
20000
40000

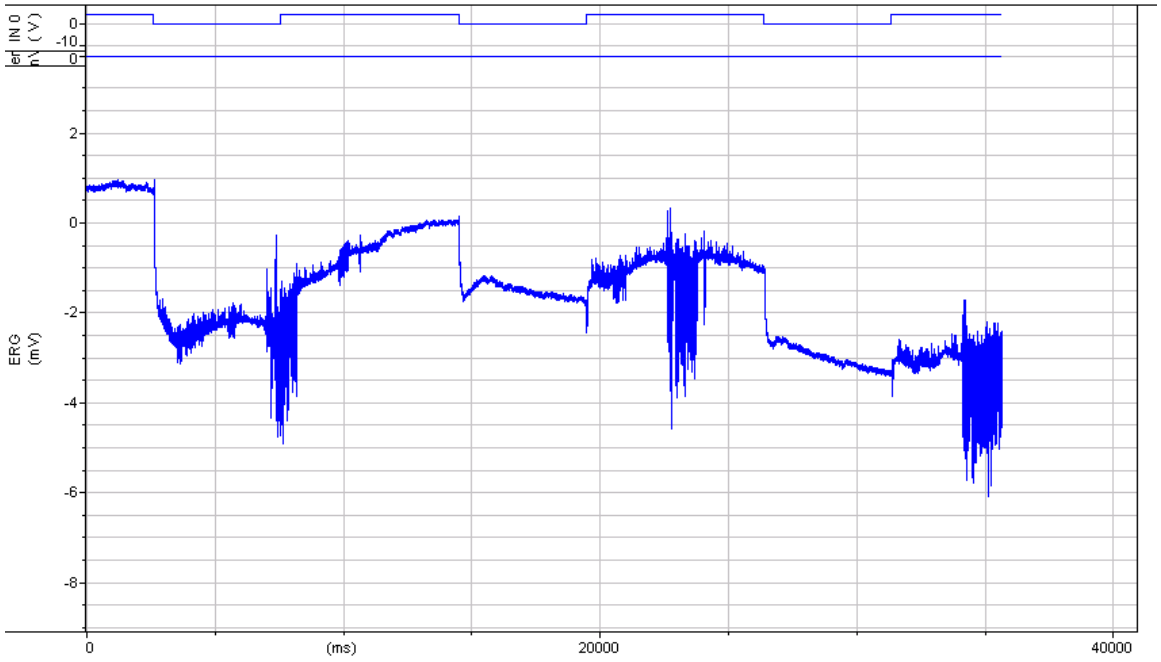
Ref IN 0
mV (V)
0
-10
0
2
0
-2
-4
-6
-8
ERG
(mV)
0
(ms)
20000
40000

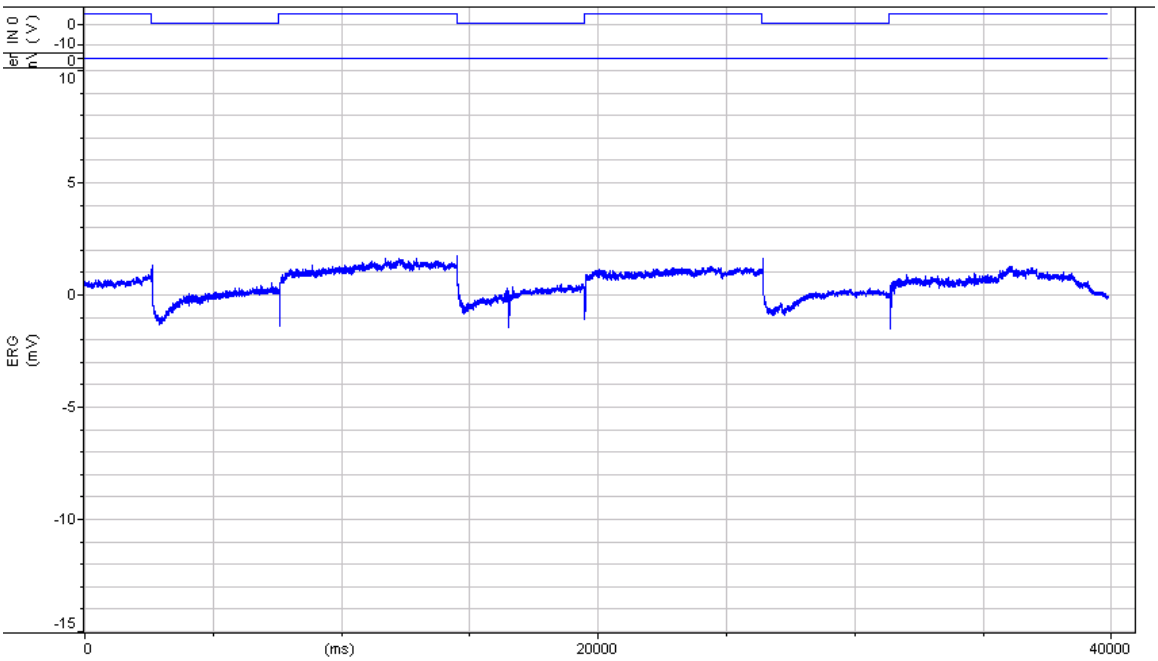
IN 0
(V)
0
-10
0
10
5
0
-5
-10
-15
ERG
(mV)
0
(ms)
20000
40000

Genotype: tubGal80ts; *repo*-Gal4> *Acsl* RNAi

Experiment: developmental heat shift, eclosion

Phenotype: with transient

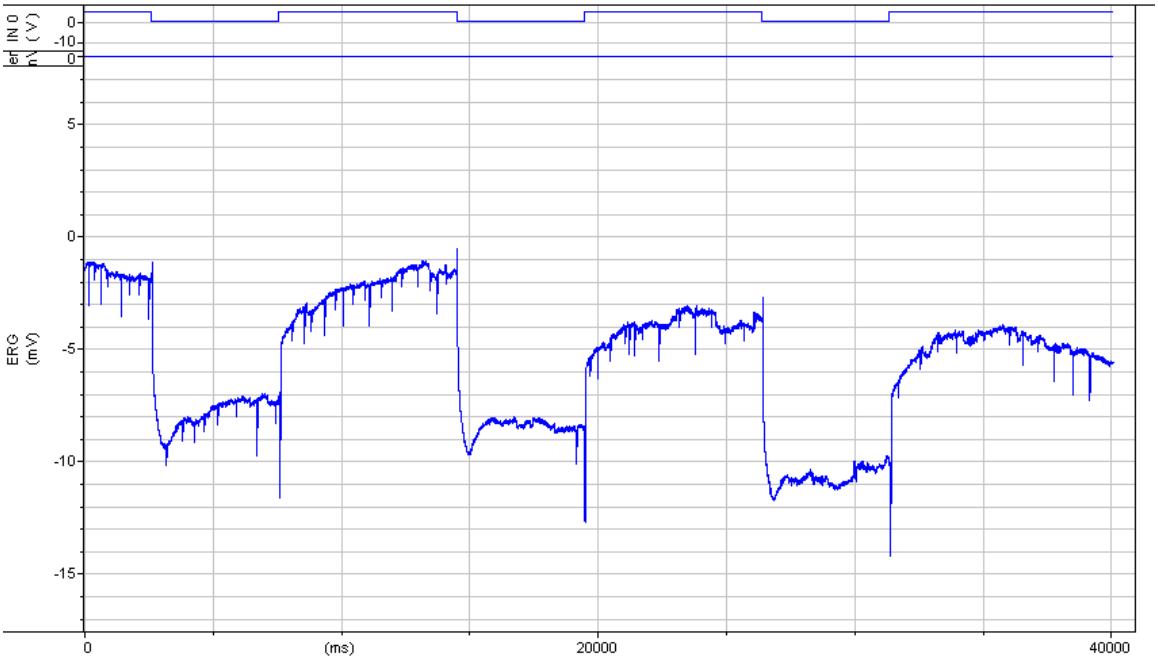

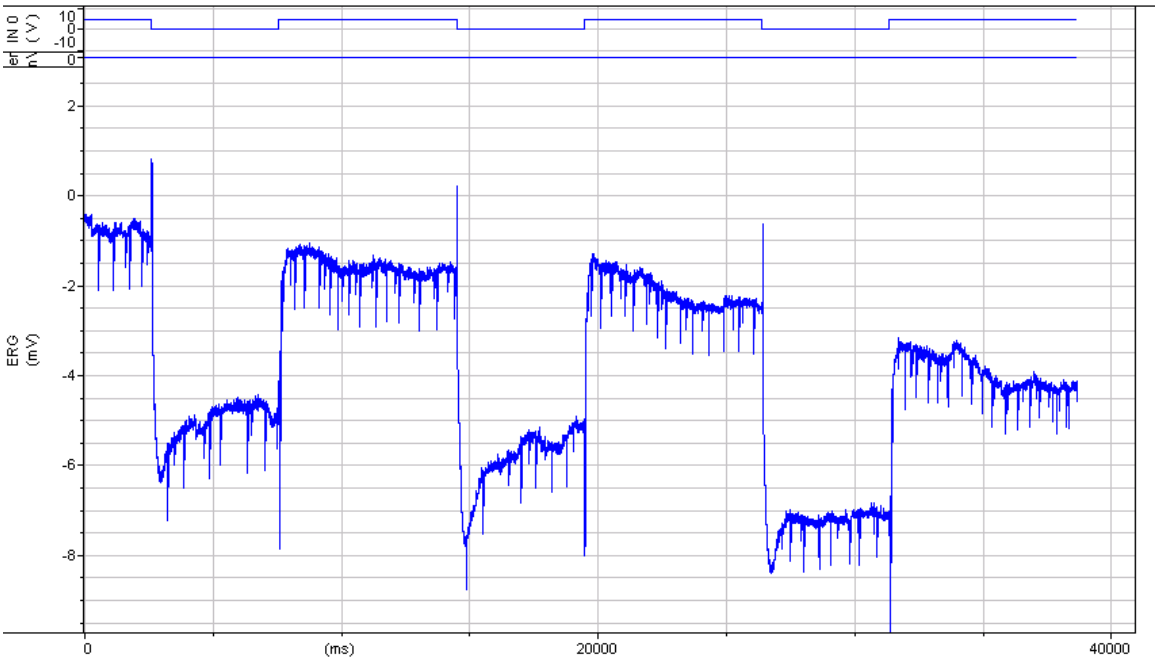

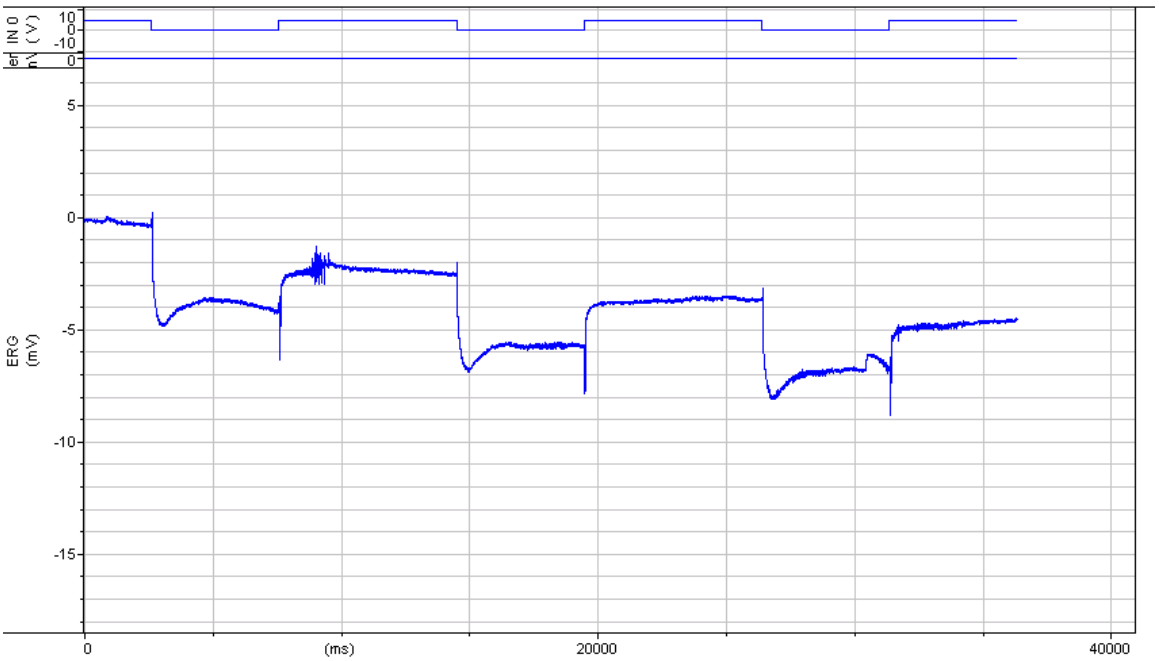
IN 0
(V)
10
0
-10
0
5
0
-5
-10
-15
ERG
(mV)
0
(ms)
20000
40000

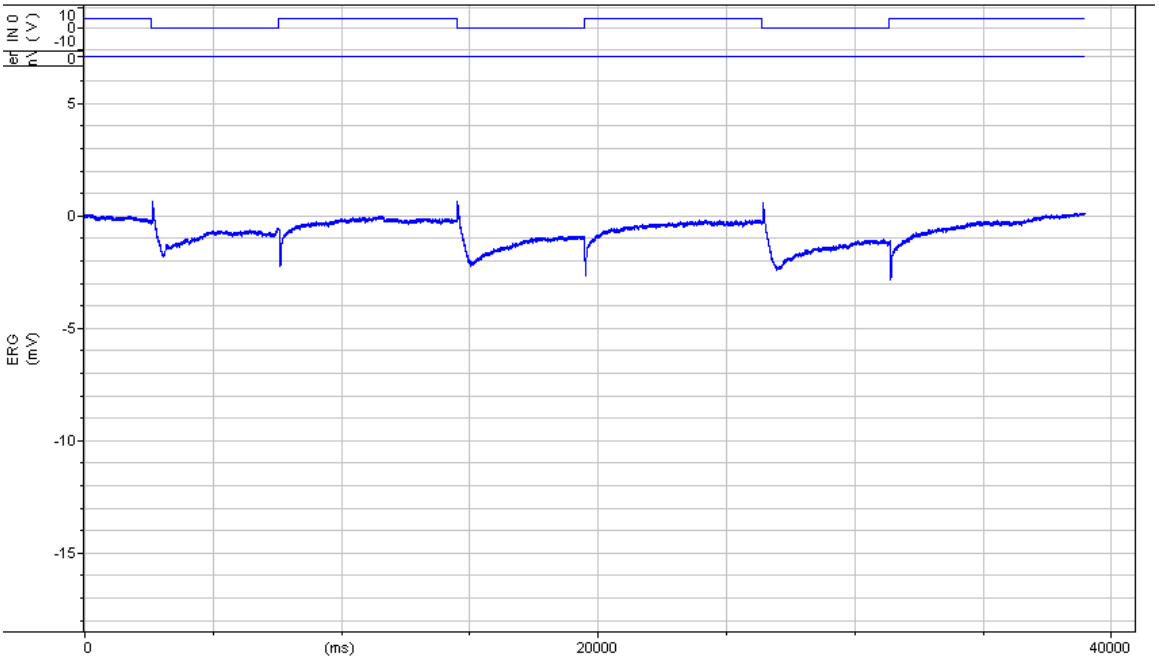
IN 0
(V)
10
0
-10
0
5
0
-5
-10
-15
ERG
(mV)
0
(ms)
20000
40000

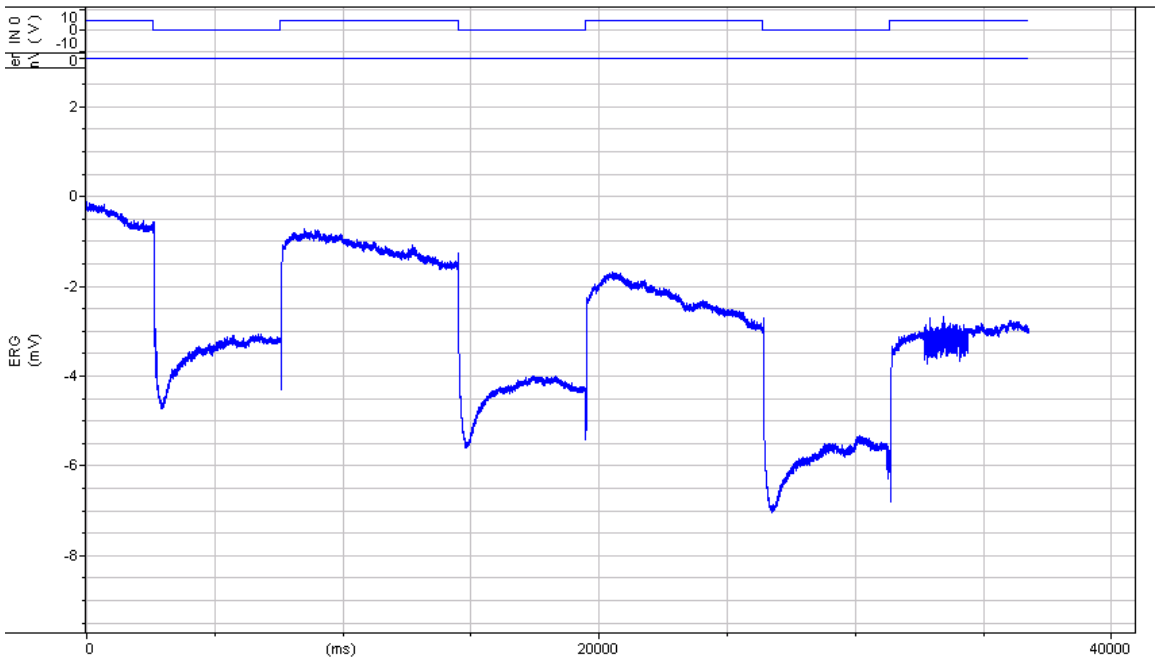
IN 0
(V)
10
0
-10
0
2
0
-2
-4
-6
-8
ERG
(mV)
0
(ms)
20000
40000

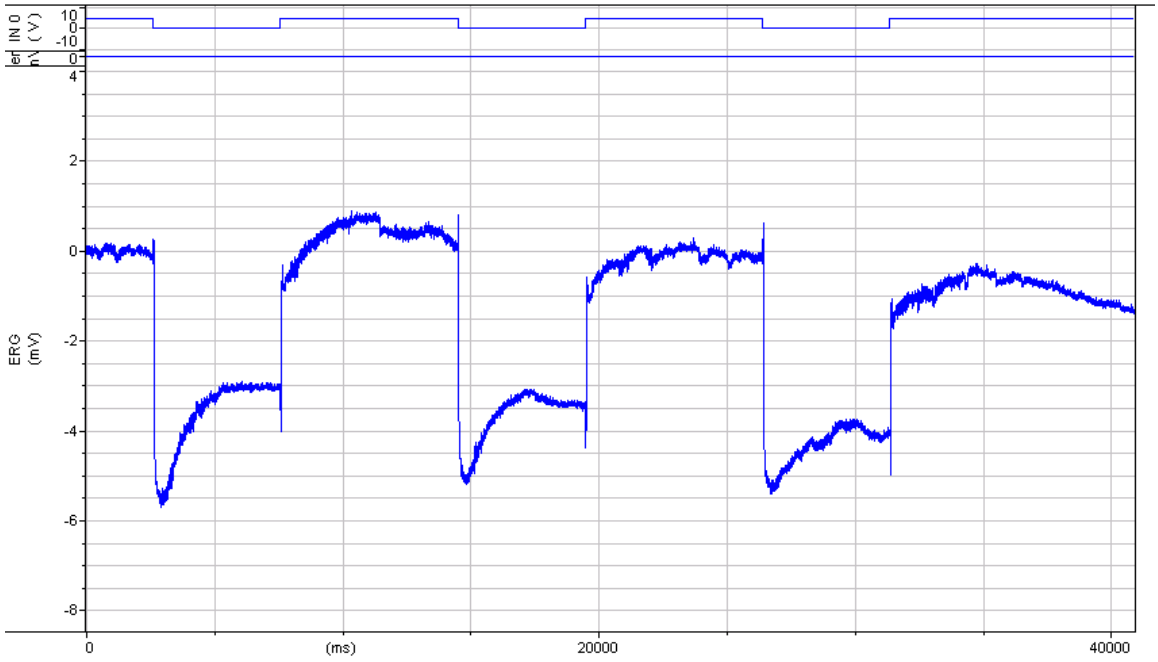
IN 0
(V)
10
0
-10
0
4
2
0
-2
-4
-6
-8
ERG
(mV)
0
(ms)
20000
40000

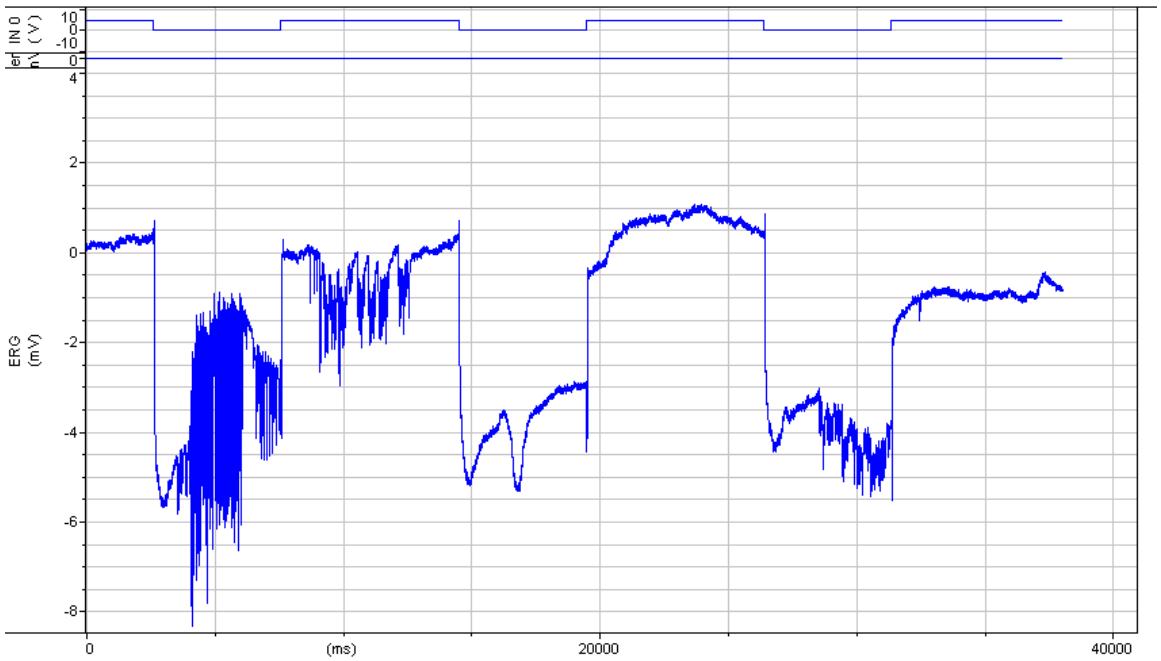
IN 0
(V)
10
0
-10
0
4
2
0
-2
-4
-6
-8
ERG
(mV)
0
(ms)
20000
40000

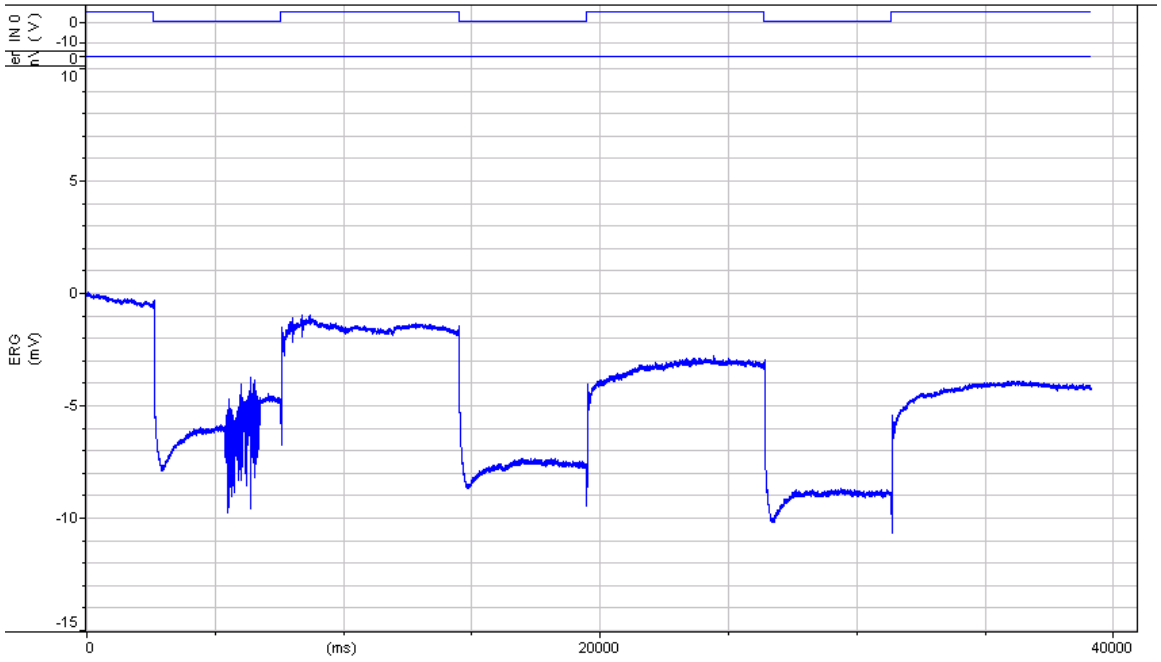
IN 0
(V)
0
-10
0
10
5
0
-5
-10
-15
ERG
(mV)
0
(ms)
20000
40000

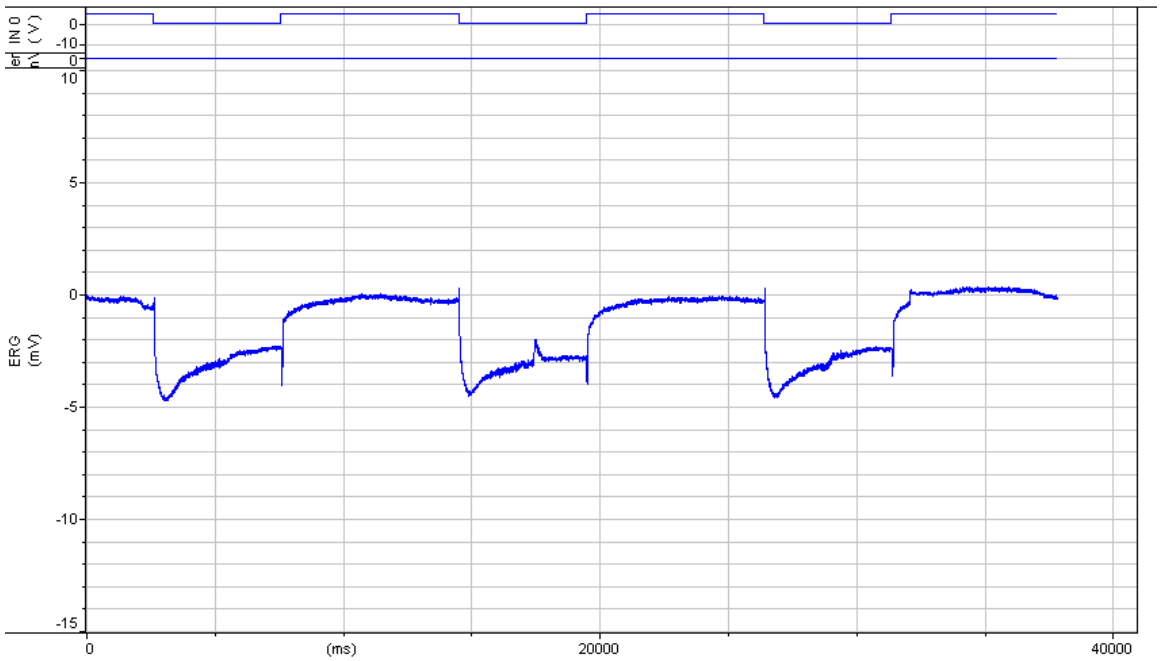
ref IN 0
nV (V)
0
-10
0
10
5
0
-5
-10
-15
ERG
(mV)
0
(ms)
20000
40000

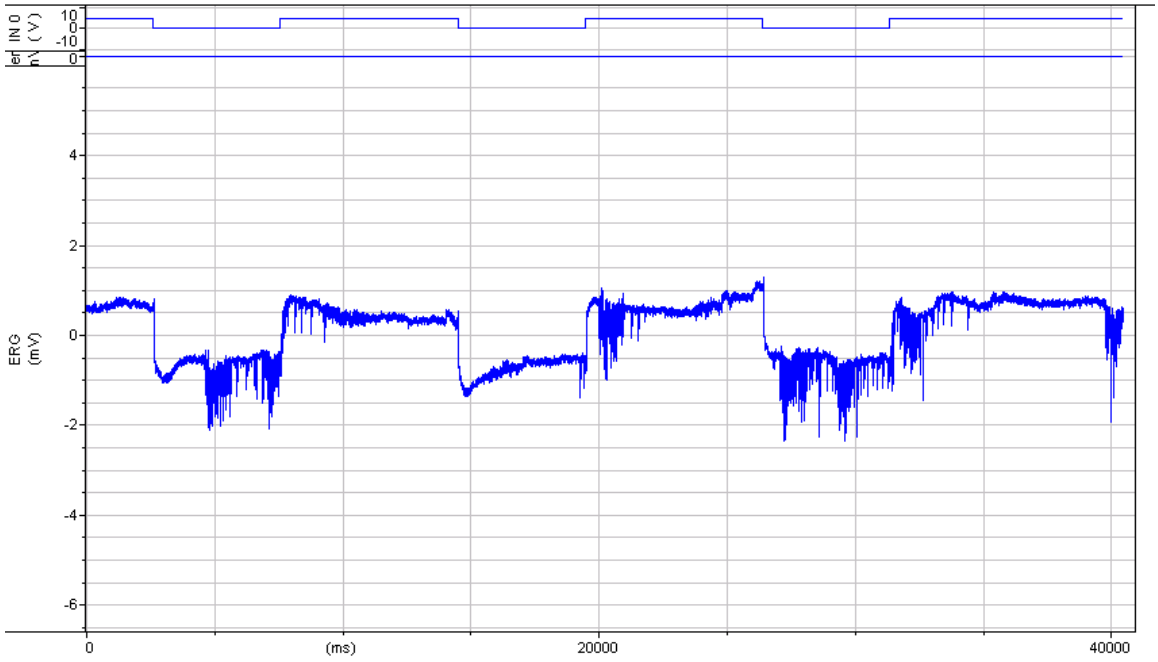
ref IN 0
nV (V)
10
0
-10
0
4
2
0
-2
-4
-6
ERG
(mV)
0
(ms)
20000
40000

Genotype: tubGal80ts; *repo*-Gal4> *Acsl* RNAi

Experiment: developmental heat shift, eclosion

Phenotype: loss of ‘on transient’

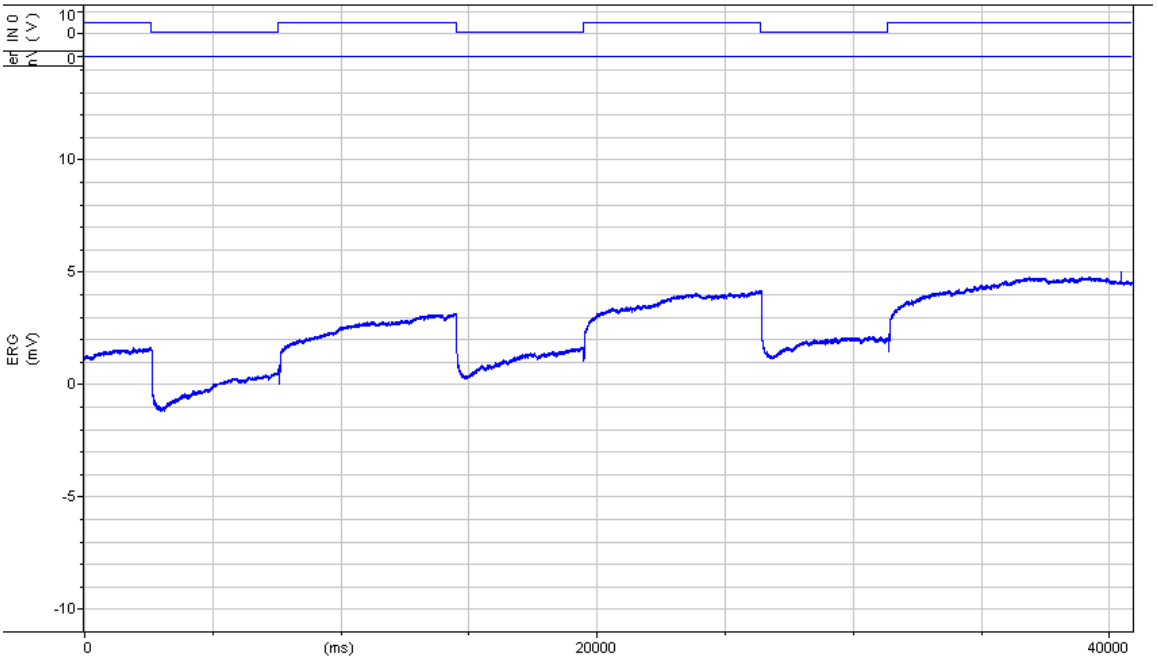

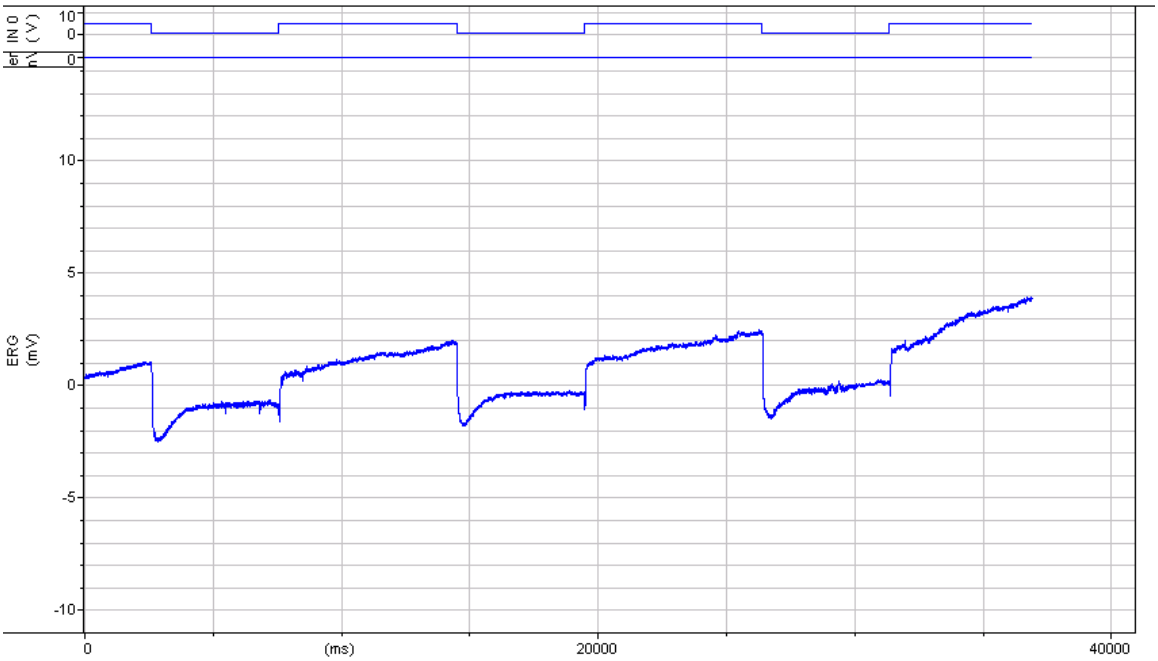

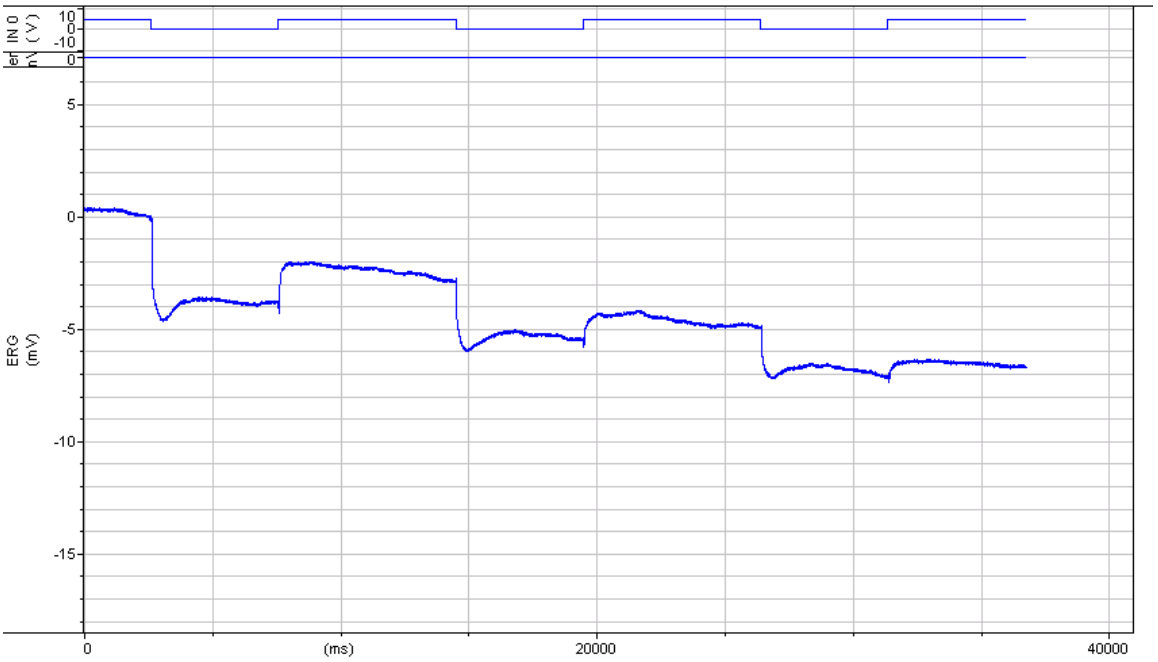
IN 0 (V)
10
0
-10
0
5
0
-5
-10
-15
ERG (mV)
0
(ms)
20000
40000

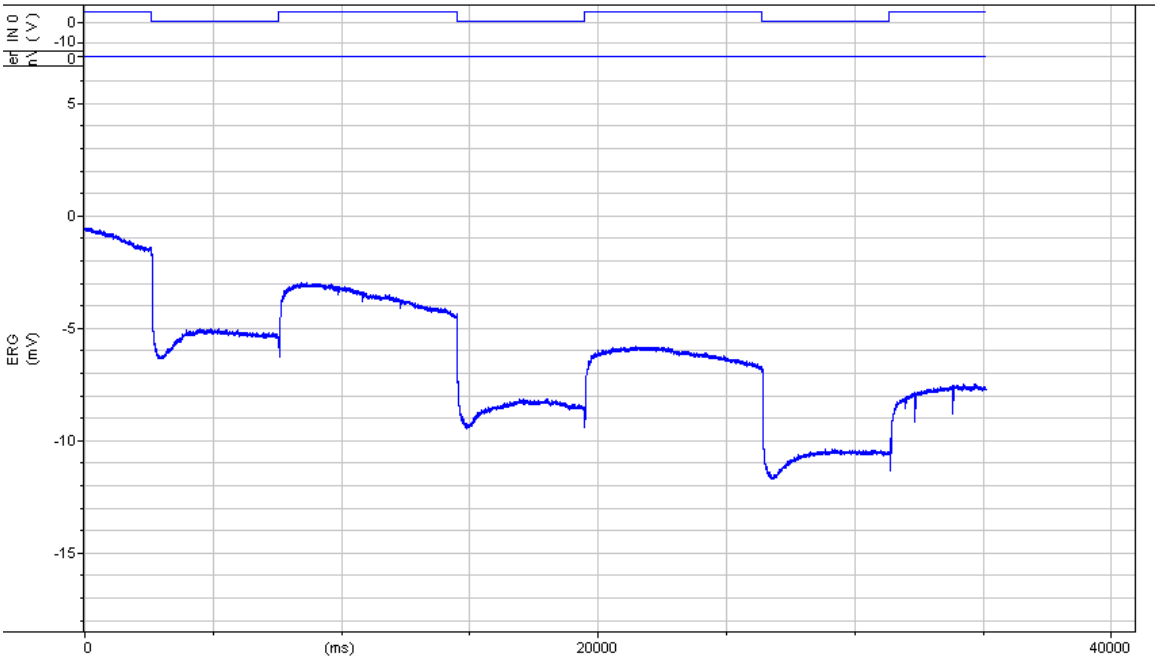
IN 0 (V)
0
-10
0
5
0
-5
-10
-15
ERG (mV)
0
(ms)
20000
40000

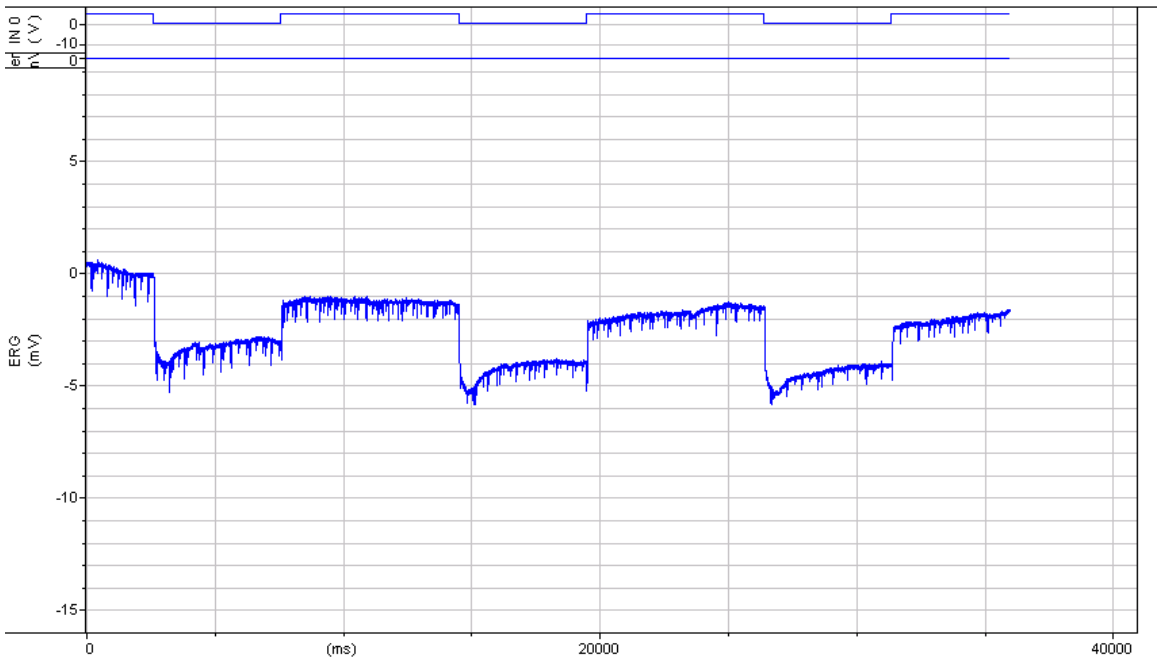
Ref IN 0
(V)
0
-10
0
5
0
-5
-10
-15
ERG
(mV)
0
(ms)
20000
40000

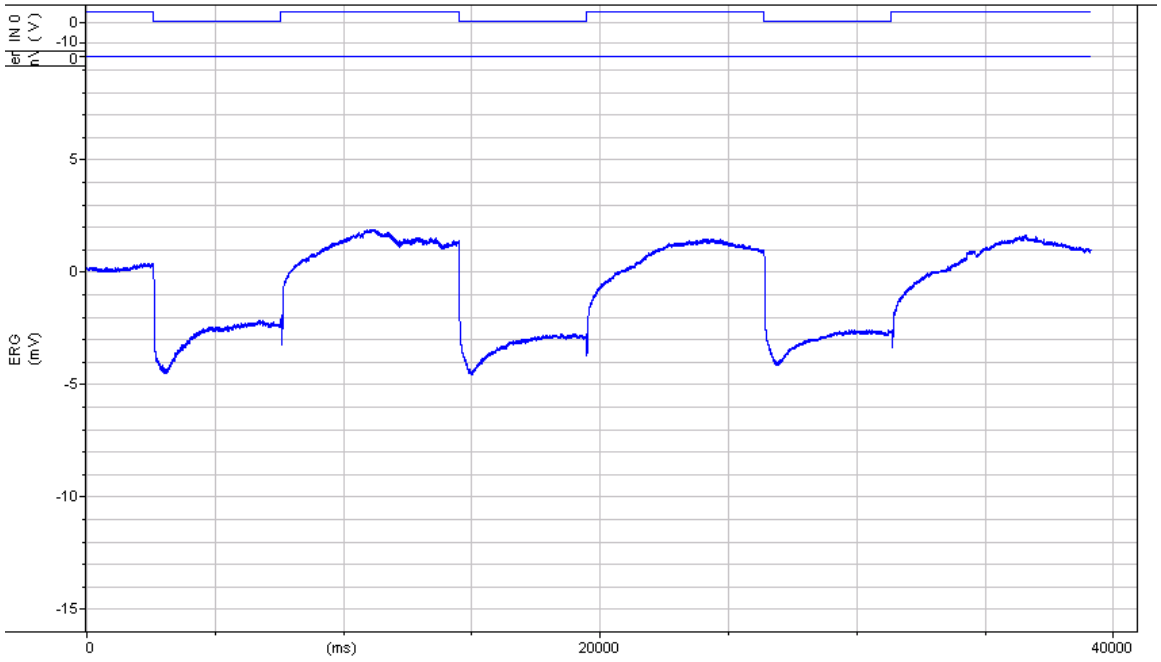
Ref IN 0
(V)
0
-10
0
5
0
-5
-10
-15
ERG
(mV)
0
(ms)
20000
40000

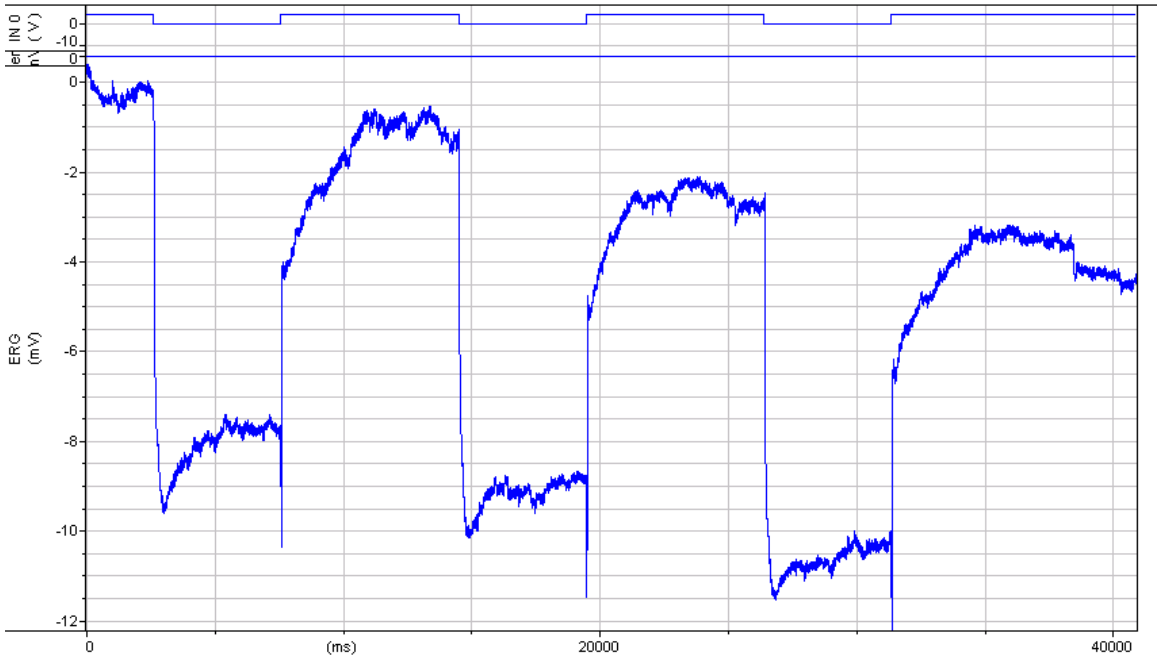
Ref IN 0
mV (V)
0
-10
0
0
-2
-4
-6
-8
-10
-12
ERG (mV)
0
(ms)
20000
40000

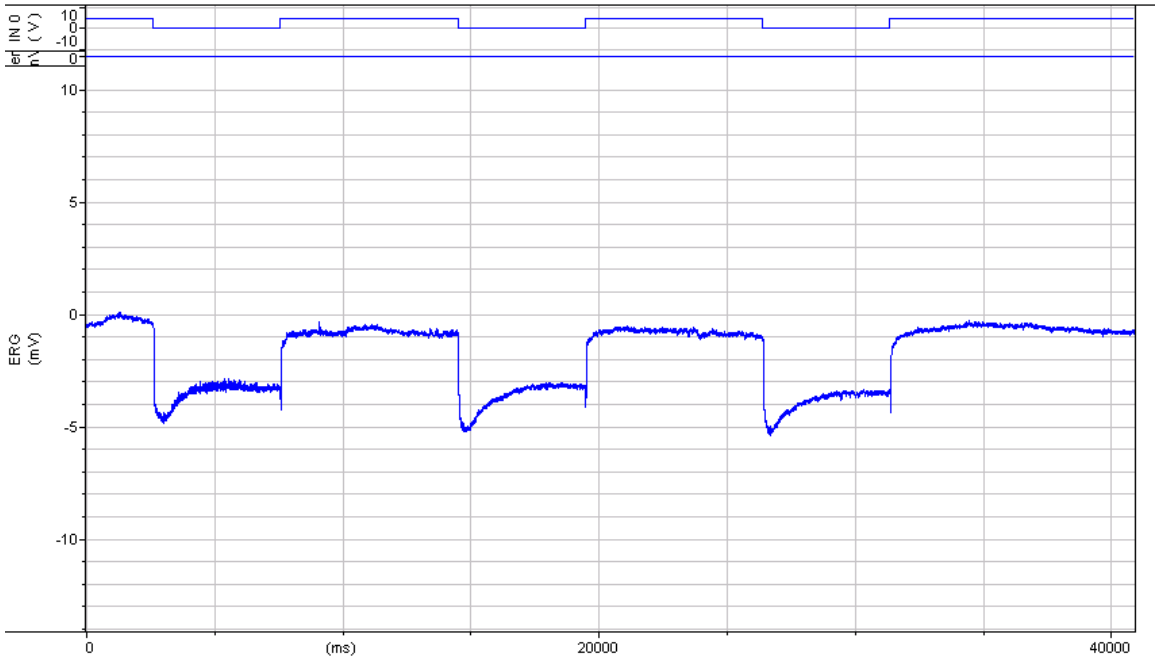
Ref IN 0
mV (V)
10
0
-10
0
10
5
0
-5
-10
ERG (mV)
0
(ms)
20000
40000

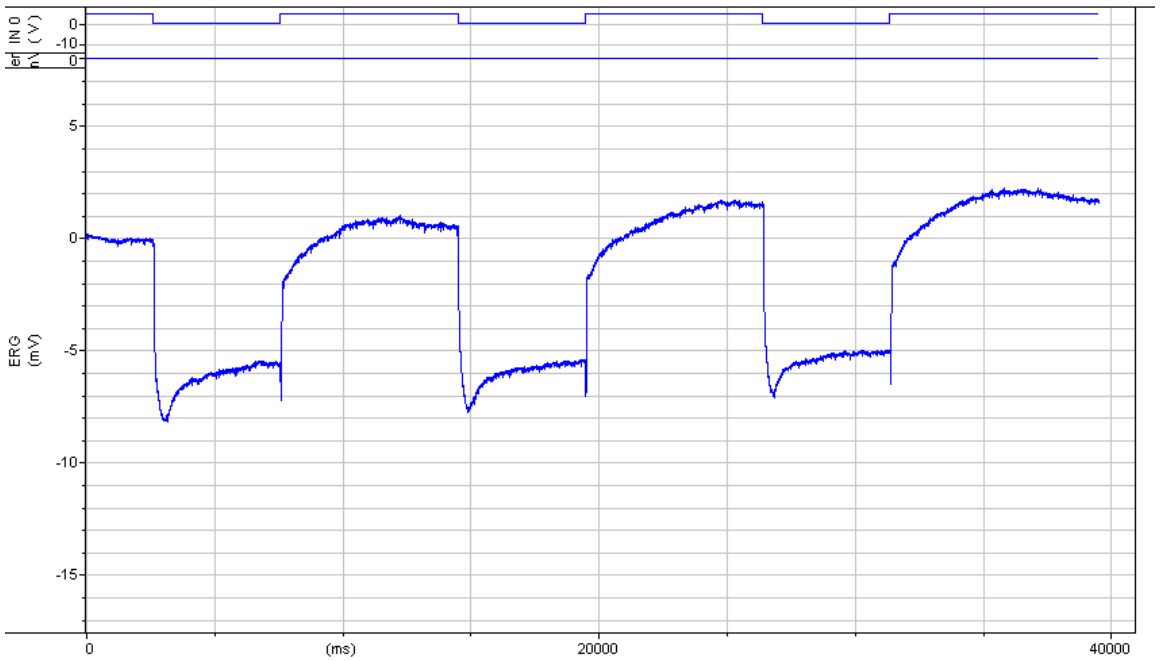
ef IN 0
n\ (V)
0
-10
0
5
0
-5
-10
-15
ERG
(mV)
0
(ms)
20000
40000

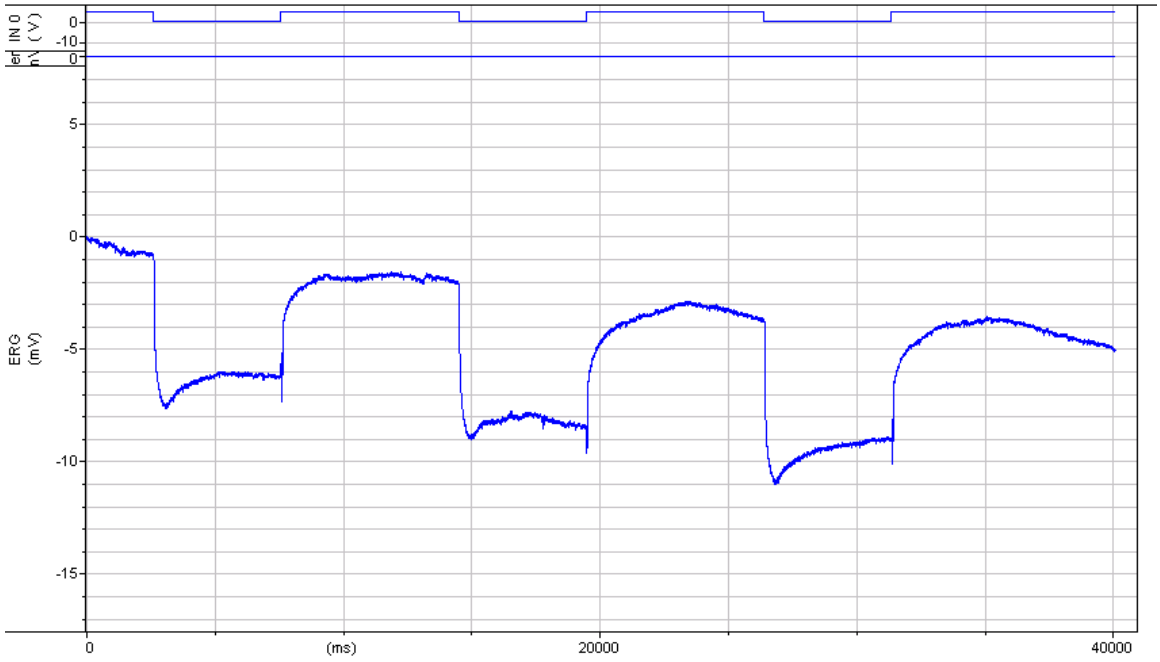
ef IN 0
n\ (V)
0
-10
0
5
0
-5
-10
-15
ERG
(mV)
0
(ms)
20000
40000

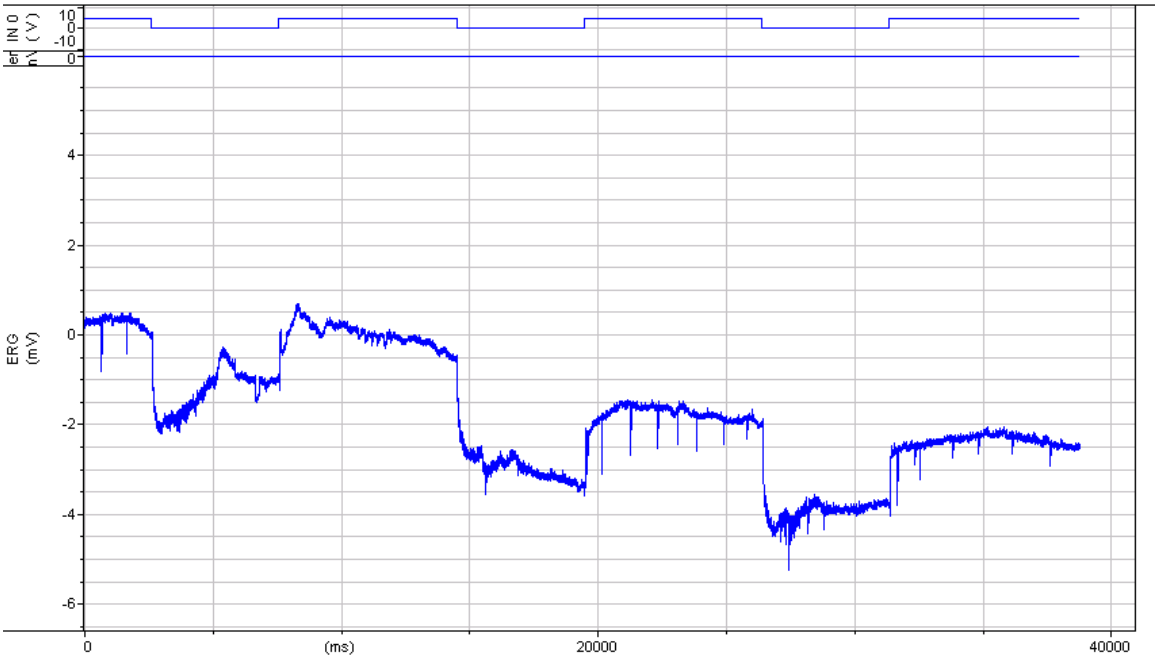
IN 0 (V)
10
0
-10
ref
0
4
2
0
-2
-4
-6
ERG (mV)
0
(ms)
20000
40000

Genotype: tubGal80ts; *repo*-Gal4> *Luc* RNAi

Experiment: developmental heat shift, 10 day

Phenotype: with transient

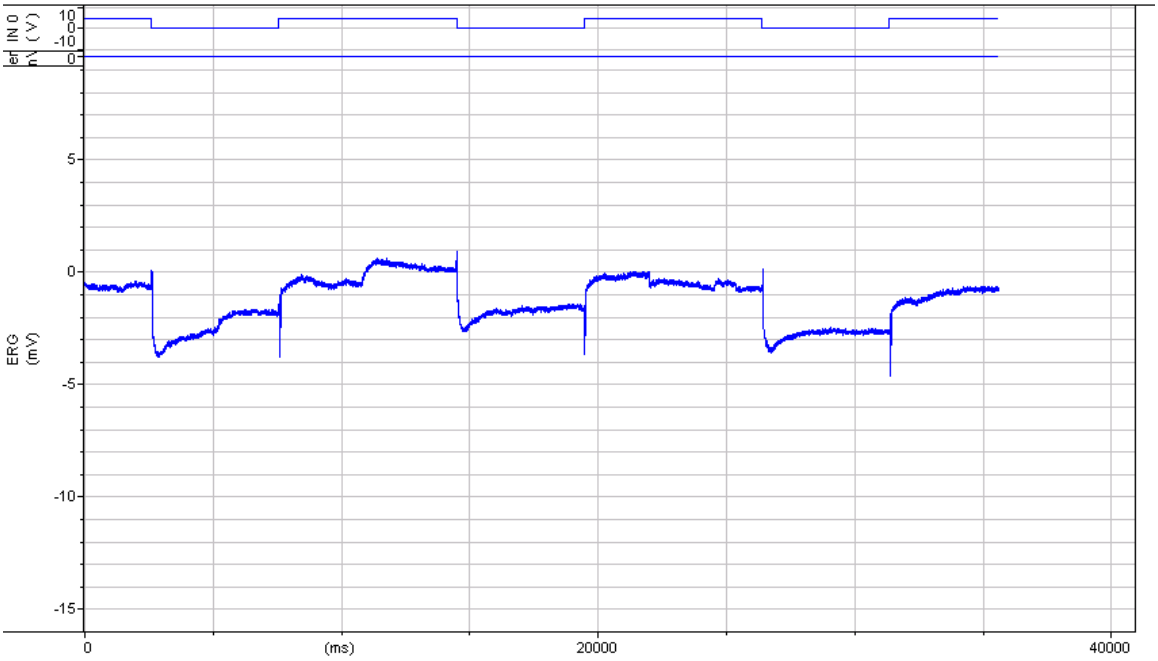

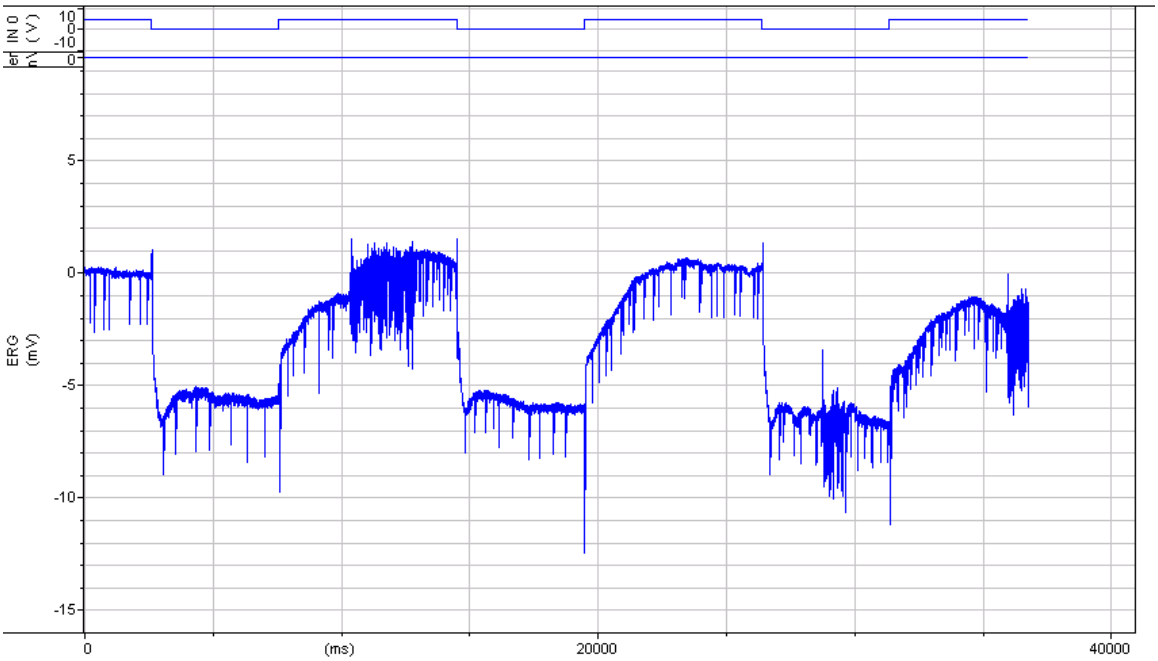

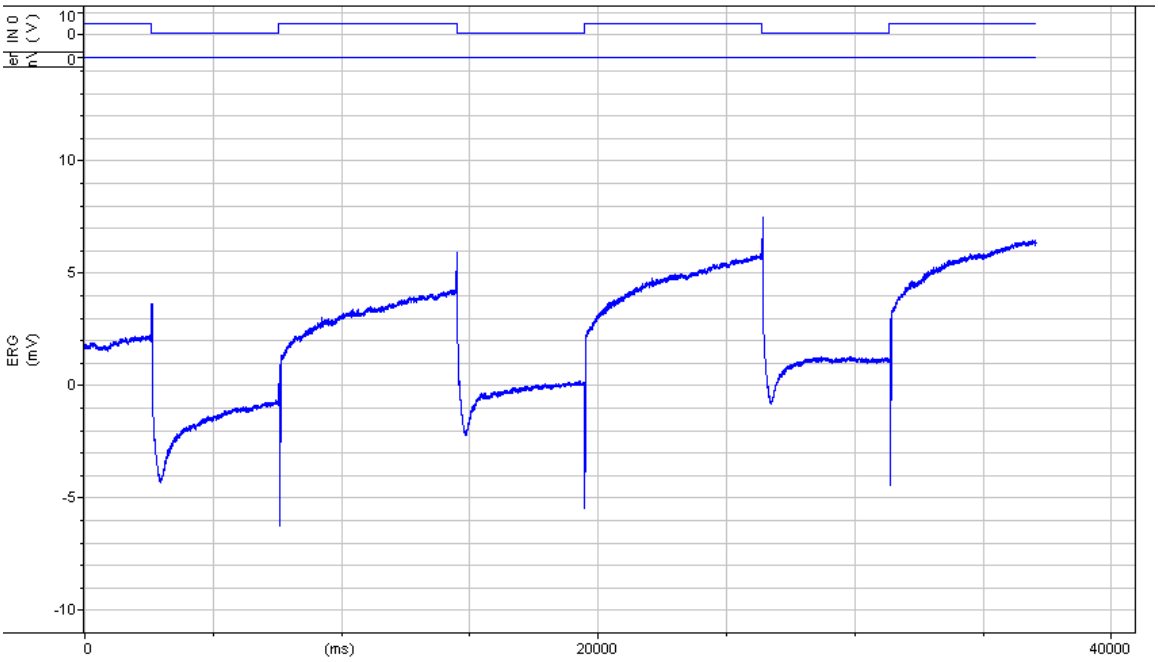
IN 0 (V)
10
0
0
10
5
0
-5
-10
ERG (mV)
0
(ms)
20000
40000

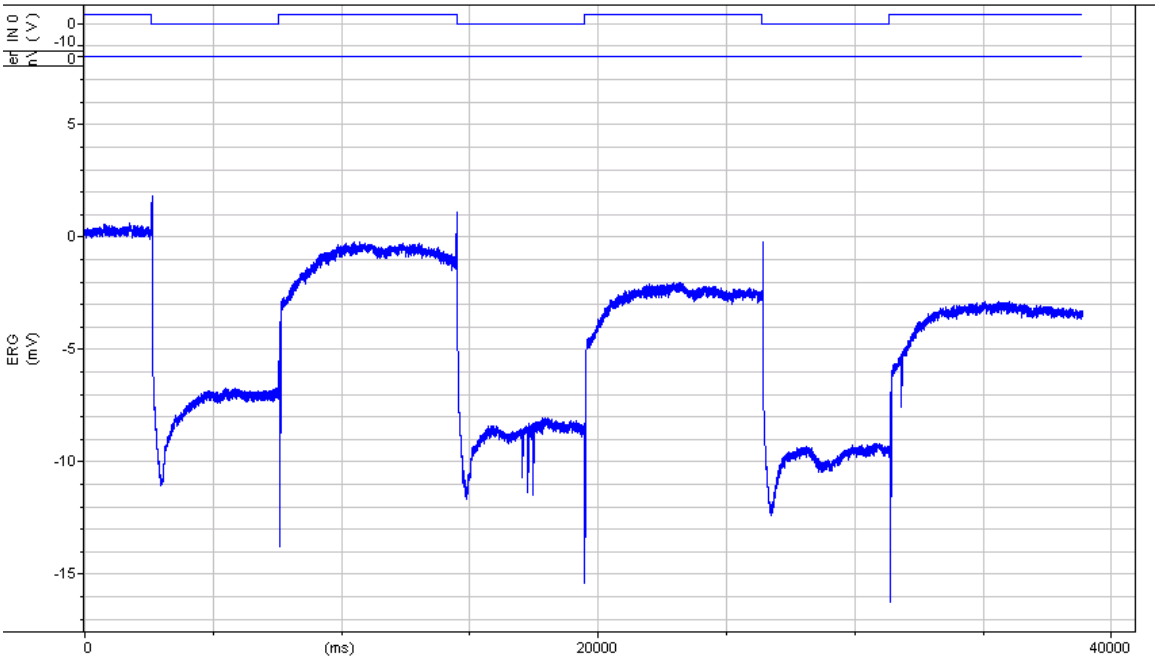
IN 0 (V)
0
-10
0
5
0
-5
-10
-15
ERG (mV)
0
(ms)
20000
40000

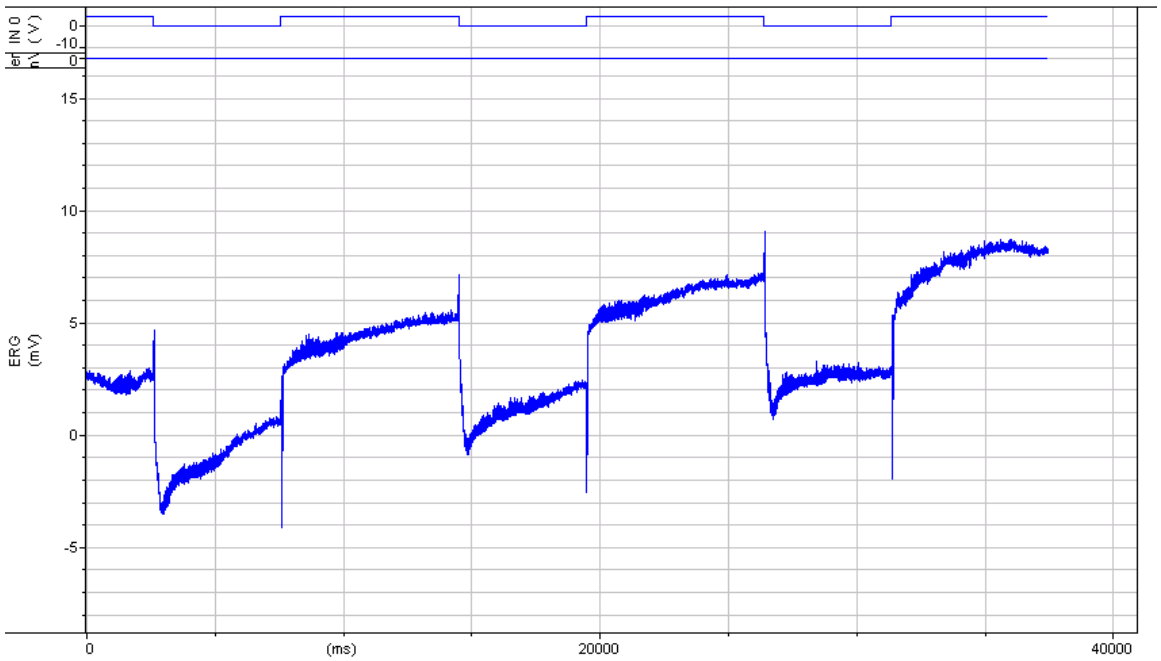
IN 0
(V)
0
-10
0
15
10
5
0
-5
ERG
(mV)
0
(ms)
20000
40000

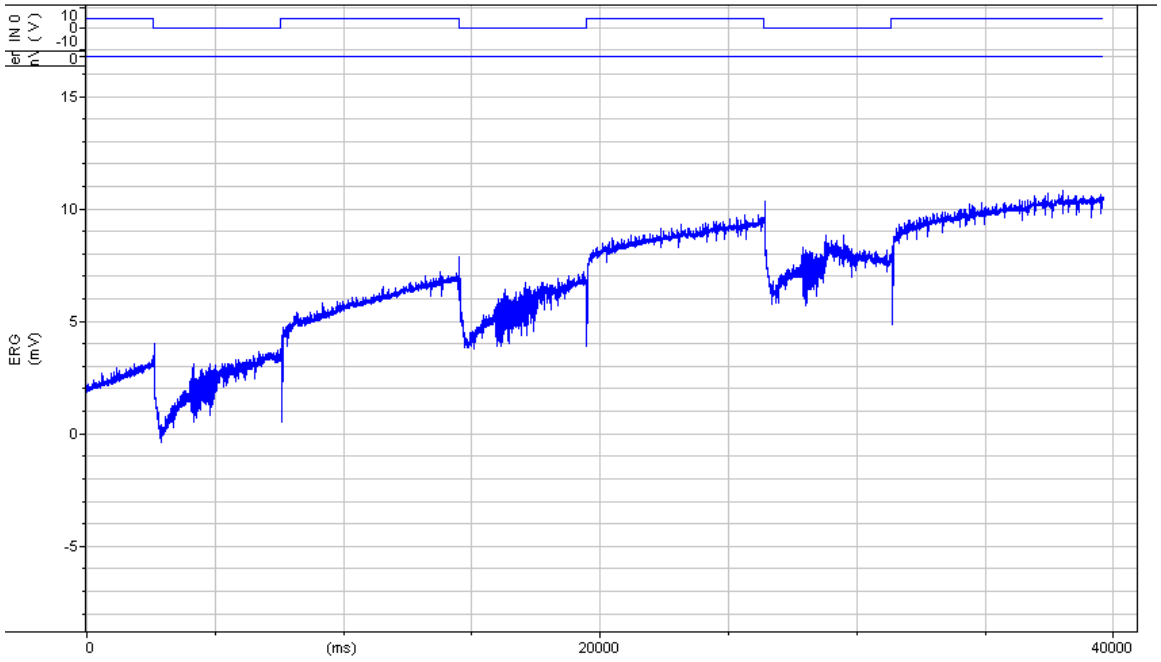
IN 0
(V)
10
0
-10
0
15
10
5
0
-5
ERG
(mV)
0
(ms)
20000
40000

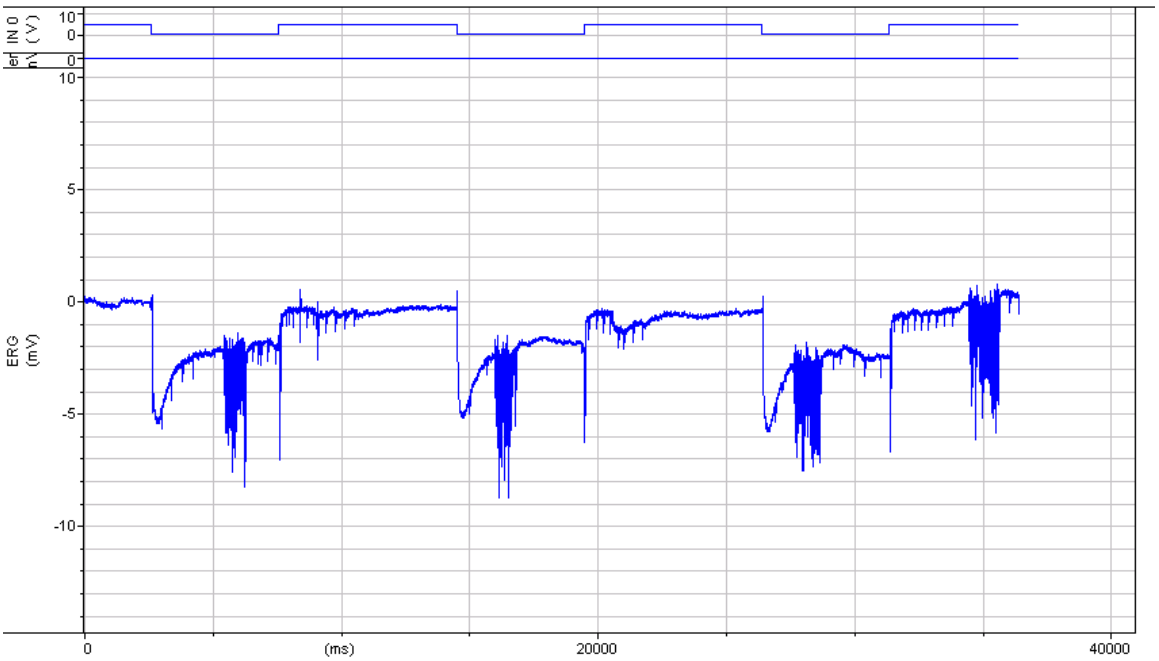
IN 0 (V)
10
0
0
10
5
0
-5
-10
ERG (mV)
0
(ms)
20000
40000

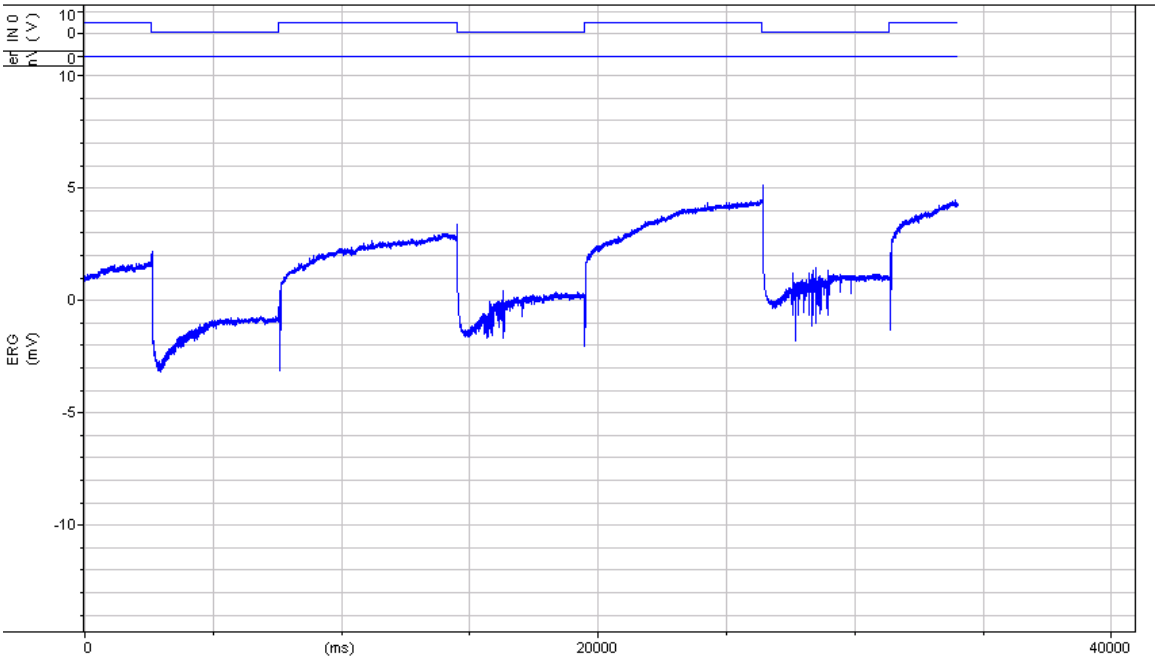
IN 0 (V)
10
0
0
10
5
0
-5
-10
ERG (mV)
0
(ms)
20000
40000

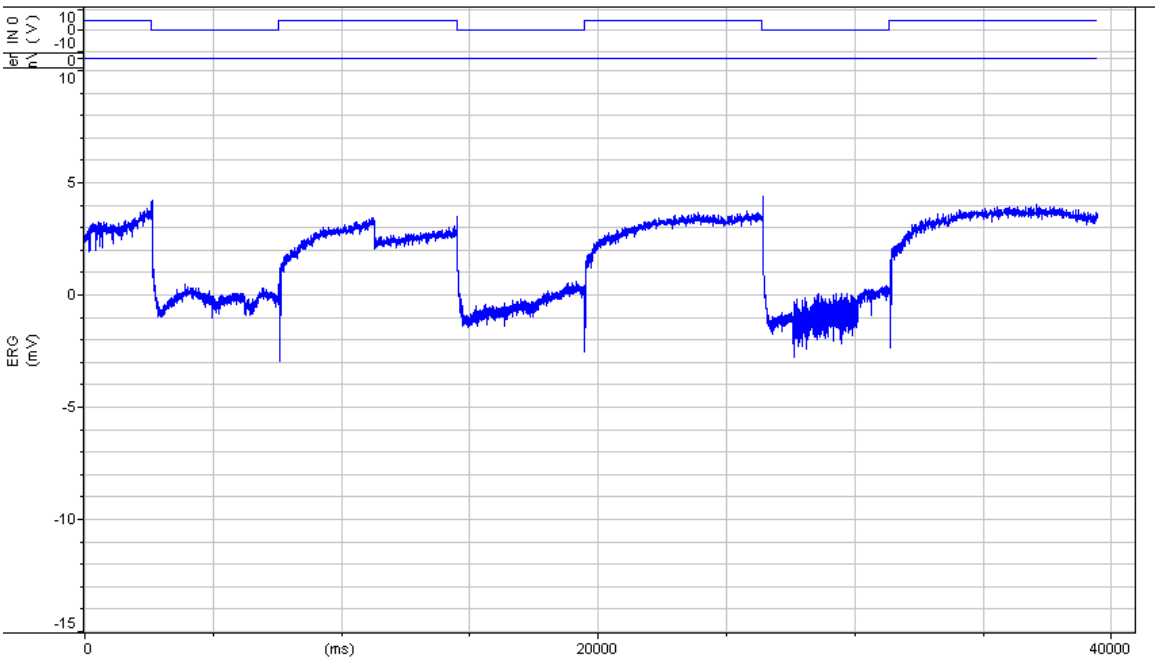
IN 0
(V)
10
0
-10
0
10
5
0
-5
-10
-15
ERG
(mV)
0
(ms)
20000
40000

Genotype: tubGal80ts; *repo*-Gal4> *Acsl* RNAi

Experiment: developmental heat shift, 10 day

Phenotype: with transient

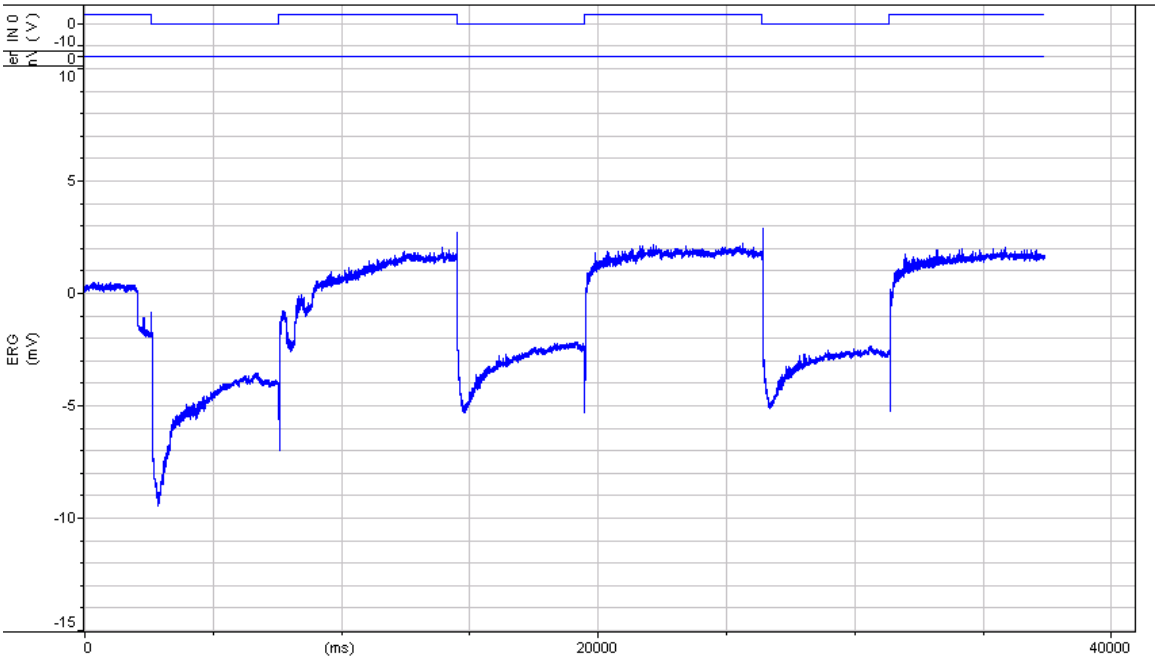

Genotype: tubGal80ts; *repo*-Gal4> *Acsl* RNAi

Experiment: developmental heat shift, 10 day

Phenotype: loss of ‘on transient’

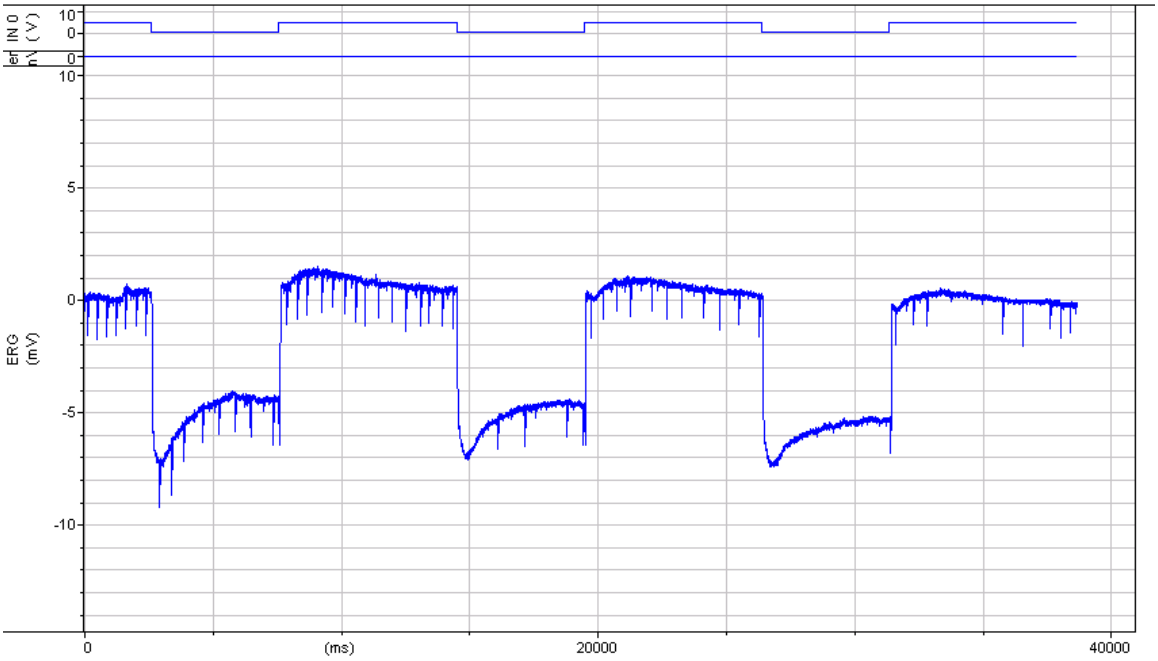

Genotype: tubGal80ts; *repo*-Gal4> *Acsl* RNAi

Experiment: developmental heat shift, 10 day

Phenotype: loss of ‘on’ and ‘off’ transients

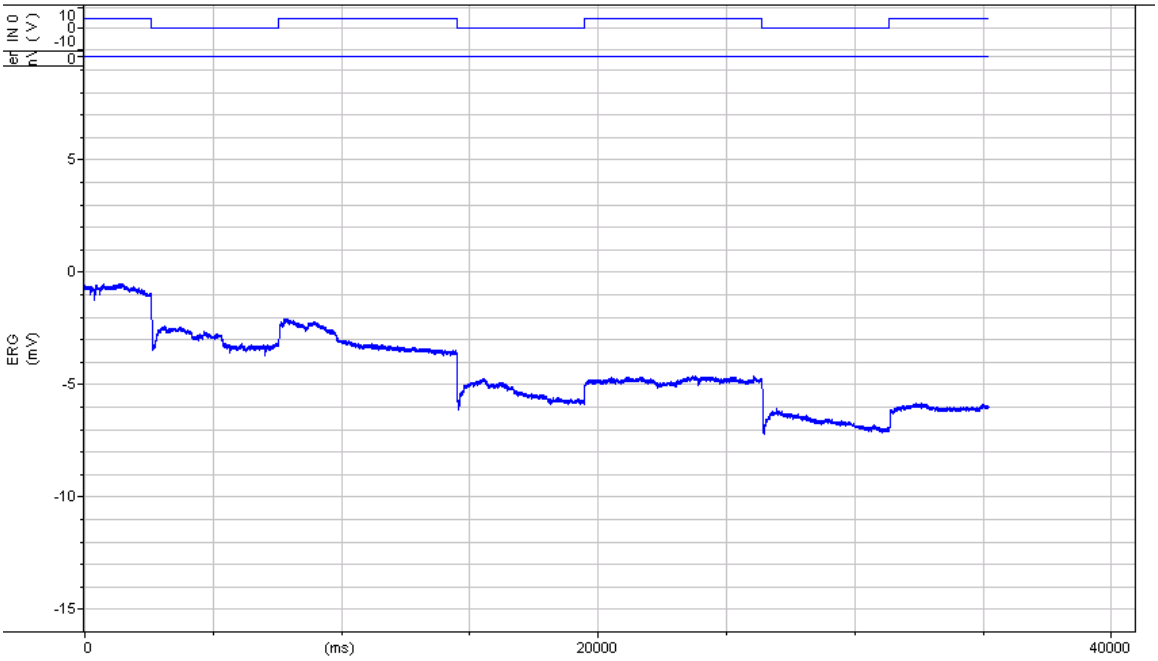

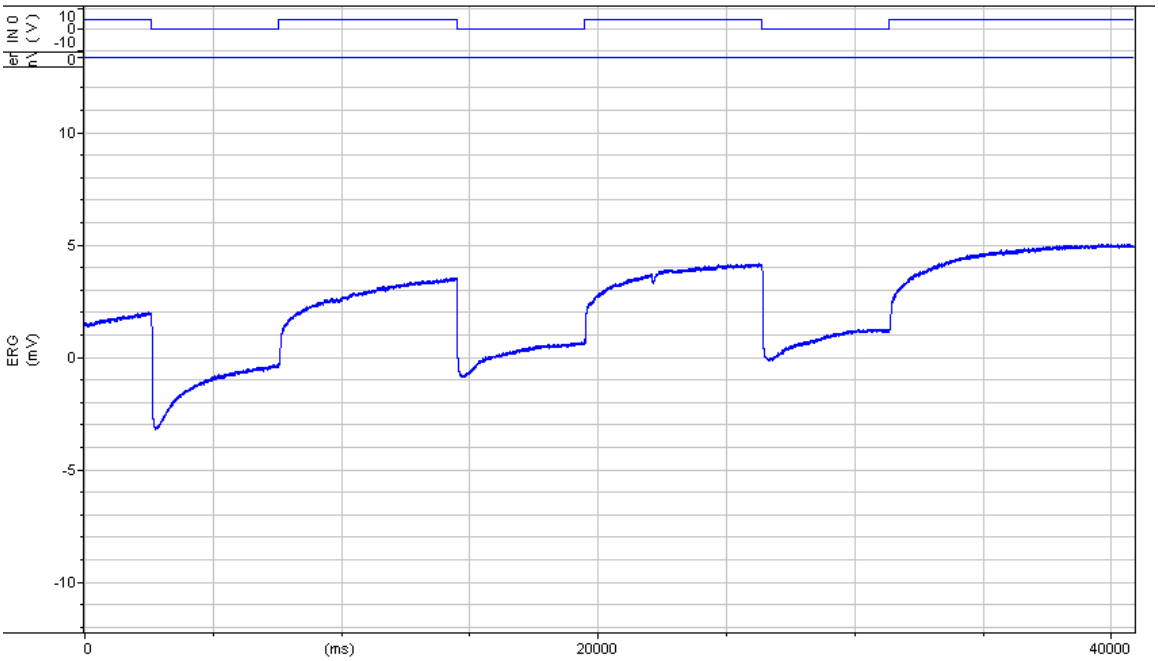

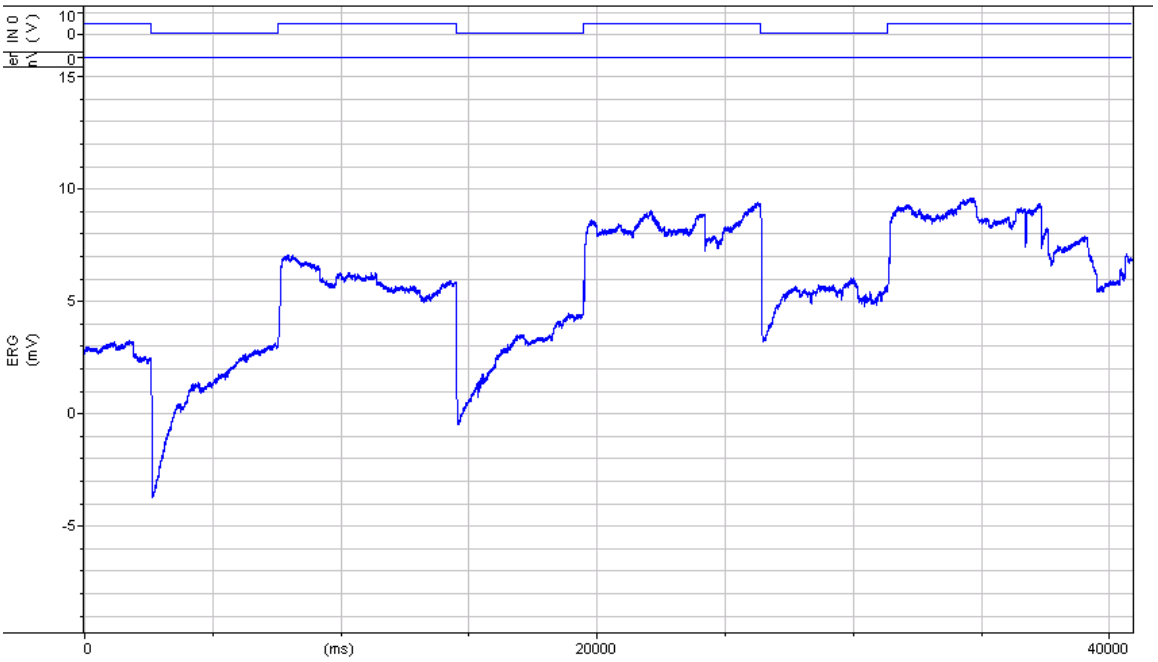
IN 0 (V)
ERG (mV)
10
0
15
5
-5
(ms)
20000
40000

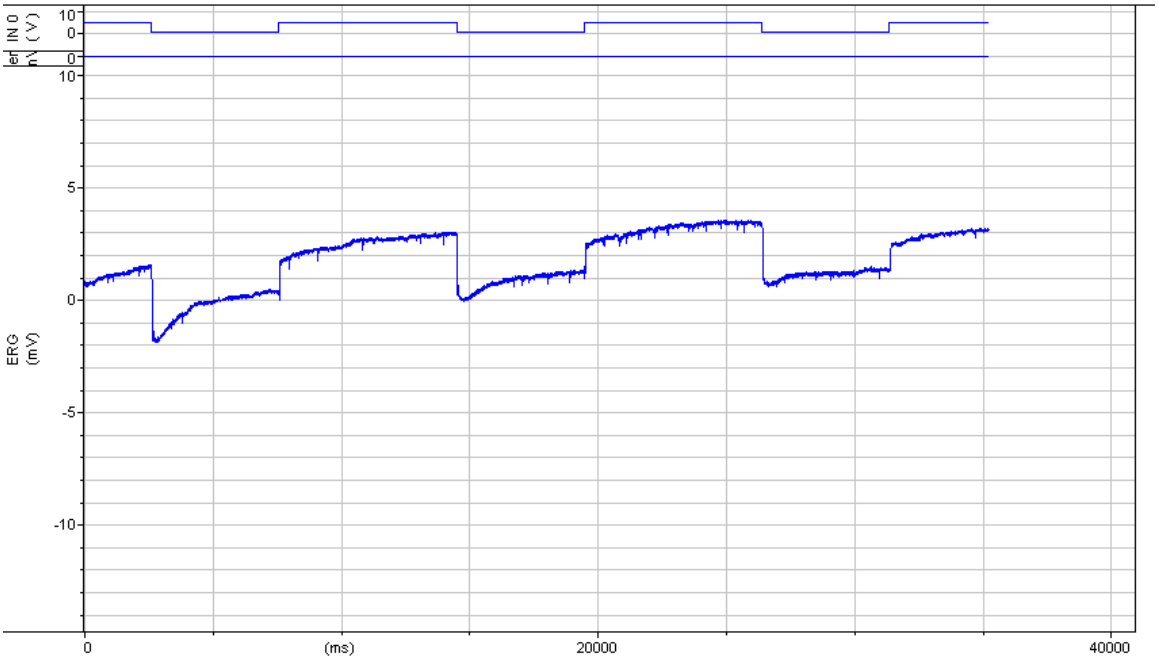
IN 0 (V)
ERG (mV)
10
0
5
-5
-10
(ms)
20000
40000

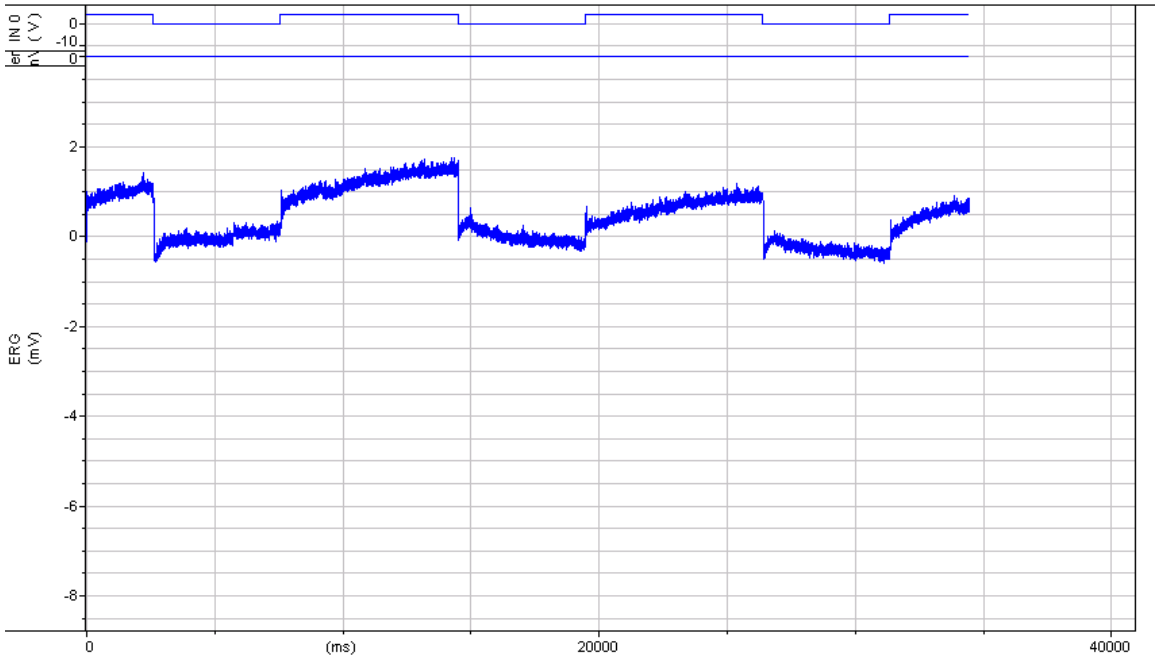
ef IN 0
nV (V)
0
-10
0
2
0
-2
-4
-6
-8
ERG
(mV)
0
(ms)
20000
40000

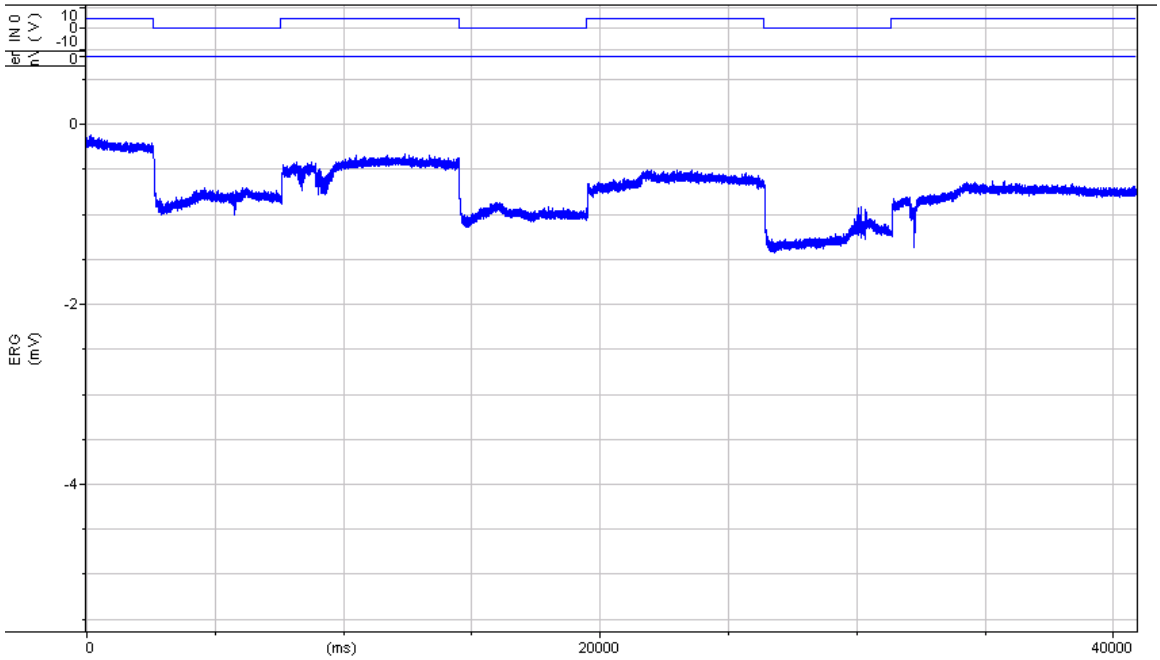
ef IN 0
nV (V)
10
0
-10
0
0
-2
-4
ERG
(mV)
0
(ms)
20000
40000

Genotype: tubGal80ts; *repo*-Gal4> *Luc* RNAi

Experiment: adult heat shift, eclosion

Phenotype: with transient

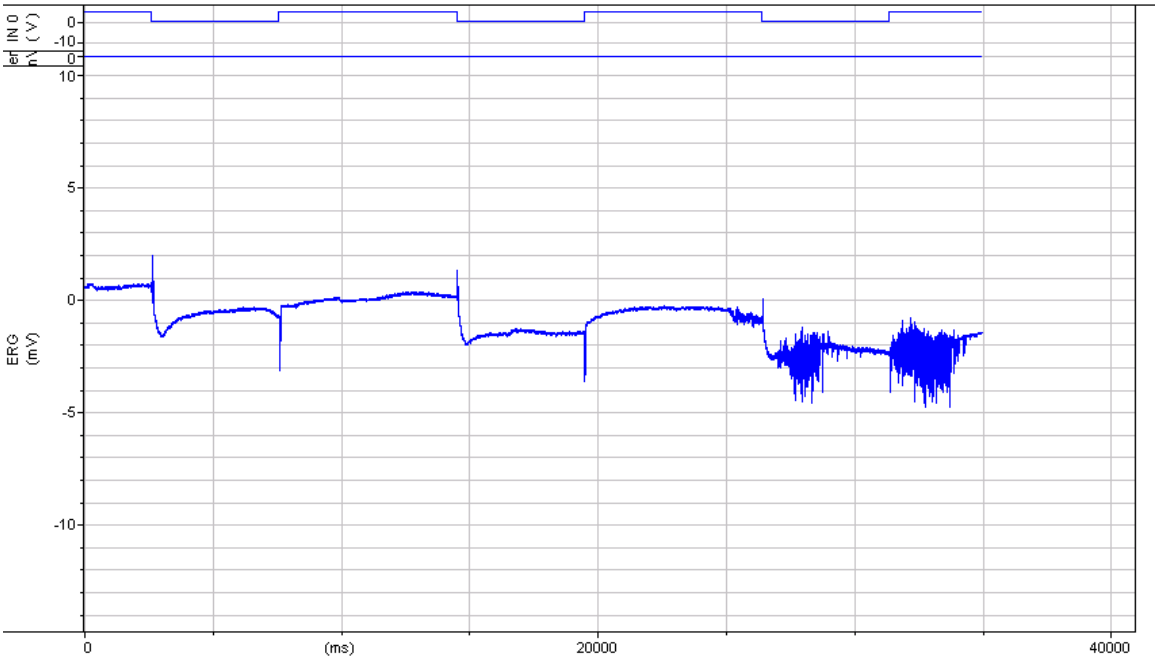

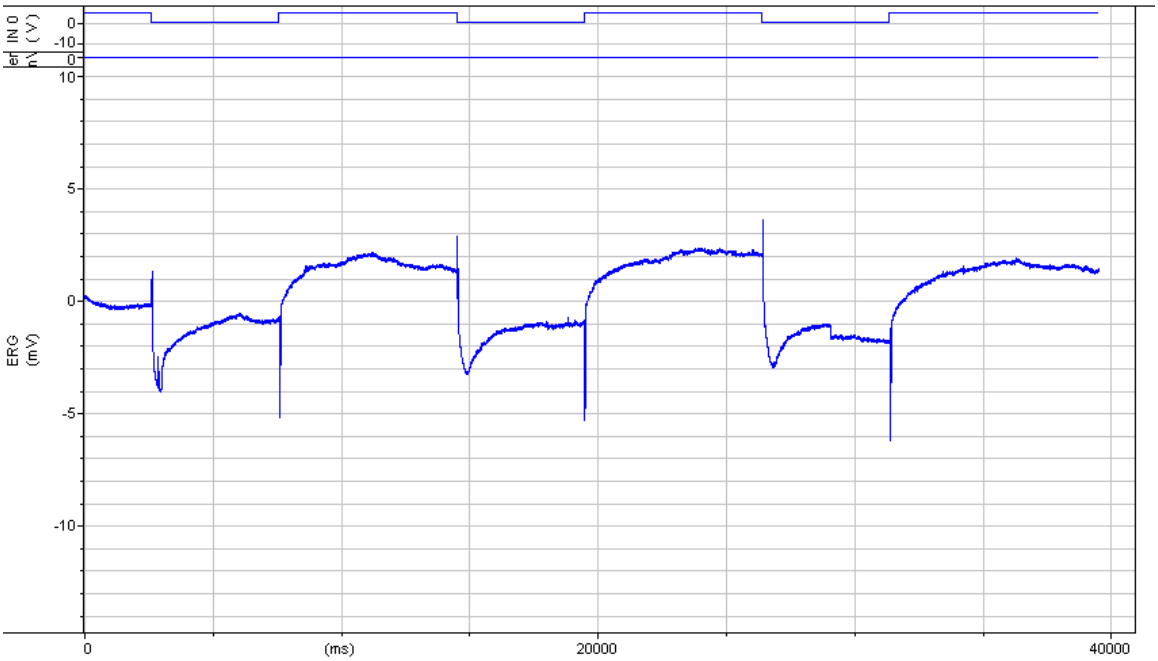

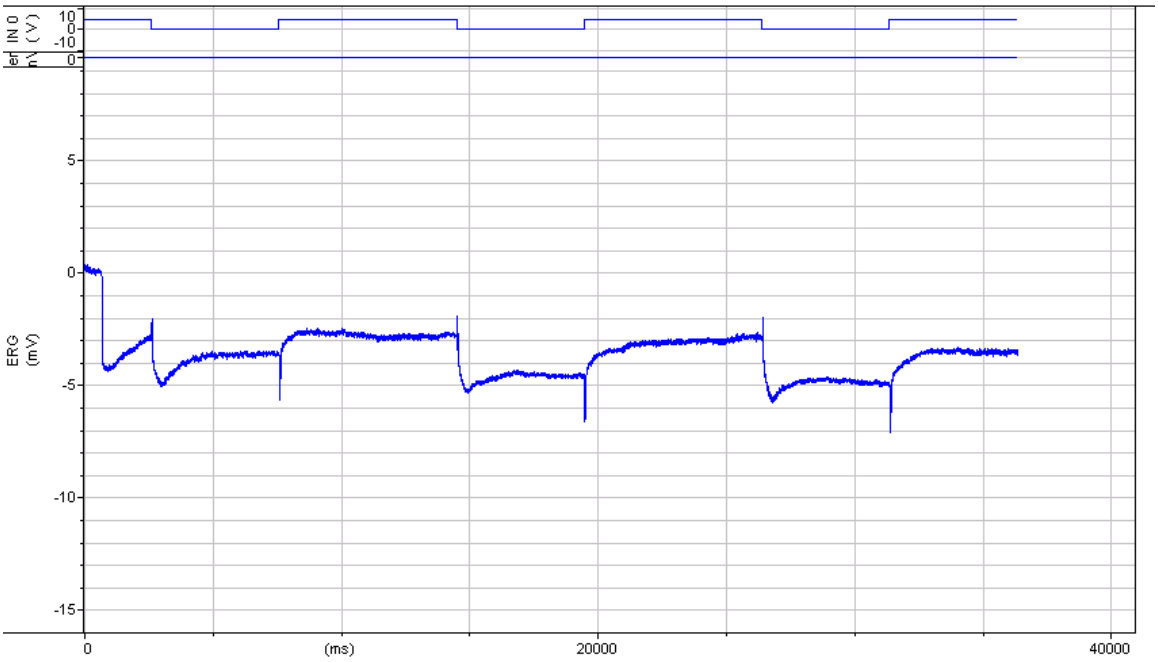
IN 0
(V)
10
0
-10
0
5
0
-5
-10
-15
ERG
(mV)
0
(ms)
20000
40000

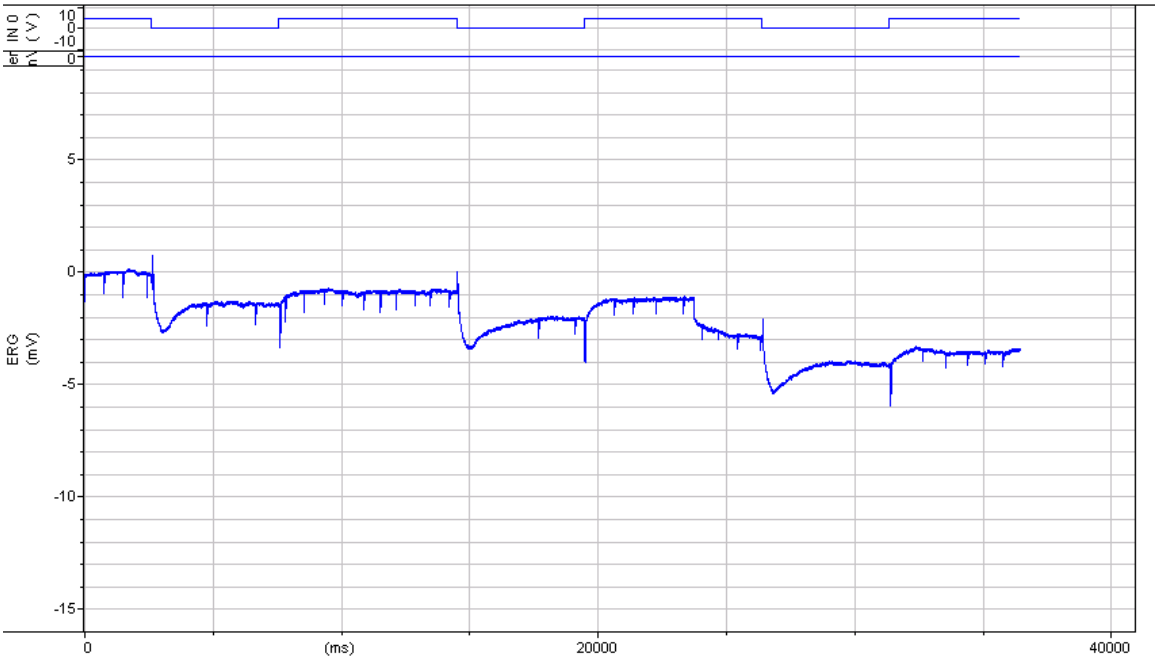
IN 0
(V)
10
0
-10
0
5
0
-5
-10
-15
ERG
(mV)
0
(ms)
20000
40000

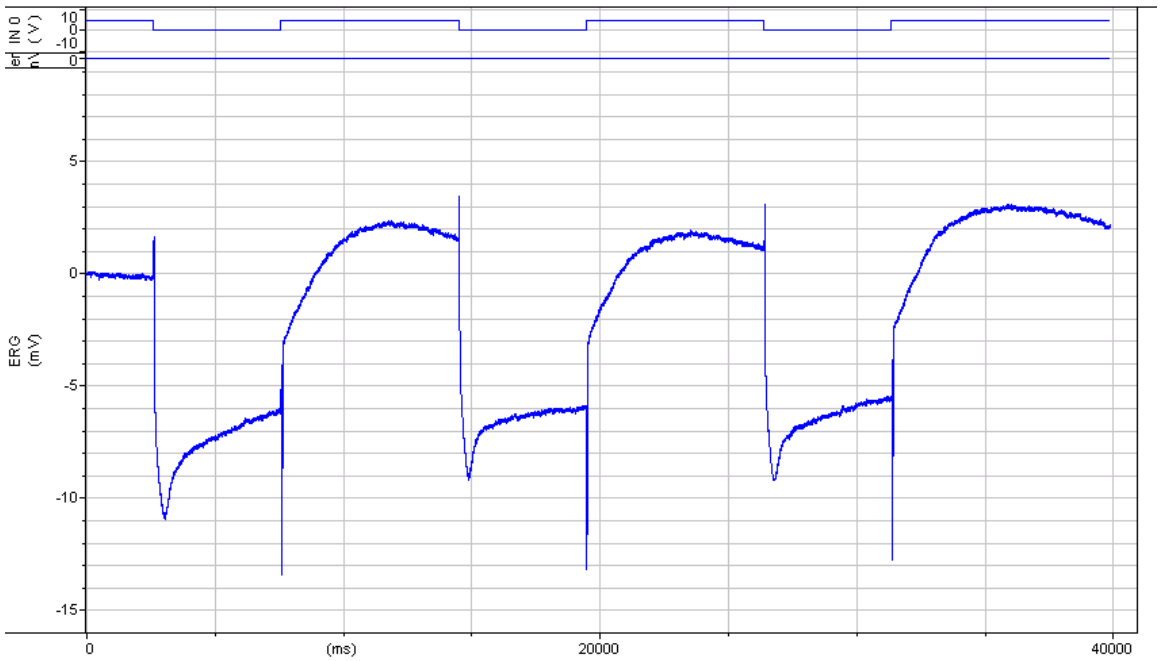
IN 0
(V)
10
0
-10
0
5
0
-5
-10
-15
ERG
(mV)
0
(ms)
20000
40000

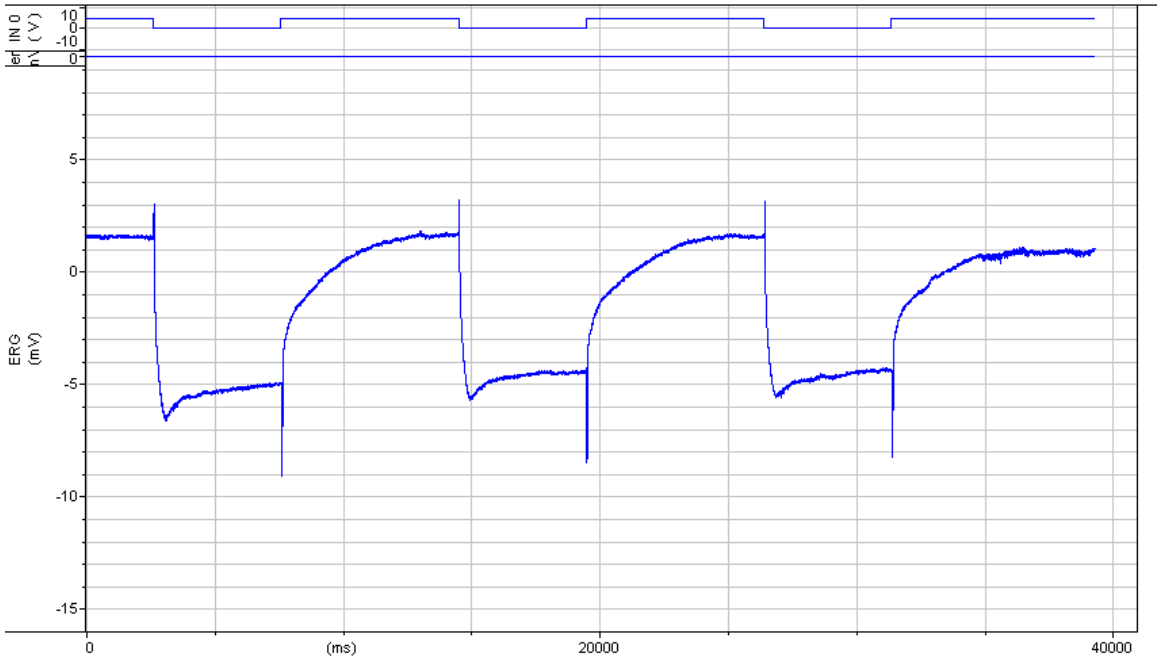
IN 0
(V)
10
0
-10
0
5
0
-5
-10
-15
ERG
(mV)
0
(ms)
20000
40000

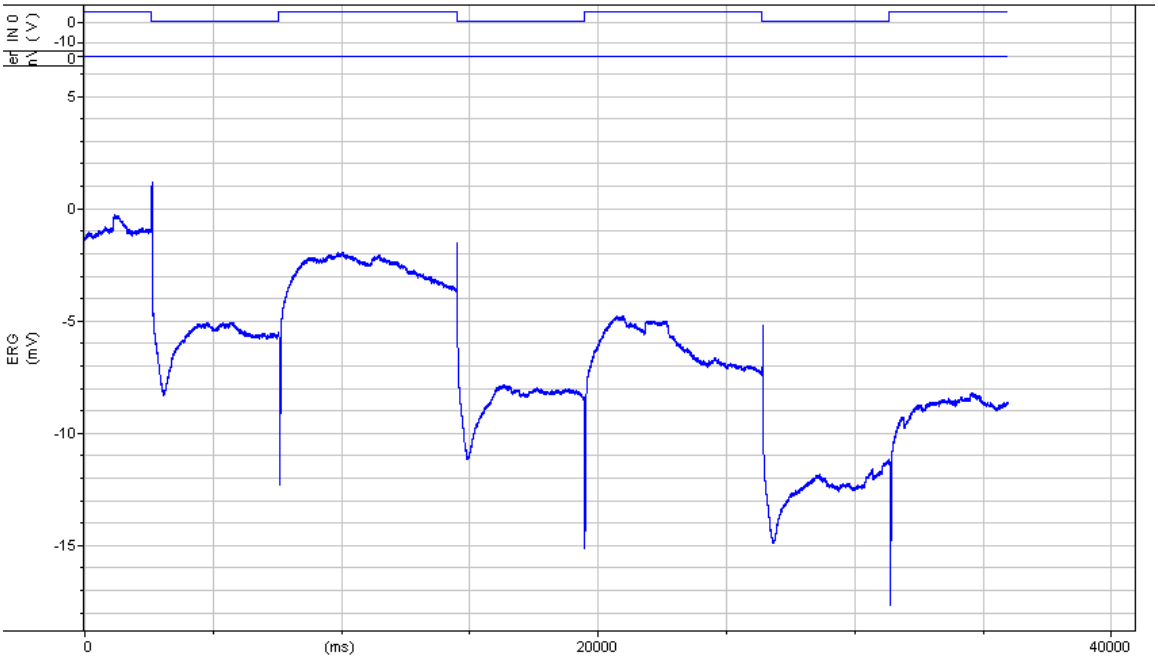
ef IN 0
nV (V)
0
-10
0
5
0
-5
-10
-15
ERG
(mV)
0
(ms)
20000
40000

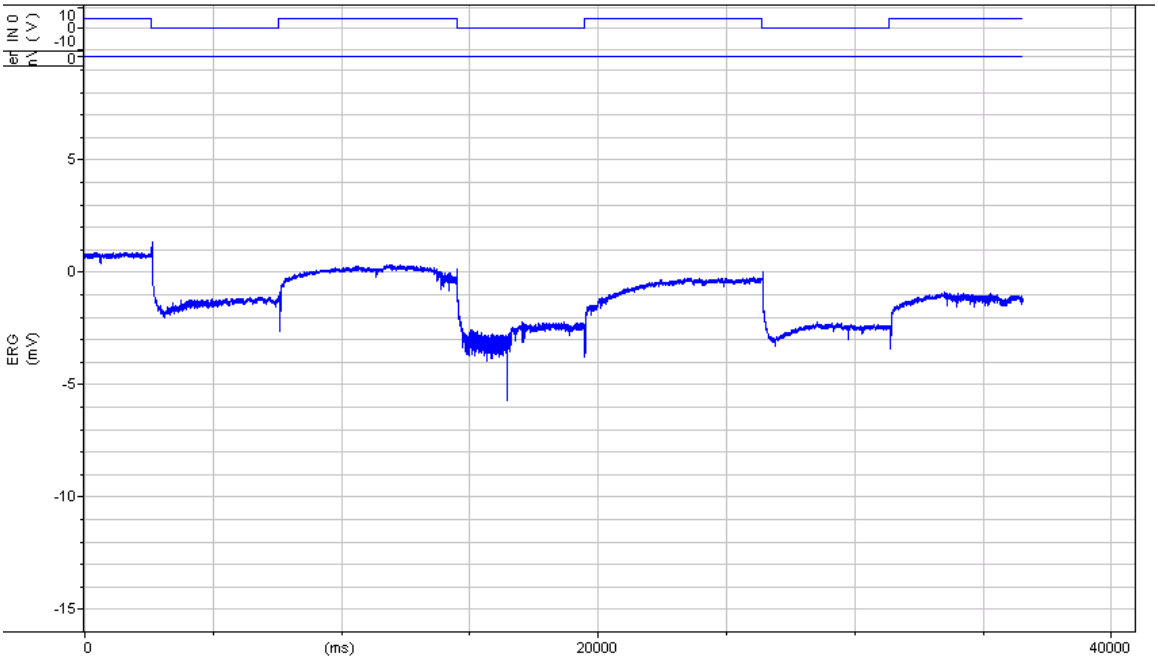
ef IN 0
nV (V)
10
0
-10
0
5
0
-5
-10
-15
ERG
(mV)
0
(ms)
20000
40000

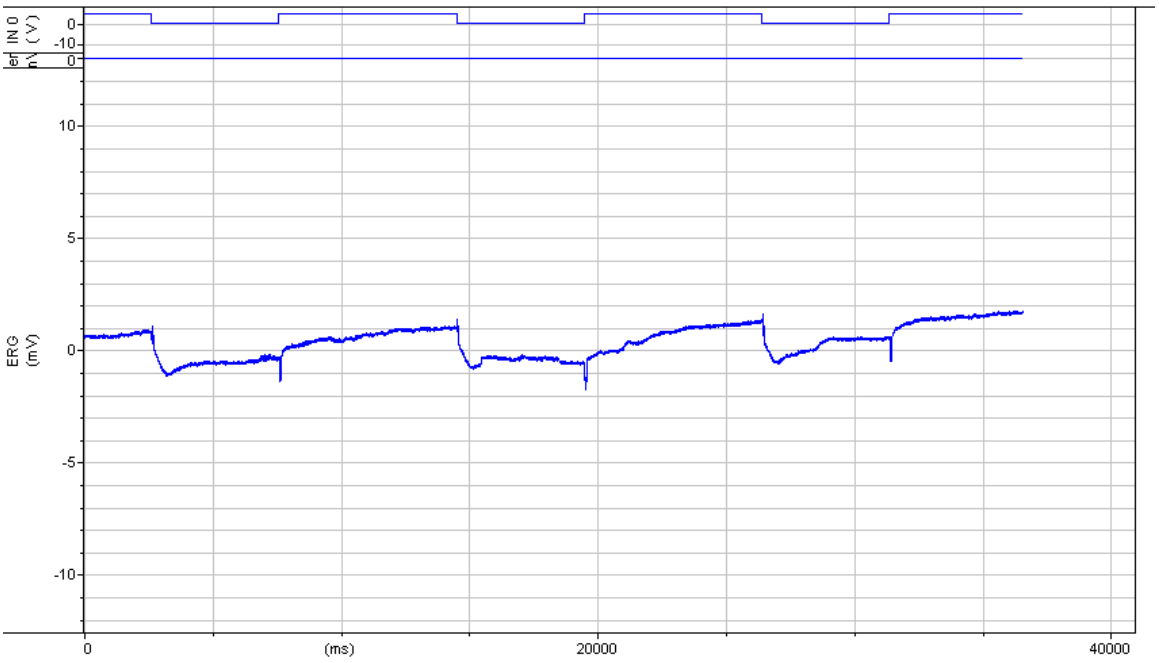
IN 0
(V)
0
-10
0
10
5
0
-5
-10
ERG
(mV)
0
(ms)
20000
40000

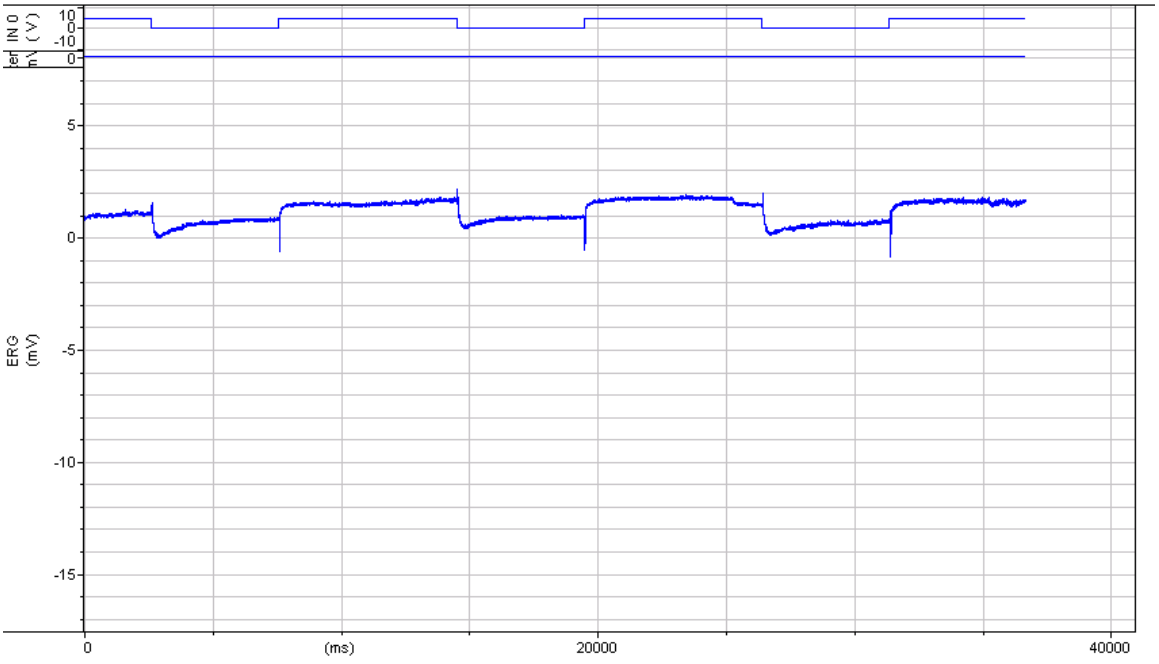
IN 0
(V)
10
0
-10
0
5
0
-5
-10
-15
ERG
(mV)
0
(ms)
20000
40000

Genotype: tubGal80ts; *repo*-Gal4> *Acsl* RNAi

Experiment: adult heat shift, eclosion

Phenotype: with transient

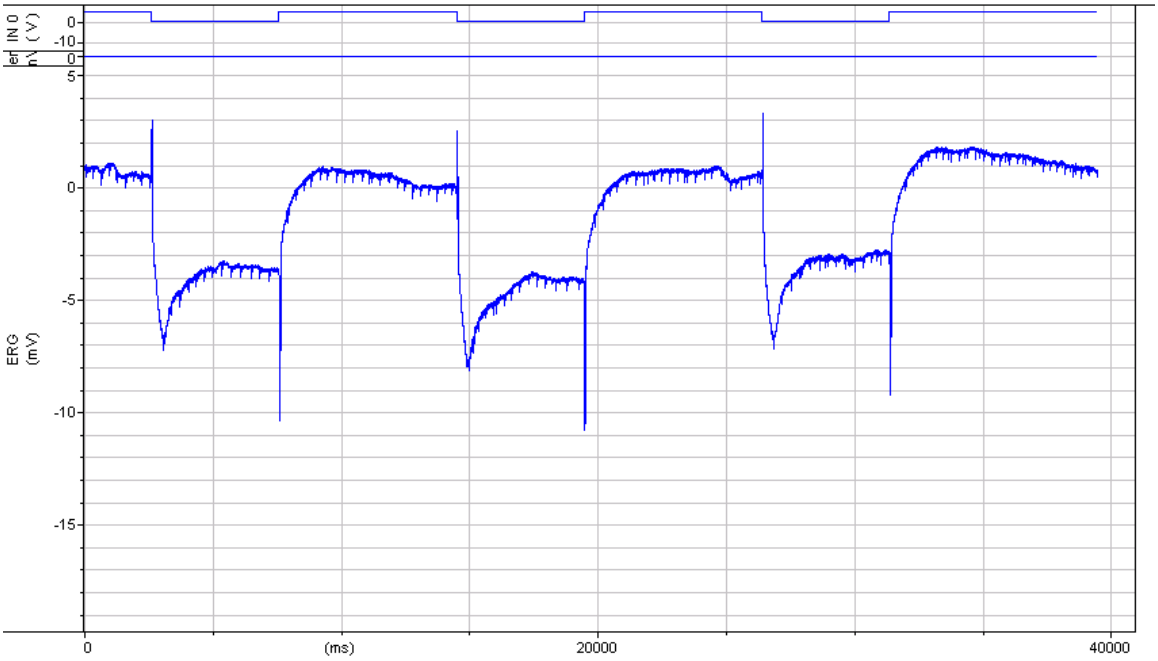

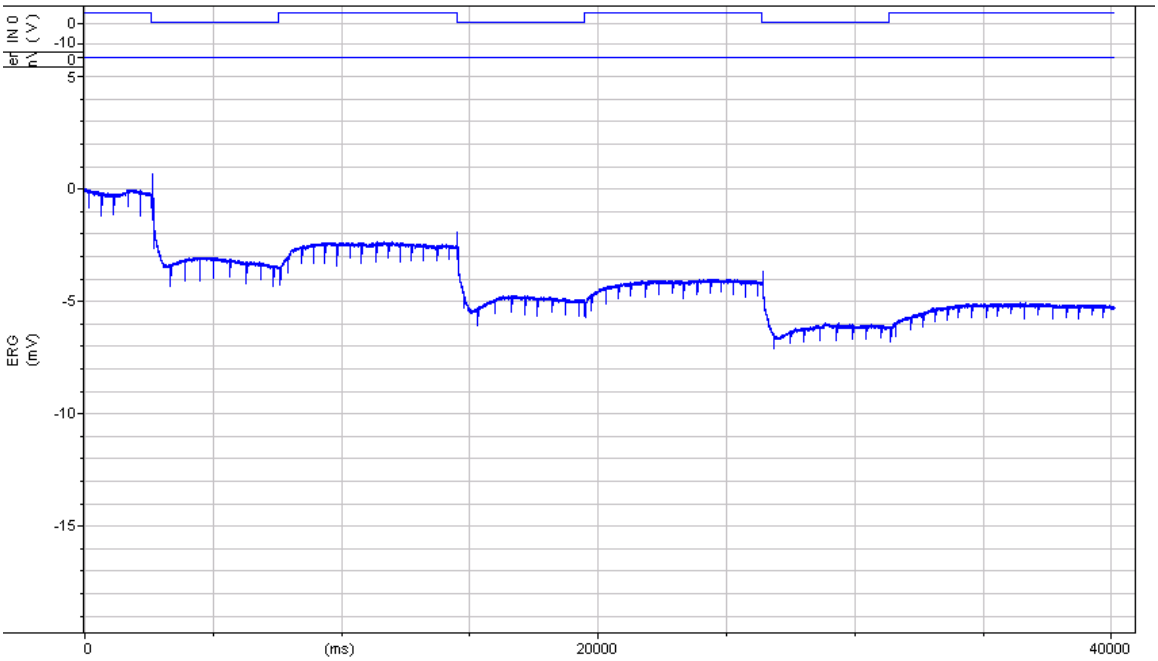

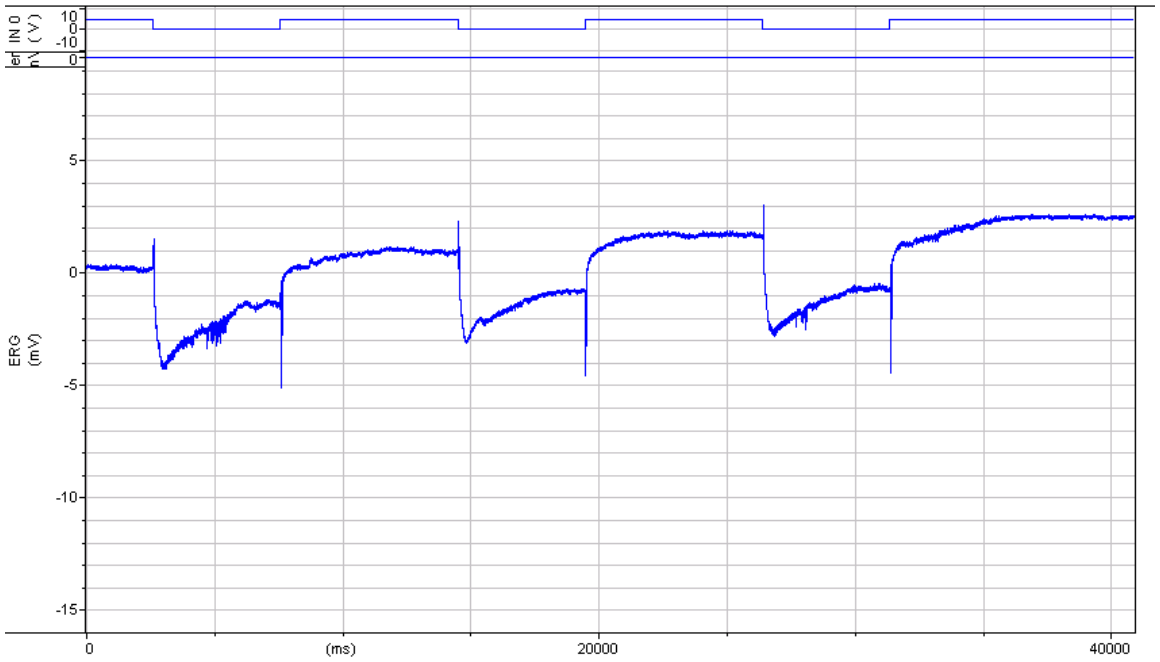
IN 0 (V)
10
0
-10
0
5
0
-5
-10
-15
ERG (mV)
0
(ms)
20000
40000

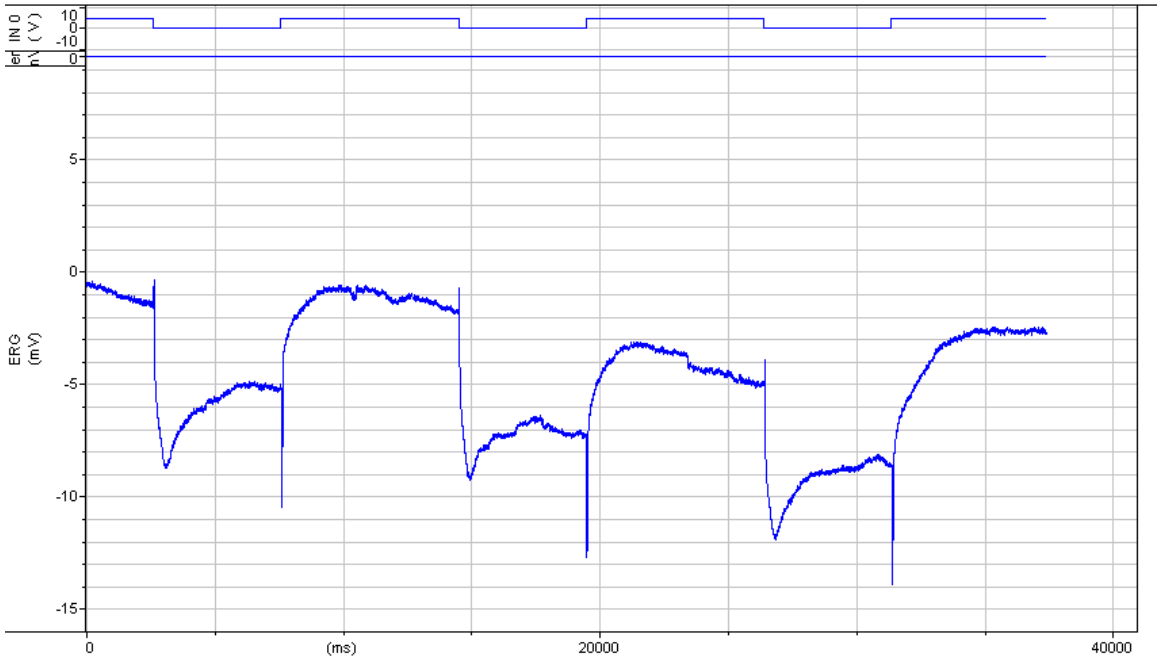
IN 0 (V)
10
0
-10
0
5
0
-5
-10
-15
ERG (mV)
0
(ms)
20000
40000

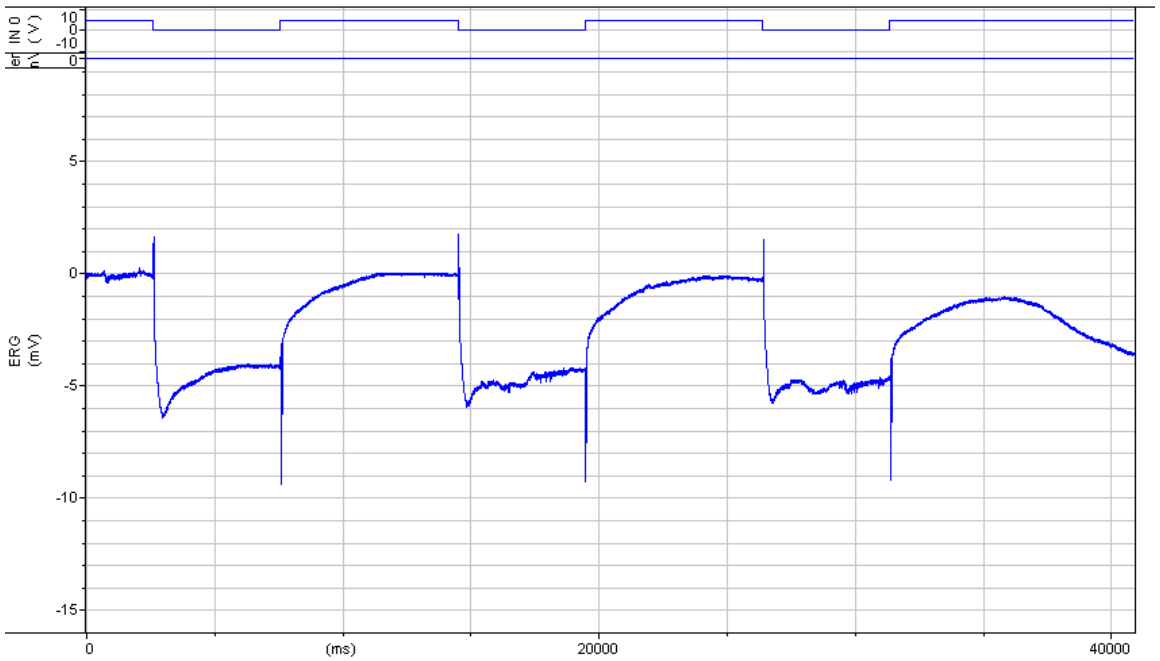
IN 0
(V)
10
0
-10
ref
0
5
0
-5
-10
-15
ERG
(mV)
0
(ms)
20000
40000

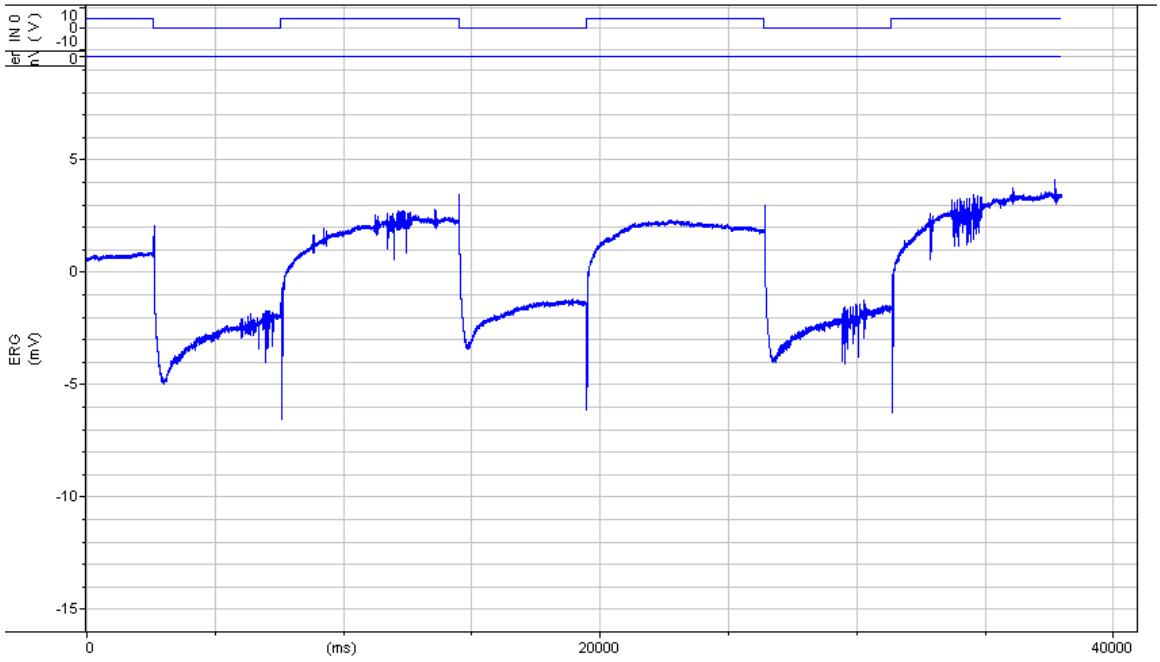
IN 0
(V)
10
0
-10
ref
0
5
0
-5
-10
-15
ERG
(mV)
0
(ms)
20000
40000

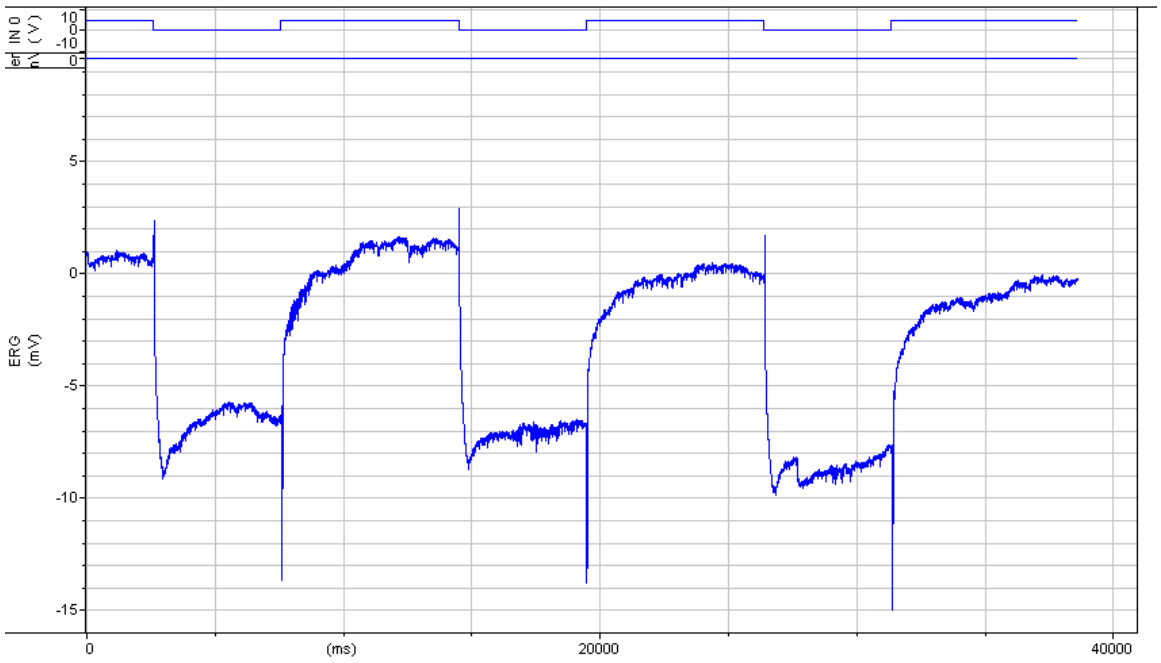
ref IN 0
(V)
10
0
-10
0
5
0
-5
-10
-15
ERG
(mV)
0
(ms)
20000
40000

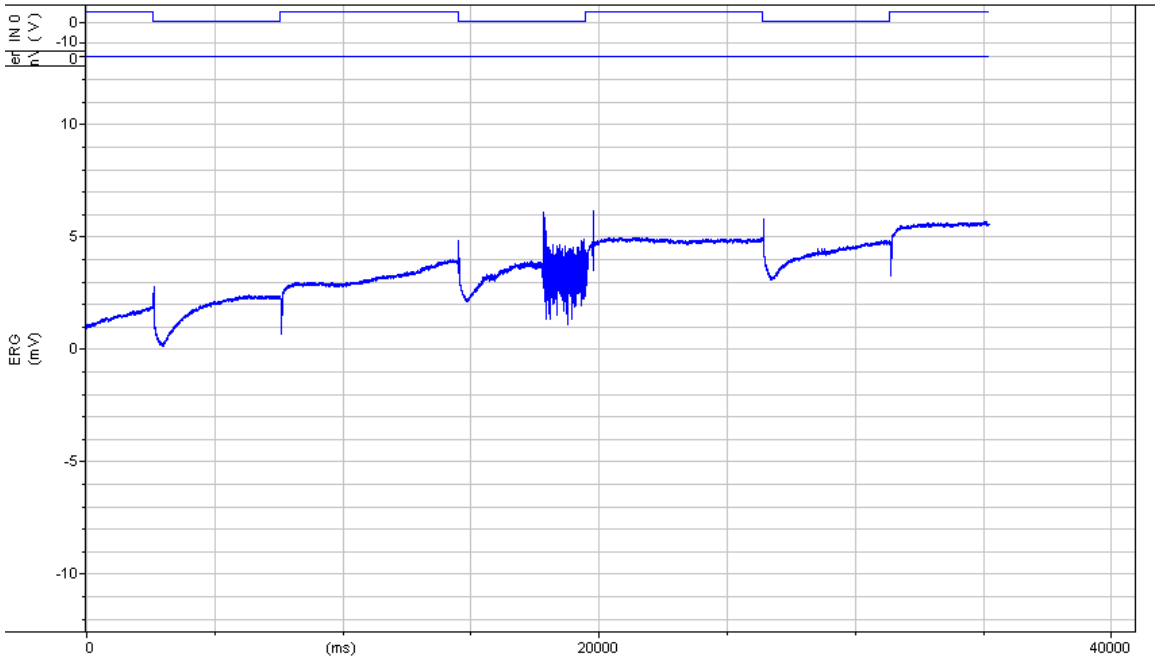
ref IN 0
(V)
0
-10
0
10
5
0
-5
-10
ERG
(mV)
0
(ms)
20000
40000

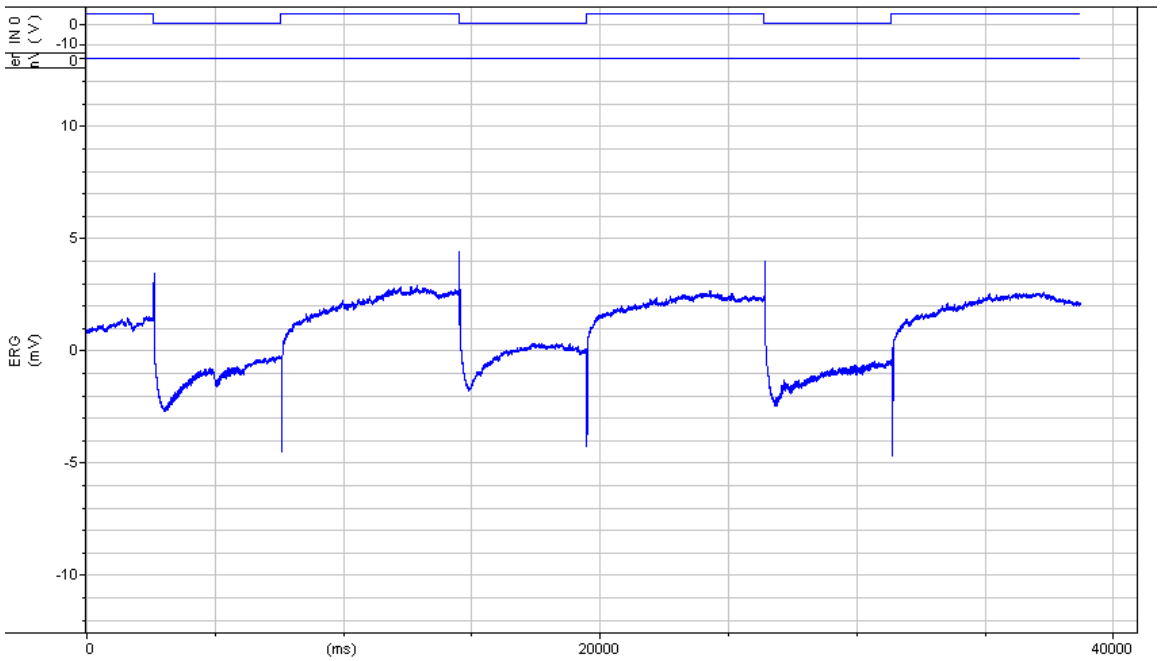
ef IN 0
n\ (V)
0
-10
0
10
5
0
-5
-10
ERG
(mV)
0
(ms)
20000
40000

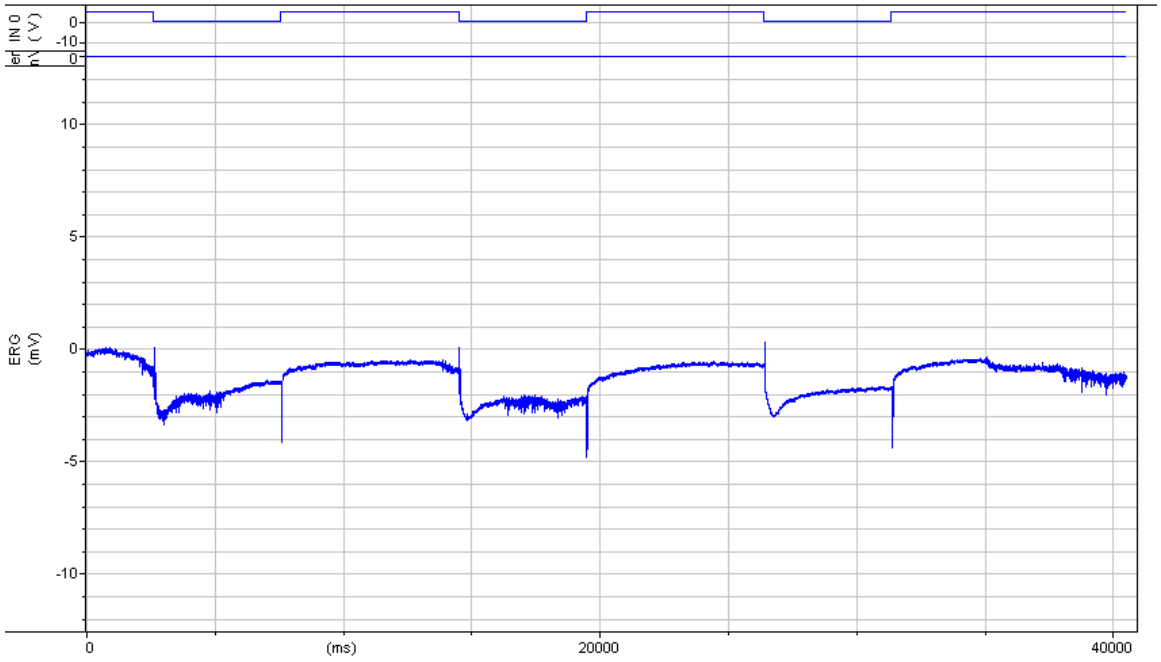
ef IN 0
n\ (V)
0
-10
0
10
5
0
-5
-10
ERG
(mV)
0
(ms)
20000
40000

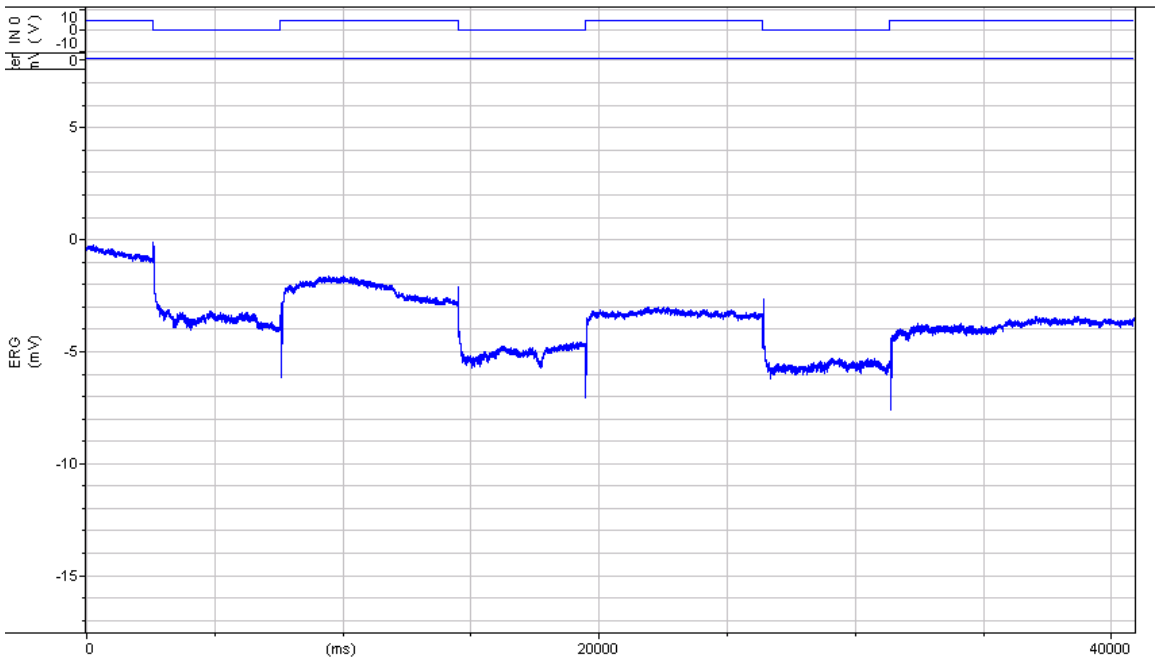
IN 0
(V)
10
0
-10
ref
mV
0
5
0
-5
-10
-15
ERG
(mV)
0
(ms)
20000
40000

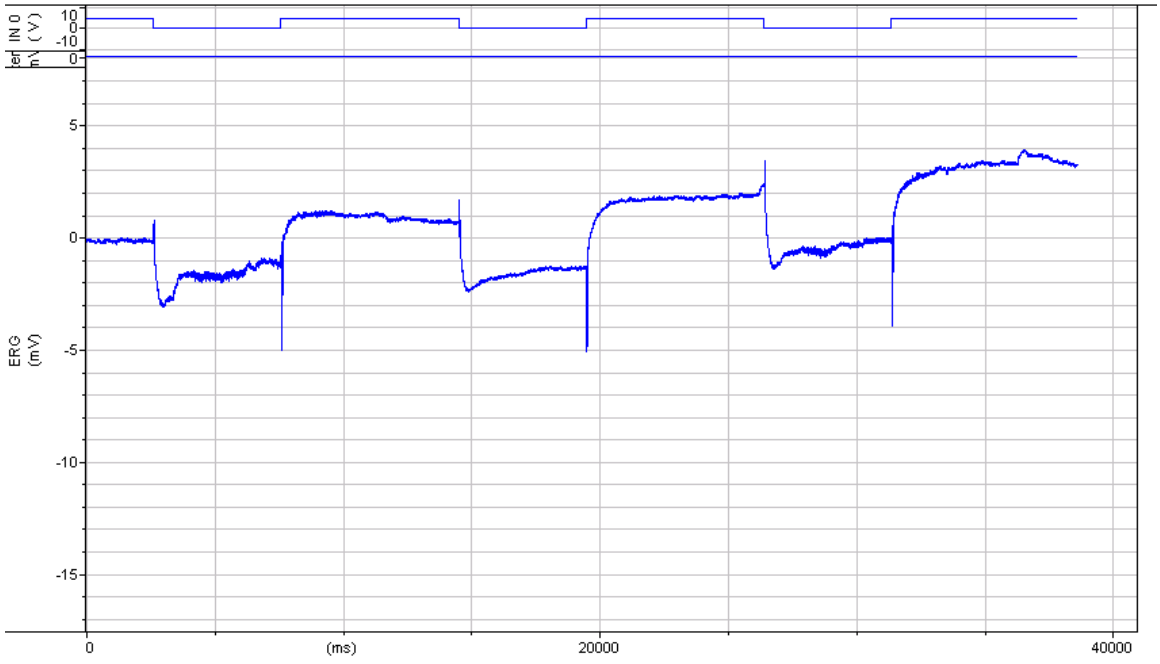
IN 0
(V)
10
0
-10
ref
mV
0
5
0
-5
-10
-15
ERG
(mV)
0
(ms)
20000
40000

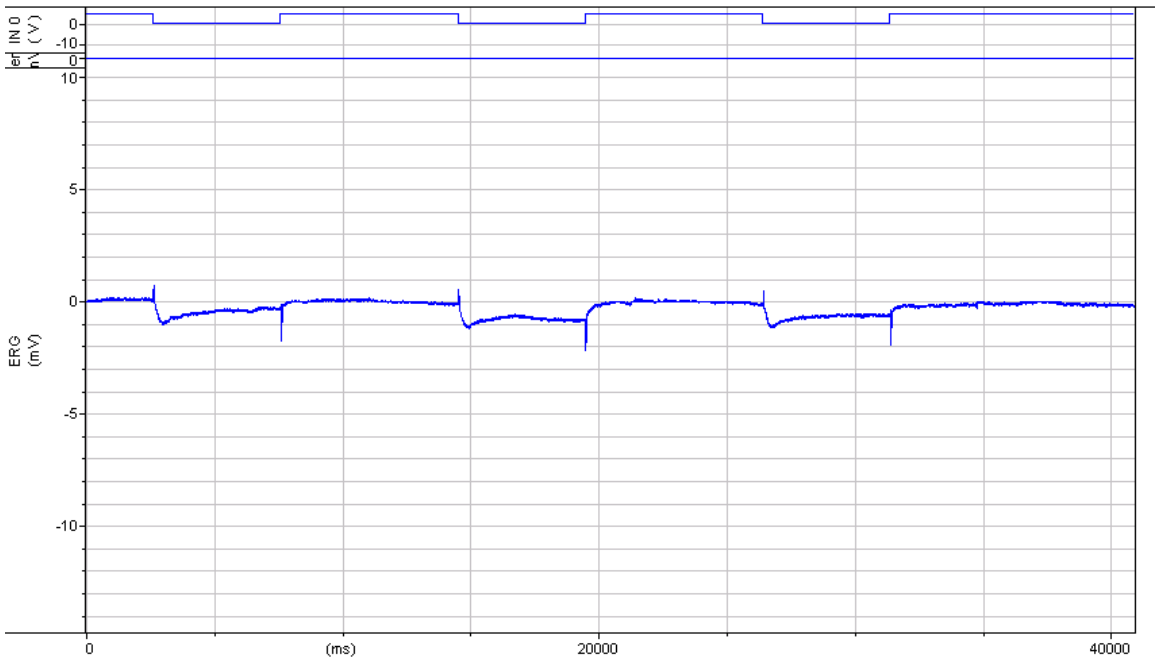
IN 0
(V)
0
-10
0
10
5
0
-5
-10
ERG
(mV)
0
(ms)
20000
40000

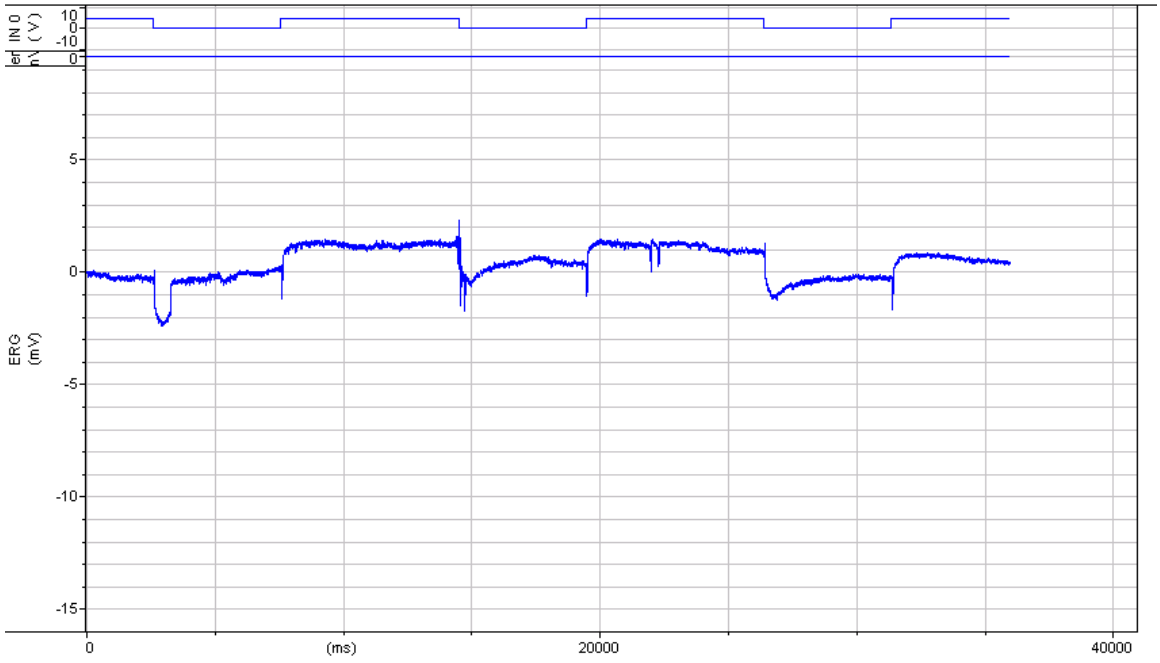
IN 0
(V)
10
0
-10
0
5
0
-5
-10
-15
ERG
(mV)
0
(ms)
20000
40000

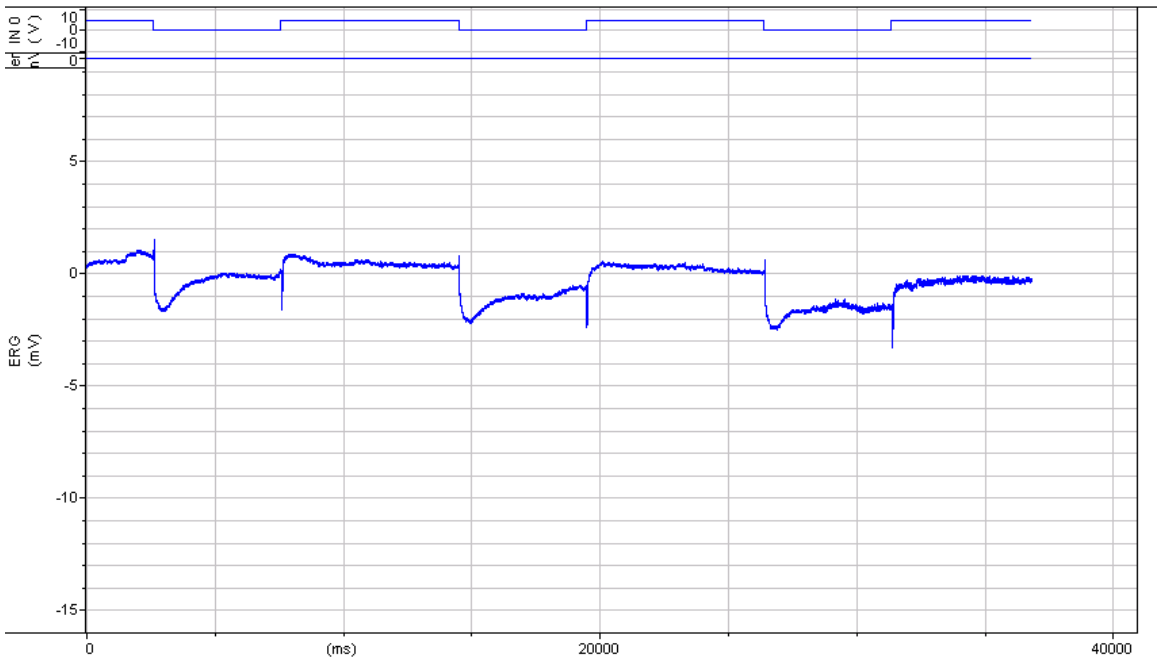
IN 0 (V)
ref
10
0
-10
0
5
0
-5
-10
-15
ERG (mV)
0
(ms)
20000
40000

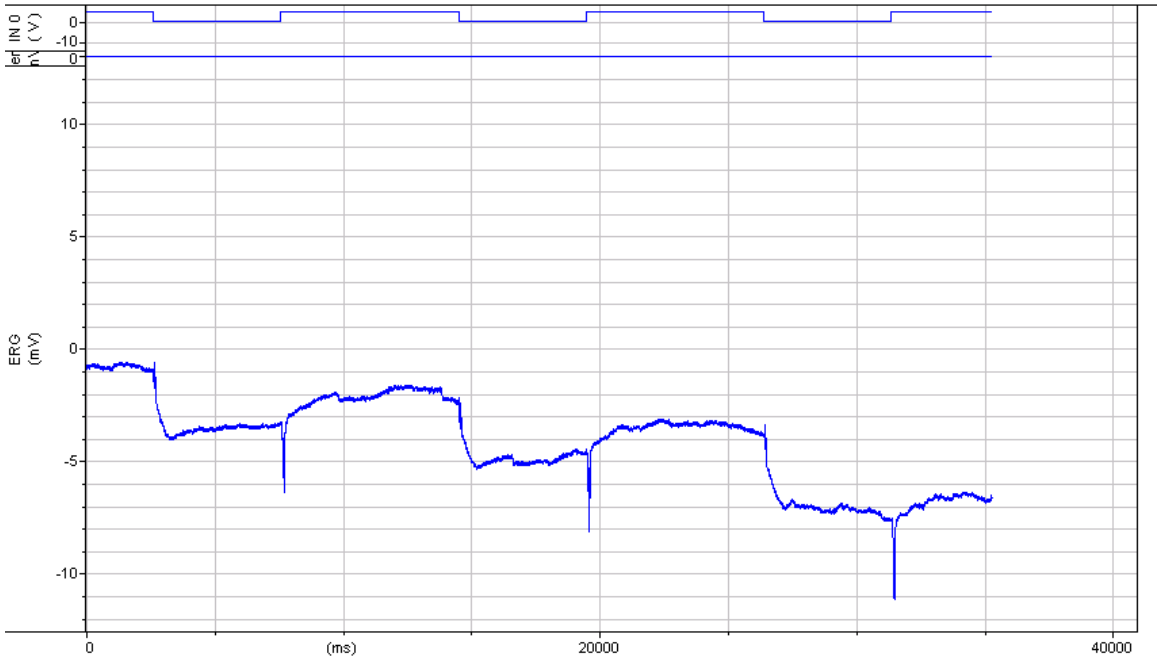
IN 0 (V)
ref
0
-10
0
10
5
0
-5
-10
ERG (mV)
0
(ms)
20000
40000

Genotype: tubGal80ts; *repo*-Gal4 > *Luc* RNAi

Experiment: adult heat shift, 10 day

Phenotype: with transient

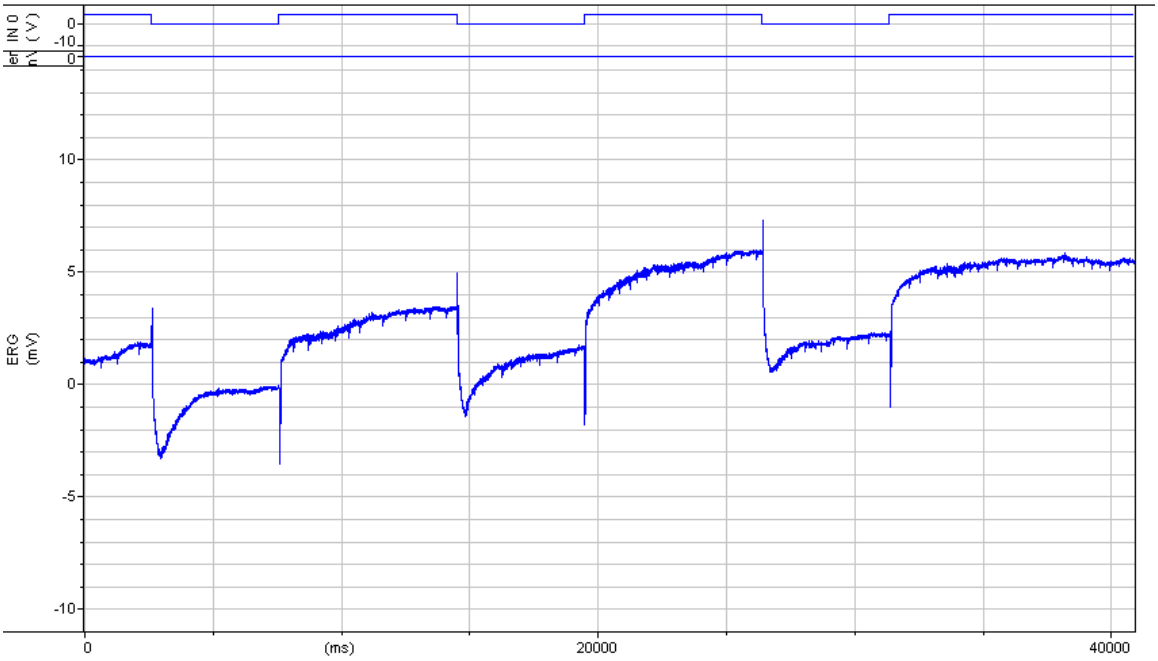

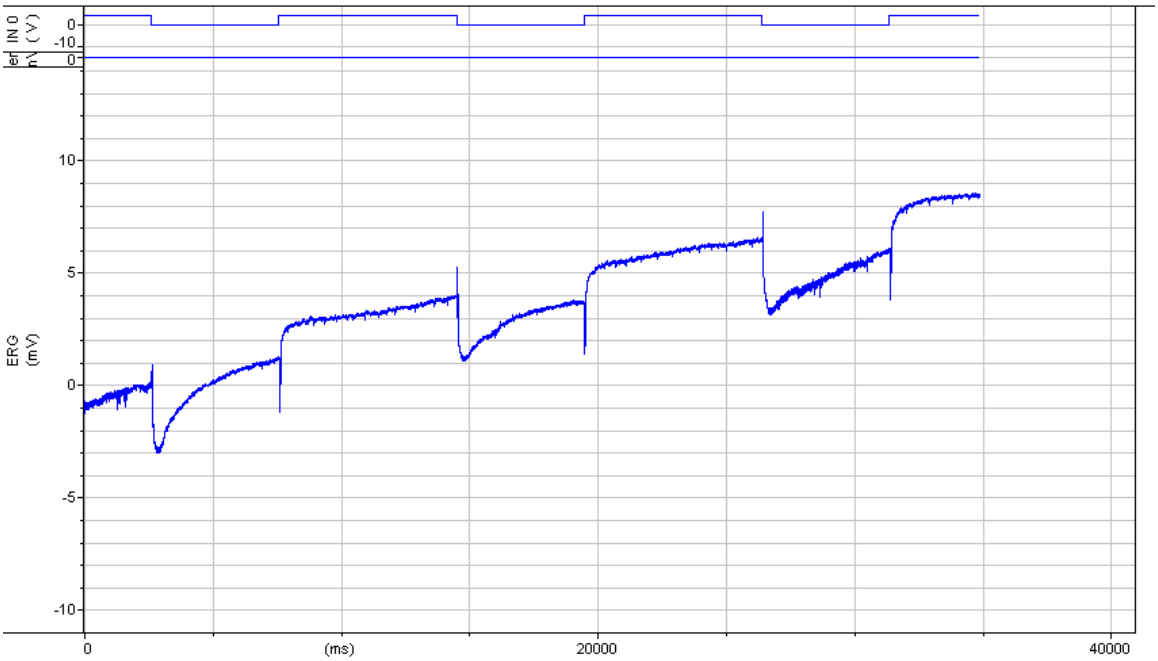

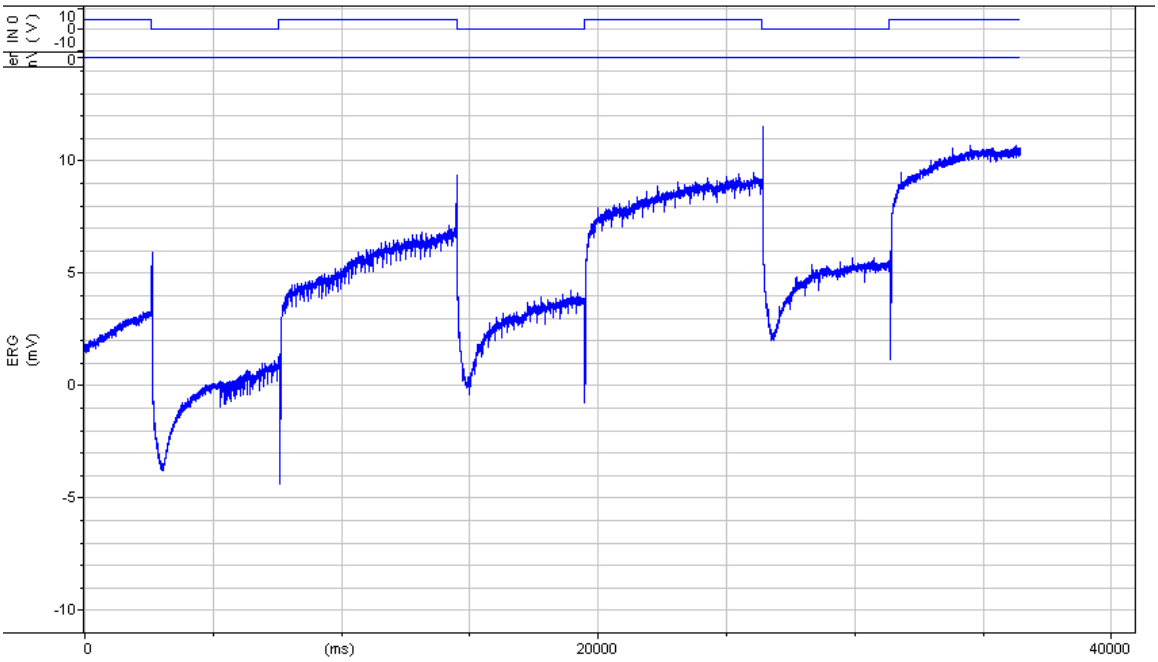
IN 0
(V)
10
0
-10
0
10
5
0
-5
-10
ERG
(mV)
0
(ms)
20000
40000

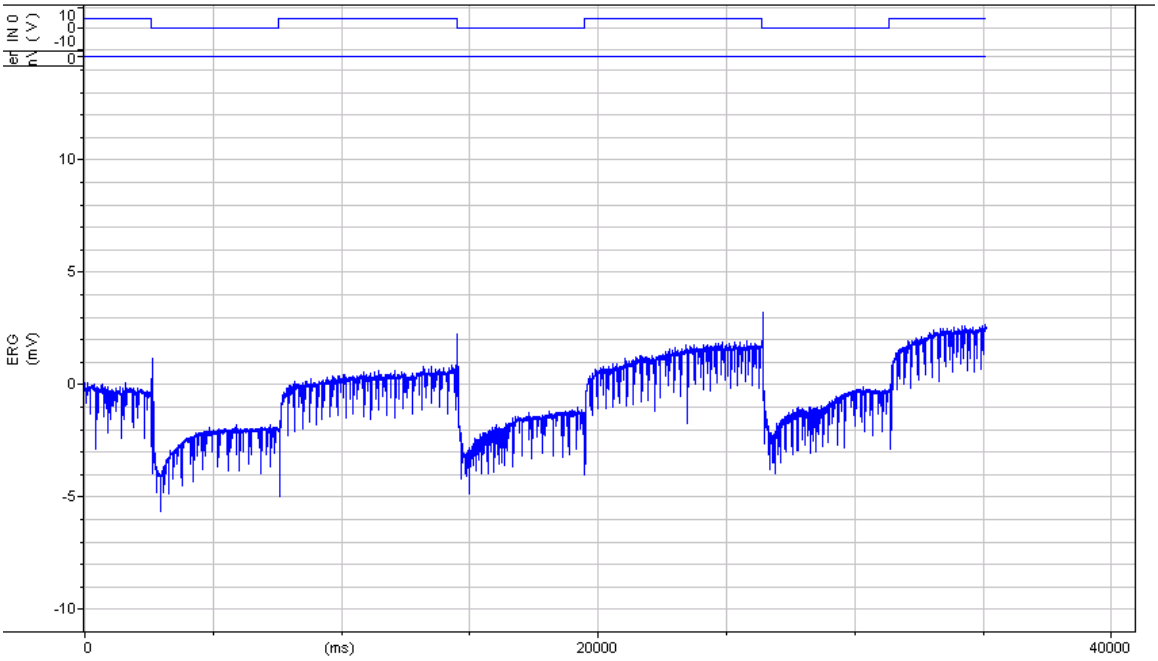
IN 0
(V)
10
0
-10
0
10
5
0
-5
-10
ERG
(mV)
0
(ms)
20000
40000

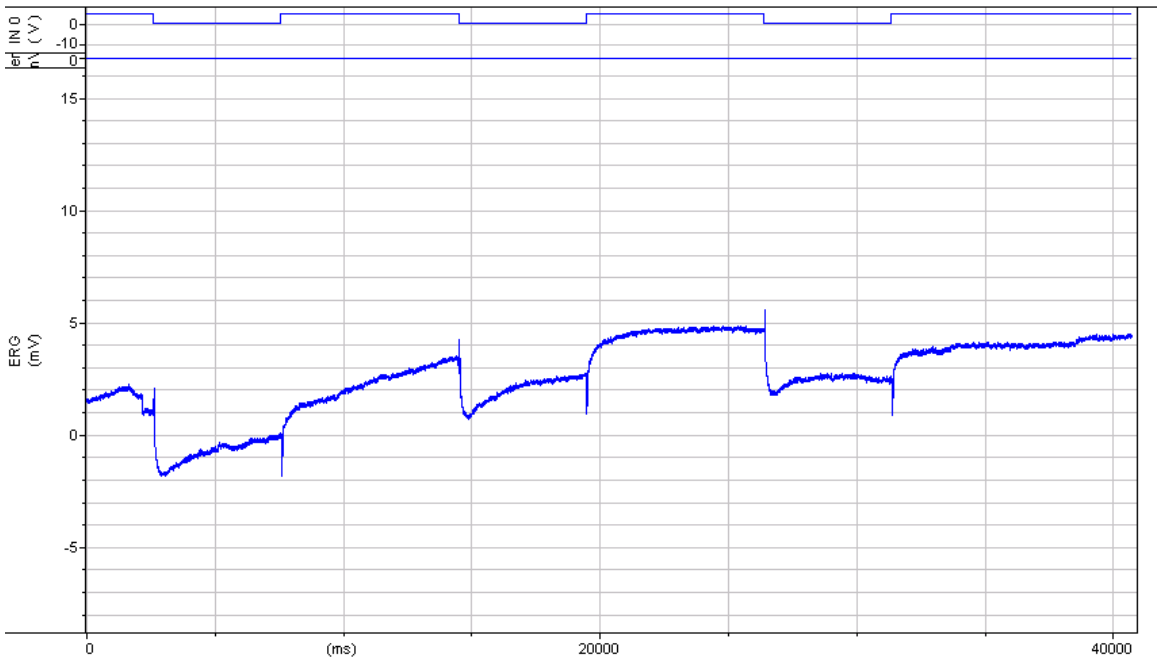
ef IN 0
nV (V)
0
-10
0
15
10
5
0
-5
ERG
(mV)
0
(ms)
20000
40000

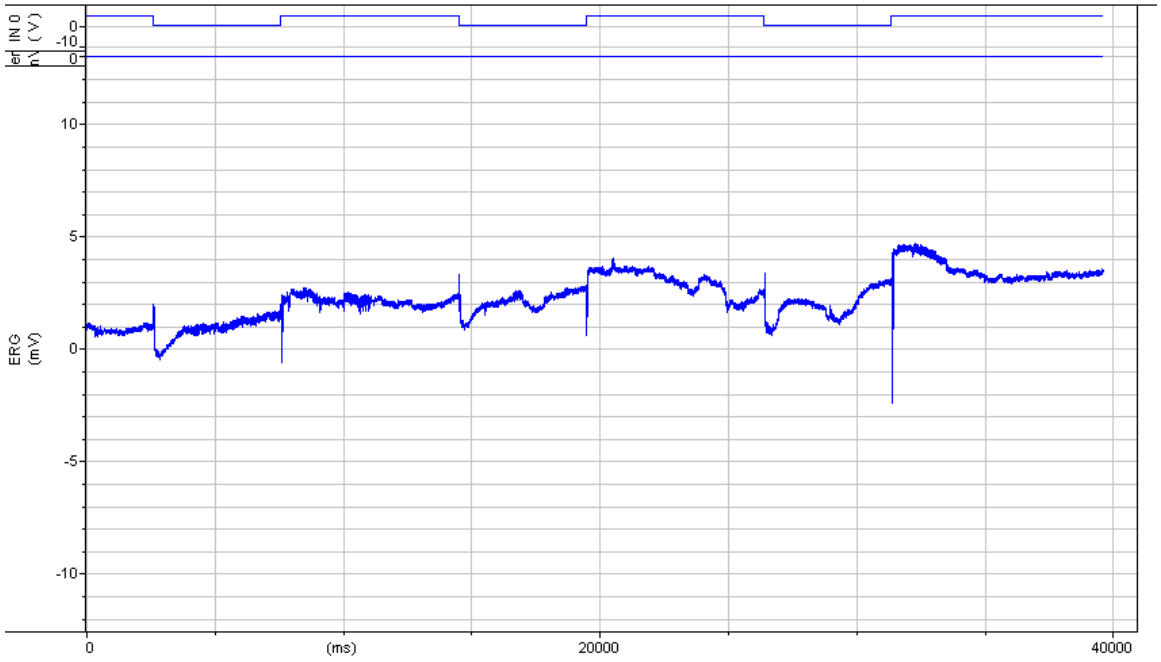
ef IN 0
nV (V)
0
-10
0
10
5
0
-5
-10
ERG
(mV)
0
(ms)
20000
40000

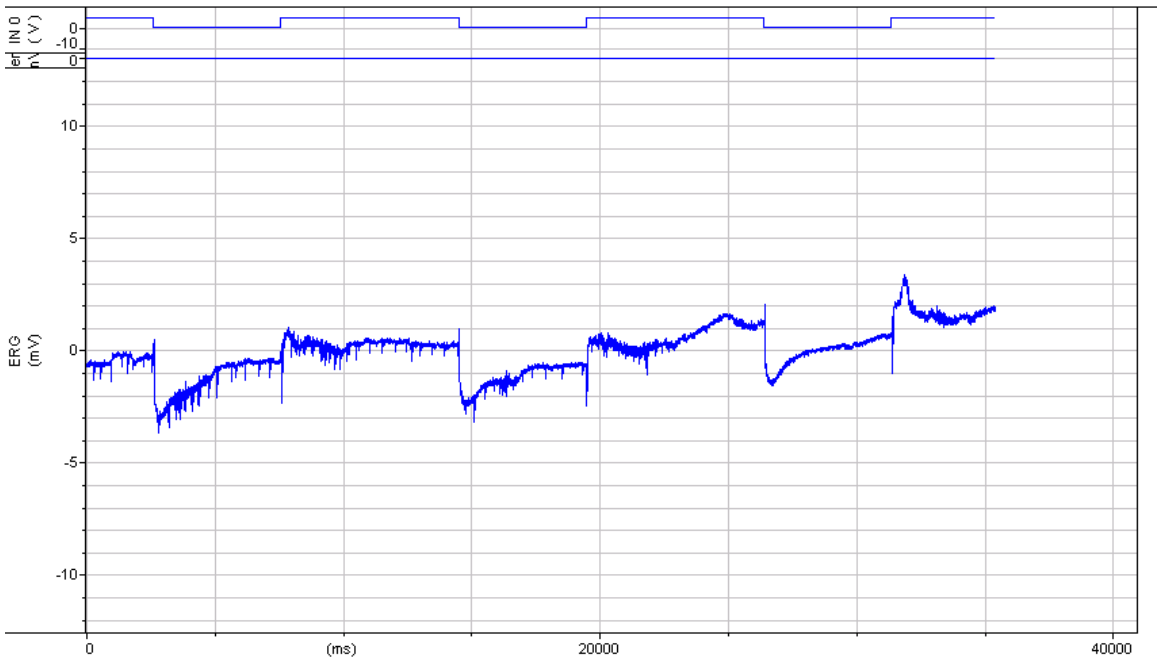
ef IN 0
nV (V)
0
-10
0
10
5
0
-5
-10
ERG
(mV)
0
(ms)
20000
40000

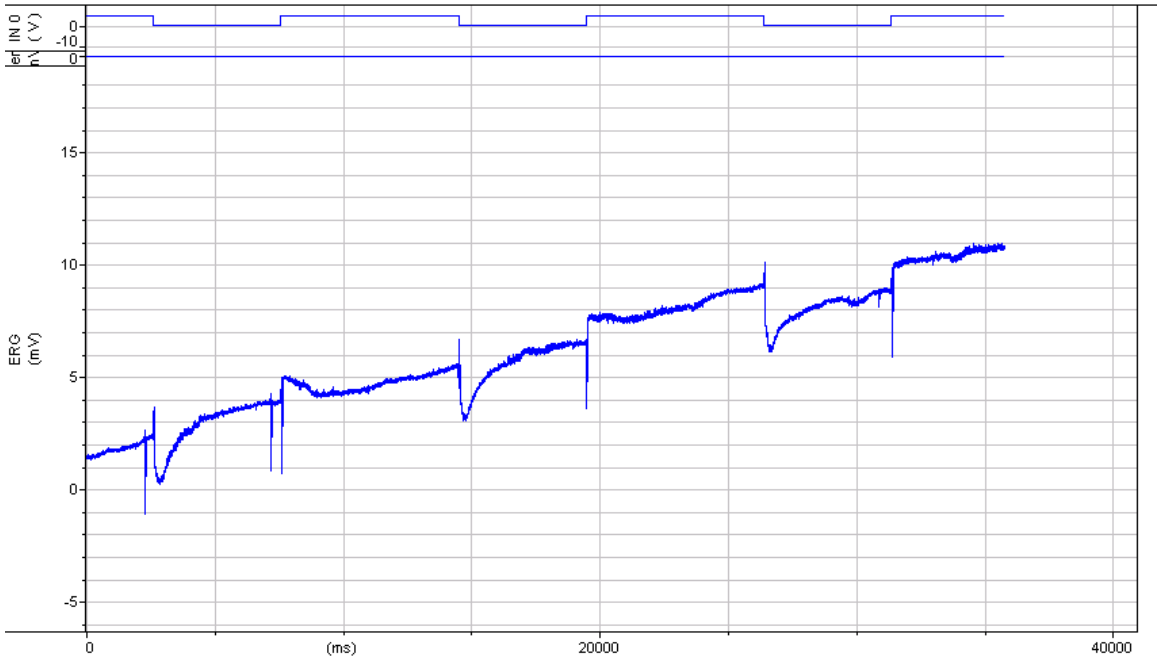
ef IN 0
nV (V)
0
-10
0
15
10
5
0
-5
ERG
(mV)
0
(ms)
20000
40000

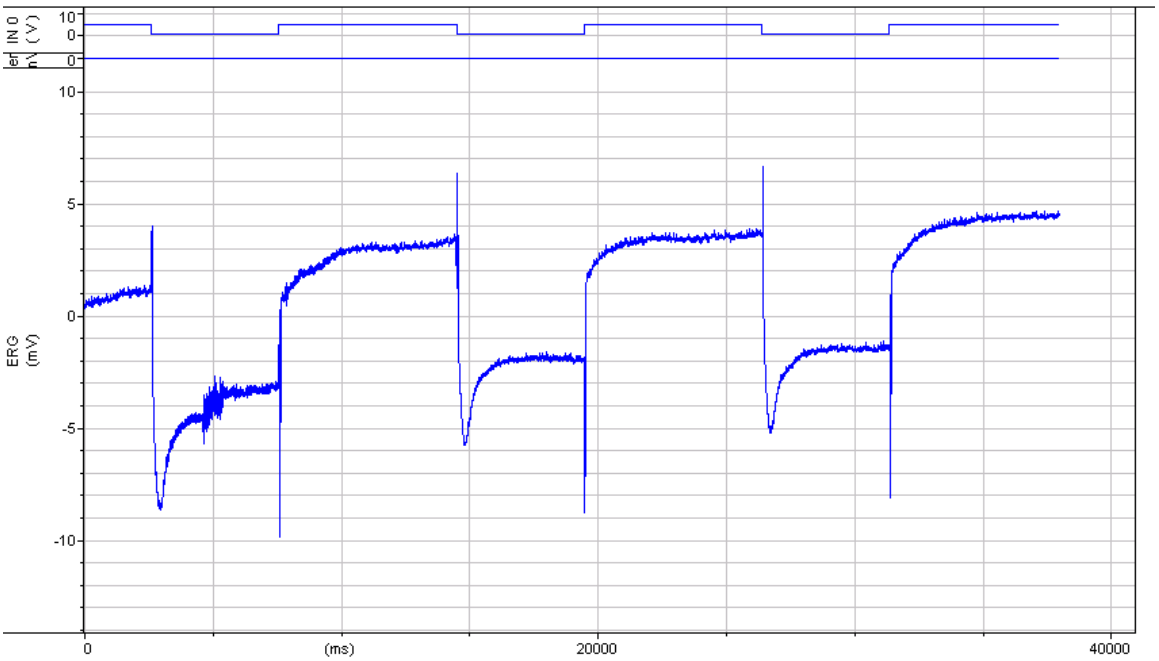
IN 0 (V)
10
0
0
10
5
0
-5
-10
ERG (mV)
0
(ms)
20000
40000

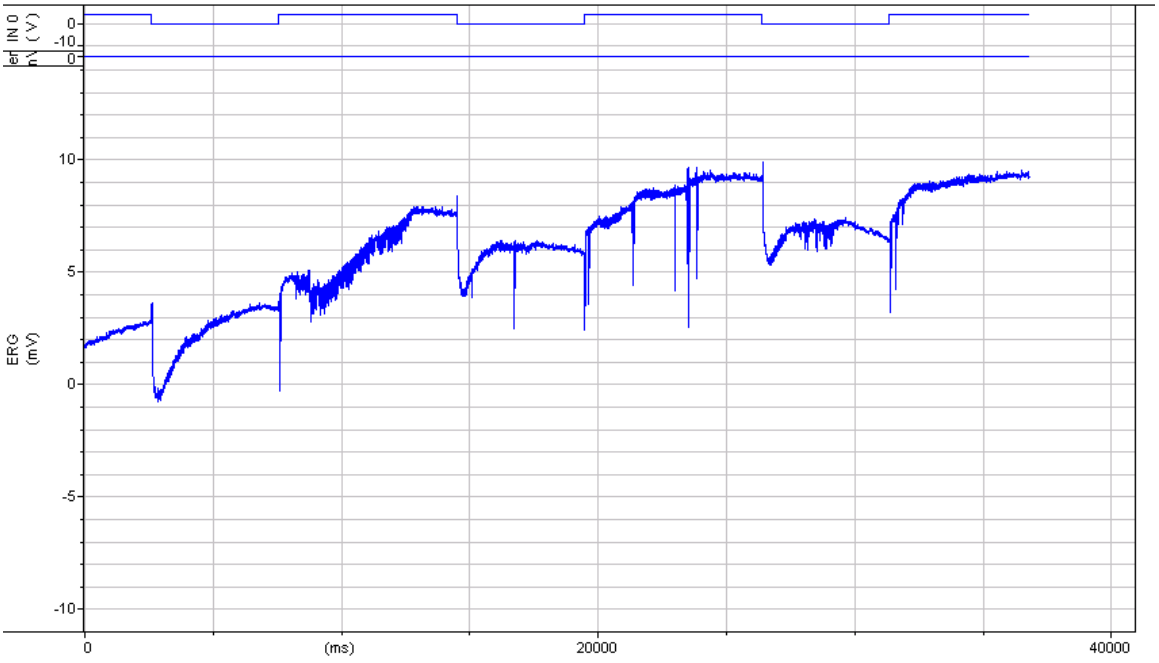
IN 0 (V)
0
-10
0
10
5
0
-5
-10
ERG (mV)
0
(ms)
20000
40000

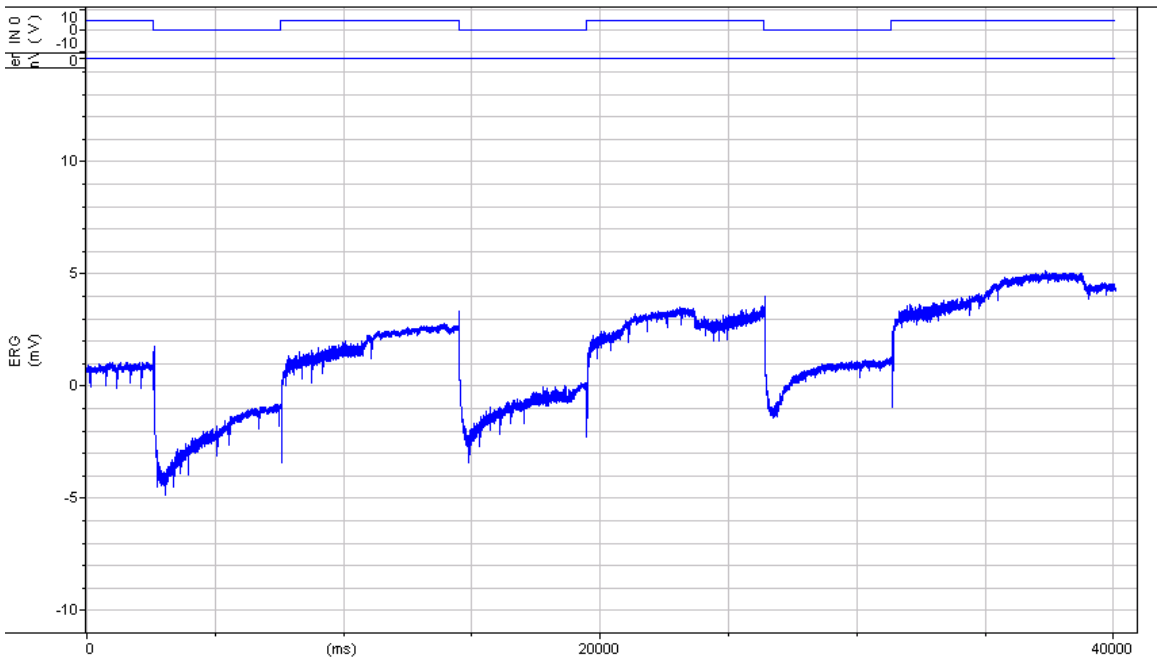
IN 0
(V)
10
0
-10
0
10
5
0
-5
-10
ERG
(mV)
0
(ms)
20000
40000

Genotype: tubGal80ts; *repo*-Gal4> *Acsl* RNAi

Experiment: adult heat shift, 10 day

Phenotype: with transient

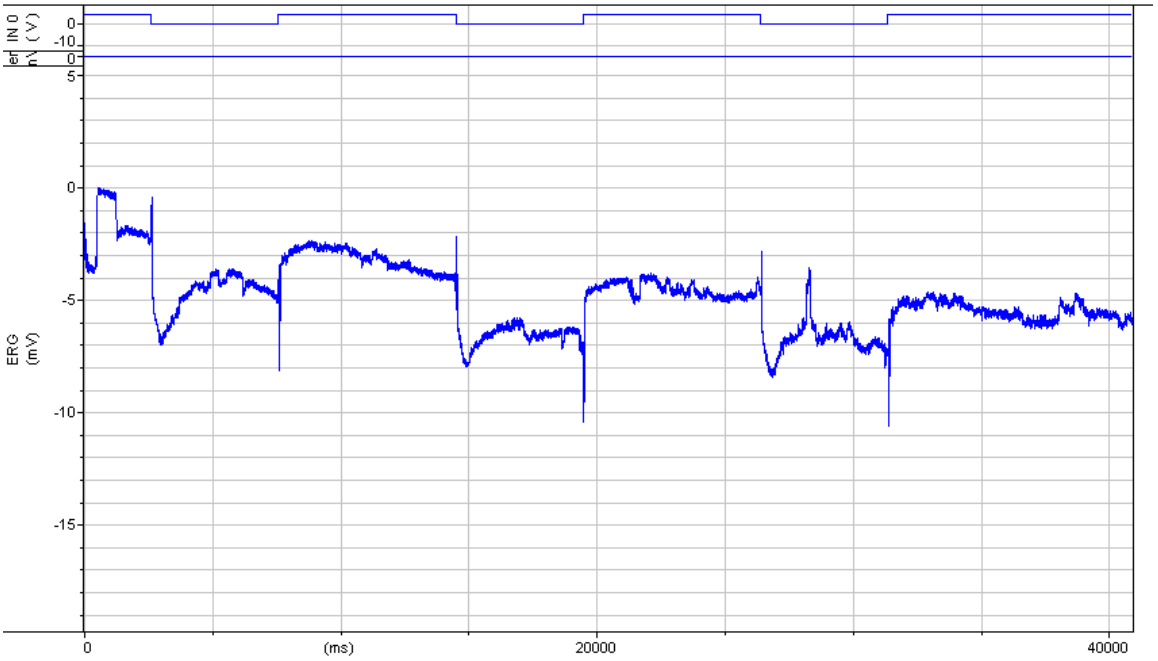

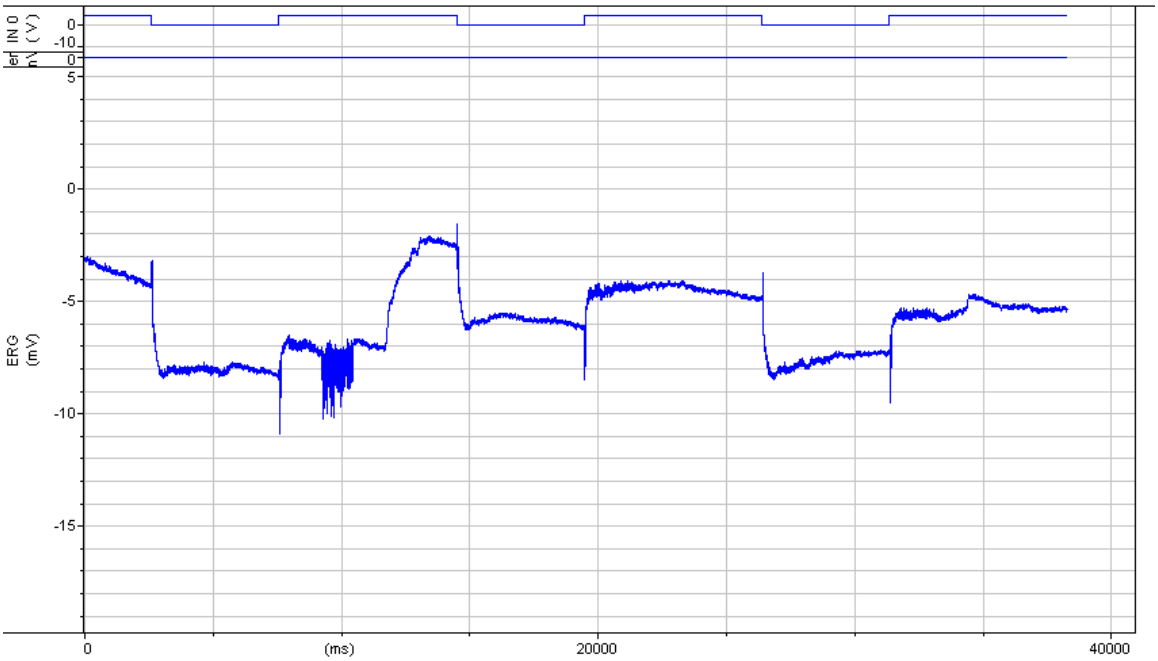

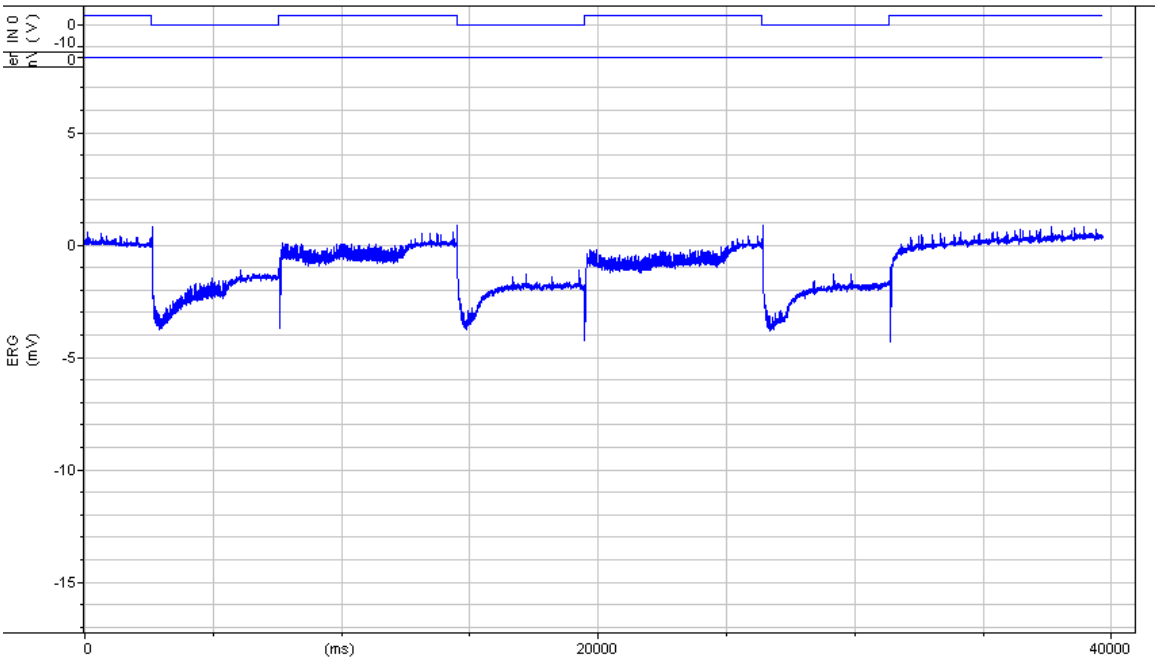
IN 0
(V)
0
-10
0
5
0
-5
-10
-15
ERG
(mV)
0
(ms)
20000
40000

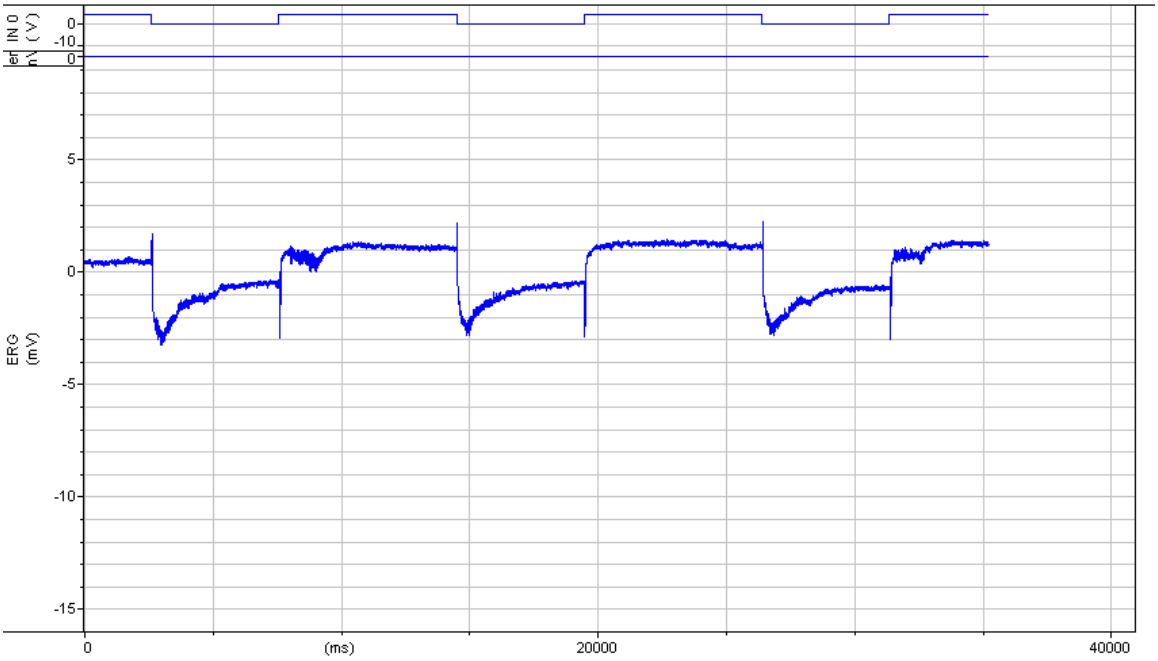
IN 0
(V)
0
-10
0
5
0
-5
-10
-15
ERG
(mV)
0
(ms)
20000
40000

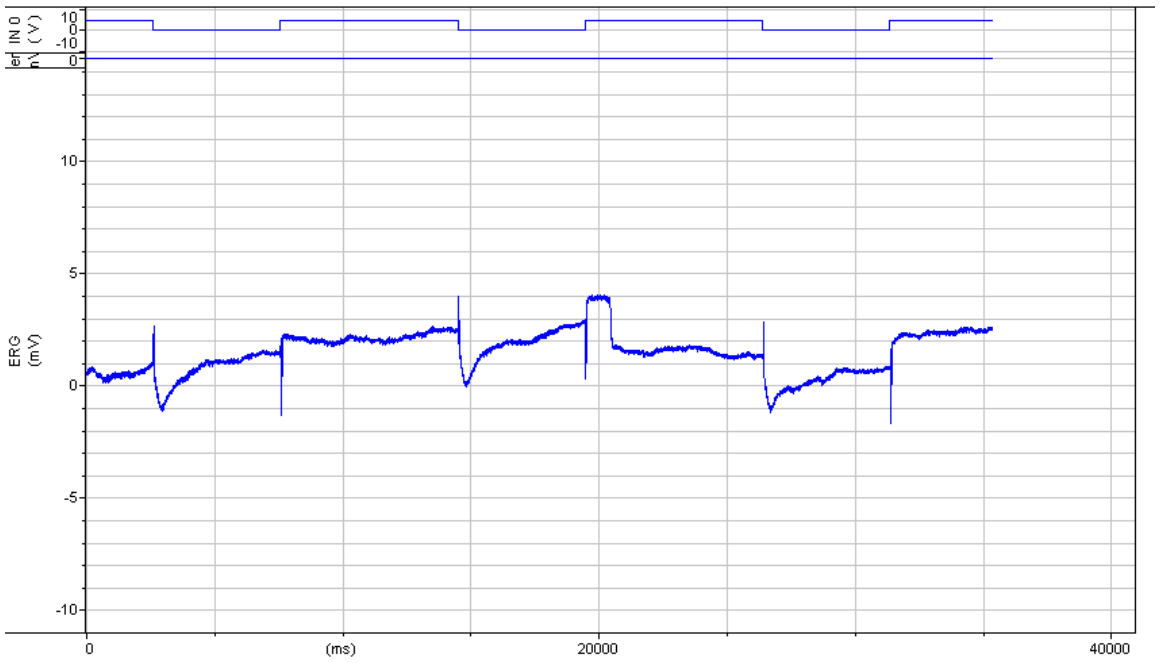
IN 0
(V)
10
0
-10
0
10
5
0
-5
-10
ERG
(mV)
0
(ms)
20000
40000

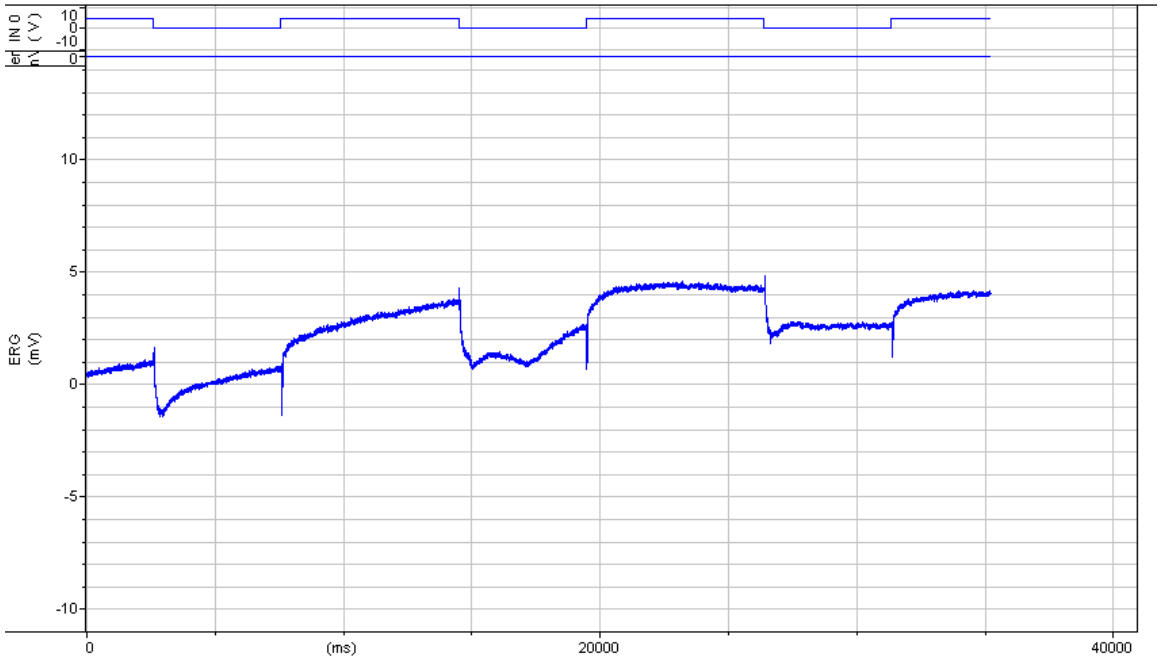
IN 0
(V)
10
0
-10
0
10
5
0
-5
-10
ERG
(mV)
0
(ms)
20000
40000

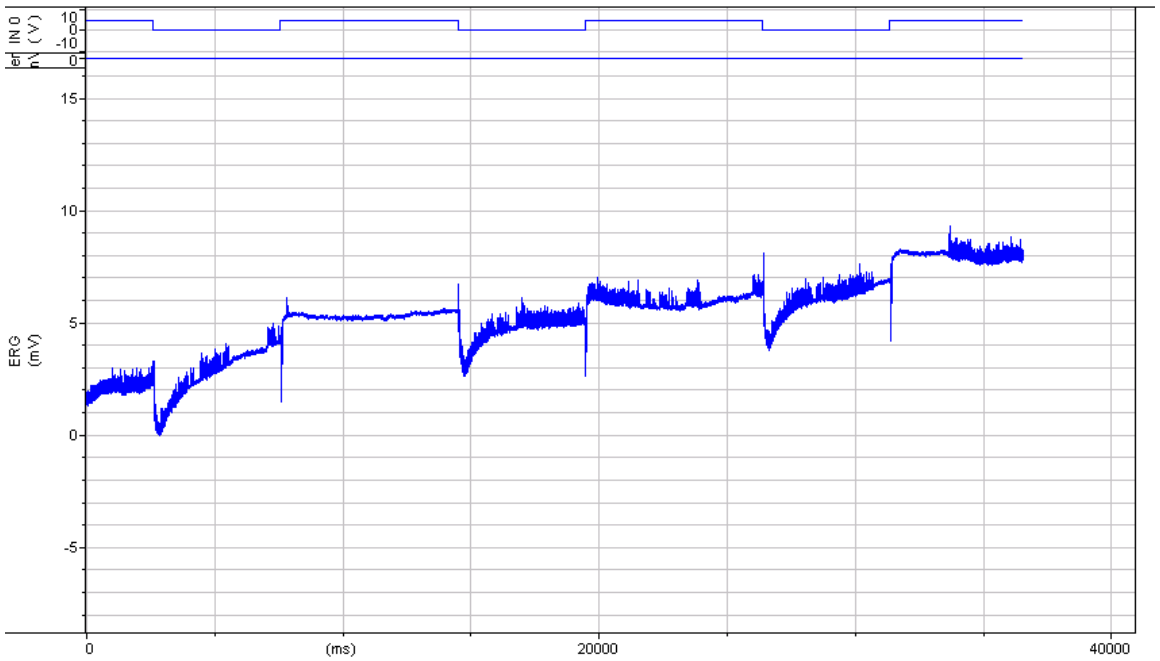
Ref IN 0
(V)
10
0
-10
0
15
10
5
0
-5
ERG
(mV)
0
(ms)
20000
40000

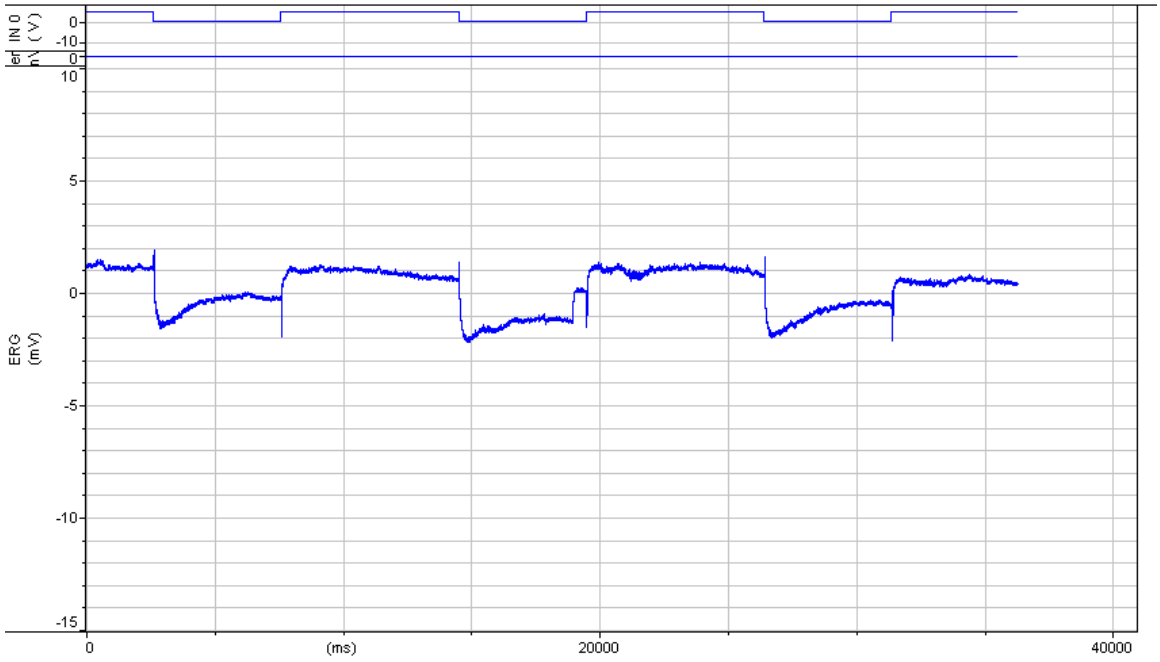
Ref IN 0
(V)
0
-10
0
10
5
0
-5
-10
-15
ERG
(mV)
0
(ms)
20000
40000

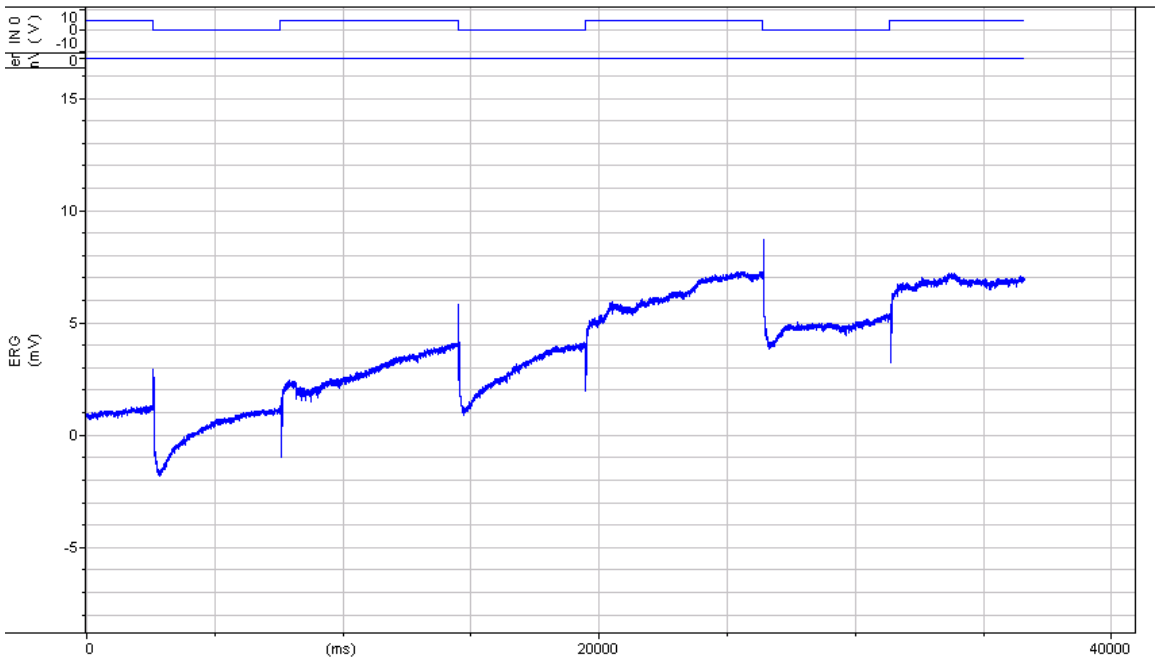
ef IN 0
nV (V)
10
0
-10
0
15
10
5
0
-5
ERG
(mV)
0
(ms)
20000
40000

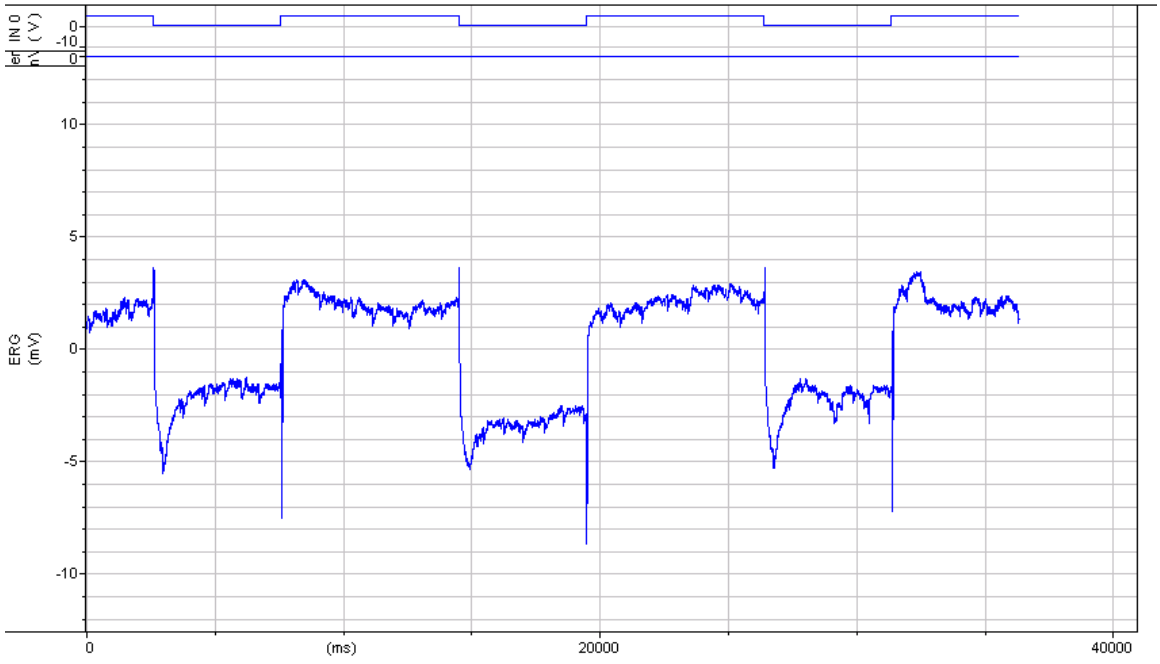
ef IN 0
nV (V)
0
-10
0
10
5
0
-5
-10
ERG
(mV)
0
(ms)
20000
40000

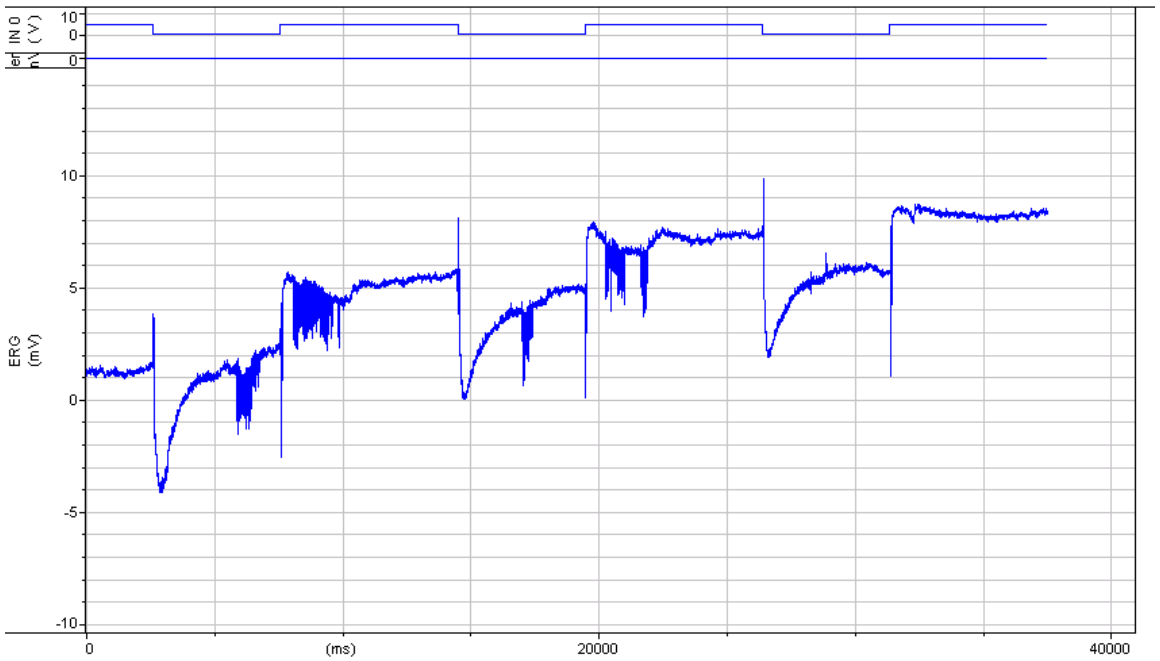
IN 0 (V)
ERG (mV)
10
0
10
5
0
-5
-10
0
(ms)
20000
40000

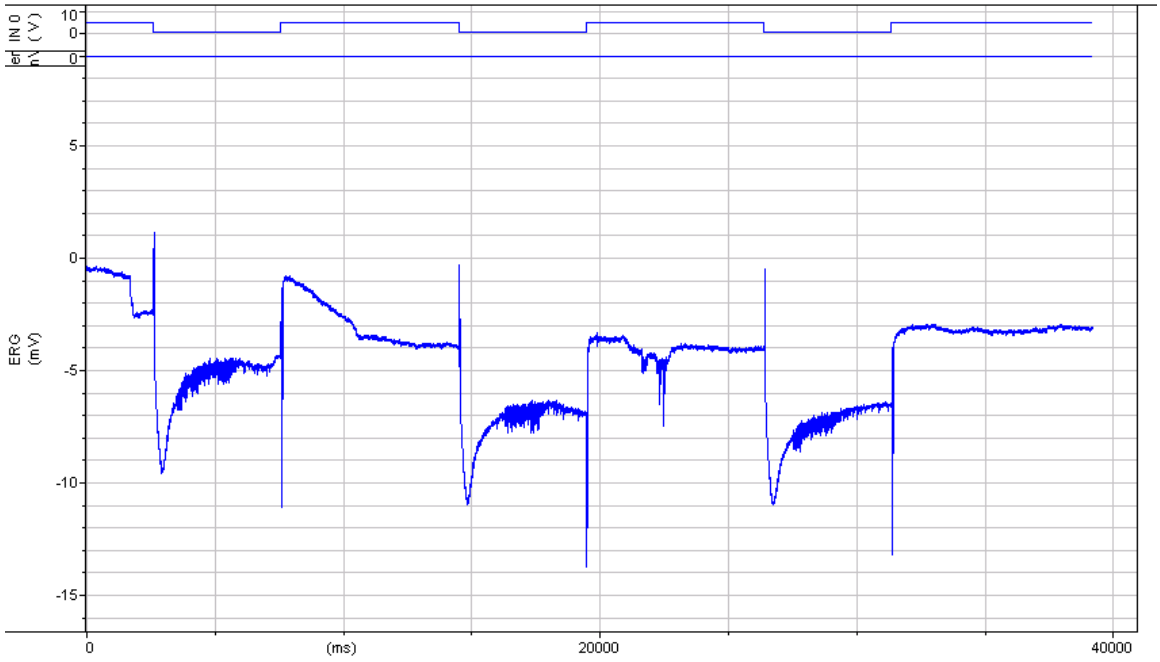
IN 0 (V)
ERG (mV)
10
0
5
0
-5
-10
-15
0
(ms)
20000
40000

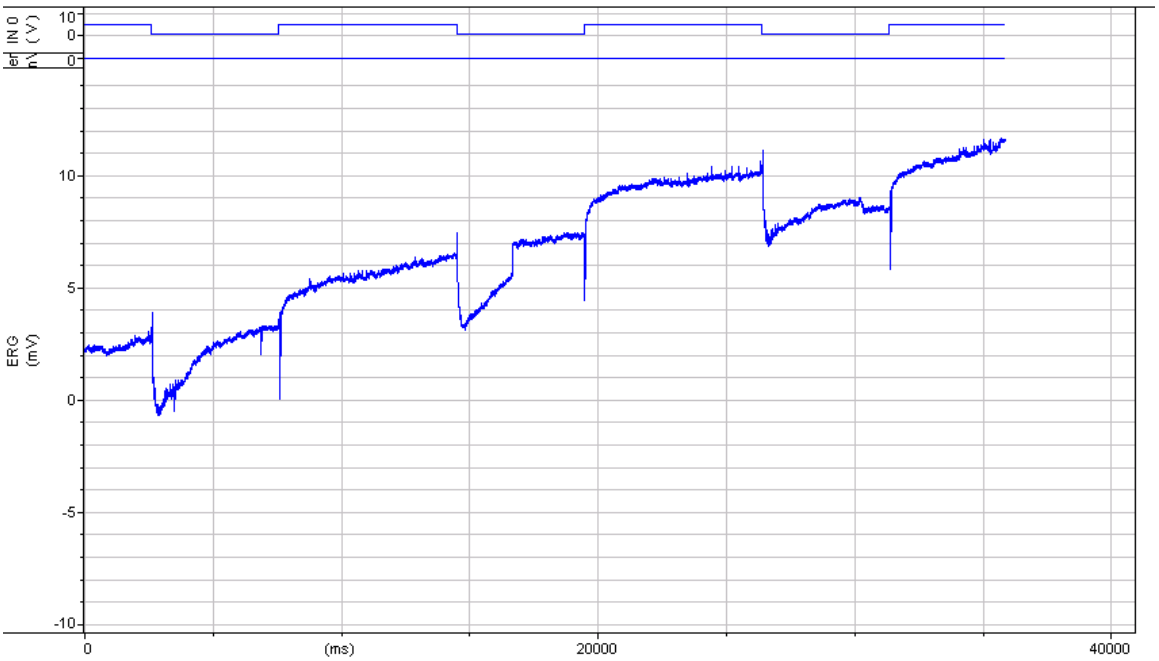
IN 0 (V)
10
0
0
10
5
0
-5
-10
ERG (mV)
0
(ms)
20000
40000

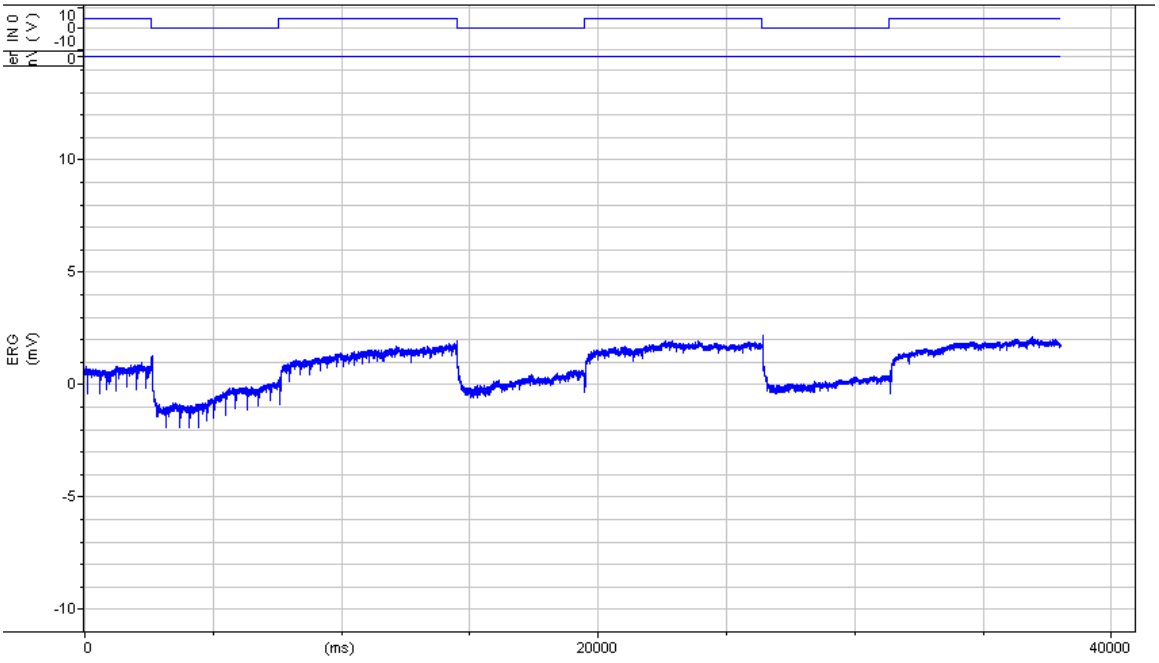
IN 0 (V)
10
0
-10
0
10
5
0
-5
-10
ERG (mV)
0
(ms)
20000
40000

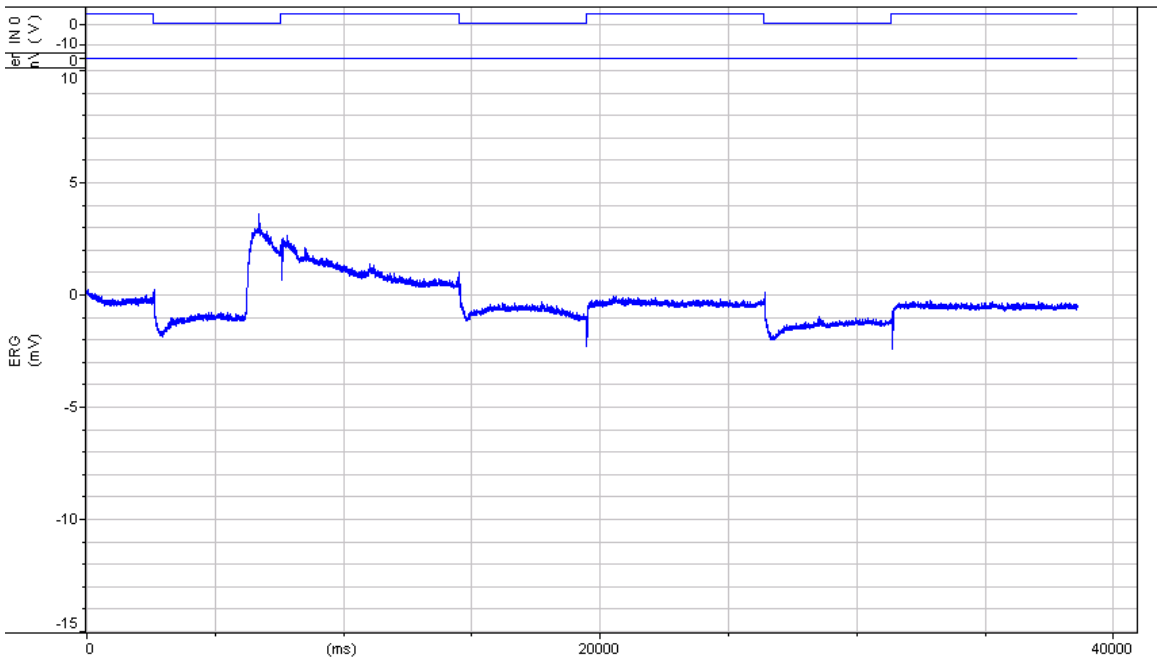
ef IN 0
n\ (V)
0
-10
0
10
5
0
-5
-10
-15
ERG
(mV)
0
(ms)
20000
40000

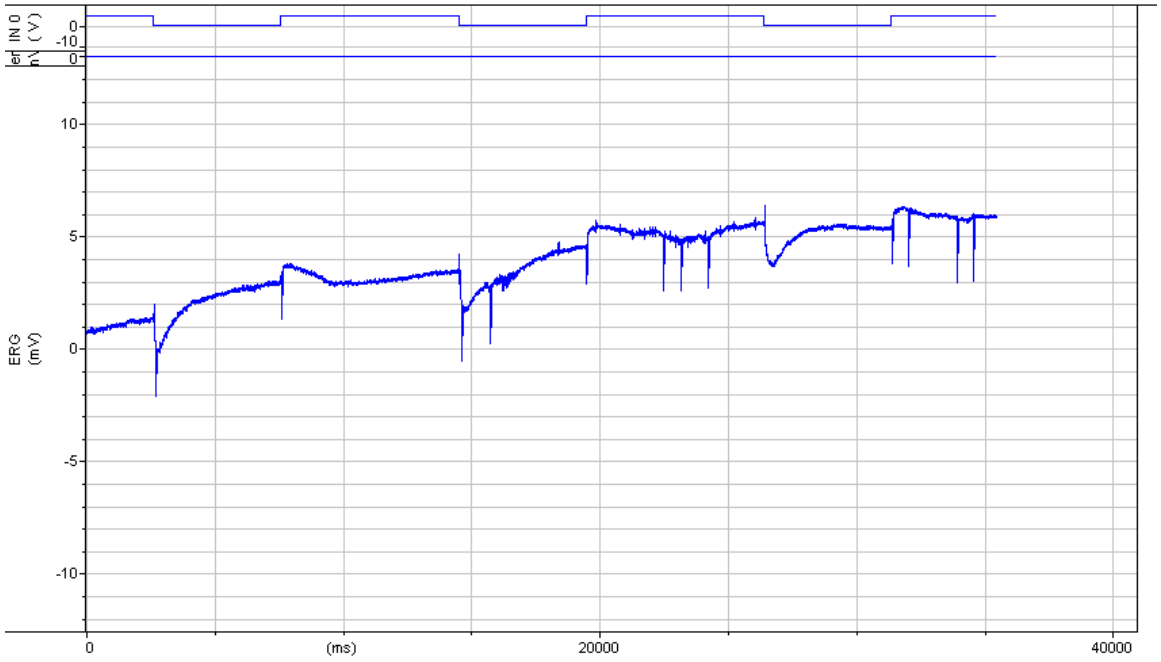
ef IN 0
n\ (V)
0
-10
0
10
5
0
-5
-10
ERG
(mV)
0
(ms)
20000
40000

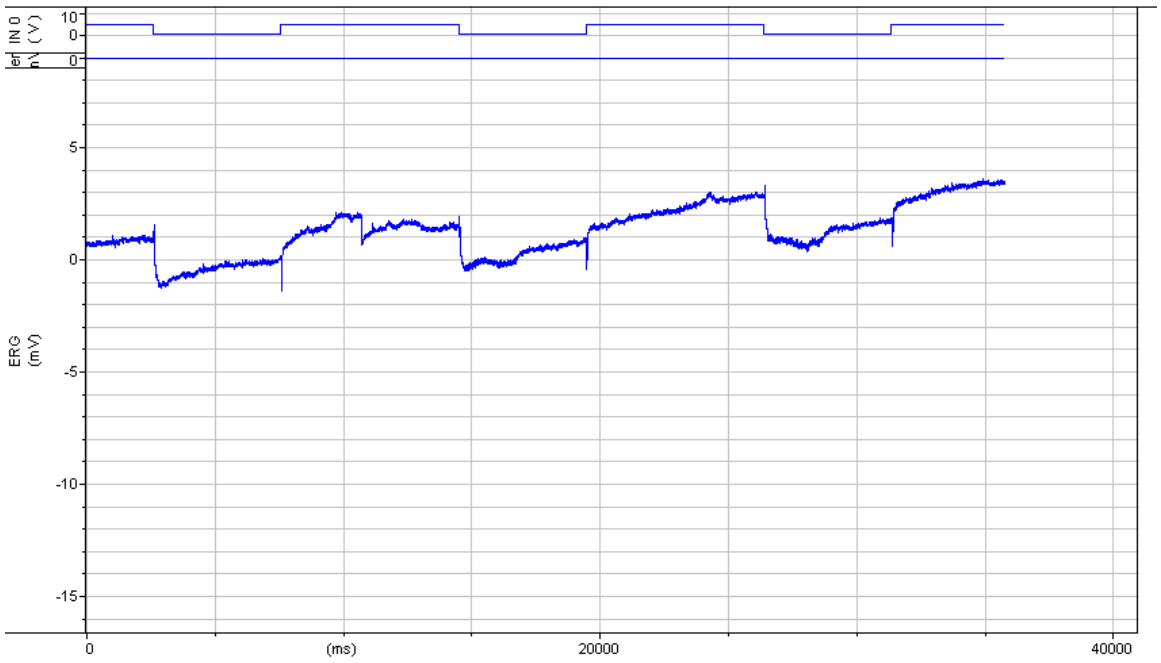
ef IN 0
nV (V)
10
0
0
5
0
-5
-10
-15
ERG
(mV)
0
(ms)
20000
40000

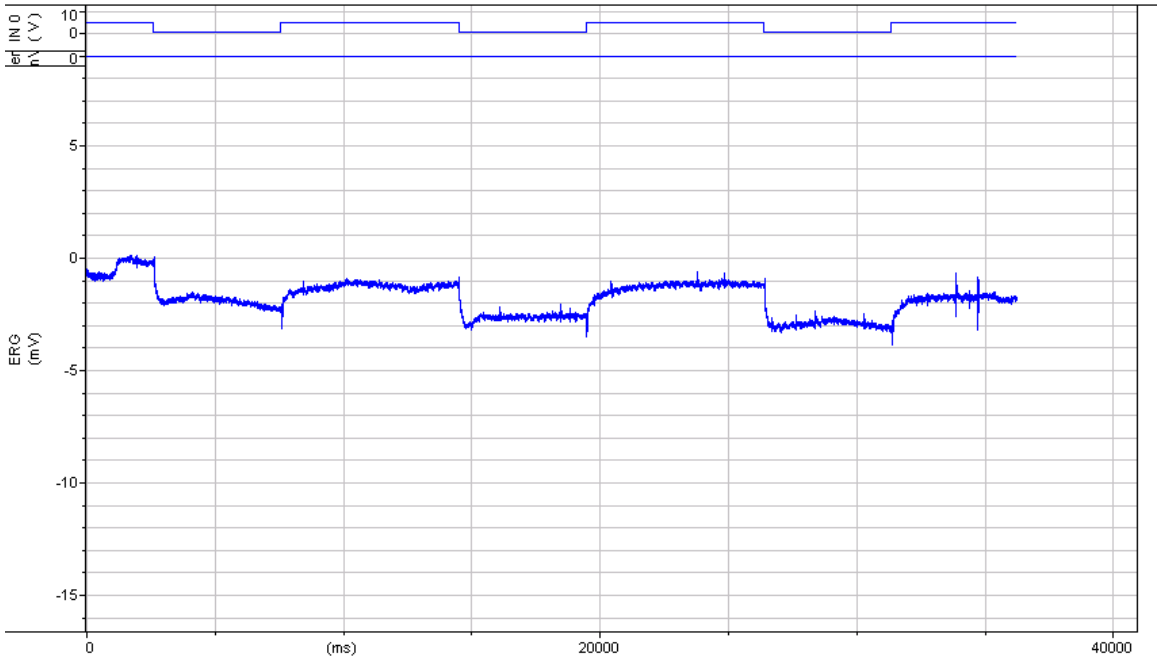
ef IN 0
nV (V)
10
0
0
5
0
-5
-10
-15
ERG
(mV)
0
(ms)
20000
40000